NASA-CR-191318

FINAL REPORT

PHASE B STUDY FOR A UV-MW HORIZON SENSOR ORBITAL EXPERIMENT

BY

J. F. FARRELL, A. R. HALBARDIER, M. A. CANTOR

FEBRUARY 1970

"This document was prepared under the sponsorship of the National Aeronautics and Space Administration. Neither the United States Government nor any person acting on behalf of the United States Government assumes any liability resulting from the use of information contained in this document or warrants that such use will be free from privately-owned rights."

PREPARED UNDER CONTRACT NO. NAS12-2224

BY

SPACE DIVISION, NORTH AMERICAN ROCKWELL CORPORATION
DOWNEY, CALIFORNIA

ELECTRONIC RESEARCH CENTER

NATIONAL AERONAUTICS AND SPACE ADMINISTRATION

SD 70-49

N73-70541
Unclas
00/14 0172845
(NASA-CR-191318) PHASE B STUDY FOR UV-MW HORIZON SENSOR ORBITAL EXPERIMENT Final Report (North American Rockwell Corp.) 347 p
COPY NO. 1

Mr. Mark Gorstein
Technical Monitor
NAS12-103
Electronics Research Center
575 Technology Square
Cambridge, Massachusetts 02139

Requests for copies of this report should be referred to:

NASA Scientific and Technical Information Facility
P.O. Box 33, College Park, Maryland 20740

Space Division
North American Rockwell

FINAL REPORT

PHASE B STUDY FOR A UV-MW HORIZON SENSOR ORBITAL EXPERIMENT

BY

J. F. FARRELL, A. R. HALBARDIER, M. A. CANTOR

FEBRUARY 1970

PREPARED UNDER CONTRACT NO. NAS12-2224

BY

SPACE DIVISION, NORTH AMERICAN ROCKWELL CORPORATION
DOWNEY, CALIFORNIA

ELECTRONIC RESEARCH CENTER

NATIONAL AERONAUTICS AND SPACE ADMINISTRATION

SD 70-49

FOREWORD

Between November, 1969, and January, 1970, the Space Division of North American Rockwell Corporation performed a Phase B study for a UV-MW horizon sensor orbital experiment satellite. This work was conducted under NASA Contract NAS12-2224. The study manager was J. F. Farrell and was assisted by M. A. Cantor. The project engineer was A. R. Halbardier. Major NR contributers to the study included D. Adamski, T. Rudiger, W. Lanning, S. Mercadante, B. Rogers, S. Nalbandian, J. Ambrose, L. Ule, J. Ashley, W. Myers, T. McClintic, R. Thompson, D. Peebles, F. Chapel, and N. Williams. EOCOM Corp. and Exotech, Inc., contributed in the areas of attitude determination and fine sun sensors.

The appendix contains a list of the Interim Reports (TDR's) submitted to NASA ERC during the study period.

CONTENTS

Section	Page
INTRODUCTION	1
SUMMARY AND CONCLUSIONS	3
Spacecraft Concepts and Missions for Flying Experiments	3
Orbital Analysis	5
Attitude Determination and Experiment Pointing	6
Mission Success Probability Analysis	7
Data Acquisition and Transmission Analysis	8
Attitude Control System	9
Telemetry, Tracking, Command and Data Handling System	11
Electrical Power Generation and Distribution System	13
Instrument Alignment Error Analysis	14
Satellite Structures Analysis	16
Thermal Control Analysis and Design Requirements	17
Mission Operations Plan	18
Program Implementation Plan for Phases C and D	18
EXPERIMENT OBJECTIVES	20
Study Objectives	20
DESCRIPTION OF EXPERIMENT SENSORS	26
UV Radiometer	26
MW Radiometer	26
SPACECRAFT CONCEPTS AND MISSIONS FOR FLYING EXPERIMENTS	29
Flight Techniques Review	30
Spin Stabilized vs. Local Vertical Experiment Configurations	39
Experiment Complexity	46
Experiment Integration on 3-Axis Stabilized Spacecraft	55

Section Page

Summary of Flight Alternatives Eliminated 66

Recommended Flight Mode and Available Missions 75

MISSION ANALYSIS 77

Orbital Analysis 77

Attitude Determination and Experiment Pointing Analysis 149

Mission Success Probability Analysis 224

Data Acquisition & Transmission Analysis 231

SPACECRAFT SYSTEMS ANALYSIS 246

Attitude Control System 248

System Analysis 250

Tradeoff Analysis of Onboard vs. Ground Controlled Error Computer for Attitude Control 283

System Description 289

Size, Weight, & Power Requirements 309

Performance Specifications 317

Operations Plan 320

Telemetry, Tracking, Command, and Data Handling System 360

Data Handling System Analysis 361

Telemetry, Tracking, & Command System Description 380

Performance Specifications, TT&C System 403

Communications Link Analysis 410

Data Reduction Requirements 417

Electrical Power Generation and Distribution System 420

System Analysis & Description 422

Section | Page

Power Profile 448

Performance Specifications 448

Increased Power Tradeoff Analysis 457

Instrument Alignment Error Analysis and Effects of Launch on Alignment 459

Satellite Structures Analysis 463

Spacecraft Design 464

Critical Interface Requirements Between Reference Satellite and Launch Vehicle 468

Mass Distribution Within the Satellite 475

Balancing Requirements 478

Thermal Control Analysis & Design Requirements 483

MISSION OPERATIONS PLAN 492

Prelaunch. 492

Launch 494

Operational 494

Task/Time Sequence 498

PROGRAM IMPLEMENTATION PLAN 505

Project Management Plan 507

Work Breakdown Structure and Program Development Schedule . . . 513

Subsidiary Program Plans 521

GSE Requirements 563

Hardware Utilization List 566

Program Cost Estimates 569

Section | Page

BIBLIOGRAPHY 572

APPENDIX A-1

List of Interim Reports (TDR's) Submitted to NASA ERC A-1

ILLUSTRATIONS

Figure		Page
1	Ultraviolet Sensor	27
2	Microwave Sensor	28
3	Study Elements	32
4	Selection of Preferred Approach	40
5	Major Categories of Experiment Operations	43
6	Function Analysis of Launch Operations	44
7	Experiment Ground Operations Functional Analysis	45
8	Predicted Failure Rates for Spin Stabilized and Vertical Satellites	56
9	UV Horizon Sensor with Scanning Mechanism	58
10	Vertically Oriented Space Pointing Geometry	60
11	Functional Block Diagram of Attitude Determination Subsystem	62
12	Determination of the Locator Point	80
13	Orbit Characteristics Versus Repeat Cycle for 90-Degree Polar Orbits	83
14	Locator Point, Range Circle Relationship	86
15	Nimbus Orbit Trace with Polar Equatorial Range Circles (Overlay for Figure 16)	90
16	Polar World Map	91
17	Horizon Point Map (Constant True Azimuth Contours)	92
18	Horizon Point Map (Constant Satellite Latitude Contours)	93
19	Horizon Point Map (Constant Relative Azimuth Contours) Relative Azimuth = 30°, 60°, 90°	94
20	Horizon Point Map (Constant Relative Azimuth Contours) Relative Azimuth = 120°, 150°	95

Figure		Page
21	Horizon Point Map (Constant Relative Azimuth Contours) Relative Azimuth = 180°, 210°, 240°	96
22	Horizon Point Map (Constant Relative Azimuth Contours) Relative Azimuth = 270°, 300°, 330°, 360/0°	97
23	True Azimuth of Spacecraft	99
24	Variation in Angle Between Sun and Orbit Plane (ERTS Orbit)	105
25	Variation in Angle Between Sun and Orbit Plane (ITOS Orbit)	106
26	Variation in Angle Between Sun and Orbit Plane (Nimbus Orbit)	107
27	Sun Elevation Angle - ITOS (790 n.mi., 9 AM, D.N., February Launch)	110
28	Sun Elevation Angle Every 15 Degrees in the Orbit - ERTS (496 n.mi., June Launch)	111
29	Sun Elevation Angle - ITOS (790 n.mi., 3 PM, A.N., February Launch)	112
30	Sun Elevation Angle (600 n.mi., Noon D.N., May 1 Launch)	113
31	ERTS Ground Trace	115
32	ITOS Ground Trace	116
33	Nimbus Ground Trace	117
34	Polar World Map	118
35	STADAN Tracking Circles for 600 n.mi. Altitude	119
36	STADAN Tracking Circles for 790 n.mi. Altitude	120
37	Ground Trace Repeat Cycle Versus Orbit Period	122
38	Percent Time in Sunlight Versus Time From Launch	123
39	Delta Injection Errors	125
40	3 σ Altitude Variation Delta Launch Vehicle 600 n.mi. Circular Orbit	126

Figure		Page
41	Orbit Parameter Variation Due to Injection Error (In Altitude) of Delta Vehicle	128
42	SCOUT Injection Errors	129
43	One-Standard Deviation in Injection Condition	130
44	Burner II Injection Errors	131
45	Variation in Angle Between Orbit Plane and Sun Line	132
46	Altitude/Inclination Trade-Off for Fixed Nodal Period	139
47	Altitude/Inclination Trade-Off for Fixed Nodal Period	140
48	Altitude Versus Inclination for Sun Synchronism	141
49	Sensitivity of Node Precession to Inclination	142
50	Sensitivity of Node Precession to Altitude	143
51	Slip of Ground Trace at Equator to Altitude Error	144
52	Slip of Ground Trace at Equator due to Inclination Error	145
53	Sun Plane and Vector	151
54	Geometry of Sun/Spin Axis Reference	152
55	Chord Geometry	152
56	Sun Sensor Field of View	155
57	Orientation of Sun Sensor Planes	156
58	Sun Sensing Geometry	158
59a	Body Axes X' Y' Z'	160
59b	Local Axes X Y Z	160
60	Experiment Data Flow Diagram	165
61	Sample Output of Synthesis Program	167
62	Effect of Undetected Roll of Satellite on Horizon Point Measurement	170

Figure		Page
63	Horizon Error at Satellite	172
64	Angles Defining Sun's Position	174
65	Recommended Orientation of Sensor Axes	180
66	Displacement of Vehicle System From Real Spin Axis	183
67	Coordinate Systems	185
68	Block Diagram of Reference Attitude Determination System	187
69	Sun Orientation	190
70	Principal Coordinate Systems	194
71	Angles Between Coordinate Systems	195
72	Sun 7° From Orbit Plane - Standard Case	198
73	Error in Horizon Altitude	200
74	Sensor Axes Lines of Sight	202
75	Located Horizon Error Due to Sun Clock Angle	203
76	Indicated Horizon Error for Sun Portion Due to Sun Cone Angle Error	205
77	Geometry of Cross-Axis Sun-Sensing System	208
78	Error in Horizon Measurement Due to Error in Sun Sensing	209
79	Position of Sun on Scan Plane	211
80	Sun Sensor Error	212
81	Ground Trace - IR Horizon Sensors	214
82	IR Horizon Sensor	216
83	Simplified Block Diagram - Energy Balancing Sensor	217
84	Non-Imaging Sensor	219
85	SEAS Details	223

Figure		Page
86	Reliability Logic Diagram - UV/MW Horizon Sensor Experiment Satellite	226
87	Reliability Summary for Electrical Power and Generation System 1.0.	227
88	Reliability Summary for TTC & Data Handling System 2.0	228
89	Reliability Summary for Attitude Control and Determination System 3.0	229
90	Five Degree Mask (Transparancy).	233
91	Polar Projection.	234
92	System Block Diagram of MW-UV Satellite	247
93	Orientation of Damper Tubes in TIROS IX..	256
94	DME-A Nutation Damper Configuration	257
95	Coordinate System Definition.	260
96	Attitude Error Orientation in Orbit Coordinates	263
97	Attitude Sensor Geometry	264
98	Sensor Scanning Pattern and Output Signals	265
99	QOMAC Coil Current Torquing Profile in Attitude Correction Mode	272
100	Compensated and Uncompensated Dipole-Moment Programs Compared with Ideal Quarter-Orbit Switching.	275
101	Orientation of MASC Coil in Orbit	278
102	Block Diagram of Dynamic Control System	290
103	TEAM Precession-Damping Devices.	292
104	Orbital Attitude and Spin Rate Control Actuator	295
105	Magnetic Dipoles Associated with QOMAC, MBS and MASC Coils.	296
106	Orbital Attitude and Spin Rate Controller	299
107	Preliminary Location Equipment Sensors	306

Figure		Page
108	V-Head Attitude Sensor Geometry and Outputs	307
109	Mission Mode-Size Profile for Dynamic Control System	314
110	Mission-Mode Weight Profile for Dynamic Control System	315
111	Mission Mode - Power Profile for Dynamic Control System	316
112	Dynamic Control System Status and Control Panel	323
113	Marking of Raw Attitude-Sensor Data	329
114	Two-Degree Roll Angle Nomogram	332
115	Example of 2-Degree Sine-Wave Template	335
116	Example of 10-Degree Sine-Wave Template	336
117	Example of 90-Degree Sine-Wave Template	337
118	Sample Polar Graph	341
119	Correction Required to Compensate λ for Effect of Inclined Earth Dipole	344
120	Residual Dipole Moment Versus Drift Rate	346
121	Format of Teletype Message (WALACO)	351
122	Format of Teletype Message (ALASKA)	352
123	Example of Reduced Attitude Data Derived from WALACO Attitude Message	355
124	Example of Graphical Determination of Γ and λ	357
125	Satellite Geometry	364
126	UV Horizon Sensor Output Signal	367
127	Error Reduction Techniques	368
128	Error Versus Encoded Bits	372
129	Microwave Sensor Output Signal	374
130	Avionics System Block Diagram	381
131	PCM Formatter	384

Figure		Page
132a	Analog Signal Format	385
132b	Signal Format	386
133	UV-MW Timer	389
134	Sensor Registers	391
135	Turnstile Antenna	394
136	Dipole Antenna	395
137	Sleeve Antenna	396
138	Monopole Antenna	397
139	Monopole Antenna Radiation Pattern - Principal Plane	398
140	Monopole Radiation Pattern - Conical Cut	399
141	Electrical Power Generation and Distribution Functional Block Diagram	423
142	Baseline Electrical Load and Battery Charge Profile (Sensors = 8.5 W)	427
143	Simplified EPGDS Block Diagram.	429
144	Simplified Boost Voltage Battery Charger Schematic	433
145	Peak Power Tracking Circuit.	434
146	Pulsewidth Modulated (PWM) Bucking Regulator Block Diagram	436
147	DC-DC Converter Block Diagram	437
148	Comparison of Nickel-Cadmium and Silver-Cadmium Battery Weights	439
149	Battery Charging Cycles as a Function of Percent Discharge.	440
150	Battery Weights for Duty Cycle Mode	441
151	Physical Dimensions for Nickel-Cadmium 20-Cell Hermetically Sealed Batteries	442

Figure		Page
152	Physical Dimensions for Silver-Cadmium 22-Cell Batteries.	443
153	Wire and Harness Candidates for UV-MW Sensor Satellite.	446
154	Alternate Electrical Load and Battery Charge Profile (Sensors = 30 and 50 W)	458
155	Drawing 3026-2A, Satellite Configuration	466
156	Thor/Delta Second-Stage Engine (DSV 3L-4 T-III-C Transtage) Compartment	469
157	Drawing 3026-1 Canister Configuration and Installation (DSV 3L-4 T-III-C Transtage)	471
158	Incident Heat Flux on Solar Panels	488
159	Solar Panel and Equipment Temperature	489
160	Temperature-Time History of Equipment After Maximum Power is Turned On.	490
161	Operations Plan, Prelaunch Phase	499
162	Operations Plan, Prelaunch Phase, Final 48 Hours.	500
163	Operations Plan, Launch Phase	501
164	Telemetry Contracts for a Typical Day of Operation (Orbits 27-41)	502
165	Program Development Planning	506
166	Work Breakdown Structure Phase C - Design	514
167	Work Breakdown Structure Phase D - Development Operations	515
168	Development Schedule	517
169	Program Engineering Process.	523
170	Manufacturing Breakdown - Satellite	530
171	Manufacturing Breakdown - Canister	532
172	Proposed Manufacturing Composite Schedule	534

Figure		Page
173	Prelaunch Test Operations Schedule	551
174	Major Quality Assurance Functions.	556
175	F&IE Property Management Systems	562

TABLES

Table		Page
1	Missions Which Cannot Meet Experiment Data Requirements	34
2	Flight Approaches, Alternate Experiment Concepts, and Required Experiment Attitude Determination Concepts	36
3	Alternate Approaches to Attitude Determination	41
4	A General Comparison of the Relative Complexities of Spin Stabilized and Vertical Satellites	50
5	Attitude Control Tradeoffs, Roll, Yaw, Torquing	52
6	Component Sample Weights	54
7	Candidate Orbits for Mid-Summer or Mid-Winter	88
8	STADAN Stations for Horizon Sensor Satellite	109
9	Rates in Inertial Space	137
10	Key to Program Headings	168
11	Coordinate Systems	184
12	Principal Attitude Quantities	186
13	Transformation Matrices	196
14	Error Contributions to Horizon Point Altitude Determination	199
15	Error Contributors to Sun Angle Determination	204
16	Characteristics of Barnes Sensor	215
17	Tracking Stations	232
18	Orbit Characteristics	232
19	Computer Printout Typical Data Acquisition Period - Night	236
20	Computer Printout Typical Data Acquisition Period - Day	237
21	Orbits of Near-Continuous Data Acquisition and Transmittal (No Data Storage)	239
22	Typical Operations Cycle	244

Table		Page
23	Command Programs	301
24	Dynamic Control System Size, Weight and Power	310
25	Up-Link Signal Format	325
26	Down-Link Signal Format	325
27	MASC Performance (WALACO Contacts Only)	347
28	Attitude Control Command Word Format	349
29	Sample Calculations of Normalized Time Increment	353
30	Sample Calculations of Normalized Time	353
31	Sample Tabulation of Instantaneous Roll Angle	354
32	Measurement List	363
33	Tradeoff Summary	373
34	Command List	378
35	TT&C System Characteristics	383
36	Calculated Minimum Requirements for Telemetry	411
37	OSO Transmitter Link Margin - Telemetry	413
38	Tracking Margin (OSO Transmitter)	414
39	Command Link Margins	416
40	Electrical Load Requirements	449
41	Preliminary Satellite Weight Statement	476
42	Preliminary Satellite Mass Properties	479
43	Equipment Temperature Limits	483
44	Mean Temperature Effects of Candidate Orbits	491
45	Launch Sequence - Delta Booster	495
46	GSE Requirement List	564
47	UV-MW Sensor Experiment Spares List	567

INTRODUCTION

Although horizon sensors for vehicle guidance and control have been in existence since 1958 and are used on the majority of orbital spacecraft, the state of the art in their design has been limited because many characteristics of the earth's horizon are not well known. These characteristics must be accurately determined in order to realize the ultimate design and maximum accuracy of horizon sensors. Given a comprehensive knowledge of the horizon profile, an optimum sensor mechanization can be designed by incorporating signal processing logic with optical and electronic filtering, electronic compensation, and computer modeling techniques.

Many significant experiments have been conducted in both the infrared spectrum and in the UV regime. Some of these experiments are the NASA D-61 Program, the Air Force Infrared Atmospheric Transmission Evaluation Program (IRATE), the Eastman Kodak experiment, the X-15 experiments, and Suborbital Scanner Probe. All of these programs have added knowledge of the horizon and, in so doing, have directed further research towards the 14-16 micron band, UV, and MW spectra.

An experiment has been proposed to orbit UV and MW horizon sensors to provide for additional data on the earth's horizon and demonstrate the principle of autonomous navigation. The objectives of flight-testing the two sensors are:

1) To evaluate the capability of the UV sensor to detect the ultraviolet horizon.
2) To evaluate the capability of the microwave sensor to detect the molecular oxygen horizon.

3) To determine the stability of the detected horizons.

To meet these objectives, data must be gathered for the following conditions:

1) Diurnal variation. Measurements must be adequate to determine the variations during the day at a fixed geographic location.
2) Seasonal variation. Measurements must be adequate to determine the variations from month to month over the four seasons of the year taken at the same position.
3) Latitude variation. Measurements must be obtained at latitude separations no greater than 5 degrees, including, if possible, both poles.
4) Geographical and meteorological conditions. Measurements must be obtained over land masses, oceans, and large weather systems and their transitions.
5) Sun zenith angle. Measurements must be adequate to determine the variations as the angle between sun line and zenith varies from 0 to 70 degrees at position of the locator altitude.

The goal of this study is to provide NASA ERC with information concerning viable alternatives and associated costs for the space flight test of an ultraviolet (UV) horizon sensor and a microwave (MW) horizon sensor sometime during the period CY 1970 through the end of CY 1973.

SUMMARY AND CONCLUSIONS

This report describes the study results of viable alternatives and associated costs for the space flight of (1) an ultraviolet horizon sensor, and (2) a microwave horizon sensor, for the gathering of data on their respective horizons. A detailed description of the study goals is presented in the section EXPERIMENT OBJECTIVES.

The major conclusion derived in the study is that the reference approach proposed by ERC (a small spin-stabilized satellite), launched piggyback in the Thor/Delta transtage engine compartment, is the most cost-effective approach to fly the experimental sensors and gather the desired data.

A brief summary is presented here of the major study elements. Detailed descriptions are contained in the report text.

SPACECRAFT CONCEPTS AND MISSIONS FOR FLYING EXPERIMENTS

An investigation was conducted of suitable flight alternatives for gathering data on the earth's ultraviolet and microwave horizons. The primary purpose of this investigation was to determine whether flight alternatives could be configured which are more cost-effective than the referenced approach which was configured by ERC.

The mission characteristics and flight techniques of 10 different space programs were reviewed. Over 15 specific flights which are scheduled within the time frame of interest were analyzed for applicability to this experiment. In each case, the salient features of the mission/experiment are identified and an evaluation was made as to

whether or not the mission is a candidate for further analysis. Promising alternative approaches were configured to specifically determine the relevant factors in cost and complexity, and these were compared to the reference spinning satellite.

Three alternate approaches, (1) a piggyback earth-oriented satellite, (2) integrate experiments on NIMBUS, and (3) integrate experiments on ERTS, are described which can supply the required data; however, the attitude determination subsystems are significantly more complex than for the spinning satellite and involve techniques which have yet to be flight proven. Also, in the piggyback vertical satellite a number of subsystems are more complex than for the spinning reference satellite. This study indicates the referenced approach is the most cost-effective manner in which to gather the required data.

The recommended flight mode is the reference concept presented by NASA-ERC and further defined in this study, integrated into the Delta second-stage engine (DSV 3L-4 TIIIC transtage) compartment. The satellite systems are similar to those used on TIROS IX. Changes are made only to reflect the use of current and more reliable components. Only minimum redundancy is used for critical components.

Viable flights for this satellite in the order of preference are:

a. NIMBUS E, 1st half 1972

b. NIMBUS F, 1st half 1973

c. ITOS C, February 1972

d. ITOS D, February 1973

e. ITOS E, February 1974

f. ERTS A, June 1972

g. ERTS B, June 1973

To carry the satellite in the Delta engine compartment requires that a new piggyback payload adapter truss be designed by the McDonnell Douglas Delta Program Office through NASA. A canister must also cover the satellite to protect it from the engine rocket exhaust during Delta/Thor staging. Since the satellite in its canister is too large to fit through existing access doors, it will be necessary to integrate the satellite/canister with the Delta prior to its mating with the Thor. This will be approximately 30 days before launch. A nitrogen purge of the canister during the on-pad period is recommended to protect the satellite from the humid atmosphere at the launch site.

The use of a separate launch vehicle for the reference concept satellite is considered a secondary flight mode. Specific launch vehicles investigated in this study are the SCOUT and Thor/Burner II.

ORBITAL ANALYSIS

The overall objective of the orbital analysis was to provide data as part of the basis for selection of the orbit and launch vehicle for the proposed horizon sensor satellite and to provide a basis for the preliminary system design. It was first necessary to scrutinize the satellite system requirements in order to determine what data were required. The two chief guidelines were the required distribution in space and time of the observations, and the measurement accuracy required. In addition to comparing orbits and launch vehicles on the basis of accuracy and distribution of the acquired data, the solar

lighting associated with each alternative was evaluated. The impact of variations in sun angles throughout the orbit and over the one-year satellite lifetime on the system design (e.g., the electrical power supply) and on the overall system accuracy was evaluated, using the data generated in the orbit analysis. These evaluations are described in detail. A comparison was made of candidate launch vehicles and orbits in terms of the aforementioned factors and gives a recommended choice. Information is also provided to permit the analysis of the data load for any of the candidate orbits.

ATTITUDE DETERMINATION AND EXPERIMENT POINTING SYSTEMS

A theoretical analysis has been made of the reference concept for a horizon sensor satellite. The results of that analysis are contained in this section. A functional description of the system concept is provided, followed by a detailed presentation of the equations and a description of the data flow and operational sequence. A description is given of the computer program created for the horizon sensor satellite studies and of more detailed programs being proposed. The application of these programs to the horizon sensor satellite problem is clearly identified. The error sensitivities of the proposed system are derived and values presented. In addition, the conditions for minimizing the error are given in terms of the orbit and the physical orientation of sensors in the satellite.

The error analysis indicates that the specified 1-km accuracy in determination of the horizon altitude can be met using a precise (10 $\widehat{\text{sec}}$)

crossed-axis sun sensor system and a pair of state-of-the-art IR horizon sensors. It appears necessary, however, to hold the dip angle of the vehicle spin axis to a small value (0 to 2°). The chief error contributors are the dip angle uncertainty and the satellite position determination error. The latter can apparently be sufficiently reduced by the use of the Manned Space Flight Network or the laser tracking stations.

MISSION SUCCESS PROBABILITY ANALYSIS

A preliminary reliability analysis of the UV/MW Horizon Sensor Experiment (UV/MW HSE), as presently configured, indicates that the reliability of the entire system is approximately 0.69 for a one-year mission. The analysis was performed under the conditions that no redundancy was to be considered. Therefore, reference to "single-point failures" is not applicable since each subsystem (and components within each subsystem) provides a potential "single-point failure".

A numerical reliability estimate of the design, as currently defined, indicates a reliability of approximately 0.647 for a one-year mission, given a successful launch. Failure rates utilized were obtained from estimates provided by hardware suppliers, contemporary satellite analyses (ERTS, TIROS, etc.), reliability data reports ("STUDY OF RELIABILITY DATA FROM IN-FLIGHT SPACECRAFT"), and from the Apollo Applications Program (as appropriate). The reports indicated above cover data gained from 225 launches from 32 U.S. space programs (all unmanned and of varying durations). The reliability prediction

was based on the assumptions that subsystem failure rates were constant during the total mission time duration, and that any failures that might occur would be of a random nature. These assumptions permitted application of the standard exponential equation which defines reliability as a function of the failure rate and operating time. Since it is recognized that any given subsystem in a "standby" mode must be capable of operation when called upon to do so, and must withstand the environment during this "standby" mode, the failure rate assigned to this subsystem was set to ten percent of the failure rate of the same subsystem in the "operational" mode.

DATA ACQUISITION AND TRANSMISSION ANALYSIS

A computer program was utilized to determine satellite time vs. latitude and longitude, whether over a tracking station (and which one) and time of entry and exit into tracking circle. A 600 nm, noon sun-synchronous orbit with a 17-day repeat cycle was assumed. With no onboard data storage, near-continuous data can be obtained between -60° and +80° latitude over a portion of the Western Hemisphere. This data could be acquired on 35 night passes and 21 day passes out of a total of 228 orbits in the 17-day cycle.

Approximately 90 minutes of data storage must be provided if data coverage of the entire world is to be obtained. If 60 minutes of data storage are provided, complete coverage can be obtained on all orbits except 60 out of the 228.

A polar projection of the world with tracking circles shown and

an overlay representing the satellite ground trace is provided to show all areas where data can be acquired and orbit times between tracking station contacts.

A data acquisition plan is recommended which acquires sensor data over the North and South America tracking station network for 50 minutes at night and 35 minutes in daylight approximately 12 hours later. This is done every seven to nine days, or as desired over the year.

ATTITUDE CONTROL SYSTEM

The Attitude Control System study is presented in six separate sections.

1. Systems Analysis. A mathematical discussion is presented of magnetic Dynamic Control System (DCS) theory. Additionally, mechanization concepts were studies where performance and/or cost criteria were implicated. Extensive use was made of the TIROS IX wheel mode spinning satellite and the DME-A satellite flight test data which are flight-proven hardware from which mechanization concepts were evaluated in terms of relative parametric sensitivities, reliability, expected cost, lifetime estimates, and potential problem areas. The TIROS IX magnetic attitude control system was concluded to be superior in every way for this mission to the DME-A system, and is proposed. Being relatively independent of the sensing and error computation aspects of the DCS, it can be employed with either ground control or onboard error computation, as the results of that independent evaluation dictate.

The TIROS IX magnetic attitude control system concept, it was concluded, is inexpensive, reliable, and highly accurate in pointing capability with good design lifetime characteristics which will provide an effective system in support of the sensor evaluation mission requirements.

2. Tradeoff Analysis of Onboard Versus Ground Controlled Error Computer for Attitude Control. The possibility of modifying the baseline system error computer from a ground-controlled, open-loop controller to an onboard, closed-loop controller was investigated. The relative merits of the two system concepts for the proposed mission indicate a definite preference for the open-loop, ground-based controller. The onboard system is an over-design, and would result in size, weight, power, reliability and cost penalties.

3. System Description. A subsystem definition of the DCS is delineated. Interface requirements between subsystem elements and between the system and other systems are defined. Physical and functional descriptions of the major components are provided with particular emphasis on operating mode considerations.

4. Size, Weight and Power Requirements. This section identifies the size, weight and power requirements of the candidate system for dynamic control of the satellite. The dynamic requirements as a function of mission mode and the static requirements as a function of subsystem elements clearly indicate the applicability of the system with respect to the figures of merit required.

5. Performance Specifications. The performance specifications of the satellite are defined by the mission requirements and the

vehicle operational requirements associated with the selected attitude control system.

6. Operations Plan. The on-orbit operations plan required for the DCS is described. Ground support equipment, logistics, data reduction, and data analysis requirements are given for maintaining the required attitude and spin rate accuracy of the satellite in both automatic and manual modes of operation. The automatic mode is considered the primary mode of operation.

TELEMETRY, TRACKING, COMMAND AND DATA HANDLING SYSTEM

The Telemetry, Tracking, Command, and Data Handling system study is presented in five separate sections.

1. Data Handling System Analysis. The UV-MW satellite measurement system must acquire and format the performance data of the experiment sensors, attitude control and determination sensors, and the various on-board status sensors for subsequent transmission to the STADAN ground stations for analysis and corrective action. The UV sensor data, transmitted in real time, constrains the system bit rate while the fine sun sensor and IR horizon sensors constrain timing accuracy. The data handling techniques and accuracies required for the experiments and attitude determination devices necessitates digital data transmission. Systems implementation does not require spacecraft or ground station development or modification.

2. Telemetry, Tracking, and Command (TT&C) System Description. The TT&C system consists of a PCM transmission system, a command

unit, and a timer. All hardware described is available as space-qualified with little or no modification. The system is fully compatible with the selected STADAN stations. The timing unit provides accurate range time and events correlation, and the telemetry transmitter serves the dual purpose of tracking beacon and data transmission. Some unique features are incorporated in the design of the data subsystem used for processing attitude determination sensor signals, to reduce sample rates while increasing timing precision.

3. Performance Specifications for TT&C System. Performance specifications are presented for the components of the TT&C subsystem. These consist of the sensor registers, timer, data conditioner, PCM encoder, premodulation filter, transmitter, diplexer, command receiver, and command decoder.

4. Communications Link Analysis. The communications link analysis was performed for the telemetry transmitter, tracking, and the command link. Adequate margins were obtained in all cases.

5. Data Reduction Requirements. Data reduction requirements are considered for the test and operational phases of the program. The telemetry signal content is described along with the planned method of data reduction and evaluation during the test phase. It is shown that the total data reduction task can be accomplished with existing equipment and software.

ELECTRICAL POWER GENERATION AND DISTRIBUTION SYSTEM (EPGDS)

The Electrical Power Generation and Distribution System is presented in four separate sections.

1. System Analysis and Description. The recommended electrical power source for the orbiting earth satellite consists of eight solar panels with a two-piece secondary storage battery supplying the electrical power for the dark periods. A major feature of the recommended EPGDS is the use of a fully automatic adaptive power duty cycle that permits a highly-flexible accommodating and efficient method for meeting the power requirements of the satellite. A low-voltage solar array with boost voltage regulation and peak power tracking provisions is used with a nickel-cadmium battery. The unique adaptive duty cycle relaxes the interfaces between solar arrays, battery, and the power conditioning equipment. Current limiters and microminiature latch relays are used for the control and protection of satellite loads. The satellite harness assembly features hard-wiring, wrapped kapton (H-film) nickel-clad copper wire and a wrapped, spot-tie configuration.

2. Power Profile. The baseline electrical load requirement for the orbiting earth satellite is predicated on a sensor load of 8.5 watts. Maximum power demand (19.80 watts) occurs during daytime data acquisition with the required power being supplied by both the solar array and battery. Nighttime data acquisition power (16.40 watts) is supplied entirely by the battery. The system cannot charge the receiver-decoder

battery during data acquisition periods. Satellite standby loads average less than 7 watts and the power required for the data acquisition period is around 16.70 watts. Maximum power requirements for initial orbit acquisition is about 15.85 watts.

3. Performance Specifications. Performance specifications are presented for the major components of the EPGDS - the Solar Array, the Peak Power Monitor, the Boost Voltage Battery Charger, the Nickel-Cadmium Battery, the Battery Status and Charge Monitor, and the DC-DC Converters.

4. Increased Power Tradeoff Analysis. An analysis was performed using an experiment sensor system requiring 30 watts of power while operating and a second system requiring 50 watts of power. Using the mode of data acquisition formulated, the proposed satellite and its power system are adequate with no revision. In the case of the 50-watt sensor system, the battery would be discharged to a maximum depth of 45% and will be fully recharged in 17 orbits, or approximately $1\frac{1}{4}$ days.

INSTRUMENT ALIGNMENT ERROR ANALYSIS OF CRITICAL STRUCTURAL LOADS DURING BOOST AND THEIR EFFECT ON INSTRUMENT ALIGNMENT

One approach is to use simpler and more economical structures and mounting techniques which results in moderate alignment shifts through a space flight environment and to monitor these shifts using a small precise instrument of lower overall cost and complexity.

A candidate system with great flexibility utilizes a device developed by Exotech, Inc., which consists of a pair of angular sensors

fabricated within a monolithic quartz structure, or within several quartz blocks cemented together. Because of their small size and low coefficient of thermal expansion, mechanical and thermal problems are minimized. Extensive tests and analysis show that the optical axes of the two sensors maintain their relative alignment within a fraction of an arc second over a wide range of thermal and mechanical environments. These sensors may be solar sensors, autocollimators, collimated light sensors, or any combination of these with very stable axes relative to each other. Such devices could be employed in the following manner.

For this experiment, the sensor combines a solar sensor with an integral electronic readout autocollimator in a monolithic quartz structure. Since the optical axes of the solar sensor and the autocollimator are rigidly maintained, the device can measure the angle between the solar vector and a reflective mounting surface on an experiment to a precision independent of minor mounting errors and deflections induced by the launch environment. This concept was successfully implemented in a program for NASA Ames Research Center which is described in "A Precision Autocollimating Solar Sensor", AIAA Guidance Control and Flight Mechanics Conference, August 1969.

It is assumed that the reflective surface on the UV horizon sensor is rigidly attached to the UV and MW horizon sensor's line of sight. The monolithic quartz sun sensor-autocollimator provides accurate aspect data despite alignment changes between the experiment and the solar sensor. This approach has the additional benefit of relaxing the mounting requirements of each device, and relaxing rigidity and stabil-

ity of the spacecraft structure. Previous experience has indicated that the alignment error can be measured by this approach to an accuracy of 3 arc seconds.

SATELLITE STRUCTURES ANALYSIS

The satellite structures analysis is presented in four separate sections.

1. Spacecraft Design. The spacecraft was configured to assure an economical and reliable satellite. The microwave and the ultraviolet horizon sensors, along with the fine sun sensor, the coarse sun sensor and the IR sensors are mounted to a common structural platform. This platform also supports the solar panels, the attitude control magnetic coils, the power packages and telemetry equipment.

2. Critical Interface Requirements between Reference Satellite and Launch Vehicle. This section of the study identifies the critical design interface requirements for the protective satellite canister and the launch vehicle. The canister provides for nitrogen purging of the satellite during the 30-day period of integration into the Delta second-stage engine (DSV 3L-4 TIIIC transtage) compartment prior to launch. Provision is made for connection of a battery charger and status monitor during this time period. Thermal and contamination protection for the satellite is also provided by the canister during second-stage motor firing. Launch loads are absorbed by the canister through the structural interface support frame of the launch vehicle. Spacecraft separation occurs by releasing the stored energy in a spring and is commanded and monitored through the launch vehicle

command and telemetry systems. The canister and hinged door covers remain with the launch vehicle after satellite ejection.

3. Mass Distribution Within the Satellite. A preliminary mass properties analysis was performed. The resultant spacecraft weighs 85 pounds, has a roll inertia of 1.28 slug-feet squared and yaw and pitch inertias of 0.85 slug-feet squared. The center of gravity and principal axes inclinations are within differential equipment shifting and ballasting limits.

4. Balancing Requirements. A procedure of final spacecraft balancing has been established and is well within the capability of current analytical and mechanical equipment requirements.

THERMAL CONTROL ANALYSIS AND DESIGN REQUIREMENTS

The object of the thermal control design is to ensure a long-life reliability of all components by maintaining their temperatures within specified limits. The approach taken in the study was to demonstrate the feasibility of a thermal design which is passive, employs state-of-the-art techniques having a long life with high reliability, and presents a minimum impact on the other satellite subsystems.

The thermal environment of the temperature-sensitive equipment carried by the UV/MW satellite can readily be controlled passively, with little or no impact on the major subsystems of the satellite. Only state-of-the-art techniques are required to maintain the equipment between 30 and 95°F during flight in the reference orbit.

MISSION OPERATIONS PLAN

A mission operations plan containing the required tasks from the prelaunch phases through a portion of the orbital data-collecting period, sufficient to establish a repetitive cycle, was developed to establish the feasibility of the spacecraft concept and the procedures for its utilization. The operational phases are identified and described followed by a task/time sequence yielding an operational plan.

The UV and MW Horizon Sensor Orbital Experiment mission functions can be conducted in a compatible, chronological manner as established by the operational plan. The actual tracking telemetry and command functions will be established at approximately weekly intervals, according to the priorities in existence at the time.

PROGRAM IMPLEMENTATION PLAN FOR PHASES C AND D

A program implementation plan consisting of preliminary plans, schedules, and cost estimates for the C and D phases of the UV/MW Horizon Sensor Satellite program are presented. Included is a Work Breakdown Structure, Program Development Schedule, Subsidiary Program Plans, Hardware Utilization List and Program Cost Estimates. The philosophy for preparation of this plan was for an inexpensive, fast schedule method of meeting the experimental objectives of the program. A minimum program with one test vehicle and a combined prototype/flight vehicle is suggested.

Results of the cost study indicate a program cost as follows:

Phase C	$ 330,000	
Phase D	1,480,000	
Total Spacecraft	$1,810,000	
Launch Integration	200,000	(Delta Contractor)
Spacecraft & Launch Integration	$2,010,000	

NR has a high confidence in the Phase C estimates. The Phase D estimate, however, does include some non-firm vendor quotes.

The ordering of certain long lead-time items (especially the fine sun sensor and the IR horizon sensors) early during Phase C is a requirement in order to meet the program schedule. Potential supplier sources have quoted delivery estimates of eight months for these items.

The launch integration cost of $200K was a verbal estimate by McDonnell Douglas Corp. (Delta Contractor) personnel and cannot be considered firm.

Launch on a Scout or Thor/Burner II increases the launch costs by $1.4M. The canister for the reference concept is not required, and therefore represents a spacecraft cost decrease of about $100,000.

Of the $1.8M spacecraft program cost, approximately 30 percent is for material and spares, and 44 percent is for engineering and development. The total management and management software costs have been held to less than seven percent.

EXPERIMENT OBJECTIVES

The ultraviolet and microwave horizons of the earth are largely unexplored phenomena that hold the possibility of providing more accurate and more reliable references for the attitude and position of near-earth spacecraft. In order to determine the utility of the phenomena as an attitude and navigation reference, the Electronics Research Center is developing low power, solid state ultraviolet (UV) and microwave (MW) horizon sensors, and has determined that an experimental in-orbit test of them is desirable and feasible. This report describes the results of a Phase B study of such an experiment performed by the Space Division of North American Rockwell Corporation.

STUDY OBJECTIVES

The experiment objectives are: (1) to evaluate the capability of the UV sensor to detect the ultraviolet horizon and to evaluate the capability of the microwave sensor to detect the molecular oxygen horizon; and (2) to determine the stability of those horizons. The expected accuracy of the horizon determinations obtained from the experiment (along the earth radius) is 1 km, including both instrument and horizon uncertainties.

The UV horizon sensor detects a particular color condition of the sunlit horizon as defined by the ratio of horizon intensity at two separate wavelengths. According to theory, variations in the horizon flux intensity, due to sun zenith angle, local albedo, polarization, season, time of day, and latitude, do not significantly effect this color ratio since color is affected primarily by spectral changes. In order to verify the theory,

measurements must be scheduled and sufficient observational data accumulated to determine the variation of the horizon altitude for the following conditions:

(1) Diurnal variation. Measurements must be adequate to determine the variations during the day at a fixed geographic location.

(2) Seasonal variation. Measurements must be adequate to determine the variations from month to month over the four seasons of the year taken at the same position.

(3) Latitude variation. Measurements must be obtained at latitude separations no greater than 5°, including, if possible, both poles.

(4) Geographical and meteorological conditions. Measurements must be obtained over land masses, oceans, and large weather systems and their transitions.

(5) Sun zenith angle. Measurements must be adequate to determine the variations as the angle between sun line and zenith varies from 0 to 70 degrees at position of the locator altitude.

The MW horizon sensor utilizes the discrete emission characteristics of atmospheric oxygen (at 60.8 GHz) as a reference for earth atmosphere limb sensing. The microwave sensor differenciates signals from opposite horizons to produce a null as a local vertical indication. The atmospheric earth limb viewed by the oxygen sensor is determined by judicious selection of the observing frequency. In addition to the variations (1) to (5) described for the two-color UV phenomena, data must be obtained adequate to determine the MW variations due to:

(6) Day-night changes.

The purpose of this study was to provide NASA with information on the flight alternatives and associated costs for implementing the UV and MW horizon sensor experiment. The following flight alternatives were evaluated.

(1) The reference concept is a small spin-stabilized satellite launched in a piggyback configuration or launched independently.

(2) The integration of the experiment on missions such as NIMBUS E & F, ITOS, Atmospheric Explorer, Orbital Scanner, ERTS, the Air Force project SPARS (Space Precision Attitude Reference System), and other suitable missions.

Implementation of flight alternatives were chosen from flight opportunities in the 1970 to 1973 period. The study considered more than one mission for integration. It also considered instrumentation to meet the experimental objectives other than the sensors whose characteristics were specified.

Reference Concept

A preliminary description of the reference concept, was refined during the study. The horizon sensors and the sun sensors are body-mounted on a small spin-stabilized satellite specifically designed for this experiment which has its spin vector normal to the orbit plane. The horizon sensor viewing lines are contained within the orbital plane and rotate about the spin axis at a nominal spin rate.

In this spinning satellite configuration, the UV and MW sensors are swept through the horizon twice per rotation. The times at which the horizon sensors pass through the horizon are transmitted to the ground. In order to locate the points of tangency to the horizon of the lines of sight of the sensors at these passage times the following information is used:

(a) The position of the vehicle at each passage time, obtained from NASA STADAN tracking network.

(b) The attitude of the satellite at the passage times, obtained indirectly from the sun sensors and IR horizon sensors mounted on the satellite.

From these two pieces of information it is possible to determine a unique point in the horizon through which the line of sight of the UV or MW sensors have passed. The satellite will be launched into a sun synchronous, near-circular orbit of 600 nautical miles.

The most critical characteristics of the orbiting vehicle are pitch, roll, and yaw. Variations in these parameters, in their composite, must be consistent with the experimental observational data requirements.

The subsystems which comprise the total satellite vehicle include:

- UV and MW sensors.
- Attitude Determination System with performance requirements compatible with the proposed scheme.
- Attitude Control System which provides re-orientation of the spin axis of the satellite by ground command, as well as adjustment of the spin rate in the range from 1 rpm to 4 rpm, also by ground command.
- Source of experiment power uses solar cells and batteries to provide the necessary power.
- Data handling subsystem includes signal conditioning and data transmission equipments (telemetry) for continuous real time encoding and transmission of observational data.

- Experiment Program Command Unit provides real-time on-off command signals to the satellite systems.

Detailed Requirements for Reference Concept

The study included an investigation of the following specific items for the reference concept.

(1) Orbital analysis to include orbit parameters, and their changes over the satellite lifetime, horizon data acquisition (longitude, latitude, sun angle, and seasonal), ground stations coverage, sun occulation periods, and sun angle data so as to determine the extent to which the experiment objectives can be achieved.

(2) System and subsystem description and performance specifications for attitude control system, power system, data handling system, and for all other systems and subsystems of the satellite.

(3) Program implementation plans and schedules for Phase C and D including detailed cost estimate, acceptance test schedule and flight test qualification schedule, quality assurance reliability assessment, manpower and facility requirements.

(4) Summary of mass distribution within the satellite.

(5) Time profile of power requirements.

(6) Mission operations plan including mission sequence and a plan for operational support.

(7) Instrument alignment error analysis.

(8) Communications link analysis.

(9) Thermal control analysis.

(10) Analyses of critical structural loads during boost and their effect on instrument alignment.

(11) System block diagram.

(12) List of GSE requirements, TTC requirements, and other necessary logistic support requirements.

(13) Mission success probability analysis.

(14) Attitude Control System Analysis.

(15) Data reduction requirements.

(16) Attitude determination and experiment pointing.

Refinement of Reference Concept

Trade-off analyses were conducted on the following aspects of the reference concept:

(1) The effect on satellite size and weight on providing continuous power in steps of 30 and 50 watts.

(2) The desirability of data storage on the satellite to accumulate observational data on a nearly continuous basis for transmission in non-real time.

(3) The desirability of ground command rather than a vehicle contained preset program sequence unit for attitude control.

(4) An investigation of critical interface requirements between the satellite of the reference concept and the launch vehicle.

DESCRIPTION OF EXPERIMENT SENSORS

This section of the report describes the ultraviolet (UV) and microwave (MW) sensors, which represent the experiment equipment to be flown. The following data on these sensors are reported by the manufacturers to be accurate and up-to-date. These sensors are still in the development phase and the following data is considered tentative.

ULTRAVIOLET SENSOR

The UV sensor description and characteristics are shown in Figure 1.

MICROWAVE SENSOR

The MW sensor description and characteristics are shown in Figure 2.

SENSOR DIMENSIONS AND ALIGNMENT

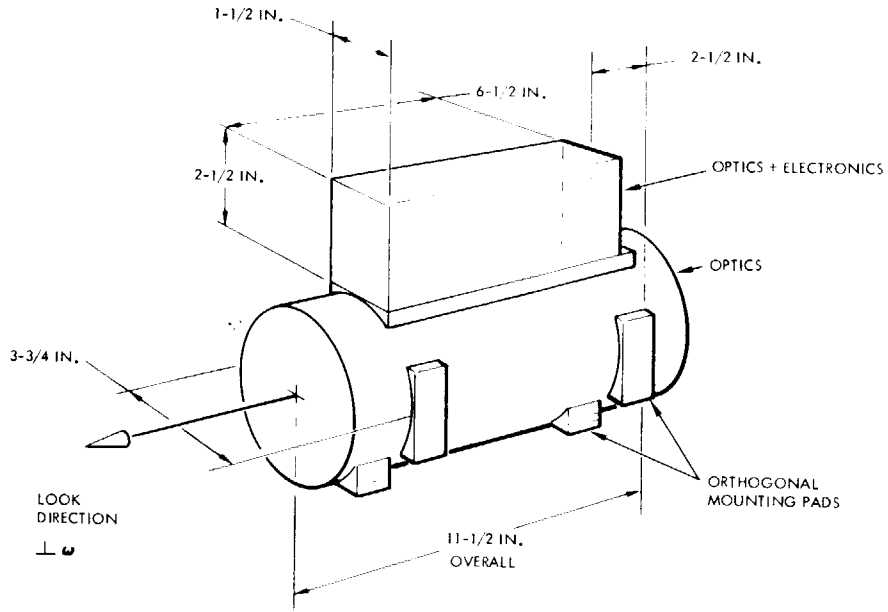

SENSOR SPECIFICATIONS

WEIGHT (MAXIMUM)	= 5 POUNDS
POWER (MAXIMUM)	= 1 WATT
VOLTAGE (INPUT)	= +14 VDC AND -14 VDC
COMMANDS	= ON-OFF (2)
TEMPERATURE LIMITS	= -50 C TO +50 C

LAUNCH ENVIRONMENTAL LIMITS DICTATED BY LAUNCH VEHICLE

OUTPUT SIGNAL
(ASSUMING 4 RPM SATELLITE SPIN RATE)

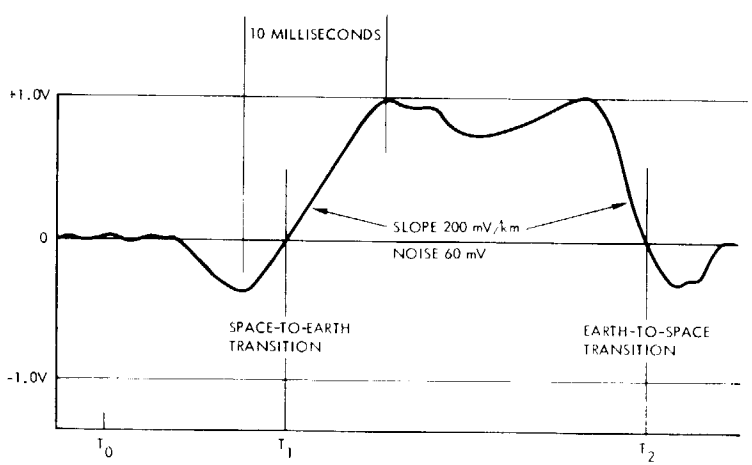

OUTPUT SIGNAL - EXPANDED SCALE
(ASSUMING 4 RPM SATELLITE SPIN RATE)

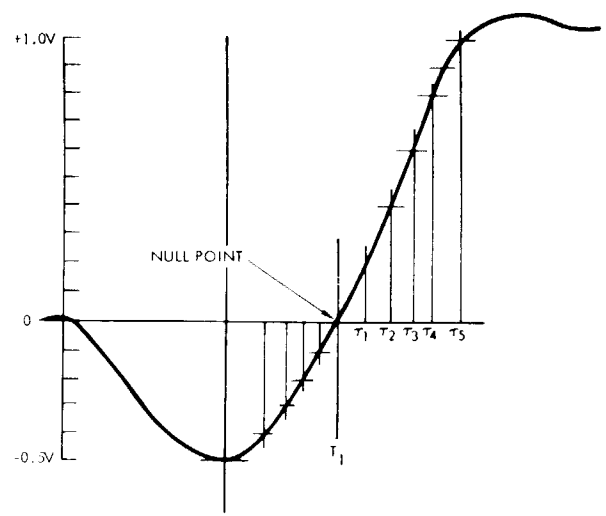

FIGURE 1. Ultraviolet Sensor

Space Division
North American Rockwell

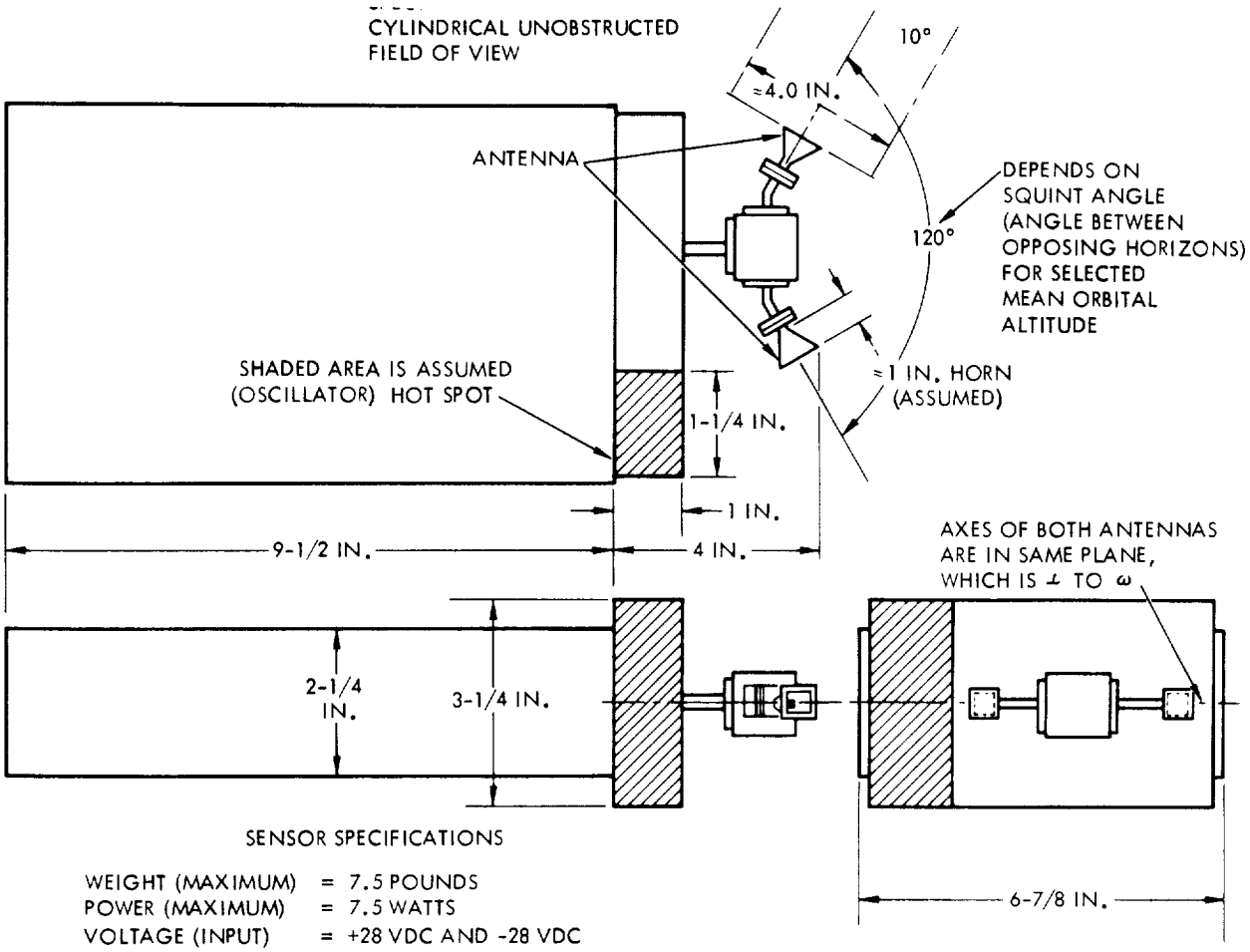

SENSOR SPECIFICATIONS

WEIGHT (MAXIMUM) = 7.5 POUNDS
POWER (MAXIMUM) = 7.5 WATTS
VOLTAGE (INPUT) = +28 VDC AND -28 VDC
COMMANDS = ON-OFF (2)
LAUNCH ENVIRONMENTAL LIMITS DICTATED BY LAUNCH VEHICLE

MICROWAVE SENSOR OUTPUT SIGNAL
(4 RPM SATELLITE SPIN RATE)

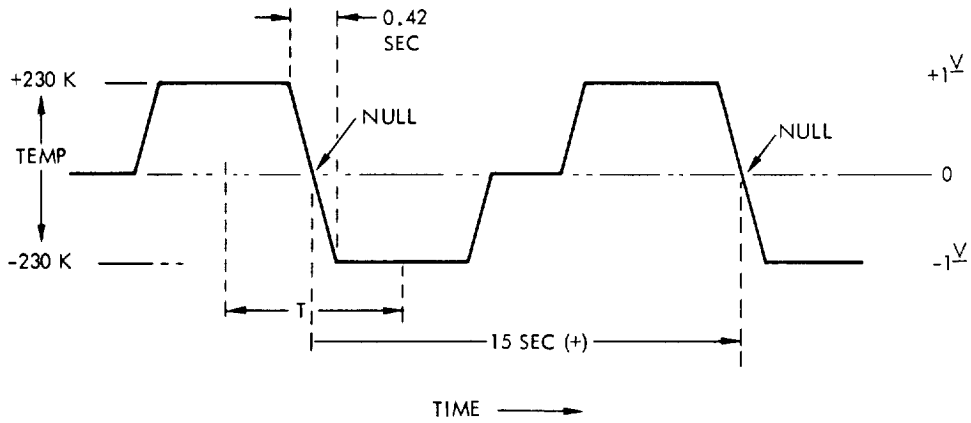

FIGURE 2. Microwave Sensor

SPACECRAFT CONCEPTS FOR FLYING EXPERIMENTS

This section describes the investigation of suitable flight alternatives for gathering of data on the earth's ultraviolet and microwave horizons. The primary purpose of this investigation was to determine whether flight alternatives could be configured which are more cost effective than the referenced approach configured by ERC. The referenced approach is a spin-stabilized satellite in the 50-pound weight class which is carried into orbit piggyback.

The mission characteristics and flight techniques of 10 different space programs are reviewed. Over 15 specific flights which are scheduled within the time frame of interest were analyzed for applicability to this experiment. In each case, the salient features of the mission/experiment were identified and an evaluation was made as to whether or not the mission is a candidate for further analysis. Promising experiments are configured to specifically determine the relevant factors in cost and complexity and these are compared to the reference spinning satellite.

Three alternate approaches, (1) a piggyback earth-oriented satellite, (2) integrate experiments on NIMBUS, and (3) integrate experiments on ERTS, are described which can supply the required data; however, the attitude determination subsystems are significantly more complex than for the spinning satellite and involve techniques which have yet to be flight proven. In the piggyback vertical satellite, a number of subsystems are more complex than for the spinning reference satellite.

This study indicates the referenced approach is the most cost effective manner in which to gather the required data.

FLIGHT TECHNIQUES REVIEW

This section reviews and examines several flight techniques for gathering information on the characteristics of the earth's horizon. Viable alternatives for the collection of this data include:

1. As a piggyback payload: an add-on payload in the launch vehicle of another program such as ITOS (improved TIROS operational satellite) B through C, NIMBUS E and F, ERTS A and B, etc.
2. On a multiple payload launch: as one payload of several on a DOD Space Experiments Support Program (SESP) launch or in a NASA-procured launch vehicle shared with other NASA or DOD payloads.
3. As a primary payload: a single payload on a suitable launch vehicle specifically supplied for the mission.

The basic data requirements of latitudinal data over four seasons eliminate suborbital probes or balloons as possible candidates for the experiment. The study was developed in the following steps:

1. A review of all missions currently planned by either the Air Force or NASA in the time period of interest.
2. Elimination of all missions which will not collect the required data.
3. A detailed review of the characteristics of those missions which will gather most of the data required.
4. Grouping of similar mission/experiment configurations so as to allow for a detailed trade-off between several candidate types rather than detailed trade studies of all possible missions.

5. Selection of a preferred technique through an analysis of the detailed trade-off study.

These steps and the order in which they were executed are illustrated in Figure 3.

Over twenty different flights in ten different programs are planned in the 1970 to 1974 time period. The actual number of flights may be much larger, but information on classified missions was not available. The following is a breakdown by program.

Program	No. of Flights
NASA	
NIMBUS	2 Flights
ITOS	5 Flights
ERTS	2 Flights
Atmos. Exp.	2 Flights
Orbital Scanner*	2 or 3 Flights
Air Force	
SPARS	1
SESP	4 + Flights
Classified	Unknown

*Not a line item

A detailed review of these missions indicated certain of the flights could be eliminated from further consideration because of experiment/mission incompatabilities, or because the mission cannot collect the required data. The principal reason for rejection is described below.

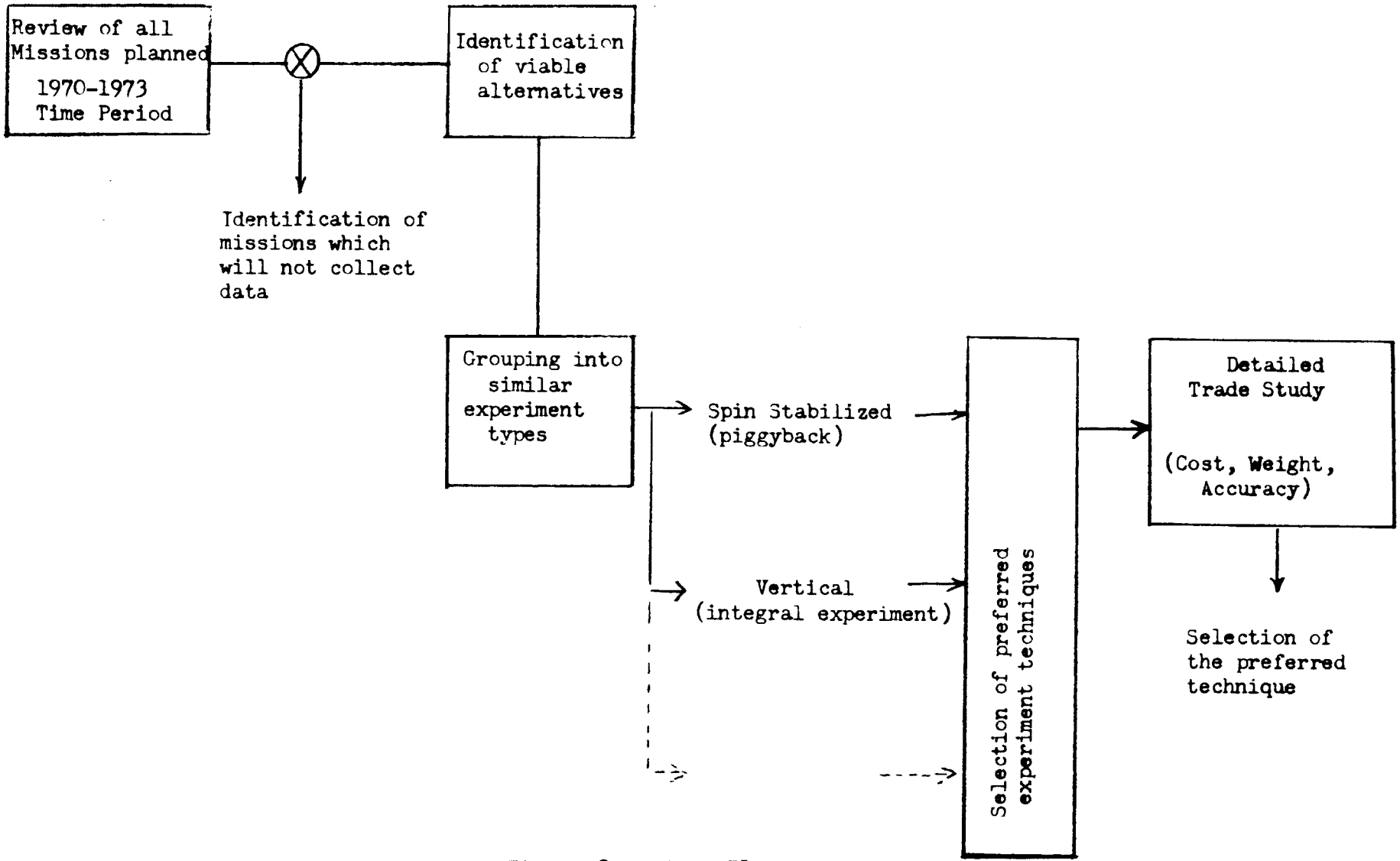

Figure 3. Study Elements

Space Division
North American Rockwell

Mission	Primary Reason For Rejection
ITOS A	Schedule
ITOS B	Payload Frozen
Atmospheric Explorer C	Orbital Eccentricity
Atmospheric Explorer D	Orbital Inclination (18°)
ISIS B	Weight, Orbital Eccentricity
ISIS C	Weight, Orbital Eccentricity
SESP (Thor Burner)	Life (7 hrs), Weight
SESP (Atlas F)	Weight, Orbital Eccentricity
Orbital Scanner	Not a line item
SPARS	Life (2 weeks)
NIMBUS E	Experiments have been selected and are under contract.

(Additional constraints these missions would place on the experiment are presented in Table 1.

The remaining missions which were considered for the ERC UV-MW Horizon Sensor Orbital Experiment are:

NIMBUS E	- piggyback experiment
NIMBUS F	- integrated payload
ERTS A	- piggyback experiment or integrated payload

TABLE 1

MISSIONS WHICH CANNOT MEET EXPERIMENT DATA REQUIREMENTS

Launch Date	Program	Reason
Feb 70	ITOS A	• Launch date too early. • Integration into ITOS requires hardware delivery date ≈ 1 year before launch.
4th qt CY 70 to 1st qt CY 71	SESP* THOR Burner II	• Current payload uses all payload weight capability. • Burner II carries a celestial IR experiment and is 3-axis-stabilized for only 7 hours. Payload dies at end of this period due to lack of power. • Initial orbit is 250 to 400 nautical miles near polar with twilight launch. Orbit is not sun synchronous; will regress and create potential thermal-control problems.
4th qt CY 70 to 1st qt CY 71	SESP Atlas F	• Orbit is direct-inject, 75 by 800 nautical miles, 94° inclination, with twilight launch. • No excess capability. The two satellites it carries requires kick stages to increase orbit apogee to 1500 nautical miles.
Mar 71	ISIS B	• Canadian-built satellite launched by NASA; integration into satellite itself not advisable. • Satellite carries several 100-ft booms. • Spin axis inertially oriented in orbit plane. • Launched on Delta E (3 stages); second stage not orbital. Therefore, piggyback satellite launch on Delta second stage not possible. • Piggyback satellite integration on third stage not advisable.
Oct 72	Atmospheric Explorer C	• Low perigee (65 to 81 nautical miles) and high apogee (2160 nautical miles) make sensor design complicated. • Variable spin rate (0.5 to 10 rpm) when in spin mode will be dictated by primary atmospheric payload. • Altitude stability in 3-axis-stabilized mode is specified at 2° rms about all axis. Attitude rates are undefined. Altitude measuring accuracy is specified at 1° rms about all solar aspects. Requires adding fine sun sensors and star mapper to system. • Contractor not selected; therefore satellite details not available.
Oct 73	Atmospheric Explorer D	• Near equatorial inclination (18°). • Cannot obtain complete earth coverage or data over poles.
Mar 73	ISIS C	• Canadian-built satellite launched by NASA; integration into satellite itself not advisable. • Program not approved by Canadian government. • Orbit apogee too high; global horizon coverage not adequate. (Orbit is 150 by 27,600 nautical miles or 69,000 nautical miles near polar.) • Satellite carries several 100-ft booms. • Spin axis inertially oriented in orbit plane.

*Air Force Space Experiments Support Program.

ERTS B	- piggyback experiment or integrated payload
ITOS C	- piggyback experiment or integrated payload
ITOS D	- piggyback experiment or integrated payload
SESP Multiple Payload	- integrated payload

Examination of the characteristics of these missions (See Table 2) indicates the following:

1. All three NASA programs could carry the experiment piggyback or as an integral experiment.
2. The SESP multiple payload launch could carry the experiment as an integral experiment.
3. If the preferred approach is piggyback, the experiment could be vertically stabilized or spin-stabilized.
4. If an integral experiment approach is preferred, all experiments would be vertically stabilized.
5. None of the vehicles have sufficiently accurate attitude systems.
6. The orbital characteristics of all of the missions would place constraints on the kind of data delivered.

The constraints each mission will place on the experiment are illustrated in the following paragraphs.

FOLDOUT FRAME

FRAME

pts,

Launch Date	Program Name	Orbit Alt (n mi)	Orbit Incl (deg)	Orbit Nodal Pt	Remarks
Feb 71	ITOS-B	790 circ (sun sync)	101.75	9 a.m descend or 3 pm ascendi	• Program funded • Secondary payloads have been integrated into TIROS satellites before. • Payload configuration (ITOS-B) currently frozen. • No room in satellite, launch vehicle adapter for small satellite. • Orbit may be changed to ≈ 900 nmi circular sun synchronous on future missions.
Feb 72	ITOS-C				• Same as for ITOS-B except payload not frozen. Integration of experiment sensors into ITOS-C remotely possible.
Feb 73 Feb 74	ITOS-D ITOS-E				• Same as ITOS-C except integration of experiment sensors more likely.
Mar-May 72	NIMBUS E	600 circ (sun sync)	99.98	12 noc ±15 m	• Program funded • Use of Delta instead of Agena almost certain at this date. • Payload currently frozen. • No room in Nimbus/launch vehicle adapter for piggyback satellite.
Mar-May 73	NIMBUS F				• Same as Nimbus E except integration possible. • Experiment submission date to NASA hq has passed; will require late submission by ERC.
June 72 June 73	ERTS-A ERTS-B	496 circ (sun sync)	99.1	9:29 a.r descend	• Mission not planned in FY 70 budget request. • Phase B/C studies currently under evaluation—Contractor not selected; details on spacecraft design not available to NR except for the NR SD proposal. • Candidate contractors are NR, GE, TRW, RCA, Lockheed.

• Data sources
ITOS - NASA Goddard ITORS program office and McI
Nimbus - NASA Goddard Nimbus program office, Ma
ERTS - NASA Goddard ERTS program office, NR p
Orbital scanner - Personal visit NASA Langley prog bers indicated are keyed to Table 2.

ERTS Orbit/Mission Parameters

Present ERTS requirements call for a sun-synchronous orbit with a 496.2 nautical miles altitude, 99.1 degrees inclination angle, and an eccentricity of less than 0.006. The ground trace repeat period is 18 days with 13 - 17/18 orbits per day. Nominal time of the descending node is 0929 LST (i.e., 9:29 a.m. orbit). The altitude and inclination angle of the orbit will be trimmed and maintained after boost injection and during the mission, resulting in a highly accurate sun-synchronous orbit with an equally accurate repeat period. The high accuracy of these parameters may significantly enhance the quality of the data obtainable from the UV/MW experiments (beyond a realistic minimum requirement). The ERTS orbit/mission parameters will, in other respects, meet the experiment requirements, with the following exceptions and limitations:

1. The ERTS mission profile does not allow the spacecraft to scan out of the orbit plane. Thus a 90-degree change of the sensor scan plane by reorientation of the spacecraft is not possible for the spinning or "dual-spin" vehicles and improbable for non-spinning spacecraft (see Table 2). This does not, however, preclude the possibility of changing the scan plane on non-spinning vehicles by appropriately gimbaling the sensors. As a result of this limitation, the capability of taking data relative to diurnal variations and/or taking data at the poles is quite problematic.
2. The 9:29 a.m. orbit timing does not provide the desired sun zenith angle variation of 0 to 70 degrees; due to the orbit altitude of 496 nautical miles, this limitation applies, to

a lesser extent, even if a 90-degree scan plane change capability is provided.

ITOS Orbit/Mission Parameters

The ITOS will be launched into a sun-synchronous 790 nautical mile circular orbit. It is anticipated that the orbit achieved will be similar to the ERTS orbit with regards to injection accuracy, eccentricity, etc. The basic difference will be the altitude 790 miles, inclination 101.75 degrees, and the nodal point 9:00 a.m. or 3:00 p.m. ascending.

These changes will affect the experiment in the following ways:

1. The increased altitude will reduce the resolution of the experiment. This has a significant impact on the accuracy of the attitude determination subsystem.
2. The 9:00 a.m./3:00 p.m. orbit timing does not provide the desired sun zenith angle variation of 0 to 70 degrees.

NIMBUS Orbit/Mission Parameters

The NIMBUS orbit (600 nautical miles - sun synchronous) with an inclination of 99.98 degrees and 12:00 noon launch is the preferred orbit of those considered for this experiment. The altitude is sufficiently high to avoid the effects of atmospheric drag, yet sufficiently low to provide for experiment resolution. The orbit will not allow for diurnal effects at a given latitude and longitude or polar measurements unless out-of-plane scan maneuvers are allowed.

These constraints, however, are less than those of either ERTS and ITOS. The principal problem of integrating the experiments on NIMBUS is the schedule constraints.

Since none of the missions planned will gather all of the data set forth in the experiment objectives, the possible candidates include the following viable alternatives:

1. Piggyback - spin stabilized
2. Piggyback - vertically stabilized
3. Integration - vertically stabilized

A detailed tradeoff study is made to compare the complexity of a vertical experiment with a spin-stabilized experiment, and then the favored approach is compared to integration (see Figure 4).

An examination of the mission and flight characteristics indicates an attitude determination system will have to be designed for any approach. S1 (see Table 3) is the most likely candidate for a piggyback spin-stabilized experiment, and S3 is the most likely candidate for a piggyback or integrated vertical experiment.

Spin-Stabilized vs. Local Vertical Experiment Configurations

A piggyback experiment which is ejected after insertion into orbit could be configured for either a local vertical orientation or spin-stabilized orientation. The latter is the case in the referenced experiment concept in this study. The requirements for long life and low cost in this experiment dictate a review of the tradeoffs associated with both these two experiment orientations to ensure the right choice. It is also important to look at the total experiment not just the orbital operations in the event selection of either orientation might affect the costs of the experiment on the ground.

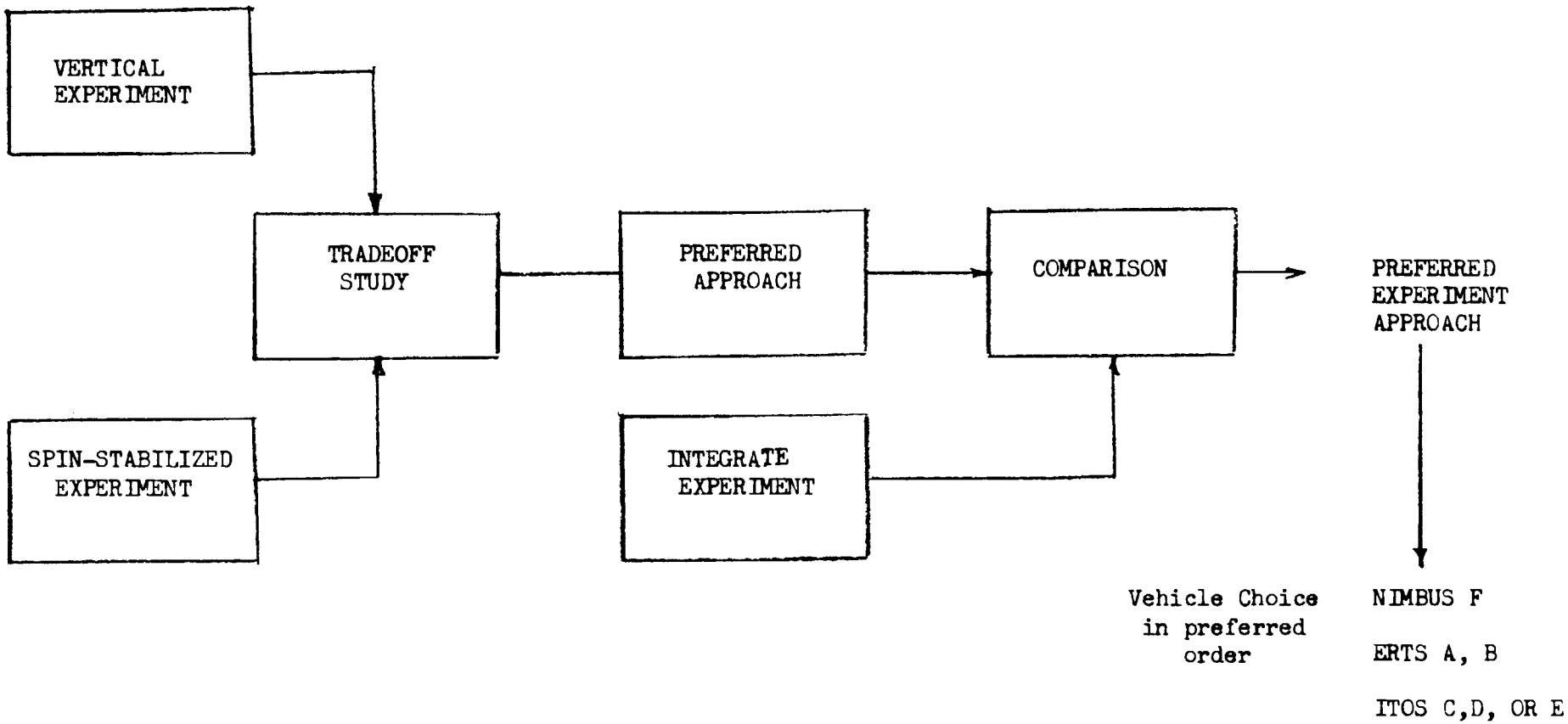

Figure 4. Selection of Preferred Approach

Space Division
North American Rockwell

FOLDOUT FRAME 1

FOLDOUT FRAME 2

Table 3. Alternate Approaches to Attitude Determination

			5 pounds and requires ≈ 1.5 watts of power. Gyro weighs 8 pounds and requires ≈ 10 to 15 watts.
S-4	Star mapper only	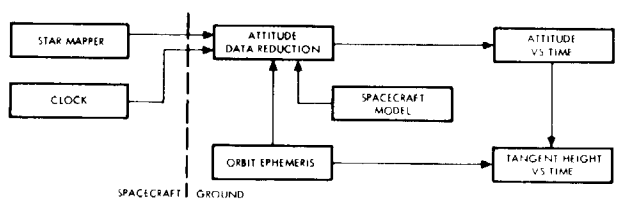	Relies on precise model of spacecraft motion to predict attitude from widely spaced star sightings. Compared with Systems 2 and 3, star mapper must sense dimmer stars (requires more frequent sightings), hence will tend to be larger and heavier (≈10 pounds). Power requirements are ≈1.5 watts.
S-5	Sun sensor—single-axis gyro	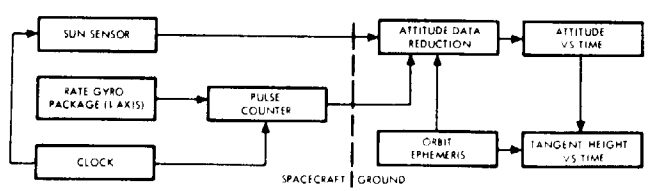	Used as in S-1 (and would profit with addition of horizon sensors). Gyro removes need for predictive modelling of spacecraft motion through eclipse portion of orbit.

A functional analysis of the experiment was conducted. Three basic operations are involved: (1) launch operations, (2) orbital operations, and (3) ground operations. The principal elements of each operation are shown in Figure 5 . A cursory examination of the different functions readily indicates certain functions in the orbital operations will be different for the vertical experiment vs. the spin-stabilized experiment; the attitude control function is an example. The manner in which launch and ground operations might be affected is not so obvious.

A detailed breakout of the launch and ground operations are illustrated in Figure 6 and Figure 7 . An evaluation of the different functions and how they might be affected by the two experiment configurations indicated three functions are affected in the launch operations and one function is affected in ground operations. A brief discussion of each follows.

Special Test Equipment Requirements

Minor differences would occur in the test equipment between the two configurations. These differences would be caused by the differences in control techniques which include different devices and by the required active scanning of the primary scanners. The vertical experiment would require more complex test methods.

Spacecraft Separation Interface

The complexity of the spacecraft separation interface for either the vertically stabilized spacecraft or the spin-stabilized spacecraft is highly dependent on the piggyback location of the spacecraft mother craft. Two experiment locations have been tentatively selected:

(1) Delta engine compartment
(2) Satellite launch vehicle adapter

LAUNCH	ORBITAL OPERATIONS	GROUND OPERATIONS
• LAUNCH VEHICLE	• SPACECRAFT STRUCTURE	• MISSION ANALYSIS
• LAUNCH SITE	• ELECTRICAL POWER	• TRACKING
• GROUND SUPPORT	• ATTITUDE CONTROL	• DATA ACQUISITION
• CHECKOUT	• MEASUREMENT SYSTEM	• DATA REDUCTION
	• DATA HANDLING	• SPACECRAFT COMMANDS
	• COMMAND & TRACKING	
	• TRANSMISSIONS	

Figure 5. Major Categories of Experiment Operations

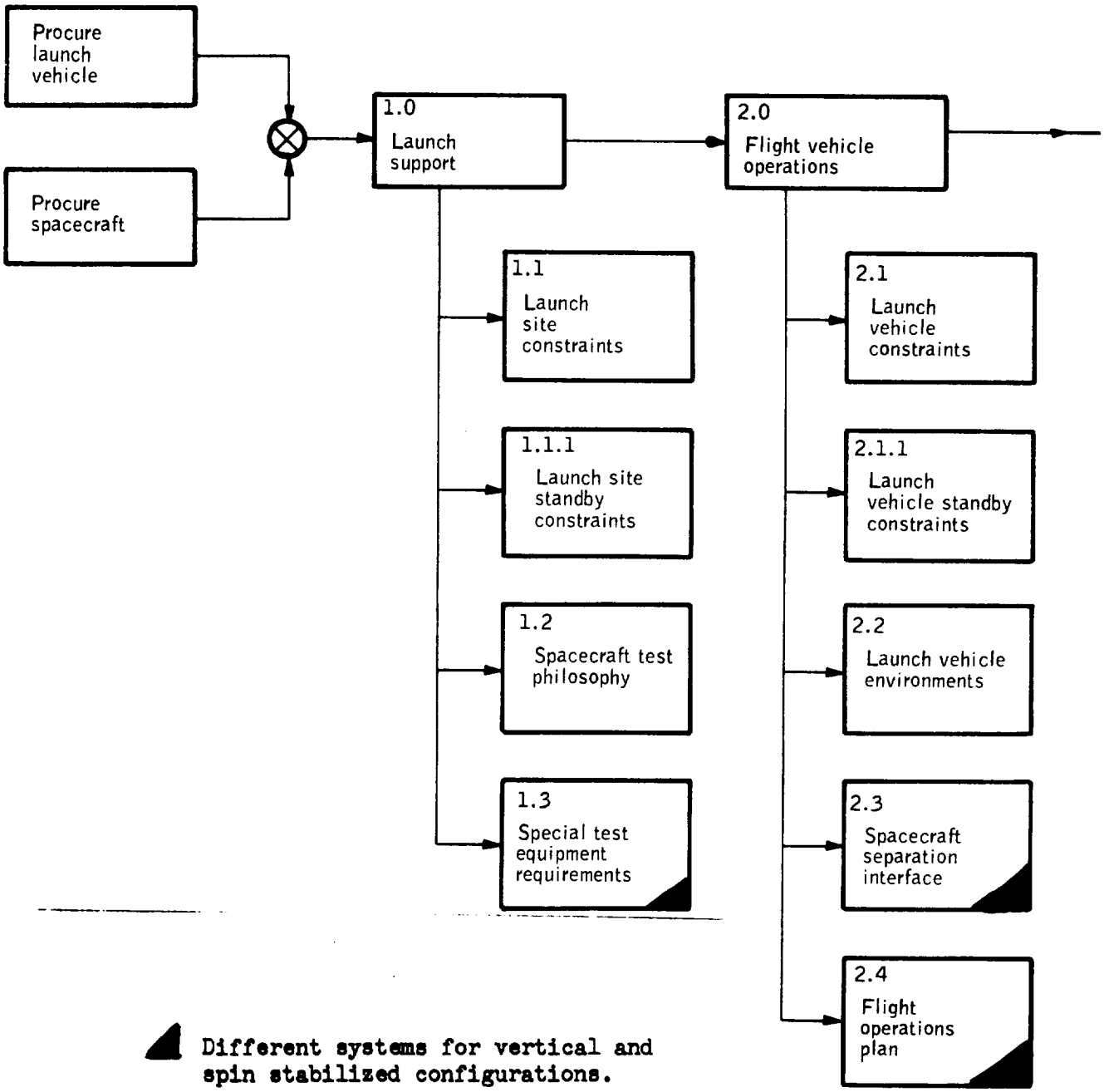

◢ Different systems for vertical and spin stabilized configurations.

Figure 6. Functional Analysis of Launch Operations

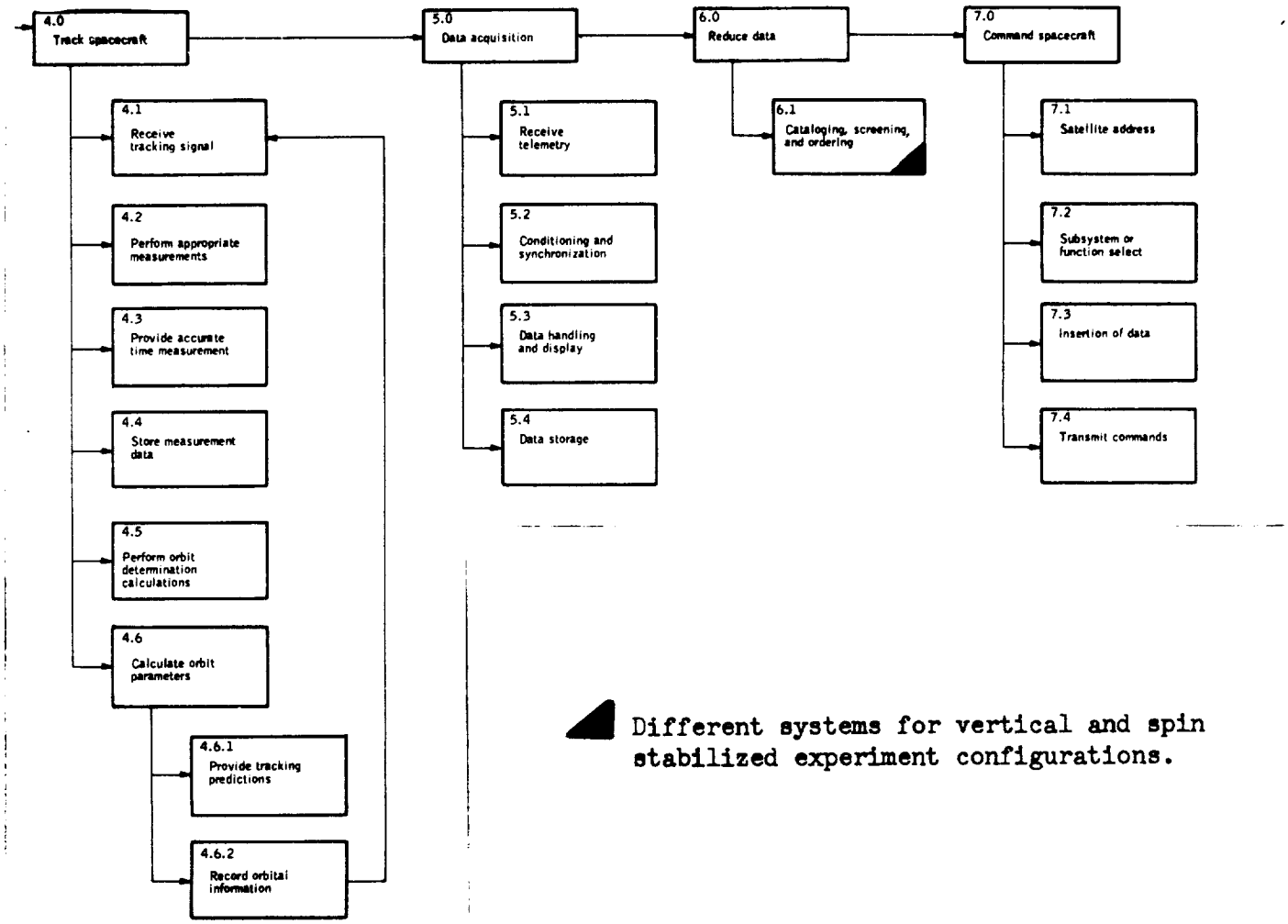

Figure 7. Experiment Ground Operations Functional Analysis

Flight Operation Plan

Minor differences in the flight operations would occur. These are obvious from an inspection of the events for the example of a stabilized experiment illustrated in Figure 6. It does not appear any basic differences in complexity would occur to the extent that costs would clearly favor one approach over the other.

Reduce Data

The data reduction task would be significantly more complex and costly in the case of the vertical experiment. The active scanning and the requirement to locate the instantaneous position of the scan relative to a celestial reference requires taking more data than in the spinning case. This concept also adds the requirement to acquire alignment information more often. This becomes significant because of the one-year life.

Experiment Complexity

A general review of the differences in experiment complexity for each of the above cases indicates none of the functions associated with a vertical experiment orientation or spin-stabilized orientation in either launch operations or ground operations would be so significant as to favor one experiment over the other. The most serious difference is the data processing problem and should be studied further to determine its significance relative to overall experiment complexity and cost.

The experiment functions associated with the orbital operations in which significant changes exist between a vertical experiment and a spin-stabilized experiment include:

(1) Power subsystem

(2) Attitude control

(3) Attitude determination

Obviously there are differences in the other subsystem concepts but they would not result in gross changes in weight, power, cost, etc.; therefore, a detailed discussion of these are not consistent with the objectives set forth in this part of the study.

The major characteristic of the spin-stabilized experiment concept is the passive scan of the measurement system. This allows for direct use of the experimental sensors without any extensive modifications or complicated mounting structure. It also provides for simplified control system techniques. The principal disadvantages of the spin-stabilized technique is the scan rate and bandwidths are constrained by the vehicle motion.

Earth stabilized experiment orientation concepts provide for the advantages of a scan rate which is independent of the vehicle motion; however, the scan must be active (moving parts). This orientation also requires a much more complicated control system and attitude determination concept. To compare these two concepts, two experiment configurations were identified. These two configurations were then compared in those cases where differences were identified. The comparison highlights the significant areas of differences in complexity and their resultant effect. The two configurations are indicated below.

Configuration No. 1

This experiment package includes the experiment sensors oriented to scan in accordance to the referenced concept. The spacecraft will be rotating so that the sensors will scan directly in front and back of the spacecraft. The sensors will then scan at the rate of four scans forward

and four scans rearward per minute. This sensing system is advantageous because of its simplicity and low failure rate. The experiment also includes a sun sensor for attitude determination. The sun sensor is used because the spacecraft rotation is conducive to sun line determination once per revolution.

The telemetry, tracking, and command communication (TT&C) subsystem can be similar to that used for TIROS. This system will include the telemetry, tracking transmitter, and diagnostic data handling equipment.

The data management system could employ core storage for data compilation. A 32 k-bit to 64 k-bit core memory would provide sufficient storage capability with high reliability.

The attitude control system will be magnetic. It will include torque coils for both spin rate adjustments and spin axis orientation. This system also includes horizon sensors and its required electronics and nutation dampers.

The power system will consist of body mounted solar cells and batteries. While rotating, the solar panels are mounted such that they are exposed to the sun. The batteries are used to provide a stable source and storage capability.

The structure will be essentially similar to the TIROS structure except for size.

Configuration No. 2

The second configuration is earth stabilized; i.e., in a local vertical orientation with spacecraft azimuth stabilized. This orientation allows for the sensors to scan in any fixed direction. The active sensors merely indicate that the sensors have an active scanning mechanism. The scan rate would be four scans per minute.

The experiment would have to include a star tracker and/or a star mapper with a gyro package (IRP) for continuous data for attitude determination. The star tracker through its own mechanism would track stars from a non-rotating spacecraft. The remainder of the experiment is made up of the necessary support electronics. The TT&C system would be similar to Configuration No. 1. The data storage system would also be similar.

The attitude control system would be more complex than the spin-stabilized system and consists of CO_2 horizon sensors and joint utilization of yaw data from the star tracker. Control is provided for by control moment gyros or a pneumatic system. Gravity gradient is desired; however, the shape of the satellite and the view factors of the experiment would probably prohibit its use.

The power system would consist of body mounted panels and batteries as noted in the first configuration. These panels would be mounted in several directions so that some portion of the total panel area is exposed to the sun whenever the spacecraft is in sunlight.

The structure for this configuration will be similar to that used in NIMBUS except for size.

These two experiment subsystem concepts are not necessarily an optimum configuration for either the vertical or spin-stabilized experiment orientation; however, the important thing here is to compare the general characteristics of the two configurations to ensure selection of the least complex configuration.

Table 4 summarizes the differences in spacecraft complexity in the vertical and spin-stabilized cases by a relative comparison of each subsystem's failure rate. No attempt was made to provide for a vigorous

1.

FOLDOUT FRAME

2.

FOLDOUT FRAME

TYPE	CONFIGURATION	MAJOR SUBSYSTEMS	E	THERMAL CONTROL	TOTALS $R = Ce^{-\lambda t}$
Orbital Spacecraft	Wheel	Pa[illegible] sat[illegible] vi[illegible]	[illegible]/orbit [illegible]e [illegible]/orbit	Insignificant	Core: $\lambda \approx 100$ Tape: $\lambda \approx 150$
	Tiros Type	λ			
	Earth oriented	Ac[illegible]	[illegible]/orbit [illegible]e [illegible]/orbit	Insignificant	Core: $\lambda \approx 200$ Tape: $\lambda \approx 300$
	Nimbus Type	λ			

determination of the absolute magnitude as this study is only interested in the differences to enable a correct choice. It should also be pointed out that the failure rates indicated would be more applicable to a larger satellite than that envisioned in the referenced concept of the ERC UV-MW Horizon Sensor Orbital Experiment Satellite.

The active scan of the vertical experiment configuration has a failure rate 10 times the failure rate of a spinning experiment. In addition, another concern is holding the alignment tolerances over a one-year experiment. It is also estimated that the power subsystem would be more complex in the vertical satellite. This would be caused by the requirement to rotate the paddles (a probable experiment concept) for the vertical case.

A qualitative review of the tradeoffs in attitude control are illustrated in Table 5 . The advantages of a magnetic control system are apparent, and the general applicability of the magnetic torquing to a spinning vehicle are well-known and need not be presented here. These advantages in simplicity are estimated to result in failure rates four times lower than comparable simple vertical control systems. Obviously the requirement of one-year life is more easily met with a magnetic system also.

Attitude determination is the other area in which there is a significant difference between the two cases. Other studies[1] have indicated a simple system consisting of horizon pipers and sun sensors can determine line of

---

[1] UV-MW Horizon Sensor Orbital Experiment - Phase B Study, NR-SD Technical Proposal SD 69-524, dated 12 September 1969.

TABLE 5

- ATTITUDE CONTROL TRADEOFFS, ROLL, YAW, TORQUING

Concepts	Disadvantages	Advantages
Momentum interchange • Inertia wheels • Control moment gyros	• Continuous power consumption (or wheel rundown) • Complicated spacecraft motions due to cross-couplings • Bearing wear-out • Requires (practically) additional torquing source to take care of long time effects (such as orbit precession)	• Continuous control possible • Can provide damping of undesired motions
Mass expulsion • Reaction jets	• Moving parts wear-out • Gas leakage generates unknown torques • Possible mass shifts upon depletion of gas supply	• Quick correction of attitude errors • Weight compatible with one-year life
Magnetic	• Continuous control impossible • Requires commutation to match earth's field • Limited practical torque capability	• No moving parts • Can compensate for residual magnetic moment • No rundown or similar limitation to life • Spacecraft motions highly predictable during no-torque period

Magnetic torquing

- Simplest - no moving parts
- Most reliable
- Highly predictable spacecraft motions
- Compensation for residual magnetic moments possible

sight of the experimental sensors to the required control accuracy. In the vertical experiment, the experimental sensors must be tethered and line-of-sight to a celestial reference must be obtained by other means. These could include:

- star trackers
- star mappers
- sun sensors

The differences in complexity can be estimated by a direct comparison of weights for devices which have been developed (see Table 6). Note that devices which are applicable to vertical systems are substantially heavier than those applicable to spinning vehicles. It is conservatively estimated this would result in a 10-times difference in failure rates assuming you can achieve the required accuracies in both cases. Three basic operations are involved in the ERC UV-MW horizon sensor orbital experiment:

(1) Launch operations

(2) Orbital operations

(3) Ground operations

These data indicate that there are no significant differences in complexity; i.e., cost, for either a vertical or spinning experiment in either the launch or ground operations. There are significant differences in complexity and cost in orbital operation, with the spinning spacecraft clearly being superior. A spin-stabilized experiment offers clear-cut advantages over a vertically oriented experiment in attitude control, experimental sensor complexity, alignment, and attitude determination. There are lesser advantages in power, ground data processing, and special test equipment; however, they are not considered critical. This data is also verified by

TABLE 6

COMPONENT SAMPLE WEIGHTS

	Weight, lbs
Star Trackers	
OAO star tracker Two axis	20.5
Dual mode star tracker Electronically gimballed	9.5
Canopus star tracker	7.0
Star Mappers	
Star Mapper	7.0
Scanner star mapper (with baffles)	20.0
Horizon Sensors	
Non-dithering	3.75
Earth sensor for spinning vehicle	1.0
Horizon sensor for vertical vehicles 4 horizon sensors Tracking servo (mirrors) Associated electronics	36.0
AOSO Sun Sensors	
One degree accuracy	3.0
One arc minute accuracy	5.0
One arc second accuracy	22.0
Radiometers	
Tiros (MRIR) (passive optics)	5.5
Scanner (active scan)	45.0

studies recently published by NASA[2] which is shown in Figure 8 . In the figure the predicted failure rate and failure rate improvement for successive launches is compared to the actual experience on early NIMBUS (earth oriented) and TIROS (wheel-spin stabilized) flights.

Experiment Integration on 3-Axis Stabilized Spacecraft

The NIMBUS and ERTS spacecraft were selected as typical spacecraft bus systems on which the UV and MW horizon sensors could be flown as experiments. Each of these spacecrafts were examined from a standpoint of experiment support systems, attitude control, attitude determination, etc. In order to compare the reference system to the NIMBUS or ERTS spacecraft, it is necessary to do a fairly detailed analysis of the experiment configuration as it might be flown on one of these buses. It is interesting to note that NIMBUS, ERTS and even other major spacecraft systems like ITOS can all be lumped into the same class and the experiment configuration is roughly the same for all these spacecraft.

The NIMBUS and ERTS spacecrafts are vertically oriented vehicles. Both these spacecraft provide an earth-oriented platform with basic systems such as power and communications adequate to support the experiment. However, the fact that the vehicles are vertically stabilized requires that some scanning technique be added to the basic UV and MW horizon sensors. The attitude control of neither the NIMBUS nor the ERTS spacecraft is sufficiently accurate to determine the line-of-sight of the UV and

---

[2]Evaluation of several mission approaches for use in defining experimentally the earth's 15 μ infrared horizon dated 15 October 1966 - NASA CR 66181.

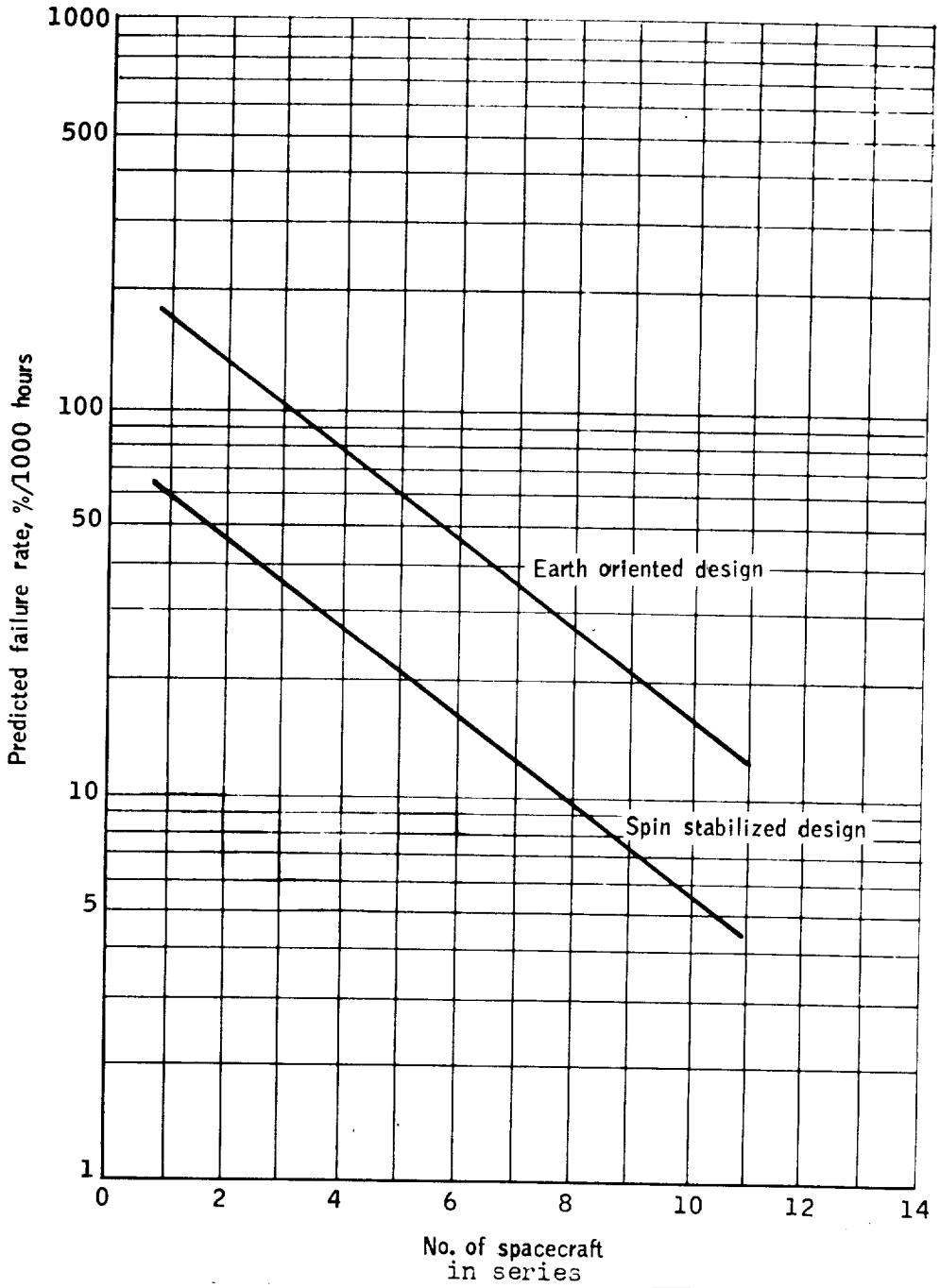

Figure 8. Predicted Failure Rates for Spin Stabilized And Vertical Satellites

MW horizon sensors to 1 km. Therefore, it will be necessary to add an accurate attitude determination system to these spacecrafts. The following paragraphs describe one possible method of modifying the UV and MW sensors for vertical orientation and describe an attitude determination approach.

Experiments Scanning Approach

UV Horizon Sensor Scanning Mechanism

The UV horizon sensor could be modified with a relatively lightweight scanning mirror that would be positioned to provide a total scan of 10 degrees. This would provide a scan of $\pm$ 5 degrees about the profile mid-point, which will provide a good cold space reference and will provide sufficient coverage for variations in orbit injection altitude, slight spacecraft pitch, etc. The position of the scanning mirror would be measured with a high resolution optical encoder. The optical encoder alignment will be calibrated by including a six point optical flat on the back surface of the scanning mirror. Periodically, an autocollimator of the PASS* type would be used to generate a precise set of six time hacks from these optical flats that would be correlated to the optical encoder angle readings against time. A sketch of the system is shown in Figure 9 .

MW Horizon Sensor Scanning Mechanism

It will be necessary to add a scanning platform to the MW horizon sensor. The entire MW sensor would be mounted on the platform and scanned identical to the UV sensor. Attached to the rotating axis would be a high resolution optical encoder. The encoder would be periodically calibrated by an autocollimation system off of six optical flats that would be rigidly attached to the side of the MW horizon sensor. The necessity to scan the

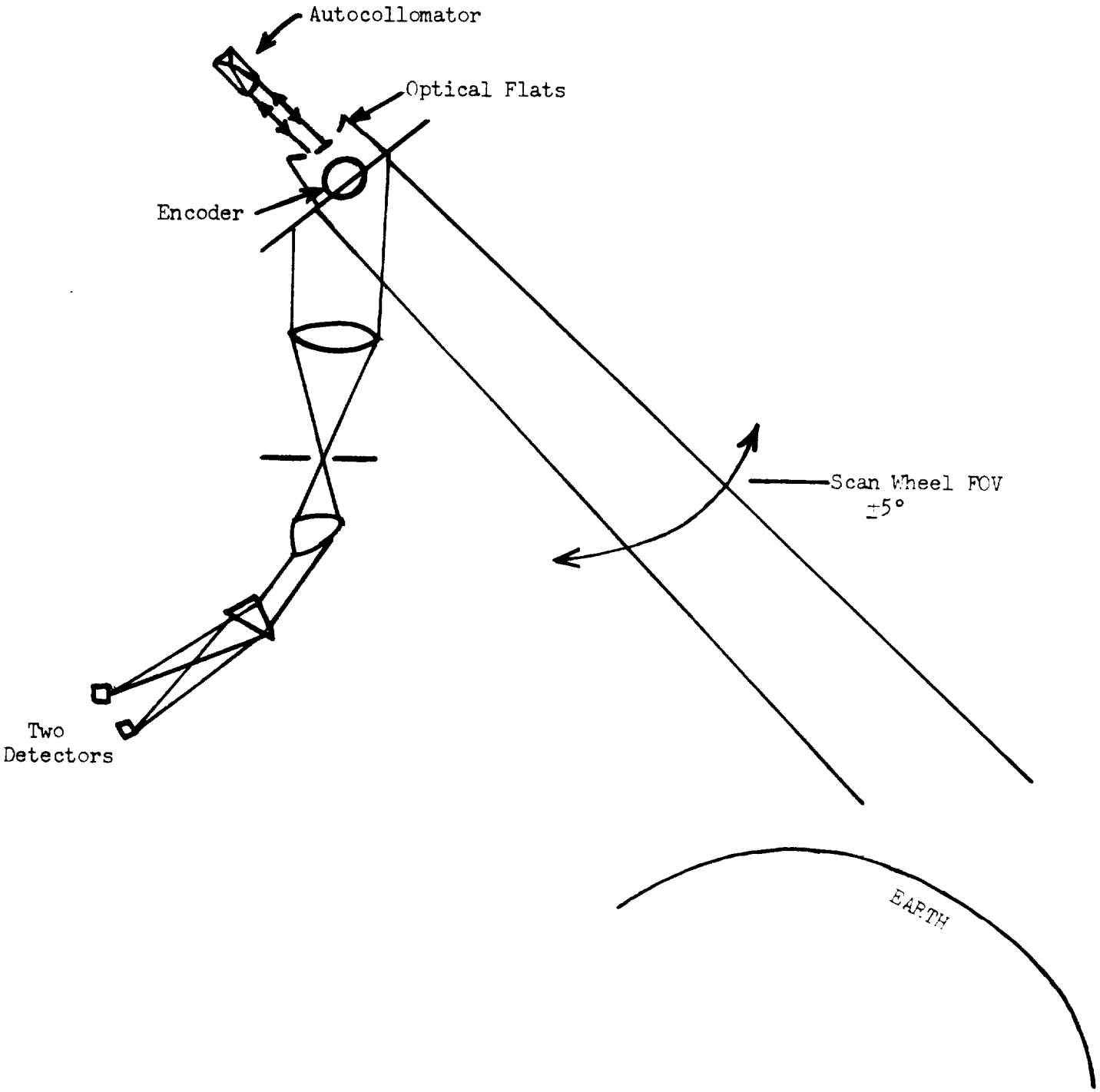

Figure 9 . UV Horizon Sensor With Scanning Mechanism

entire MW sensor forces the use of a large and heavy scanning mechanism. Alternate experiment configurations were considered using flexible waveguide and rotating joints. All of those were discarded because of both reliability and compromise of the basic experiment goals.

Determination of Horizon Sensor Pointing

The determination of the sensor pointing axis is more difficult in the vertically stabilized spacecraft than in the reference rolling wheel design. The sun sensor-horizon sensor concept as applied in the rolling wheel will not work in the vertically stabilized vehicle. An attitude determination system is required in the vertically stabilized spacecraft unless another experiment on-board already contains one.

The purpose of this attitude determination system would be to determine the horizon sensor line-of-sight in an inertial reference frame. Then, the horizon sensor pointing direction is transformed into an earth-based reference frame, and the tangent height of the line-of-sight above the earth's surface is computed. To compute the tangent height, knowledge of the spacecraft position vector, $\bar{R}$, and the horizon sensor line-of-sight vector, $\hat{s}$, is required (Figure 10). The position vector, $\bar{R}$, is determined by the NASA tracking facilities and equipment already in existence. The on-board attitude determination system is required to determine the horizon sensor line-of-sight.

As in the spinning vehicle, the sun is an attractive reference for the attitude determination system. Use of the sun as a single reference places almost impossible restrictions on a vertically stabilized spacecraft. After

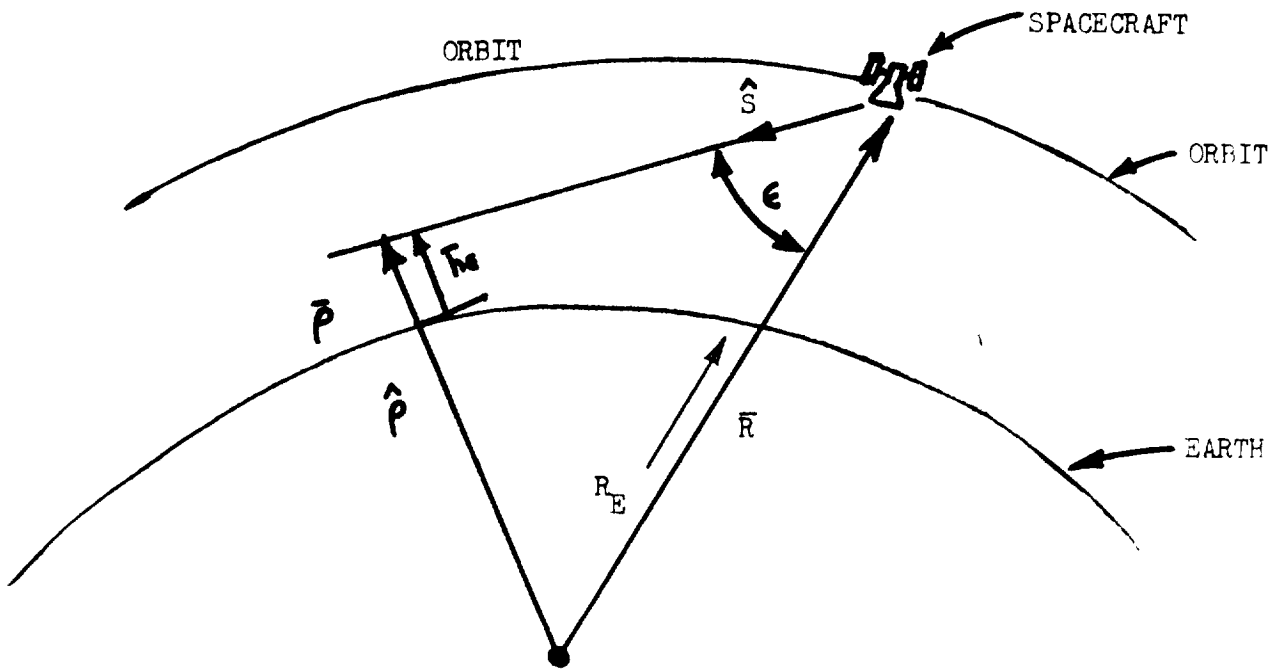

$$\bar{h}_t = (|\rho| - R_E)\,\hat{\rho} = \text{Tangent Height}$$

$$\bar{\rho} = \bar{R} - |\bar{R}|\,\hat{S}\,\cos\epsilon$$

Figure 10. Vertically Oriented Space Pointing Geometry

examining several alternate approaches, a star mapper with a three-axis gyro package was selected for the vertically stabilized spacecraft. A functional block diagram of such a system is shown in Figure 11.

The advantage of using star mapping for attitude reference is that stars are available throughout the orbit. The moving mechanisms required on the vertically stabilized vehicle cause sufficient perturbations to the spacecraft to require each horizon sensor data point to be supported by an almost simultaneous line-of-sight fix. It will not be possible to take advantage of updating the vehicle position based on predictable spacecraft motions. In theory, continuous information can be obtained by sampling a succession of stars. In practice, however, studies have shown that to assure the continuous presence of at least two stars within a 40-degree field-of-view, a star detection down to 4.5 magnitude is required. Reliable star detection during daylight is generally limited to between second and third magnitude for a reasonable star light shielding requirement. Thus it is necessary to use gyros for interpolation between star sightings and reduce the data sampling requirements by requiring only intermittant star fixes.

The star mapper 3-axis gyro system can measure all the spacecraft rates and provide continuous 3-axis attitude data. Also, the use of the 3-axis gyro system relieves the star sighting problem to the point that a completely passive star mapper scanning at orbital rates can be used.

An error analysis of the statistical and bias error associated with determining the line-of-sight of the horizon sensor shows that the total 1σ RSS error can be held within 45 arc seconds, which corresponds to approximately 0.8 km tangent height. The error budget is as follows:

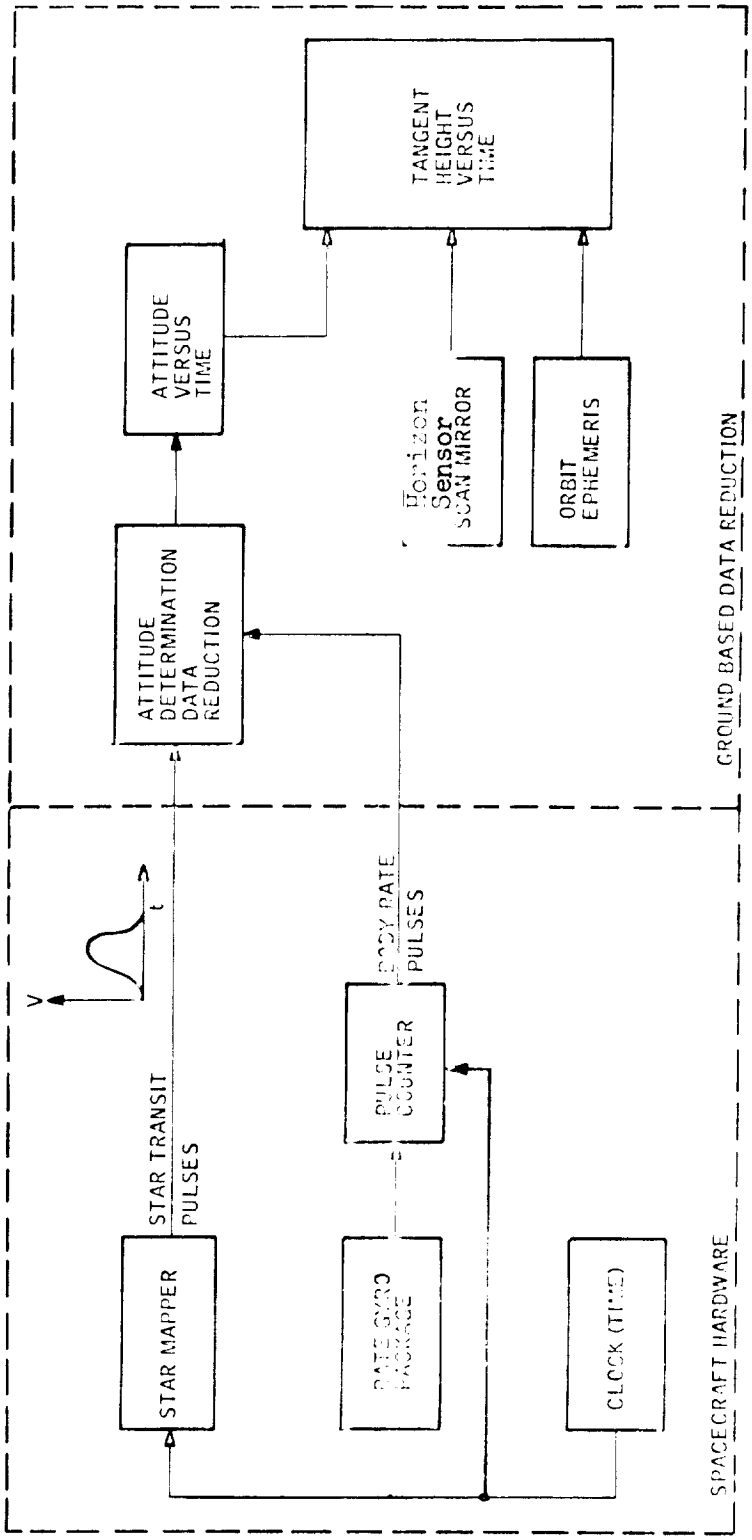

Figure 11 Functional Block Diagram of Attitude Determination Subsystem

	Statistical	Bias
Alignment:		
Star Mapper - 3-axis gyro system		20 $\widehat{\text{sec}}$
UV Horizon Sensor (MW same)	$\pm$10 $\widehat{\text{sec}}$	$\pm$15 $\widehat{\text{sec}}$
Star Mapper		$\pm$10 $\widehat{\text{sec}}$
Orbit Determination	$\pm$15 $\widehat{\text{sec}}$	
Star Ephemeris	$\pm$ 2 $\widehat{\text{sec}}$	
Time Correlation	$\pm$ 3 $\widehat{\text{sec}}$	
Error due to Gyro Drift	$\pm$30 $\widehat{\text{sec}}$	
RSS	$\pm$35.2 $\widehat{\text{sec}}$	$\pm$26.9 $\widehat{\text{sec}}$
Total RSS System = 44.3 $\widehat{\text{sec}}$ 1σ		

Comparison of Reference Satellite to 3-Axis Integration

The preceding paragraphs have described in general one method whereby the UV and MW horizon sensors could be modified for a NIMBUS or ERTS spacecraft. In the vertically stabilized spacecraft, the rather straightforward UV and MW sensors of the referenced system become very complicated with scanning mechanisms and optical alignment readout devices. The very simple straightforward line-of-sight determination system of the referenced system becomes extremely sophisticated with a 3-axis gyro system being calibrated by a precise star mapping technique. The fore and aft horizon crossings provided automatically in the referenced system are lost in the vertically stabilized vehicle unless two complete sensor packages are used. Assuming that the other instrumentation systems onboard a NIMBUS or ERTS spacecraft will allow it, the vertically stabilized vehicle does provide a rather

versatile pointing arrangement to obtain alternate azimuth points of the sensors by simply rotating the spacecraft. A comparison of the reference system to the NIMBUS-ERTS is as follows:

System	Horizon Sensors	Experiment Scanning Mechanisms	Optical Alignment Sensors	Sensor Line-of-Sight Determination	Spacecraft Support Systems (Power, Comm., etc.)
Ref. System	UV&MW	Not required	2 required (1 UV to Sun Sensor, 1 MW to Sun Sensor)	Sun Sensor & Horizon Sensor	Must furnish all.
ERTS	UV&MW	UV Scanning & MW Scanning	5 required (1 for each scanning, 1 for each sensor to S.M. & 1 for S.M. to gyros)	Star Mapper & 3-axis gyro package	Onboard systems OK
Nimbus	UV&MW	UV Scanning & MW Scanning	5 required	Star Mapper & 3-axis gyro package	Onboard systems OK

A partially hidden factor in the vertically stabilized spacecraft is the lengthy and difficult alignment verification of the scanning mechanism. Previous jobs of this task have shown that 50 percent of the total cost is required for testing. The pre-flight and post-flight data reduction and interpretation is at least an order of magnitude more complicated with the vertically oriented system with its attitude determination system than the referenced spinning wheel spacecraft.

An estimated weight summary of the subsystems that must be added to the basic UV and MW horizon sensors for a vertically stabilized spacecraft is as follows:

Gyro Package - IRP	10 pounds
Star Mapper	8 pounds
Star Mapper Baffling	4 pounds
Scanning Mechanism for UV Sensor	2 pounds
Scanning Mechanism for MW Sensor	10 pounds
Alignment Devices	3 pounds
	37 pounds

Conclusion

This examination of using the NIMBUS, ERTS or any vertically stabilized spacecraft for the UV and MW horizon sensor experiment has shown that the vertically stabilized spacecraft (1) is more expensive, (2) is more complex, (3) compromises the experiment, and (4) provides better azimuth alignment than a spin-stabilized spacecraft.

SUMMARY OF FLIGHT ALTERNATIVES ELIMINATED

Twenty promising NASA and Air Force flight alternatives for the MW and UV instruments have been investigated. Of these, six were rejected during the proposal effort as defined in NR/SD Proposal, SD 69-524. An additional nine flight alternatives have been rejected. Data on these alternatives and reasons for their elimination are presented.

The missions discussed are:

Atmospheric Explorer C

Orbital Scanner

SPARS

SESP Multiple Payload Launch 71-2

Air Force Classified Launches

SESP Multiple Payload Launches

TD-1 (Thor Delta-1)

Each flight alternative is discussed in a succinct outline form as follows:

Program Name

Integration Mode

Launch Date

Orbit

Reason for Elimination

Program Data Source

Some of the missions offer two flight alternatives which are discussed separately; (1) integration of the instruments into the primary spacecraft and (2) integration of a piggyback satellite carrying the instruments on the launch vehicle for the primary spacecraft.

1. PROGRAM NAME: Atmospheric Explorer C

INTEGRATION MODE: Add to primary spacecraft

LAUNCH DATE: October 1972 - April 1973

ORBIT: Initial: 65 to 81 x 2160 n.mi., 108° incl., sun sync, 2 PM descending node.

Others: Let initial orbit decay in circular steps of 600, 500, 400, etc. Stay at each step 1-2 weeks. Can take full orbits of data.

REASON FOR ELIMINATION:

(a) Cannot use experiments during initial phases of mission since low perigee (65 to 81 nautical miles) and high apogee (2160 nautical miles) makes sensor design complicated if not impossible (would require variable squint angle and sensitivity).

(b) Spin rate during the circular orbit step phases will be stable and controllable in the range 0.5 to 10 RPM as required by the experiments. Integration of the experiments into the primary spacecraft for use during one of these mission phases should be technically feasible. Requires adding a fine sun sensor and possibly a star mapper to the spacecraft. Will get only 1-2 weeks of data in the orbit for which the MW sensor squint angle has been set prior to launch.

(c) MW and UV horizon sensing not in keeping with objectives of program.

(d) Cannot investigate the effect of diurnal variations, conditions directly over the earth's poles, or cannot achieve 0° sun line locator zenith angle unless out-of-orbit plane scan

maneuvers of the total spacecraft are allowed. Current program does not include such maneuvers.

(e) Program beginning 9-month Phase B/C study soon. Contractors have not been selected. Configuration of flight spacecraft will not be known until after the B/C study. Therefore, cannot perform integration studies at this time.

(f) Submission of experiments for flight is past due. Announcement of Flight Opportunity (AFO) was released in mid-1969. Many requests are currently being turned down and others are being eliminated. NASA/HQ, Mr. F. Gaetano, AE Prog. Mgr. feels it is not possible to obtain flight approval on C at this time. Mr. Gaetano will send Mr. Grostein (ERC) AFO for AE D when it is issued.

PROGRAM DATA SOURCE: D. W. Grimes, NASA/GSFC (301) 982-6519
F. Gaetano, NASA/HQ, (202) 963-6929

2. PROGRAM NAME: Atmospheric Explorer C

INTEGRATION MODE: Piggyback satellite (Delta engine compartment)

LAUNCH DATE: October, 1972 - April, 1973

ORBIT: Initial: 65 to 81 x 2160 n.mi., 103° incl., sun sync, 2 PM descending node.

Others: Let initial orbit decay in circular steps of 600, 500, 400, etc. Stay at each step 1-2 weeks. Can take full orbits of data.

REASON FOR ELIMINATION

Initial perigee is low and the orbit will decay rapidly. If the satellite does not have an orbit makeup capability like

AE C, it will not be possible to obtain data over a 1-year period. Could modify orbit by incorporating satellite into an orbital shuttle (Ref: Adamski, D. F., "Orbital Shuttle," Astronautics & Aeronautics, May 1968), but the added complication and cost are not justified in view of other visible flight opportunities in more favorable orbits which do not require the use of the orbital shuttle.

PROGRAM DATA SOURCE: D. Grimes, NASA/GSFC (301) 982-6519
F. Gaetano, NASA/HQ. (202) 963-6929

3. PROGRAM NAME: Orbital Scanner

INTEGRATION MODE: Add to Primary Spacecraft

LAUNCH DATE: CY 1973 to 1974 (estimated)

ORBIT: 270 n.mi. circ., 97.4° incl., sun sync, 3:00 PM descending node (based on Honeywell Pre-Phase A Study). Lockheed study used 340 n.mi. Space General study used 286 n.mi.

REASON FOR ELIMINATION:

(a) Program not approved by NASA OART ARTEP so that it does not currently exist as a NASA approved and funded program.

(b) Configuration of spacecraft currently undefined. Pre-Phase A studies have identified at least four technically feasible approaches (Honeywell, Lockheed, Space General and RCA) to the spacecraft design. Langley has not requested ARTEP approval and funding of initial work on Phase B toward a flight program. Therefore, integration studies cannot be performed.

(c) Cannot achieve 0° sun line locator zenith angle even with 90° out-of-plane maneuver for 3:00 PM nodal crossing.

(d) Cannot investigate the effect of diurnal variations as required by UV sensor unless the Scanner experiment accepts relatively frequent out-of-plane maneuvers. This point has not been factored into any existing Scanner studies. It cannot be answered since program details are unknown at this time.

PROGRAM DATA SOURCE: J. Dodgen, NASA/Langley (703) 827-1110
T. Michaels, NASA/HQ. (202) 962-7294

4. PROGRAM NAME: Orbital Scanner

INTEGRATION MODE: Piggyback Satellite (Delta engine compartment)

LAUNCH DATE: CY 1973 to 1974 (estimated)

ORBIT: 270 n.mi. circ., 97.4° incl., sun sync. 3:00 PM descending node (based on Honeywell Pre-Phase B Study). Lockheed study used 340 n.mi. Space General study used 266 n.mi.

REASON FOR ELIMINATION:

(a) Program not currently approved by NASA OART ARTEP so that it does not currently exist as a NASA approved and funded program.

(b) Projected orbit too low. Effects of atmosphere drag on vehicle stability still exist at 270 n.mi. Better to choose viable alternative with higher orbit to eliminate the problem rather than try to design or model (software) around it.

PROGRAM DATA SOURCE: J. Dodgen, NASA/Langley (703) 827-1110
T. Michaels, NASA/HQ. (202) 962-7294

5. PROGRAM NAME: SPARS (Orbital portion of PEPSY)

INTEGRATION MODE: Add to primary spacecraft or as piggyback satellite

LAUNCH DATE: CY 1972 - 1973

ORBIT: 200 $\pm$100 n.mi. circ., 90° incl., not sun sync.

REASON FOR ELIMINATION:

(a) PEPSY mission has upper altitude limit of 300 n.mi. due to limitations of ground laser power output used to establish accurate ground line-of-sight.

(b) Mission requires an orbit life of two to four weeks. Cannot investigate effect of seasons on MW and UV.

(c) SPARS is classified. To integrate with it as a separate spacecraft or hard mounted on an Agena or Burner II would be politically complicated. Would have to give experiment to the Air Force for flight so as not to compromise national security.

(d) SPARS flight hardware is not yet approved. Date of flight is not defined. SESP is not planning the mission as yet.

(e) SPARS program office personnel (J. Alberts and Lt. J. Lyons) are interested in MW experiment. They advise that the experiment not be integrated into the SPARS vehicle due to projected power (supplied by large primary batteries) and weight limitations. The use of the large batteries creates the weight limitation.

(f) Mission orbit cannot be sun synchronous due to requirements of the primary experiment. This means that sun can illuminate satellite from any angle. This complicates the solar array and the thermal subsystem analyses and design. These complications are not worth addressing in view of available viable sun synchronous missions.

PROGRAM DATA SOURCE: J. E. Alberts, Air Force, SAMSO/SMTAG (213) 643-2656

Lt. J. K. Lyons, Air Force, SAMSO/SMTAG (213) 643-2656

Lt. N. Anderson, SESP Office, SAMSO/SMTEE (213) 643-0841

6. PROGRAM NAME: SESP Multiple Payload Launch, 71-2

INTEGRATION MODE: Add to primary spacecraft or as piggyback satellite.

LAUNCH DATE: 3 qt. CY 1971 to 3 qt. CY 1972

ORBIT: 350 to 400 n.mi. circ., 90° incl., not sun sync.

REASON FOR ELIMINATION:

(a) Project currently in state of flux. Lockheed Agena integration price too high. General Hedrich has directed a competitive procurement for the project. RFP was issued in December, 1969, with a 35-day response period. Mission details will not be available until a contractor is selected several months from now.

(b) SESP has more payloads identified for this launch than the capabilities of probable launch vehicles to be used.

(c) To obtain flight through SESP, NASA must submit experiment for review and approval by the DOD/SESP payload review board through established channels. Best change to obtain ride exists in submitting a small piggyback satellite since integration interface is simplified.

(d) Mission orbit cannot be sun synchronous due to requirements of primary experiments. This means that the sun can illuminate a piggyback satellite from any angle. This complicates solar array and thermal subsystem analysis and design. These complications are not worth addressing in view of available viable sun synchronous missions.

PROGRAM DATA SOURCE: Maj. J. F. Hoelscher, SESP Office, SAMSO/SMTEE (213) 643-0841

Lt. N. Anderson, SESP Office, SAMSO/SMTEE (213) 643-0841

7. PROGRAM NAME: Air Force Classified Launches

INTEGRATION MODE: Add to primary spacecraft or as piggyback satellite.

LAUNCH DATA: Classified

ORBIT: Classified

REASON FOR ELIMINATION:

(a) Cannot obtain data on satellites or boosters due to classifications.

(b) Experimenter must interest Air Force in the experiment.

PROGRAM DATA SOURCE: Classified

8. PROGRAM NAME: SESP Multiple Payload Launches

INTEGRATION MODE: Add to primary spacecraft or as piggyback satellite.

LAUNCH DATE: CY 1973 - 1974

ORBIT: Unknown at this time.

REASON FOR ELIMINATION:

No planning data on the launches as yet.

PROGRAM DATA SOURCE: Maj. J. E. Hoelscher, SESP Program Office, Air Force, SAMSO/SMTEE (213) 643-0841

9. PROGRAM NAME: TD-1 (Thor Delta - 1)

INTEGRATION MODE: Piggyback satellite (Delta engine compartment)

LAUNCH DATE: 2nd Quarter 1972

ORBIT: 297 n.mi. circ., 97.4° incl., sun sync.

REASON FOR ELIMINATION:

(a) Will launch ESRO satellite. Would have to negotiate agreement with ESRO to fly a piggyback satellite.

(b) Orbit is too low. Effects of atmospheric drag on vehicle stability still exists at 297 n.mi. Better to choose a viable alternative with a higher orbit to aliminate this potential problem than try to design or model (software) around it.

PROGRAM DATA SOURCE: T. La Valle, NASA-McDonnell Douglas In-Plant Representative (213) 391-0311, Ext. 6293

Delta Missions Summary, 1 November 1969, obtained from J. Tomersillo, NASA/GSFC (301) 982-2272

RECOMMENDED FLIGHT MODE AND AVAILABLE MISSIONS

The recommended flight mode is the reference concept presented by NASA-ERC and further defined in this study, integrated into the Delta second-stage engine (DSV 3L-4 TIIIC transtage) compartment. The satellite systems will be similar to the TIROS IX systems. Changes are made in this study only to reflect the use of current and more reliable components and only minimum redundancy is used for critical components.

Viable flights for this satellite in the order of preference are:

a. NIMBUS E, 1st half 1972

b. NIMBUS F, 1st half 1973

c. ITOS C, February 1972

d. ITOS D, February 1973

e. ITOS E, February 1974

f. ERTS A, June 1972

g. ERTS B, June 1973

To carry the satellite in the Delta engine compartment requires that a new piggyback payload adapter truss be designed by the McDonnell Douglas Delta Program Office through NASA. A canister must also cover the satellite to protect it from the engine rocket exhaust during Delta/Thor staging. Since the satellite in its canister is too large to fit through existing access doors, it will be necessary to integrate the satellite/canister with the Delta prior to its mating with the Thor. This will be approximately 30 days before launch. A nitrogen purge of the canister during the on-pad period is recommended to protect the satellite from the humid atmosphere at the launch site. These parameters are discussed in detail elsewhere in this report.

The use of a separate launch vehicle for the reference concept satellite is considered a secondary flight mode. Specific launch vehicles investigated in this study are the SCOUT and Thor/Burner II.

ORBITAL ANALYSIS

The overall objective of the orbital analysis is to provide data as part of the basis for selection of the orbit and launch vehicle for the proposed horizon sensor satellite and to provide a basis for the preliminary system design. It was first necessary to scrutinize the satellite system requirements in order to determine what data were required. The two chief guidelines were the required distribution in space and time of the observations and the measurement accuracy required. In addition to comparing orbits and launch vehicles on the basis of accuracy and distribution of the acquired data, the solar lighting associated with each alternative was evaluated. The impact of variations in sun angles throughout the orbit and over the one-year satellite lifetime on the system design (e.g., the electrical power supply) and on the overall system accuracy was evaluated, using the data generated in the orbit analysis. These evaluations are described in detail separately. This section compares candidate launch vehicles and orbits in terms of the aforementioned factors and gives a recommended choice. Information is also provided to permit the analysis of the data load for any of the candidate orbits.

Orbit Selection

General Criteria

The analysis of orbit applicability to the mission objectives is in two parts:

1. General consideration of orbit types.
2. Consideration of the orbits involved in other satellite missions which might accommodate a piggyback satellite (specifically, ERTS, NIMBUS, and ITOS).

In the following discussion, the two parts of the problem are considered in sequence.

The first part reviews the stated objectives of the mission and the application of various orbits to achieve these objectives. It shows the technical basis on which NR/SD has approached the problem of orbit selection, pointing out the key factors.

The objective of the proposed mission is to map the UV and molecular oxygen altitude boundaries over the earth's surface for several times of day over the four seasons of the year. The interval of time over the year has not been specified. The interval of time over the day has not been specified, but should be less than two hours if a reasonably smooth curve is to be obtained. It has been specified that the points over the earth must be ≤ 5 degrees apart in latitude and extend from pole to pole. The required separation of these points in longitude was not specified; but this separation is closely related to the frequency with which measurements at any given point are made, as indicated in the following discussion.

It is shown that the less frequently tests at identical points are made, the closer together in longitude are the orbital passes which provide measurement opportunities. It is also indicated that conditions can exist which will provide more data than required. Consequently, it is possible that a data discrimination rule should be adopted to avoid unnecessary data handling problems.

The orbit of the proposed satellite is defined by its altitude, inclination, and node orientation. In the following discussion, some criteria are presented for the selection of these orbit parameters.

It is shown in the following discussion that the sensitivity of horizon height measurements to pointing errors in the vertical plane increases as the nominal orbit altitude is increased and that the sensitivity of the locator geographic position to such errors is independent of the orbit altitude. In Figure 12 point B represents the location of the locator point (or point of tangency) at altitude h, and point E represents a low-altitude satellite with look angle θ, orbit radius b, range angle ϕ, and range R to the point B. Point A represents a high-orbit satellite with associated quantities θ', b', ϕ', and R'. Points Q and Q' represent erroneous locator points at altitudes h_e and h_e', respectively, resulting from a pointing error Δ in the look angles at E and A. The altitude error ($\Delta h'$) corresponding to the pointing error at A is proportionately larger than that (Δh) corresponding to the same pointing error at E' that is, $\frac{\Delta h'}{\Delta h} = \frac{R'}{R}$ because the altitude error is approximately equal to the product of the range and the pointing error (in radians). Since the range increases with orbital altitude, it follows that the altitude error sensitivity to pointing error also increases with orbital altitude.

The geographic position of the locator point is represented by the range angle at C subtended by the locator point and the satellite. This angle is computed from a knowledge of the orbit altitude, the pointing angle at the satellite, and the angle at B, which is by definition equal to 90 degrees. Any pointing error Δ will result in an error, of the identical magnitude in the range angle, regardless of the altitude from which the horizon measurement is being made because the sum of the three angles of the triangle must equal 180

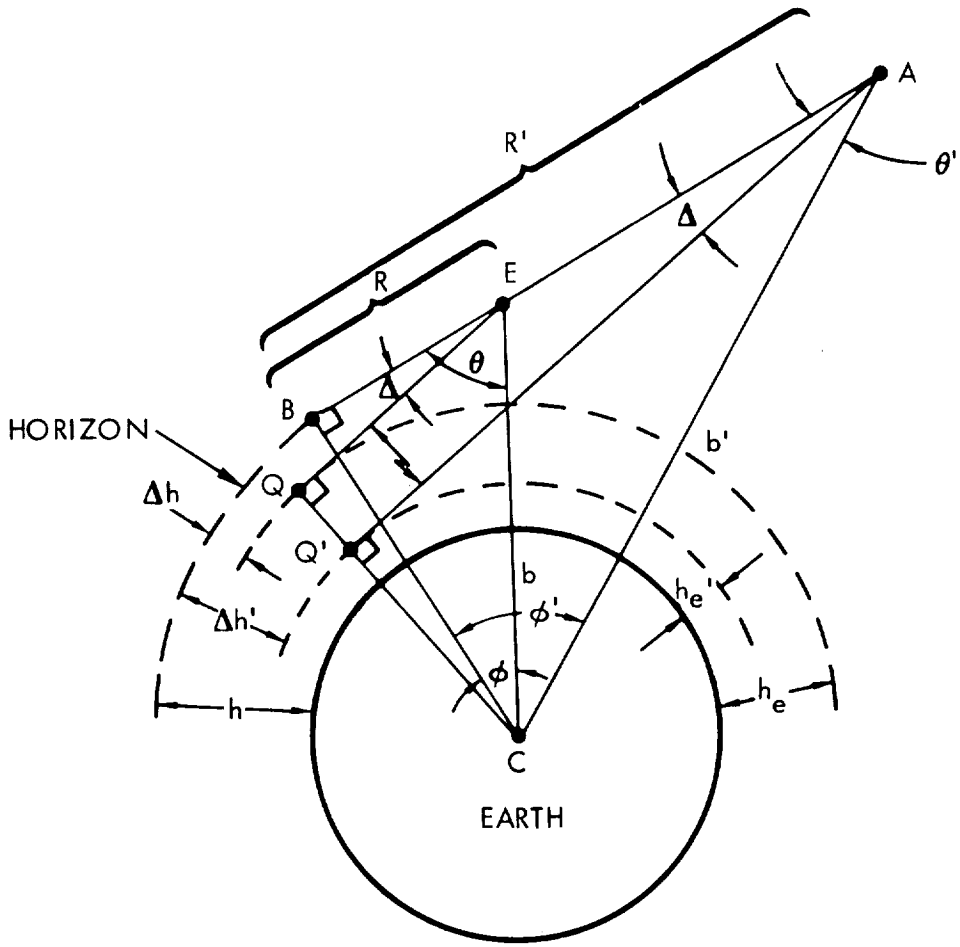

	SATELLITE	
	E	A
POINTING ANGLE	θ	θ'
ORBIT RADIUS	b	b'
HORIZON ALTITUDE	h	h'
RANGE	R	R'
RANGE ANGLE	ϕ	ϕ'
ERRONEOUS HORIZON ALTITUDE	h_e	h_e'

POINT B REPRESENTS THE LOCATOR POINT.
POINTS Q AND Q' REPRESENT ERRONEOUS LOCATOR POINTS GENERATED BY A POINTING ERROR Δ AT E AND A, RESPECTIVELY.

Figure 12 Determination of the Locator Point

degrees. Therefore, the sensitivity of the geographic location of the locator point to pointing error in the vertical plane is independent of orbit altitude.

The higher orbit altitudes provide greater visibility of points that are not in the orbit plane. This is advantageous for obtaining data points with local times different from those available in the orbit plane. These factors must be considered, along with the sensor performance variation, in selecting the orbit altitude.

Two major mission parameters which are strongly dependent on the orbit selected are the frequency with which the satellite will repeat its ground trace and the variation in local time with each passage over the same point. The former is essentially dependent only on the orbital altitude, and the latter is dependent on the combination of orbit inclination and altitude. A detailed discussion of these dependencies will be found subsequently. To obtain seasonal variations, it is necessary to observe the same point repeatedly under the same conditions at different times of the year. The orbital motion can be synchronized with earth rotation to provide a repeatable ground trace by the appropriate selection of orbit altitude. The orbit can then be synchronized with the apparent motion of the sun to control the local time of equatorial crossing by selecting the appropriate orbit inclination.

If the local time of successive passages of the same point is to be kept constant throughout the year, the rotation of the nodes in inertial space (in the equatorial plane) must be made equal to the rate of the earth around the sun (sun synchronism). However, if this rotation rate of the nodes were made equal to zero, then the local time of passage would change at the rate of 24 hours in a year, or 3.94 minutes/day. In this way, each test point in the orbit plane would be observed at a different local time every time it was observed.

The rate of change in local time is dependent on the nodal rate created by adjustment of orbit inclination. Zero nodal rate is obtained when the inclination is 90 degrees. Under this condition, if the repeat cycle were four sidereal days, the local time would be 15.76 minutes later every time the satellite passed over a given point. The increment of local time is 3.94T where T is the elapsed time in sidereal days (1 sidereal day = 23 hours, 56.07 min). To obtain small increments of local time, therefore, the repeat cycle should be made small (for a given orbit inclination). However, the number of different longitude positions covered on the earth will reduce correspondingly. The minimum number of longitudinal positions along the equator that will be covered is 28 for a one-day repeat cycle and altitude below about 800 nautical miles. Fourteen of these passages will be in sunlight and 14 in the dark. The local time will advance by 0.286 minute with each successive orbit. The relationship between repeat cycle, orbital altitude, orbit period, and earth coverage is shown in Figure 13 for a polar ($i=90°$) orbit.

In the foregoing analysis, the local time of passage over any given point undergoes one 24-hour cycle in one year. The local time could be made to pass through a 24-hour cycle in one year by causing the orbit to regress at a multiple (m) of the earth's rate about the sun. That is,

$$n - 1 + m$$

The quantity m is positive for posigrade orbits ($0 < i < 90°$), which regress, and negative for retrograde orbits, which progress. The sun-synchronous case, for which $m = 1$, causes n to equal zero and the local time to be constant. The polar orbit case described above corresponds to $m = 0$. For $n = 2$, the required posigrade orbit is nonpolar by the same amount (about 10°) as is the retrograde orbit necessary to produce $n = 0$ (sun synchronism).

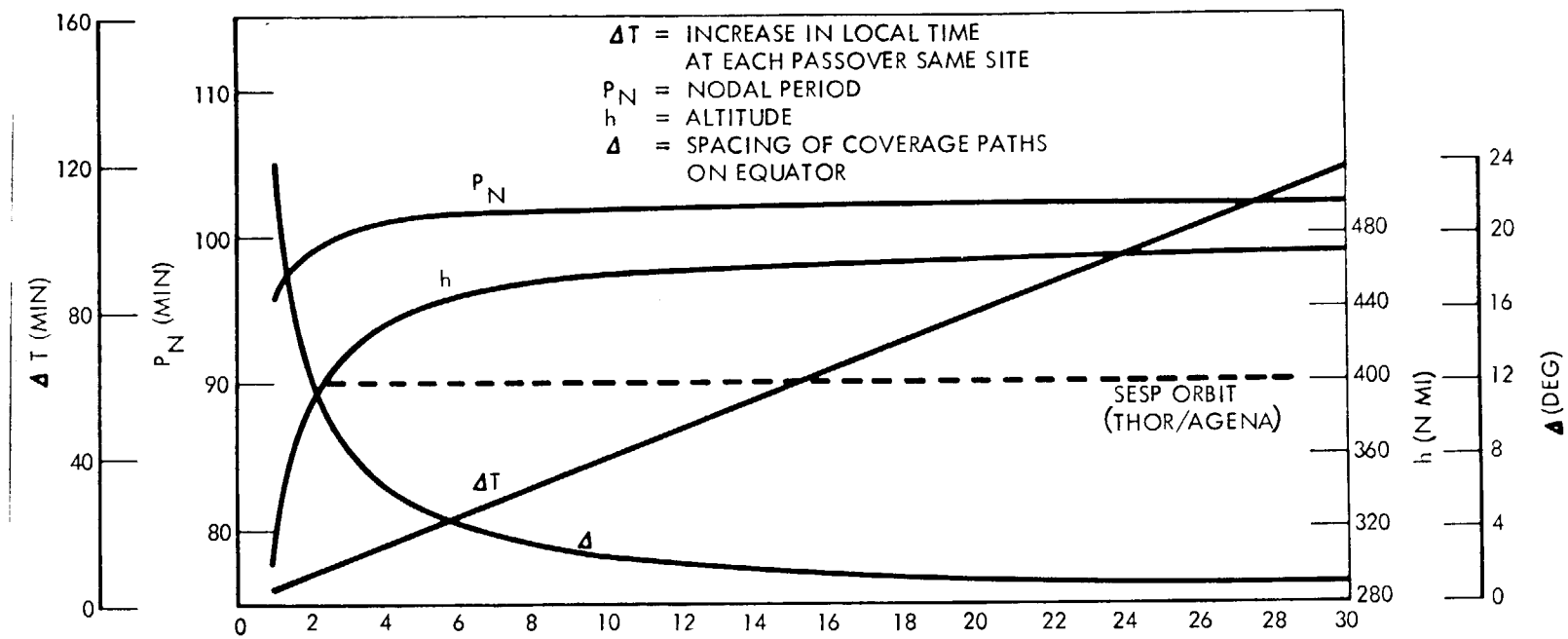

Altitude: 350/400 circular
Inclination: ≈ 90°

Figure 13. Orbit Characteristics Versus Repeat Cycle for 90-Degree Polar Orbits

Space Division
North American Rockwell

The diurnal (local time) variations described above are correlated with the time of year. That is, any one local time of passage over a point occurs only once or twice during the year. The 6 a.m. value of a measurement at a given point may be made six months after the 6 p.m. measurement at the same point. It has been assumed the diurnal variation be observed over a real day, in which case a stationary sensor suspended over the earth would be the theoretically ideal solution. Observation from a 24-hour equatorial earth-synchronous satellite is the only way this requirement can be met. However, this type of orbit is impractical because of its inability to provide global coverage and its high altitude (19,323 nautical miles).

Measurements of the same point at different local times may be made over a relatively short time period if the sensor is permitted to "look" outside the orbit plane. Studies indicate that the satellite would have to be reoriented each time a different local time of observation is required. The range of local time variation obtainable is discussed in detail.

The Application of Sun-Synchronous Orbits

In-Plane Observations

The use of a sun-synchronous orbit for the proposed satellite has the advantage of providing a relatively invariant thermal cycle over the year. However, if the satellite is constrained to a sun-synchronous orbit, the local time at each latitude in the orbit will remain essentially constant over the mission lifetime so that diurnal variations at the same point cannot be observed by a fore-and-aft looking sensor. Also, the use of a sun-synchronous orbit, or any other nonpolar orbit, precludes the observation of polar points except by destroying the alignment between the vehicle spin axis and the normal to the orbit plane.

The variation in the sun-zenith angle over one orbit (for in-plane observations) changes over the year. For example, at the time of the vernal equinox, the sun lies directly in the plane of the 12 o'clock orbit (NIMBUS) and on the equator so that the value of sun-zenith angle passes through zero. At other times of the year, the minimum value is several degrees. The minimum sun-zenith angle is on the order of 30 degrees in the instance of orbits whose sunlit nodes are at local times of about 3 p.m. (ITOS) or 9 a.m. (ERTS). The sun-zenith angle is approximately equal to 15 degrees for every hour that the local time of the sunlit node departs from 12 noon. The sun-zenith angle will, of course, pass through the specified maximum (70 degrees) in every instance except that in which the spacecraft is always in sunlight.

For any given point over the earth, the sun-zenith angle at the time of measurement will change only to the extent that the local time of the measurement changes. For sun-synchronous orbits and in-plane measurements, this change is very small - a few degrees.

Out-Of-Plane Observations

This section illustrates methods and conditions for obtaining observations of a point at different time of day and for observing points directly beneath the sun (zero zenith sun angle). Figure 14 shows a locator (Point A) at an arbitrary fixed geographic position which can be observed from any point (X) on a range circle, B (only a circle when drawn on a spherical surface), which is intersected by the orbital traces of the satellite. For a sun-synchronous orbit (sun essentially fixed with respect to the orbit trace), the local time of each observation will be different; but the look azimuth from any point X to point A is different at each point (X). Also, point A is only one of an infinite number of points that can be observed from each point (X)

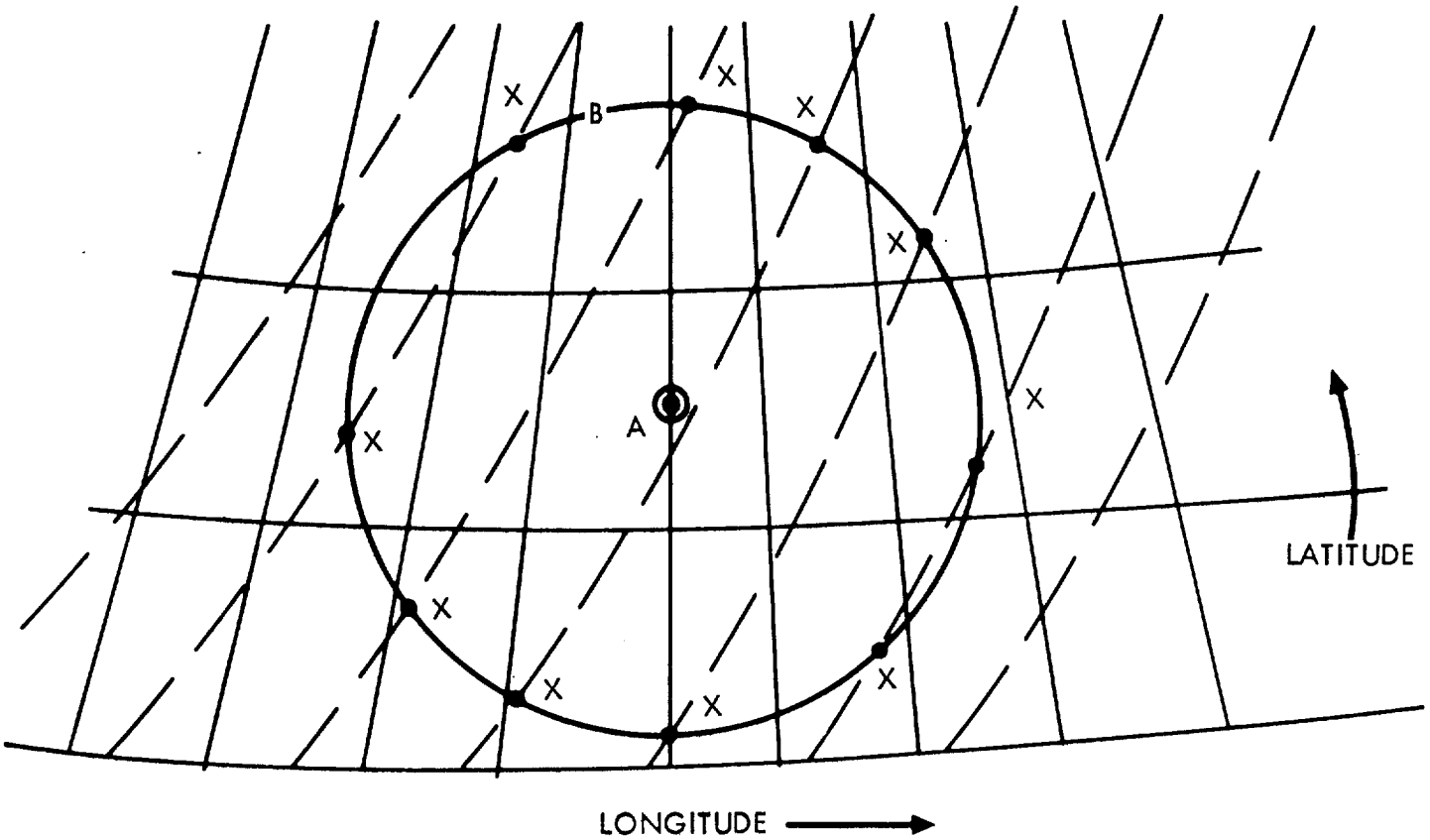

Figure 14 Locator Point, Range Circle Relationship

on the circle of Figure 14. A logical basis for determining the direction of observation at each point in the orbit must therefore be established.

To observe a point that is directly beneath the sun (zero Sun-Zenith angle), the satellite must pass within a certain minimum range of that point and, in general, the sensor must look out of the orbit plane, as in the preceding discussion. The minimum range is determined by the altitude of the locator point and the altitude of the satellite. The orbit plane of a sun-synchronous orbit is displaced from the sun line (and, therefore, the locator point) by a relatively fixed angle and, contrary to the previous case of a general point of fixed position, the sub-solar test point never gets any closer to the orbit trace. If the angle is too great, the satellite will never pass close enough to the sun line to observe a zero-zenith-angle point. The best opportunity occurs in mid-summer or mid-winter, depending on the orbit. The following brief discussion evaluates candidate orbit from the standpoint of their inherent opportunities for such observations.

With a locator point on a horizon of altitude h_1 and directly beneath the sun assumed, horizontal lines drawn from the locator point will intersect a sphere, representing the orbital altitude, h_s, at a series of points, which form a circle around the locator-sun axis (Figure 14). The satellite must pass within this circle in order to observe a point which has a zero-zenith-sun angle. The radius of the circle can be defined by the angle ϕ subtended by the sun (or locator) and a point on the circle, at the center of the earth. This radius is shown for four candidate orbits in Table 7 .

Three of the four candidate orbits which have been considered offer opportunities for zero-zenith-sun angle observations in varying degrees. The

TABLE 7. CANDIDATE ORBITS FOR MID-SUMMER OR MID-WINTER

Orbit Altitude h_s (nmi)	Orbit Plane Orientation	Circle Radius Ø (deg)		Project Name
		h_L = 27 nmi	h_L = 15.65 nmi	
270	3:00 p.m. desc node sun sync	21	21.5	Orbital Scanner
496	9:29 a.m. desc node sun sync	28	28.6	ERTS
600	12 noon sun sync	30.7	31.3	Nimbus
790	9:00 a.m. D.N. or 3:00 p.m. A.N. sun sync	34.8	35.2	ITOS

270 nautical mile orbit does not intersect the range circle at all; the ERTS and ITOS orbits barely intersect their circles, and only in the middle of the summer, when the sun is in the northern hemisphere.

A satellite in the noon orbit of the Nimbus satellite passes through its range circle on every orbit and therefore has two opportunities every orbit to observe sub-solar locators. However, the local time variation of other points that can be observed from this orbit (using out-of-plane observations) is as low as two hours (approximately 30 degrees, the radius of the circle). The range of local time that can be obtained corresponds to the range of longitude that can be spanned by the range circle with its center at the satellite location. Near the North Pole, for example, locators can be observed at all values of local time because the circle encompasses all of the time zones.

Figure 15 shows a Nimbus orbit with the range circles (31 degrees radius) at the equator and near the North Pole. Figure 16 is a polar map drawn to the same scale as Figure 15 , which relates the orbit and circles to time zones and geographic locations. The figures of the next section show the available variation in local time and location of the test point for various spacecraft latitudes and looking directions in the Nimbus orbit.

Horizon Point Maps

For the 600 nautical mile orbit, maps were made of the horizon point locations obtainable from the satellite throughout its orbit and for any orientation of its line-of-sight. These maps indicate the latitude of the horizon points and the difference in longitude (and thus the difference in local time) from the satellite to the horizon point. The maps (Figures 17 through 22) are drawn with contours of satellite latitude, true azimuth of the line-of-sight, and relative azimuth of the line-of-sight so that any program of horizon observation can be synthesized. The maps are drawn for an assumed horizon altitude of 23.1 nautical miles ($\approx$ 43 km).

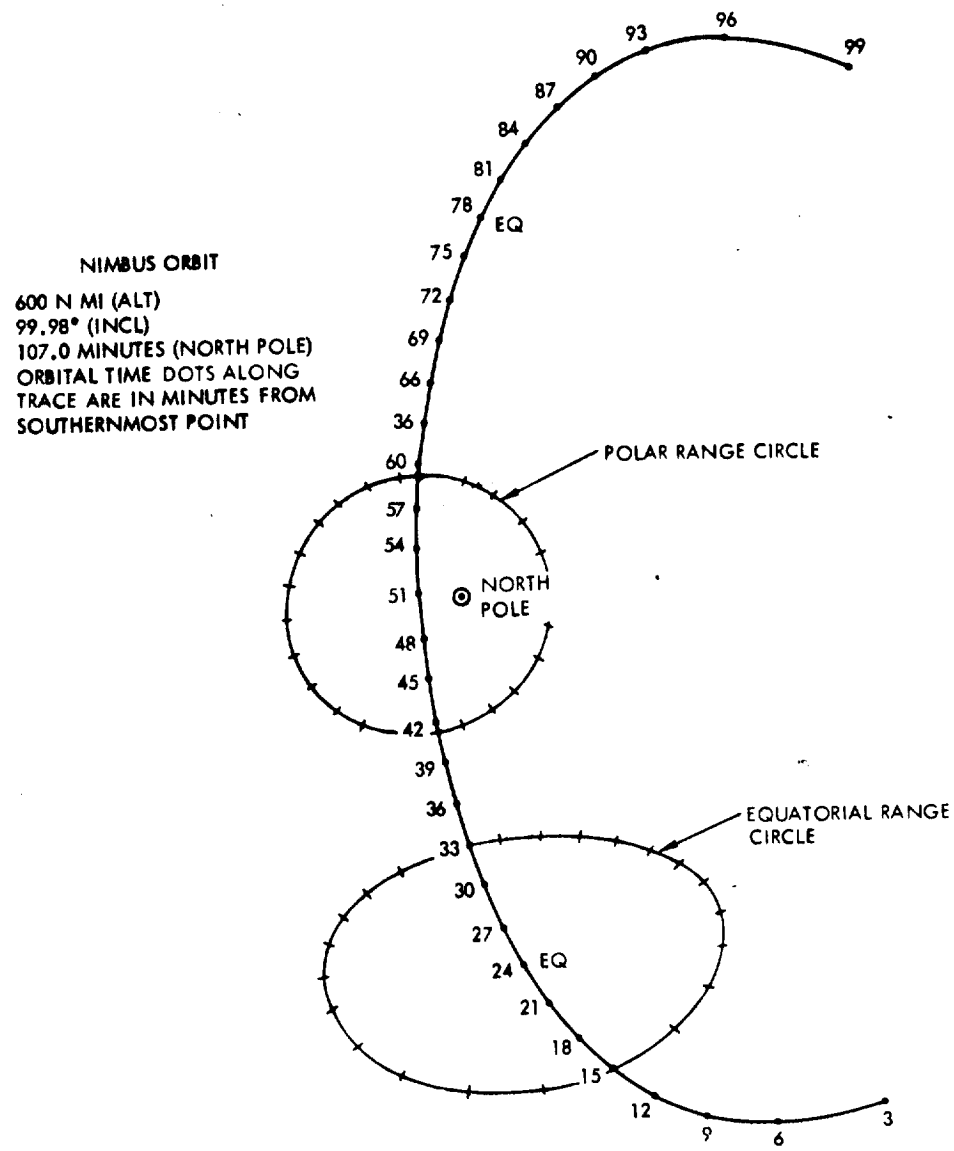

Figure 15. Nimbus Orbit Trace With Polar and Equatorial Range Circles (Overlay for Figure 16)

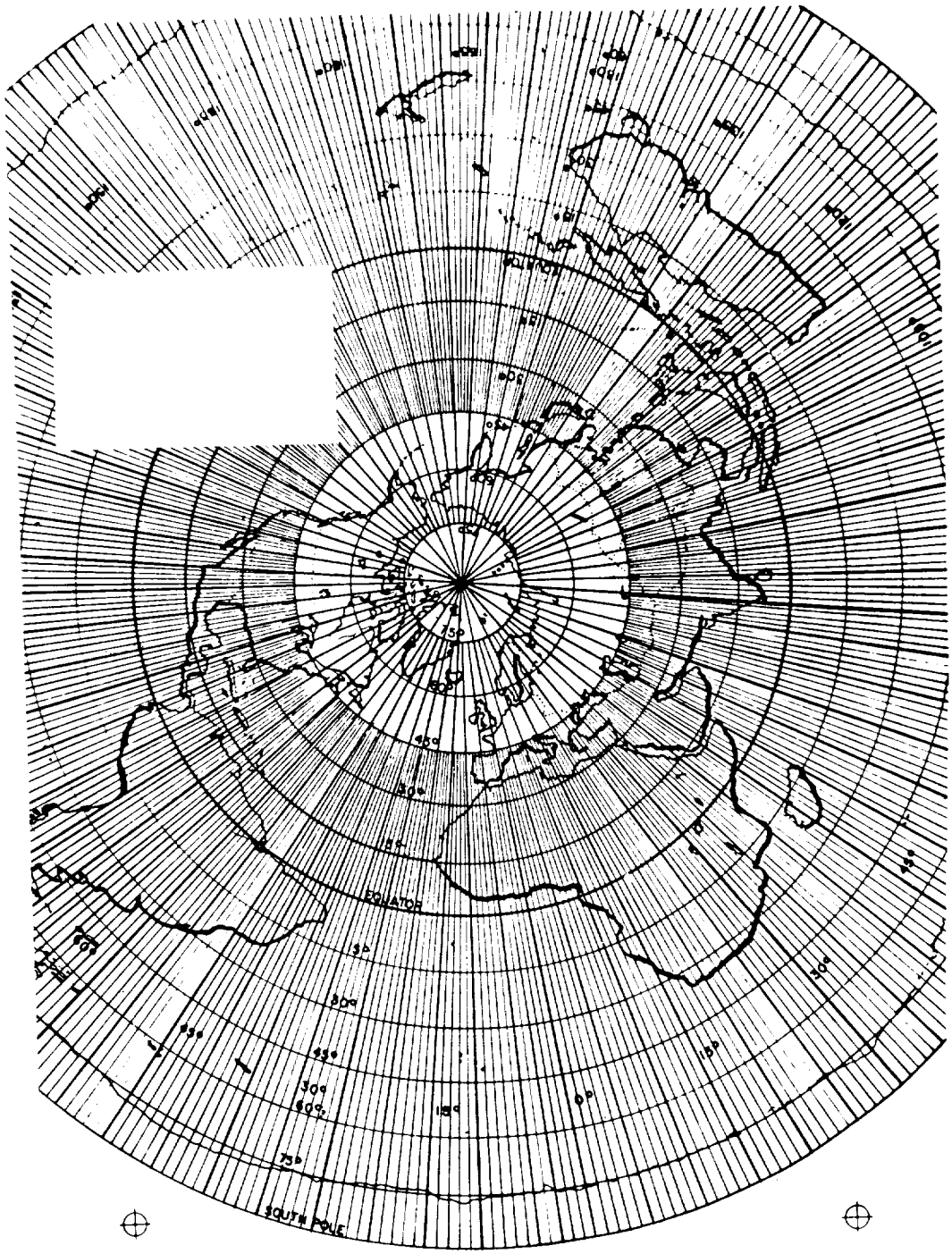

Figure 16. Polar World Map

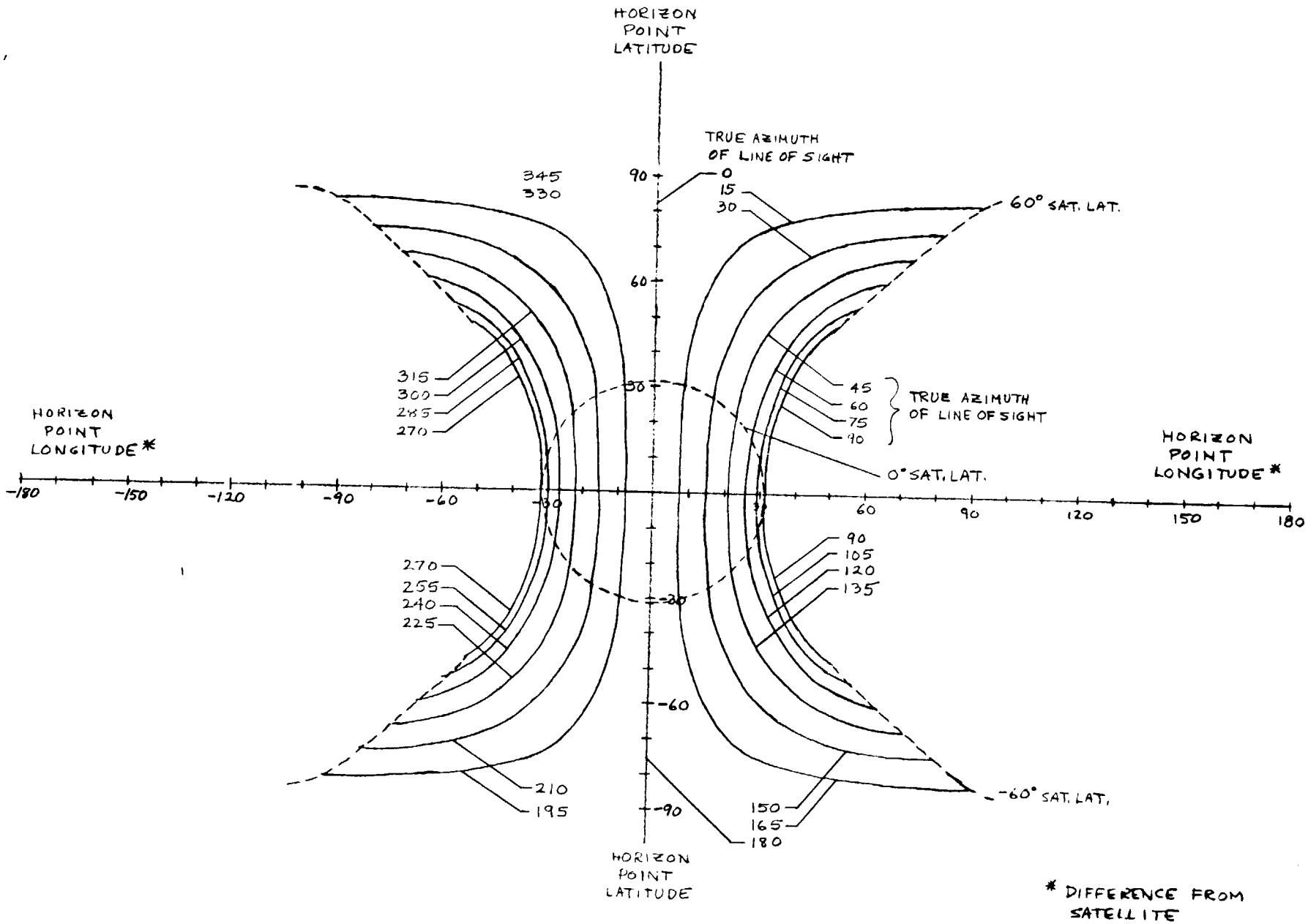

Figure 17. Horizon Point Map
(Constant True Azimuth Contours)

Space Division
North American Rockwell

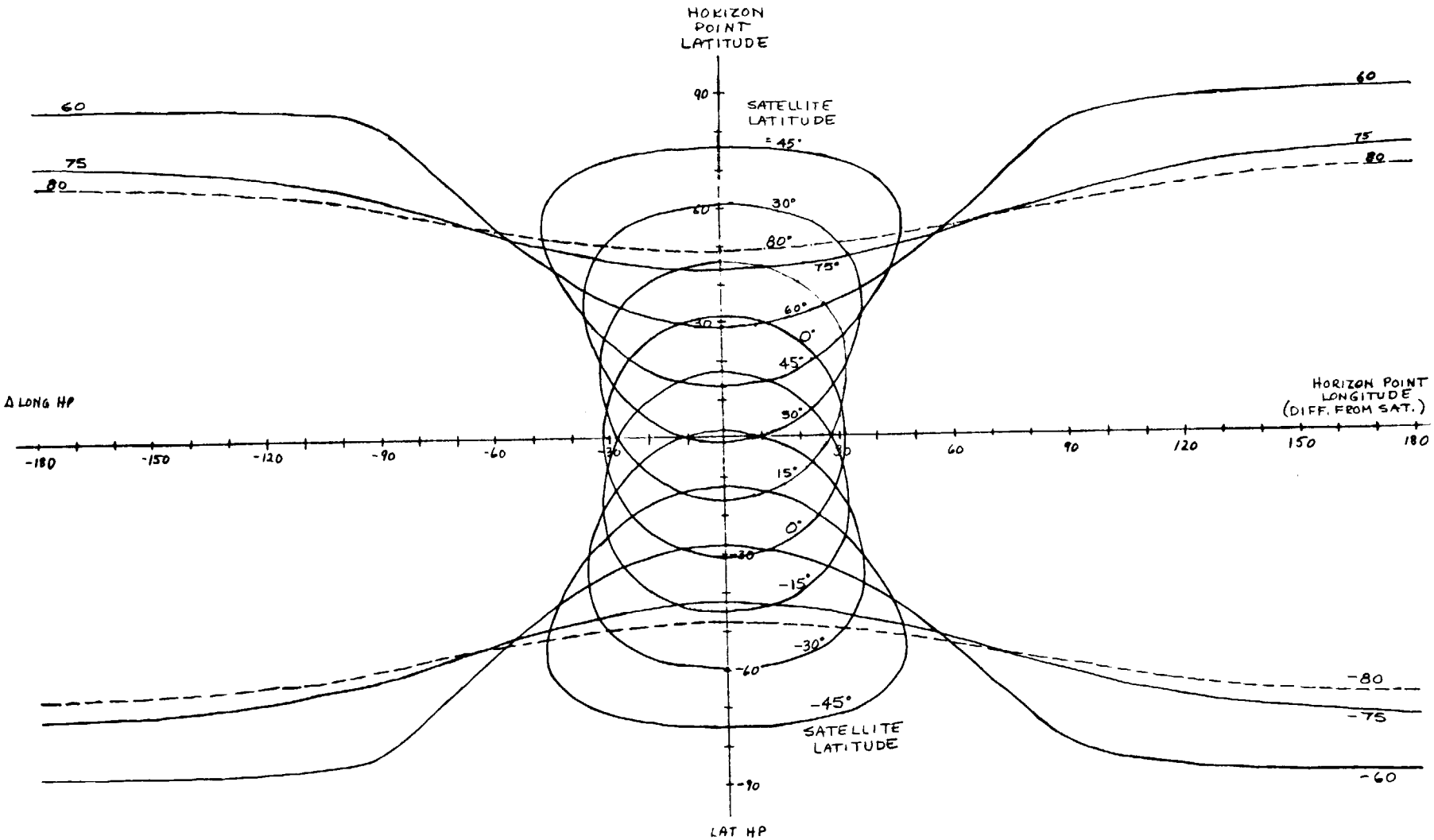

Figure 18. Horizon Point Map
(Constant Satellite Latitude Contours)

Space Division
North American Rockwell

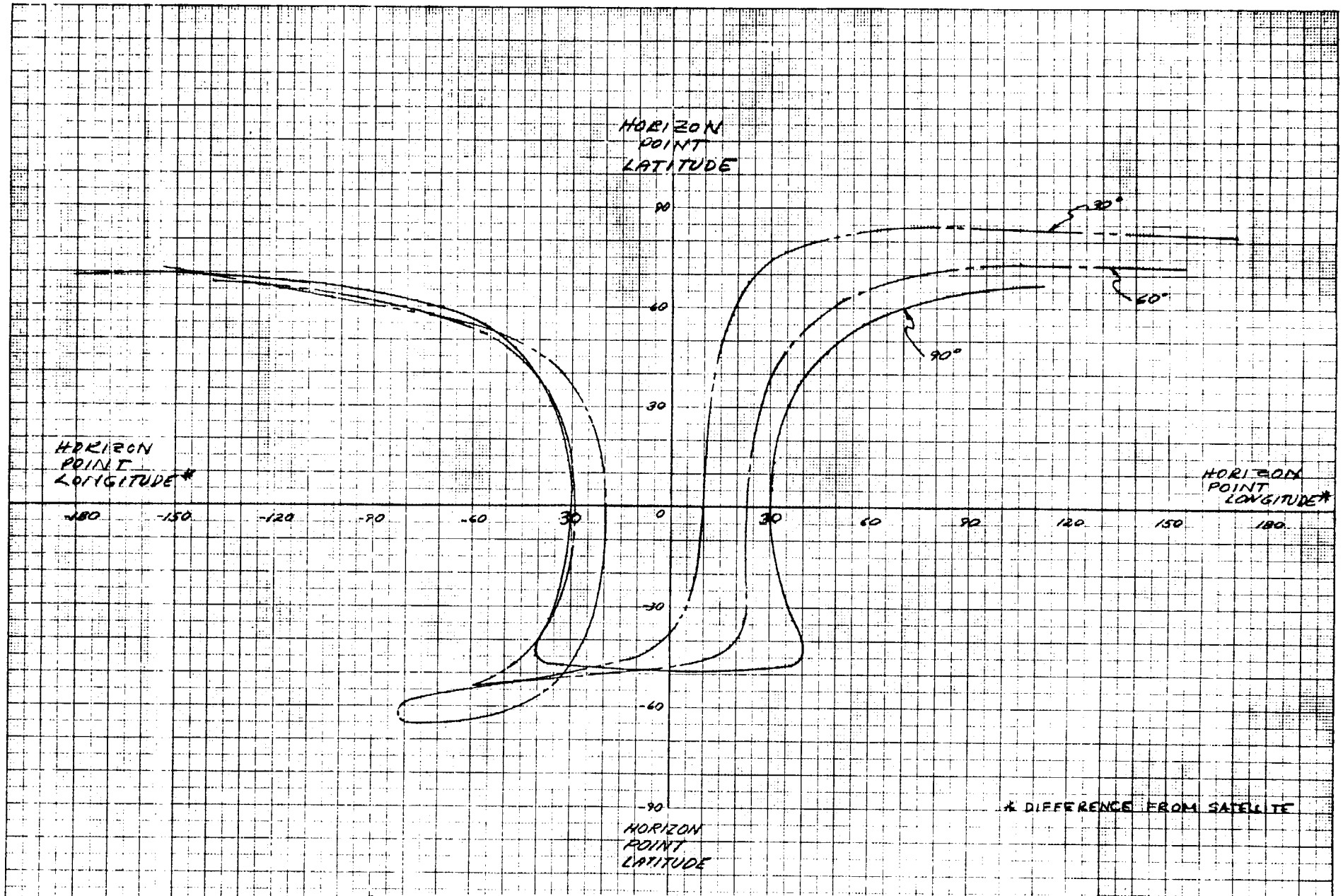

Figure 19 Horizon Point Map
(Constant Relative Azimuth Contours)
Rel. Az. = 30°, 60°, 90°

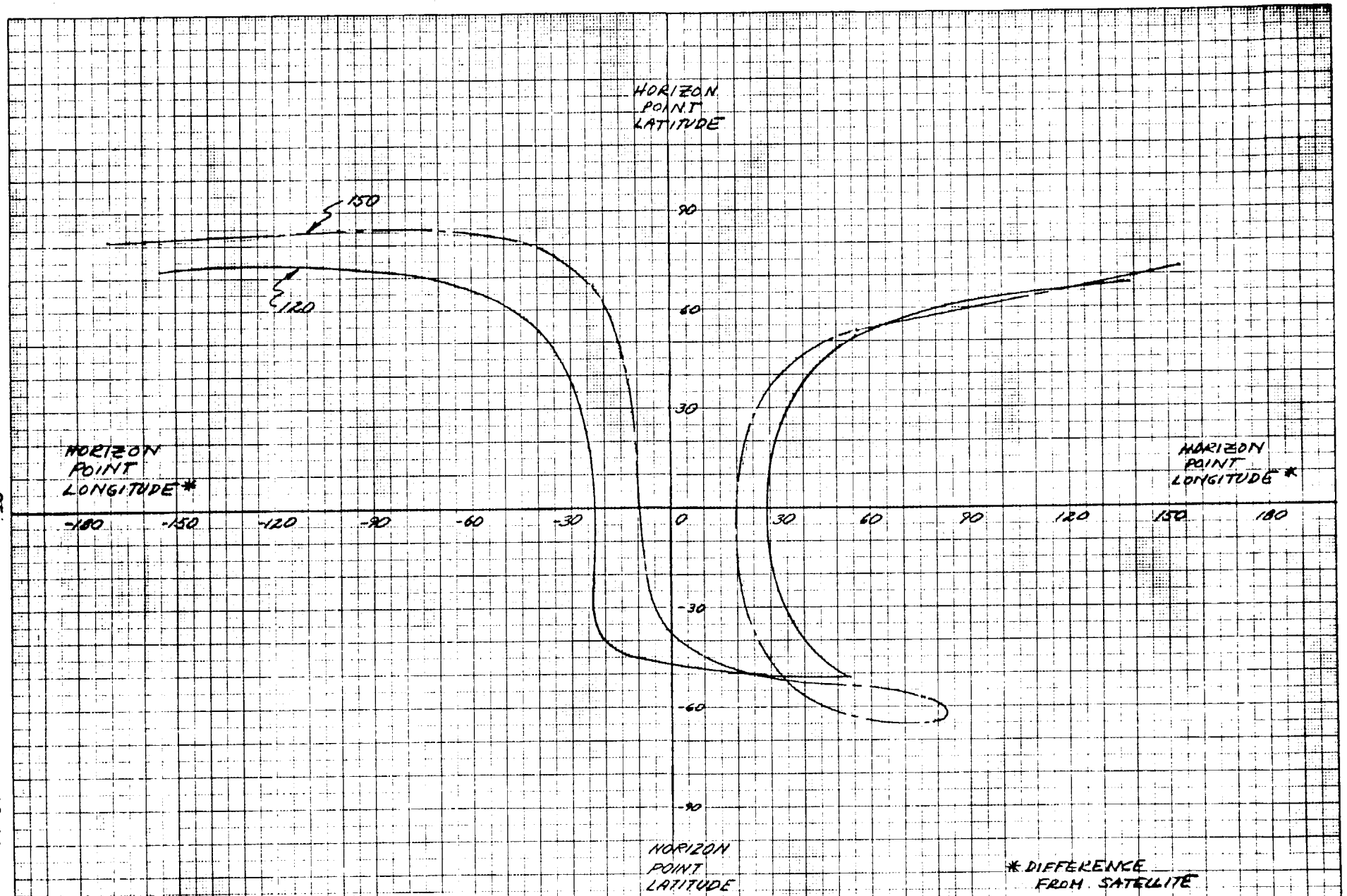

Figure 20 Horizon Point Map
(Constant Relative Azimuth Contours)
Rel. Az. = 120°, 150°

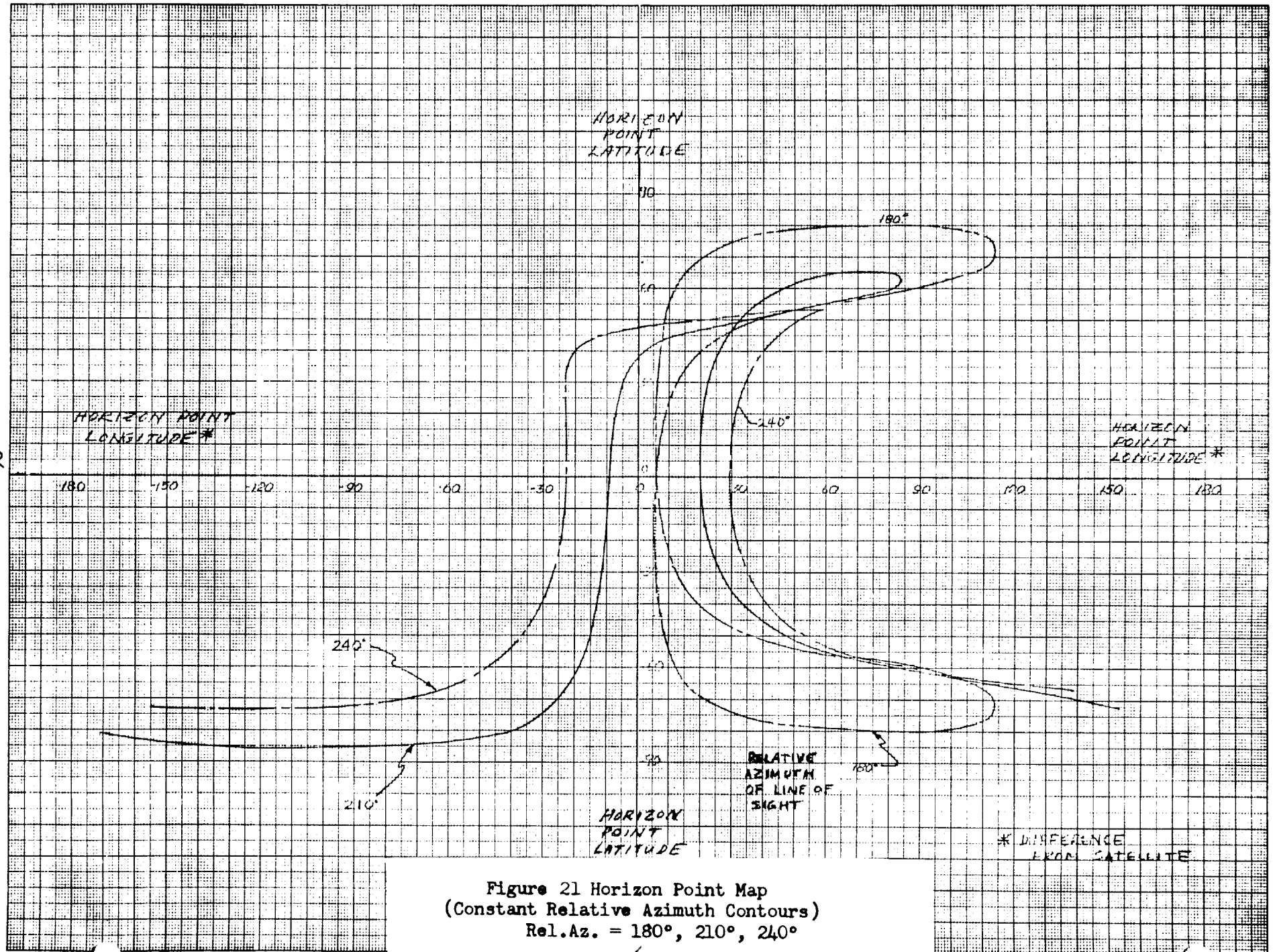

Figure 21 Horizon Point Map
(Constant Relative Azimuth Contours)
Rel.Az. = 180°, 210°, 240°

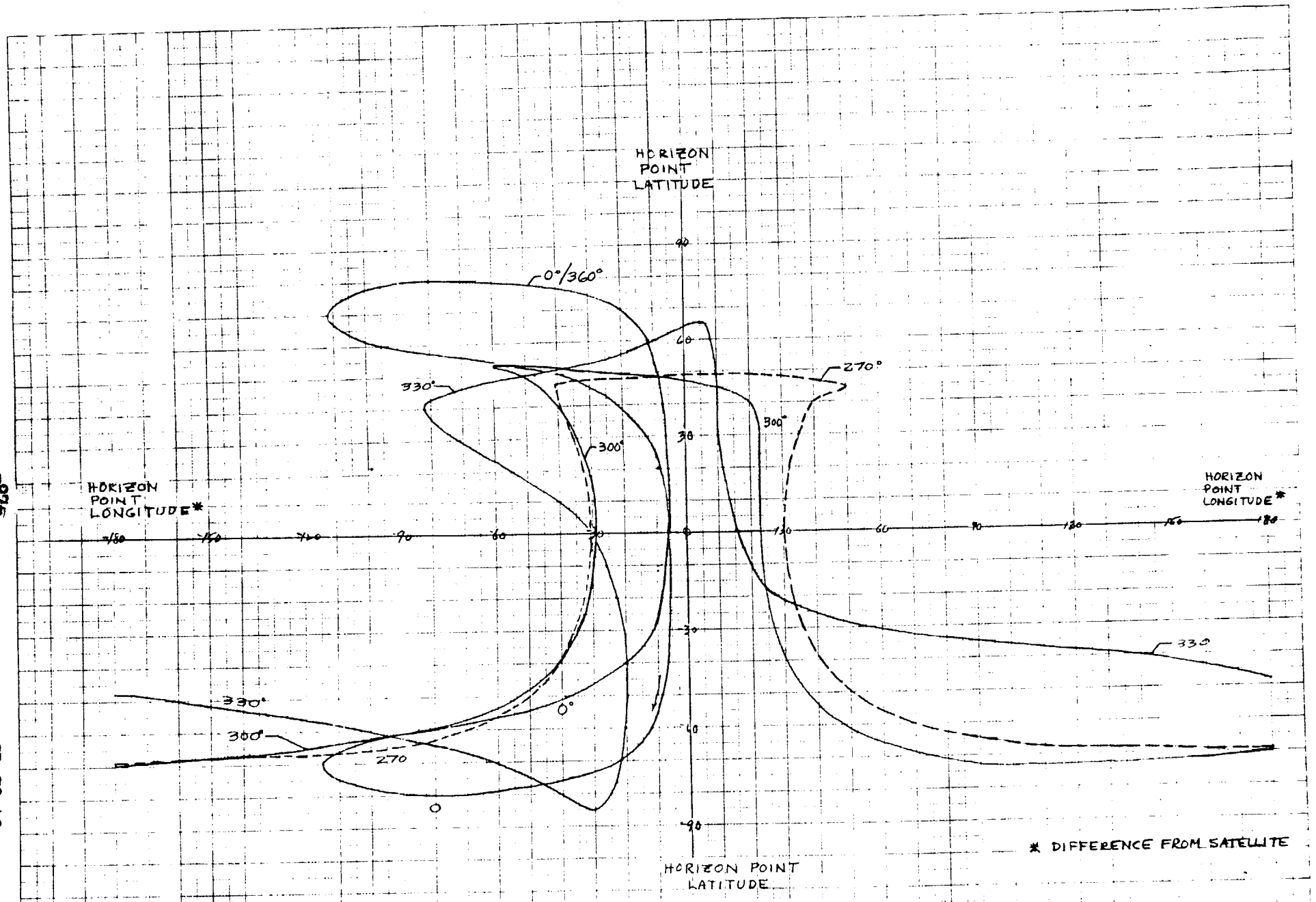

Figure 22 Horizon Point Map
(Constant Relative Azimuth Contours)
Rel.Az. = 270°, 300°, 330°, 360°/0°

The use of the horizon point maps can be illustrated by a simple example. Assume it is required to observe a series of points during an orbit, all of which differed by two hours in local time from the local time of the satellite and were five degrees apart in latitude. The satellite's latitude and looking azimuth (with respect to true north) at each observation is identified, by reference to Figures 18 and 17 respectively, by the intersection of the two-hour (or 30°) line on the abscissa and the appropriate value of the test point, or locator, latitude on the ordinate. In like manner, the relative aximuth can be found by reference to Figures 19, 20, 21, and 22. By reference to the computed ground trace of the satellite, the time of each observation can be added to these maps.

The maximum difference in local time of any horizon point measurement at the equator is approximately two hours (30 degrees of longitude). Therefore, the diurnal variation in horizon altitude from 10 a.m. to 2 p.m. can be observed on the equator if the scan plane of the satellite is rotated 90 degrees in either direction. Variations over a much greater range of local time can be observed at the extreme latitudes, but diurnal variations are less significant at those latitudes. Figures 17 and 18 combined show the points that can be observed using any combination of satellite latitude and azimuth of the line-of-sight. The curves for constant relative azimuth of the line-of-sight are considerably less uniform than the others because of the changing satellite heading. However, these curves are probably the most applicable because the scan plane will have one or more fixed relative azimuth values, each for an extended period of time and covering the whole range of latitudes. The curve of satellite heading, or true azimuth of the velocity vector, which relates the relative azimuth plots of Figures 19 through 22 to the true azimuth plot of Figure 17 is shown in Figure 23.

FOLDOUT FRAME 1.

FRAME X.

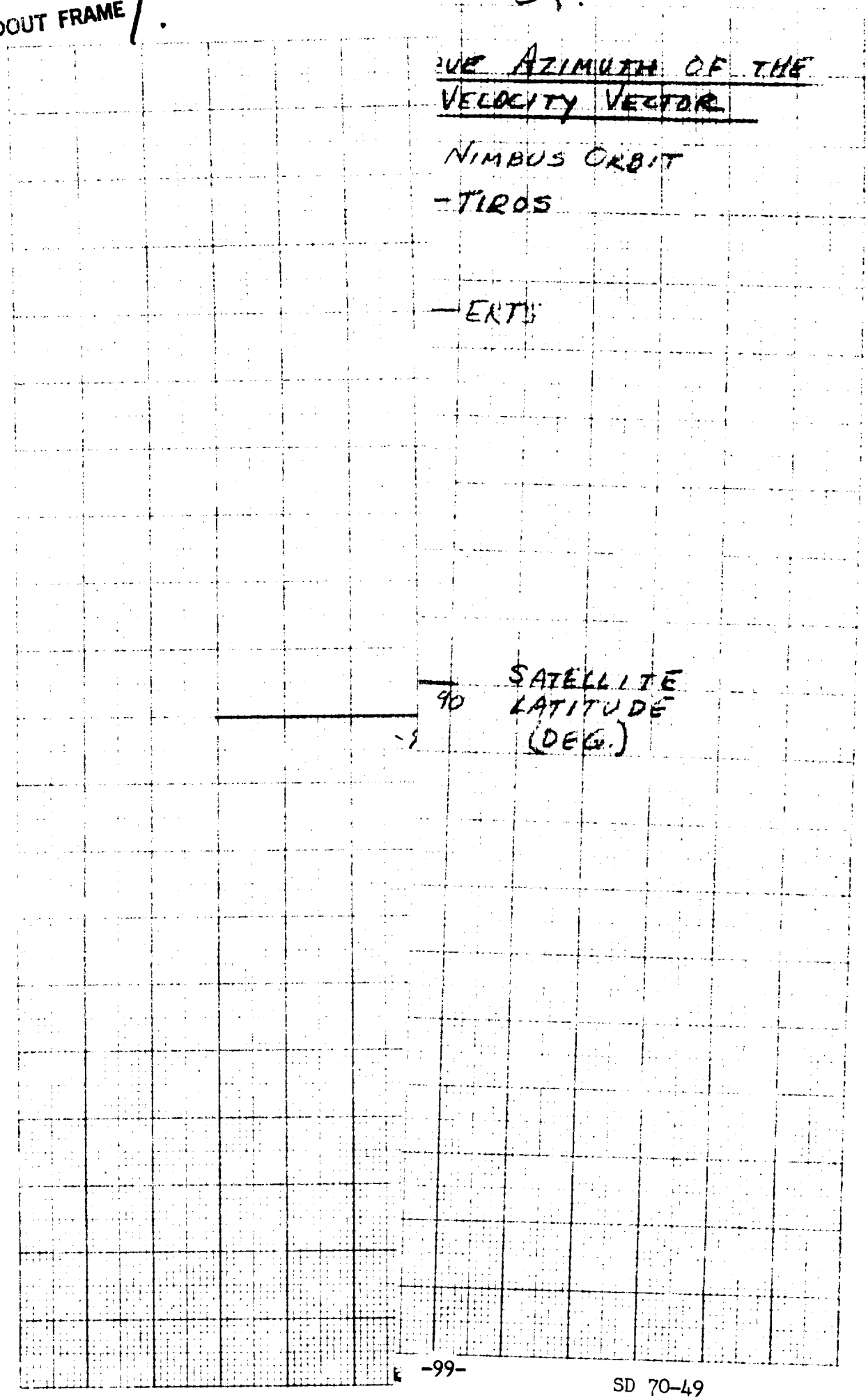

Impact of Performance Requirements on Orbit Selection and Pointing Requirements

This section discusses primarily the relationship of the vehicle orientation policy to the data-gathering process and the fulfillment of stipulated performance requirements. The discussion encompasses three conditions and the effect of each on the sun-synchronous satellite and on a satellite in a non-sun-synchronous polar orbit. The candidate orbits are of both types. The three conditions are inertially fixed attitude, continuously processed attitude, and periodic reorientation so that there are six possible combinations of orbit type and orientation policy. There are several important factors to be considered in selecting the six combinations. These factors fall into two categories:

1. Performance requirements

   Seasonal variations

   Diurnal variations

   Sun-Zenith angle variation

   Geographic coverage range

2. Impact on the vehicle design problem

   Vehicle torquing systems

   Satellite thermal balance

   Solar-electric power systems

   Data handling and utilization

The factors in Category 1 are considered briefly in the succeeding discussion, after which the impact of orbit selection and orientation policy selection on factors of Category 2 are briefly mentioned. More detailed discussion of these design factors can be found elsewhere in this report.

The analysis leads to the following conclusions:

- It is essential to observe points directly over the poles; either a non-sun-synchronous orbit with in-plane observation or a sun-synchronous orbit with a satellite having an out-of-plane observation capability is required.
- If the diurnal variation over the same geographic point must be observed in a sufficiently short period that the seasonal change is negligible, out-of-plane observations are needed and each diurnal time point requires a different looking azimuth. This statement applies to both polar and sun-synchronous orbits.
- If the seasonal variation at a given point at the same time of day is required, the orbit must be sun-synchronous and must have a ground trace that is repeatable at least once a month.
- A point with zero-sun-zenith angle lies in the orbit plane only twice a year for a noon sun-synchronous orbit and not at all for sun-synchronous orbits whose local time departs more than one-half hour from a noon orbit. To extend the viewing time of such a point for the noon orbit or to make viewing possible from other sun-synchronous orbits, out-of-plane viewing is required.
- Polar orbits (non-sun-synchronous) permit in-plane viewing of sub-solar points twice a year and the sun moves out of the plane at approximately one degree per day. In comparison, the sun moves out of the orbit plane at the rate of approximately

1/16-degree per day in the case of a noon sun-synchronous orbit. In the latter case, the maximum departure of the sun from the orbit plane is about six degrees, while in the former, the maximum is 180 degrees.

Impact on Vehicle Design Factors

The data-gathering capabilities associated with various types of orbits and constraints on the viewing direction have been discussed. The vehicle orientation program implied by each of the viewing philosophies now will be considered.

Since the horizon sensor derives its information by rotating through the horizon, it is assumed that optimum results are obtained when the plane of rotation is normal to the horizon. For in-plane viewing, this occurs when the sensor spin axis is normal to the orbit plane. This condition can be maintained indefinitely without applied torque in the absence of perturbations. However, if the orbit is deliberately subjected to a perturbation which causes it to rotate through 360 degrees in a year (sun synchronism), the satellite will effectively rotate 360 degrees with respect to the orbit plane in one year if left uncorrected. Consequently, the alignment of the spin axes can be maintained in a sun-synchronous orbit only if a continuing torque is applied to the satellite. This requirement does not exist in the case of a polar orbit.

However, if the sensor is to observe points outside of the orbit plane, the sensor spin axis must be kept at least close to the horizontal plane. This would require continuous torquing even in the case of the polar orbit. To alter the out-of-plane angle of the sensor, or to change its orientation from in-plane to out-of-plane, requires a separate attitude maneuver in any case.

Conclusions:

- Continuous or frequently repeated attitude torquing is required in a sun-synchronous orbit for in-plane viewing and for out-of-plane viewing.
- Continuous attitude torquing is not required in a polar orbit except for out-of-plane viewing.

The use of a sun-synchronous orbit presents the satellite with a relatively constant cycle of exposure to the sun. This simplifies the analysis and solution of the problems of thermal balance and solar-electric power system design. However, some of the sun-synchronous orbits (particularly the noon orbit) offer a lower total exposure to the sun over the year than a polar orbit and, consequently, a lower average amount of solar-electric energy.

One of the chief tasks in planning the proposed satellite mission is that of programming the observation of data points and formulating a logical method of correlating the data. In the case of in-plane observation, the procedure is relatively simple because there is only one pair of points to be observed at any given time; but if out-of-plane viewing is permitted, an infinite number of points are available for each position of the satellite. A relatively simple plan would be to fix the sensor line-of-sight to one relative azimuth value and take data every five degrees of satellite travel for a complete repeat cycle, then alter the azimuth and repeat the process for another cycle (With a repeat cycle of five days, six data points of the diurnal variation could be obtained in one month and the points would be a maximum of five degrees apart in longitude). This would require continual adjustment of the satellite's attitude.

If, on the other hand, the attitude were allowed to drift, successive test points would correspond to continuously varying values of local time; this would complicate the task of obtaining the same set of conditions for each data point. It appears, however, that continuous control of satellite attitude will be necessitated by the pointing accuracy requirement and, therefore, will preclude this complication. The problem of controlling attitude and pointing accuracy is described elsewhere in this report.

Piggyback Missions

Sun/Orbit - Plane Angle

The foregoing analysis was performed to determine types of orbit that would be preferable for the proposed experiment from the standpoint of horizon measurement accuracy if the horizon sensor satellite had its own launch vehicle. Using the aforementioned criteria, orbits of known satellites were evaluated for their applicability to this problem, considering the possibility that the horizon sensor satellite might fly as a piggyback payload. The results of that evaluation follow.

Figures 24, 25 , and 26 show the sun/orbit plane angle over the mission lifetime of one year for ERTS, ITOS, and NIMBUS launches, respectively, considering their probable launch dates. As is shown in the error analysis, the large angles associated with the ERTS and ITOS orbits reduce the accuracy with which the horizon measurement can be made because they place the sun, which is used as a pitch reference, too far out of the orbit plane. They also would create the need for a sun sensor with a wide field-of-view. In addition, the ERTS and ITOS orbits aggravate the solar cell power supply design problem because in such orbits the sun's rays are never normal to any of the satellite's principal surfaces. Since the most likely candidate

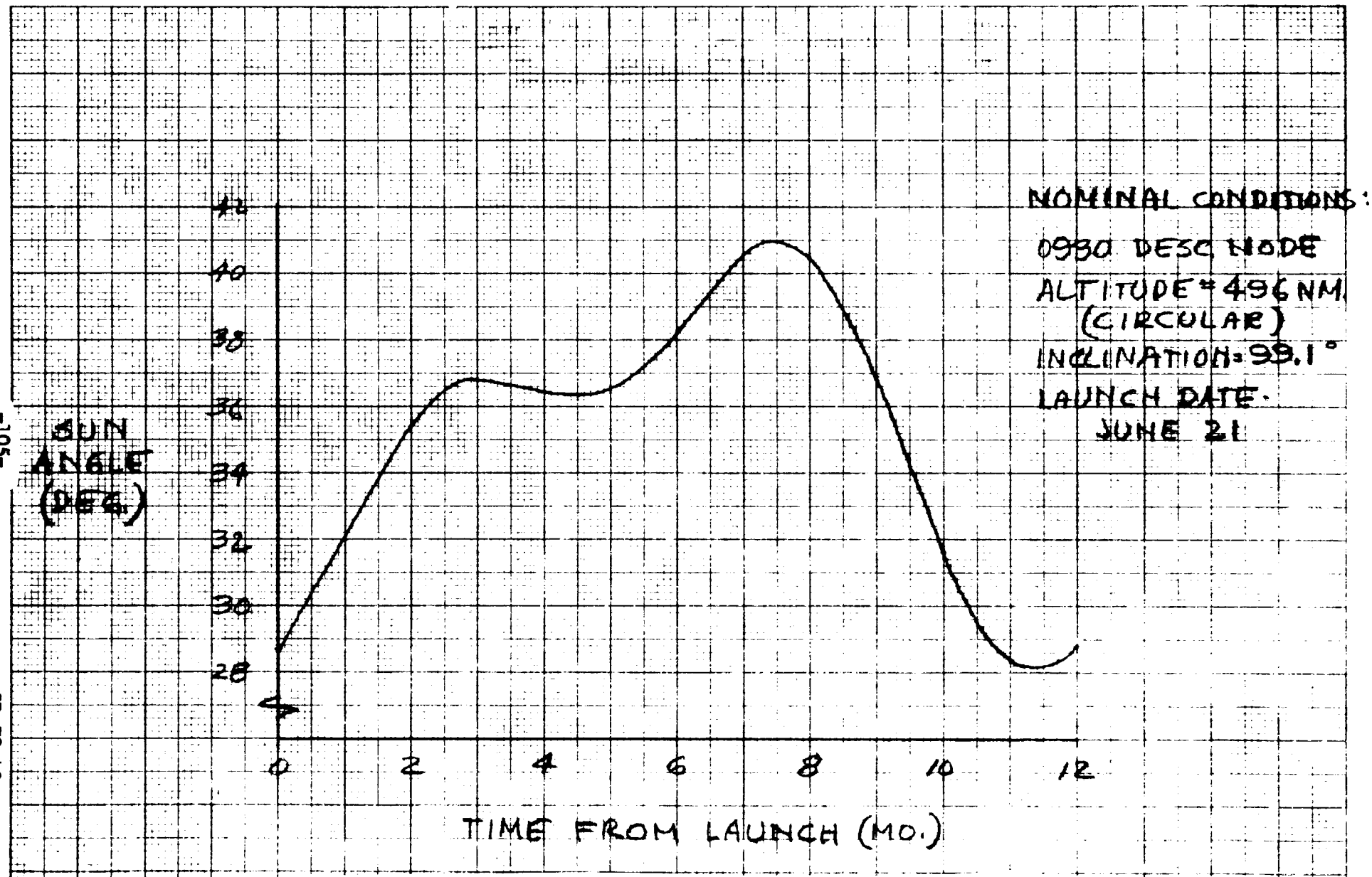

Figure 21 Variation in Angle Between Sun and Orbit Plane
(PTS Orbit)

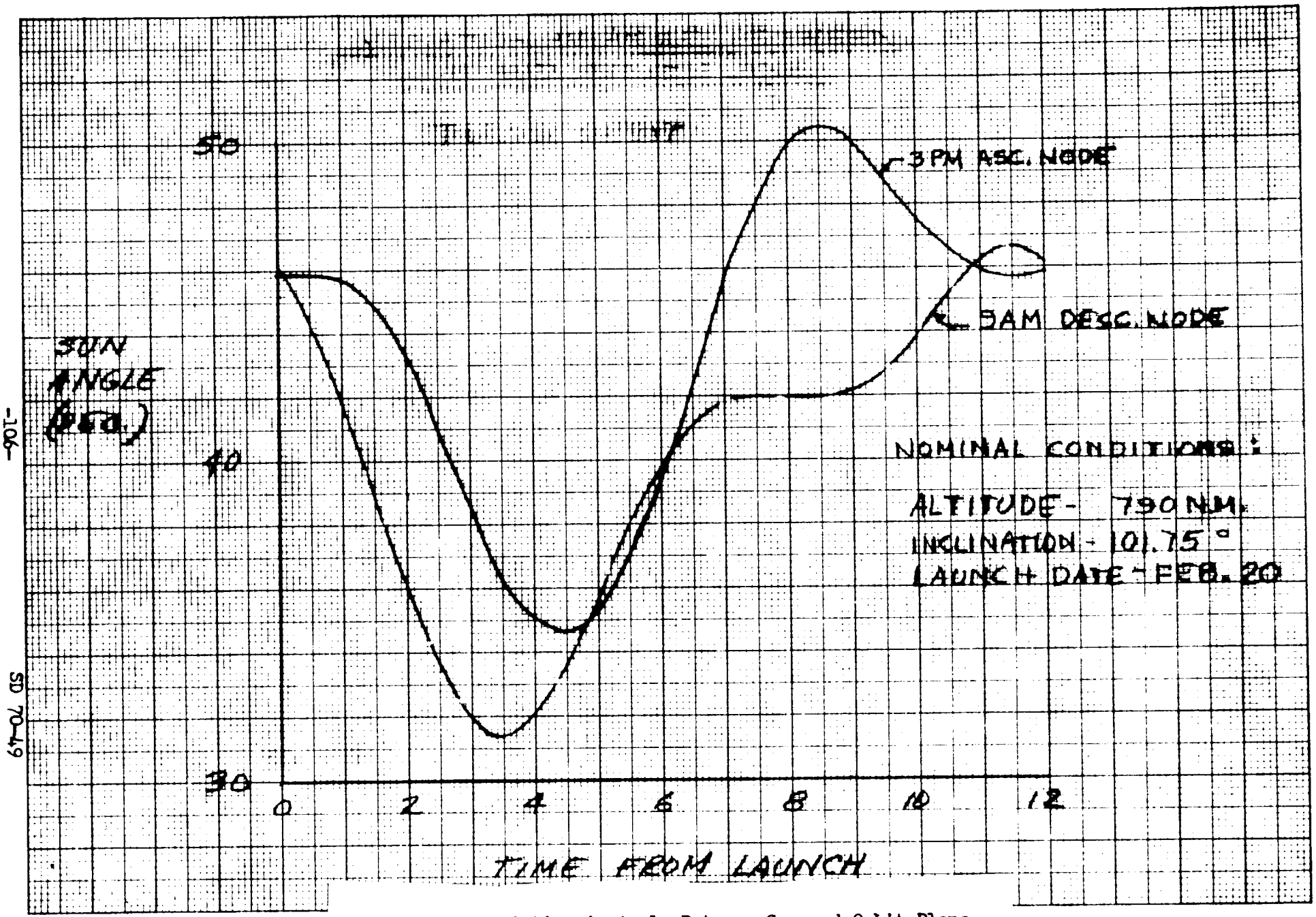

Figure 25 Variation in Angle Between Sun and Orbit Plane
(ITOS Orbit)

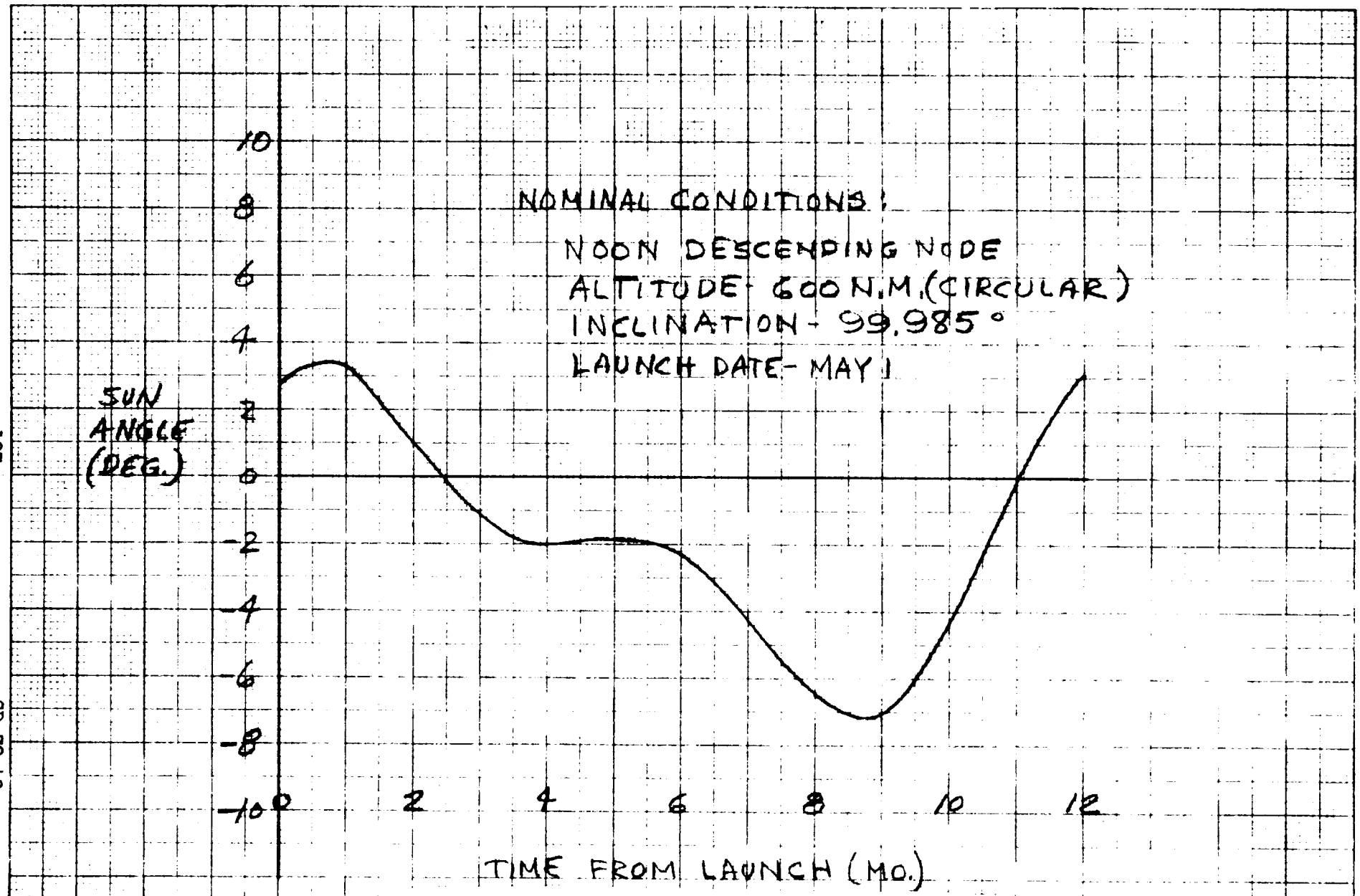

Figure 26 Variation in Angle Between Sun and Orbit Plane (NIMBUS Orbit)

system concept entails the alignment of the satellite spin axis normal to the orbit plane, the most desirable location for the sun will probably be in the spin plane or orbit plane. This suggests a noon orbit which is characteristic of the NIMBUS mission, and which will result in the greatest vehicle cross-section to solar energy.

Tracking Circles

It has been assumed that the satellite will be tracked by the STADAN network (See Table 8) using Minitrack. These stations will also be used to receive the data transmitted by the satellite. In order to analyze the data handling schedule, visibility circles were constructed for each station corresponding to two altitudes (600 nautical miles and 790 nautical miles) and two mask angles (minimum elevation at which satellite is visible from the station). These are shown in Figures 35 and 36. These are drawn on the same scale as the map and ground traces of Figures 31 through 34. From the standpoint of tracking station coverage, the higher altitude orbit (ITOS) is superior because it allows communication of data throughout a greater portion of the orbit than that permitted by either the 600 nautical miles NIMBUS orbit or the 496 nautical miles ERTS orbit.

The selected tracking stations provide continuous coverage from the North Pole to latitudes below the southern tip of South America. Therefore, collection and transmission of data in real time over this whole range can be accommodated.

TABLE 8

STADAN STATIONS FOR HORIZON SENSOR SATELLITE

NAME	LATITUDE	LONGITUDE
1. Johannesburg	-25.88	27.71
2. Orroral	-35.63	148.96
3. Alaska	64.99	212.49
4. Rosman	35.20	277.13
5. Quito	-.26	281.42
6. Santiago	-33.15	289.33
7. Winkfield	51.45	359.30

Sun Elevation Angle

It is required to obtain horizon data for points on the earth which have various values of sun elevation angle. Figures 27, 28 , 29 , and 30 show the variation of the sun elevation angle with the latitude for either the satellite or the horizon point (In the nominal case of looking fore and aft at the horizon, the satellite passes over the inertial location of every horizon point). Using the NIMBUS orbit, a much greater range of sun elevation angle is available. The three-month intervals depicted in Figure 24 show elevation angles approaching 90 degrees. They do not show the 90-degree elevation angle which is obtainable twice a year (at the equinox) when the sun/orbit plane angle is zero (Figure 27). In contrast, the ERTS and ITOS orbits provide sun elevation angles up to only 60 degrees.

Ground Traces

The orbits considered have been primarily sun-synchronous orbits so that the satellite could observe the same point at regular intervals and under the

FOLDOUT FRAME 2.

FOLDOUT FRAME 1.

- TIME 0 MO
OR MAR. - TIME 3 MO AND 9 MO.
- TIME 6 MO

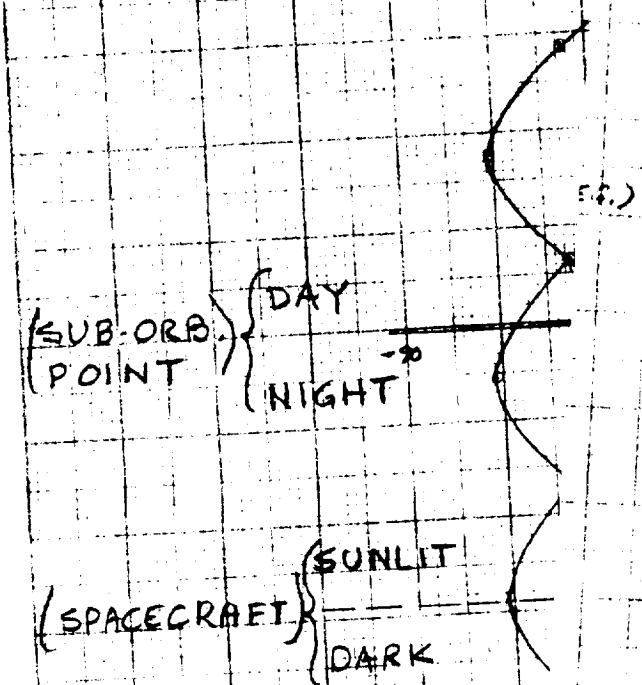

1 POINTS EVERY 15 DEGREES IN ORBIT
ORBIT EVERY 3 MO.

FOLDOUT FRAME 1.

FOLDOUT FRAME 2.

FEB - TIME 0 MO.
MAY - TIME 3 MO.
AUG - TIME 6 MO.
NOV - TIME 9 MO.

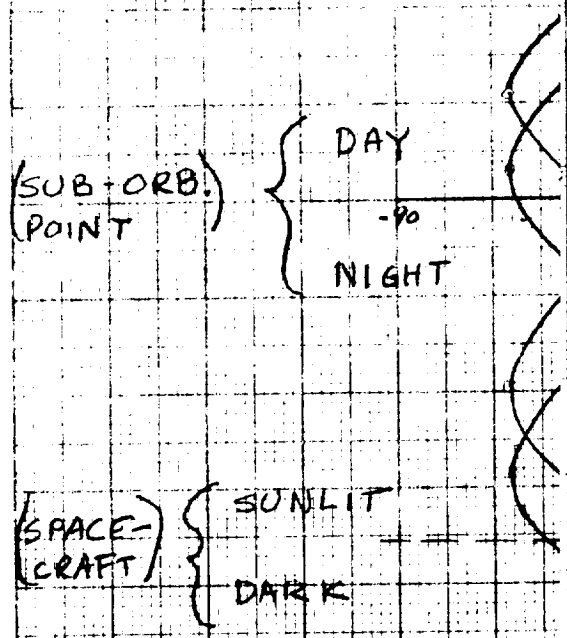

(DEG.)

~~DATA POINTS~~ EVERY 15 DEGREES IN ORBIT
ONE ORBIT EVERY 3 MO.

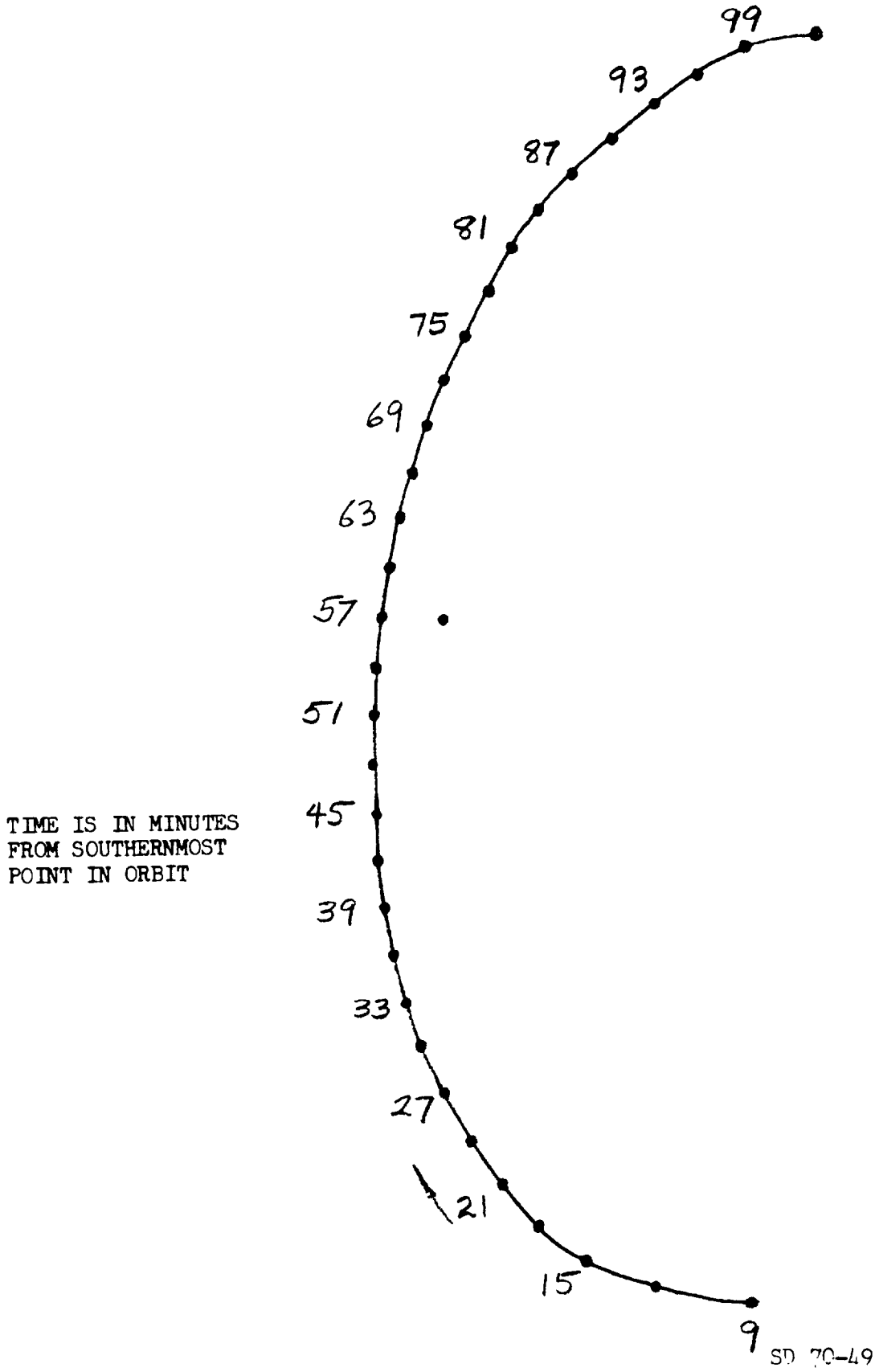

SD 70-49

Figure 32 ITOS Ground Trace

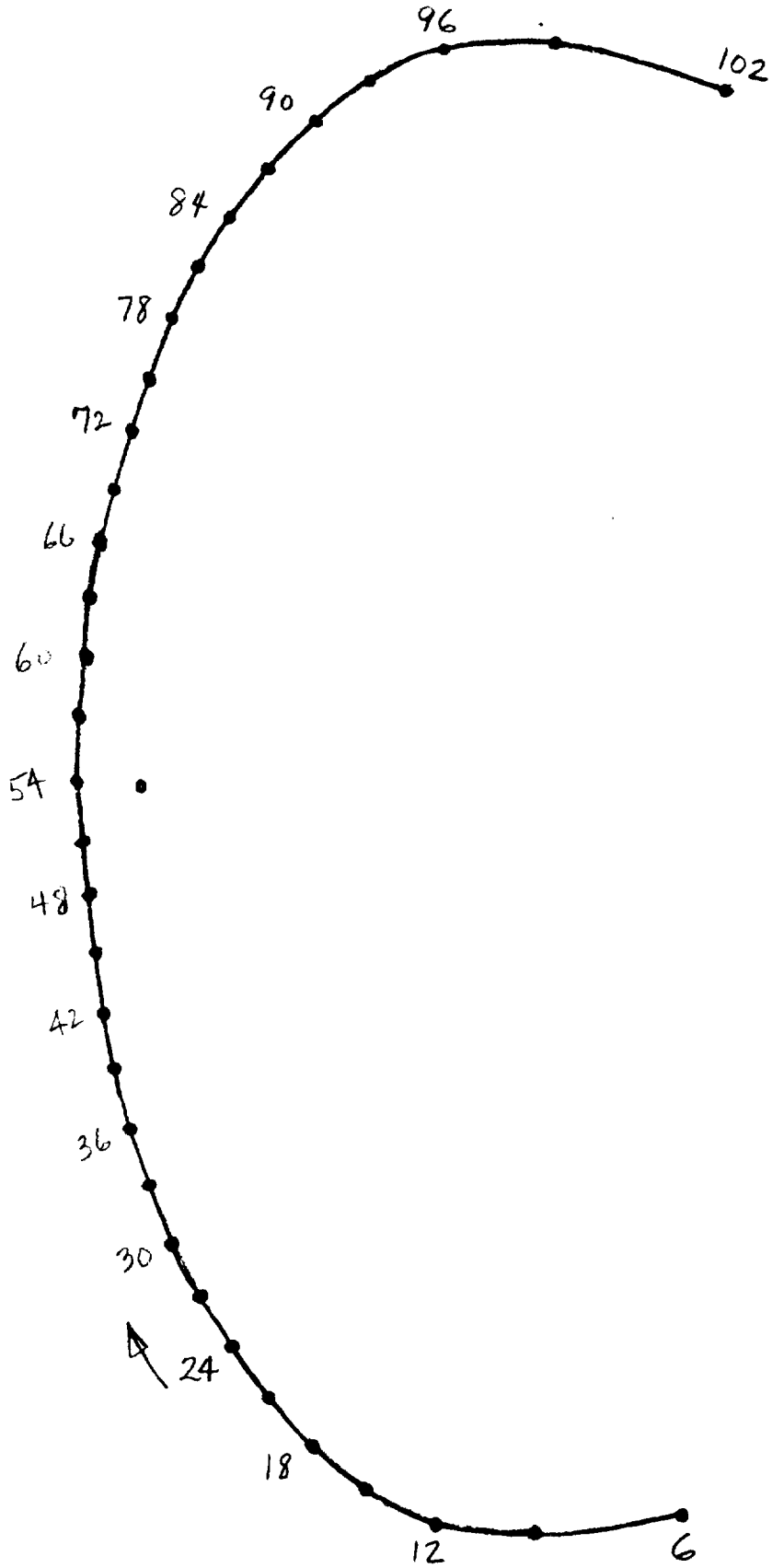

TIME IS IN MINUTES
FROM SOUTHERNMOST
POINT IN ORBIT

SD 70-49

Figure 33 NIMBUS Ground Trace

1.

FOLDOUT FRAME

2.

FOLDOUT FRAME

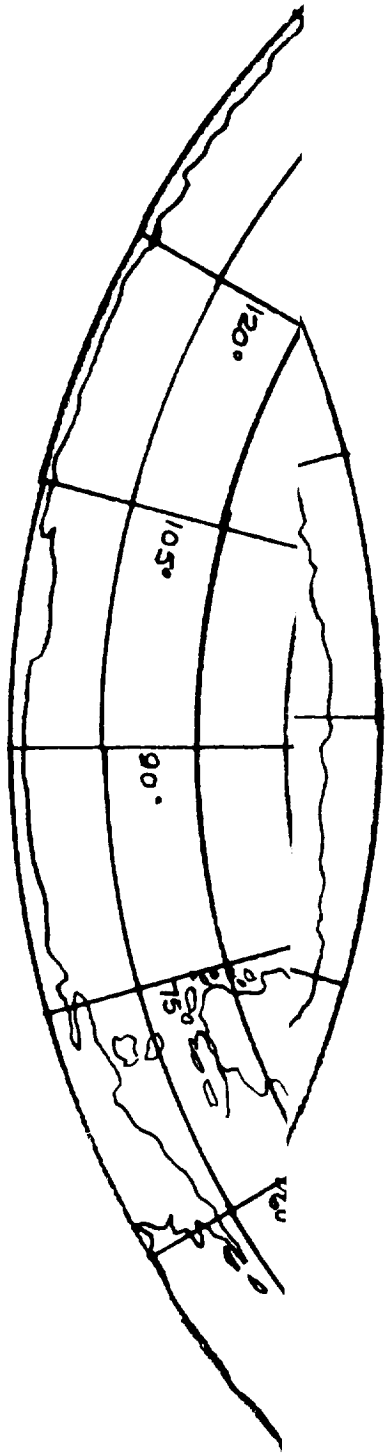

Figure 34. Polar World Map

FOLDOUT FRAME 1.

FOLDOUT FRAME 2.

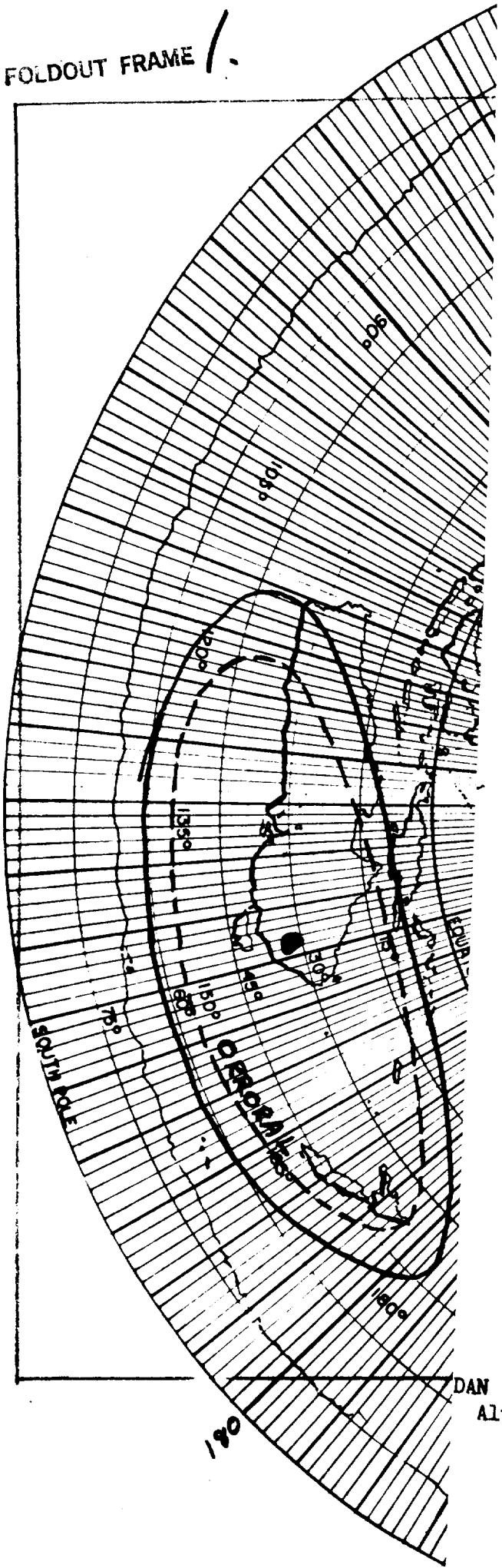

- - - ELEV. ANGLE = 10° Min.
——— ELEV. ANGLE = 5° Min.

ALASKA
ROSMAN
QUITO
SANTIAGO
WINKFIELD
JOHANNESBURG
ORRORAL

DAN Tracking Circles for Altitude = 600 N.M.

1.

FOLDOUT FRAME

2.

FOLDOUT FRAME

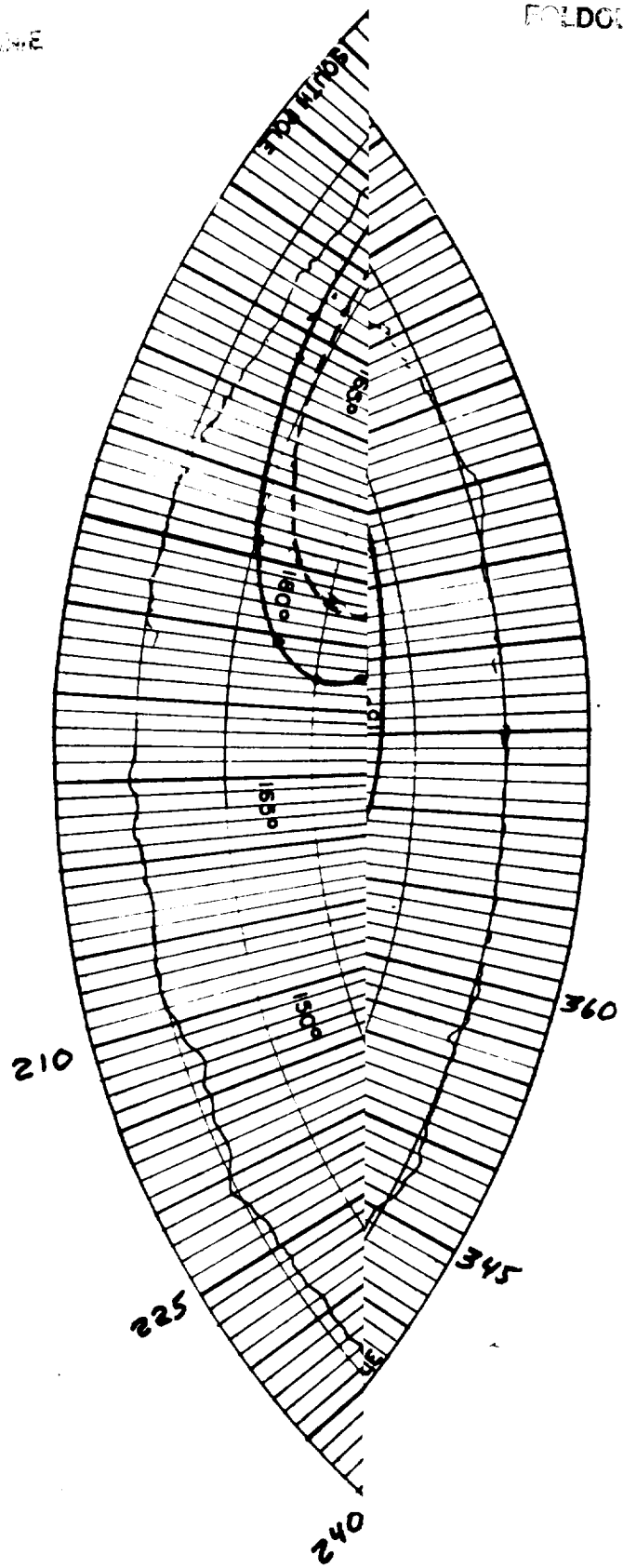

- - - ELEV. ANGLE = 10° MIN.

——— ELEV. ANGLE = 5° MIN.

ALASKA

ROSMAN

QUITO

SANTIAGO

WINKFIELD

JOHANNESBURG

ORRORAL

igure 36 STADAN Tracking Circles for Altitude = 790 NM

Figure 37 shows the repeat cycle for orbits up to approximately 900 nautical miles altitude, assuming the ground traces on consecutive days move in the same direction along the equator by an increment equal to the smallest longitude difference between test points. This synchronism with the earth's rotation is not necessarily important in all missions in which sun-synchronism is required.

Percent Time in Sunlight

It is necessary to know the direction from which the sun's rays hit the satellite and the amount of time that the satellite is exposed to the sun in order to design the electric power system of a satellite. Figure 38 is a graph of the percent time in sunlight for ERTS, ITOS, and NIMBUS orbits. While the value is lowest for the NIMBUS orbit, it is also the least variable, thereby presenting a relatively easy task for analysis of power supply and thermal problems.

Perturbations to the Orbit

The satellite orbit is affected to a small degree by natural perturbations due to solar radiation pressure, atmospheric drag, earth ablateness, and the gravitational fields of the sun and moon. These perturbations affect the longitude of the ground trace and the sun-synchronism primarily. The shift in longitude is of relatively little significance and the shift in local time is small (less than an hour). The atmospheric drag effect is negligible for the 600 and 790 nautical miles orbital altitudes, especially in view of the large m/C_DA ratio ($\approx .6$) of the satellite. A discussion of perturbations on the orbital elements and a detailed analysis of the effect of orbit variations of the ground trace and sun-synchronism are discussed subsequently.

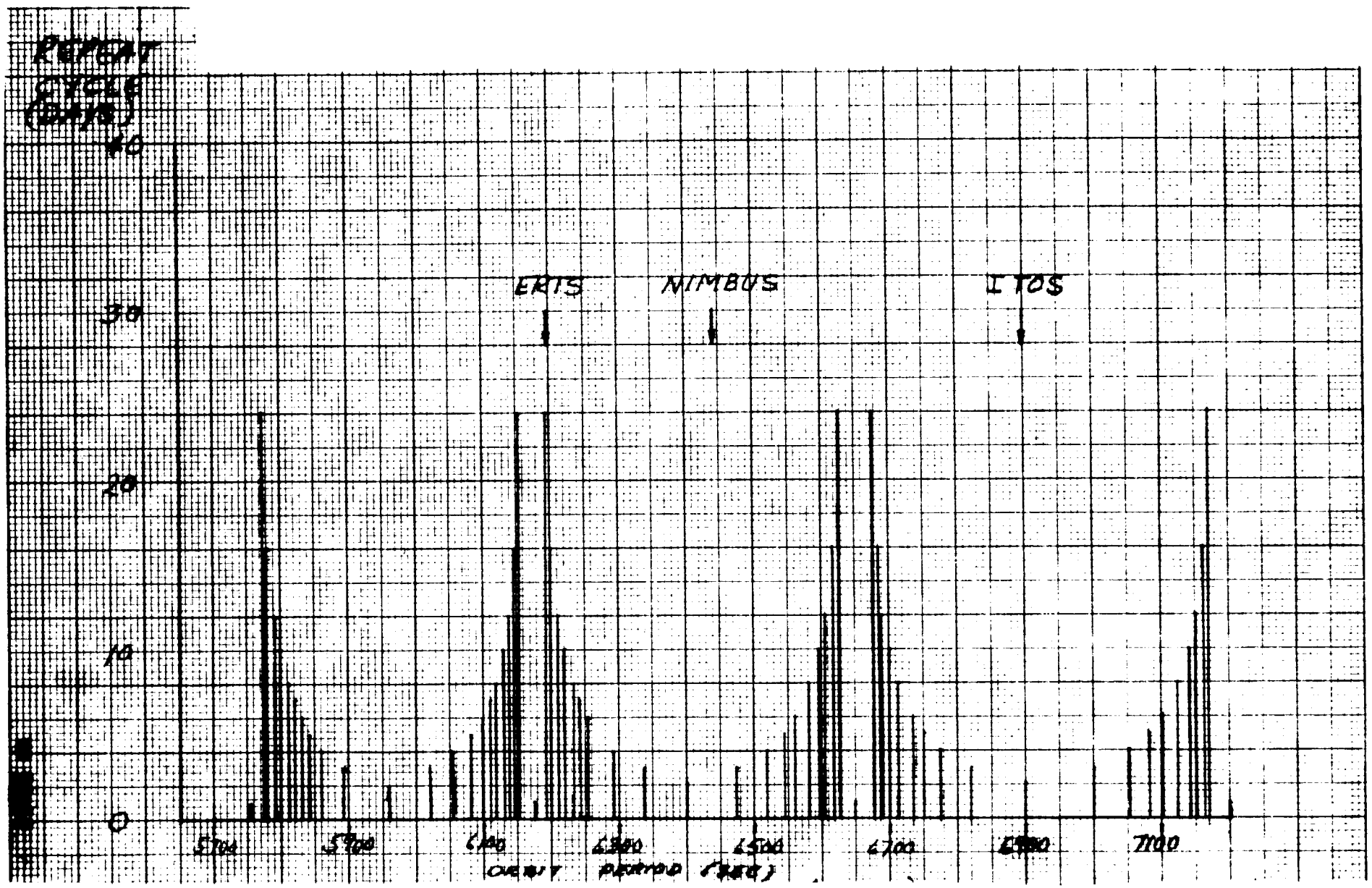

Figure 37 Ground Trace Repeat Cycle vs. Orbit Period

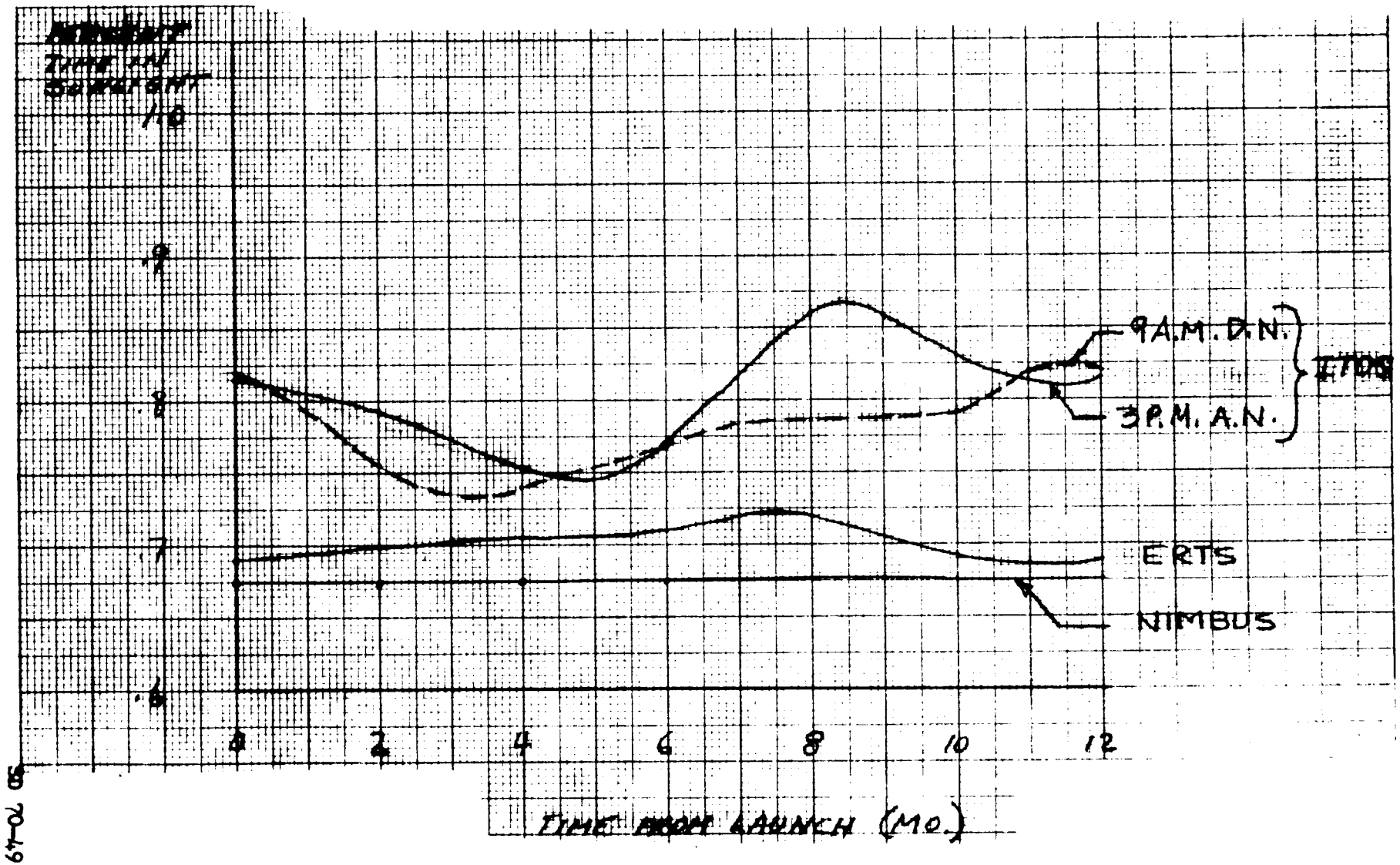

Figure 38 Percent Time in Sunlight vs. Time from Launch

Launch Vehicle

The candidate launch vehicles included the Delta, Scout, and Thor/Burner II. From the orbital standpoint, the Delta was judged superior because its relatively good control of the initial orbit assures a reasonably small variation in the sun/orbit plane angle. A large variation could impose a prohibitive requirement on the field-of-view of the fine sun sensor. The study showed that the orbit variation associated with either the current Delta or the advanced-guidance Delta would be within the capabilities of a realizable fine sun-sensor system. A review of the injection errors of the candidate launch vehicles and an analysis of the consequences of the Delta injection errors in terms of the sun/orbit plane angle follows.

Injection Errors

The injection errors for the Delta vehicle entering a circular orbit are stated in terms of the deviation from circularity and the orbit inclination error. These are shown in Figure 39 for a range of nominal orbit altitude from 100 - 900 nautical miles. The injection altitude will be within one or two nautical miles of the nominal, but the velocity error will be such as to cause a relatively large deviation in the altitude of the opposite apsis (approximately 180 degrees downrange from the injection point). The 3-sigma value of this deviation is ± 14.85 nautical miles for a nominal 600 nautical miles orbit using the advanced Delta guidance. The corresponding inclination error is 0.04 degree, independent of orbital altitude. The current Delta vehicle produces altitude errors approximately twice as large and inclination errors approximately four times as large. The combinations of altitudes consistent with these errors are shown in Figure 40 . These

• Circular Retrograde (100° Incl.) Orbits

• WTR Launches

Ref. S. J. Harris, McD.-Douglas

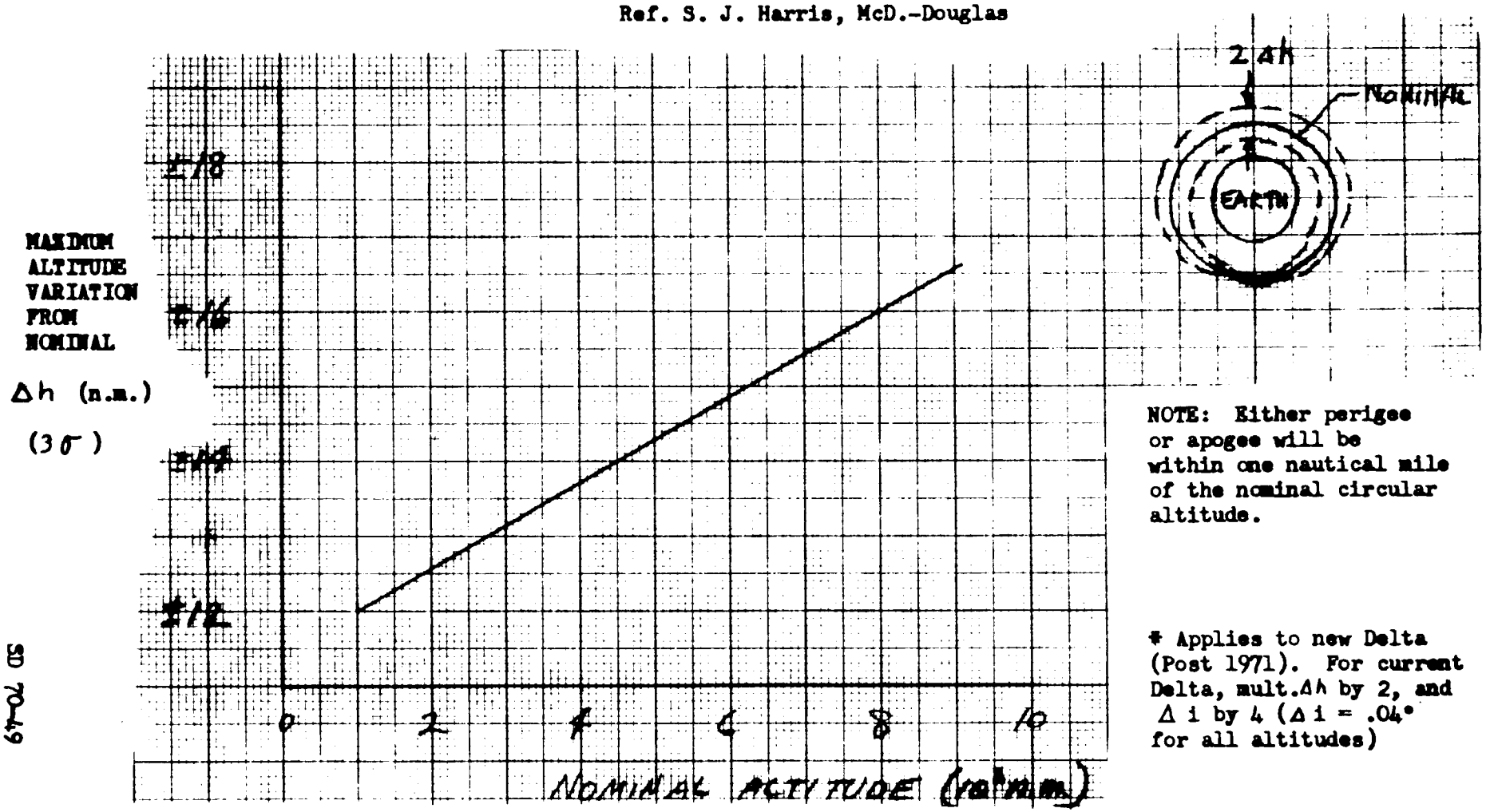

NOTE: Either perigee or apogee will be within one nautical mile of the nominal circular altitude.

* Applies to new Delta (Post 1971). For current Delta, mult. Δh by 2, and Δ i by 4 (Δ i = .04° for all altitudes)

Figure 39 Delta Injection Errors*

ORIGINAL PAGE IS OF POOR QUALITY

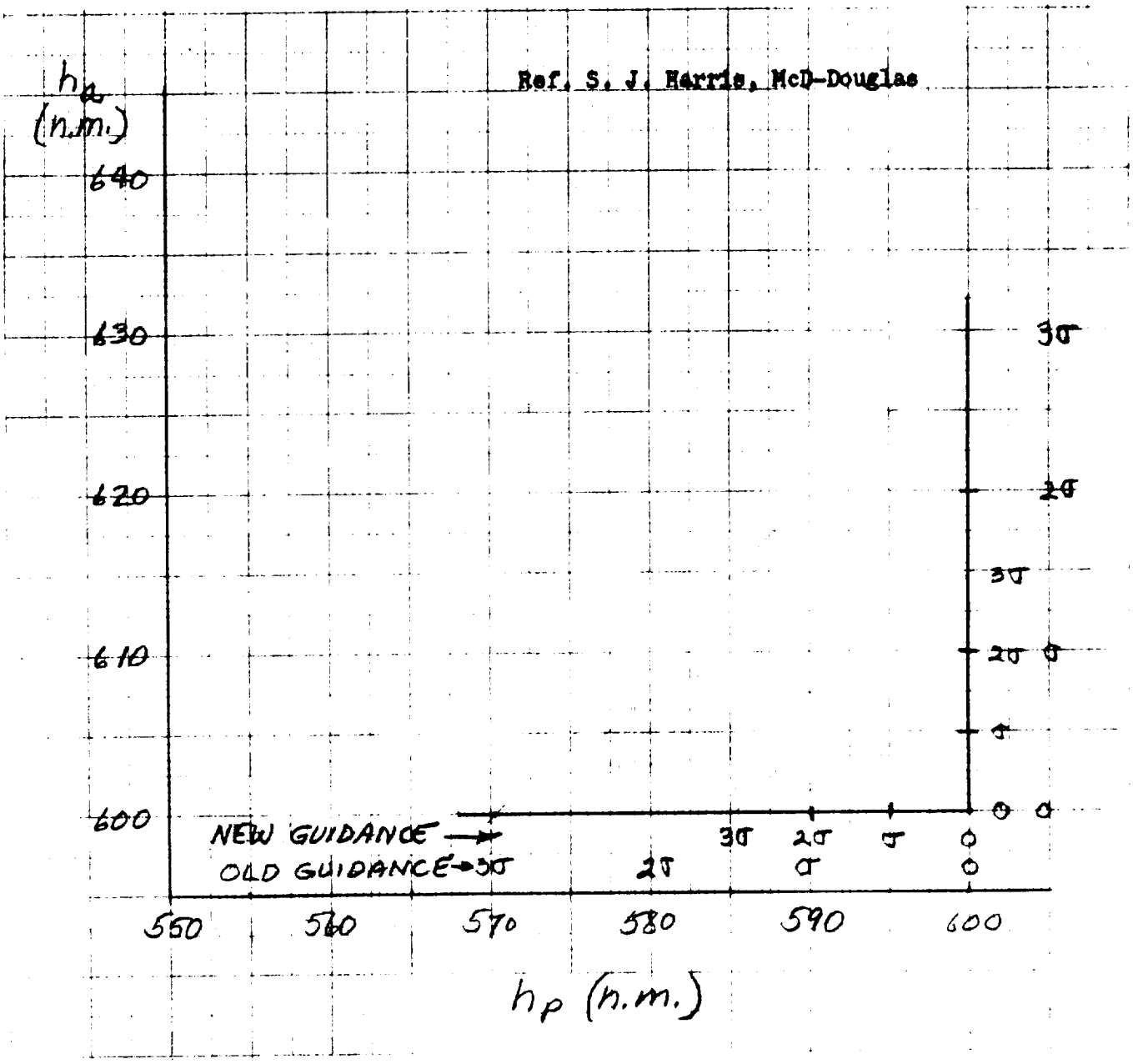

Figure 40

3 σ Altitude Variation
Delta Launch Vehicle
600 NM Circular Orbit

values were used in the computer analysis of sun/orbit plane angle variation described later in this report.

The injection errors for the Scout vehicle are shown in Figure 42 , in the same form as the Delta errors of Figure 39 , for easy comparison. These errors were immediately judged as prohibitively high. Uncorrected, they place too high a demand on satellite versatility, and correction of the errors imposes the additional requirement of in-orbit propulsion on the satellite. Errors of this magnitude preclude sun synchronism or predictable ground trace repetition. The corresponding one-sigma errors at injection, from which Figure 42 was derived, appear in Figure 43 .

The three-sigma errors of the Thor Burner II are shown in Figure 44 . The error in average altitude, or semi-major axis, is approximately ± 26 nautical miles for a 600 nautical miles orbit. The error is approximately 1.7 times that of the current Delta, which is 15 nautical miles (Figure 41), and 3.5 times that of the advanced Delta, which is 7.5 nautical miles.

In the following discussion, it is shown that the variations in sun/orbit plane angle due to the worst Delta errors are commensurate with obtainable sun sensor hardware while the errors of the other two vehicles suggest a possible design problem.

Figure 45 shows the variation in the angle between the sun and the orbit plane with time, for a year after the launch date (May 1 was chosen as typical). The example is that of a piggyback mission in a NIMBUS orbit. The effects of 3-sigma errors in altitude and inclination are included for the current (worst case) Delta vehicle. The maximum angle occurs about nine months after launch. The maximum (3σ) deviation from the nominal value at nine months is about 4 degrees due to inclination and 3 degrees due to altitude. The combined

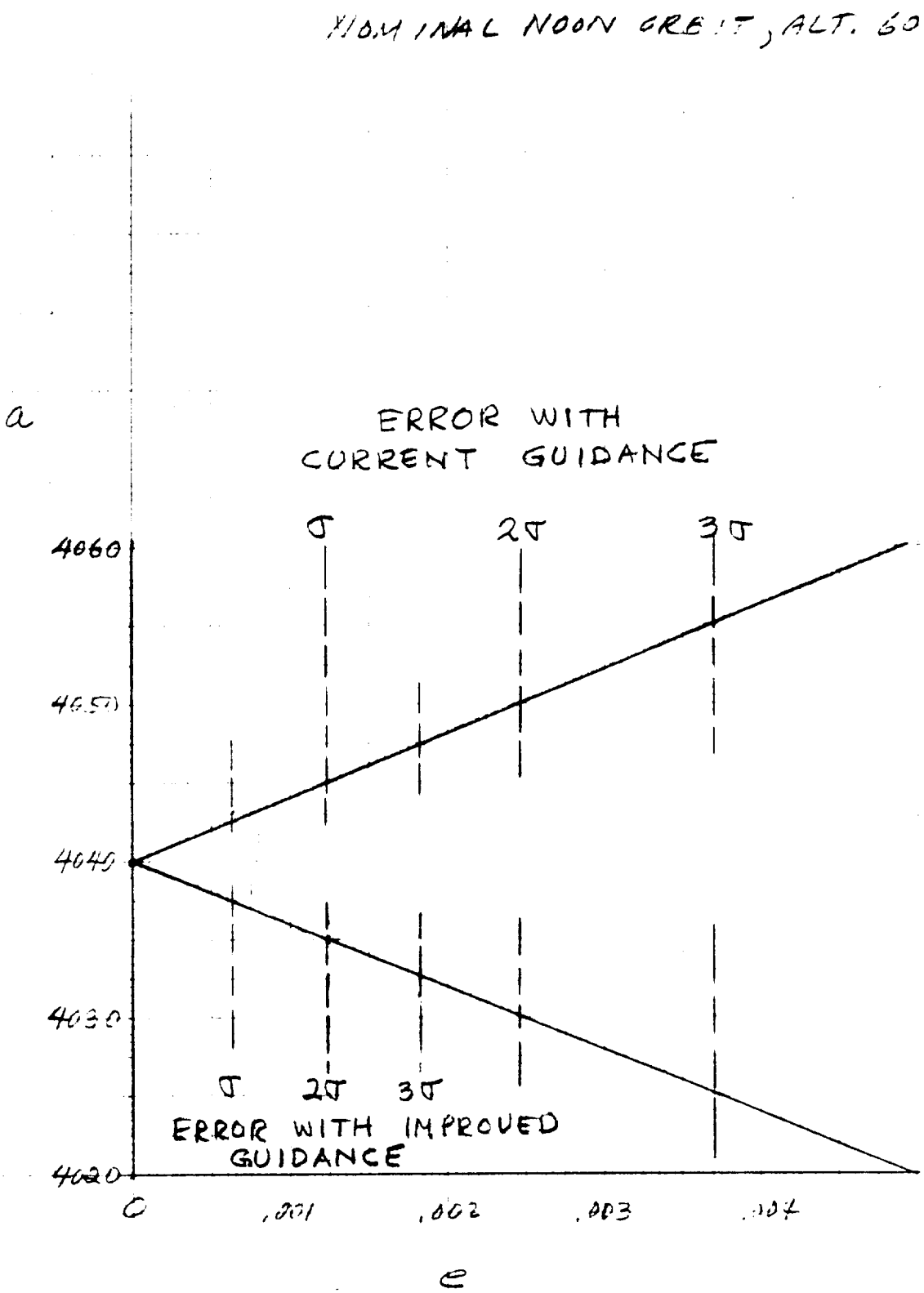

Figure 41

Orbit Parameter Variation due to
Injection Error (In Altitude)
of Delta Launch Vehicle

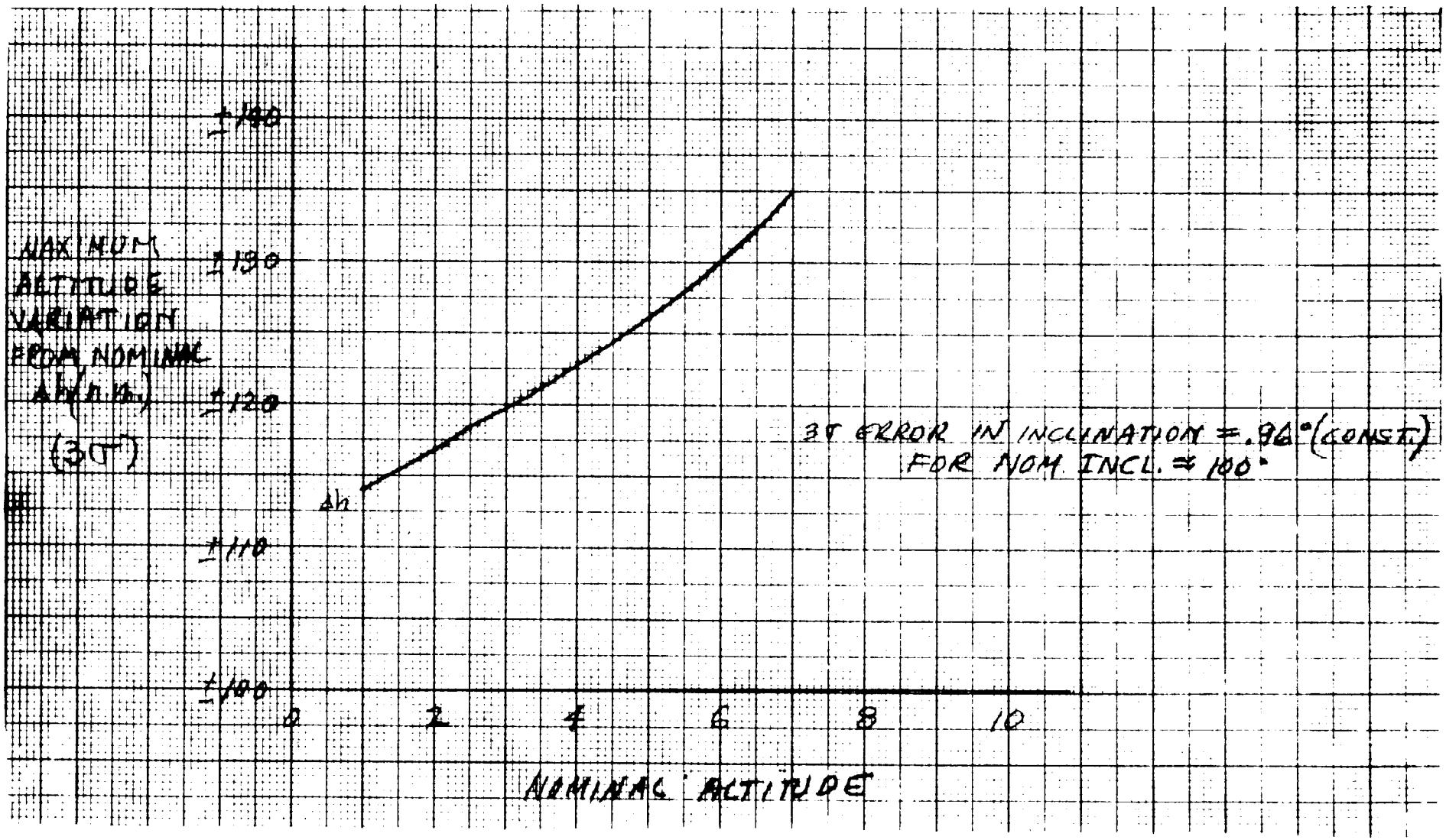

Figure 42 Scout Injection Errors

ORBIT MISSIONS

INJECTION ACCURACY

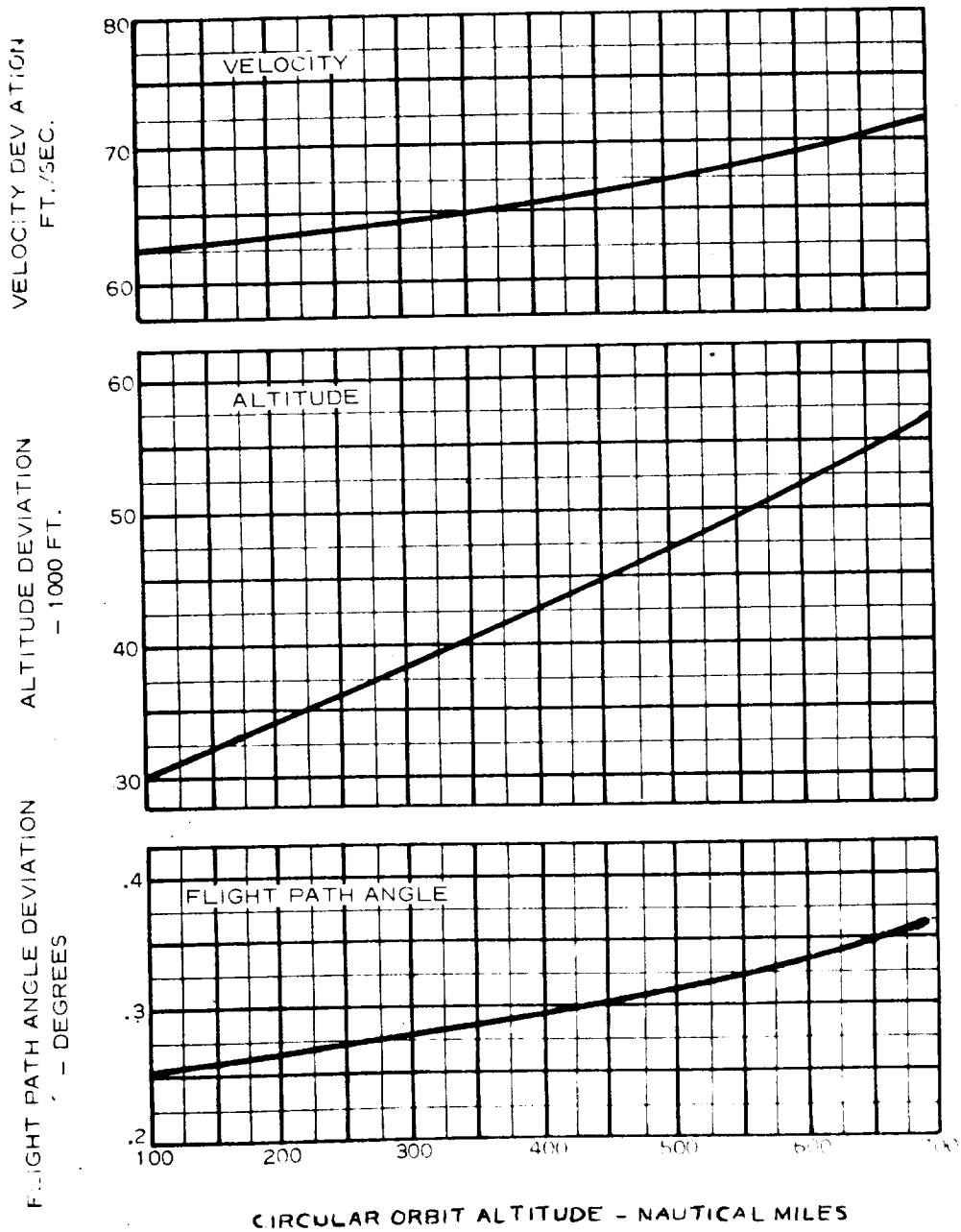

Figure 43 One-Standard Deviation in Injection Condition

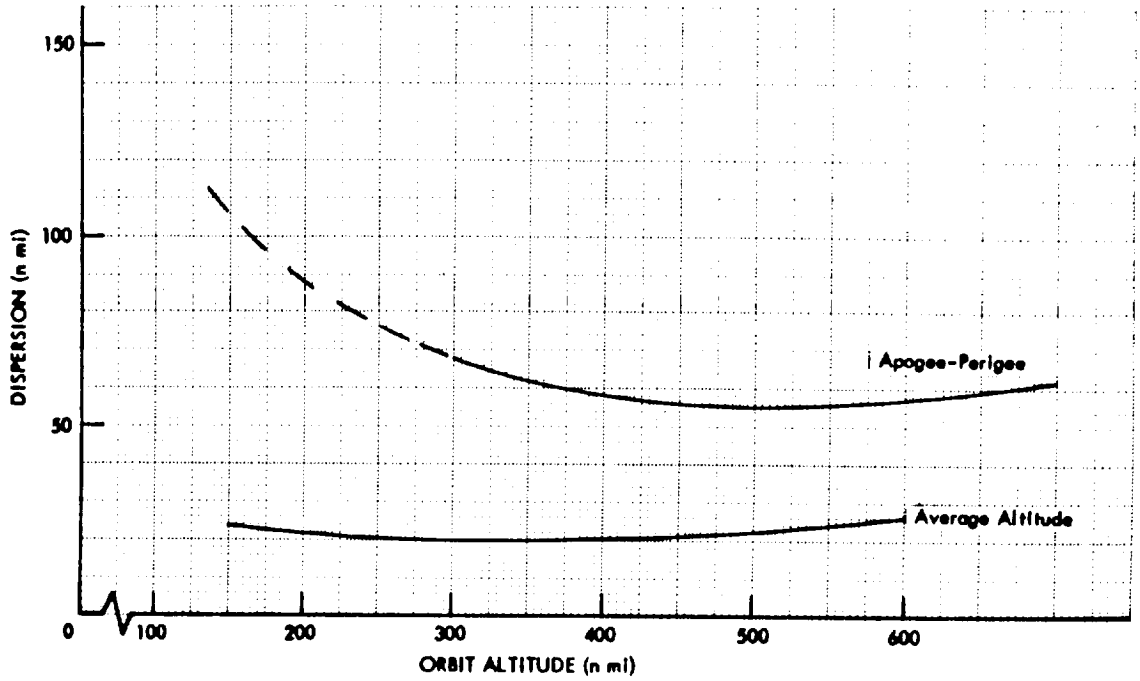

a. SLV-2A (LESS SOLIDS)/BURNER II ERRORS (3-Sigma)

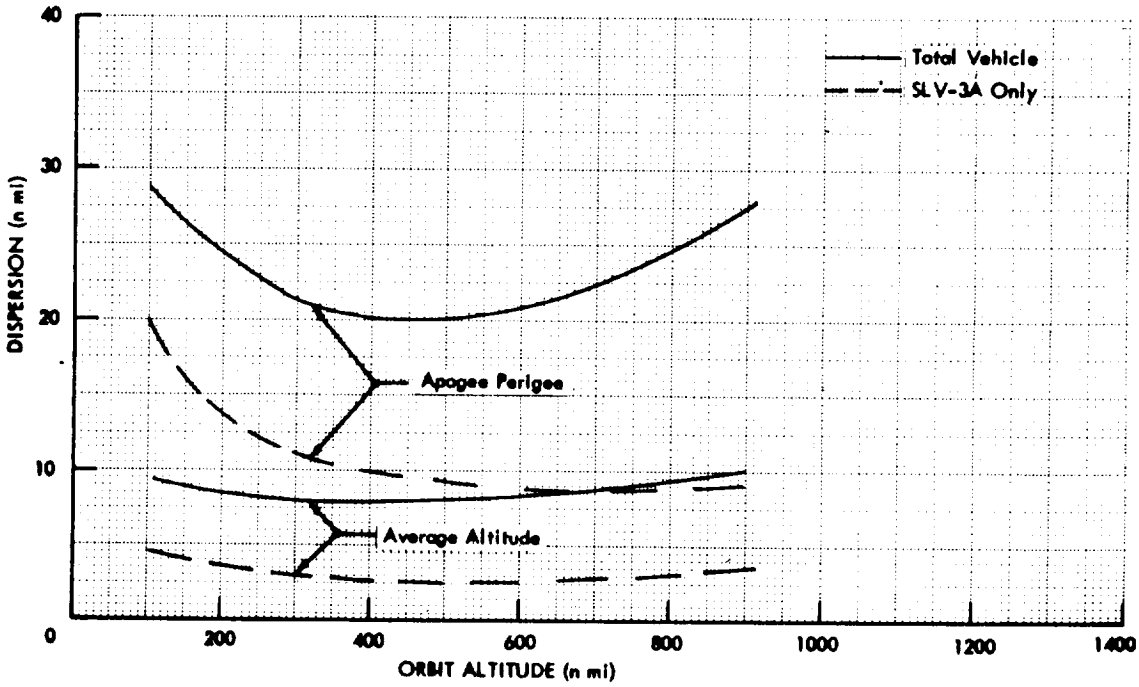

b. ATLAS (SLV-3A)/BURNER II ACCURACY (3-Sigma) (Radio Guidance of the SLV-3A)

Figure 44 Burner II Injection Errors

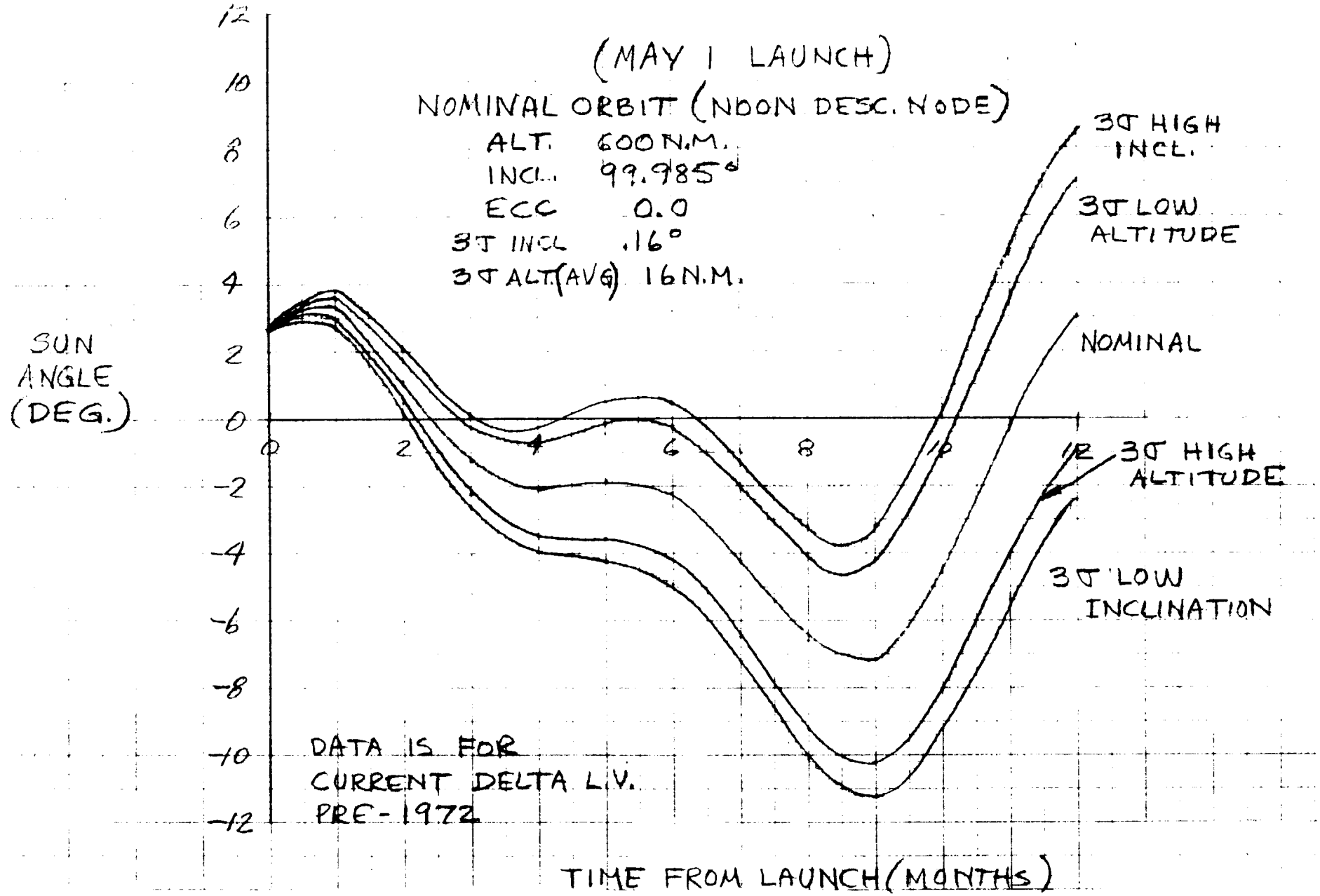

Figure 45 Variation in Angle between Orbit Plane and Sun Line

Space Division
North American Rockwell

maximum is about 5 degrees. Thus, the total angle between the sun line and the orbit plane could be about 12 degrees, which would be consistent with the use of a sun sensor whose field-of-view extends 15 degrees either side of the zenith. Figure 45 shows that applying a slight bias to the orbit could result in a smaller maximum angle if required. However, in the event that most of the required data will have been obtained in the early part of the mission, such a deliberate bias would be of little value and would degrade the data taken in the early phase.

Conclusions

Based on a comparison of the candidate satellite piggyback orbits, it is concluded that the noon sun-synchronous orbit of the NIMBUS best serves the purpose of the horizon sensor satellite mission. This conclusion concurs with that obtained in the attitude error analyses.

It is recommended that the mission requirement nominally call for the spin axis to be oriented normal to the orbit plane, but that the option of turning the satellite in azimuth to "look" out of the orbit plane be retained.

Using the aforementioned orbit data over the full latitude range can be obtained and sun elevation angles from zero to 90 degrees can be achieved. Full seasonal variations can be observed at all latitudes, but diurnal variations are limited. As little as four hours (± 2 hours) variation in local time at the test point can be experienced. The minimum possible local time variation occurs at the equator and can be achieved only by yawing the satellite ± 90 degrees.

The proposed orbit permits a spinning vehicle to present a sufficient cross-section to solar rays to provide adequate electrical power. The orbit also allows sufficiently long periods of exposure to the sun and results in a relatively uniform thermal cycle.

The proposed orbit will produce ground traces which leave spaces only 1-1/2 degrees (90 nautical miles) apart in longitude at the equator. Therefore, points between the traces can be observed by applying a very slight yaw maneuver.

The proposed orbit has a sufficiently high altitude to render the effect of atmospheric drag negligible for the size and weight of the proposed vehicle. The orbit is compatible with obtainable sun sensors from the standpoint of sun aspect angle, and minimizes the pitch error of the system due to the sun aspect angle.

Ground Trace Drift and Local Time Shift for Deviations in Inclination and Altitude

This section presents a detailed analysis of the relationship of ground trace and local time of node passage to orbital period and the precession effect of earth ablateness. It shows the requirements, in inclination and altitude, necessary to produce a desired combination of ground trace repeat cycle and sun synchronism and describes the effect, on both, of errors in inclination and altitude.

The altitude of a satellite can be selected so that the satellite will complete each orbit in any required period of time, to synchronize with any other event. The altitude of the orbit in the absence of perturbations does not, however, affect the inertial orientation of the orbit plane. Under these circumstances, an orbiting satellite cannot be expected to cross over the same point on the equator of a rotating globe unless the point has traversed exactly 360 degrees in the course of one or more complete orbital periods. If this condition is met, the local time will be different each time the coincidence of subsatellite point and earth target occurs, due to the eastward relative motion of the sun. The inclination of the orbit has

no effect (perturbations are neglected). To obtain rendezvous every sidereal day, therefore, the relationship of orbital rate to earth rotation rate would be

$$\omega_o = n\,\omega_1 \tag{1}$$

Now, if coincidence need occur only once out of every m times that the target appears in the orbit plan (m sidereal days), the coefficient of ω_1 can be a non-integer $(\frac{n}{m})$. Coincidence will occur every m resolutions of the earth, and the satellite will have traversed n orbits.

If the point of coincidence must be eastward of the original orbit plane, the plane must undergo the appropriate eastward displacement in the interval of time between coincidences, and the total time between coincidences must be increased by the length of time required by the point on the earth to travel the additional distance eastward. If either of these fails to occur, then coincidence will not take place on the required orbital pass. If the orbital period is increased and the plane is not rotated, the satellite will pass to the west of the point; and if the plane is precessed without increasing the period, the satellite will pass to the east of the point. Assume that the eastward displacement of the rendezvous point keeps it beneath the sun. Then, in the former case the target will be under the sun at rendezvous time, and the satellite will be on the equator at rendezvous time but at a different longitude and local time (forenoon). In the latter case, the satellite will have passed the equator before the target arrives beneath the sun. The equatorial passage of the satellite and the passage of the target beneath the sun will have occurred at the same local time (12 noon), but not simultaneously.

If the period and plane precession are compatible for rendezvous, but the orbit precession rate is not equal to the rate of the sun's relative motion,

then each rendezvous will take place at a different local time, the difference depending upon the rate difference. If a day is defined as the elapsed time between alignments of the target with the sun's meridian, then the elapsed time between rendezvous cannot be an exact integer number of days in this case.

The equations describing the aforementioned conditions follow. For the purposes of this analysis, rendezvous is defined as the alignment of the satellite with the target point on the earth, along the local vertical through the point.

Let i = the number of (inertial) revolutions of the earth for rendezvous without sun-synchronism

N_i = the number of orbits before rendezvous.

The number of orbits before rendezvous is

$$N_i = N_1 + (i - 1)(N_1 + 1) \tag{2}$$

The above equation does not assure rendezvous, but it assures that the satellite will be on the equator at the appointed time; that is, it is a necessary, but not a sufficient condition. Assurance that the node will have moved along the equator by the required amount is given by

$$N_i \, d\Omega = \omega_3 t \tag{3}$$

where t is the elapsed time

$d\Omega$ is inertial motion of the node per orbit.

ω_3 is the rate per unit time of the Sun line or other reference line in inertial space.

This is the Sun-synchronism criterion.

Now, in order that the point on the Earth appear beneath the satellite at the time of nodal crossing, it is necessary that

$$\omega_1 t = \omega_3 t + 360i \tag{4}$$

or

$$t = \frac{360i}{\omega_1 - \omega_3} \tag{5}$$

where ω_1 is the Earth rotational rate. This is the repeat cycle criterion. When i = 1, the time t is the length of one solar day.

The nodal period of the satellite must be

$$P = \frac{t}{N_i} \tag{6}$$

Substituting and combining,

$$P = \frac{360i}{(\omega_1 - \omega_3)\ (N_1 + (i - 1)\ (N_1 + 1))} \tag{7}$$

and $d\Omega = \omega_3 P$ inertial degree/orbit.

TABLE 9

RATES IN INERTIAL SPACE

MOTION	DEGREE/	DEGREE/HOUR	DEGREE/DAY (24 HOURS)	DEGREE/YEAR (365.25 DAYS)
Earth (ω_1) Point	.250684	15.04105	360.9852	131849.8
		.00011408		1
		.00001901		1/6
Earth about Sun (ω_3)	.00068446	.0410678	.9856263	360

The nodal period can be obtained by the correct selection of orbit altitude and inclination. Values of ω_1 and ω_3 are shown, for reference, in Table 9 .

Although the nodal period is a function of altitude and inclination, there are more than one combination of altitude and inclination that will produce the same nodal period (Figure 46). The required combination is that which produces, in addition, a node precession sufficient to satisfy Equation (3). The precession of the node is also a function of altitude and inclination. There is only one combination of altitude and inclination that provides both the sun-synchronism and the required repeat cycle.

The required precession rate of the node to track the sun is represented by the value of ω_3. If $\omega_3 = 0$, the orbit is inertially fixed. It can be seen from Equation (7) that any orbit period requirement can be satisfied by selecting the appropriate value of ω_3, without changing i or N_1. Therefore, if sun-synchronism is not required, a whole range of orbit period will provide the same repeat cycle. The attendant degradation in sun-synchronism is shown in Figures 47 and 48.

Figures 49 and 50 show for a typical sun-synchronous orbit, the contributions of inclination and altitude, respectively, to node precession or local time variation. Figures 51 and 52 show the drift of the ground trace in response to uncompensated inclination and altitude errors, respectively. The drift of the ground trace is derived from the change in nodal period only, associated with errors in inclination and altitude.

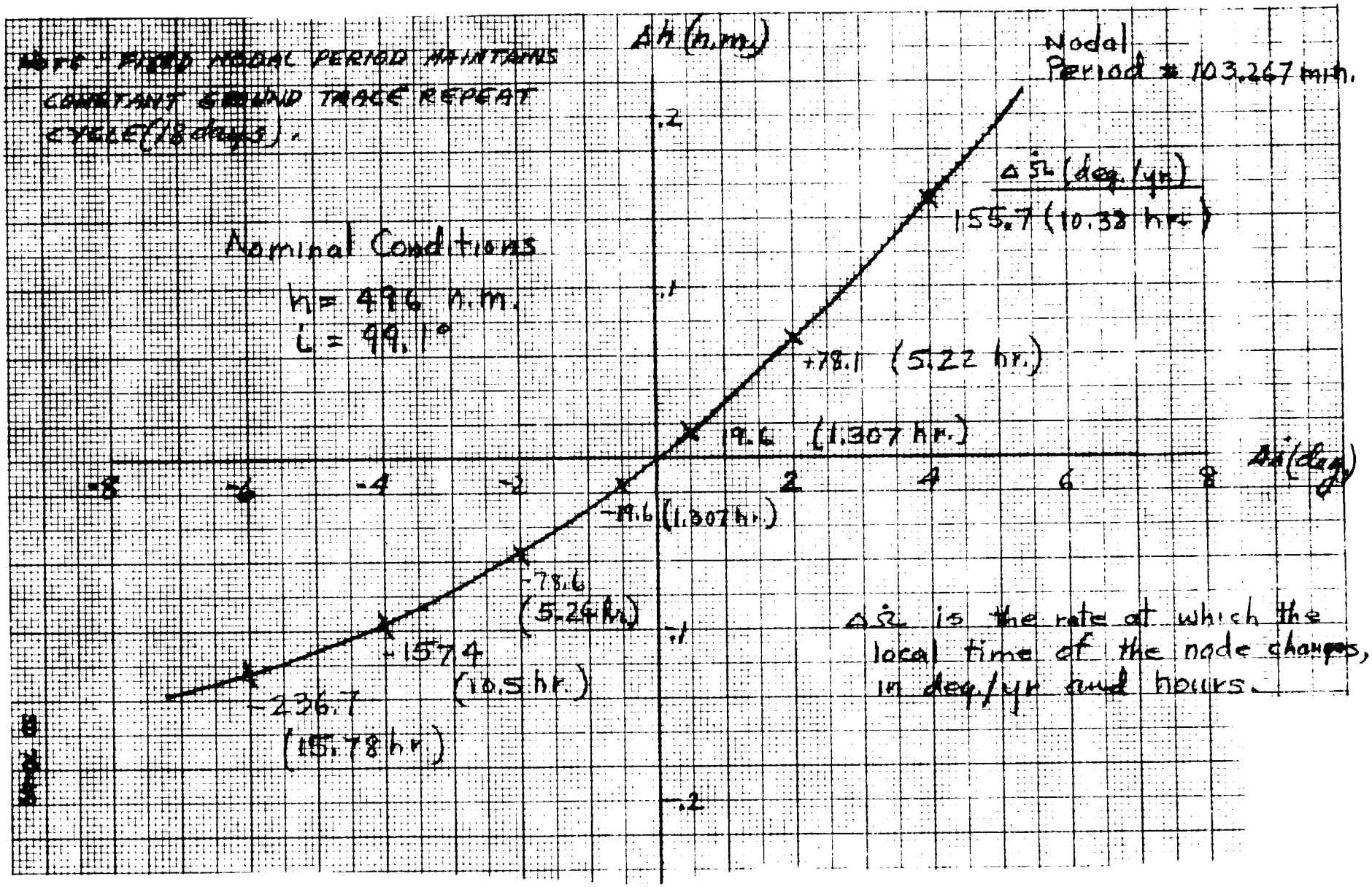

Figure 46 Altitude/Inclination Trade-Off for Fixed Nodal Period

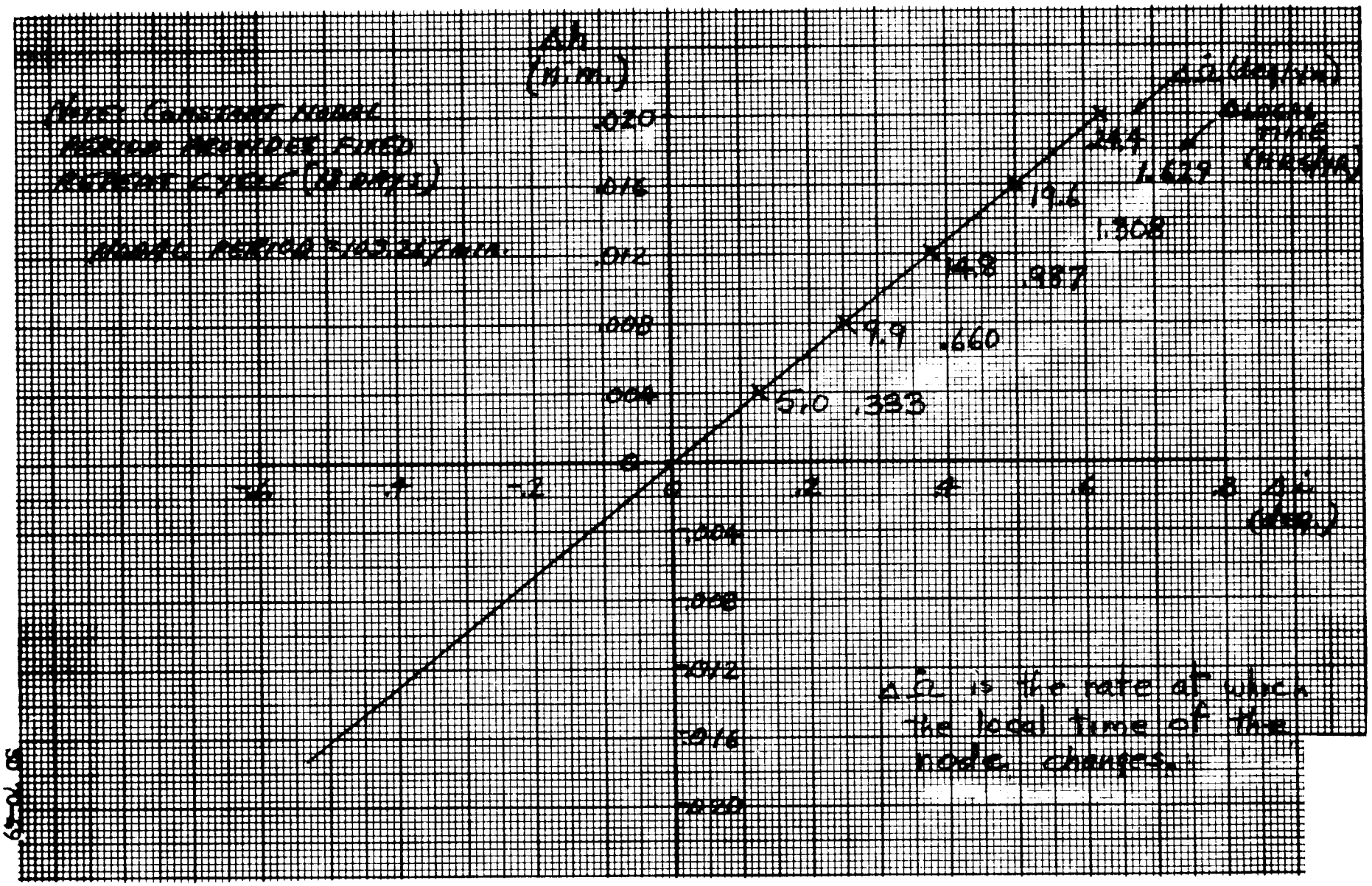

Figure 47 Altitude/Inclination Trade-Off for Fixed Nodal Period

ORIGINAL PAGE IS OF POOR QUALITY

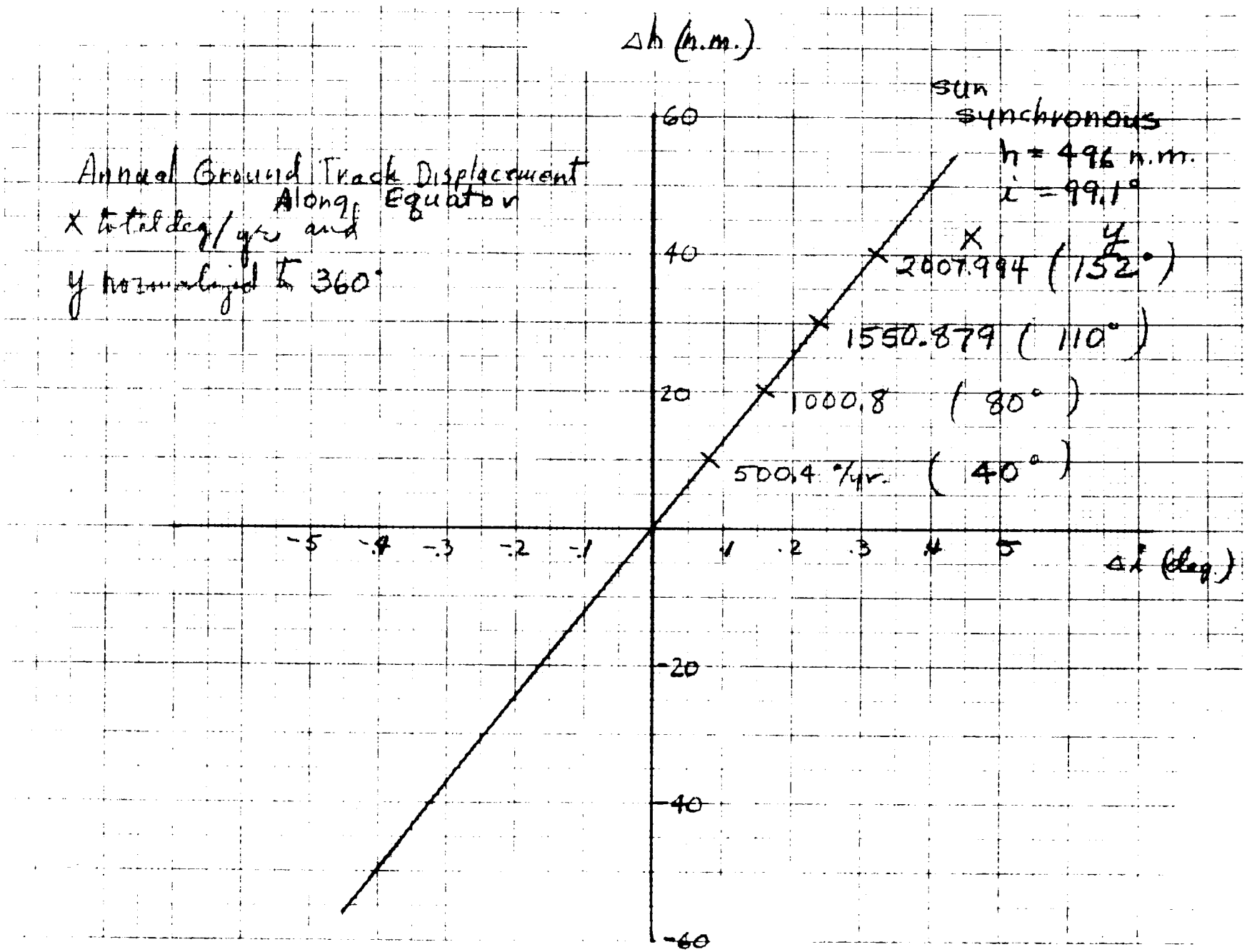

Figure 48 Altitude vs. Inclination for Sun Synchronism

Space Division
North American Rockwell

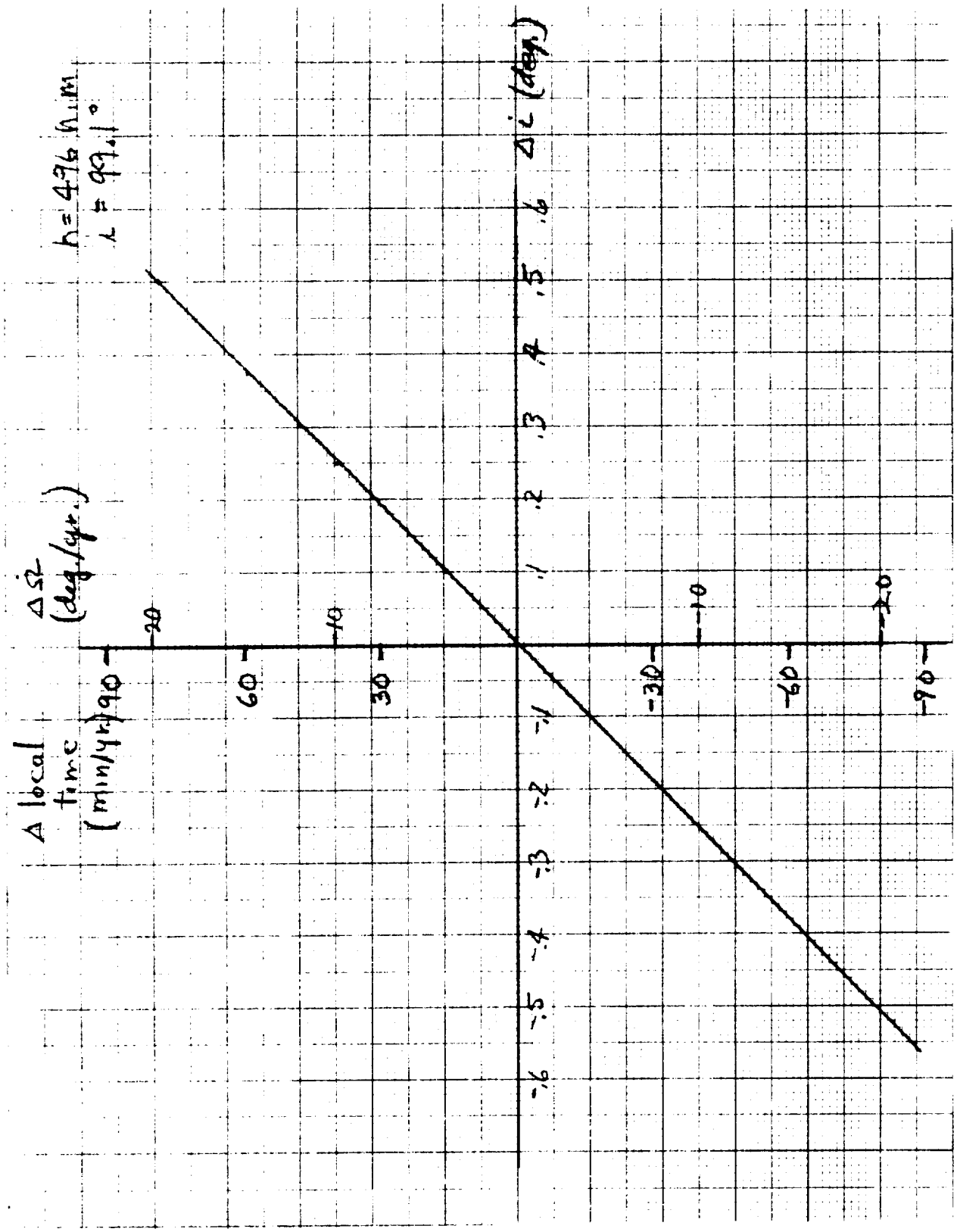

Figure 49 Sensitivity of Node Precession to Inclination

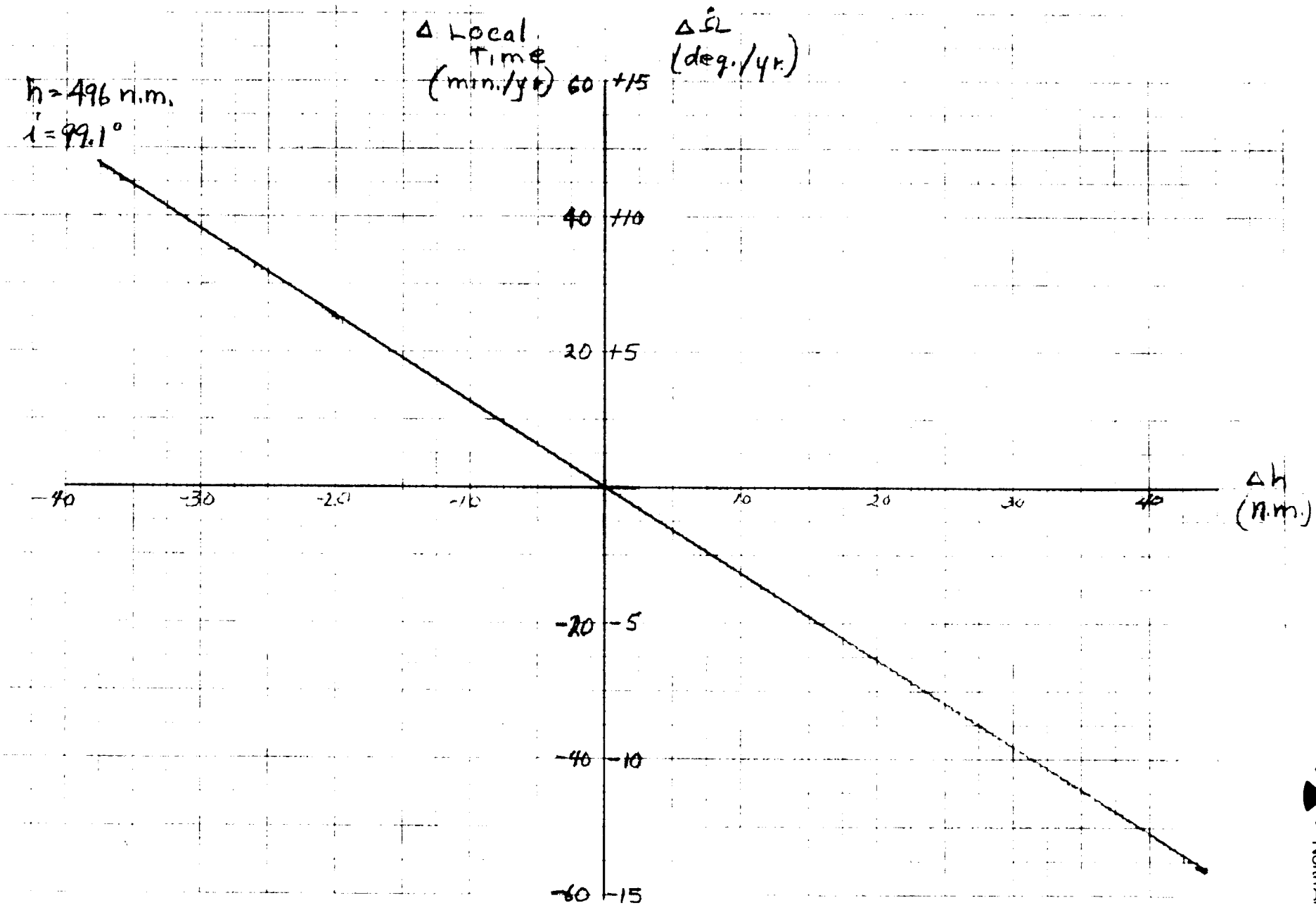

Figure 50 Sensitivity of Node Precession to Altitude

Space Division
North American Rockwell

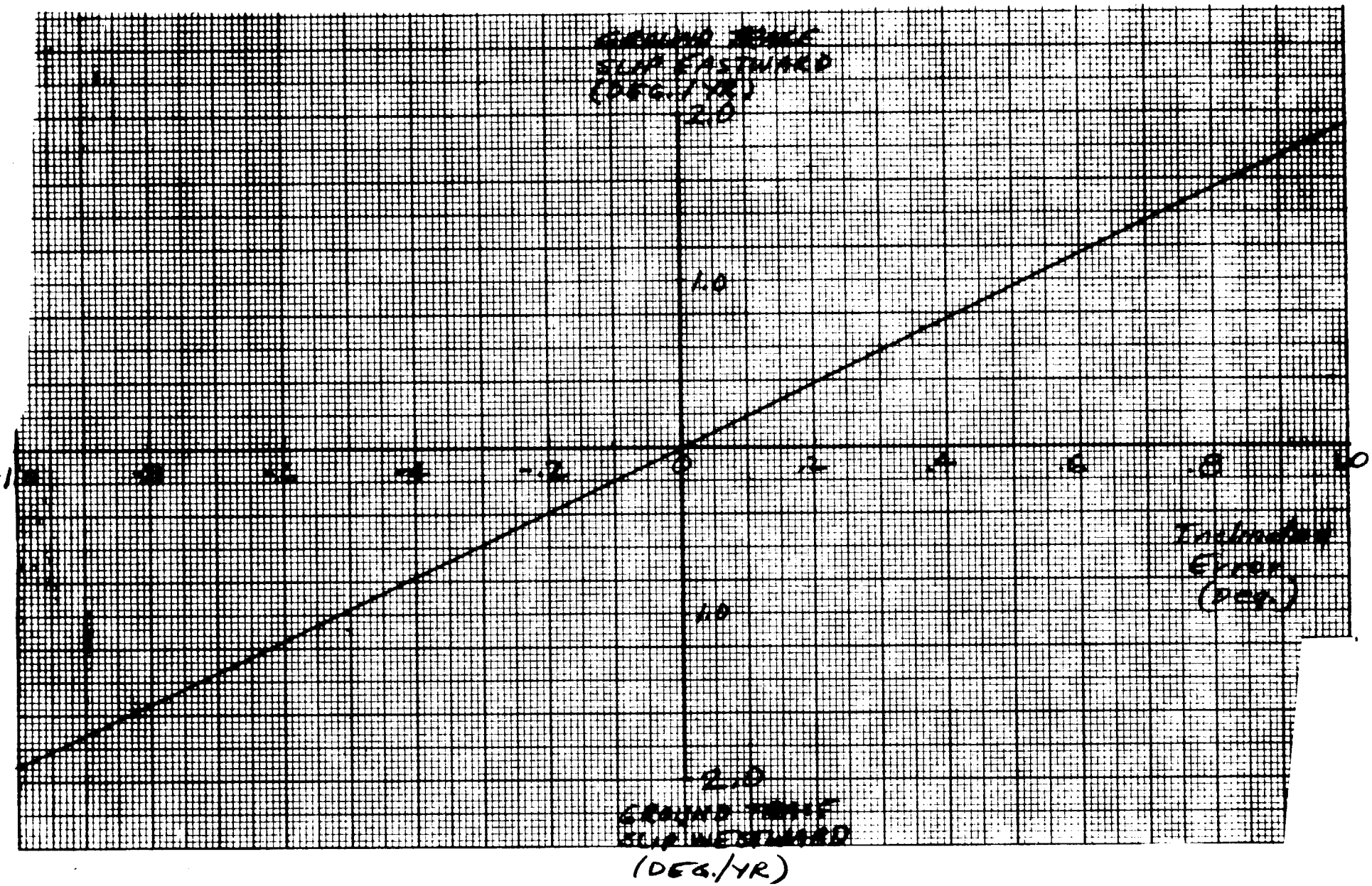

Figure 51 Slip of Ground Trace at Equator due to Altitude Error

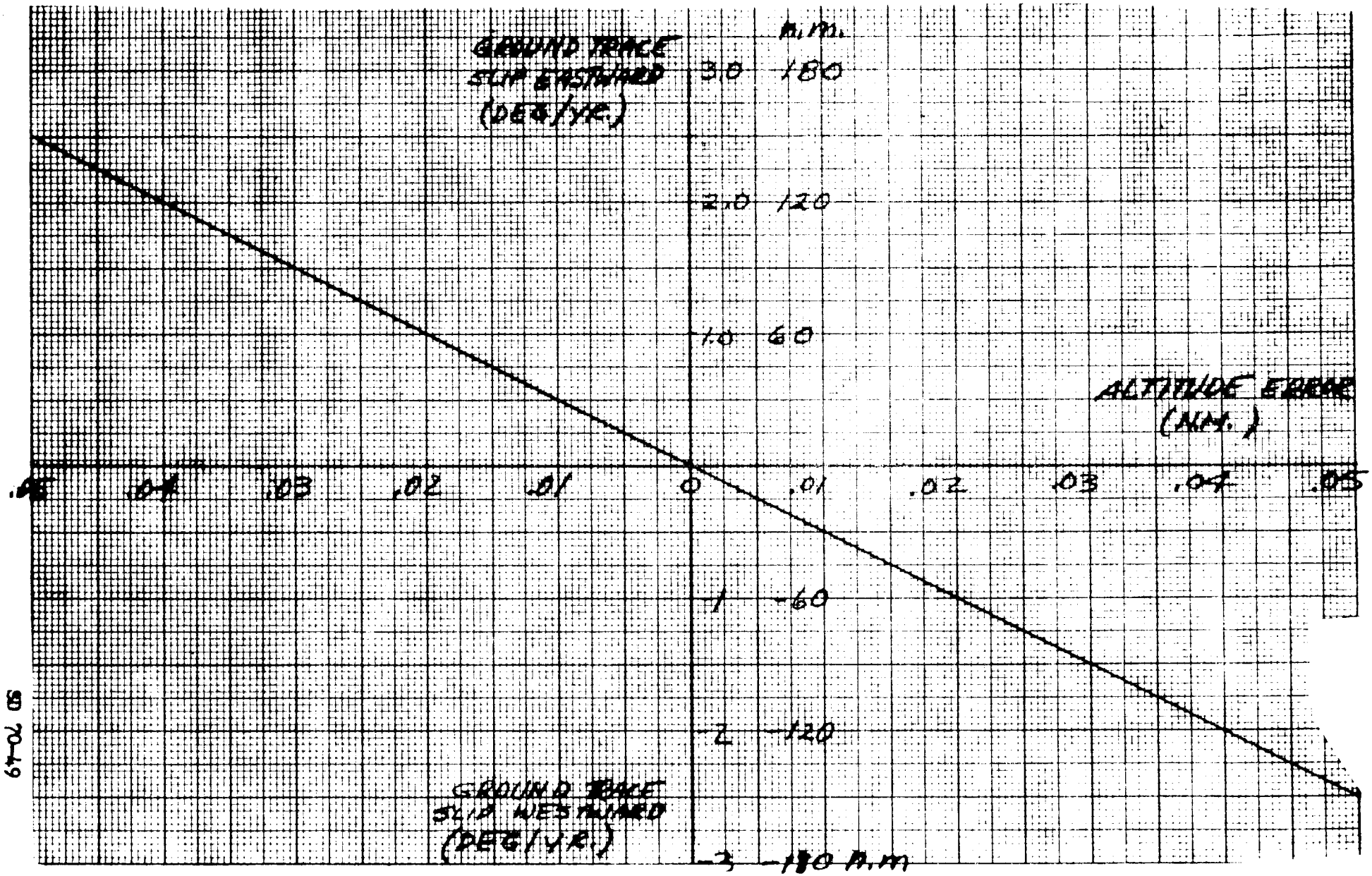

Figure 52 Slip of Ground Trace at Equator due to Inclination Error

ORIGINAL PAGE IS
OF POOR QUALITY

Orbit Deterioration

This section shows the magnitude of changes that can be expected in the orbit orientation parameters (node and inclination) over the lifetime of the horizon sensor satellite, due to natural perturbations. These two parameters constitude an index of the sun-synchronism and the ground trace repeat period of the satellite. The effects of changes and of initial errors in these parameters on the sun-synchronism of the orbit and the repeat period of the satellite's ground trace are described in the previous section.

The four most significant perturbative forces acting on an earth satellite are solar radiation pressure, earth oblateness, atmospheric drag, and the gravitational attraction of the sun and the moon.

Solar Radiation Pressure

The rate of node rotation due to solar radiation pressure is:

$$\Omega = \frac{a^2 FW}{\sin i} \left[- \cos E \right]_{E_1}^{E_2} \quad \text{rad/rev.}$$

where $W = \sin i \quad \cos^2 \frac{\epsilon}{2}$

and $F = Ap/m\mu e$

a is the orbit radius

p is solar pressure at 1 a.u. (19×10^{-8} lb/ft^2)

ϵ = 23.5 (obliquity)

A = satellite cross-sectional area (2.5 ft^2)

m = satellite mass (slugs) (3.0)

μe = earth's grav. const. ($1.40766 \times 10^{16} \frac{ft^3}{sec^2}$

The quantities E_1 and E_2 are the angles at which the satellite leaves the shadow and re-enters it, respectively. The total value of $\Delta \Omega$ for one year in the case of the horizon sensor satellite is approximately 3.73 degrees.

The change in inclination is

$$\Delta i = a^2 FW (\sin E) \Big|_{E_1}^{E_2}$$

which, for the horizon sensor, is approximately .00275 degree/year.

Earth Oblateness

The altitude and inclination of the orbit are selected to create the required sun-synchronism and ground trace repeat frequency. The sun-synchronism is ac ieved by virtue of the earth's oblateness. Therefore, the displacement of the node due to oblateness does not represent an error, but a deviation from the correct displacement does. The correct nodal motion is approximately .985 degree/day. Since the equation for nodal motion is

$$\Delta \Omega = -3\pi J_2 \left(\frac{R}{p}\right)^2 \cos i \quad \text{deg/orbit.}$$

where: J_2 = earth's gravitational coefficient (1082.28×10^{-6})

R = earth radius - 3440 nmi

p = semi-latus rectum of orbit

the displacement per day is therefore

$$\Delta \Omega = -5.68 \cos i \quad \text{deg/day}$$

and the sensitivity of $\Delta \Omega$ to changes in i is

$$\frac{\partial \Delta \Omega}{\partial i} = .096 \quad \frac{\text{deg/day}}{\text{deg}}$$

Oblateness does not affect orbit inclination.

Atmospheric Drag

The shift of the node due to atmospheric drag at 500 nautical miles is approximately .000109 degree/day or .03978 degree/year (2.4 n.m./yr) for the horizon sensor satellite. For this altitude and any higher altitude, the effect can be considered negligible.

Solar and Lunar Gravity

The approximate perturbations of the node and inclination due to lunar and solar gravities for the circular orbit are

$$\Delta \Omega = -K_1 \; a^3 \; \cos i \quad \text{deg/day}$$

$$\Delta i = \frac{-K_1}{2} \; a^3 \; \sin i \quad \text{deg/day}$$

where a is the orbital radius in earth radii and K_1 (sun) = .02025

K_1 (moon) = .04404

For a 500 nautical miles orbit, the values are

$$\left.\begin{aligned} \Delta \Omega &= .01147 \quad \text{deg/yr} \\ \Delta i &= -.03260 \quad \text{deg/yr} \end{aligned}\right\} \text{MOON}$$

$$\left.\begin{aligned} \Delta \Omega &= .00527 \quad \text{deg/yr} \\ \Delta i &= .01498 \quad \text{deg/yr} \end{aligned}\right\} \text{SUN}$$

Conclusions

The magnitudes of all of the natural perturbations have been found to be extremely small in the case of the horizon sensor satellite at 500 nautical miles altitude. At higher altitudes, up to 800 nautical miles, the oblateness and atmospheric drag effects are much smaller, and the effects due to solar radiation pressure and lunar and solar gravity appear negligibly larger. In view of the mission requirements, these perturbations cannot be said to significantly degrade or hiner the performance of the horizon sensor satellite.

ATTITUDE DETERMINATION AND EXPERIMENT POINTING SYSTEMS

A theoretical analysis has been made of the reference concept for a horizon sensor satellite. The results of that analysis are contained in this section. A functional description of the system concept is provided, followed by a detailed presentation of the equations and a description of the data flow and operational sequence. A description is given of the computer program created for the horizon sensor satellite studies and of more detailed programs being prepared. The application of these programs to the horizon sensor satellite problem is clearly identified. The error sensitivities of the proposed system are derived and values presented. In addition, the conditions for minimizing the error are given, in terms of the orbit and the physical orientation of sensors in the satellite. Lastly, a numerical evaluation of the errors and a sensor hardware description are presented.

Outline of System Concept

The proposed satellite design concept consists of two experimental instruments (a microwave horizon sensor and a UV horizon sensor) with an attitude reference provided by a pair of operational IR sensors and an operational sun-sensor. The satellite rotates nominally about an axis normal to the orbit plane, with the axes of the experimental sensors and the sun sensor located in the spin plane. The times of sensing the horizons are recorded and correlated with vehicle orientation to determine the indicated directions of the horizons. Vehicle orientation is indicated by the sun sensor (pitch and azimuth) and the IR horizon sensors (roll).

The proposed concept entails correcting the measured horizon data to account for measured deviations of the vehicle axes from the local space axes. The measurement of these deviations is described below. It is fitting at this point, however, to point out that these deviations should be kept as small as possible in order to keep the horizon error component due to attitude uncertainty down to a reasonably low level. This problem is discussed further in the error analysis.

The attitude deviations must be measured using the sun sensor and the IR sensors. The IR sensors are used to indicate the degree to which the plane in which they rotate differs from a vertical plane based on the line of sight from the satellite to the geometric center of the earth. They also could indicate, with low accuracy, the orientation of the line of intersection of these two planes, and thereby define the local horizontal plane. However, the sun sensor provides a reference plane (A) and a directional reference line in that plane (B, Figure 53) (as long as the sun does not lie on or near the vehicle spin axis). And since the sun can be sensed by a sun sensor more accurately than the center of the earth can be sensed by the IR horizon sensors, the sun reference is used to determine the orientation of the line of intersection, and thus the local horizontal plane. A description of the method by which the sun sensor and the IR sensors establish the local horizontal plane follows:

The location of the axis of intersection of the two planes can be defined (Figure 54) by its angle from the sun/spin axis plane (ν). If A, B, and C are unit vectors along the vehicle spin axis, the intersection and the sun line, respectively, the lengths of their chords are (Figure 55):

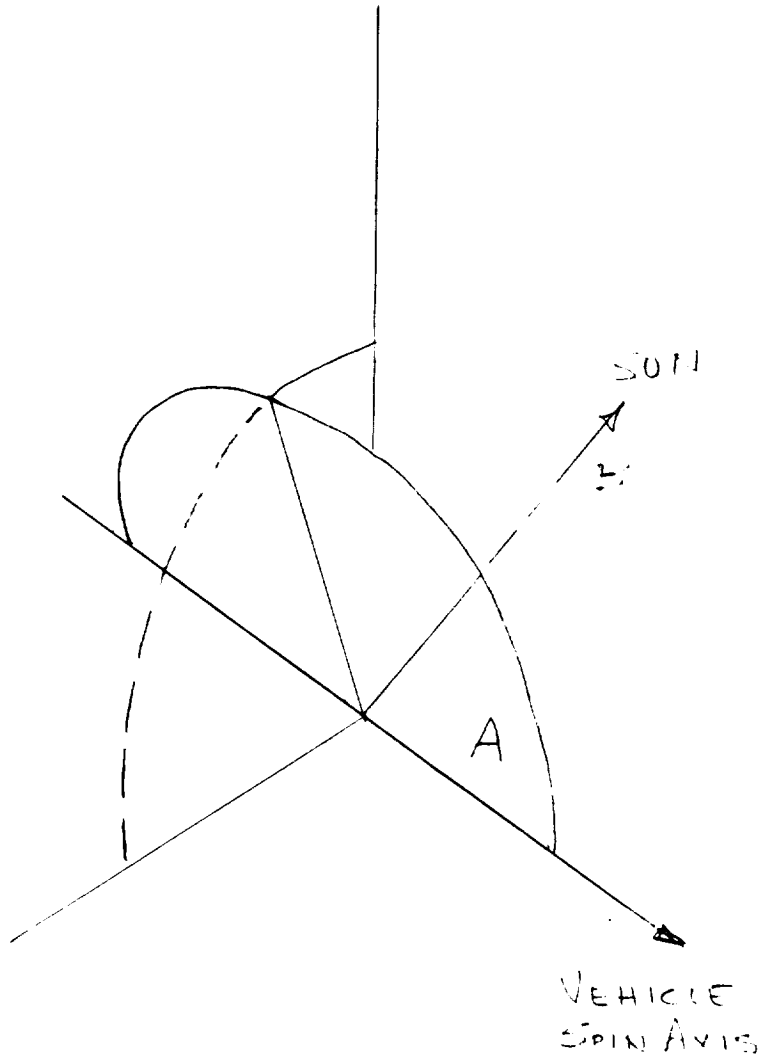

FIG. 53 - SUN PLANE AND VECTOR

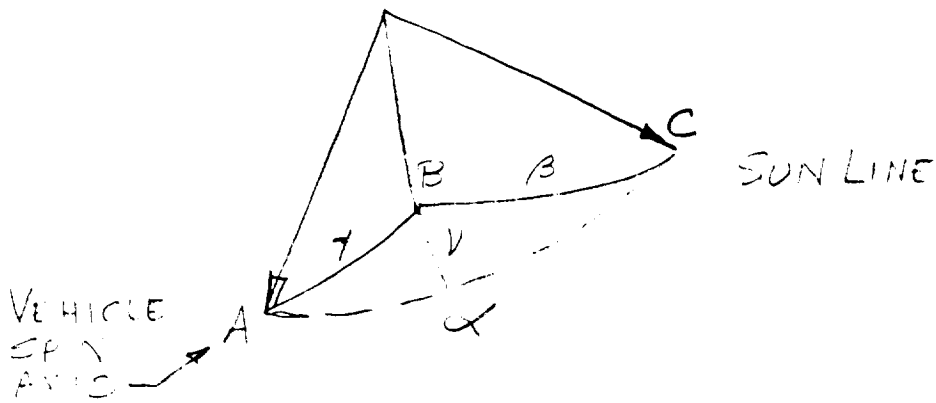

FIG. 24 - GEOMETRY OF SUN/SPIN AXIS REFERENCE

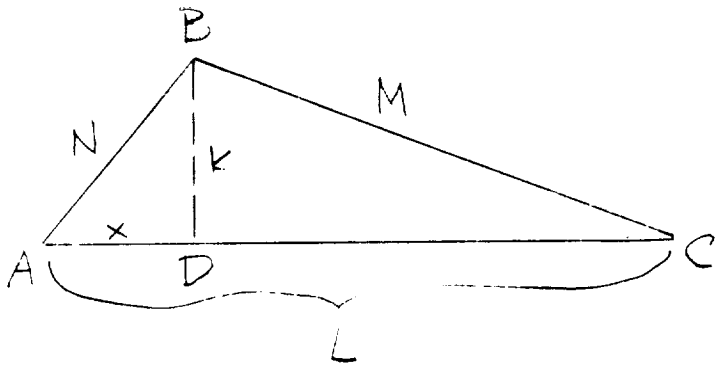

FIG. 25 - CHORD GEOMETRY

ORIGINAL PAGE IS
OF POOR QUALITY

$$N = 2 \sin \left(\frac{\gamma}{2}\right)$$

$$M = 2 \sin \left(\frac{\beta}{2}\right)$$

$$L = 2 \sin \left(\frac{\alpha}{2}\right)$$

The chords form the triangle ABC, in which K is the chord of the required angle (ν). By plane geometry,

$$K = \left[N^2 - \left(\frac{M^2 - L^2 - N^2}{-2L} \right)^2 \right]^{1/2}$$

$$\nu = 2 \sin^{-1} \frac{K}{2}$$

This equation has two solutions. The correct one is that which is closest to the coarse solution given by the IR sensors.

The reference direction in the horizontal plane just defined is given by the projection of the sun line on the plane. By reference to the sun's ephemeris and the satellite's ephemeris, the component of satellite orbital motion in the horizontal plane can be located. The yaw of the satellite is the angular difference between this component and the intersection of the vehicle spin plane with the horizontal plane.

The calculated yaw is used to ascertain the latitude and longitude of the horizon point. The pitch reference (sun sensor) is used to determine the difference between a pair of consecutive horizon measurements. Without a pitch reference, the radii to both horizons would have to be assumed equal. When the satellite has a dip (roll) with respect to the horizontal plane, the UV horizon sensor cuts the horizon at an angle and calculation of the horizon point location (in three dimensions) is made more difficult

than when there is no dip. Approximate equations have been programmed, for a fixed range angle to the horizon point.

More precise and inclusive equations are being added, which can be used in the operational system.

Determination of Sun-Line Vector

In the previous section, a method of determining the orientation of a vector with respect to the spin-axis/sun-line plane was described. The method requires, as input, the knowledge of the angles β and γ which are the angles from the vector to the sun-line and the vehicle spin axis, respectively. In order to orient the vector with respect to the local system, the location of the sun vector and the spin-axis/sun-line plane in that system must be known. This section describes the method for determining the orientation of the sun vector and the plane.

The sun vector is located by the system in terms of (1) its projection on the spin plane and (2) the aspect angle or angular distance out of the spin plane ϕ.

Sun Aspect Angle

The sun aspect angle can be determined by means of two sun sensors whose fields of view are ℓ° by m° where $\ell^\circ \gg m^\circ$ (Figure 56). The planes are oriented at right angles to each other with their intersection normal to the vehicle spin axis (Figure 57). As the vehicle spins, the sun describes a path across the sensors generating an electrical impulse in each. The time between impulses is Δt, which generates the angle $2\,\theta$ by multiplication with the spin rate ω.

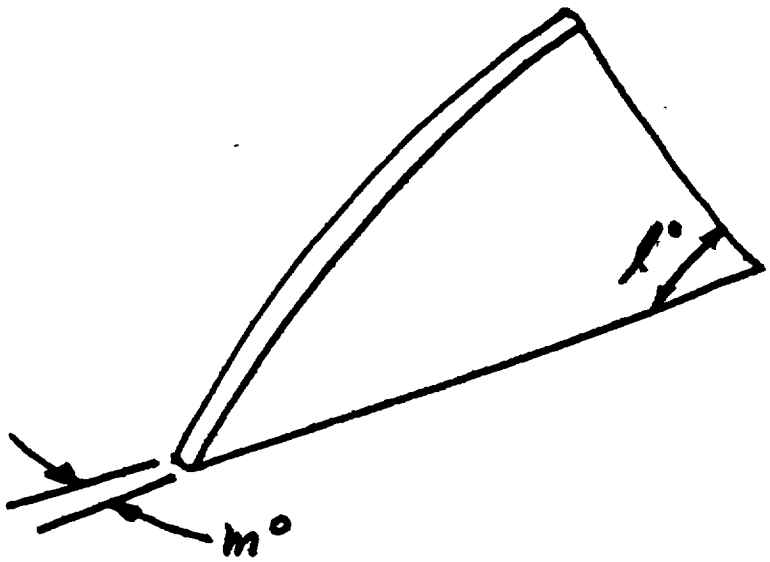

Figure 56. Sun Sensor Field of View

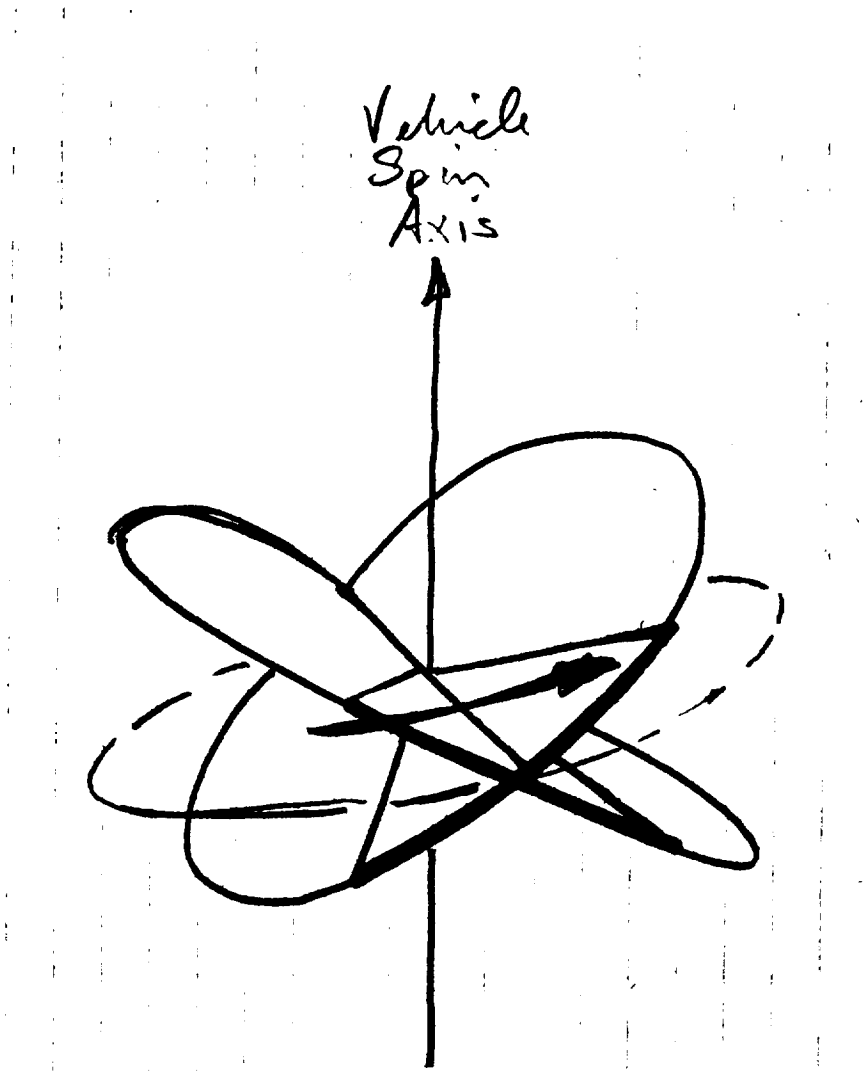

Figure 57. Orientation of Sun Sensor Planes

A unit vector through O (Figure 58) has components

$$X = \cos \delta$$
$$Y = -\sin \delta \sin \gamma \qquad (1)$$
$$Z = \sin \delta \cos \gamma$$

and

$$X = \cos \phi \cos \theta$$
$$Y = \cos \phi \sin \theta \qquad (2)$$
$$Z = \sin \phi$$

so that

$$\cos \delta = \cos \phi \cos \theta$$
$$-\sin \delta \sin \gamma = -\cos \phi \sin \theta \qquad (3)$$
$$\sin \delta \cos \gamma = \sin \phi$$

from which it follows that,

$$\tan \phi = \frac{\sin \theta}{\tan \gamma} \qquad (4)$$

which is sufficient as long as,

$$-90 \leq \phi \leq +90$$

The angle θ is 1/2 the product of the spin rate (ω) and the time (Δt) between sun signals from A and B. That is,

$$\theta = \frac{\omega \Delta t}{2} \qquad (5)$$

which identifies the location of the sun-line projection on the spin plane.

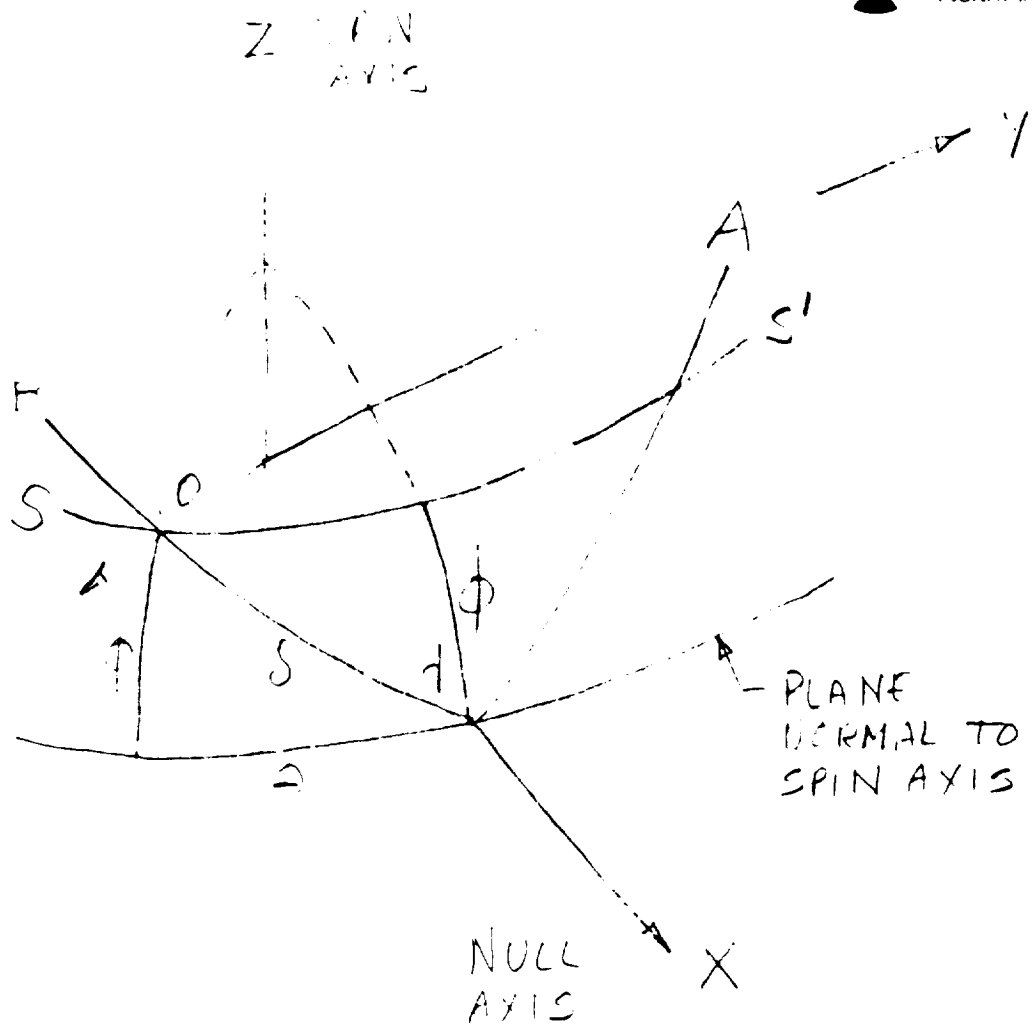

Figure 58. Sun Sensing Geometry

γ is the angle between the spin axis and the sensor planes A and B

SS' is the path of the sun line as it cuts the sensor planes due to the spin of the vehicle

ϕ is the aspect angle of the sun

θ is 1/2 the angle through which the vehicle spins between sun signals from planes A and B.

Determination of the Vehicle Spin Axis Vector

The orientation of the vehicle spin axis is defined by two angles, (1) yaw, or azimuth, and (2) dip angle or roll about the line of intersection between the spin plane and the horizontal plane. The equation for calculating dip angle is derived as follows. The calculated value of the dip angle is used in conjunction with the sensed sun data to determine the yaw of the satellite.

Dip Angle (ψ)

Assume an X' Y' Z' system with X' in the direction of motion and Y' along the spin vector of the satellite (Figure 59a). Let the angles ξ and ρ define the orientation of the coarse horizon sensor line of sight. Assume an XYZ system (Figure 59b) with X in the direction of motion and Y along the orbital spin axis. Let the vector to a horizon be defined by the angles σ and θ (the angle (θ - 90) is shown in the figure for clarity).

The line-of-sight vector has components:

$$X' = \cos \rho \sin \xi \tag{6}$$

$$Y' = \sin \rho \tag{7}$$

$$Z' = \cos \rho \cos \xi \tag{8}$$

and the horizon vector has components:

$$X = \cos (\theta-90) \cos \sigma \tag{9}$$

$$Y = \cos (\theta-90) \sin \sigma \tag{10}$$

$$Z = \sin (\theta-90) \tag{11}$$

and, due to the dip angle,

$$X = X' \tag{12}$$

$$Y = Y' \cos \psi - Z' \sin \psi \tag{13}$$

$$Z = Y' \sin \psi + Z' \cos \psi \tag{14}$$

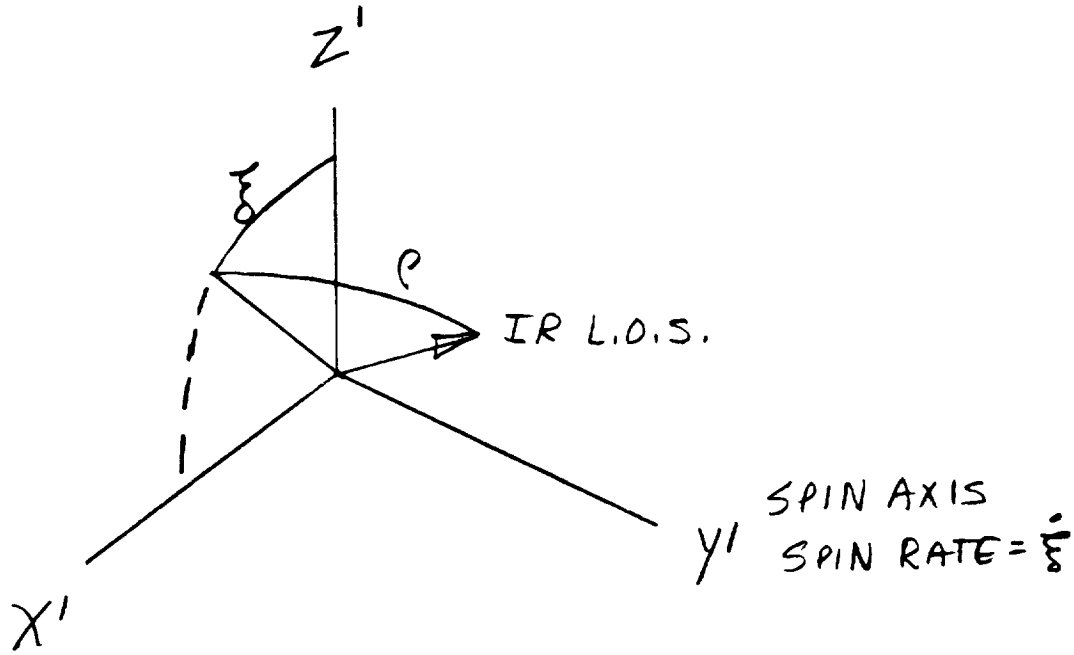

FIG. 59 a - BODY AXES, X'Y'Z'

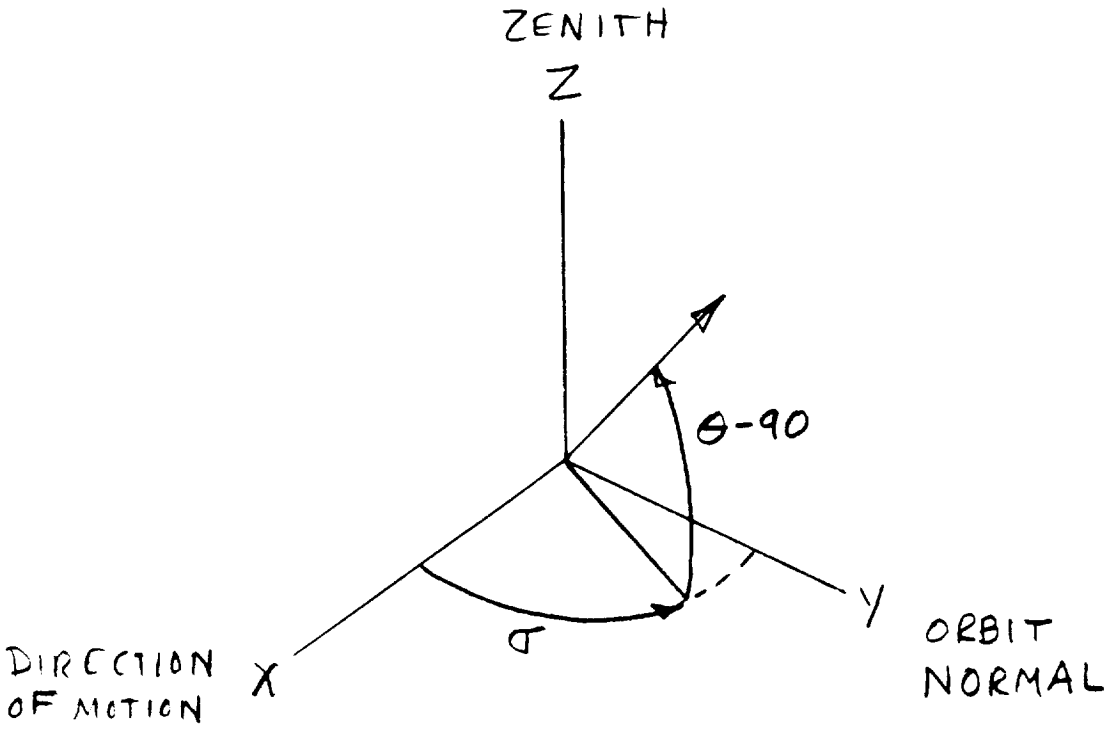

FIG. 59 b - LOCAL AXES, XYZ

When the horizon sensor line-of-sight encounters the horizon the aforementioned vectors are coincident.

Therefore,

$$X = \cos(\theta-90)\cos\sigma = \cos\rho\sin\xi \tag{15}$$

$$Y = \cos(\theta-90)\sin\sigma = \sin\rho\cos\psi - \cos\rho\cos\xi\sin\psi \tag{16}$$

$$Z = \sin(\theta-90) = \sin\rho\sin\psi + \cos\rho\cos\xi\cos\psi \tag{17}$$

or,

$$\sin\theta\cos\sigma = \cos\rho\sin\xi \tag{18}$$

$$\sin\theta\sin\sigma = \sin\rho\cos\psi - \cos\rho\cos\xi\sin\psi \tag{19}$$

$$-\cos\theta = \sin\rho\sin\psi + \cos\rho\cos\xi\cos\psi \tag{20}$$

The quantity θ can have values only between 0 and 90°, while the quantity ρ can lie between -90° and $+90^\circ$. For a pair of sensors canted at equal angles, $\rho_2 = -\rho_1$. For each value of ξ there are two values of ξ, such that,

$$\xi_{n+1} = 360 - \xi_n \tag{21}$$

Corresponding to ρ_1,

$$\xi_2 = 360 - \xi_1 \tag{22}$$

and corresponding to ρ_2,

$$\xi_4 = 360 - \xi_3 \tag{23}$$

so that four equations result from (20):

$$-\cos\theta = \sin\rho_1\sin\psi + \cos\rho_1\cos\xi_1\cos\psi \tag{24}$$

$$-\cos\theta = \sin\rho_1\sin\psi + \cos\rho_1\cos\xi_2\cos\psi \tag{25}$$

$$-\cos\theta = -\sin\rho_1\sin\psi + \cos\rho_1\cos\xi_3\cos\psi \tag{26}$$

$$-\cos\theta = -\sin\rho_1\sin\psi + \cos\rho_1\cos\xi_4\cos\psi \tag{27}$$

Solving one of the equations (24),

$$-\cos \xi_1 = \cos \theta \sec \rho_1 \sec \psi + \tan \rho_1 \tan \psi \qquad (28)$$

But since,

$$-\cos \xi_1 = \cos \frac{\xi_1 - \xi_2}{2} \qquad (28a)$$

equation (28) becomes,

$$\cos \frac{\xi_1 - \xi_2}{2} = \cos \theta \sec \rho_1 \sec \psi + \tan \rho_1 \tan \psi \qquad (29)$$

Also since

$$\xi_n = \dot{\xi} t_n$$

$$\cos \left[\frac{\dot{\xi}}{2} (t_1 - t_2) \right] = \cos \theta \sec \rho_1 \sec \psi + \tan \rho_1 \tan \psi \qquad (30)$$

which is in agreement with previous analyses.

Similarly it follows from (26) that:

$$\cos \left[\frac{\xi}{2} (t_3 - t_4) \right] = \cos \theta \sec \rho_1 \sec \psi - \tan \rho_1 \tan \psi \qquad (31)$$

Subtracting (31) from (30) results in:

$$\tan \psi = \left[\frac{1}{2} \cot \rho_1 \right] \left[\cos \left[\frac{\xi}{2}(t_1 - t_2) \right] - \cos \left[\frac{\xi}{2}(t_3 - t_4) \right] \right] \qquad (32)$$

The dip angle ψ is always in the first or fourth quadrant and, therefore, is sufficiently defined by (32).

Yaw Calculation

The foregoing sections showed how the sun sensor and the IR horizon sensors can be used to provide a reference frame in which to measure the

horizon height. The orientation of the reference frame can be conveniently described in terms of the yaw angle and the dip angle of the spin axis. The calculation of dip angle has already been described. This section describes the calculation of the yaw angle. The yaw angle is derived by combining the equations describing the sun's known position in local coordinates with those which describe it according to the sun sensor data. This is done by means of the transformation matrices presented in a subsequent section on system error magnitudes. The equations for yaw angle are

$$\sin \alpha = \frac{f_a - dc}{f_b - ec} \tag{33}$$

$$\cos \alpha = \frac{ea - db}{ce - f_b} \tag{34}$$

where

$$a = X_{2s} \cos \theta_H + Z_{2s} \sin \theta_H \tag{35}$$

$$b = Y_s \tag{36}$$

$$c = X_s \tag{37}$$

$$d = Y_{2s} - Z_s \sin \beta \tag{38}$$

$$e = -X_s \cos \beta \tag{39}$$

$$f = Y_s \cos \beta \tag{40}$$

and

X_{2s}, Y_{2s}, Z_{2s} are the components of the sun vector in the vehicle system.

X_s, Y_s, Z_s are the components of the sun vector in the local system.

β is the dip angle.

θ_H is the pitch angle at which the horizon is encountered.

System Data Flow and Operational Plan

The foregoing section described functionally how the proposed system provides the required output data. This section presents a logical data flow diagram, showing the interrelation of the system elements and functions, essentially a concise summary of the proposed system.

A preliminary data flow diagram of the proposed system is presented in Figure 60. The operational plan of the experiment, as far as it has been developed, is summarized below.

1. Vehicle spins nominally around axis normal to scan plane. Successive encounters of sun on the same sun sensor half-plane establishes spin rate.
2. Presence of sun in plane containing spin axis is sensed.
3. UV senses one horizon then the other, indicating time difference between sun sensing and horizon sensings. From this data and knowledge of relative orientation of UV and sun sensor axes in the vehicle, the angles between sun-sensing and horizon sensings are computed.
4. MW senses vertical for the same orbital point to which UV sightings correspond. Recording the time of MW vertical indicates angle between sun and the indicated vertical, measured in scan plane, which is nominally vertical.
5. IR sensors sense both horizons. Times are used to determine average roll angle existing during horizon measurements.
6. Sensed sun position is compared with ephemeris sun position, accounting for vehicle roll, and vehicle azimuth is determined.

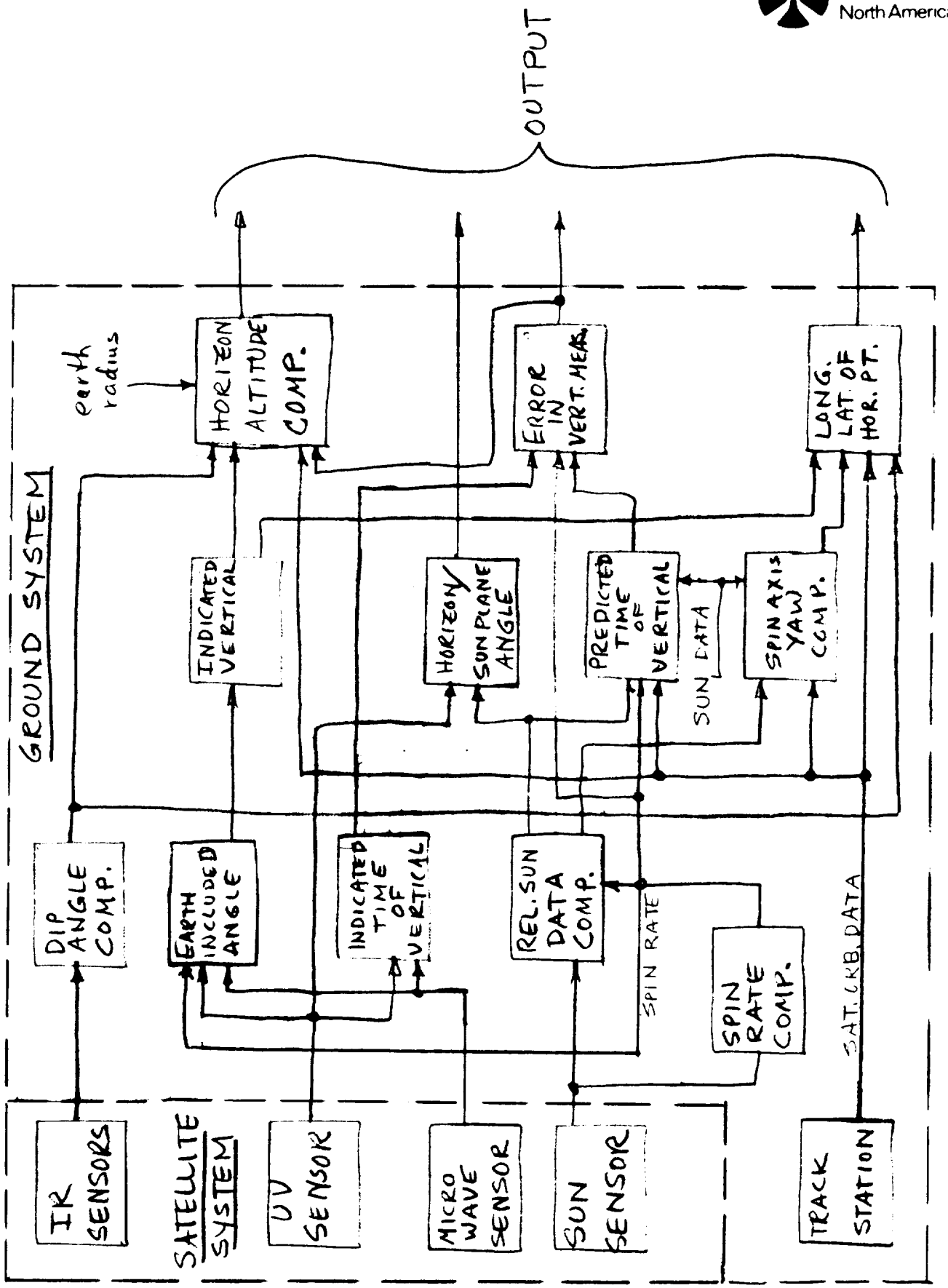

FIG. 60 - EXPERIMENT DATA FLOW DIAGRAM

7. From the above, the angles from the vertical to the horizons are determined and the altitudes and locations of the horizon points are determined.
8. Vectors to the midpoints between the horizons are determined and compared with the theoretical ephemeris vertical.

Horizon Sensor Synthesis Program

A program has been written which computes the approximate latitude, longitude, and altitude of the horizon point for any satellite position and orientation of the line-of-sight. This program as designed primarily to generate the horizon point maps and was used to determine the sensitivity of the horizon point measurement to various error sources (such as satellite position, orbit parameters, and pointing angles). However, the range angle to the horizon point does not vary with roll angle as it should for correct assessment of roll error sensitivity.

Program Description

There are basically two versions of the program. In one version, the azimuth of the line-of-sight can be selected as an input, and the two angles by which the sun sensor will identify the location of the sun will be outputs. In another version, these two angles θ_{sm} and ϕ_{sm} are inputs so that they may be perturbed, and the effect, observed. In both versions the spacecraft position can be incremented automatically through the orbit.

Figure 61 is a sample output of the program, and Table 10 is a key to the heading names. The first line of headings is the input line; the second is the output line. The first output line of data is separated from the input line of data by a double space. The output lines represent 10° increments in orbital position, but orbital position is not printed in the output.

OMGS	INCL	NODE	F	H	BET	THH	ALFA
LATSAT	THSM	PHISM	DLHP	LATHP	LTHP	HHP	TIME
.00001	100	180	.00001	600	.00001	31	.00001
0.0000	59.0000	-0.0000	-5.9566	30.4784	23.602	22.9558	0.000
9.8465	49.0000	-0.0000	-6.8302	40.2476	23.427	22.9558	0.023
19.6835	38.9999	-0.0000	-8.4866	49.9372	23.193	22.9558	0.046
29.4987	28.9999	-0.0000	-11.6691	59.4665	22.840	22.9558	0.069
39.2734	18.9999	-0.0000	-18.4722	68.6154	22.215	22.9558	0.093

FIG 61

Space Division
North American Rockwell

TABLE 10. KEY TO PROGRAM HEADINGS

Input

OMGS	Celestial longitude of sun (measured in ecliptic plane from first point of aries, with earth as center).
INCL	Orbit inclination.
NODE	Right ascension of ascending node.
F	Orbital position of satellite from ascending node.
H	Satellite orbital altitude.
BET	Dip angle.
THH	Pitch angle to horizon.
ALFA	Yaw of vehicle spin axis.

Output

LATSAT	Satellite latitude.
THSM	Clock angle of sun from horizon point (in scan plane).
PHISM	Out-of-plane angle of sun.
DLHP	Longitude difference from satellite to horizon point.
LATHP	Latitude of horizon point.
LTHP	Local time at the horizon point.
HHP	Altitude of the horizon point.
TIME	Orbital time in days.

The initial orbital position is input as F, which in the example is approximately zero. An alternate version of the program has sun zenith angle as an output.

In the present configuration of the computer program, the depression angle (θ_H), measured in the scan plane from the horizontal plane to the UV line of sight when it is on the horizon, is an input. Consequently, when a dip angle is inserted, the horizon point will shoft but the line of sight will still be constrained to the original value of θ_H which is now measured in a tilted plane. This is not the way the system would actually behave. The line of sight would seek the horizon and change the value of θ_H to the extent necessary. If the dip angle is known, the degree of change in θ_H can be predicted and no error need result. However, if the dip angle is undetected, the difference in θ_H manifests itself as a horizon error (in altitude, longitude and latitude). The program is being changed to make the actual depression of the horizon from the horizontal an input (P_H), and the value of θ_H necessary to achieve it, an output.

The attitude error can be expressed as follows (Figure 62):

$$\Delta h = \theta_H - P_H \tag{41}$$

where

$$P_H = \cos^{-1}\left[\frac{H_{HP} + R}{R + h_s}\right] \qquad 0 \leq P_H \leq 90 \tag{42}$$

$$\theta_H = \sin^{-1}\left[\frac{\sin P_H}{\cos \beta}\right] \qquad 0 \leq \theta_H \leq 90 \tag{43}$$

P_H IS ACTUAL DEPRESSION ANGLE OF HORIZON

θ_H IS MEASURED DEPRESSION ANGLE

β IS UNDETECTED ROLL OF SATELLITE

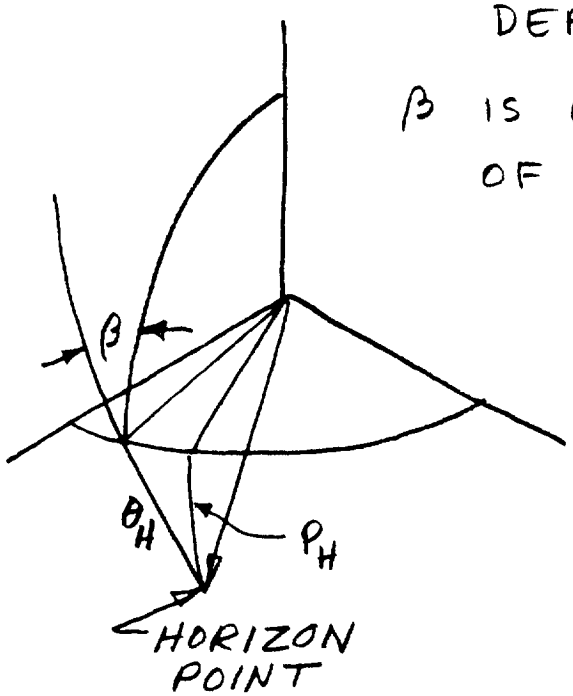

FIG. 62 - EFFECT OF UNDETECTED ROLL OF SATELLITE ON HORIZON POINT MEASUREMENT

Figure 63 is a graph of the error in pitch angle of the horizon due to the dip angle. If the vehicle dip angle is set to zero with an uncertainty of 0.5°, the error in the horizon altitude measurement at the satellite will be about 5 sec of arc. If the dip angle is 3° the error would be 171 seconds if uncorrected. If corrected, using perfect knowledge of the dip angle, the horizon error would be zero. However, if the dip angle were measured as 3 deg and there were a 0.5° uncertainty, the net error in the horizon attitude determination could be 61 seconds, which is objectionable. It appears, therefore, that a substantial reduction in probable error would result from adopting a nominal dip angle of zero.

Error Sensitivities

The components, functions, and operation of the proposed system have been described. This section describes the sensitivity of the output data to error in measurements as related to the orbit parameters, position in orbit, and the time of year. Actual error magnitudes are not considered. Those are contained in the section devoted to the error budget.

The direction of the local vertical and the height of the horizons could be determined using only horizon sensors. One earth centerline lies midway between the horizons indicated by any of the horizon sensors; and the orthogonal centerline is indicated by the assymetry of the scan patterns of the two auxiliary sensors. The sun, however, provides a reference for comparison, in the following way. If the position of the satellite is known, the correct elevation of the sun from the nadir $(90 + \beta)$ and the correct sun zenith angle (ϕ) can be calculated. The error in the horizon system can be found by measuring the angle swept through by the vehicle between the sensed vertical and a plane containing the sun, and comparing this with the reference value (Figure 64).

Figure 63 HORIZON ERROR AT SATELLITE

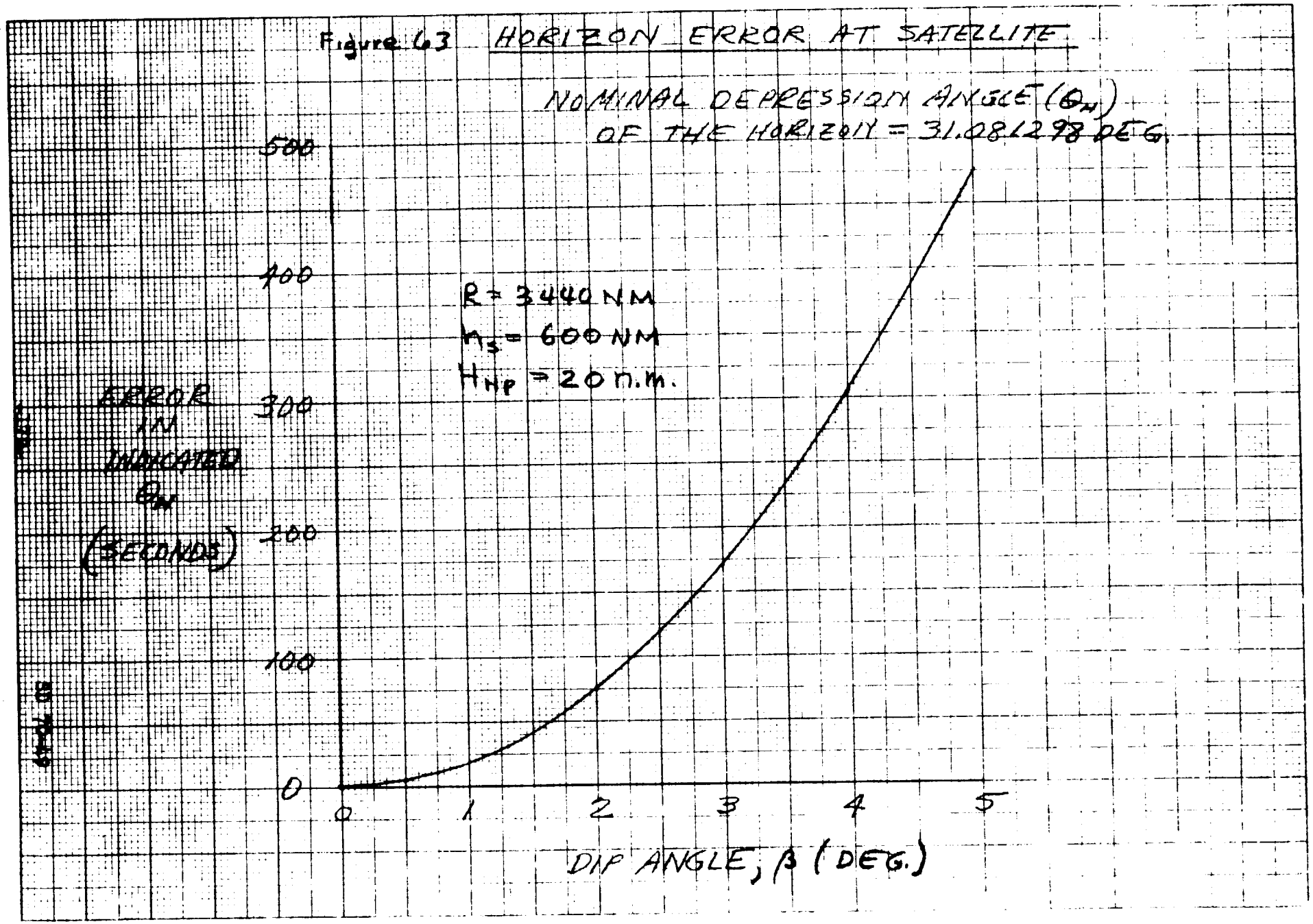

The use of the sun for this purpose is most effective when the line from the satellite to the sun is normal to the spin axis of the vehicle. Since it is desirable, for several other reasons, for the spin axis to be normal to the orbit plane, it follows that the sun should be in the orbit plane or close to it. The elevation of the sun in this plane is not critical as far as this consideration is concerned. However, for the purposes of determining azimuth (which is necessary for calculating the latitude and longitude of the tangent point) the elevation of the sun above the horizontal plane should be small. The accuracy of the azimuth determination, however, is not required to be very high.

The effects of sun position (relative to the satellite) on the accuracy of principal measurements in the experiment are discussed below.

Pitch Sensitivity to Sun Position

The accuracy of measurement of the angle from the sun's projection in the scan plane to the horizon depends on the angle ϕ between the plane and a line to the sun. In Figure 64 the sun's position is described in terms of azimuth and elevation (α and β) at the satellite and the instrument angles (ξ and ϕ) at the satellite. An error in ξ is propagated directly as an error in the critical measurement. The sensitivity of ξ to azimuth (α) errors and elevation errors (β) in sighting on the sun is derived below.

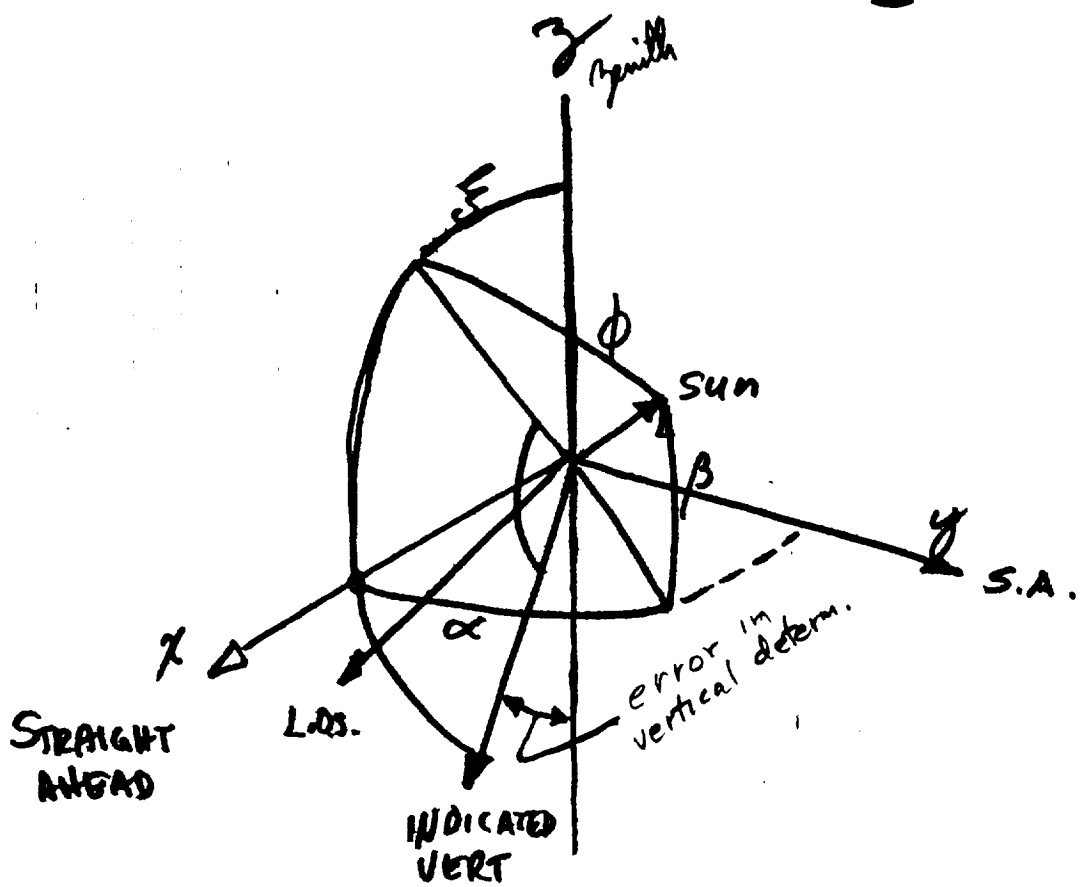

Fig 64 - Angles Defining Sun's Position

From Figure 64,

$$\cos\beta\cos\alpha = \cos\phi\sin\xi$$
$$\cos\beta\sin\alpha = \sin\phi \qquad (44)$$
$$\sin\beta = \cos\phi\cos\xi$$

Thus,

$$\phi = \sin^{-1}(\cos\beta\sin\alpha) \qquad -90 < \phi < 90 \qquad (45)$$

Also,

$$\sin\xi = \frac{\cos\beta\cos\alpha}{\cos\phi} \qquad (46)$$

and

$$\cos\xi = \frac{\sin\beta}{\cos\phi} \qquad (47)$$

Combining (46) and (47),

$$\tan \xi = \frac{\cos \beta \cos \alpha}{\sin \beta} \tag{48}$$

or

$$\tan \xi = \frac{\cos \alpha}{\tan \beta} \tag{49}$$

which relates the sun azimuth and elevation to the pitch reference plane. Differentiating (49),

$$\partial \tan \xi = \sec^2 \xi \, \partial \xi = \frac{-\sin \alpha \; \partial \alpha}{\tan \beta} \tag{50}$$

from which,

$$\frac{\partial \xi}{\partial \alpha} = \frac{-\sin \alpha}{\tan \beta \sec^2 \xi} = \frac{-\sin \alpha \cos^2 \xi}{\tan \beta} \tag{51}$$

But

$$\cos^2 \xi = \frac{\sin^2 \beta}{\cos^2 \phi} \tag{52}$$

$$\cos \phi = (1 - \sin^2 \phi)^{1/2} \tag{53}$$

$$\sin^2 \phi = \cos^2 \beta \sin^2 \alpha \tag{54}$$

$$\cos \phi = (1 - \cos^2 \beta \sin^2 \alpha)^{1/2} \tag{55}$$

Therefore,

$$\cos^2 \xi = \frac{\sin^2 \beta}{1 - \cos^2 \beta \sin^2 \alpha} \tag{56}$$

Combining (56) and (51), the sensitivity of the pitch measurement to errors in sun azimuth is,

$$\frac{\partial \xi}{\partial \alpha} = \frac{-\sin \alpha \sin^2 \beta}{\tan \beta \, (1 - \cos^2 \beta \sin^2 \alpha)} \tag{57}$$

The sensitivity to sun elevation is obtained by differentiating (49) with respect to β,

$$\partial \tan \xi = \sec^2 \xi \, \partial \xi = (\cos \alpha)(-\csc^2 \beta) \tag{58}$$

$$\frac{\partial \xi}{\partial \beta} = \frac{-\csc^2 \beta \cos \alpha}{\sec^2 \xi} \tag{59}$$

$$\sec^2 \xi = \frac{1 - \cos^2 \beta \sin^2 \alpha}{\sin^2 \beta} \tag{60}$$

$$\frac{\partial \xi}{\partial \beta} = \frac{-\cos \alpha}{1 - \cos^2 \beta \sin^2 \alpha} \tag{61}$$

Therefore the sensitivity to error in sun elevation is,

$$\frac{\partial \xi}{\partial \beta} = \frac{-\cos \alpha}{1 - \cos^2 \beta \sin^2 \alpha} \tag{62}$$

From the above equations, it can be seen that a small value of α results in low sensitivity of the critical measurement to errors in sighting the sun.

Yaw Error Sensitivity to Sun Position

The determination of the yaw angle is affected by the accuracy with which the sun angles θ and ϕ are measured, as follows.

$$\sin \xi = \frac{\cos \alpha \cos \beta}{\cos \phi} \tag{63}$$

where

$$\cos \beta = \frac{\sin \phi}{\sin \alpha} \tag{64}$$

Thus,

$$\sin \xi = \frac{\cos \alpha \sin \phi}{\cos \phi \sin \alpha} = \cot \alpha \tan \phi \tag{65}$$

and

$$\cot \alpha = \frac{\sin \xi}{\tan \phi} \tag{66}$$

Differentiating,

$$-\csc^2 \alpha \partial \alpha = \frac{\cos \xi}{\tan \phi} \partial \xi \tag{67}$$

from which,

$$\frac{\partial \alpha}{\partial \xi} = \frac{\cos \xi}{-\csc^2 \alpha \tan \phi} = \frac{\cos \xi \sin^2 \alpha}{-\tan \phi} \tag{68}$$

But

$$\sin^2 \alpha = \frac{\sin^2 \phi}{1 - \cos^2 \phi \cos^2 \xi} \tag{69}$$

so that,

$$\frac{\partial \alpha}{\partial \xi} = \frac{\cos \xi}{-\tan \phi} \left[\frac{\sin^2 \phi}{1 - \cos^2 \phi \cos^2 \xi} \right] \tag{70}$$

Therefore, the sensitivity of the azimuth determination to pitch error is,

$$\frac{\partial \alpha}{\partial \xi} = \frac{-\cos \xi \sin^2 \phi}{\tan \phi \, (1 - \cos^2 \phi \cos^2 \xi)} \tag{71}$$

From this equation it is seen that pitch error affects the measurement of azimuth most seriously when $\xi \approx 0$.

The sensitivity of the azimuth computation to error in the aspect angle ϕ is derived as follows:

$$\cot \alpha = \frac{\sin \xi}{\tan \phi} = \sin \xi \cot \phi \tag{72}$$

$$-\csc^2 \alpha \partial \alpha = \sin \xi \, (-\csc^2 \phi \, \partial \phi) \tag{73}$$

$$\frac{\partial \alpha}{\partial \phi} = \frac{\sin \xi \csc^2 \phi}{\csc^2 \alpha} = \sin \xi \csc^2 \phi \sin^2 \alpha \tag{74}$$

$$\frac{\partial \alpha}{\partial \phi} = \frac{\sin \xi}{1 - \cos^2 \phi \cos^2 \xi} \tag{75}$$

$$\frac{\partial \alpha}{\partial \phi} = \frac{\sin \xi}{1 - \cos^2 \phi \cos \xi} \tag{76}$$

From this equation it is seen that error in ϕ affects the azimuth measurement most at large values of ξ.

Since the main horizon sensor provides data in a single plane its accuracy can be evaluated most satisfactorily by having the sun in or near that plane. Vertical sensing errors in the orthogonal plane contributed to the coarse horizon sensors will have a relatively small effect on this evaluation.

Aspect Angle Error Sensitivity

In order to calculate the aspect angle accurately, it is necessary to have accurate knowledge of the vehicle spin rate and the time interval between sun pips. The sensitivity of the aspect angle determination to error in both of these is given below. Substituting, in the equation for aspect angle, the relationship,

$$\theta = \frac{\omega \Delta t}{2}$$

results in,

$$\tan \phi = \frac{\sin \left(\frac{\omega \Delta t}{2}\right)}{\tan \gamma} \tag{77}$$

Differentiating with respect to ω,

$$\frac{\partial \phi}{\partial \omega} = \frac{\Delta t \cos \left(\frac{\omega \Delta t}{2}\right)}{2 \tan \gamma \sec^2 \phi} \tag{78}$$

and with respect to the time interval,

$$\frac{\partial \phi}{\partial \Delta t} = \frac{\omega \cos\left(\frac{\omega \Delta t}{2}\right)}{2 \tan \gamma \sec^2 \phi} \tag{79}$$

The spin rate is related to the spin period by

$$\omega = \frac{360}{T} \tag{80}$$

Differentiating with respect to T,

$$\frac{\partial \omega}{\partial T} = -\frac{360}{T^2} \tag{81}$$

Therefore the sensitivity of ϕ to error in period measurement is,

$$\frac{\partial \phi}{\partial T} = -\frac{360}{T^2}\left[\frac{\Delta t \cos\left(\frac{\omega \Delta t}{2}\right)}{2 \tan \gamma \sec^2 \phi}\right]$$

$$= -\frac{\omega^2}{360}\left[\frac{\Delta t \cos\left(\frac{\omega \Delta t}{2}\right)}{2 \tan \gamma \sec^2 \phi}\right] \tag{82}$$

Sensor Orientation Recommendations

In the previous section, the sensitivity of the output data to errors in input data was discussed. The time delay between measurements, however, was not considered directly. Changes in vehicle position and attitude during such time intervals, of course, does contribute to system error. An arrangement of sensors has been designed to minimize such time lapses without creating a lopsided data schedule or unreasonable vehicle mass distribution (Figure 65).

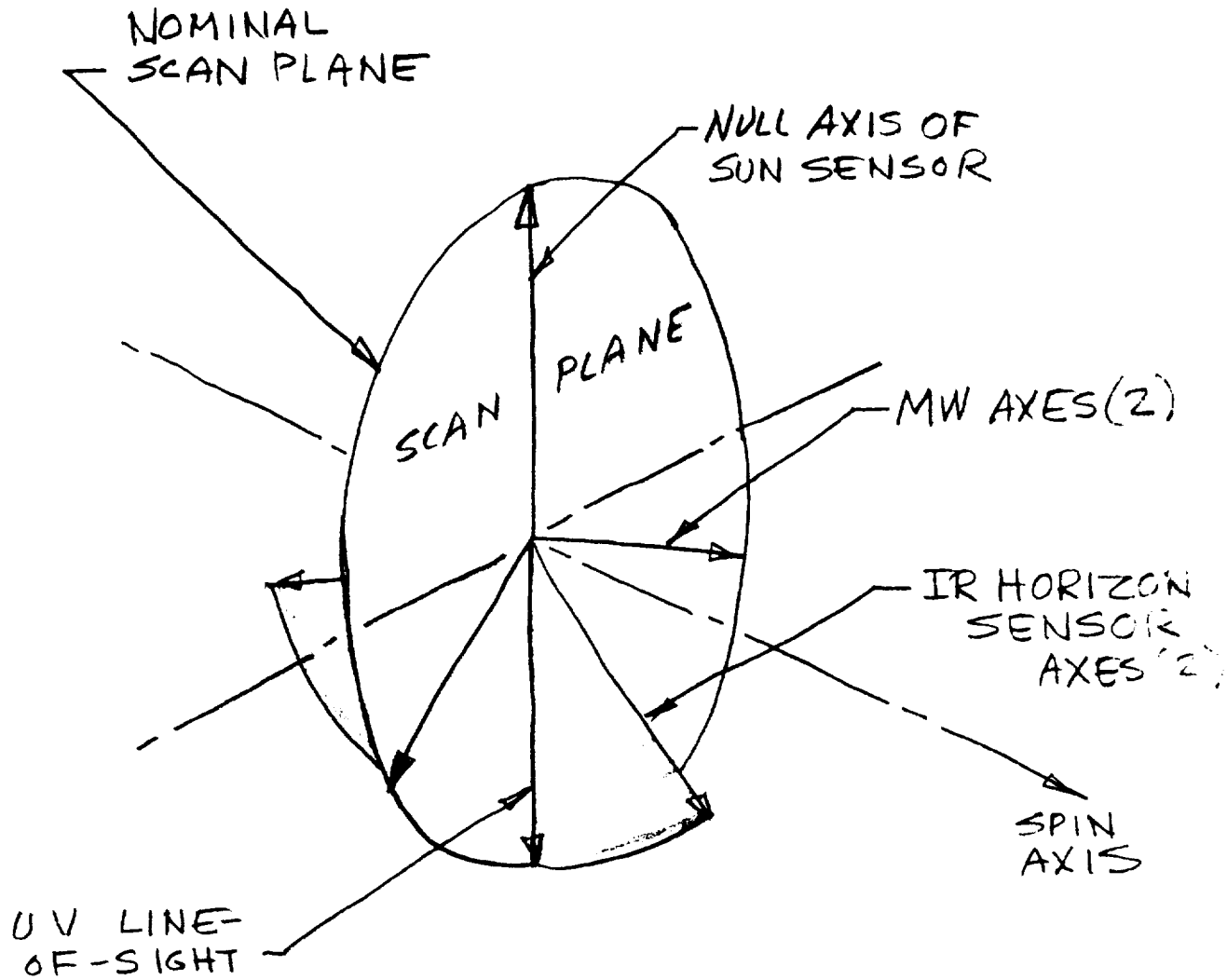

FIG. 65 - RECOMMENDED ORIENTATION OF SENSOR AXES

In this arrangement, the IR sensors provide dip-angle data corresponding to the exact time for which the experimental sensors provide local vertical information. The IR sensor axes are co-planar with the UV axis and the spin axis. The plane so defined bisects the angle between the MW horn axes. The sun sensor null axis lies in the same plane, but is oriented opposite to the direction of the UV line-of-sight. The sun elevation angle varies throughout the orbit; therefore, the (time) spacing between acquisition of sun data and other data cannot be controlled by selecting sun sensor orientation. Justification for the selected orientation of the sun sensor lies in the fact that the error effect is equal for both fore and aft horizon observations. This is true also if the null axis points in the same direction as the UV axis. However, such an arrangement increases the error and appears to aggravate the packaging problem.

In the proposed arrangement, the vertical indications of both experimental sensors (UV and MW) correspond to the same instant of time, or position in orbit, so that they may be compared and/or combined. Also the IR sensors provide roll data for the instant for which the horizons are measured.

It is recommended that the arrangement of Figure 65 be adhered to as closely as possible within the constraints of good packaging practices.

Spin Axis Misalignment

The previous error discussion indicated the sensitivity of the system to errors inherent in the instruments, such as the sun sensors, the IR horizon sensors, and the satellite tracking equipment. Errors must also be attributed to misalignment of the axes within the satellite and misalignment of the vehicle with respect to the spin axis in space. The magnitudes of the errors caused by these misalignments vary as the satellite translates and rotates. Equations and procedures for determining how these errors propagate in time have been developed and are being programmed. Neglecting

perturbing torques, the precise orientation of any axis in the satellite can be calculated in closed form for any given point in time. However, in the presence of disturbing torques the equations describing vehicle attitude must be numerically integrated over the time period of interest. The latter equations are presented and discussed in the System Analysis Section. The closed form solution is presented below.

Closed Form Solution of Vehicle Attitude vs. Time

A program is being written which will compute the instantaneous orientation of all vehicle axis of interest for any time in order for any given spin rate and inertial orientation of the spin axis. The equations have been written and the coding is in process. The need for such a program became evident during the horizon sensor satellite study. In the proposed satellite system, the misalignment of the vehicle spin axis with respect to the real spin axis in space is not sensed nor compensated for. This program provides a means of estimating the effect of such a misalignment as the satellite progresses in its orbit neglecting disturbance torques. The program also will compute the instantaneous local coordinate system orientation and the nominal vehicle orientation.

Key Equations

Assuming that the satellite rotates at constant speed about an arbitrary axis that is fixed in space, (Figure 66) and initially displaced from the vehicle system by the angles R and S, it is seen that unit vectors along the vehicle axes X'Y'Z' describe cones about the Y axis. The spin vector includes applied spin plus that due to orbital motion. The conical motion may be readily integrated and compared with the integrated motion of a vehicle without misalignment. The result is a running record of the attitude deviations due to the misalignment.

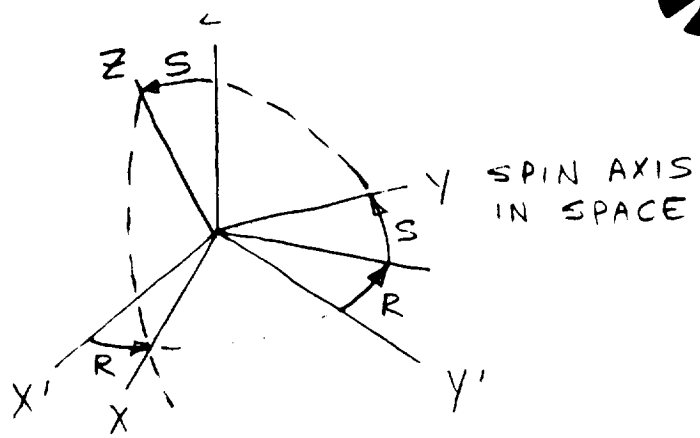

Figure 66. Displacement of Vehicle System From Real Spin Axis

The direction cosines of the moving axes on the fixed axes are as follows:

		Moving Axes X'	Moving Axes Y'	Moving Axes Z'
Fixed Axes	X	$r \cos Q$	$\sin \psi \cos \nu$	$\cos S \sin \omega t$
	Y	$-\cos S \sin R$	$\cos \psi$	$\sin S$
	Z	$r \sin Q$	$-\sin \psi \sin \nu$	$\cos S \cos \omega t$

where

$$\nu = \nu_o + \omega t$$

$$\cos \nu_o = \sin R / \sin \psi$$

$$\psi = \cos - 1 (\cos R \cos S)$$

and

$$Q = Q_o - \omega t$$

$$r = \sqrt{\cos^2 R + \sin^2 R \sin^2 S}$$

$$\sin Q_o = \frac{\sin R \sin S}{r}$$

$$\cos Q_o = \frac{\cos R}{r}$$

For the case of zero misalignment, the values of R and S are set to zero, and the same spin rate is assumed.

A third set of coordinate axes may be set in motion about the Y axis to represent the local coordinate system. The spin of this system is equal to the orbital rate, and the spin vector is aligned with the X axis, except in the case of a sun-synchronous orbit, when the precession rate of approximately .985 deg/day is added vectorially.

By combining the instantaneous data pertaining to the appropriate pair of systems, it is possible to determine all necessary information; for example,

a) the instantaneous misalignment of the axes from their nominal position.

b) the instantaneous nominal position with respect to the local coordinate system.

In the following discussion the expressions for quantities of general interest are given in terms of the inertial system X Y Z. Nomenclature is as in Table 11.

TABLE 11 - COORDINATE SYSTEMS

Coordinate System	Unit Vectors
Local Space	X_o Y_o Z_o
Aligned Vehicle	X_r Y_r Z_r
Misaligned Vehicle	X_p Y_p Z_p

Thus, for example, the X component of Y_o would be X_{Yo}.

Of principal importance are the three attitude quantities roll (or dip), azimuth, and pitch, defined in Figure 67 as β, α, and P_H, respectively. These quantities are determined from knowledge of the components of the vectors, as shown in Table 12.

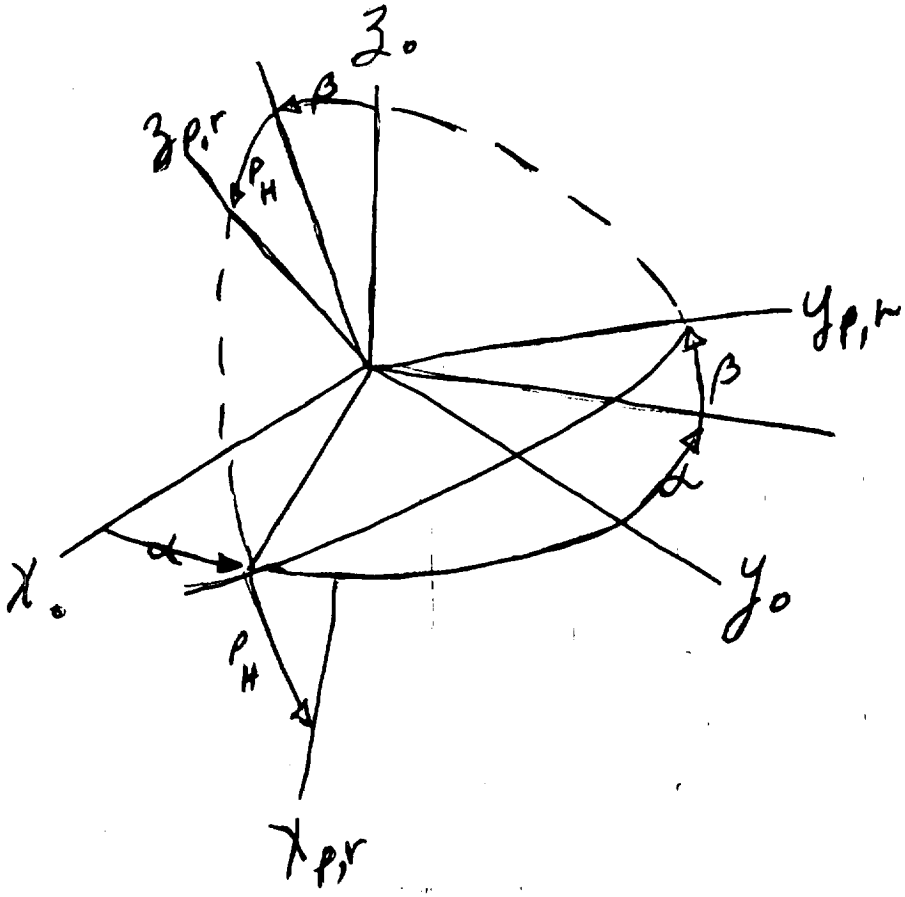

X_o Y_o Z_o are local coordinates

X_o in orbit plane and horizontal in the direction of motion

Y_o normal to orbit plane

Z_o vertical upward

$(XYZ)_{p,r}$ are satellite body axes misaligned (p) and aligned (r).

FIGURE 67

Coordinate Systems

TABLE 12. PRINCIPAL ATTITUDE QUANTITIES

Symbol	Name	Equation	Description
β	roll (dip)	$\beta = \sin^{-1} Z_{Y_o}$	perpendicular distance from X_o Y_o plane to Y axis
α	azimuth	$\alpha = \sin^{-1} \left[\frac{X_{Y_o}}{(X_{Y_o}^2 + Y_{Y_o}^2)^{1/2}} \right]$	angle CCW from Y_o axis to projection of Y on X_o Y_o plane
P_H	pitch	$P_H = \cos^{-1} (J \cdot X)$	angle CCW about Y axis from horizontal plane to X axis

The inclination of all three body axes to the zenith is easily obtained from the direction cosines of their unit vectors on the Z_o axis.

The aforementioned data can also be obtained for axes on the vehicle which are not aligned with the body axes X Y Z, but whose orientation with resepct to them is defined by a set of angles. Each angle may have a known part and an unknown part, or uncertainty.

System Error Magnitudes

The purpose of the attitude determination system is to locate the unique point at which the UV and MW horizon sensors indicate the earth's limbs. The required accuracy for locating this point is 1 km measured along the earth's radius to the point of tangency. The proposed system consists of a fine sun sensor and a V-head IR horizon sensor. A block diagram of this system is shown in Figure 68. The sun sensor line of sight lies in the spin plane. The sun sensor reticle is in the form of

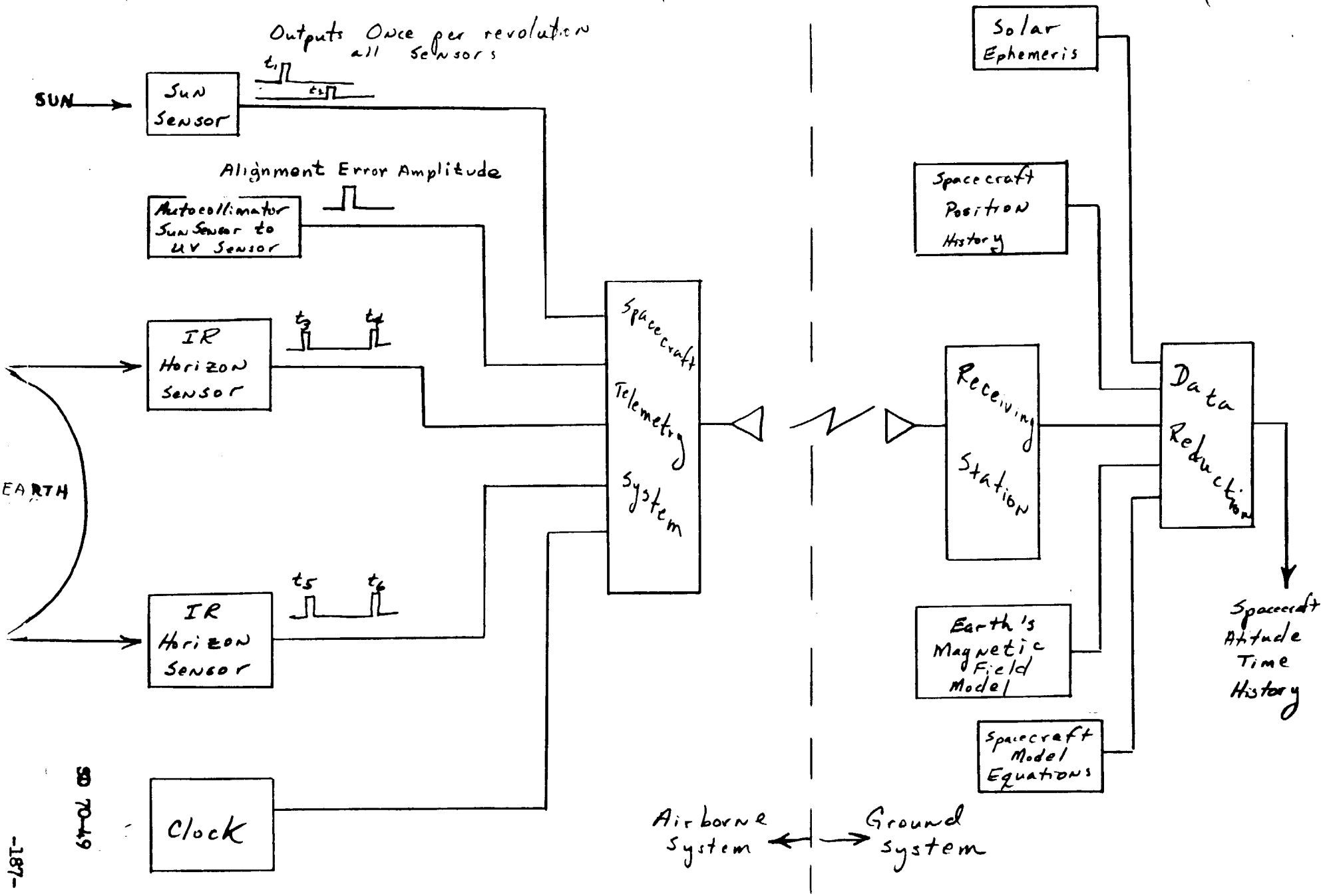

Figure 68 Block Diagram of Reference Attitude Determination System

an X. As the vehicle rotates, the sun is scanned across this reticle. As the sun crosses each side of the X, a time hack is recorded. The vector to the sun can be determined from these two time measurements. In the V-head horizon sensor, two IR earth horizon crossing indicators are utilized. Each IR sensor is mounted at 30° to the spin plane. As the vehicle rotates, the line of sight of both sensors is scanned across the earth. A time hack is generated as each sensor crosses the earth's limbs. By comparing the times generated by one sensor to the times generated by the other sensor, it is possible to determine the vector to the local vertical.

An extensive effort is required to completely analyze the motion, torques, and filtering techniques that come into play in determining the attitudes. A set of equations that describe spacecraft motions in a dynamic environment is provided in this report, but the magnitude of the job of modeling and analyzing the problem in depth is beyond the scope of this study. The approach taken to evaluate the reference system was to model a static condition of the spacecraft and exercise one variable at a time, examining its effect on the indicated tangent height. Each of the error sources is discussed in the subsequent error analysis section of this report. An examination of these errors shows that the direct output data is marginal for providing 1 km altitude information unless the dip angle is kept to 2° of less. The accuracy deteriorates when the sun is out of the plane or not visible, but can be improved by modeling vehicle motions and curve-fitting data points. The error magnitudes contributed by the IR sensors and the minitrack-STADAN orbit determination appear to be the most significant. From the analysis performed to date, it appears that a precise sun sensor (10-15 sec) working with a $.5^{\circ}$ IR horizon sensor local vertical reference system can provide 1 km altitude resolution.

Since the referenced concept is based on a noon orbit, the sun is never more than 7° from the orbit plane. A tradeoff study showed that a star mapping technique working in conjunction with the precise sun sensor will provide much improved accuracy. A preliminary analysis of the problem indicates that the star mapper need operate only on the dark side of the earth, and the sun would provide sufficient up-date due to its favorable location with respect to the orbit plane.

It would be necessary to develop a complete free-body model of the spacecraft, its motions, associated torques, and their relationships to inertial space, in order to make a rigorous analysis of the accuracy of either the sun-IR system or the sun-star mapper system.

System Analysis

The spacecraft reference concept for the UV and MW experiment is a spinning spacecraft in a sun-synchronous circular orbit at 600 n.mi. altitude whose spin axis is normal to the orbit plane. For a rolling wheel in space the following differential equations describe its rotary motion in the presence of torques:

$$\dot{W}_x = W_y W_z \left(1 - \frac{I_z}{I_y}\right) + \tau_x \frac{I_y}{I_x}$$

$$\dot{W}_y = W_x W_z \left(\frac{I_z}{I_y} - \frac{I_x}{I_y}\right) + \tau_y$$

$$\dot{W}_z = W_x W_y \left(\frac{I_x}{I_y} - 1\right) + \tau_z \frac{I_y}{I_z}$$

$$\dot{\psi} = \left[W_z \cos\theta - W_x \sin\theta\right] \frac{1}{\cos\phi}$$

$$\dot{\phi} = W_x \cos\theta + W_z \sin\theta$$

$$\dot{\theta} = W_y - \dot{\psi} \sin\phi,$$

where:

W_x, W_y, W_z	=	Vehicle angular rates along the principal body axes.
τ_x, τ_y, τ_z	=	Disturbing torques divided by I_y.
I_x, I_y, I_z	=	The spacecraft moments of inertia measured along the principal body axes.
ψ, ϕ, θ	=	Euler angles relating the principal axes to inertial space.

If a sensor on this rolling wheel senses the vector to a celestial body (Star, Sun, Moon, Earth, Planets), the vector, S, can be expressed in terms of direction cosines with respect to inertial space (Figure 69):

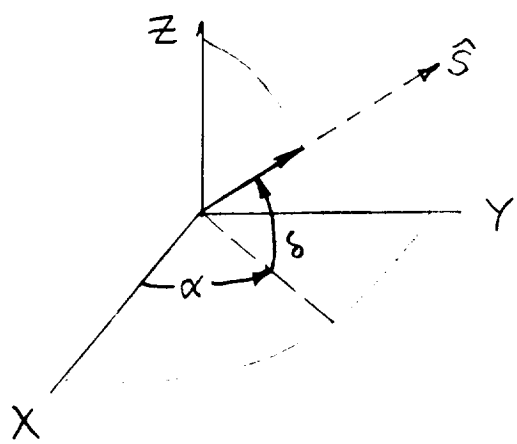

$$S = \begin{bmatrix} \cos\delta \cos\alpha \\ \cos\delta \sin\alpha \\ \sin\delta \end{bmatrix}$$

Figure 69. Sun Orientation

The vector S in inertial coordinates can be transformed through the transformation matrix E (ψ , ϕ, θ) where

$$S_B = E\, S_I$$

and

$$E = \begin{bmatrix} (\cos\theta\cos\psi - \sin\theta\sin\phi\sin\psi) & (\cos\theta\sin\psi + \sin\theta\sin\phi\cos\psi) & -\sin\theta\cos\phi \\ -\cos\psi\sin\psi & \cos\phi\cos\theta & \sin\phi \\ (\cos\theta\cos\psi + \cos\theta\sin\phi\sin\psi) & (\sin\theta\sin\psi = \cos\theta\sin\phi\cos\psi) & \cos\theta\cos\phi \end{bmatrix}$$

Ignoring other coordinate transformations such as a possible misalignment between the UV and MW experiment coordinates and the principal body coordinates, this set of equations relates the celestial sighting to the spacecraft coordinate system.

If the only spacecraft motion is W_y ($W_x = W_z = 0$) and if no other torques affect the vehicle (τ_x, τ_y, $\tau_z = 0$), then the motion equations reduce to

$$\theta = W_y - \psi \sin\phi$$

These are the assumptions made in the analysis on Appendix B to the statement of work.

The basic sources of unwanted torque acting on the spacecraft are:

- Solar pressure
- Aerodynamic pressure
- Gravity gradient
- Meteoroid disturbances
- Vehicle outgassing
- Magnetic interaction
  - a. Eddy current
  - b. Residual magnetic moment

An analysis of these forces was made on a vehicle in a 500 n.mi. orbit on the Horizon Definition Study under Contract NAS1-6010. The study showed that all of these forces except the Magnetic Interaction were small and could be neglected. It is reasonable to extrapolate this report and assume that the only external force that needs to be modeled for the UV-MW experiment is the magnetic interactions. The equations for the magnetic interaction would be as follows:

$$\tau_x = B_z \frac{M_y}{I_2} - By \frac{M_z}{I_2} + \frac{K}{I_2} \left[B_x(B_y W_y + B_z W_z) - W_x B_y^2 + B_z^2 \right]$$

$$\tau_y = B_z \frac{M_z}{I_2} - B_z \frac{M_x}{I_2} + \frac{K}{I_2} \left[B_y (B_x W_x + B_z W_z) - W_y (B_x^2 + B_z^2) \right]$$

$$\tau_z = B_y \frac{M_x}{I_2} - B_x \frac{M_y}{I_2} + \frac{K}{I_2} \left[B_z (B_x W_x + B_y W_y) - W_z (B_x^2 + B_y^2) \right]$$

Where:

M_x, M_y, M_z	=	Magnetic Moment Coefficients
K	=	Eddy current coefficient
B_x, B_y, B_z	=	Earth's magnetic field components in the satellite body coordinates

It can be seen that these forces can be large enough to introduce undesirable perturbations to the spacecraft motion. The presence of these torques and the initial torques of separation necessitate the use of a system to control satellite attitude. An estimate of the degree to which the attitude (primarily dip angle) must be controlled is indicated in the subsequent discussion of system error.

The error sensitivities were determined by synthesizing the system computations and varying the input quantities in small increments. The mathematical relationships used to synthesize the system are presented below.

The principal coordinate systems are shown in Figure 70. The angles relating the coordinate systems are shown in Figure 71, and the transformation matrices are presented in Table 13. The position of the sun relative to the earth in the ecliptic plane is transformed into the roll/yaw system (x, y, z); and the angles at which the sun is sensed are transformed into the same system. Roll is known from the dip angle solution, so that yaw and pitch can easily be calculated. The position of the sun in the ecliptic and in the body system are, respectively,

$$x_E = \sin \omega_s$$

$$y_E = 0$$

$$z_E = \cos \omega_s$$

and

$$x_2 = \cos \phi_{sm} \cos \theta_{sm}$$

$$y_2 = \sin \phi_{sm}$$

$$z_2 = -\cos \phi_{sm} \theta_{sm}$$

The pitch angle at which the horizon is sensed determines the angular displacement, or great circle distance, from the satellite to the horizon point. This quantity combined with the spacecraft position and the azimuth of the line of sight (yaw) identifies the geographic location of the horizon point. The satellite altitude and the pitch angle of the horizon sensor combine to define the horizon point altitude.

FIG. 70, Principal Coordinate Systems

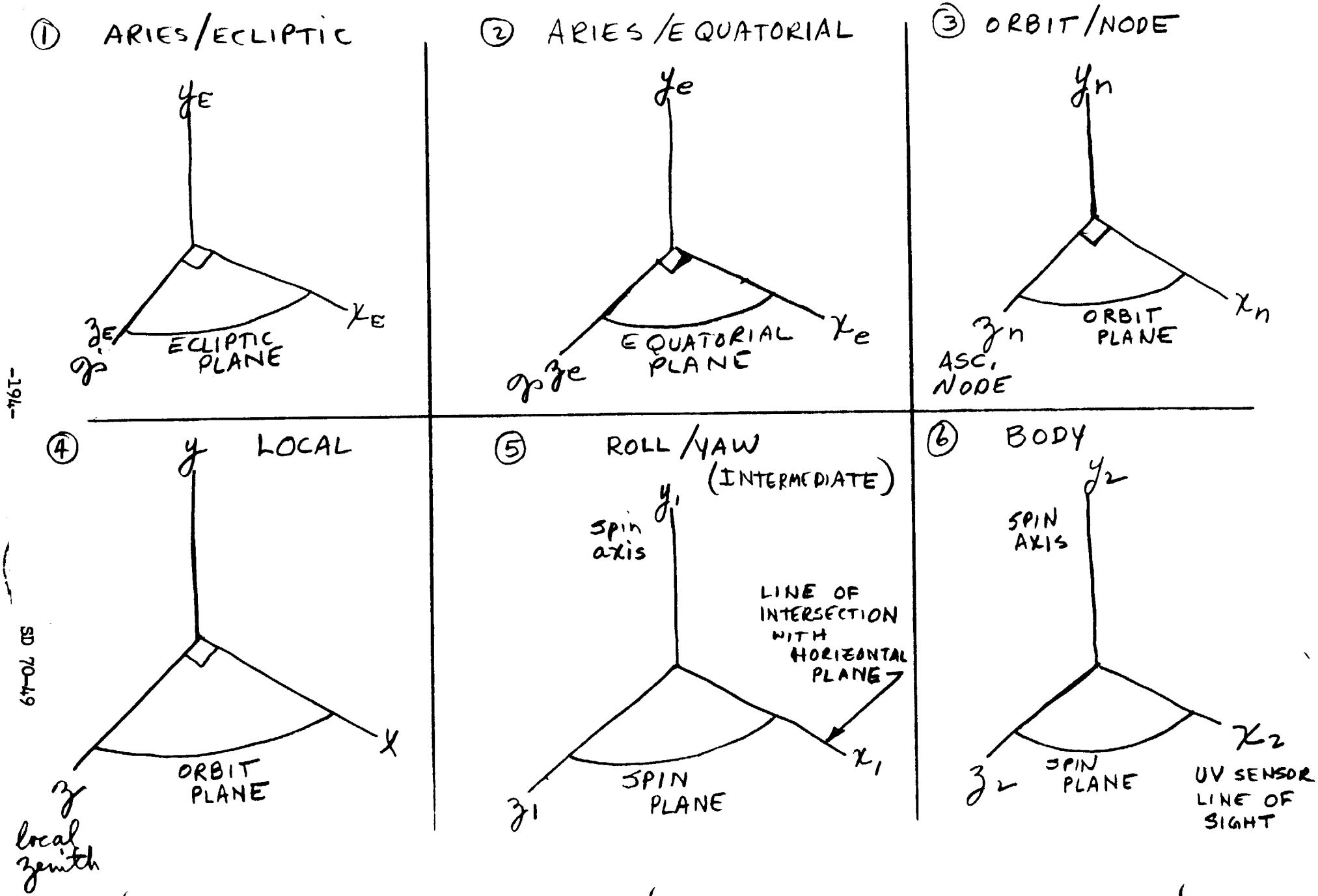

FIG 71, ANGLES BETWEEN COORDINATE SYSTEMS

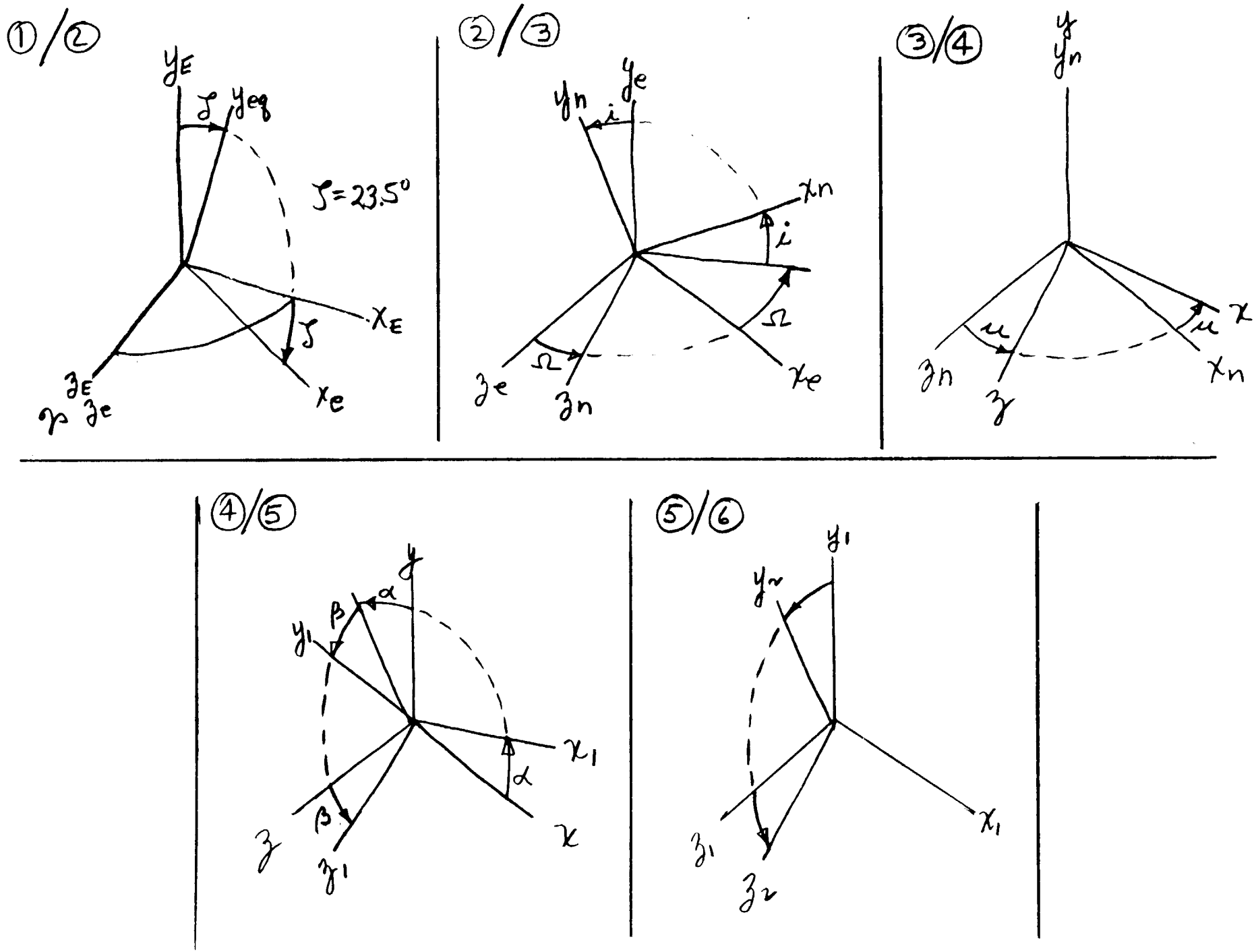

TABLE 13

TRANSFORMATION MATRICES

M_1

$$\begin{vmatrix} x_E \\ y_E \\ z_E \end{vmatrix} = \begin{vmatrix} \cos\zeta & \sin\zeta & 0 \\ -\sin\zeta & \cos\zeta & 0 \\ 0 & 0 & 1 \end{vmatrix} \begin{vmatrix} x_e \\ y_e \\ z_e \end{vmatrix}$$

M_2

$$\begin{vmatrix} x_e \\ y_e \\ z_e \end{vmatrix} = \begin{vmatrix} \cos\zeta & -\sin\zeta & 0 \\ \sin\zeta & \cos\zeta & 0 \\ 0 & 0 & 1 \end{vmatrix} \begin{vmatrix} x_E \\ y_e \\ z_E \end{vmatrix}$$

M_3

$$\begin{vmatrix} x_e \\ y_e \\ z_e \end{vmatrix} = \begin{vmatrix} \cos i \cos\Omega & -\sin i \cos\Omega & \sin\Omega \\ \sin i & \cos i & 0 \\ -\cos i \sin\Omega & \sin i \sin\Omega & \cos\Omega \end{vmatrix} \begin{vmatrix} x_n \\ y_n \\ z_n \end{vmatrix}$$

M_4

$$\begin{vmatrix} x_n \\ y_n \\ z_n \end{vmatrix} = \begin{vmatrix} \cos i \cos\Omega & \sin i & -\cos i \sin\Omega \\ -\sin i \cos\Omega & \cos i & \sin i \sin\Omega \\ \sin\Omega & 0 & \cos\Omega \end{vmatrix} \begin{vmatrix} x_e \\ y_e \\ z_e \end{vmatrix}$$

M_5

$$\begin{vmatrix} x_n \\ y_n \\ z_n \end{vmatrix} = \begin{vmatrix} \cos u & 0 & \sin u \\ 0 & 1 & 0 \\ -\sin u & 0 & \cos u \end{vmatrix} \begin{vmatrix} x \\ y \\ z \end{vmatrix}$$

M_6

$$\begin{vmatrix} x \\ y \\ z \end{vmatrix} = \begin{vmatrix} \cos u & 0 & -\sin u \\ 0 & 1 & 0 \\ \sin u & 0 & \cos u \end{vmatrix} \begin{vmatrix} x_n \\ \\ z_n \end{vmatrix}$$

M_7

$$\begin{vmatrix} x \\ y \\ z \end{vmatrix} = \begin{vmatrix} \cos\alpha & -\cos\beta \sin\alpha & \sin\beta \sin\alpha \\ \sin\alpha & \cos\beta \cos\alpha & -\sin\beta \cos\alpha \\ 0 & \sin\beta & \cos\beta \end{vmatrix} \begin{vmatrix} x_1 \\ y_1 \\ z_1 \end{vmatrix}$$

M_8

$$\begin{vmatrix} x_1 \\ y_1 \\ z_1 \end{vmatrix} = \begin{vmatrix} \cos\alpha & \sin\alpha & 0 \\ -\cos\beta \sin\alpha & \cos\beta \cos\alpha & \sin\beta \\ \sin\beta \sin\alpha & -\sin\beta \cos\alpha & \cos\beta \end{vmatrix} \begin{vmatrix} x \\ y \\ z \end{vmatrix}$$

M_9

$$\begin{vmatrix} x_1 \\ y_1 \\ z_1 \end{vmatrix} = \begin{vmatrix} \cos\theta_H & 0 & \sin\theta_H \\ 0 & 1 & 0 \\ -\sin\theta_H & 0 & \cos\theta_H \end{vmatrix} \begin{vmatrix} x_2 \\ \\ z_2 \end{vmatrix}$$

M_{10}

$$\begin{vmatrix} x_2 \\ y_2 \\ z_2 \end{vmatrix} = \begin{vmatrix} \cos\theta_H & 0 & -\sin\theta_H \\ 0 & 1 & 0 \\ \sin\theta_H & 0 & \cos\theta_H \end{vmatrix} \begin{vmatrix} x_1 \\ y_1 \\ z_1 \end{vmatrix}$$

Space Division
North American Rockwell

The aforementioned relationships were programmed on a computer, and error sensitivities were determined for various cases in the range of expected orbital parameters. The values of the sun angles were inserted as angles rather than derived from time values as would be done in the real system. The equations relating the angles to time were later derived and are being added to the program. Also, the computer calculation of error due to inserted values of dip angle is misleading as it contains a fixed value of the scan-plane angle to the horizon point. This is an unrealistic case as described previously in the Error Sensitivity section. The equations of that section are therefore used in the subsequent analysis of dip angle effects.

Figure 72 is the computer printout for the case where the spin axis is normal to the orbit plane and the sun is seven degrees out of the orbit plane. Computed data were based perturbation of the inputs of this case.

Error Analysis

Error Contributions

For a satellite altitude of 600 n.mi. and a horizon altitude of 20 n.mi the range from satellite to horizon point is 2086 n.mi. or 3863 km. The line of sight to the horizon is approximately 31.1° below the horizontal plane. Under these conditions a 1 km altitude error corresponds to approximately 53.4 sec of arc at the satellite. Reference to the horizon error graph in the previous discussion of the system synthesis (Figure 63) shows that a roll uncertainty of .5 when a dip andlg of 2 degrees or more is measured can result in an error of at least 45 seconds or .842 km. Therefore, it appears that allowing too great a dip angle can in itself cause a prohibitive error in horizon altitude.

Figure 73 shows the altitude error due to dip angle uncertainty for various measured values of dip angle. For a given horizon error, the larger dip angle uncertainties (due to IR measurement inaccuracy or spin axis misalignment) require smaller values of allowable dip angle, and consequently more frequent attitude correction.

The computer program (containing the static model) was employed to generate error data for the proposed system. Errors in the sun position determination, the dip angle and the satellite position were included. The estimated horizon altitude errors due to these and other sources are listed in Table 14 as follows:

TABLE 14. ERROR CONTRIBUTIONS TO HORIZON POINT ALTITUDE DETERMINATION

Sun Pitch (clock) Angle	.3 km
Sun Azimuth (Cone) Angle	.1 km
IR dip angle measurement*	.85 km
Orbit Determination - Minitrack	.5 km
S/C Data Processing	.1 km
Sun Ephemeris and Ground Reduction	.2 km
Timing	.1 km

*Assuming a $.5^{\circ}$ uncertainty and an allowable dip angle of 2°.

The RSS value of these is approximately 1.06 km. This error varies with the sun angle to the orbit plane and with the azimuth angle to the sun during the experiment. With reasonable care in instrument design and selection of data - taking times in the orbit the error can be reduced from this value.

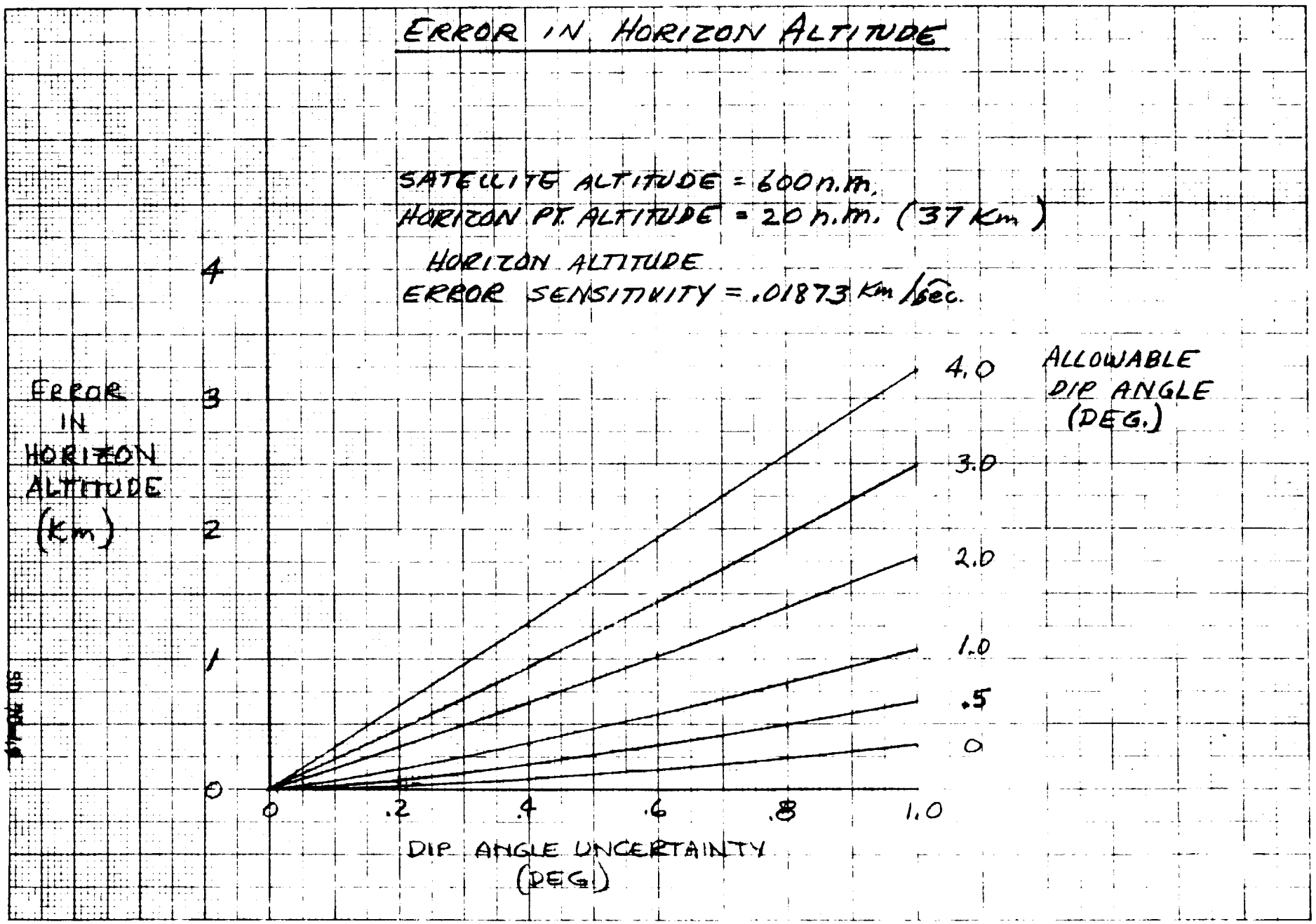
ERROR IN HORIZON ALTITUDE
SATELLITE ALTITUDE = 600 n.m.
HORIZON PT. ALTITUDE = 20 n.m. (37 Km)
HORIZON ALTITUDE ERROR SENSITIVITY = .01873 Km/sec.
ERROR IN HORIZON ALTITUDE (Km)
0
1
2
3
4
0
.2
.4
.6
.8
1.0
DIP ANGLE UNCERTAINTY (DEG.)
4.0
3.0
2.0
1.0
.5
0
ALLOWABLE DIP ANGLE (DEG.)

Fig. 73

The orbit determination error is based on Minitrack capabilities of 100 meters altitude, 300 meters in track, and 700 meters cross track accuracy. Improved accuracy could be obtained through the use of the Manned Space Flight Tracking Network or through the use of laser tracking which GSFC states is presently being accomplished. Either of these techniques is stated to provide better than 50 feet tracking accuracy. This would reduce the orbit determination error to less than 0.1 km.

The error associated with the spacecraft data processing is the accuracy with which a pulse output can be sensed and recorded. This error is tied to the timing error which is the accuracy with which the clock time can be read and correlated to the occurrence of a separate event such as the sun crossing a reticle in the sun sensor. The sun emphemeris is based on the accuracy estimate of present knowledge of the sun-earth relationship and the ability to accurately program this knowledge into the ground computer.

Sun Angle Error

Two angles are measured with respect to the sun, the clock sun angle and the sun azimuth angle. The sun clock angle is defined to be in the plane normal to the spin axis. It is the angle between the sun vector and the UV horizon vector projected in the spin plane (Figure 74).

The sun clock angle is a function of the time of sun sighting to the time of UV or MW horizon sensor sighting the earth's limb. To evaluate this error all other parameters were held constant and the sun clock angle error was evaluated with a variation of 0.004° to $.010^{\circ}$ (15 sec to 36 sec). The resultant tangent height error is shown in Figure 75 .

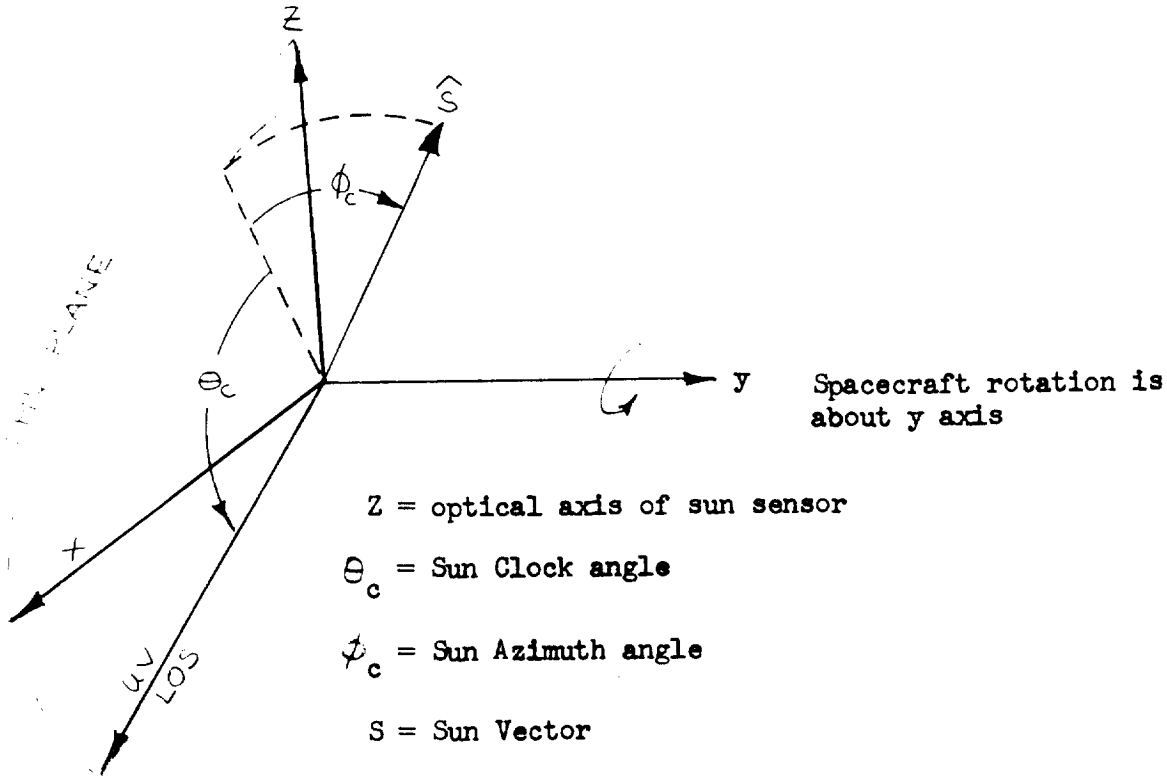

Figure 74. Sensor Axis Lines of Sight

K+E 10 X 10 TO ½ INCH 46 1323
7 X 10 INCHES MADE IN U.S.A.
KEUFFEL & ESSER CO.

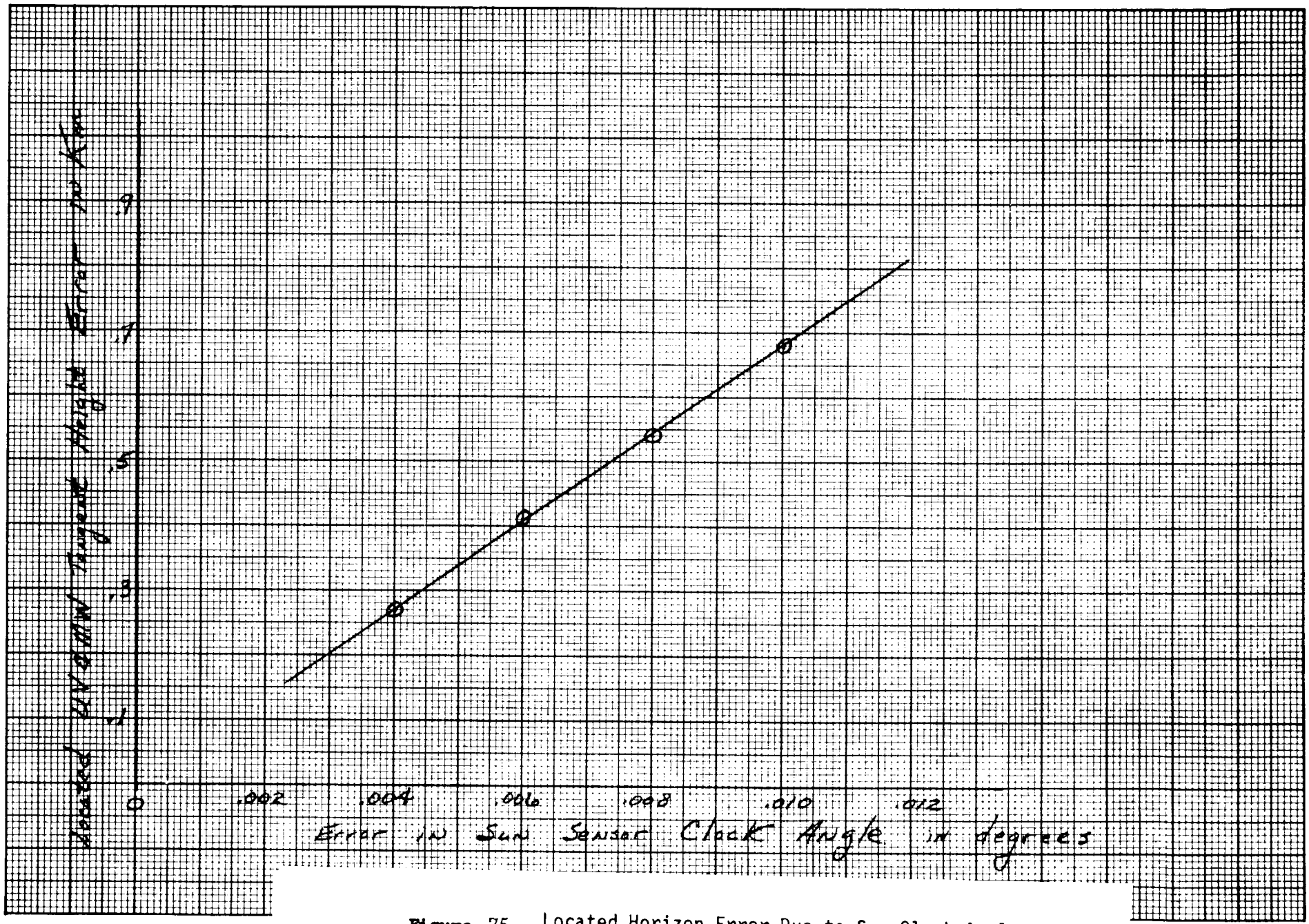

Figure 75 Located Horizon Error Due to Sun Clock Angle

Any single measurement of the sun clock angle will be influenced by the following error sources in Table 15,

TABLE 15. ERROR CONTRIBUTORS

TO SUN ANGLE DETERMINATION

Sun Sensor Accuracy	15 $\widehat{\text{sec}}$
UV to Sun Sensor Alignment	3 $\widehat{\text{sec}}$
Timing	3 $\widehat{\text{sec}}$
S/C Data Processing	3 $\widehat{\text{sec}}$
Sun Ephemeris	3 $\widehat{\text{sec}}$
Spin Rate Degradation	Neglible
Vehicle Motion	Neglible

An RSS evaluation of which shows:

$$\Delta \theta_c = \sqrt{15^2 + 3^2 + 3^2 + 3^2 + 3^2} \simeq 16.2 \text{ sec} = .0042^\circ$$

From Figure 75 it can be seen that the expected tangent height error due to the clock sun angle would be approximately .28 km.

The sun azimuth angle is a measure of the angle between the sun vector and its projection in the spin plane. The effect on the UV-MW experiment located tangent height by the accuracy of this measurement is related to the spacecraft's location in orbit. Figure 76 is a plot of the sunlight portion of the orbit showing the error in located tangent height for a .01 degree and .005 degree error in measuring the sun azimuth angle (which is actually a measure of yaw). The sun sensor measures this angle to 0.005 degrees and the indicated tangent height error is less than 0.1 km.

Local Vertical Measurement

The error in measuring the local vertical is directly related to the horizon sensor accuracy. If each horizon sensor is accurate to 1/2 degree, then the accuracy with which local vertical to be measured can be approximateed by the RSS error of the horizon crossing. A system having 1/2 degree horizon sensors can locate the local vertical to an accuracy of approximately 0.7 degree. It has been shown that by working in the 14-16 μ CO_2 band it is possible to obtain very good local vertical knowledge; and for the purposes of this study it was assumed that local vertical could be determined by the horizon sensors to 0.5 degree. It is possible that by doing some ground interpretation of the data and updating the data based on time of year and location of horizon crossing on the earth's surface, an accuracy of 0.2 to 0.3 deg can be realized.

Sun Sensor Error Functions - Approximate Analysis

The foregoing analysis adopted a single characteristic error for the sun sensing system. This discussion describes the magnification of the error in the sun-sensor as the out-of-plane angle of the sun increases and as the misalignment between the real spin axis and the vehicle spin axis (normal to scan plane) increases. The error magnification is shown to be small within the range represented by a noon orbit and a 2° maximum spin axis dip angle. The cross-axis sun-sensing system was assumed to have a minimum error of 10 sec at its null point. The determination of the error equation and the resulting data are given below. It should be noted that the error considered is purely the pointing error. Timing errors are not considered.

Assuming that the sensitive planes A and B of the crossed-axis sun-sensing system are inclined by angles $\pm\gamma$ to the spin axis (Figure 77) and a line to the sun is inclined to the spin axis by the angle $(90 - \phi)$,

$$\sin\delta = \frac{\sin\phi}{\cos\gamma}$$

It is assumed that the sensing error of either plane varies inversely as the cosine of δ ; that is,

$$\Sigma = \frac{\Sigma_o}{\cos\delta} = \frac{\Sigma_o}{\left(1 - \frac{\sin^2\phi}{\cos^2\gamma}\right)^{1/2}}$$

becoming infinite when $\phi = \gamma$. As the vehicle spins, the line to the sun describes a cone of half angle $(90 - \phi)^\circ$. If the plane inclination angle (γ) is greater than this half angle, the rays of sun will never fall on the sensors at all. Theoretically, when $(90 - \phi) = \gamma$ the sun will not cut across the sensor, but will move along its edge. Therefore, in the region where $(90 - \phi) \simeq \gamma$, the accuracy of the sensor would be relatively poor. The error in determining the position of the sun on the scan plane is shown in Figure 78 as a function of the out-of-plane angle (ϕ) for a minimum error (Σ_o) of 10 arc sec and a plane inclination of 45°. Figure 78 indicates that the error magnification is relatively small for $-30^\circ \leq \phi \geq +30^\circ$.

The foregoing analysis pertains to a system in which the intersection of the sun-sensitive planes of the sun-sensors lay in the scan plane (90° to the spin axis). It was shown that when the sun line was within an angle γ of the spin axis, the sun would not be sensed and thus would be useless in determining the accuracy of the horizon measurement. In addition, when

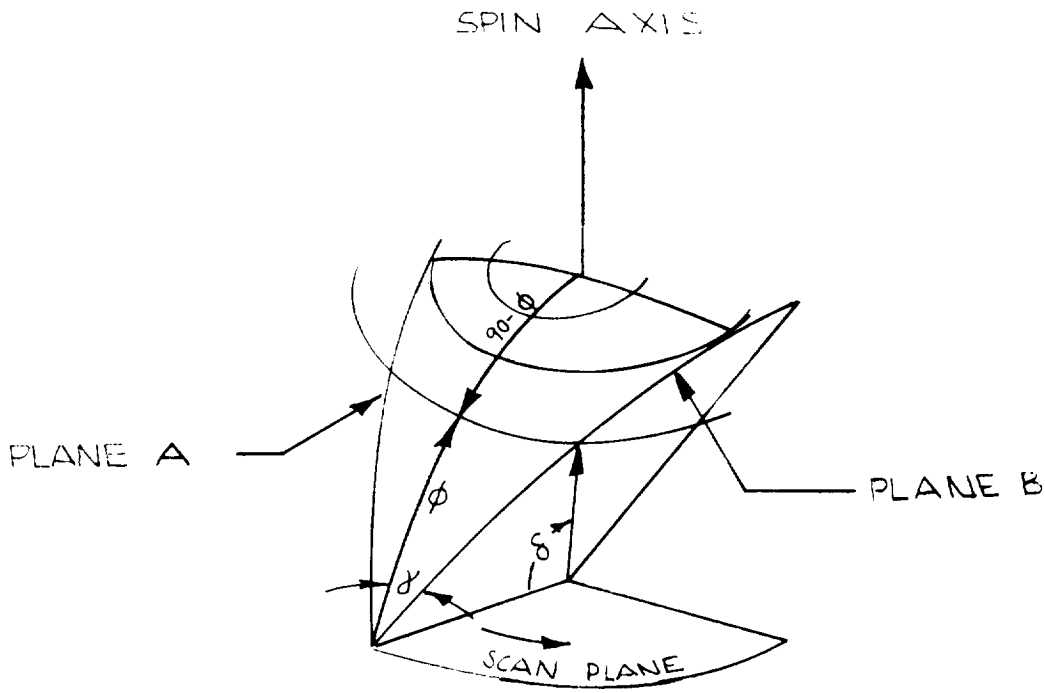

Figure 77. Geometry of Cross-Axis Sun-Sensing System

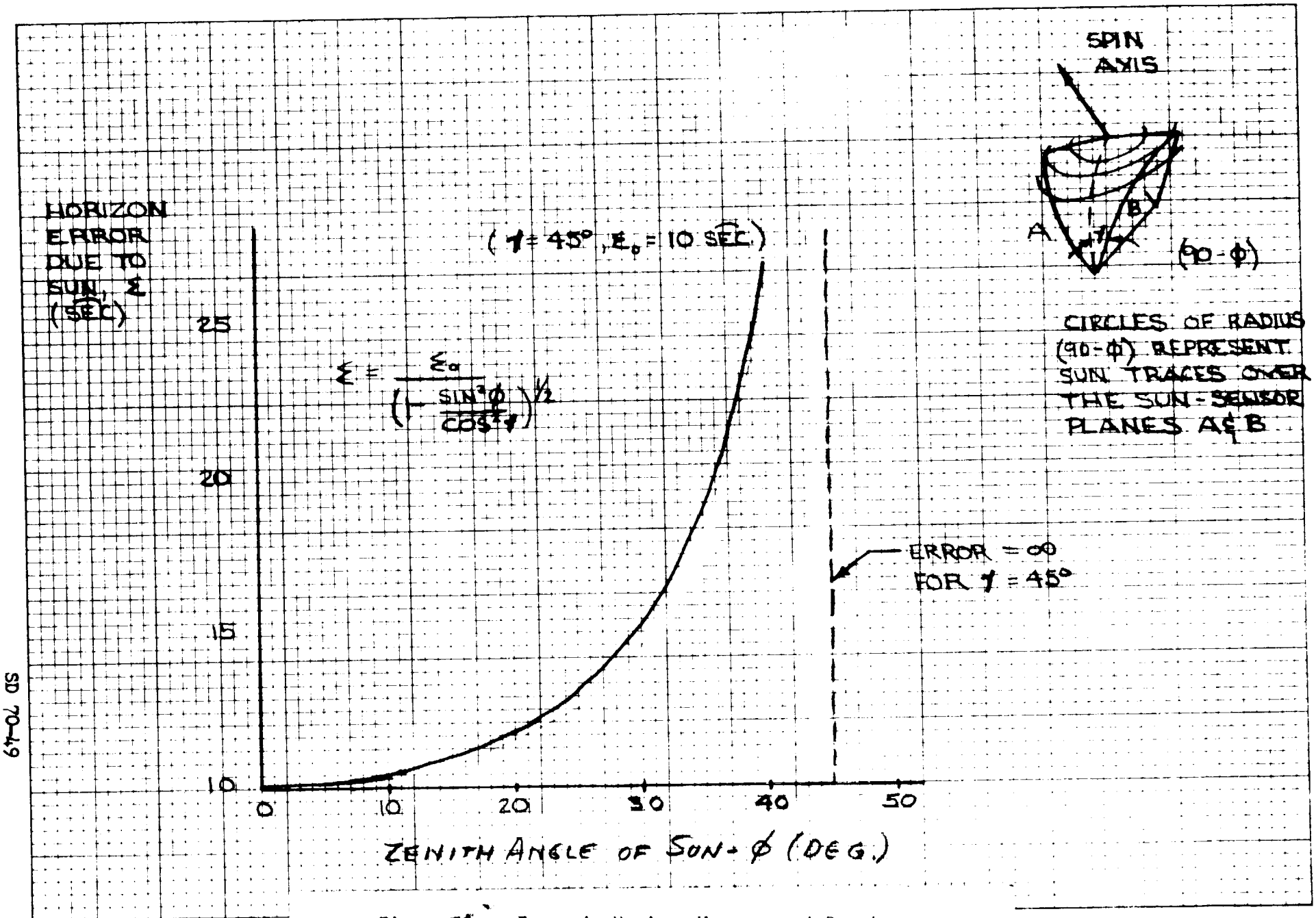

Figure 78. Error in Horizon Measurement Due to Error in Sun-Sensing

the difference angle between sun line and spin axis is only slightly greater than γ , the accuracy of the sun as a reference is poor. A question was raised as to the overall accuracy resulting when the sensor (intersection) axis is rotated to increase this difference. The following analysis pertains to the general case (Figure 79) when the intersection is displaced from the scan plane by an angle (η) either intentionally or due to spin axis misalignment. Equations are given first for the determination of ϕ and then for the sensitivity of the horizon measurement to an inaccuracy in θ. The coordinate systems involved are shown in Figure 79 .

If the previous error equation is modified to account for the tilt of the null axis out of the orbit plane by an angle η , then,

$$\Sigma = \frac{\Sigma_o}{\left(1 - \frac{\sin^2(\phi - \eta)}{\cos^2 \gamma}\right)^{1/2} \cos \phi}$$

where ϕ is the angle between the sun and the orbital, or scan, plane.

The error thus determined is plotted in Figure 80 for various combinations of ϕ and η . The figure indicates that the minimum error occurs when $\phi = 0$ and $\eta = 0$. But the minimum error does not increase appreciably as the value of η departs from zero. The minimum error increases only 50% as η goes from zero to 60°. In the proposed system and orbit the sum of η and ϕ will not exceed 10°.

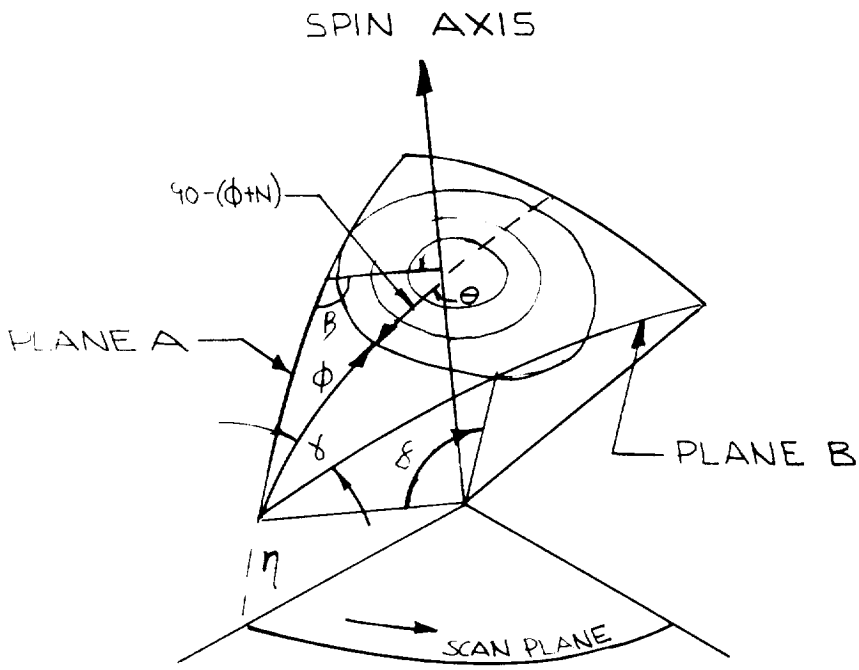

Figure 79. Position of Sun on Scan Plane

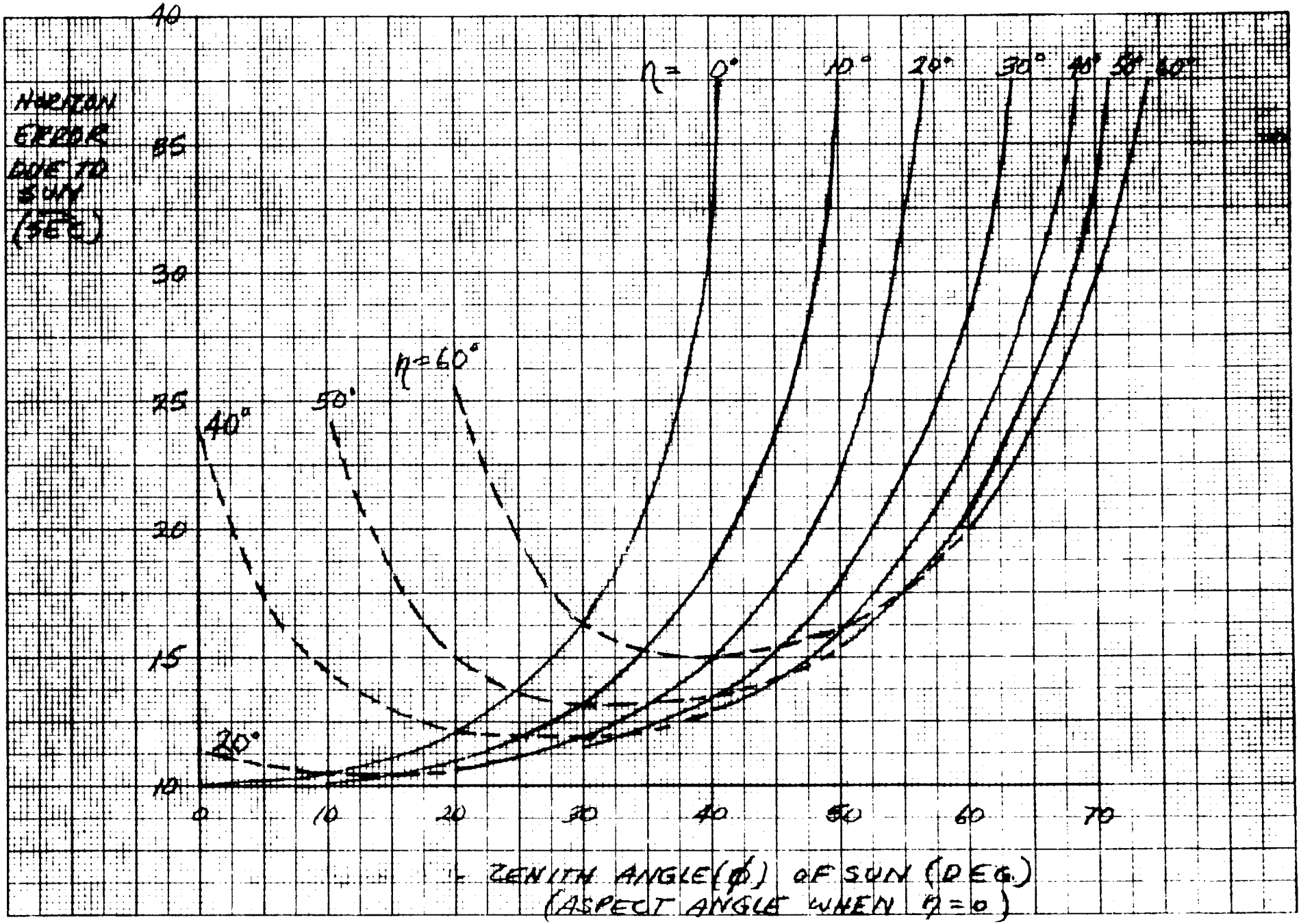

Figure 80 . Sun Sensor Error

Conclusions

The error analysis indicates that the specified 1 km accuracy in determination of the horizon altitude can be met using a precise (10 $\widehat{sec}$) crossed-axis sun sensor system and a pair of state-of-the-art IR horizon sensors. It appears necessary, however, to hold the dip angle of the vehicle spin axis to a small value (0 to 2°). The chief error contributors are the dip angle uncertainty and the satellite position determination error. The latter can apparently be sufficiently reduced by the use of the Manned Space Flight Network or the laser tracking stations.

IR Horizon Sensor Design

In the proposed system the IR horizon sensors are used to measure the roll angle, ψ. The operational concept is identical to that shown in the UV and MW Horizon Sensor Experiment Statement of Work. Two IR horizon sensors are mounted in the spacecraft with their optical axes canted at an angle of 60°. The plane defining the two optical axes is perpendicular to and centered about the orbit plane with each sensor 30° from the orbit plane. As the spacecraft rotates, the line of sight of each instrument produces a circular scan. If the spacecraft spin plane is perfectly aligned with the orbit plane, the trace of the IR sensors' optical axes across the earth appears as shown in Figure 81 .

The thermal discontinuity between the earth and outer space generates a signal as the field of view is scanned across the horizon. The time of the horizon crossing is recorded. If the spin plane is aligned with orbit plane, then

$$(t_2 = t_1) - t_4 - t_3) = 0$$

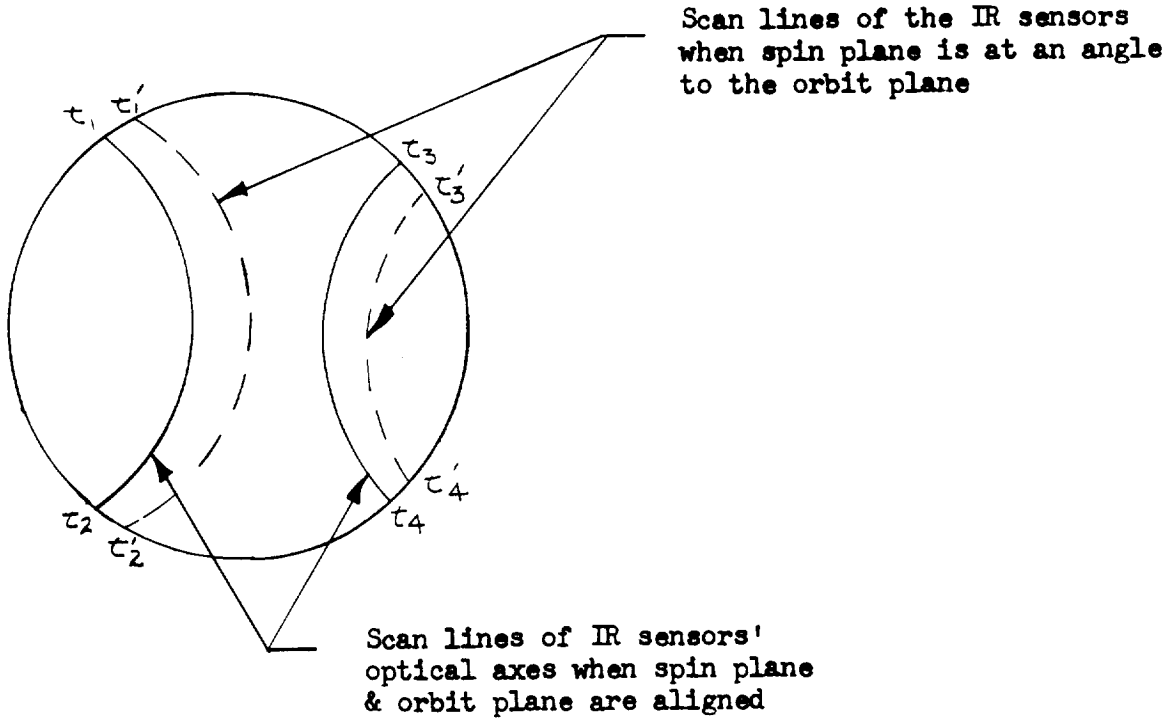

Figure 81 Ground Trace - IR Horizon Sensors

If the spin plane is at angle to the orbit plane, then:

$$(t_2' - t_1') - (t_4' - t_3') = \Delta T$$

and ΔT is a measure of the angle between the spin plane and the orbit plane. There are two sources of error in this measurement, (1) the alignment of the IR horizon sensor and (2) the alignment of the IR horizon sensors to the spin plane. The magnitude and effect of these errors is discussed in the section System Error Analysis.

A survey was made of off-the-shelf IR horizon sensors. None were found with $1/2^\circ$ accuracy for this mission. Barnes Engineering Company proposed using the electronic package from their 13-205 (TIROS) sensor and the optics from their 13-210 sensor will be enlarged to provide the larger aperture required for the 14-16 μ CO_2 spectral band. Figure 82 is a layout of the Barnes System and Table 16 is a list of its principle properties.

TABLE 16. CHARACTERISTICS OF BARNES SENSOR

Weight:	12 oz	
Power:	.250 MW max .50 MW max, with DC to DC converter (required for power system)	
Input Voltage:	$\pm$28 VDC	
Size:	See figure	
Optics:	Spectral Band 14-16 Field of View 1.5° x 1.5°	
Detector:	Immersed thermistor	
Output:	Rectangular wave with leading and trailing edges corresponding to space-earth and earth-space crossings. Amplitude is +15 volts, rise and fall time approximately 50 microseconds.	
Environment:	Vibration:	-25 g's random
	Acceleration:	100 g's
	Temperature:	0 to 60°C
	Vacuum:	1×10^5 TORR

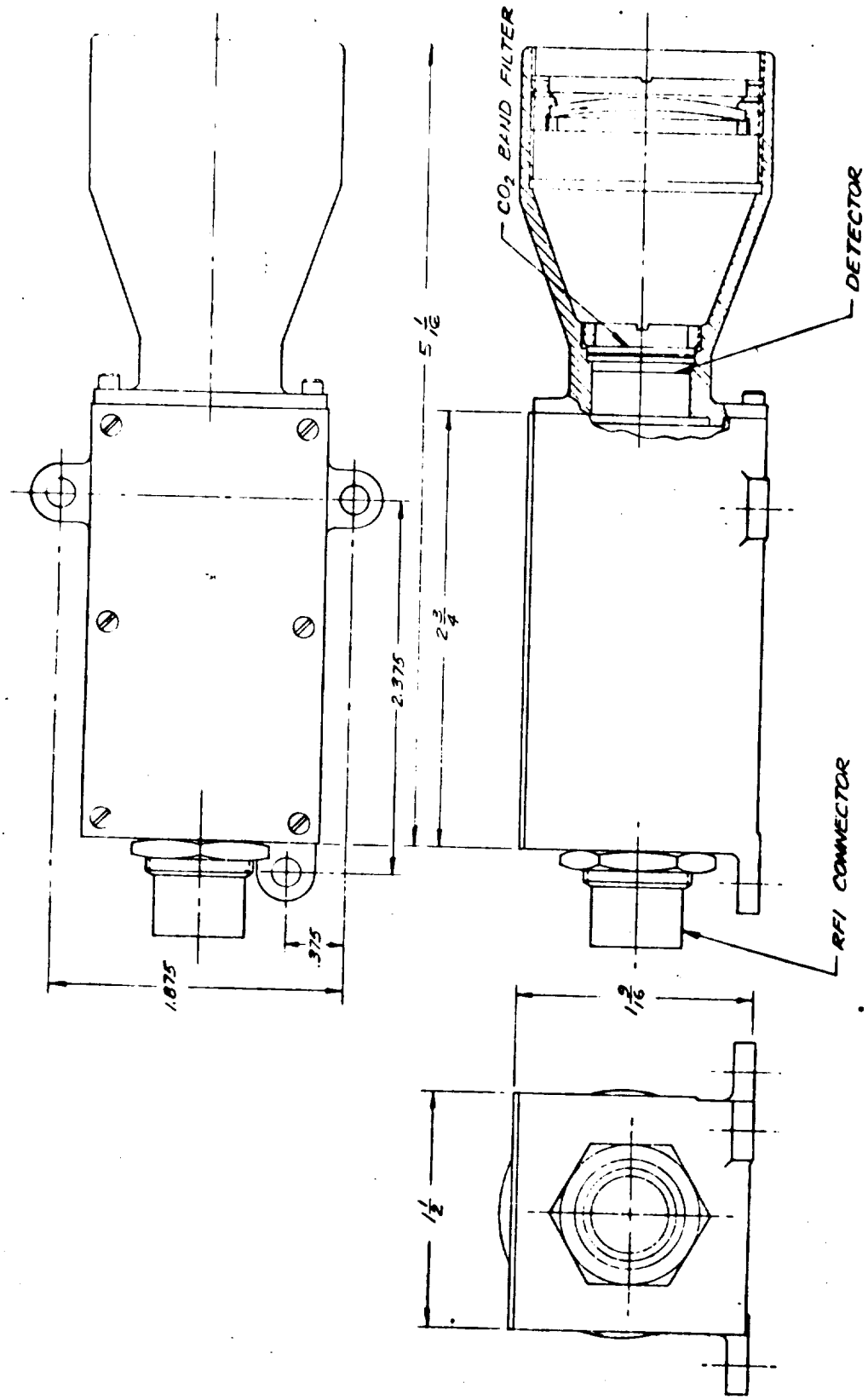

Figure 82 IR Horizon Sensor

Sun Sensor Design

In the proposed system, the sun sensor measures the vector direction to the sun. The spacecraft rotation scans the field of view of the sun sensor across the sun. If the reticle was a simple line perpendicular to the spin plane, one angle is measured each time the sun crosses this line. If this line is now rotated at some angle to the spin plane and a second line is placed on the reticle at an equal and opposite angle from the spin plane as the first line, an X reticle is formed. The time between the two reticle lines defines the position of the sun in the X reticle and provides the second angle to sun, defining the vector direction. This is the approach that was taken in design of the sun sensor.

Sun sensors of the energy-balance type are most advantageous for an application of this nature because an on-axis indication is given by a null output eliminating any requirement for precise intensity calibration. The generalized energy balancing sensor can be considered as a combination of filters and detectors as shown on the following block diagram (Figure 83).

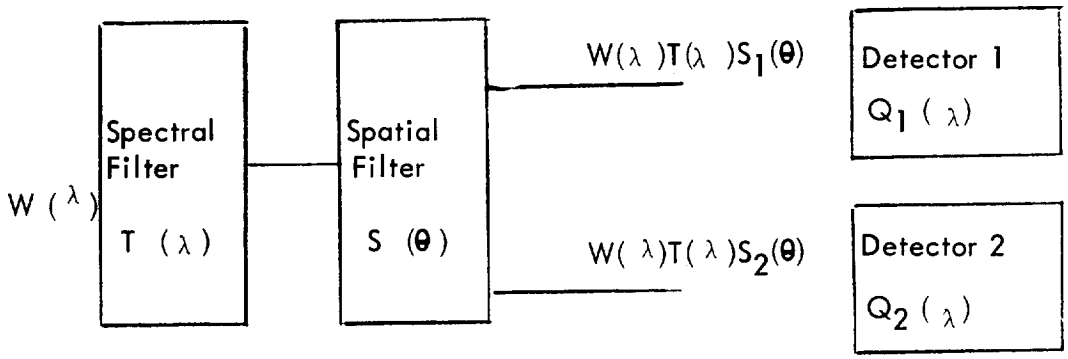

Figure 83. Simplified Block Diagram-Energy Balancing Sensor

Actually, by using this diagram, we have restricted the sensor to those systems in which a single spectral filter and a single spatial filter are used for both detectors. There are notable exceptions to this procedure, however, the basic considerations are similar albeit complicated by possible differences in the filters for each detector.

The spatial filter can be a lens and mask, a combination of two masks, etc; in any case, the function is to divide the incoming light between the two detectors according to the part of the field from which the light originated. The spatial filter is assigned a characteristic function, $S(\theta)$ which is some function (depending on the characteristic of the specific filter) of the angle between a reference axis and the line-of-sight to the center of the sun, θ.

The spectral filter is defined by a function, $T(\lambda)$, where the value of the function represents the transmission of the filter.

Several basic types of energy balance sensors exist:

1) <u>The imaging sensor</u> - in which the spatial filter maps a point on the sun into a point in the imaging plane. An example of this type is a lens located to focus an image of the solar disc onto two detectors separated by a narrow occulting strip with straight parallel edges.

2) <u>The non-imaging sensor</u> - in which the spatial filter maps a point on the sun into an area of finite dimensions in an "image" plane, such that the energy distribution is a function of aspect angle. An example of such a sensor is a slit in an opaque material spaced a short distance from two detectors as shown in Figure 84.

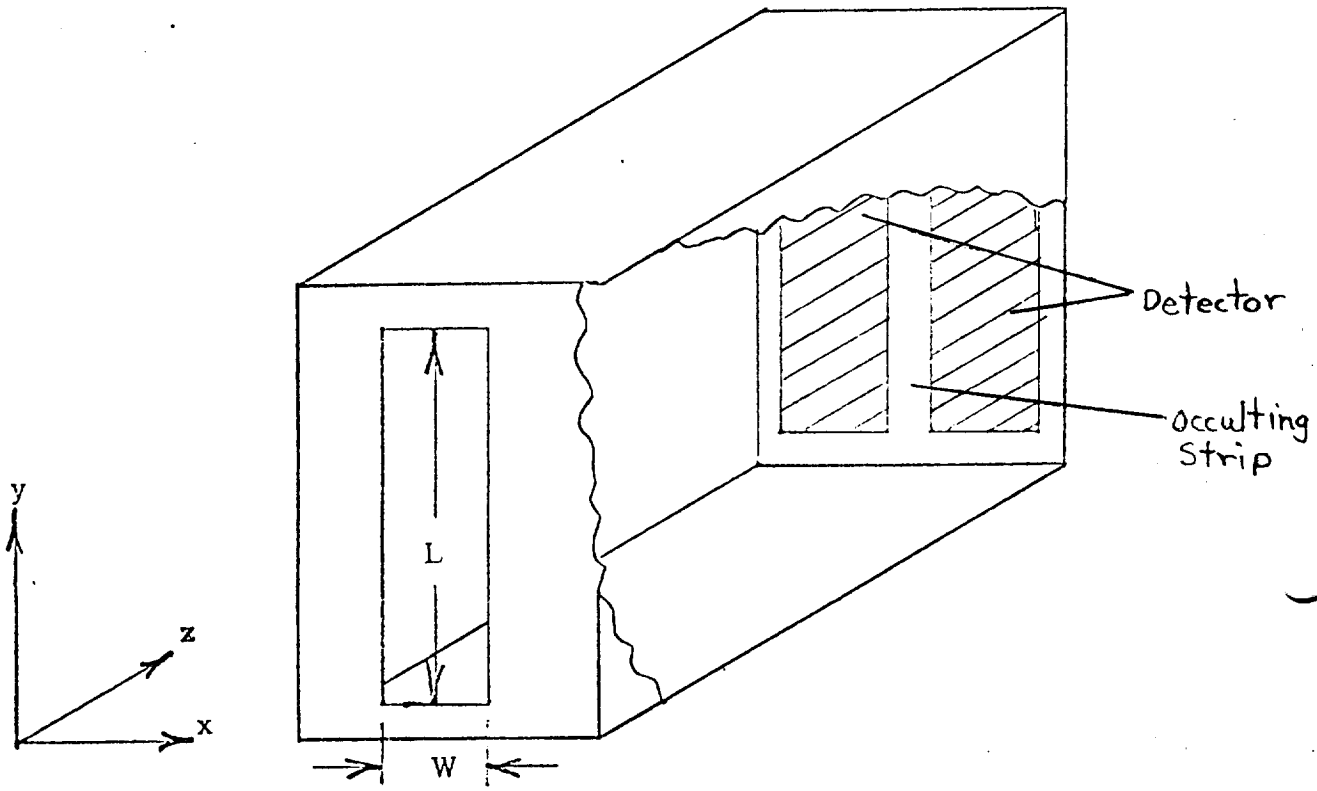

Figure 84 Non-Imaging Sensor

The first of these, the imaging sensor, has the advantage of high sensitivity with reasonable aperture sizes. However, it is undesirable for the present application because the sharply focused image falls on a small portion of the occulting strip and very small edge irregularities produce errors when the sensor is rotated in the non sensitive axis - (Cross-coupling errors). Furthermore, unless special design features are included, the sharply focused image falls on a small area of the detectors whose responsivity may vary significantly from place to place, again resulting in cross-coupling errors.

The non imaging sensor overcomes these problems by having its energy spread out over the entire occulting strip as well as over a relatively large detector area. Cross coupling errors may still arise due to curvature of the occulting strip edges but these will be smooth, repeatable functions of offset angle, and can be taken into account when calculating the experiment attitude.

Stability of this sensor is dependent on the spatial stability of the occulting strip relative to the slit edges. If a small dust speck falls on the slit edge, a null shift results. This problem is not insuperable but it does impose additional cleanliness requirements in testing and application.

All of the previously mentioned objections can be overcome by using a combination of the two approaches, in which the slit of the non-imaging sensor is replaced by a cylindrical lens. This distributes incident solar energy along the entire occulting strip and over a relatively large detector area. At the same time, dust particles on the lens cause intensity variations which are symmetric about the occulting strip axis so they do not contribute to null shifts, to the extent that lens aberrations affect symmetry.

Based on system design criteria and an analysis of the error budget, a Solar Aspect Sensor, having a $\pm 22^{\circ}$ FOV in the nonsensitive axis and an accuracy of ± 15 arc seconds including autocollimator errors, appears to be satisfactory. To achieve this level of performance, attention must be given to the following:

Null Accuracy - Since attitude measurements are obtained from the relative timing of sensor nulls, only the null accuracy is important and the shape of the sensor transfer characteristic is not critical, and it need not be linear. This provides additional design flexibility although attention must be given to thermal and mechanical stability.

Cross Coupling - In any sensor which operates off-axis in the nonsensitive direction, cross-coupling errors arising from non linearity or misalignment of energy controlling reticles must be considered as a significant source of error.

Radiation Environment - A careful selection of optical materials must be made to ensure no significant optical property changes in the presence of direct solar radiation.

Sensor Bandwidth - With the satellite spinning at approximately 4 rpm, the effective scan rate is approximately 10^5 arc seconds/second. To avoid angular aspect errors, the sensor system must be very fast or any delays must be stable, within a few microseconds (i.e., $< 10\ \mu$ sec).

Testing - Testing difficulties should be minimized, and the final sensor design should be capable of operating in a precision tungsten solar simulator beam.

Several companies were contacted concerning sun sensor design. There are no off-the-shelf sensors that adapt themselves directly to this application. After discussing different ideas with several companies, Exotech, Inc., was selected as the tentative vendor for the sun sensor and the airborne autocollimator. The design concept discussed is based on an Exotech concept to modify their SEAS system to this application. A detail discussion of Exotech's PASS system (the fore-runner to SEAS) can be found in AIAA Paper No. 69-858, published at the AIAA Guidance, Control, and Flight Mechanics Conference held August, 1969. Figure 85 shows a detail layout of the SEAS system. A detail report on the "Design, Development and Fabrication of a Solar Experiment Alignment Sensor (SEAS)" is provided in Exotech's Final Report to Ames Research Center on contract NAS2-4835, Report No. TR 1CD39.

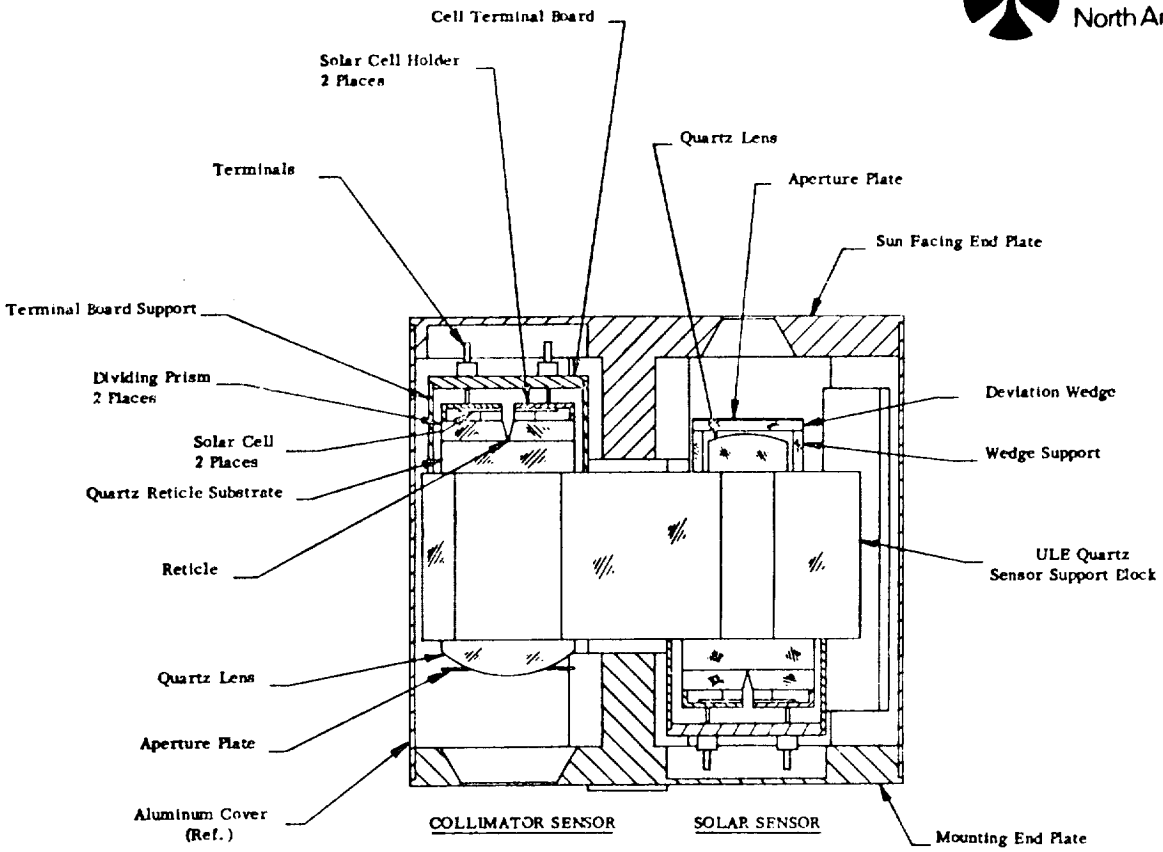

SECTION A-A

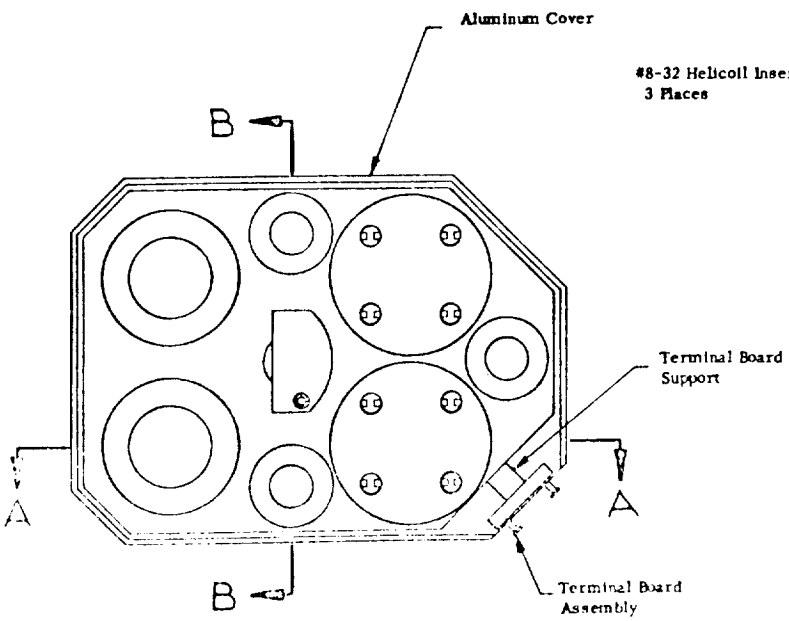

VIEW WITH MOUNTING END PLATE REMOVED

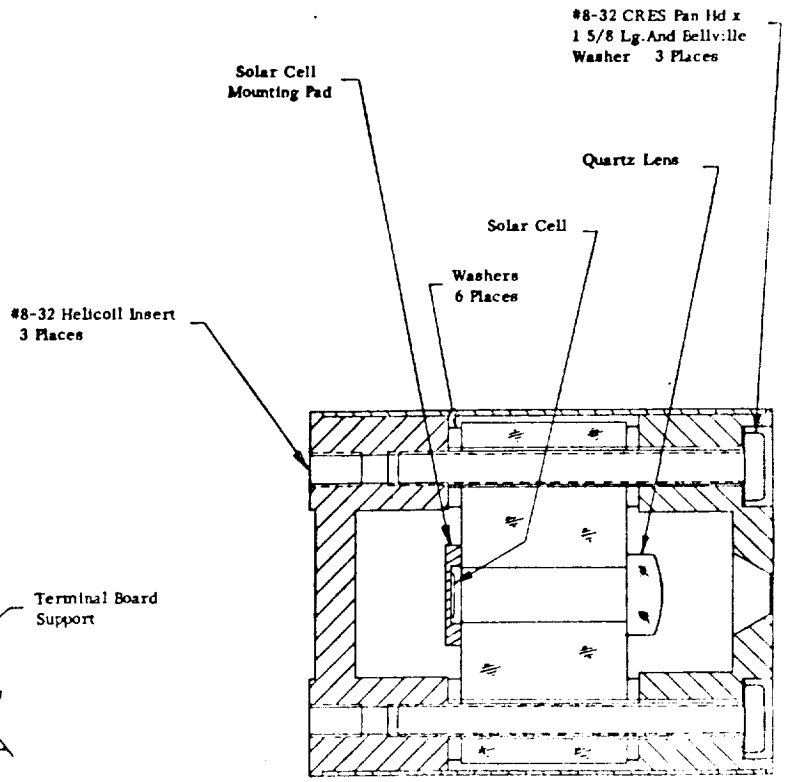

SECTION B-B
DETAILS OF AGC SENSOR

Figure 85 SEAS Details

MISSION SUCCESS PROBABILITY ANALYSIS

A preliminary reliability analysis of the UV/MW Horizon Sensor Experiment (UV/MW HSE), as presently configured, indicates that the reliability of the entire system is approximately 0.69 for a one-year mission. The analysis was performed under the conditions that no redundancy is to be considered. Therefore, reference to "single-point failures" is not applicable since each subsystem (and components within each subsystem) provides a potential "single-point failure".

Reliability Prediction

A numerical reliability estimate of the design, as currently defined, indicates a realiability of approximately 0.647 for a one-year mission, given a successful launch. Failure rates utilized were obtained from estimates provided by hardware suppliers, contemporary satellite analyses (ERTS, TIROS, etc.), reliability data reports ("STUDY OF RELIABILITY DATA FROM IN-FLIGHT SPACECRAFT"), and from the Apollo Applications Program (as appropriate). The report indicated above covers data gained from 225 launches from 32 U.S. space programs (all unmanned and of varying durations). The reliability prediction was based on the assumptions that subsystem failure rates were constant during the total mission time duration, and that any failures that might occur would be of a random nature. These assumptions permitted application of the standard exponential equation which defines reliability as a function of the failure rate

and operating time. Since it is r cognized that any given subsystem in a "standby" mode must be capable of operation when called upon to do so, and must withstand the environment during this "standby" mode, the failure rate assigned to this subsystem was set to ten percent of the failure rate of the same subsystem in the "operational" mode.

Figure 86 shows the system logic used for the UV/MW satellite. Figures 87, 88 , and 89 show the subsystem logic for the Electrical Power System, the TTC and Data Handling System, and the Attitude Control and Determination System, respectively, together with the details relative to the failure rates used, the estimated percentage of time each component within a given system is operational (or in "standby"), and a tabulation of the predicted reliabilities of each subsystem within each system.

Although there have been no reports of payload failures during launch, the probability of such an occurrence cannot be ignored. Consequently, the effects of the activities (launch, coast, etc.) preceeding spacecraft separation are outlined below:

System reliability for one year (8760 hours) = $e^{-8760\lambda} = 0.647$

From which ---- $\lambda = (\ \ n\ 0.647)/8760 = 4.9703 \times 10^{-5}$

Estimated time-line of launch (including all burns) = 0.25 hours

Estimated time-line for coast prior to spacecraft separation = 1.5 hours

Environmental stress factor for launch (and burn) portion = 80.0

Environmental stress factor for coast = 1.0

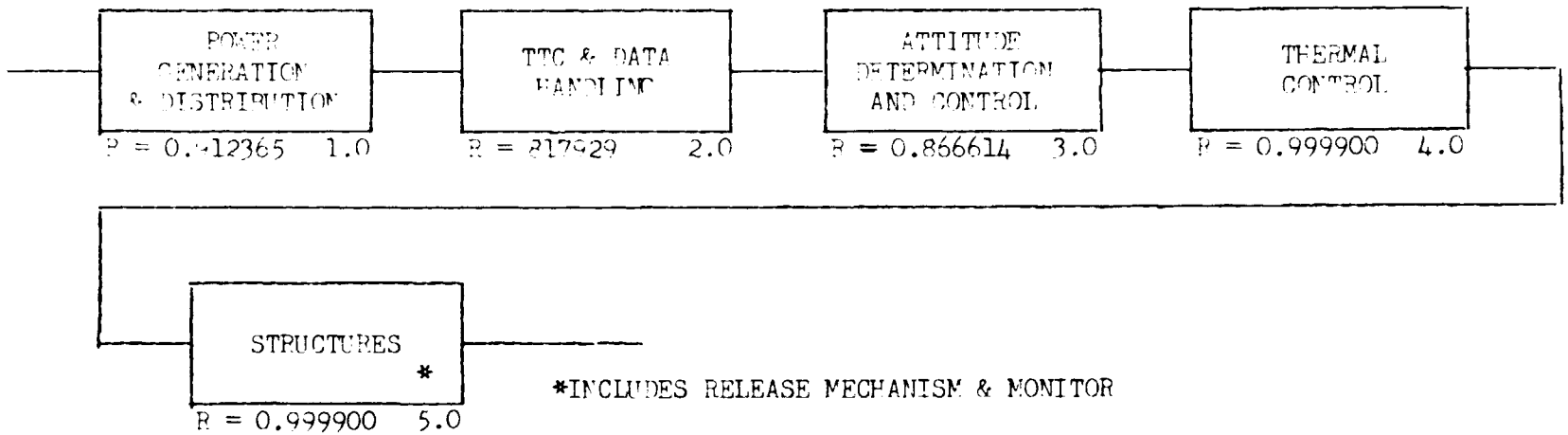

TOTAL SYSTEM RELIABILITY (ESTIMATED) = 0.646581

Figure 86. Reliability Logic Diagram - UV/MW Horizon Sensor Experiment Satellite

Space Division
North American Rockwell

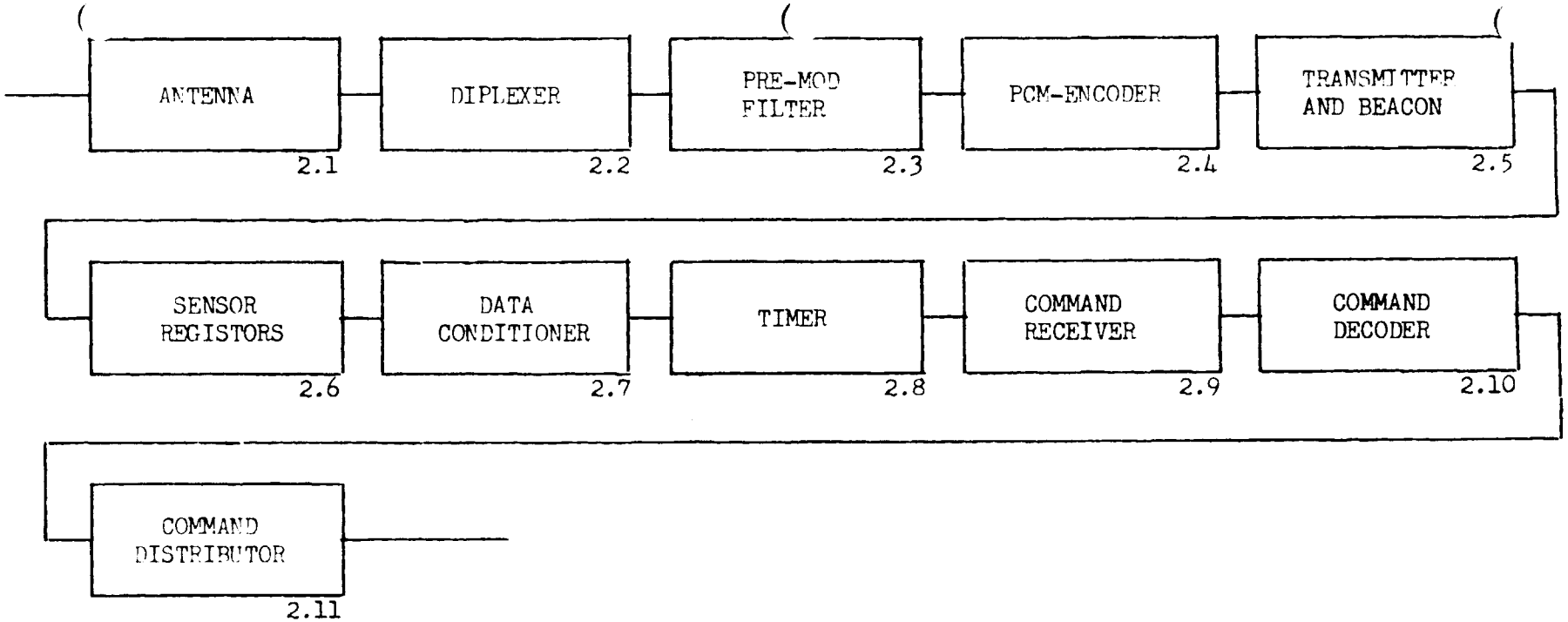

COMPONENT	$\lambda \times 10^{-6}$	OPER. TIME	STAND-BY	RELIABILITY
2.1	0.4000	10%	90%	0.999335
2.2	2.0000			0.996672
2.3	0.1000			0.999046
2.4	8.0000			0.986774
2.5	6.0000			0.990014
2.6	10.0000			0.983495
2.7	10.0000			0.983495
2.8	8.0000			0.986774
2.9	1/			0.910000
2.10	1/			0.985000
2.11	10.0000	10%	90%	0.983495

1/ RELIABILITY ESTIMATES SUPPLIED BY EQUIPMENT MANUFACTURER

TOTAL FOR SUBSYSTEM #2 = 0.817929

Figure 88. Reliability Summary for TTC & Data Handling System 2.0

Space Division
North American Rockwell

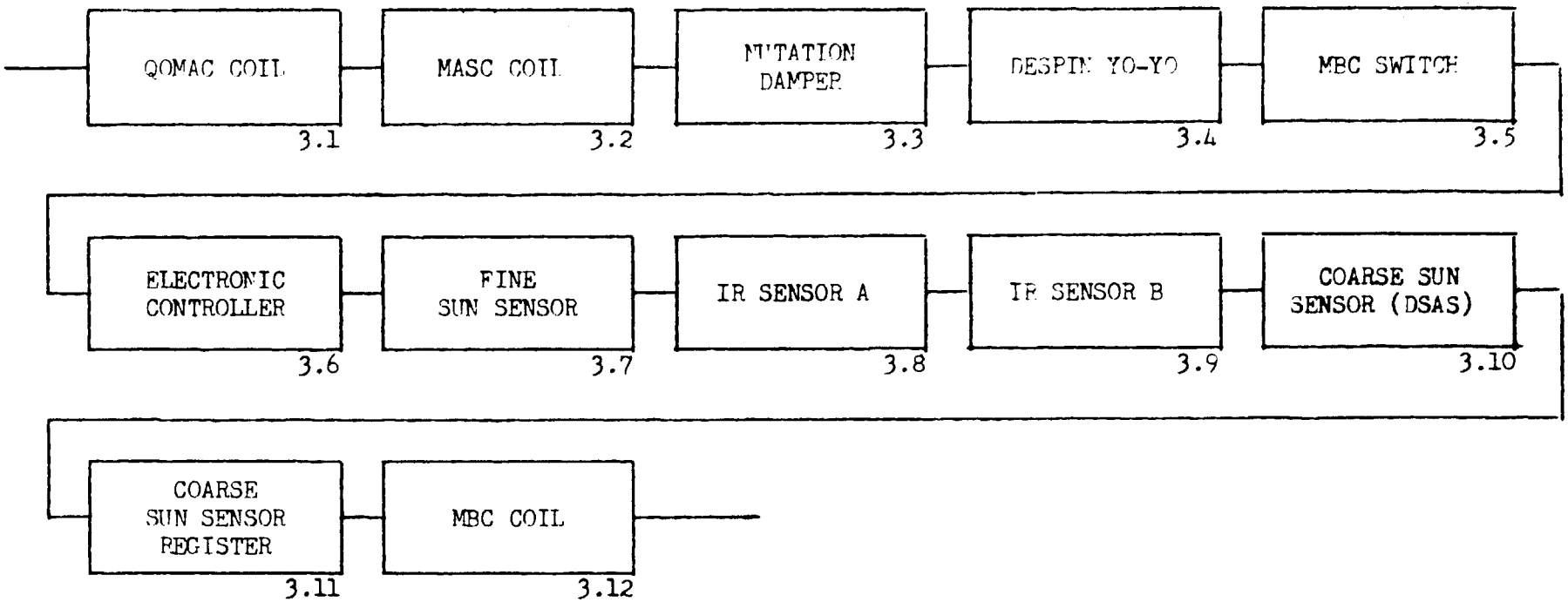

COMPONENT	$\lambda \times 10^{-6}$	OPER. TIME	STAND-BY	RELIABILITY
3.1	1.0000	10%	90%	0.990452
3.2	0.5000	10%	90%	0.999168
3.3	2.0000	100%	-	0.982633
3.4	2.0000	1/	1/	1/
3.5	1.0000	1%	99%	0.999045
3.6	2.0000	1%	99%	0.999652
3.7	1.0000	10%	90%	0.990452
3.8	28.0000	10%	90%	0.954483
3.9	28.0000	10%	90%	0.954483
3.10	1.0000	< 1%	> 99%	0.999900
3.11	10.0000	< 1%	> 99%	0.999000
3.12	1.0000	100%	-	0.990004

1/ THIS COMPONENT WILL ONLY BE USED IF THE SCOUT/THOR BURNER II BOOSTERS ARE USED. IN THIS EVENT, THE RELIABILITY WILL BE FACTORED IN AT THAT TIME.

TOTAL FOR SYSTEM 3.0 = 0.866614

Figure 89. Reliability Summary for Attitude Control and Determination System 3.0

Space Division
North American Rockwell

Therefore, the reliability of the launch (burn and coast) portion of the mission is given by

$$R_L = e^{-(80 \times 0.25 \times 4.9703 \times 10^{-5} + 1.0 \times 1.5 \times 4.9703 \times 10^{-5})}$$

$$= e^{-(9.9406 \times 10^{-4} + 7.4555 \times 10^{-5})}$$

$$\cong e^{-(1.0686 \times 10^{-4})} \cong 0.999$$

Factoring this reliability estimate into the system reliability calculated above, the reliability of the entire system (including probability of failure during launch) = 0.647 x 0.999 = 0.646353 ≅ .646.

DATA ACQUISITION AND TRANSMISSION ANALYSIS

A computer program was utilized to determine satellite time vs. latitude and longitude, whether over a tracking station (and which one), and time of entry and exit into tracking circle. A 600 nmi, noon sun-synchronous orbit with a 17-day repeat cycle was assumed. With no onboard data storage, near-continuous data can be obtained between -60° and +80° latitude over a portion of the Western Hemisphere. This data could be acquired on 35 night passes and 21 day passes out of a total of 228 orbits in the 17-day cycle.

Approximately 90 minutes of data storage must be provided if data coverage of the entire world is to be obtained. If 60 minutes of data storage are provided, complete coverage can be obtained on all orbits except 60 out of the 228.

A polar projection of the world with tracking circles shown and an overlay representing the satellite ground trace is provided to show all areas where data can be acquired and orbit times between tracking station contacts.

A data acquisition plan is recommended which acquires sensor data over the North and South America tracking station network for 50 minutes at night and 35 minutes in daylight approximately 12 hours later. This is done every 7 to 9 days, or as desired over the year.

Data Acquisition and Transmission Opportunities

Coverage Analysis

A computer program previously developed at NR for ERTS was modified to provide ground coverage and tracking station information for this study. Seven STADAN tracking stations, Table 17, were assumed to be available.

TABLE 17

TRACKING STATIONS

1	Johannesburg
2	Ororal
3	Alaska
4	Rosman
5	Quito
6	Santiago
7	Winkfield

The range circles (with a 5-degree mask, Figure 90) are shown for these stations on a polar projections of the world in Figure 91 along with an orbit trace overlay for a typical orbit. A mission simulation of this orbit was performed using the computer program and the orbit characteristics which are shown below in Table 18 (The data is for the period May 1-17, 1972):

TABLE 18

ORBIT CHARACTERISTICS

Altitude	600 NM
Inclination	99.9 Deg
Period	107.37 Min
Mean Motion	3.353 Deg/Min
Rev/Day	13.4118
Repeat Period	17 Days
Nodal Shift/Orbit	-26.9 Deg/Orbit
Local Time (descending) Nodal Crossing	12:00 Noon
Time/Orbit in Shadow	34.8 Min/Orbit (32.5%)

Daylight was assumed on the descending pass.

The 3.353 deg/min orbital motion indicates that 5 degrees will be covered in 1.5 minutes. For the mission simulation performed, a satellite rotation of 4 revolutions per minute was assumed with data acquired every 5 degrees of orbital motion or 1.5 minutes (or 6th revolution of the satellite). A full 17-day cycle was run.

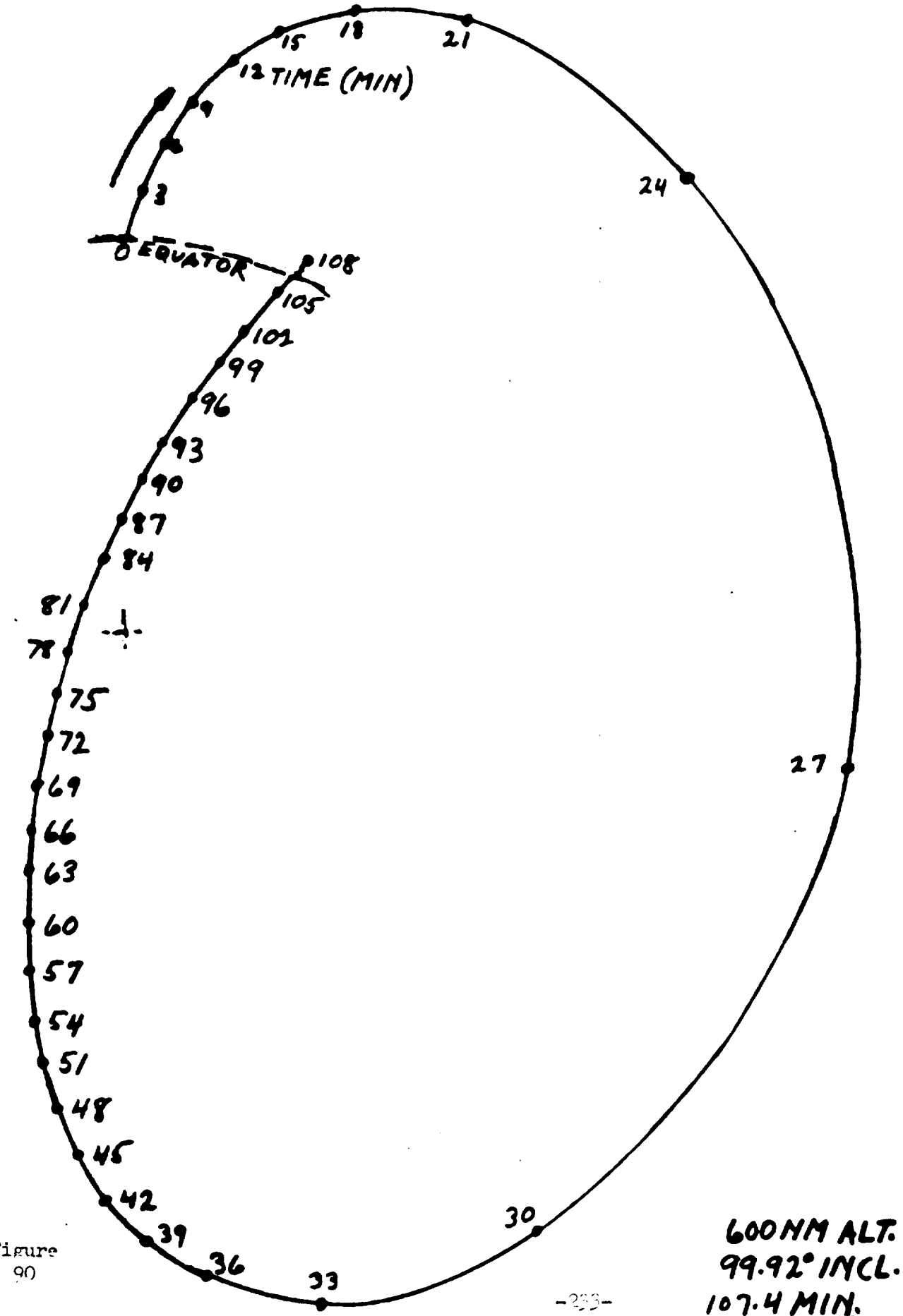

600 NM ALT.
99.92° INCL.
107.4 MIN.

Figure
90

The computer printout included satellite orbit number (228 orbits) for a complete cycle), satellite time (sampled every 1.5 minutes), latitude, longitude, light or dark on ground, satellite revolution in that orbit (427 revs/orbit), whether over a tracking station and which one (numbers keyed to those in Table 17, time (from start of that orbit) of entry into tracking circle and exit from tracking circle. Two typical pages showing parts of Orbit 32 and 38/39 from the computer printout are shown in Tables 19 and 20. As the program was modified from an existing program, superfluous data is printed and should be ignored. The columns of interest are:

R = Orbit Number

Enter = Time from start of that orbit

Latitude and Longitude

LD; 1 = Light on Ground; 0 = Dark

T-CR and LD - ignore

CC = Satellite revolution from start of that orbit

ST = Tracking station in view (0 = none)

ENTR = Time entered tracking circle

EXIT = Time left tracking circle

The printout was analyzed and Figure 91 and its orbit overlay, Figure 90, used to picture the results discussed below. It is to be noted that the computer program starts a new orbit at the descending node instead of at the ascending node which is the usual situation.

Real Time Data Transmission (No Onboard Storage)

Using the overlay pivoted at the North Pole through the mark shown, if data is transmitted only in real time to all seven STADAN stations, data can

TABLE 19

COMPUTER PRINTOUT TYPICAL DATA ACQUISITION PERIOD - NIGHT

MISSION SIMULATION DATA

SATELLITE NO = 1

R	C	AR	S	ENTER	LAT	LONG	EXIT	LAT	LONG	LD	T-CR	LD	%CC	ST	ENTR	EXIT	CATA-ACQ	DATA-TRA	NET-DI
32.				37.5	-53.0	-58.3				0.			151.	6.					
32.				39.0	-48.2	-60.8				0.			157.	6.					
32.				40.5	-43.3	-63.0				0.			163.	6.					
32.				42.0	-38.4	-64.9				0.			169.	6.					
32.				43.5	-33.5	-66.6				0.			175.	6.					
32.				45.0	-28.6	-68.1				0.			181.	6.					
32.				46.5	-23.6	-69.6				0.			187.	6.					
32.				48.0	-18.7	-70.9				0.			193.	6.					
32.				49.5	-13.7	-72.3				0.			199.	6.					
32.				51.0	-8.8	-73.5				0.			205.	6.	37.5	52.5			
32.				52.5	-3.8	-74.8				0.			211.	6.					
32.				54.0	1.1	-76.0				0.			217.	5.					
32.				55.5	6.1	-77.3				0.			223.	5.					
32.				57.0	11.0	-78.6				0.			229.	5.					
32.				58.5	16.0	-79.8				0.			235.	5.					
32.				60.0	20.9	-81.2				0.			241.	5.					
32.				61.5	25.9	-82.6				0.			247.	5.	54.0	63.0			
32.				63.0	30.8	-84.1				0.			253.	5.					
32.				64.5	35.7	-85.7				0.			259.	4.					
32.				66.0	40.6	-87.5				0.			265.	4.					
32.				67.5	45.5	-89.5				0.			271.	4.					
32.				69.0	50.4	-91.8				0.			277.	4.					
32.				70.5	55.2	-94.6				0.			283.	4.					
32.				72.0	59.9	-98.0				0.			289.	4.	64.5	73.5			
32.				73.5	64.6	-102.4				0.			295.	4.					
32.				75.0	69.1	-108.4				0.			301.	3.					
32.				76.5	73.4	-117.3				1.			307.	3.					
32.				78.0	77.0	-131.3				1.			313.	3.					
32.				79.5	79.5	-153.4				1.			319.	3.					
32.				81.0	79.9	177.8				1.			325.	3.					
32.				82.5	78.1	152.8				1.			331.	3.					
32.				84.0	74.7	136.3				1.			337.	3.	75.0	85.5			
32.				85.5	70.6	126.1				1.			343.	3.					
32.				87.0	66.2	119.2				1.			349.	0.					

TABLE 20

COMPUTER PRINTOUT TYPICAL DATA ACQUISITION PERIOD - DAY

MISSION SIMULATION DATA

SATELLITE NO = 1

R	C	AR	S	ENTER	LAT	LONG	EXIT	LAT	LONG	LD	T-CR	LD	%CC	ST	ENTR	EXIT	CATA-ACQ	DATA-TRA	NET-DI
38.				84.8	72.6	-30.6				1.			337.	7.					
38.				86.3	68.3	-38.9				1.			343.	7.					
38.				87.8	63.8	-44.6				1.			349.	7.	83.3	89.3			
38.				89.3	59.1	-48.7				1.			355.	7.					
38.				90.8	54.3	-52.0				1.			361.	0.					
38.				92.3	49.5	-54.7				1.			367.	4.					
38.				93.8	44.6	-56.9				1.			373.	4.					
38.				95.3	39.7	-58.9				1.			379.	4.					
38.				96.8	34.8	-60.6				1.			385.	4.					
38.				98.3	29.9	-62.2				1.			391.	4.					
38.				99.8	25.0	-63.7				1.			397.	4.					
38.				101.3	20.0	-65.1				1.			403.	4.					
38.				102.8	15.1	-66.4				1.			409.	4.	92.3	104.3			
38.				104.3	10.1	-67.7				1.			415.	4.					
38.				105.8	5.2	-69.0				1.			421.	5.					
38.				107.3	0.2	-70.2				1.			427.	5.					
39.				1.4	-4.7	-71.4				1.			1.	5.					
39.				2.9	-9.7	-72.6				1.			7.	5.					
39.				4.4	-14.6	-73.9				1.			13.	5.					
39.				5.9	-19.6	-75.3				1.			19.	5.					
39.				7.4	-24.5	-76.6				1.			25.	5.	1.4	8.9			
39.				8.9	-29.5	-78.1				1.			31.	5.					
39.				10.4	-34.4	-79.7				1.			37.	6.					
39.				11.9	-39.3	-81.4				1.			43.	6.					
39.				13.4	-44.2	-83.4				1.			49.	6.					
39.				14.9	-49.1	-85.6				1.			55.	6.					
39.				16.4	-53.9	-88.2				1.			61.	6.	10.4	17.9			
39.				17.9	-58.7	-91.4				1.			67.	6.					
39.				19.4	-63.4	-95.5				1.			73.	0.					
39.				20.9	-67.9	-101.0				1.			79.	0.					
39.				22.4	-72.3	-109.0				0.			85.	0.					

be acquired from a latitude of -60° to +80° (subsatellite point). Data can be taken and transmitted in a near-continuous pass between these ranges, in the Western Hemisphere on orbits where the descending node occurs between 85 degrees and 145 degrees west longitude. These runs occur over Santiago, Quito, Rosman and Alaska, and mainly at night. Orbit 32 (Table 19) is typical of such orbits.

On orbits whose descending nodes lie between 62 degrees and 95 degrees east longitude, the satellite passes over Winkfield, Rosman, Quito, and Santiago almost without interruption and allows data to be taken and transmitted in real time between latitudes of +81 degrees and -60 degrees. These passes occur in daylight. Orbit 38/39, shown in Table 20 is typical of these orbits. Other orbits will allow data to be transmitted in accordance with the locations shown by Figures 90 and 91 .

The computer printout shows that near-continuous data can be acquired on the orbits shown in Table 21 in a 17-day (228-orbit) cycle.

An examination of Table 21 and Figure 90 shows:

1. There are 35 orbits of night data acquisition (at least two every day).
2. There are 21 orbits of day data acquisition (at least one every day).
3. There are a total of 76 half orbits of near-continuous data acquisition out of a total of 228 orbits in the cycle.
4. The dark orbits usually occur in cycles of two consecutive orbits followed by a single light orbit 5 or 6 orbits later.
5. The data acquisition period is approximately 50 minutes in the dark cycle (Table 19) and approximately 35 minutes in the light cycle (Table 20).

TABLE 21

ORBITS OF NEAR-CONTINUOUS DATA ACQUISITION
AND TRANSMITTAL (NO DATA STORAGE)

DAY	ORBIT	LIGHT COND.
1	5 6 11/12 12/13	Night Night Day Day
2	18 19 25/26	Night Night Day
3	32 33 38/39	Night Night Day
4	45 46 52/53	Night Night Day
5	58 59 65/66	Night Night Day
6	72 73 79/80	Night Night Day
7	85 86 92/93	Night Night Day
8	99 100 106/107	Night Night Day
9	112 113 120/121	Night Night Day
10	125 126 127 132/133	Night Night Night Day
11	139 140 145/146 146/147	Night Night Day Day
12	152 153 160/161	Night Night Day
13	166 167 172/173 173/174	Night Night Day Day
14	179 180 186/187	Night Night Day
15	193 194 199/200	Night Night Day
16	206 207 212/213 213/214	Night Night Day Day
17	219 220 226/227	Night Night Day

6. Data can be obtained during the day and night from latitudes -60 degrees to +80 degrees.
7. Use of Johannesburg and Ororal will permit data to be obtained from 0 degree to -60 degrees in the Eastern Hemisphere as checkpoints; otherwise, these two stations are not required.

The above information and the computer printout can be utilized to establish optimum times to put the satellite in the standby mode for battery charging to minimize loss of data.

Increase in Capability with Onboard Data Storage

If data is required at more points than can be obtained with real time transmission, onbaord storage will be required resulting in an increase in satellite cost and complexity. If continuous data is desired all over the world, storage capability must be provided for approximately 90 minutes of data on Orbits 7, 47, 74, 77, 113, 140, 154, 168, 181, 200, and 208, or 12 of 228 orbits. If only 60 minutes of storage is provided, some data will be lost on 48 additional orbits in the cycle or a total of 60 out of 228 orbits.

As the satellite is power limited and must go on standby mode approximately one-half the time to recharge batteries if data is acquired continuously, the orbits on which data will be lost due to data storage limitation could be used for the standby mode to minimize data loss. If one hour of storage is provided, Quito would not be required and Rosman or Winkfield could also probably be dropped.

Requirements for Data Acquisition

The conditions for horizon observations are specified as:

1. Diurnal variations during the day at fixed geographic location.
2. Seasonal variations from month to month over the four seasons.
3. Latitude variations at latitude separations of no greater than 5 degrees, including, if possible, both poles.
4. Measurements over land masses, oceans, large weather systems and their transitions.
5. Variations as the sunline-zenith angle varies from 9 to 70 degrees at position of the locator altitude.
6. Day-night changes (for the MW sensor).

The reference concept utilizes a 600 NM altitude sun-synchronous orbit with the equator crossing at 12:00 noon and a 17-day repeat period.

The use of a sun-synchronous orbit for the proposed satellite has the advantage of providing a relatively invariant thermal cycle over the year. However, if the satellite is constrained to a sun-synchronous orbit, the local time at each latitude in the orbit remains essentially constant over the mission lifetime and diurnal variations at the same point cannot be observed by a fore-and-aft looking sensor. Also, the use of a sun-synchronous orbit, or any other non-polar orbit, precludes the observation of polar points except by destroying the alignment between the vehicle spin axis and the orbital spin axis.

The variation in the sun-zenith angle over one orbit (for in-plane observations) changes over the year. For example, at the time of the vernal equinox, the sun lies directly in the plane of the 12 o'clock orbit (Nimbus) and on the equator so that the value of sun-zenith angle passes through zero.

At other times of year, the minimum value is several degrees. The minimum sun-zenith angle is on the order of 30 degrees in the instance of orbits whose sunlit nodes are at local times of about 3 p.m. (ITOS) or 9 a.m. (ERTS). The sun-zenith angle is approximately equal to 15 degrees for every hour that the local time of the sunlit node departs from 12 noon. The sun-zenith angle will, of course, pass through the specified maximum (70 degrees) in every instances except that in which the spacecraft is always in sunlight.

For any given point over the earth, the sun-zenith angle at the time of measurement will change only to the extent that the local time of the measurement changes. For sun-synchronous orbits and in-plane measurements, this change is very small -- a few degrees.

The orbit selected passes over all latitudes between ± 80 degrees. As the orbit period is 107.37 minutes, it takes $(5°/360°)\ 107.37 = 1.5$ minutes to travel 5 degrees around the orbit. Measurements taken every 1.5 minutes (or every sixth revolution of a satellite rotating at 4 rpm) will satisfy the requirement of every 5 degrees of latitude.

The sun-synchronous orbit provides day-night coverage of the same general area after approximately six or seven orbits (See Table 21).

Using Figure 90 , it can be seen that the requirements of 5 degrees latitude spacing can be met in both day and night orbits by using Winkfield, Alaska, Rosman, Quito and Santiago, and data can be obtained between -60 degrees and +80 degrees latitude. During these passes, the satellite overflies land masses and oceans. From Table 21 , the dark passes over these stations occur in cycles of at least two consecutive passes followed six or seven orbits later by a daylight pass.

Recommended Data Acquisition Program

It is recommended that data be acquired on day and night passes at 7- to 9-day intervals, or twice in each 17-day cycle (approximately four times each month). The data should be taken on the dark side and then six or seven orbits later on the light side. Tables 19 and 20 are typical of such a pair of orbits (Orbits 32 and 38). This schedule will provide adequate seasonal variation. Additional data can be acquired over large weather systems as they occur during periods in between the 7-9-day normal schedule. Flexibility is provided to integrate the data acquisition periods into the tracking station schedules since data can be taken at least once every day and can therefore be obtained more or less frequently if desired.

Approximately 50 minutes of data can be obtained during the dark cycle and 35 minutes during the day cycle. The sensors would be turned OFF after the data acquisition period of 35 or 50 minutes to conserve spacecraft power. They would be turned ON at least 10 to 15 minutes before they are to acquire data to permit warmup.

With this data acquisition schedule, the satellite power requirements are minimized, onboard data storage is not required, and mission flexibility is provided. This schedule permits attitude correction maneuvers to be programmed on days between data acquisition.

A typical mission timeline for system operations using the above recommended data schedule is shown in Table 22 . It is to be noted that when the satellite is over any tracking station, housekeeping data can be transmitted, commands received, or the satellite can be tracked.

TABLE 22

TYPICAL OPERATIONS CYCLE

ORBIT	TIME (IN ORBIT) (Min.)	CYCLE TIME (Min.)	EVENT
31	87	0	Alaska commands experiments ON for sensor warmup
	87.9	0.9	Leave Alaska
32	22	42	Satellite crosses terminator into dark
	31.5	51.5	Satellite enters shadow
	37.5	57.5	Acquire Santiago and start transmitting data
	54	74	Switch to Quito
	64.5	84.5	Switch to Rossman
	66.0	86	Satellite leaves shadow
	75.0	95	Switch to Alaska
	76.5	96.5	Satellite crosses terminator into light
	85.0	105	Alaska commands experiments OFF
	85.5	105.5	Leave Alaska
33	31.5	158.9	Satellite enters shadow
	36.7	164.1	Acquire Santiago
	50.2	177.6	Switch to Quito
	56.2	183.6	Leave Quito
	60.7	188.1	Acquire Rossman
	66	193.4	Satellite leaves shadow
	69.7	197.1	Switch to Alaska
	79.4	206.8	Leave Alaska
34	8.8	243.6	Acquire Johannesburg
	14.8	249.6	Leave Johannesburg
	31.4	266.2	Enter shadow
	65.8	300.6	Acquire Alaska
	65.9	300.7	Leave shadow
	82.3	317.1	Leave Alaska
35	.4	342.6	Acquire Johannesburg
	16.9	359.1	Leave Johannesburg
	31.4	373.6	Enter shadow
	65.9	408.1	Leave shadow
	66.4	408.6	Acquire Alaska
	7.9	410.1	Leave Alaska
	87.4	429.6	Acquire Winkfield
	99.4	441.6	Leave Winkfield

TABLE 22

TYPICAL OPERATIONS CYCLE

(Continued)

ORBIT	TIME (IN ORBIT) (Min.)	CYCLE TIME (Min.)	EVENT
36	2.5	452.1	Acquire Johannesburg
	13.0	462.6	Leave Johannesburg
	31.3	480.9	Enter shadow
	65.8	515.4	Leave shadow
	71.5	521.1	Acquire Alaska
	77.5	527.1	Leave Alaska
	85	534.6	Acquire Winkfield
	100	549.6	Leave Winkfield
37	31.3	588.3	Enter shadow
	36.2	593.2	Acquire Ororal
	51.2	608.2	Leave Ororal
	65.8	622.8	Leave shadow
	84.2	641.2	Acquire Winkfield
	96.2	653.2	Leave Winkfield
38	5.3	669.7	Acquire Santiago
	18.8	683.2	Leave Santiago
	23.3	687.7	Satellite crosses terminator into dark
	31.2	695.6	Enter shadow
	35.3	699.7	Acquire Ororal
	48.0	712.4	Command experiments ON for warmup
	48.5	712.9	Leave Ororal
	65.7	730.1	Leave shadow
	75.8	740.1	Satellite crosses terminator into light
	83.3	747.7	Acquire Winkfield and start acquiring data
	89.3	753.7	Lose Winkfield
	92.3	756.7	Acquire Rossman
39	1.4	773.2	Switch to Quito
	10.4	782.2	Switch to Santiago
	17.0	788.8	Command experiments OFF
	17.9	789.7	Leave Santiago
	31.2	803.0	Enter shadow
	65.7	837.5	Leave shadow
	89.9	861.7	Acquire Rossman
	106.4	878.2	Switch to Quito

SPACECRAFT SYSTEMS ANALYSIS

This section of the report describes the reference spin stabilized satellite and the analysis performed for the systems selected. Tradeoff analyses are also presented for several of the systems. The study results presented are identified by the following subsection titles:

- Attitude Control System
- Telemetry, Tracking, Command and Data Handling System
- Electrical Power Generation and Distribution System
- Instrument Alignment Error Analysis and Effects of Launch on Alignment
- Satellite Structures Analysis
- Thermal Control Analysis and Design Requirements

A brief summary for each of these subsections presents the significant results, how they were obtained and the conclusions derived. Detailed descriptions are presented in the text.

A block diagram of the satellite, Figure [illegible], shows the major systems and their respective subsystems. The command requirements and engineering status measurements are noted in the diagram for each specific subsystem. Also shown are the satellite protective canister and its contained subsystems along with the launch vehicle and the ground STADAN stations' telemetry links.

ATTITUDE CONTROL SYSTEM

The Attitude Control System study is presented in six separate sections:

- System Analysis
- Tradeoff Analysis of Onboard Versus Ground Controlled Error Computer for Attitude Control
- System Description
- Size, Weight and Power Requirements
- Performance Specifications
- Operations Plan

A brief summary is presented for each of these sections:

Systems Analysis -- A mathematical discussion is presented of magnetic Dynamic Control System (DCS) theory. Additionally, mechanization concepts were studied where performance and/or cost criteria were implicated. Extensive use was made of the TIROS IX wheel mode spinning satellite and the DME-A satellite flight test data which are flight-proven hardware from which mechanization concepts were evaluated in terms of relative parametric sensitivities, reliability, expected cost, lifetime estimates, and potential problem areas. The TIROS IX magnetic attitude control system was concluded to be superior in every way for this mission to the DME-A system, and is proposed. Being relatively independent of the sensing and error computation aspects of the DCS, it can be employed with either ground control or onboard error computation, as the results of that independent evaluation dictate. The TIROS IX

magnetic attitude control system concept, it was concluded, is inexpensive, reliable, and highly accurate in pointing capability with good design lifetime characteristics which will provide an effective system in support of the sensor evaluation mission requirements.

Tradeoff Analysis of Onboard Versus Ground Controlled Error Computer for Attitude Control -- The possibility of modifying the baseline system error computer from a ground-controlled, open-loop controller to an onboard, closed-loop controller is explored. The relative merits of the two system concepts for the proposed mission indicate a definite preference for the open-loop, ground-based controller. The onboard system is an over-design and requires that extensive size, weight, power, reliability and cost penalties be paid.

System Description -- A subsystem definition of the DCS is delineated. Interface requirements between subsystem elements and between the system and other systems are defined. Physical and functional descriptions of the major components are provided with particular emphasis on operating mode considerations.

Size, Weight and Power Requirements -- This section identifies the size, weight and power requirements of the candidate system for dynamic control of the satellite. The dynamic requirements as a function of mission mode and the static requirements as a function of subsystem elements clearly indicate the applicability of the system with respect to the figures of merit required.

Performance Specifications -- The performance specifications of the satellite are defined by the mission requirements and the vehicle operational requirements associated with the selected attitude control system.

Operations Plan -- The on-orbit operations plan required for the DCS is described. Ground support equipment, logistics, data reduction, and data analysis requirements are given for maintaining the required attitude and spin rate accuracy of the satellite in both automatic and manual modes of operation. The automatic mode is considered the primary mode of operation.

System Analysis

This section documents the system analysis and tradeoff evaluation of a Dynamic Control System (DCS) for the UV-MW Horizon Sensor Experiment Satellite. The analyses performed during the proposal indicated a magnetic torquing system would best meet the mission requirements. Consequently, this study considers the tradeoffs for defining the type of magnetic control system to be used rather than proving the feasibility of the magnetic control concept.

The open-loop, ground control approach to error computation was accepted as baseline in this study. However, tradeoff analysis is presented of this concept in comparison to onboard, closed-loop mechanization. This analysis is relatively independent of the dynamic actuation system concept study contained in this report, and will be described subsequently as a separate tradeoff evaluation.

Maximum utilization of completed and existing work which is applicable to this mission and vehicle constraints were employed to obtain the benefit of flight-tested technology systems and concepts.

Symbols

$\overline{B}$	Instantaneous vector representation of earth's magnetic field
$B_{\ell,b,n}$	Components of $\overline{B}$ in the $\hat{\ell}$-$\hat{b}$-$\hat{n}$ system
$\hat{b}$	Unit vector perpendicular to $\hat{\ell}$ in orbital plane
H	Angular momentum
h	Orbit altitude
I_s	Spin inertia
i	Orbit inclination
i_m	Inclination of earth's magnetic dipole with respect to geographic polar axis
K	Geomagnetic dipole (8.1×10^{25} gauss-cm^3)
$\hat{\ell}$	Unit vector along orbit ascending node
M	Magnetic dipole moment
N_c	Coil normal
$\hat{n}$	Unit vector along orbit normal
R	Distance of satellite from center of earth
R_E	Mean earth radius
$\hat{r}$	Unit vector along the local vertical (positive outward)
$\hat{s}$	Unit vector along spin axis
T_s	Spin torque
T_p	Precessional torque
$T_{\ell b}$	Torque in $\hat{\ell}$ $\hat{b}$ plane

T_n	Torque along orbit normal
t	Time
t_{ei}	Earth time as viewed by horizon sensor i
t_{spin}	Spin period from AHS
x_m	Line of nodes of geographic and magnetic equatorial planes
$\hat{x}$	Vernal equinox
$\hat{z}$	Geographic north polar axis
α_i	Angle between horizon sensor optical axis and spin axis
β	Satellite anomaly
β_i	Initial β for MASC torquing
β_f	Final β for MASC torquing
β_s	Start angle for QOMAC cycle
β'_i	1/2 the earth intercept angle as viewed by horizon sensor i
γ_σ	Angle between N_c and $\hat{r}$ at time of commutation
θ_{12}	Angle between lines of sight of horizon sensors
λ	Phase of attitude error
λ'	$90° + \lambda$
Λ	Argument from ascending node of precession vector in the orbit plane
ϕ	Roll angle
ϕ_{max}	Attitude error magnitude
ψ	Yaw angle
Ω	Angle between $\hat{x}_m$ and $\hat{\ell}$
$\bar{\omega}_s$	Satellite spin rate
ϖ_p	Spin-axis precession vector
$\tilde{\omega}_{p,\ell,b,n}$	Average precession vector $\hat{\ell}$-$\hat{b}$-$\hat{n}$ system
ω_o	Rotational rate of orbit ascending node

Mission Requirements and Vehicle Constraints

In order to effectively evaluate the performance of the UV and MW horizon sensors, the following mission requirements associated with the experimental satellite Dynamic Control System (DCS) are imposed:

1. Operate in any orbit in the altitude range between 400 nm and 800 nm.
2. Operate with an orbital inclination between 80 and 102 degrees.
3. Damp the initial orbital injection spin axis nutation to less than 0.5 degree per half-cone angle.
4. Damp the initial orbital injection spin rate to less than 7 rpm.
5. Establish reference orientation of the spin vector normal to the orbit plane in 15 orbits or less.
6. Maintain the selected orbital spin rate of 4 rpm (nominal) to an accuracy of 0.5%.
7. Have the capability of changing nominal orbital spin rate between 1 and 7 rpm to an accuracy of 0.5%.
8. Provide for spin axis precession to compensate for the nominal orbit regression rate and residual satellite dipole.
9. Maintain spin-axis orientation to within 2 degrees per half-cone angle of orbit normal for the mission duration.
10. Perform all functions for a period of one year.
11. Minimize size, weight and power.
12. Minimize environmental sensitivity.
13. Minimize cost.
14. Maximize use of off-the-shelf hardware and flight-proven technology.

Candidate Dynamic Control Systems

Preliminary analysis of TIROS IX and DME-A magnetic control systems indicates a distinct advantage over other types of actuation systems which were considered, such as Reaction Jet, Inertia Wheel, or Control Moment Gyro (CMG) systems, in terms of the control requirements of a small spinning experimental satellite with a minimum lifetime of a year. Inertia wheel or CMG systems are both significantly more costly, are heavier, require more space, require significantly more power to operate, and have a lower reliability factor. In addition, they provide more capability than necessary in terms of output torque. In the case of the spin control actuator, where only three or four corrections a week are required, either the inertia wheel or CMG would have to be kept running all of the time in spite of a 0.1% utilization rate, or they would have to be spun up on command which would induce more disturbance torque than that being corrected for. Either way, the power drain is significant. Additionally, desaturation would be required for inertia wheel or CMG systems, which creates additional size, weight, and power requirements. Hence, CMG and inertia wheels were not considered serious candidates for this application, and no further analyses were performed. The penalties for using CMG or inertia wheels were excessive compared to those of the magnetic controller.

The reaction jet controller appears to be more desirable than the CMG or the inertia wheels but still does not appear competitive with the magnetic actuator system. One of the main disadvantages associated with reaction jet control is that its lifetime is limited by the amount of

propellant which is stored on board for jet utilization. Although the weight of fuel to satisfy the minimum operation time requirement of one year is estimated to be about 5 lbs, this leaves no latitude for additional maneuvering. Any additional fuel which is carried must be traded off directly in terms of dollars since the size, weight, and moment of inertia would increase with additional fuel storage. This creates a less-than-unity efficiency factor when adding fuel because the associated increase in moment of inertia causes an increase in torque required to negotiate a given maneuver or correction which is directly measurable in fuel expended. Although the size, weight, power and reliability factors of a cold gas reaction jet system are not as extreme as those of the inertia wheels or CMG systems, nevertheless those penalties still exist in significant quantity in comparison with the baseline magnetic control concept.

In addition to the savings of size, weight, and power that the magnetic actuation approach presents, extensive empirical flight test data is available from TIROS wheel flights which verifies the predictability and reliability of this concept. Results of preliminary analysis indicates that some form of magnetic actuator is the best candidate approach to be employed.

Control Systems for Orbital Injection

The philosophy and the hardware for damping orbital injection nutations and providing initial spin rate attenuation are independent of the attitude maneuver and housekeeping system employed while orbiting. Since they are independent, they can be integrated with any orbit attitude

control system selected, and are treated separately.

Nutation Damping

During the deployment phase, the satellite is injected into orbit with considerable wobble or nutation of its spin axis, which must be eliminated to effect the attitude control mission requirements. Whatever nutation damper is employed, it can and should be maintained active throughout the mission to ensure that spin axis nutation does not recur during housekeeping modes as a result of magnetic cross coupling or other disturbance torques which may be encountered.

The TIROS IX employs a very effective passive damper which consists of two diametrically opposed sliding balls which ride on curved monorails whose chord is parallel to the satellite spin axis. Friction between the oscillating masses and their respective tracks dissipates the nutational energy in the form of heat and reduces satellite wobble to less than 0.5 degree. The masses are tuned to the natural precession frequency of the satellite. After the wobble has been damped out, the two masses reside approximately in the center of their guiderails. The masses are caged until deployment, at which time they are released by a switch. Figure 93 shows the orientation of these tubes in the TIROS IX. Nutation can be damped to the required level in less than five minutes.

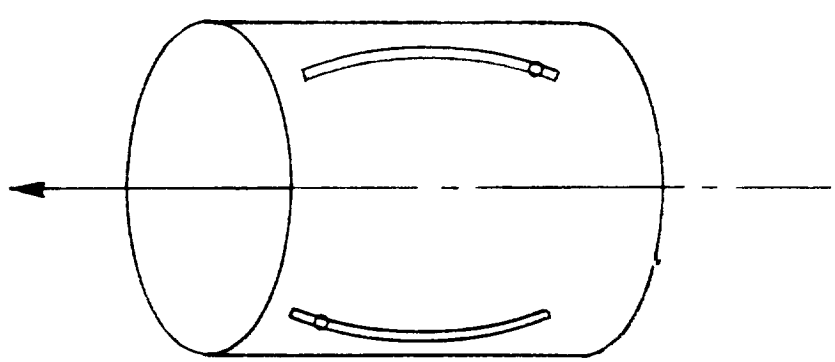

Figure 93 . Orientation of Damper Tubes in TIROS IX

An alternate approach, employed in the DME-A satellite (shown in Figure 94), consists of a pair of ball-in-tube devices mounted on its structure. Two curved aluminum tubes, each approximately one foot long and containing hardened copper balls, lie in circular arcs in planes approximately normal to the satellite spin axis. Their centers of curvature are displaced slightly off the body axis in order to provide a position of central stability for the balls. The damper plane is raised above the satellite's center of mass in order that the rolling spheres respond to nutations of the spin axis. Permanent magnets attached to the tubes creat a high-level magnetic field through the tubes directed in the damper plane. When the satellite is nutating, each copper ball is forced to move against the tube's magnetic field. Eddy currents generated in the ball result in a retardation of its motion and effect dissipation of nutational energy. The damper provides nutation decay half times in the order of 30 minutes for large nutation angles (20 degrees) and faster damping half-times for smaller angles.

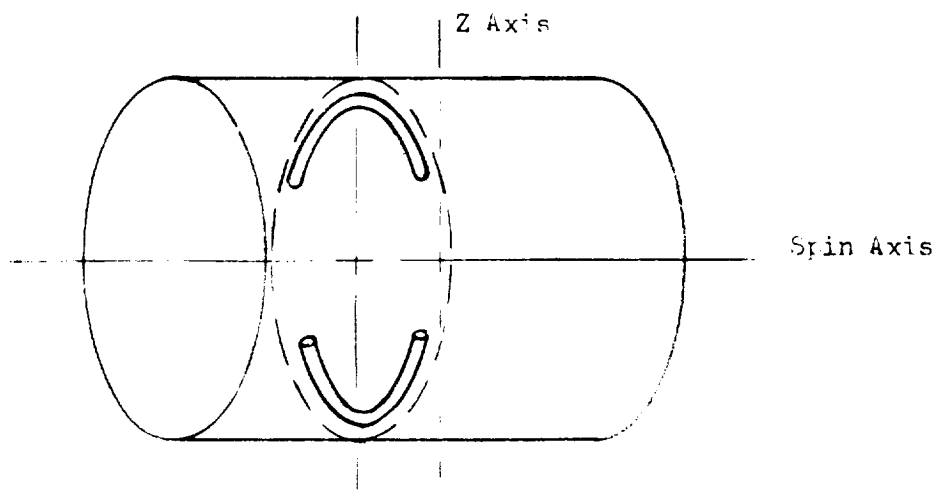

Figure 94. DME-A Nutation Damper Configuration

The DME-A system has two distinct disadvantages. The first is that it is slower to damp injection nutations than the TIROS IX system. Secondly, it requires the use of permanent magnets which will interact with the earth's magnetic field-satellite dipole relationship, creating a bias in the attitude and spin control equations. The inclusion of permanent magnets would require magnetic bias compensation.

Orbital Injection Spin Rate Attenuation

The spin rate of the satellite after orbital injection can be as high as 180 rpm depending on the launch vehicle selected for this mission. This rate must be reduced to below 7 rpm in a reasonable period of time and allow the magnetic spin control system to assume control authority. The despin mechanism consists of a pair of cable-attached masses which are released from the satellite structure after absorbing the necessary energy. The attachment point to the cables would be located 180 degrees apart on the circumference of the satellite with the cable wrapping around 360 degrees. Normally, the masses would be released at the required time by automatic firing of squibs; however, ground control manual backup would also be provided. Centrifugal force causes each cable to unwind; it extends radially from the structure, at which time it slips off an open hook and departs from the satellite which causes a spin-rate reduction of one order of magnitude in 0.5 second. Reference[1] has detailed information on the despin principles and analysis for building a De-Spin Yo-Yo.

[1]Haseltine, W. R., Nutation Damping Rates for a Spinning Satellite, Aerospace Engineering, p. 10, March 1962.

Orbit Attitude and Spin Rate Control Systems

Coordinate Definition

With the satellite having been deployed into orbit, the initial spin axis nutations damped and the injection spin rate attenuated to below 7 rpm, the remaining mission attitude and spin rate control functions are under authority of the magnetic control system.

Consider a coordinate system as shown in Figure [illegible]. The satellite must be oriented within a polar orbit of between 80° and 102° inclination such that the spin axis remains within 2 degrees of half-cone angle of coincidence with the orbit normal.

Axes $\hat{\ell}$, $\hat{b}$, and $\hat{n}$ define the orbit coordinate system where $\hat{\ell}$ is along the orbit line of nodes (toward the ascending node), $\hat{n}$ is the orbit normal, and $\hat{b}$ is orthogonal to both $\hat{\ell}$ and $\hat{n}$ and lies in the plane of the orbit completing a right-hand orthogonal coordinate system $\hat{b} = \hat{n} \times \hat{\ell}$. β is the satellite orbit angle measured counterclockwise around $\hat{n}$ from the line of nodes to the orbit radius, defining the satellite's position in the orbit plane. "i"is the orbit inclination angle measured counterclockwise around ℓ from the earth's polar axis Z. Ω_{an} is the right ascention of the line of nodes. "$\hat{r}$" is the radius vector from the center of the earth to the satellite. X, Y, and Z form a right-hand orthogonal system defining the earth's geographic coordinate system in inertial coordinates. X_m, Y_m, and Z_m define the earth's magnetic coordinate system in inertial coordinates. The angle i_m is the inclination between the earth's geographic and magnetic systems. The vector $\hat{r}$ represents local vertical.

A simple canted-magnetic-dipole of 8.1×10^{25} gauss -cm^3 is a good approximation of the geomagnetic field typical of 400 to 800 nm orbits. This dipole axis is inclined from the polar axis of the earth by an angle i_m = 11.4 degrees. It intersects the earth at a latitude of N-78.6 degrees, longitude W-70.1 degrees, and latitude S-78.6 degrees, longitude W-250.1 degrees.

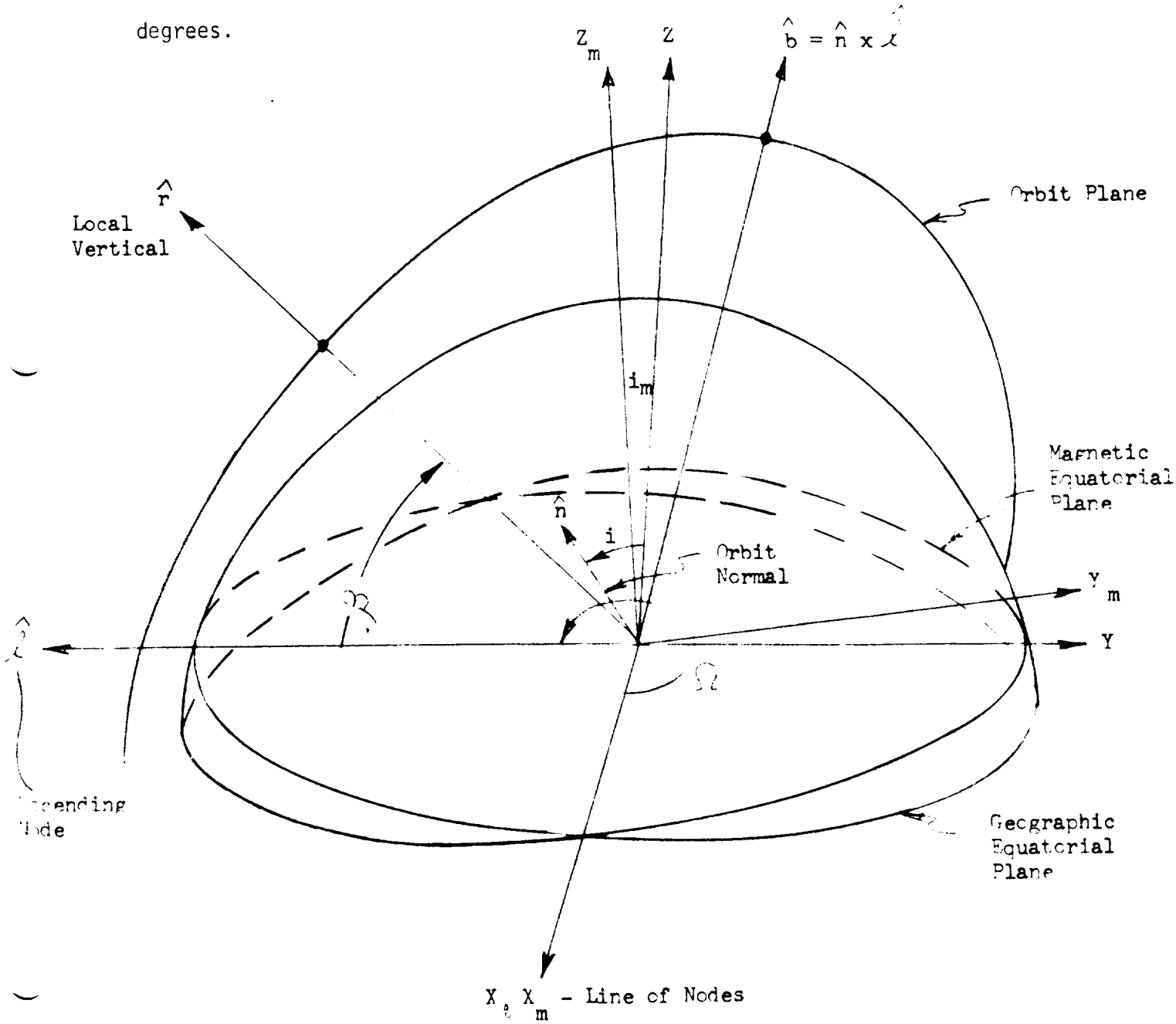

Figure 9. Coordinate System Definition

The earth's field components, due to a dipole source expressed in an orbit coordinate set, are:

$$B_{\hat{\ell}} = \frac{K}{R^3}\left\{-\frac{3}{2}\sin i \cos i_m \sin 2\beta + \sin i_m \left[\frac{1}{2}\sin\Omega + \frac{3}{4}(\cos i+1)\sin(2\beta+\Omega) + \frac{3}{4}(\cos i-1)\sin(2\beta-\Omega)\right]\right\}$$

$$B_{\hat{b}} = \frac{K}{R^3}\left\{\frac{1}{2}\sin i \cos i_m (3\cos 2\beta-1) + \sin i_m \left[\frac{1}{2}\cos i \cos\Omega - \frac{3}{4}(\cos i+1)\cos(2\beta+\Omega) - \frac{3}{4}(\cos i-1)\cos(2\beta-\Omega)\right]\right\}$$

$$B_{\hat{n}} = \frac{K}{R^3}\left\{\cos i \cos i_m + \sin i \sin i_m \cos\Omega\right\}$$

Flight test data gained on TIROS IX in conjunction with detailed non-approximated computer simulation has demonstrated that simplification of the equations representing the earth's magnetic dipole in orbital coordinates can be made with negligible error resulting in dynamic stability control performance or model effectiveness. These approximations are:

1. Consider the dipole approximation to the source of the earth's magnetic field collinear with the polar axis of the earth (i.e., $i_m = 0°$, $\Omega = 0°$).
2. The orbital regression rate for one orbit is only on the order of 0.07 degree which is insignificant in terms of the magnetic field/satellite relationship for a one-orbit analysis of spin vector magnitude or argument control. Over long periods, a definite bias is built up which must be corrected, but for a single orbit, can be neglected.

3. The orbit is near circular, such that the eccentricity can be assumed zero.

With the benefit of these approximations, the earth's magnetic field, in orbital coordinates, can be reduced to

$$B = \frac{V}{R^3} \left[\left(\frac{3}{2} \sin 2\beta \sin i\right) \hat{\ell} + \left(\frac{3}{2} \cos 2 \quad \sin i - \frac{1}{2} \sin i\right) \hat{b} + (\cos i)\, \hat{n} \right]$$

Attitude and Spin-Rate Sensing

The attitude error of a satellite in true wheel mode is zero ($\hat{s} = \hat{n}$). When $\hat{n}$ becomes non-collinear with $\hat{s}$, then an error parameter must be decided upon and monitored to indicate the magnitude and direction of the attitude. The most convenient and effective parameter to monitor and correct for is the total attitude error angle Γ. Figure 96 indicates Γ in the orbital plane.

Γ is a total attitude error between the orbital ($\hat{n}$) axis and the body spin axis ($\hat{s}$). The spin axis is inertially fixed and the roll-yaw coordinate system rotates with the local vertical. Consequently, the roll and yaw components of attitude must undergo cyclic variation in magnitude. If λ' is the angle between the projection of $\hat{s}$ on the orbit plane and the ascending node, and β is an angle which corresponds to that portion of the 360° from the ascending node which the satellite should have traveled as determined by a precession time count established for a known orbital rate, then the angles ϕ and ψ, which represent satellite body roll and yaw error angles, respectively, can be given as

$$\sin \phi = \sin \Gamma \sin (\beta - \lambda) \qquad \text{(Roll)}$$

and

$$\sin \lambda = -\sin \Gamma \cos (\beta - \lambda) \qquad \text{(Yaw)}$$

where

$$\lambda = \lambda' - 90°.$$

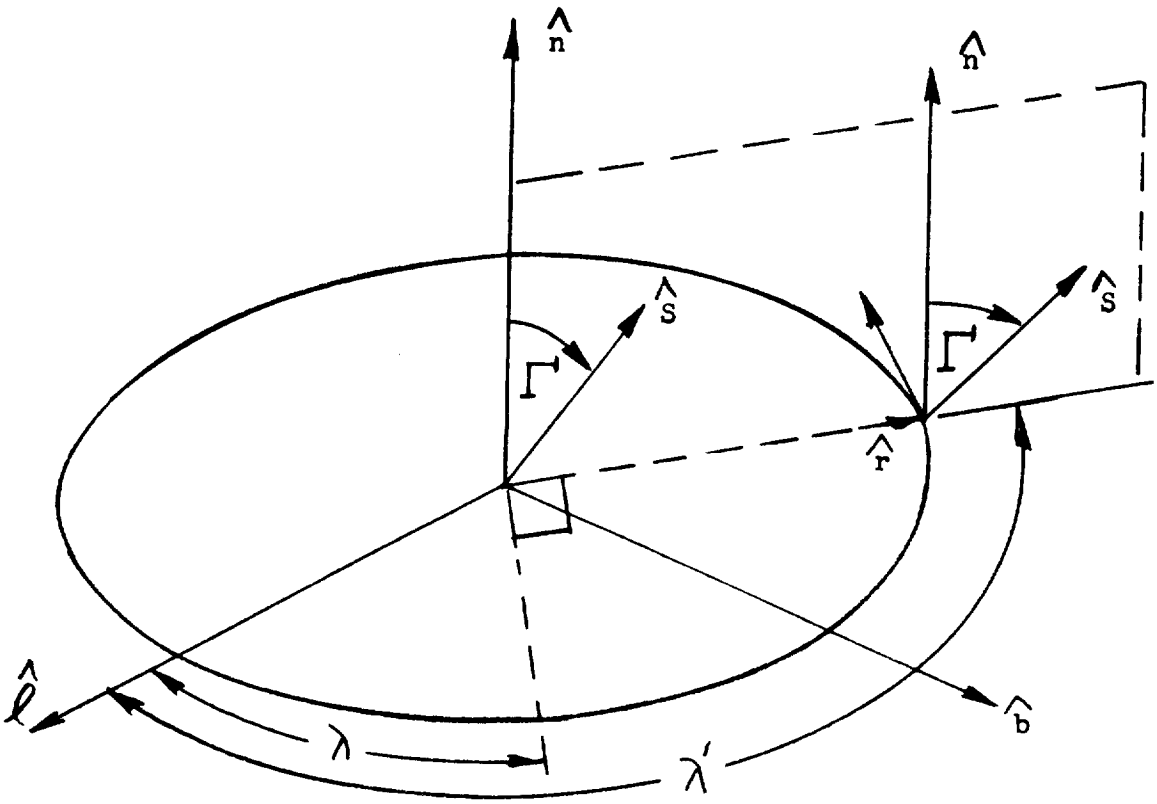

Figure 96. Attitude Error Orientation in Orbit Coordinates

It is proposed that two infrared sensors (similar to those employed on TIROS wheel) be used to obtain data which can be used to compute λ and Γ and ultimately ϕ and ψ. These sensors are rigidly mounted to the spacecraft and derive their scanning from the spinning motion of the spacecraft. The sensors generate output pulses whenever a change in radiance is observed by the optics.

The infrared sensors for determining Γ and λ are configured in a "Vee" symmetric about a plane perpendicular to the spin axis as shown in Figure 97.

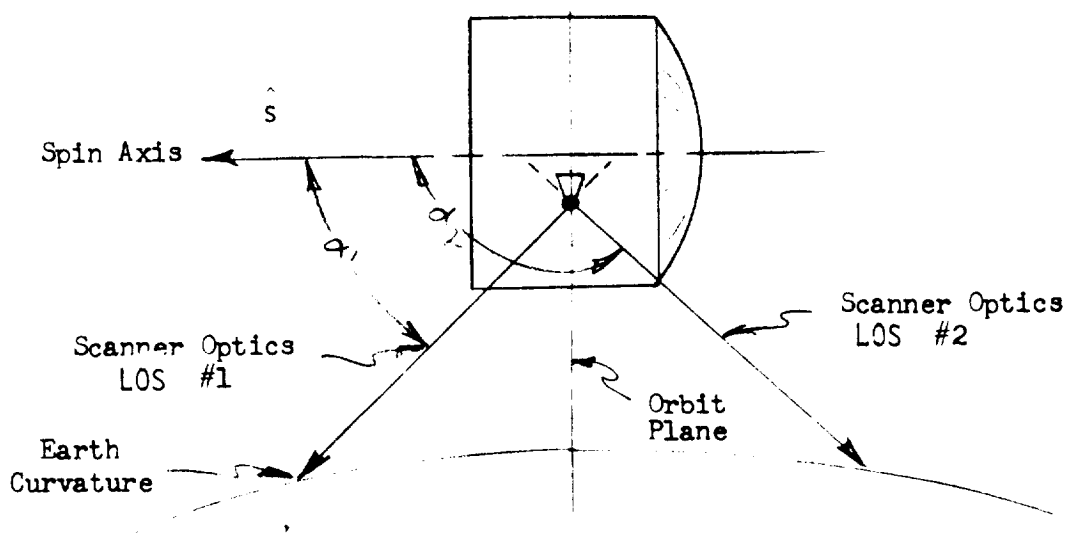

Figure 97. Attitude Sensor Geometry

As the spacecraft spins, the optical axes trace out two cones in space. The pulses resulting from the points where these cones intersect the earth's horizon are shown in Figure 98.

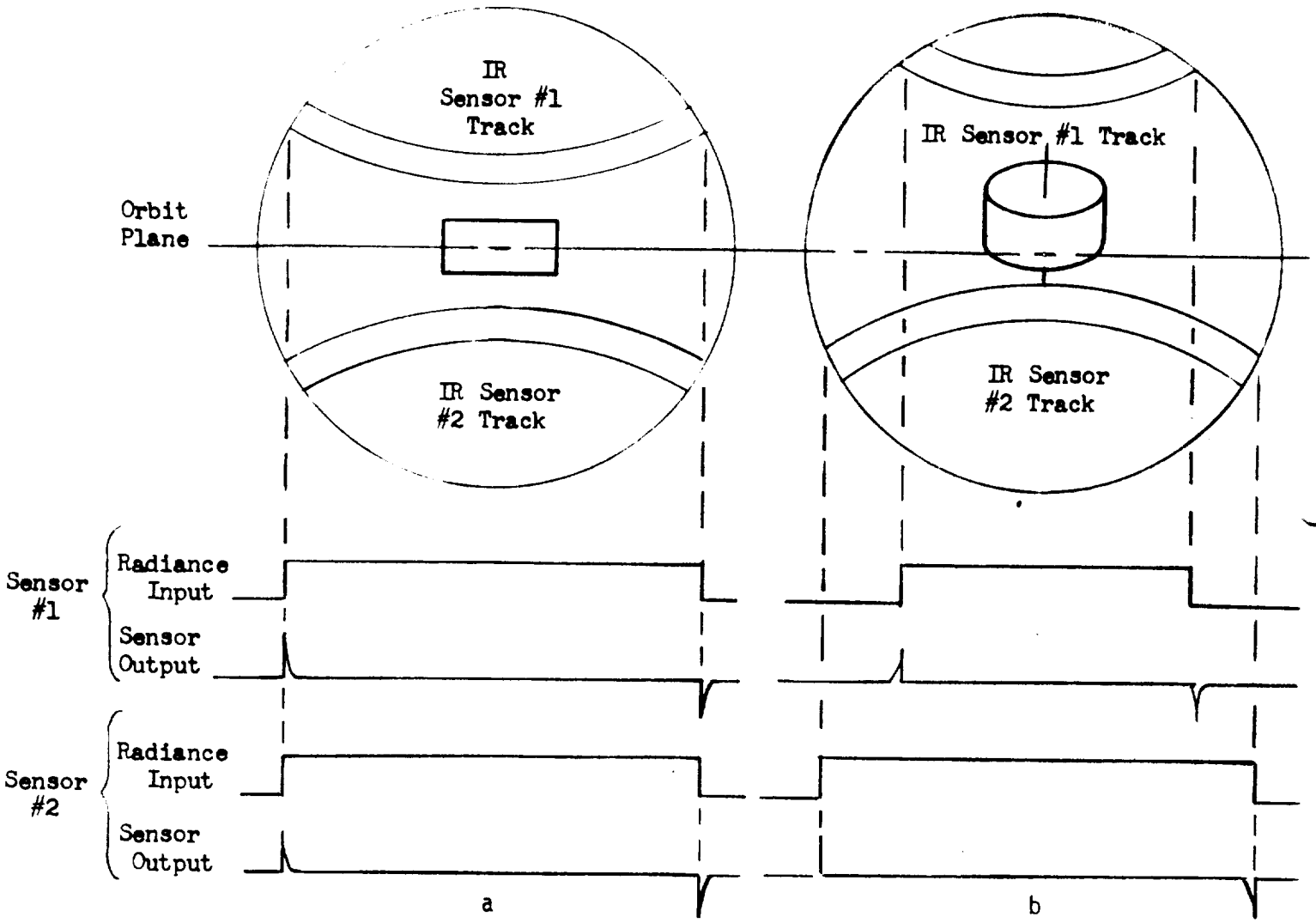

Figure 98. Sensor Scanning Pattern and Output Signals for (a) $\Gamma = 0$ and (b) $\Gamma \neq 0$ but $\Psi = 0$ (Roll error only)

When the spacecraft is in wheel mode attitude (spin axis normal to the orbit plane), the outputs of each channel will show equal time durations of the earth's intercept paths (Figure 98a). If, however, the earth's spin axis is not normal to the orbit plane, a roll error angle exists, as shown in Figure 98b. The earth intercept paths will not be of equal duration as evidenced by the unequal time spans between sky-to-earth and earth-to-sky pulses of the two channels. Roll angle ϕ is defined as the angle between the local vertical and the spin axis minus 90 degrees ($\sin \phi = \hat{s} \times \hat{r}$). With this method, the roll angle is positive if the spin axis points away from the earth and negative if it points toward the earth. Because of the earth's symmetry, the yaw error ψ of attitude cannot be detected directly by the horizon scanner. This is not a limitation since yaw data can be determined from roll data history. Yaw is defined as the angle between the spin axis and the plane defined by the orbit normal and the local vertical. This angle is negative when the spin axis points in the direction of the local orbital vector. By analyzing the time history of the relative duty cycles of the two horizon scanners, ϕ and ψ can be computed as noted earlier.

It can be shown that the equation which relates roll angle to earth time (t_e) and spin time (t_{spin}) measurements from either channel ($i = 1$ or $i = 2$) of the attitude horizon scanner is

$$\cos \beta'_i = \frac{\tan \phi}{\tan \alpha_i} + \frac{\cos h_f}{\sin \alpha_i \cos \phi}$$

where

$$h_f = \sin^{-1} \left(\frac{R_e}{R_e + h}\right) \text{ and } \beta'_i = \left(\frac{t_{e_i}}{t_{spin}}\right) (180°)$$

If data is available from both channels of the attitude horizon sensors, a more convenient expression, which is independent of altitude, may be used:

$$\tan \phi = \frac{\tan \alpha_1}{2} (\cos \beta'_1 - \cos \beta'_2)$$

assuming $\alpha_1 + \alpha_2 = 180°$ and where β_i is 1/2 the earth's intercept angle as viewed by Horizon Sensor i.

In addition to the attitude horizon sensor, there is also a Digital Solar Aspect Indicator (DSAI). This provides a digital readout of the angle between the sun vector and the spin vector once per spin while the satellite is in sunlight. This sensor is particularly useful during the early days of orbit operations when a large attitude maneuver is required. In conjunction with a single accurate roll angle measurement, the solar aspect indicator can be used to determine the attitude of the satellite without a need for time averaging. However, because the resolution of this sun sensor is one degree, it is not as accurate as the roll angle history method previously discussed.

Spin rate is also measured using the infrared sensors. The spin period can be found very accurately simply by selecting an initial and a final earth sky transition and measuring the time between them and dividing by the number of spins.

Error Computation

The total attitude error Γ can be maintained within 1° over extended periods of time by using open-loop control on the satellite. Spin rate may be controlled within 0.5% by ground control. The correction rate will be low. These values were derived from the TIROS IX

missions. However, further tradeoff studies will be conducted to determine the feasibility of an onboard error computer. A highly accurate up-link and down-link system is obviously required to implement the open-loop system.

Magnetic Actuation

The magnetic actuation of a spinning spacecraft (in wheel mode) requires that correctional control functions be performed. A Quarter Orbit Magnetic Attitude Control (QOMAC) system is required to perform spin vector argument (attitude) corrections. The magnetic field generated by this unit must be commutated at twice the spin rate in order to generate a spin-period average secular control torque. This is required since the magnetic field interaction between the satellite dipole and earth dipole is sinusoidal in nature as a function of the vehicle body coordinate rotation with respect to orbit coordinates. The second attitude function to be performed is orbital regression compensation which can be attained by applying a non-secular, non-commutated bias to the magnetic attitude control actuator which will negate the effect of regression rate. Thirdly, spin vector magnitude control must be performed. The magnetic actuation required is orthogonal to the attitude control actuators (in a plane containing the spin axis).

Attitude Control.- The control torque developed by the magnetic interaction between the satellite coil and the earth's magnetic field is given by the vector equation:

$\overline{T} = \overline{M} \times \overline{B}$ (where $\overline{M}$ is the magnetic moment generated by the satellite)

then $\dot{\overline{H}} = \overline{T} = \overline{M} \times \overline{B}$ (H is the satellite angular momentum).

The attitude coils are arranged on the satellite such that the coil axes are collinear with the spin axis;

then

$M = M\hat{s}$ (for a positive magnetic moment in the direction of the spin vector).

Hence, the magnetic torque is always perpendicular to $\hat{s}$

Now

$\overline{T} = \overline{\omega}_p \times \overline{H}_s = \overline{\omega}_p \times I_s \omega_s \hat{s}$ (where ω_p is the resultant precession rate of the applied torque),

then

$$\overline{\omega}_p \times I_s \omega_s \hat{s} = \overline{M} \times \overline{B} = M (\hat{s} \times \overline{B})$$

From analysis of general gyroscopic motion, it can be shown that, for light torque loading, the precession motion which satisfies the equation is

$$\overline{\omega}_p = \frac{-M}{I_s \omega_s} \overline{B}$$

That is, for a positive dipole moment, the spin axis will precess about an axis which is collinear with but opposite in direction to the instantaneous earth's magnetic field over the orbital path. The precession vector in orbital coordinates due to orbital precession and magnetic torquing is given by

$$\overline{\omega}_p = \frac{-M}{I_s \omega_s} \overline{B} + \overline{\omega}_o$$

where $\overline{\omega}_o$ is the orbital precession vector given by

$$\overline{\omega}_o = {}_o (\sin i)\, \hat{b} + \omega_o (\cos i)\, \hat{n}$$

Now, assuming small motion of the spin axis over an interval of time, the net motion can be predicted by average position and magnitude of the precession vector as found by standard integration techniques. The spin axis is assumed to move at a constant rate about the average precession vector during the time interval. The validity of this averaging has been verified by computer simulation as well as actual flight results.

For magnetic bias control (MBC) torquing, the coil is assumed to have constant dipole moment, magnitude and polarity throughout the entire orbit. Orbit averaging of $\bar{\omega}_p$, assuming a near circular orbit, results in the following:

$$\tilde{\omega}_{p\ell} = 0$$

$$\omega_{pb} = + \left(\frac{\mu}{2} - \omega_o\right) \sin i$$

$$\tilde{\omega}_{pn} = - \left(\mu + \omega_o\right) \cos i$$

where

$$\mu = \frac{MK}{I_s \omega_s R^3}$$

Once the spin axis is in the wheel mode, i.e., $(\hat{s} = \hat{n})$, adjusting μ to equal $2\omega_o$ by selecting a particular spacecraft dipole moment M causes the spin axis to remain in the wheel mode. That is, in spite of orbit regression, which causes a rotation rate of $\hat{n}$ equal to ω_o about the north geographic pole, the spin axis will be continuously torqued to move at the same rate. This is neglecting the effect of the uncanted dipole; however, TIROS IX flight data indicates a 75% reduction in spin axis drift with respect to orbit normal with the MBC from the uncompensated drift rate. Even though TIROS satellites were magnetically nulled before

liftoff, they nevertheless have been noted to retain a residual dipole after orbit injection. The MBC control is employed to cancel this dipole moment. For the near polar orbits of magnetically controlled spacecraft, both orbital precession and residual magnetic precession have their major component along the $\hat{b}$ axis so that residual drift of of the spin axis is expected to be about $\hat{b}$ which is shown by analysis of TIROS IX flight data.

The effective precession vector, using DC torquing, is almost totally along $\hat{b}$ in the orbit plane, and the injection conditions are such that $\hat{s}$ initially lies approximately along $-\hat{b}$. Therefore, out-of-plane motion with MBC from this initial condition is almost non-existent. However, by reversing the coil current each quarter orbit, a precession vector lying anywhere in the orbit plane can be generated. This means that the average precession vector can always be selected normal to the spin vector so the net motion of the spin vector is in a plane perpendicular to the orbit plane which will facilitate orientation of the spin vector into near coincidence with orbit normal after injection.

The quarter orbit reversal of current and a time delay from the ascending node are the fundamental elements of the Quarter Orbit Magnetic Attitude Control (QOMAC) technique. A typical coil current schedule for this approach is shown in Figure 99 . Continuous repetitive cycles may be programmed to achieve greater spin axis motion.

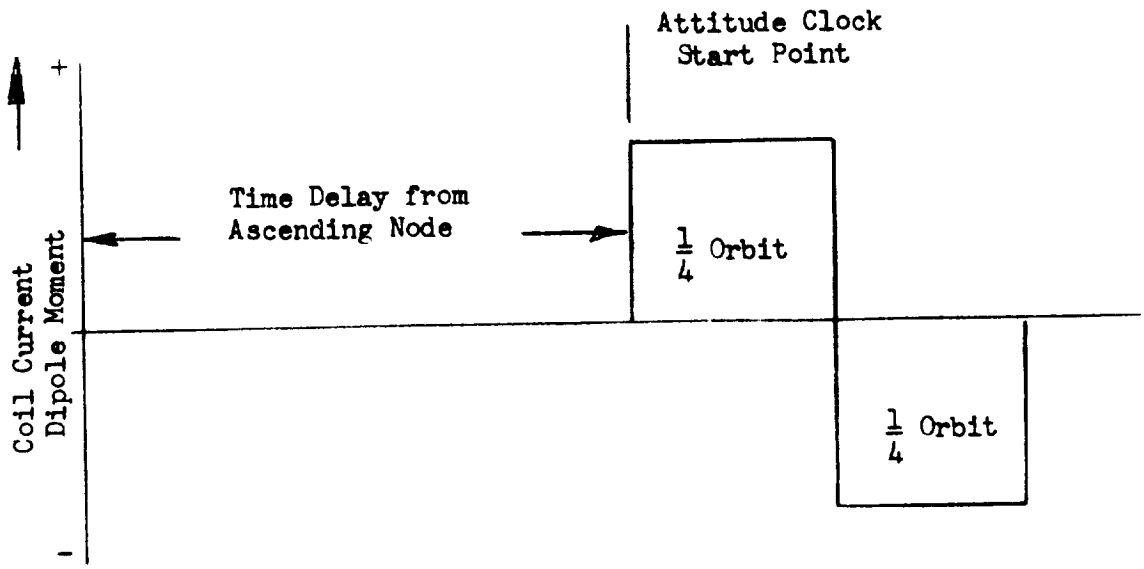

Figure 99. QOMAC Coil Current Torquing Profile in Attitude Correction Mode

Expressions for the average precession components as a function of an arbitrary starting phase for the quarter orbit torque program are subsequently developed. The delay angle from the ascending node is β_s. The convention is employed which defines the torque coil magnetic moment as positive (in the direction of the satellite spin axis) during the first quarter orbit of a torque cycle. Again, using orbit averaging techniques, the following expressions for orbital coordinate control precession rates ω_p can be developed:

$$\tilde{\omega}_{p\ell} = \frac{-\mu}{\pi}\left\{-\frac{3}{2}\sin i\left[\int_{\beta_s}^{\beta_s+\frac{\pi}{2}} \sin 2\beta \, d\beta - \int_{\beta_s+\frac{\pi}{2}}^{\beta_s+\pi} \sin 2\beta \, d\beta\right]\right\}$$

$$= \frac{3}{\pi}\mu \sin i \cos 2\beta_s$$

$$\tilde{\omega}_{pb} = \frac{\mu}{\Pi}\left\{\frac{3}{2}\sin i\left[\int_{\beta_s}^{\beta_s+\Pi/2} d\beta - \int_{\beta_s+\Pi/2}^{\beta_s+\pi} d\beta\right]\right\}$$

$$= \frac{3}{\Pi}\mu \sin i \sin 2\beta_s, \text{ and}$$

$$\tilde{\omega}_{pn} = 0$$

The axis about which the average precession motion occurs is then at an angle Λ measured counterclockwise around $\hat{n}$ from the ascending node to the precession axis. The angle Λ is defined by

$$\tan \Lambda = \frac{\tilde{\omega}_{p_b}}{\tilde{\omega}_{p_\ell}}$$

$$= \tan 2\beta_s$$

$$\beta_s = \frac{\Lambda}{2} + m\Pi, \quad (m = 0, 1, 2, \ldots)$$

This implies that a precession axis can be selected to lie anywhere in the orbit plane, at an angle Λ with respect to the ascending node. The half-orbit average precession rate about this axis is, then,

$$\left|\tilde{\omega}_p\right| = \frac{3}{\Pi}\mu \sin i.$$

To utilize the precession technique to align the spin axis coincident with the orbit normal, the precession vector must be normal to $\hat{n}$ and $\hat{s}$ which occurs at orbit angle λ. Hence, by selecting a start angle

$$\beta_s = \frac{\lambda}{2} + m\Pi \qquad (m - 0, 1, 2 \ldots\ldots),$$

the average precession vector will lie along λ.

The application of QOMAC to wheel mode satellites first requires the determination of attitude coordinates Γ and λ. Γ indicates how far the spin axis must be precessed and λ indicates the appropriate start angle (or time) for correctional torquing.

The required dipole moment history is accomplished by using a programmer which starts a QOMAC cycle with an appropriate time delay after

a command is received. The clock will run up to eight consecutive QOMAC cycles by reversing the dipole moment every quarter orbit of correction. The satellite will be designed for high torque (precession rate of 10 deg/orbit) or low torque (ω_p = 4 deg/orbit) depending on the appropriate dipole moment. If the assumption of an uncanted dipole is relaxed ($i_m \neq 0, \Omega \neq 0$), orbit averaging techniques may again be applied to yield the results

$$\tilde{\omega}_{p\ell} = \frac{3}{\pi} (a \cos 2\beta_s - b \sin 2\beta_s)$$

$$\tilde{\omega}_{pb} = \frac{3\mu}{\pi} (a \sin 2\beta_s + b \cos 2\beta_s), \text{ and}$$

$$\tilde{\omega}_{pn} = 0$$

where

$$a = \cos i \sin i_m \cos \Omega - \sin i \cos i_m, \text{ and}$$

$$b = \sin i_m \sin \Omega$$

Note than when $\Omega = i_m = 0$, these equations reduce to those for the uncanted case, and Λ is defined by

$$\tan \Lambda = \frac{\tilde{\omega}_{pb}}{\tilde{\omega}_{p\ell}}$$

$$= \frac{a \sin 2\beta_s + b \cos 2\beta_s}{a \cos 2\beta_s - b \sin 2\beta_s}.$$

By rearranging this equation and solving for β_s, it can be shown that

$$\tan 2\beta_s = \tan \left\{ \Lambda - \tan^{-1} (b/a) \right\}$$

or

$$\beta_s = 1/2 \left\{ \Lambda - \tan^{-1} (b/a) \right\}^*$$

*Note that $i_m \geq \tan^{-1} (b/a) \geq -i_m$, thus eliminating quadrant problems.

To compensate for errors in the quarter orbit clock*, a correction factor is added to the computation for β_s. The rationale of this correction is based on an attempt to spread the error over the whole cycle or the whole chain of cycles rather than permit the error to accumulate at the end of a cycle. This is shown in Figure 100.

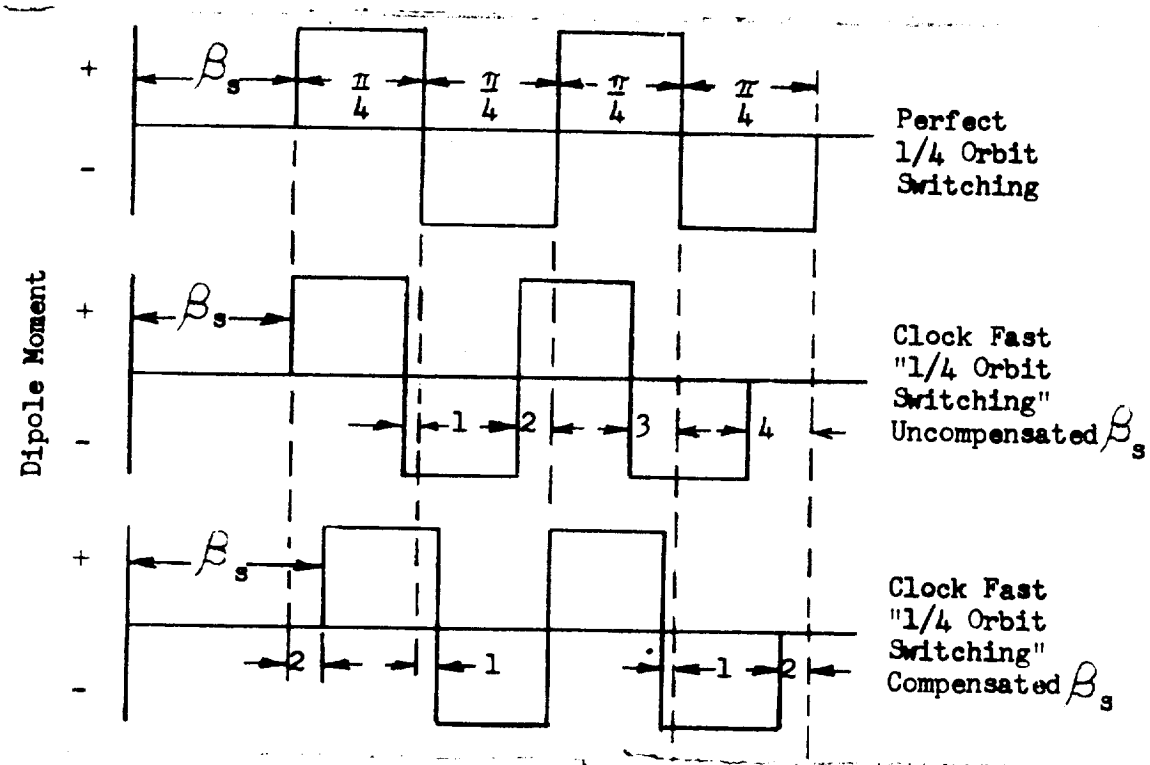

ε = clock error = $\left(\frac{-\text{p QOC}}{4}\right) \frac{360°}{}$

p QOC = period in QUARTER ORBIT CLOCK

τ = anomalistic period

Figure 100. Compensated and Uncompensated Dipole-Moment Programs Compared with Ideal Quarter-Orbit Switching

*Quarter Orbit Clock counts quarter orbit time intervals based on an orbit period which is established before launch.

β_s is then expressed by

$$\beta_s = \frac{1}{2} \{ - \tan^{-1} b/a \} + (1 - \frac{p_{QOC}}{\tau}) \; 90° \; N_Q$$

where N_Q is the number of consecutive QOMAC cycles

The MBC system serves another function in addition to nulling the residual dipole of the satellite. That is, by selecting the appropriate d-c dipole value, the residual plus the normal regression rate value, the off-orbit normal drift rate of the satellite can be reduced considerably. This is verified as follows:

The time derivative of the spin vector with respect to the rotating coordinate system fixed in the orbit plane is given by

$$\dot{\hat{s}} = \hat{s} \times \bar{a}$$

where

$$\bar{a} = \mu \hat{b} + \bar{\omega}, \text{ and}$$

$$\bar{\omega} = \text{orbital precession vector}$$

Assuming that the orbit-normal orientation is acquired, the spin vector can be made to track the orbit normal by selecting the appropriate magnetic bias for the satellite. That is, the value of μ, which is directly proportional to the magnetic moment, must be such that $\bar{a}$ is parallel to $\hat{s}$, hence $\dot{\hat{s}}$ is equal to zero (with respect to $\hat{\ell}$, $\hat{b}$, $\hat{n}$ coordinates). Assuming that the spin vector is initially aligned with the orbit normal, i.e.,

$$\hat{s} = \hat{n}$$

noting that

$$\bar{\omega} = \omega \sin i \, \hat{b} + \omega \cos i \, \hat{n}$$

and orbit averaging, it can be shown that

$$\bar{b}_{avg.} = - \frac{\sin i}{2} \hat{b} + \cos i \, \hat{n}, \text{ and}$$

$$a_{avg.} = (\omega \frac{\mu}{2}) \sin i \, \hat{b} + (\mu + \omega) \cos i \, \hat{n}$$

Therefore, if the magnetic moment is selected so that

$$\omega - \frac{\mu}{2} = 0$$

then

$\bar{a}_{avg.}$ is parallel to $\hat{n}$, and $\hat{n}$ is equal to $\hat{s}$

Therefore,

$\hat{s}$ is parallel to $\bar{a}$, and $\dot{\hat{s}}$ is zero

Due to the fact that the earth dipole is canted, there exists a finite (not infinitesimal) granularity in the MBC values. The exact orbit-normal attitude acquisition is difficult to accomplish and practically impossible to verify. It is unrealistic to expect the drift rate to be zero; however, it is possible to reduce the drift rate considerably by selecting the appropriate dipole value. This was verified using computer simulation on the TIROS IX wheel satellite program.

Spin Rate Control.- A spin-stabilized vehicle requires that a nominal angular velocity be maintained about the axis of maximum moment of inertia. A rotating vehicle sees an oscillating magnetic field which penetrates its conducting surfaces. The resulting losses due to eddy currents and hysteresis tend to despin the satellite. A magnetic spin control system (MASC) will be used for controlling spin rate to better than 0.5%.

To control spin vector magnitude, a magnetic coil whose axis is normal to the spin axis is required. Figure 101 shows the coil in an arbitrary position in orbit.

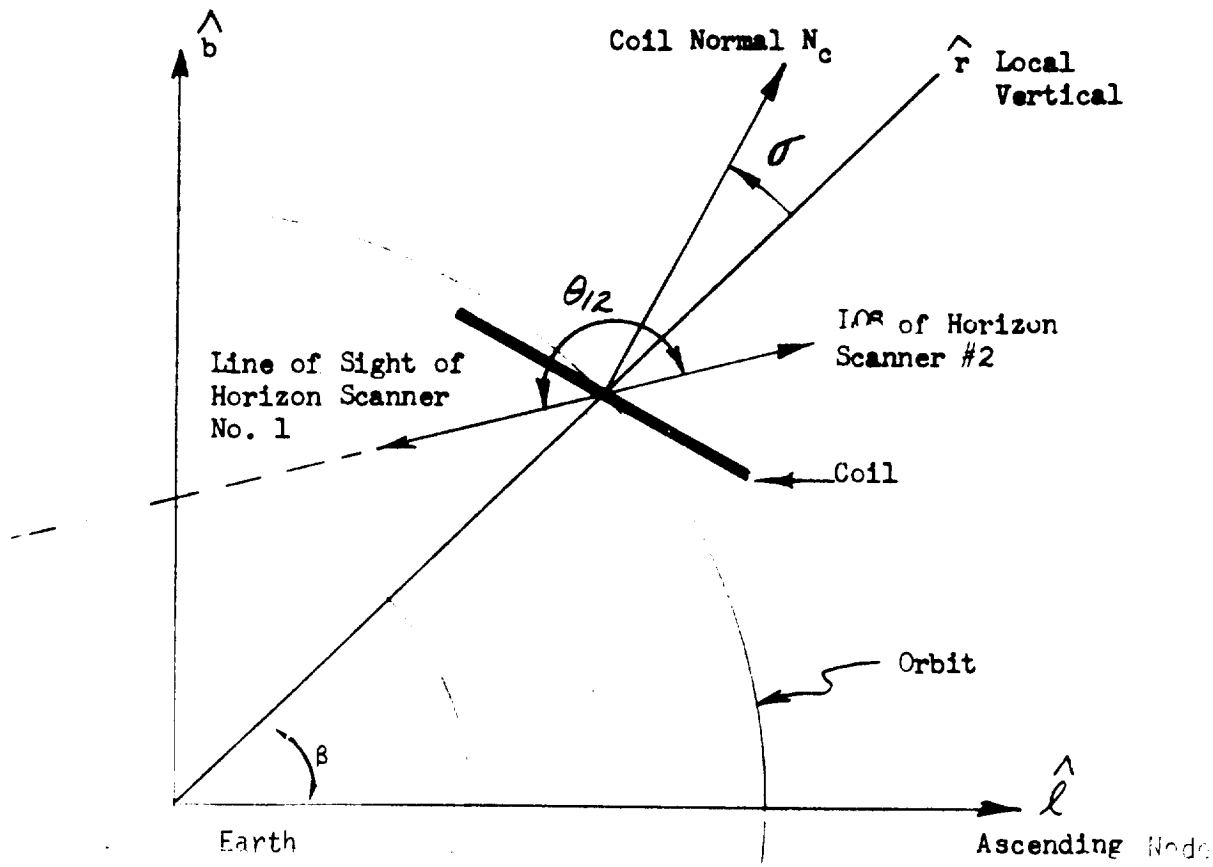

Figure 101.Orientation of MASC Coil in Orbit

The spin control algorithms given here are based on the use of two horizon sensors (the IR horizon sensor and the UV horizon sensor) with respective lines of sight θ_{12} degrees apart, as shown in Figure However, the magnetic torquing relationship between the satellite dipole and the earth's magnetic dipole could be implemented by detecting spin rate by any means.

If time, t, in one spin period is taken to be zero when Horizon Sensor No. 1 senses a sky-to-earth transition, the positive displacement of the coil normal, N_c, from the local vertical at the start of each spin cycle can be expressed by the angle σ . For a non-eccentric

orbit σ is a constant. The magnetic dipole moment generated by the satellite dipole when the spin axis is collinear with the orbit normal ($\Gamma = 0$) is

$$\overline{M} = M \left[\cos\left(\omega_s t + \sigma + \beta\right) \hat{\ell} + \sin\left(\omega_s t + \sigma + \beta\right) \hat{b} \right]$$

The earth's magnetic field components as previously given are:

$$\overline{B} = \frac{K}{R^3} \Bigg[\Bigg\{ -\frac{3}{2} \sin i \cos i_m \sin 2\beta + \sin i_m \frac{1}{2} \Big[\sin \Omega + \frac{3}{4} (\cos i + \ell) \sin (2\beta + \Omega) + \frac{3}{4} (\cos i - \ell) \sin (2\beta - \Omega) \Big] \Bigg\} \hat{\ell}$$

$$+ \Bigg\{ \frac{1}{2} \sin i \cos i_m (3 \cos 2\beta - \ell) + \sin i_m \Big[\frac{1}{2} \cos i \cos \Omega - \frac{3}{4} (\cos i + \ell) \cos (2\beta + \Omega) - \frac{3}{4} (\cos i - \ell) \cos (2\beta - \Omega) \Big] \Bigg\} \hat{b}$$

$$+ \Big\{ \cos i \cos i_m + \sin i \sin i_m \cos \Omega \Big\} \hat{h} \Bigg]$$

Substituting these relationships into the basic torque equation ($\overline{T} = \overline{M} \times \overline{B}$) and integrating over one spin period results in the net average MASC torque.

$$\overline{T}\ \text{avg/spin} = \frac{KM}{R^3} \frac{\sin \frac{\theta_{12}}{2}}{\pi} \Bigg\{ 2 \Big[\cos i \cos i_m + \sin i \sin i_m \cos \Omega \Big] \Big[\sin \left(\frac{\theta_{12}}{2} + \sigma + \beta \right) \hat{\ell} - \cos \left(\frac{\theta_{12}}{2} + \sigma + \beta \right) \hat{b} \Big]$$

$$+ \Big[3 \sin i \cos i_m \cos \left(\beta - \sigma - \frac{\theta_{12}}{2} \right) - \frac{3}{2} \sin i_m (\cos$$

$$\cos \left(\beta \ldots \frac{\theta_{12}}{2} \right) \ldots 2 \sin i_m (\cos i + 1) \cos \left(\beta + \Omega - \sigma - \frac{\theta_{12}}{2} \right)$$

$$- \sin \Omega \sin i_m \sin \left(\beta + \sigma + \frac{\theta_{12}}{2} \right) + (\cos i \sin i_m \cos \Omega$$

$$- \sin i \cos i_m) \cos \left(\beta + \sigma + \frac{\theta_{12}}{2} \right) \Big] \hat{n} \Bigg\}$$

For spin axis orientation perpendicular to the orbit plane, the $\hat{n}$ component of the $\overline{T}$ avg/spin vector provides the desired spin control torque, while the $\hat{\ell}$ and $\hat{b}$ components introduce undesirable spin axis precession. The change in spin rate occurs over an angular orbit

sector $(\beta_f - \beta_i)$ which can be obtained by integrating the n component over the sector

$$\Delta\omega_s = \int_{\beta_i}^{\beta_f} \frac{T_n}{I_s\ \omega_s}\, d\beta$$

The corresponding amount of precession occurring over this interval is

$$\psi = \frac{T_{\ell b}\ (\beta_f - \beta_i}{I_s\ \omega_s\ \omega_o}$$

Optimum commutation occurs when θ_{12} is 180 degrees (i.e., when triggering pulses resulting from sensing sky-to-earth transitions of the two horizon sensors, separated by exactly one-half spin period. Furthermore, maximum torque per spin cycle is produced when the commutation is timed to coincide with an instantaneous zero torque condition. Since the earth's magnetic field is strongest in the vicinity of the poles, current reversal through the torquing coil when the coil axis is aligned with local vertical ($\hat{N}_c \times \hat{r} = 0$) is equivalent to optimizing the commutation process in the vicinity of the strongest magnetic field. Figure 101 shows that such an implementation requires $\sigma = 0$.

Although MASC can be implemented for orbits having lower inclinations that 100 degrees, the higher inclinations (near polar orbits) result in utilization of the strong field components $\hat{B}_\ell$ and $\hat{B}_b$ for spin torquing while simultaneously reducing the normal component $\hat{B}_n$ which leads to undesirable precession.

The numerous parameters occurring in the equation for average torque per spin for MASC make a digital computer simulation desirable. This has been done for TIROS IX with performance sensitivities for all

parameters having been examined. However, the MASC performs well without computer support in a highly predictable manner. Nominal orbit variations will have a minor effect on predicted MASC performance.

The effect of the two-degree variation in spin axis orientation from nominal will have an insignificant effect in spin torque causing roughly a 1.3% change. The maximum precession angle expected through a ten-minute torquing period will be approximately 0.09 degree. A 2-degree variation of spin axis orientation during a spin vector magnitude torquing mode only results in a 22% change in the precessed angle of 0.09 degree after ten minutes.

To achieve spin rate control to $\pm 0.5\%$, the following factors must be considered:

(1) Spin rate decay due to hysteresis and eddy current effects,

(2) Horizon sensor error due to environmental sensitivity

(3) Transmission and computation error

It is estimated that three MASC corrections per week will result in a 0.1 rpm deviation from the nominal spin rate of 4 rpm. Short-term fluctuation of the horizon sensor output pulse rise time has not been found to cause a change in spin rate with the infrared sensor employed. It is feasible to measure the spin period to better than 1 millisecond by averaging a series of consecutive horizon pulses transmitted to the ground station.

Disturbance Factor.- The characteristics of the major sources of external torque which might affect a spin-controlled satellite in wheel mode are both gravitational and magnetic. A non-symmetric, rigid body

in a gravitational field will experience a measurable torque if its principal moments of inertia are unequal. The moment of inertia of a spin-stabilized satellite about its spin axis must, of necessity, be larger than its transverse moment of inertia or a passive nutation damper will not reduce the spin axis nutation. The primary disturbance to attitude is magnetic cross coupling, while spin rate decay is due primarily to eddy currents.

System Selection

In review of the conceptual design approaches and flight data analysis of the TIROS IX and DME-A magnetic control systems, it is clear that the TIROS IX actuation concept is superior if low torquing rates are acceptable.

The major difference in the two systems is that TIROS IX employs air coils for magnetic actuation, whereas the DME-A uses a magnetic core. The magnetic core provides additional torquing capability, at the expense of null resolution of spin rate and spin vector attitude. The magnetic cores in the DME-A actuator are rechargeable permanent magnets which generate a residual dipole moment of the spacecraft with the electromagnetic coils de-energized. The residual field must be sensed and compensated for by passing an appropriate amount of current through the coils to make interaction between the earth's field and the satellite dipole inactive. Although the magnetometer null calibration curve did not seem to change significantly from pre-flight adjustment, the granularity of magnetic null indication is only 20 pole-cm.

Significant drift rates were observed during flight testing of DME-A which are partially attributed to magnetic cross coupling of the earth's field with a residual satellite dipole as well as gravity gradient torque effect. Spin axis orientation was held to five-degree half-cone angles to orbit normal for long periods of time, whereas the TIROS IX maintained half-cone angles of less than 1.0° over extended periods of time (several weeks). Similarly, the DME-A satellite controlled spin rate to ±10% whereas TIROS IX controlled spin rate to 0.2%.

In addition to the obvious difference in performance, the TIROS IX magnetic control system requires less area, weighs less, and is less expensive.

Conclusion

The TIROS IX concept of magnetic actuation is superior to other flight-tested concepts for low torque applications. This concept is adaptable for use with either an open-loop (ground control) or closed-loop (onboard) error computer.

A derivative of this system will be used for the UV-MW satellite mission. The system design will be outlined subsequently.

Tradeoff Analysis of Onboard vs. Ground Controlled Error Computer for Attitude Control

The previous evaluation defines baseline sensing and actuation systems for the proposed dynamics control system. However, definition of the baseline error computer is not made. That tradeoff is made here, completing the system analysis for the dynamics control system.

In-Orbit Reference Frame

β - corresponds to the orbit angle where the S projection should point if there were no yaw error (measured in time% of one period)

λ' - the angle from the ascending node to the plane formed by and S.

λ - $\lambda' - 90°$

Γ - total attitude error

ϕ - roll error angle

ψ - yaw error angle

$\hat{\eta}$ - orbit normal

$\hat{s}$ - spin vector

Error Correction Requirements

The requirements for the dynamic control system, when functioning in the attitude hold mode, are:

(1) Measure spin rate and correct for errors larger than 0.5% from nominal.

(2) Measure the angular deviation from alignment between the satellite spin vector and the orbit normal and correct for half-cone angles of larger magnitude than $\pm 2°$ from coincidence.

Error Correction Philosophy

Existing theory and flight data verification shows the error types which may occur are:

(1) An attitude bias which is created by a constant precession rate from the effects of residual satellite magnetic

polarization reacting with the earth's magnetic field, and an attitude bias caused by the earth's regression around the sun.

(2) Attitude errors which will vary as a function of magnetic cross-coupling and gravity gradient torques which become more pronounced as a function of misalignment, non-optimal torquing algorithms and large attitude errors in the case of magnetic torques and orbital ellipticity in the case of gravity gradient.

(3) Spin rate decay as induced by the presence of hysteresis and eddy currents.

It is reasonable, then, that there should be an attitude bias control Magnetic Bias Coil (MBC), a random attitude correction controller Quarter Orbit Magnetic Attitude Coil (QOMAC), and a spin control system Magnetic Spin Coil (MASC).

The first two questions which must be advanced are the following:

(1) What are the relative merits/disadvantages of a full closed-loop, onboard controller?

(2) Is there an advantage to a hybrid error controller of some combination (partly closed-loop, partly ground control)?

It has been demonstrated from TIROS IX flight data, that if a proper value of attitude bias is selected to effectively negate the satellite residual dipole effect and compensate for orbital regression, the satellite in a nearly polar orbit can maintain an attitude error less than 2° half-cone angle and/or a spin rate within 0.5% of nominal for several weeks without a single correction. Typically, the attitude

and spin rate corrections required to maintain these accuracy specifications were no more than three times a week each. This is a very low correction rate. It would appear that any significant investment in closed-loop control would be wasted unless there was another reason why it should be considered. Additionally, since a correction is required at the most once a day for a worst case situation, there is no advantage for the attitude error to be sampled once a second, which is the slowest available frequency from the clock system which is provided for use in orbit time and spin period computation. Provision for a slower onboard frequency would still require continuous onboard power and additional hardware to implement. There is no advantage - in fact, there are four major disadvantages - to an onboard control system:

(1) With continuous, onboard error computation, the power would have to be on all of the time - thereby increasing the total power requirements of the dynamic control system by an order of magnitude.

(2) The cost of the system is significantly increased by providing the automatic error computer.

(3) Reliability decreases because additional parts have been added.

(4) Attitude errors cannot be evaluated individually. In some cases, where the attitude error is just over the tolerance limit, it may be much more desirable to allow a very small additional position error than to introduce a correctional torque, as far as the status of the onboard experiment is concerned.

This rationale would appear to apply equally well to both the attitude control system and the spin rate control system. Since the attitude bias setting will be a single or infrequent correction, it would appear not only functionally desirable but economically mandatory that all three control system error computers be ground commanded. The hybrid system hypothesis, then, apparently holds no merit either, particularly when the telemetry communication medium is established for transmission of one type of error signal for actuation. The additional logic required to accommodate the error signal from the ground to stimulate the other actuation systems is modest.

Sensing and Computational Considerations

With the "V" head attitude sensor the information available about the attitude error in orbit plane coordinates is only in one axis, roll (ϕ), on a short period sample. It takes the compilation of many cycles to extract the yaw (ψ) attitude error from the data. A reference coordinate system is provided in Figure 95 which identifies these angles.

In order to compute the error angle in attitude and the torque start time in orbit, a small digital computer would be required for the following reasons:

(1) In order to obtain the required accuracy in attitude control, average values of many cycles must be made which alludes to the fact that memory requirements exist for storing previously sampled information.

(2) An additional accuracy constraint is imposed by atmospheric conditions through which the horizon scanners must detect the actual earth horizon threshold. The error computer must be able to reject bad data which may be present on the horizon scanner for any one of a number of reasons, including:

(a) Noise;

(b) Cloud interference;

(c) Sun interference;

(d) Low amplitude signal;

(e) Jamming (crosstalk).

This implies that a sophisticated signal analyzer and/or filter be employed to screen input data. This filter would be digital to obtain the desired effectiveness, which means that more memory and a reasonable repertoire of arithmetic and logical commands must be available.

(3) At least a second order transformation between the attitude sensor information and the actual attitude error must be made, which can be implemented either by iterative solution of the equation relating the two or by a table look-up scheme, either of which requires a digital computer. Since the required attitude and spin correction rate will be very low and the inclusion of a computer would increase the size, weight, and power significantly, and the cost by an order of magnitude, onboard, closed-loop control on this mission is not cost-effective.

Conclusion

In order to effectively accomplish the attitude and spin rate control system error computations with an onboard, closed-loop controller within the specified accuracy, a digital computer is required. A computer is not justified in this application when an open-loop ground control system can be employed with no sacrifice in control accuracy and significant savings in onboard size, weight, power, reliability, and cost. Additionally, extensive empirical flight data is available from the TIROS series to add credibility to both the design concept and the associated hardware of a ground controlled system.

System Description

The System Analysis portion describes the results of a tradeoff study performed to determine the most effective method of attitude control for the Ultraviolet and Microwave Horizon Sensor Experimental Satellite. Considering the mission goals and vehicle constraints, it was concluded that a magnetic actuation concept was highly suited to this application. This report describes the system concept and mechanization approach which was selected.

System Definition and Block Diagram

The proposed dynamics control subsystem (Figure 102) consists of the following elements:

(1) Nutation Dampers

(2) Despin Device (for SCOUT or BURNER II launches)

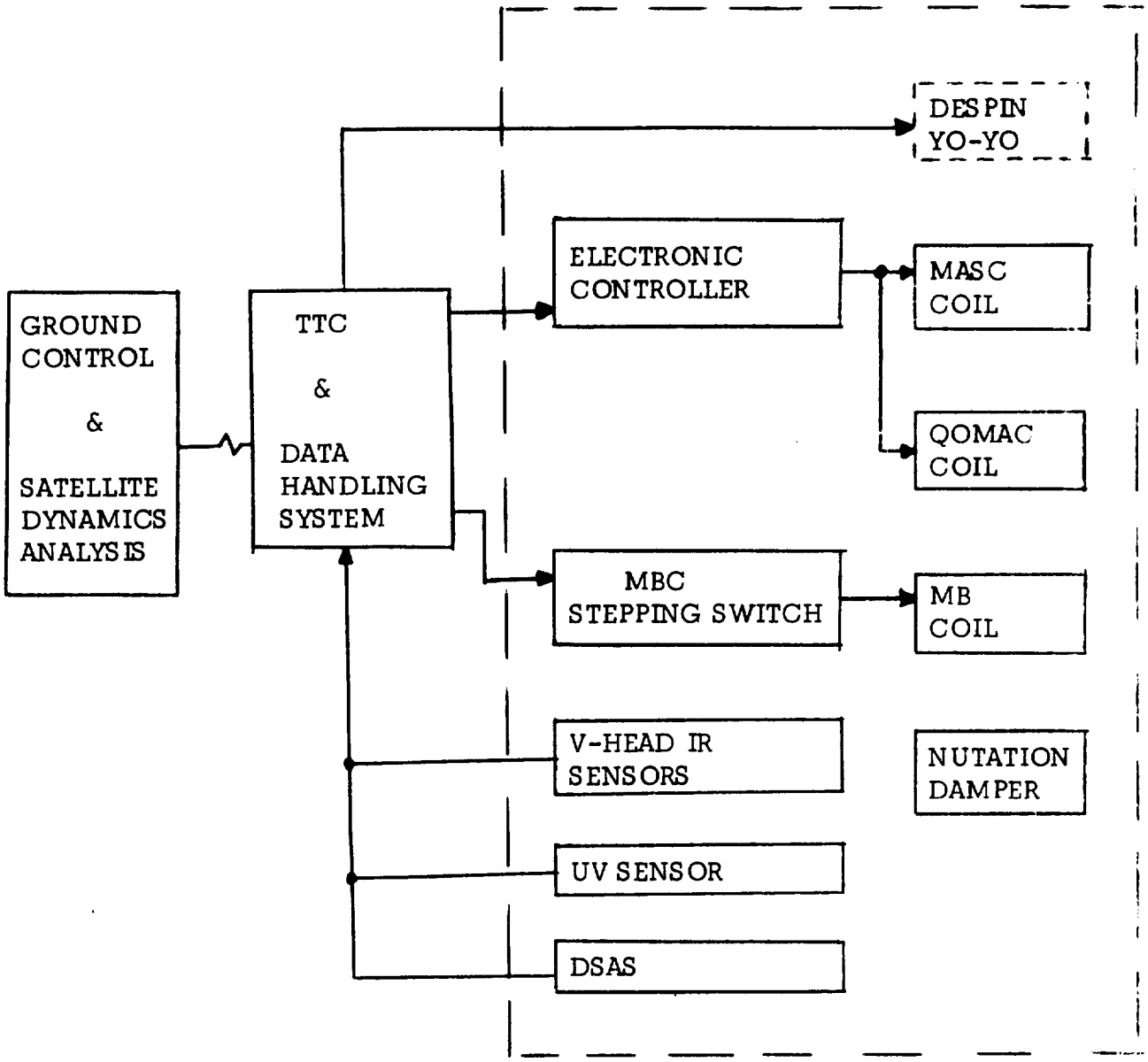

Figure 102. Block Diagram of Dynamic Control System

(3) Orbital Attitude and Spin Control Actuation Subsystems

. Dynamics Control Electronics

. QOMAC (Quarter Orbit Magnetic Attitude Control) Coil

. MBS (Magnetic Bias Control) Coil

. MASC (Magnetic Spin Control) Coil

. MBC Stepping Switch

(4) Attitude Sensors

Nutation Damping Devices

The initial nutation or wobble of the satellite, caused by tip-off torques when the satellite is ejected from the launch vehicle, is damped out rapidly by two tuned-energy absorption-masses (TEAM) that oppose the forces which oscillate the satellite. Two of the nutation damping devices (shown in Figure 103) are installed parallel to the spin axis along the inside wall of the satellite 180 degrees apart. Each mechanism weighs a little under one pound; each mass, approximately three ounces. During boost, the traveling mass is restrained by a mechanical latch which is released when the satellite separates from the launch vehicle permitting the masses to roll freely along the rods. The latches are opened by automatic firing of squibs. The device is tuned to the nutation frequency of the satellite and rapidly absorbs the energy causing the wobble, dissipating this energy in the form of heat. After damping of the nutation, the masses rest at or near the center of the rods.

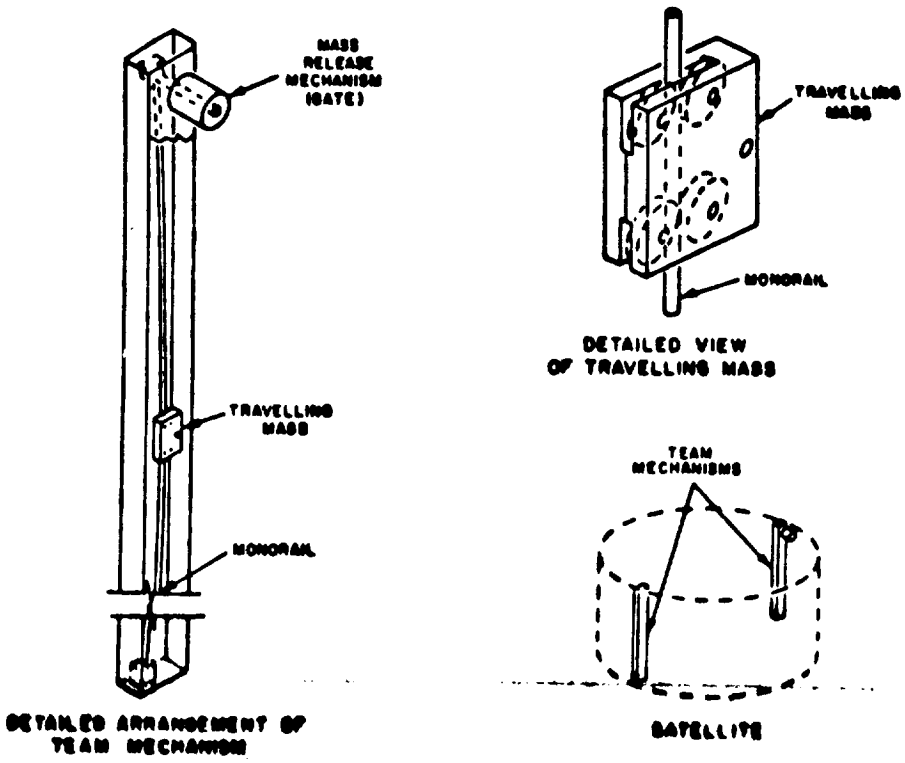

Figure 103. TEAM Precession - Damping Devices

"Yo-Yo" Despin Device

When the satellite separates from the final stage of the carrier rocket, its spin rate may be as high as 180 rpm if the SCOUT or BURNER II vehicles are used. To reduce this initial spin rate to the desired level in as short a time as possible, a despin mechanism can be used to transfer the necessary amount of kinetic energy away from the vehicle. This despin mechanism consists of a pair of cable-attached masses that are released from the satellite structure after reducing the angular velocity by increasing the moment of inertia. The attachment points to the cables are located 180 degrees apart, and the cables wrap around the satellite a full 360 degrees. The masses are released at the required time by automatic firing of squibs.

Centrifugal force causes each cable to unwind until it extends radially from the structure, at which time it slips off an open hook. This device reduces the spin rate of the satellite from a nominal 180 rpm to within 4 rpm. The yo-yo despin is only required if the satellite has a high initial angular velocity upon ejection from the launch vehicle.

Orbital Attitude and Spin Rate Actuation System

The Orbital Attitude and Spin Rate Controller (OASRC) functions as the interface between the up-link telemetry command signal and the magnetic actuation system. The magnetic actuation system includes the Magnetic Bias Control (MBC) coil which negates the residual satellite dipole and provides a magnetic bias for the desired orbit precession, the Quarter Orbit Magnetic Attitude Control (QOMAC) coil which implements

correction of spin vector argument errors with respect to the orbit normal vector, and the Magnetic Spin Control (MASC) coil which implements corrections to the spin vector magnitude. The interrelation between these coils and the Orbital Attitude and Spin Rate Controller is demonstrated in Figure 104. The orientation of these coils with respect to the vehicle geometry is shown in Figure 105 .

The OASRC is commanded from the ground by the command programmer. An OFF command turns off all but standby power to the OASRC. For QOMAC and MASC-coil operation, an ON command is first sent to the OASRC unit to condition the unit to receive programmed data, whereupon a command message consisting of 20 data bits, is issued.

Attitude Control

When the command program specifies a QOMAC coil torquing sequence, upon receipt of the command signal the OASRC proceeds to count out the programmed time delay, T_0. At the end of T_0, current is allowed to flow through one-half of the center-tapped coil for one-quarter orbit. At the end of the first one-quarter orbit, current is switched to the other half of the torquing coil and inhibited from flowing in the first half. This condition continues for another one-quarter orbit, completing one attitude correction cycle. Current is switched through each half of the coil on alternate quarter orbits, until the programmed number of attitude correction cycles have been completed. The quarter orbit time information is pre-set into the OASRC before launch and corrected after the actual orbital period has been determined. At the end of an attitude control sequence, all but standby power is removed from the OASRC.

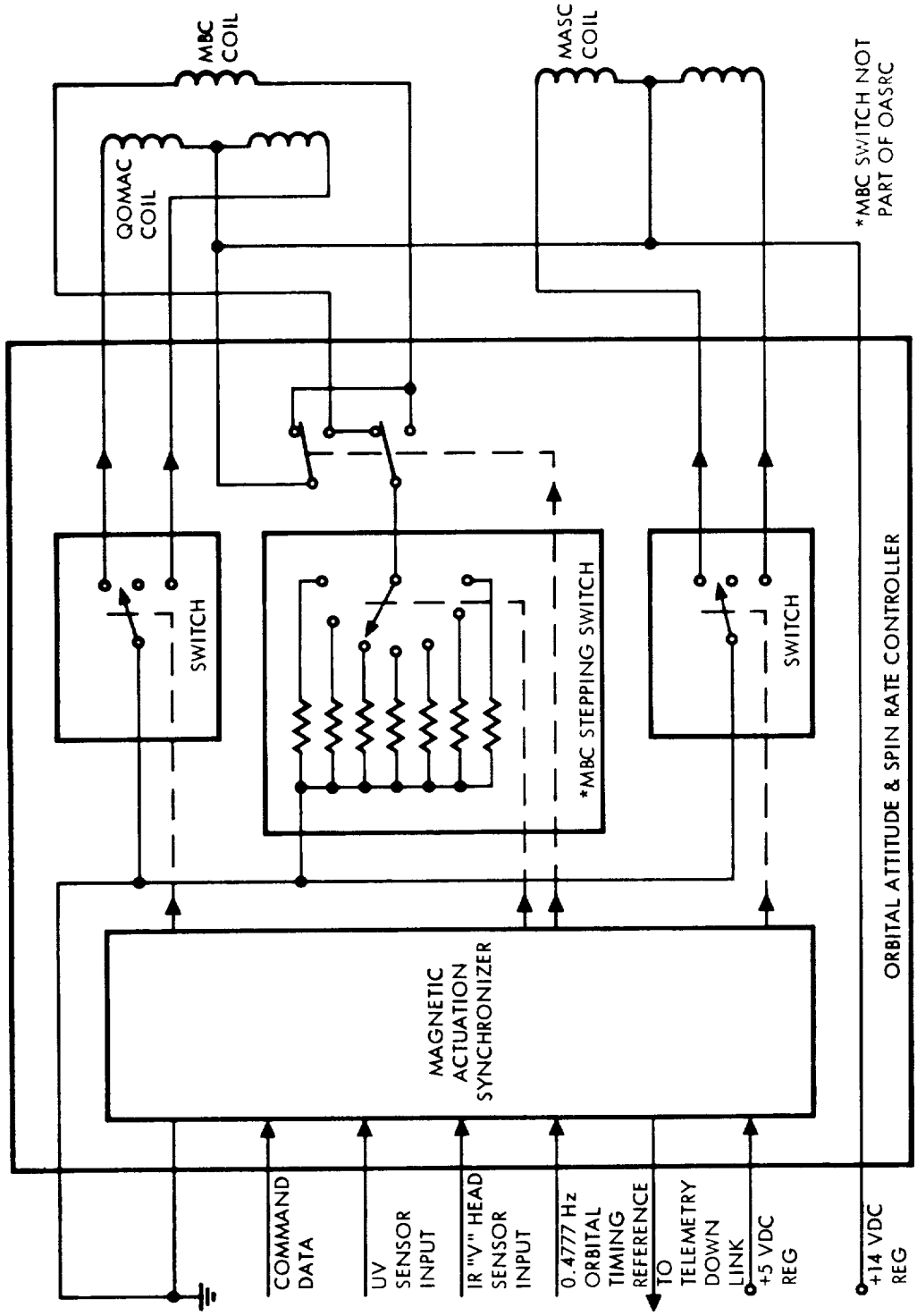

Figure 104. Orbital Attitude and Spin Rate Control Actuator

The OASRC is commanded from the ground by the command programmer. An OFF command turns off all but standby power to the OASRC. For QOMAC and MASC-coil operation, an ON command is first sent to the OASRC unit to condition the unit to receive programmed data, whereupon a command message consisting of 20 data bits, is issued.

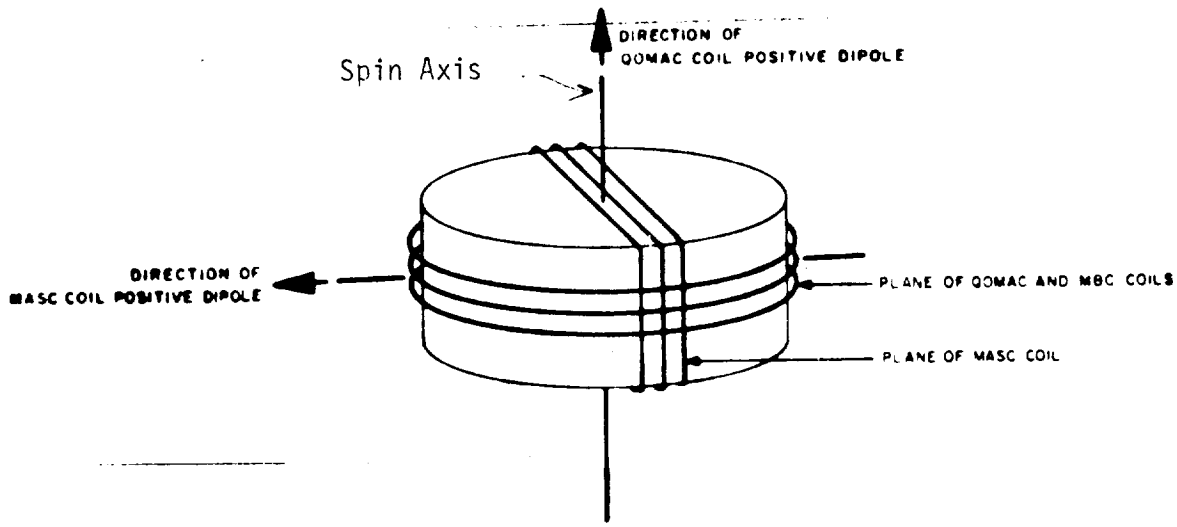

Figure 105. Magnetic Dipoles Associated with QOMAC, MBC and MASC Coils

Spin Control

When the command program specifies operation of the MASC coil, upon receipt of the command signal the OASRC counts out the programmed time delay, T_0, and then causes a MASC coil cycle to commence. A complete spin-correction cycle comprises the flow of current through the coil for a quarter orbit and the removal of the current during the next quarter orbit. During the first and third quarter orbits, direct current is applied through alternate halves of the center tapped coil, respectively, for each half of a satellite rotation.

Information indicating the completion of one-half of a satellite rotation is generated by the UV and IR horizon sensors. Spin-up or spin-down is determined by the phasing of the coil currents with respect to the output information from the opposing horizon scanners.

For spin-up, one sensor enables current through one-half of the coil for Cycles 1, 3, 5, and 7. The other sensor enables current through the other half of the coil for Cycles 2, 4, 6, and 8. For spin-down, these phase relationships are interchanged.

At the end of a spin-control sequence, all but standby power is removed from the OASRC.

Component Description

Orbital Attitude and Spin Rate Controller

An Orbital Attitude and Spin Rate Controller consists of (1) a 17-stage shift/count register, (2) a state sequencer (four control flip-

flops), and (3) miscellaneous logic configurations and interface circuits. Figure 106 is a block diagram of an OASRC unit. When an ON command is received, the register is enabled for data shifting. Upon receipt of the 17th data bit following a data "1", the register overflows and is enabled for counting. When the OASRC has been commanded in an attitude-control or a spin-control mode, T_0 is counted out at 0.4777 pps in the least significant 11 stages. A maximum T_0 of 1 hour 11 minutes and 27 seconds can be counted out in approximately 2-second increments. At the end of T_0, attitude or spin-correction currents flow in the appropriate coil and the register continues counting at 0.4777 pps input rate. A feedback gate, whose inputs are connected by means of an externally mounted plug (one quarter orbit plug) wired in conformance with the predicted orbit time, constrains the least significant 11 stages to count the time required for one quarter orbit. The one quarter orbit time is adjustable in 4-second increments with a minimum time of approximately 17 minutes and a maximum time of 34 minutes. The 12th, 13th, and 14th stages of the register tally one half orbit counts (torquing cycles). An overflow from these stages ends a torquing sequence, and all but standby power to the unit is turned off.

During an attitude-control sequence, after T_0 the state of the 11th flip-flop denotes odd or even quarter orbits and controls which half of the center tapped QOMAC coil receives current.

During a spin control sequence, after T_0, the state of the 11th flip-flop determines whether or not the MASC coil receives current. The 15th flip-flop, whose state is programmed, and a control flip-flop which receives information from opposite looking horizon sensors, determine the phasing of currents in each half of the MASC coil.

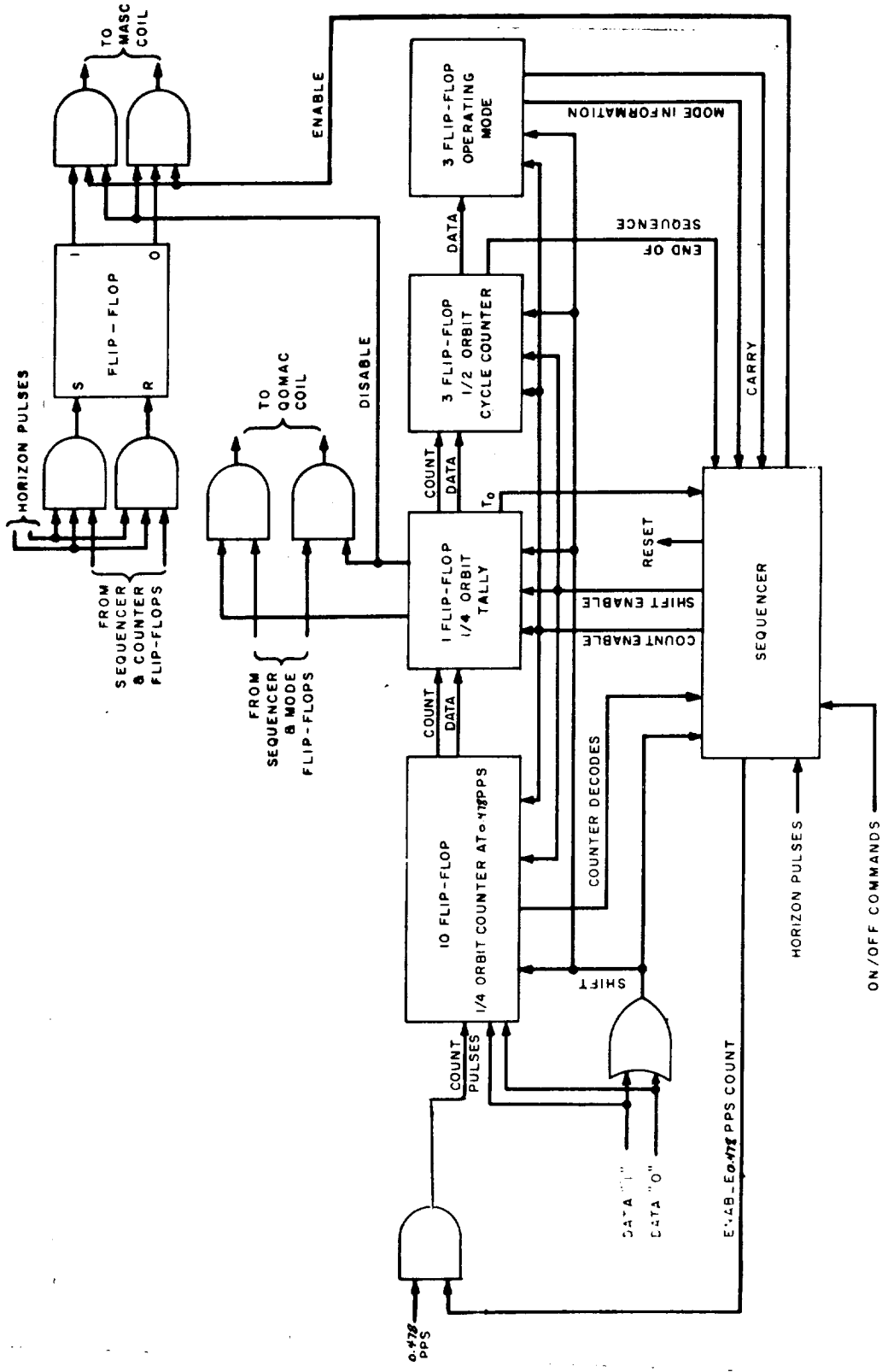

Figure 106. Orbital Attitude and Spin Rate Controller

The following inputs are supplied to the Control Electronics units:

(1) Regulated and switched dc power

(2) Data "1"s and "0"s

(3) 0.4777 register orbital timing reference signal in attitude and spin control modes

(4) Horizon pulses from both the infrared attitude sensor and the ultraviolet sensors.

Outputs from OASRC are as follows:

(1) QOMAC coil operating current

(2) MASC coil operating current

(3) Telemetry outputs

(4) MBC coil current.

The function to be performed by the OASRC is selected by ground command. In the case of attitude control or spin control functions, the torquing-current flow program is also determined by ground command.

A typical command consists of 20 data bits, the least significant 19 of which comprise the actual data required. The most significant bit is always a "1"; the overflow of this bit indicates that the programming is completed. The possible command programs for the OASRC are given in Table 23.

TABLE 23
COMMAND PROGRAMS

Mode	Bit No.						
	20 ← 8	7	6	5	4	3	2	1
Attitude Control	2's complement of T_o at 0.5 pps	No. of cycle				0	1	1
Spin Control (Increase)					0	1	1	1
Spin Control (Decrease)					1	1	1	1
MBC Step					x	x	0	1

As shown in Table 23, Bit No. 1 is always a "1". When Bit No. 2 is a "1", either the attitude-control or spin-control functions are in operation, as determined by Bit No. 3. If Bit No. 3 is a "0", the attitude control function is performed; if Bit No. 3 is a "1", the spin-control function is performed. Bit No. 4 determines whether an increase or decrease in spin rate is required. If Bit No. 4 is a "1" the spin rate would be decreased, whereas a "0" would increase spin rate. If Bit No. 2 is a "0", a magnetic bias coil correction is to be made.

Quarter Orbit Magnetic Attitude Control Coil

The basic QOMAC coil torquing cycle consists of the application of direct current through alternate halves of the center-tapped coil for two consecutive quarter orbits. The command word sent to the OASRC specifies the mode to be used. If QOMAC or MASC coil operation is

specified, the command also specifies when the torquing cycles begin, and the number of cycles to be performed.

When the counting operation begins, the programmed delay time is counted out at a rate of 0.4777 pulse per sec. At the end of the delay time, the half of the QOMAC coil is energized which produces a positive magnetic dipole when connected to ground. At the same time, the register begins counting quarter orbit periods.

The coil is mounted on the satellite with the coil normal coincident with the spin axis. This always produces a torque normal to the spin axis.

Magnetic Bias Control Coil

The MBC coil is wound on the same frame as the QOMAC coil and is orthogonal to the MASC coil.

The MBC coil cancels any magnetic dipole within the satellite due to interaction of the earth's magnetic field and the ferromagnetic materials used in the satellite.

After a number of days in orbit, the satellite begins to show an attitude drift due to interaction of the residual dipole with the earth's magnetic field. This drift is analyzed, the residual dipole is calculated, and the MBC coil switch is commanded by the ground station to step to a position to cancel the residual dipole. After cancellation of the dipole, the MBC coil is used to generate a constant dipole to cause the spacecraft attitude to drift sufficiently to compensate for the precession rate of approximately 1 degree per day that occurs with a sun-

synchronous orbit. This constant, controlled drift reduces the amount of QOMAC programming required.

Magnetic Spin Control Coil

The MASC coil consists of aluminum wire wound in a frame. The MASC coil is operated by means of the Electronic Controller which, through the MASC switch, provides programmed switching of the center tapped coil controlling both the direction of magnetic dipole induced by the coil and the period of current flow. The MASC switch also allows for read-out of switch position.

The general operation of the MASC coil is similar to the operation of the QOMAC coil. In addition to quarter orbit switching periods, half-spin switching periods synchronized with sensing of the earth's horizons are also utilized. Furthermore, the quarter orbit switching does not result in a polarity reversal. Instead, the initial quarter orbit polarity is established in response to the command message, and the current to the entire coil is turned on and off at the quarter orbit intervals. During the quarter orbit period that the coil is on, the polarity of the magnetic dipole is reversed at half-spin intervals by alternately switching the ground connection to opposite ends of the center tapped coil.

Bias Control Switch

The MBC coil switch is a solenoid-operated, three-deck, twelve-position stepping switch that controls the amount of current in the MBC coil (the magnitude of its magnetic dipole). At each of 10 positions

on Deck 1, a current-limiting resistor placed in series with the MBC coil and the 15-volt dc power supply enables the selection of magnetic moments from 0.02 to 0.2 ampere-turns-meter^2, in increments of 0.02 ampere-turns-meter^2.

Each position of the switch on Deck 2 provides an indication of switch position to the telemetry system. The telemetry voltage varies from 0 to 5.0 volts, in increments of 0.5 volt.

Deck 3 is assigned to functions involved with overall dynamic control of the satellite. Position 11 is for the high-torque mode of QOMAC coil operation; Position 12 is the "home" position. When the switch is in either Position 11 or 12, no current will flow in the MBC coil.

Reference Indicator Subsystem

The reference-indicator subsystem is comprised of the V-head IR horizon sensor, the UV horizon sensor, and the digital solar aspect sensor.

The UV horizon sensor is part of the onboard experiment to be evaluated and provides an indication of the sky-earth transitions during a rotation of the satellite. This data presents an indication of the satellite spin period, and is used in programming operation of the MASC to increase or decrease the spin rate. In addition, this data can be used to determine the satellite attitude. UV sensor data is transmitted to the interrogating STADAN ground station.

The V-head IR sensor is the basic system used to obtain an indication of the satellite attitude. This data is used in programming the operation of the QOMAC coil in both the performance of the initial wheel-orientation maneuver and in the maintenance of the wheel attitude. Data from the V-head attitude sensor is transmitted to the ground during attitude control, data acquisition, and standby modes.

The digital solar aspect sensor provides measurements of the angle between the satellite sun line and the satellite spin axis. Knowledge of this angle is required for power availability studies, and, in certain instances, is used in determining satellite attitude. Solar aspect indicator data is transmitted to the STADAN ground stations. Figure 107 indicates the proposed orientation of these sensors on the satellite.

V-Head IR Horizon

The V-head sensor consists of two IR sensors and associated electronics. The two IR sensors are arranged in a "V" configuration, as shown in Figure 108a. When the satellite is in the perfect wheel attitude, the spin axis is normal to an earth radius, and the outputs of the two heads are identical, as shown in Figure 108b. A roll error is detectable as an inequality in the pulse durations from the two heads, as shown in Figure 108c.

The orientation of the spin axis is determined from attitude sensor data derived over a discrete section of the orbit. The accuracy of the computation is determined by the resolution and reliability of

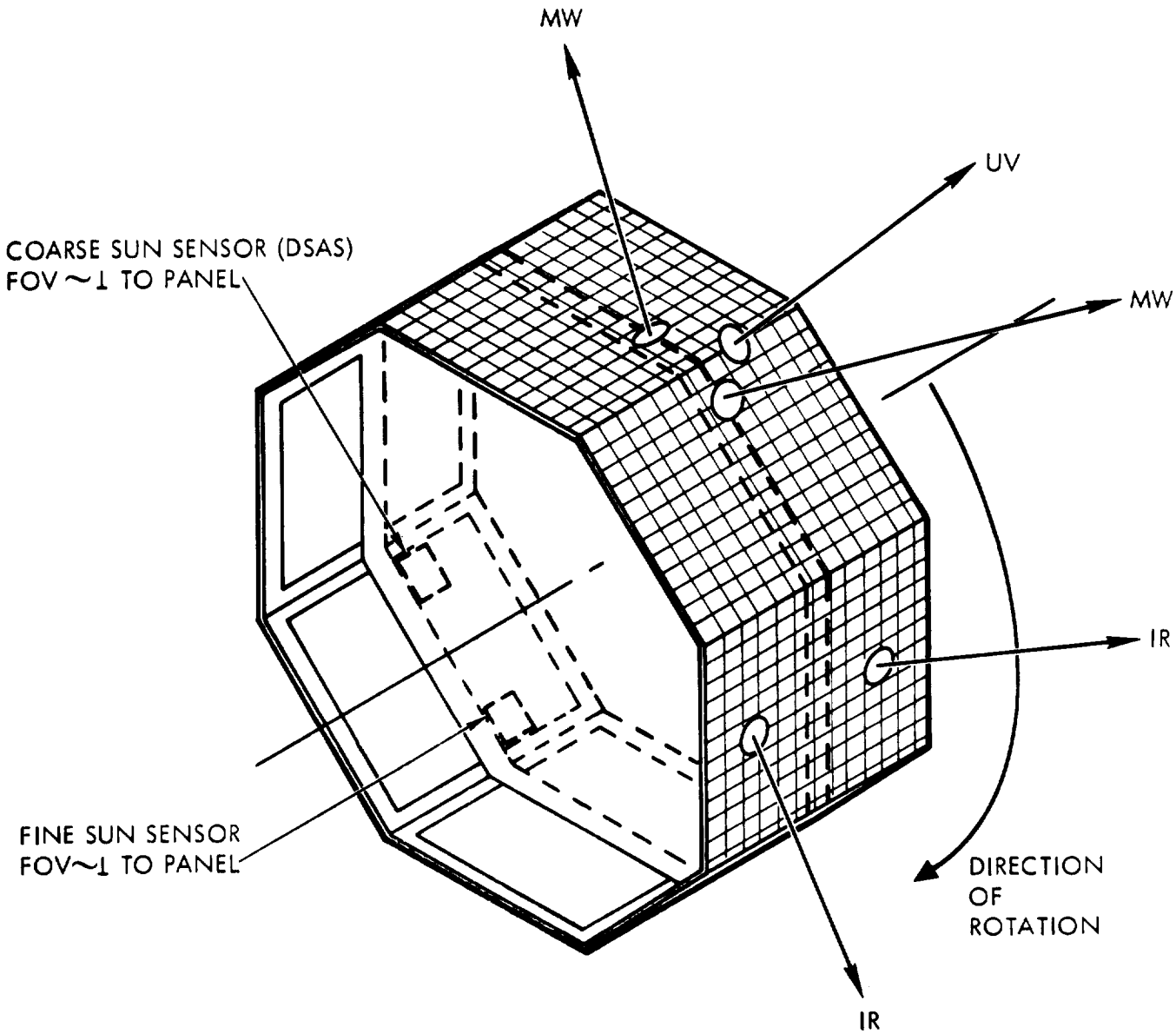

Figure 107. Preliminary Location Equipment Sensors

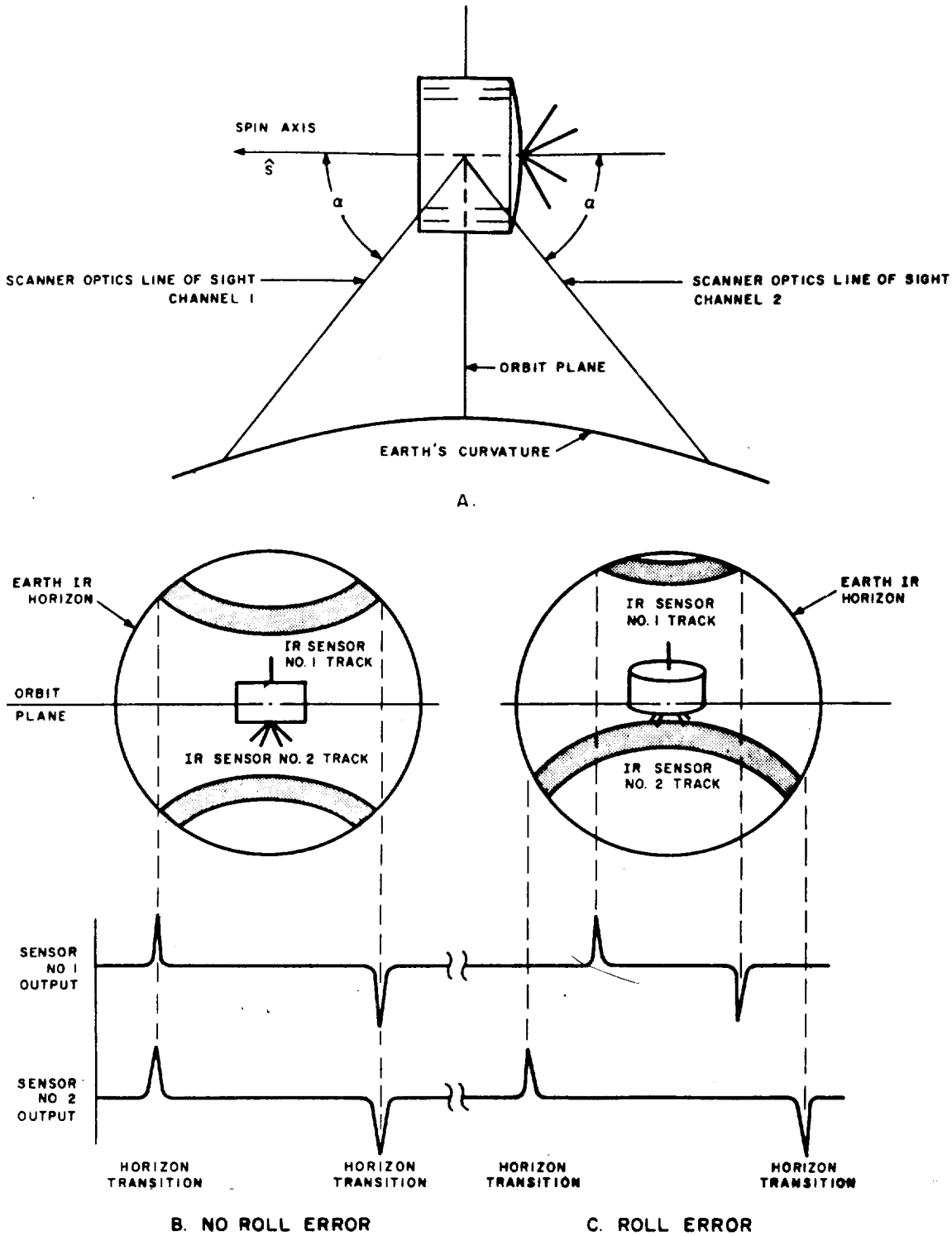

Figure 108. V-Head Attitude Sensor Geometry and Outputs

each of the data points. Consequently, at least 10 minutes of data from a pass over a given STADAN station is required for accurate determination of spin-axis attitude using V-head sensor data alone.

Digital Solar Aspect Sensor

The solar aspect sensor utilizes a gray-coded light mask which produces direct digital readings of the angle between the satellite sun line and the satellite spin axis. The readings are presented as serial, gray-coded words. The solar aspect sensor has a 1-degree resolution over a range of 180 degrees. It consists of two separate subassemblies; the sensing element and an electronics package. The sensing element consists of two 7-bit gray-coded reticles equipped with a small solar cell under each bit, and a "command" reticle which also includes a solar cell. The electronics package contains an amplifier for each bit, bi-stable multivibrators to establish thresholds and to convert the parallel input to a series output, and control circuits. The command reticle causes the angle determined by the gray-coded reticle to be read out when the sun is in a plane defined by the spin axis and the satellite-sun line passing through the aspect eye.

The reticles are small oblong blocks of fused quartz with slits centered along the top surface, and a light mask arranged in a gray-coded pattern, photographically applied to the bottom surface. Sunlight enters the indicator through the slits casting a narrow band of illumination across the light masks. The light passing through the pattern generates a seven-bit word, coded to indicate the angle of incidence of

the light on the mask. Gray code was chosen for the light mask pattern to eliminate any errors in the measurement of the gamma angle caused by errors in the synchronization of the data bits. Such errors could be easily noted in the gray-code since only one data bit would change when the measured angle changes one degree.

UV Sensor

This sensor is part of the experiment and will be employed in attitude control only to commutate the MASC coil during spin vector magnitude corrections.

Conclusion

The recommended dynamic control system mechanization is an open-loop magnetic torquing configuration. The performance of this type of system has been demonstrated by flight data from the TIROS IX and other wheel mode satellites. It is adequate in performance for this application while maintaining simplicity in design, development and test. The integration of this conceptual design with state-of-the-art microelectronic technology provides a reliable, cost-effective attitude control system.

Size, Weight & Power Requirements

The data presented is a size, weight and power requirement estimate of the system previously described.

Parametric data is given by operating mode and specific subsystem requirements and characteristics are broken out so that percentile indices can be associated with the mechanization of specific operational functions.

The subsystems contained in the Dynamic Control System (DCM) are:

(1) Quarter Orbit Magnetic Attitude Control Coil

(2) Magnetic Bias Control Coil

(3) Magnetic Spin Control Coil

(4) Nutation Dampers

(5) Despin Yo-Yo (only required for SCOUT or BURNER II launches)

(6) Magnetic Bias Control Switch

(7) Electronic Controller

The size, weight and power requirements of each of these subsystems are delineated in Table 24.

TABLE 24

DYNAMIC CONTROL SYSTEM SIZE, WEIGHT AND POWER

Evaluation Index / DCS Subsystem	Size (In.^{3})	Weight (#)	Power (w)
QOMAC & MBC Coils	150	3.0	1.5 max (+15v Reg.)
MASC Coil	65	1.5	
Nutation Dampers	50	1.2	0
Despin "Yo-YO"	150*	1.5	0
MBC Switch	50	1.0	
Electronic Controller	100	3.8	2.5 (+5v Reg.)
*Mounted external to spacecraft	565	12.0	4.0

Quarter-Orbit Magnetic Attitude Control Coil

The quarter-orbit magnetic control coil weighs 2.0 pounds, consumes 100 in.^{3} of space around the inside circumference of the vehicle, and uses 1.5 watt power when activated.

The coil is an aluminum wire wrapped around and bonded to a frame which is secured by braces to the inside of the satellite. There are 600 turns of No. 25 AWG wire required for the coil, which generates a dipole moment of 14.0 ampere-turn-meter^2 when consuming 1.50 watts of power from a voltage source of +15 VDC-regulated ($\pm$1.0%).

Magnetic Bias Control Coil

The magnetic bias control coil weighs 1.0 pound (including its portion of the frame), requires approximately 50 cubic inches, and consumes 0.1 watt of power from a voltage source of +15 VDC-regulated $\pm$1.0%, when providing 0.2 ampere-turn-meter^2 of magnetic moment. It is wound from 30 turns of No. 30 AWG aluminum wire on the same frame as the quarter-orbit coil.

Magnetic Spin Control Coil

The magnetic spin control coil weighs 1.5 pounds, occupies 65 cubic inches, and consumes 1.5 watts of power while providing a magnetic moment of 0.33 ampere-turn-meter^2 orthogonal to the spin axis. The coil is comprised of 20 turns of No. 26 gauge aluminum wire wound on a frame which is supported inside the spacecraft.

Nutation Dampers

The nutation dampers are installed vertically inside the wall of the satellite, 180° apart. The total of the two mechanisms weigh 1.2 pounds, requires about 50 cubic inches of space, and draws no power. The dampers are initiated shortly after orbit injection and remain effective throughout the mission. Two 3-oz balls are released to ride in their respective tracks while damping spin-axis nutation. The spin-axis moment of inertia, however, must be larger than the traverse moment of inertia to effect a positive damping coefficient.

Despin Yo-Yo

The despin Yo-Yo mechanism consists of two cable-attached masses which unwind, after the initial orbit injection nutations have been damped out, in order to reduce the injection spin rate to a level which can be accommodated by the magnetic actuation system. The masses and cables weigh approximately 1.5 pounds, require 150 cubic inches on the outside of the satellite canister. No power is required for operation except that involved in firing of the squibs. The cables, which are initially wrapped a full 360° around the satellite body, unwind, while reducing spin rate, ands lip off hooks on the side of the satellite into space when they are fully unwound.

Magnetic Bias Control Stepping Switch

The magnetic bias control stepping switch is a solenoid-operated, three-deck, twelve-position switch which is employed in controlling the amount of current through the MBC coil and, thereby, the magnitude of

its magnetic dipole. At each of ten positions on Deck 1, a current-limiting resistor is placed in series with the coil and its power supply enabling the selection of coil currents to provide a magnetic moment bias of 0.02 to 0.2 amp-turn-m^2 in 0.02 increments. Deck 2 of the switch is assigned to the telemetry function, and at each position of the switch a point on a voltage divider is commected to the telemetry system which provides an indication of switch position to the ground stations. Deck 3 contains logic involving the QOMAC torque level.

Electronic Controller

The electronic controller computes torquing time and effects magnetic actuation based on ground command input data (see previous analysis). It requires approximately 100 cubic inches of space and weighs 3.8 pounds. When in the operation mode, it consumes 2.5 watts of power from a voltage source of +5 VDC-regulated ($\pm$1.0%).

Figures 109, 110, and 111relate the subsystem size, weight and power requirements as a function of mission mode. The time associated with each mode is not in proportion to its space allotment. The attitude hold mode will comprise about 99% of the mission time with the other three modes lasting from a few seconds to a few hours. The size and weight mission profiles are seen to reduce at the point of release of the despin cables accounting for about 15% of orbit injection value. On the other hand, there is virtually no power consumed until the vehicle is despun and the reorientation maneuver commences, at which time the power supplies to the Dynamic Control System (DCS) are turned on and

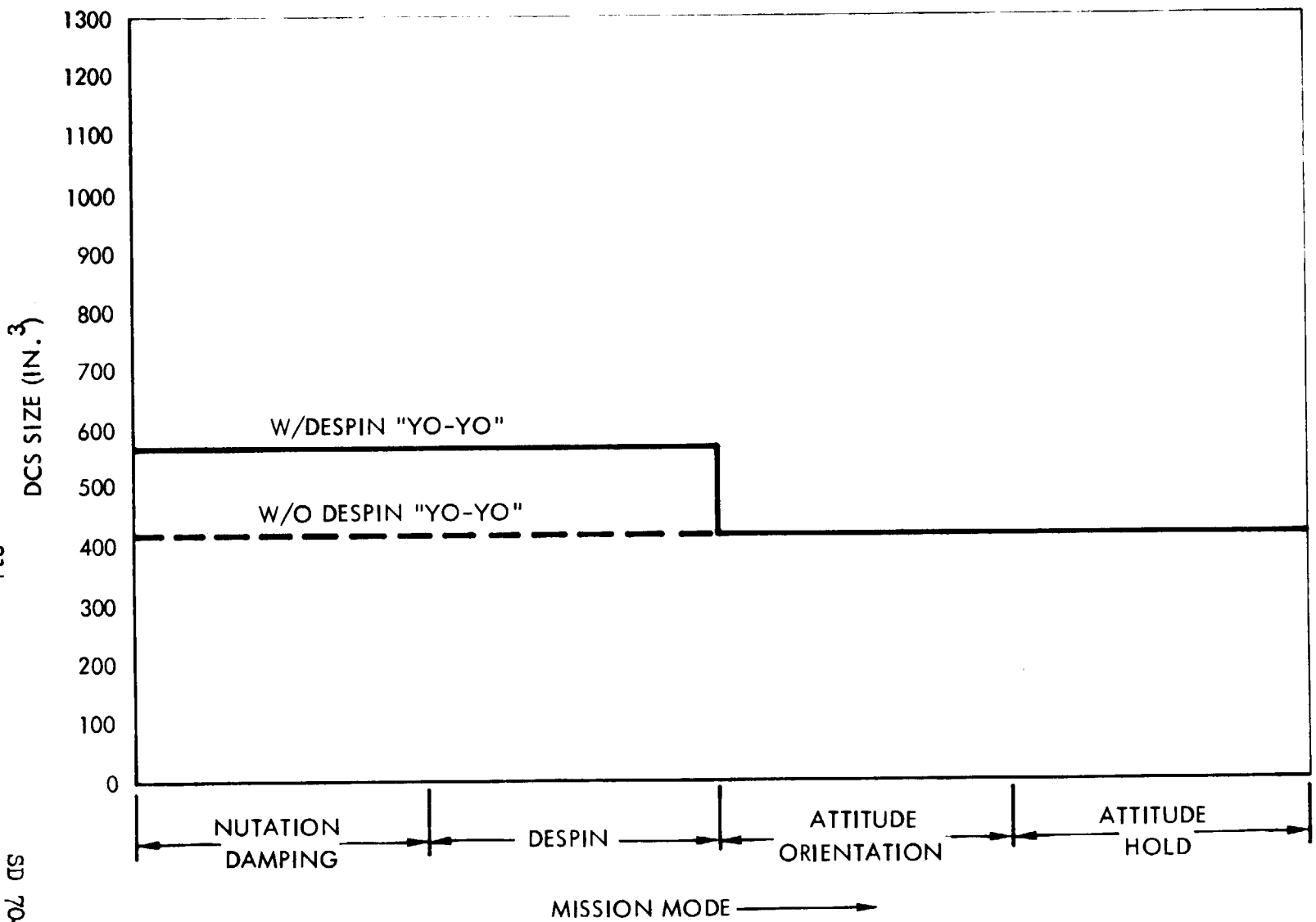

Figure 109. **Mission Mode Size** Profile for Dynamic Control System

Space Division
North American Rockwell

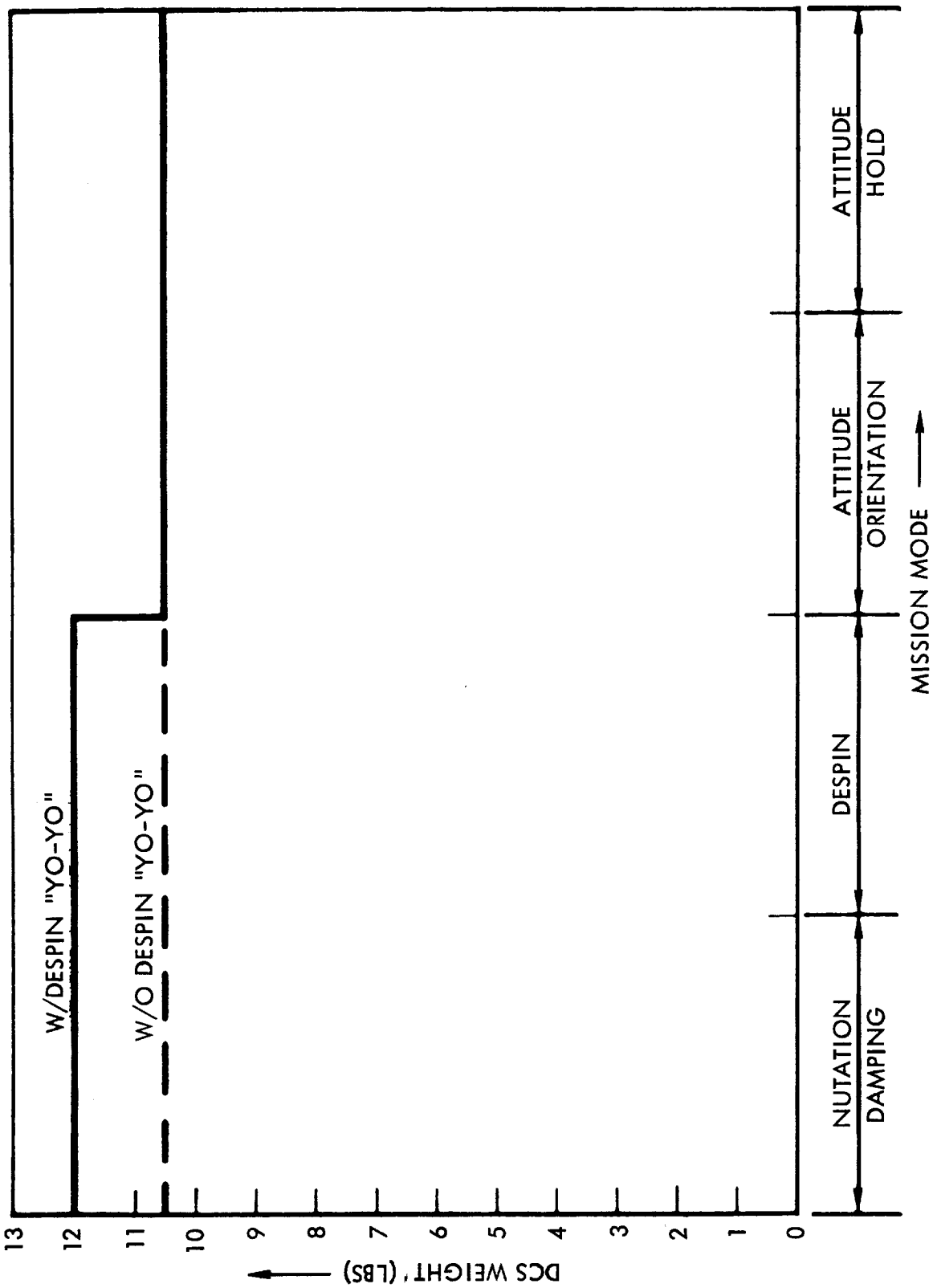

Figure 110. Mission Mode/Weight Profile for Dynamics Control Systems

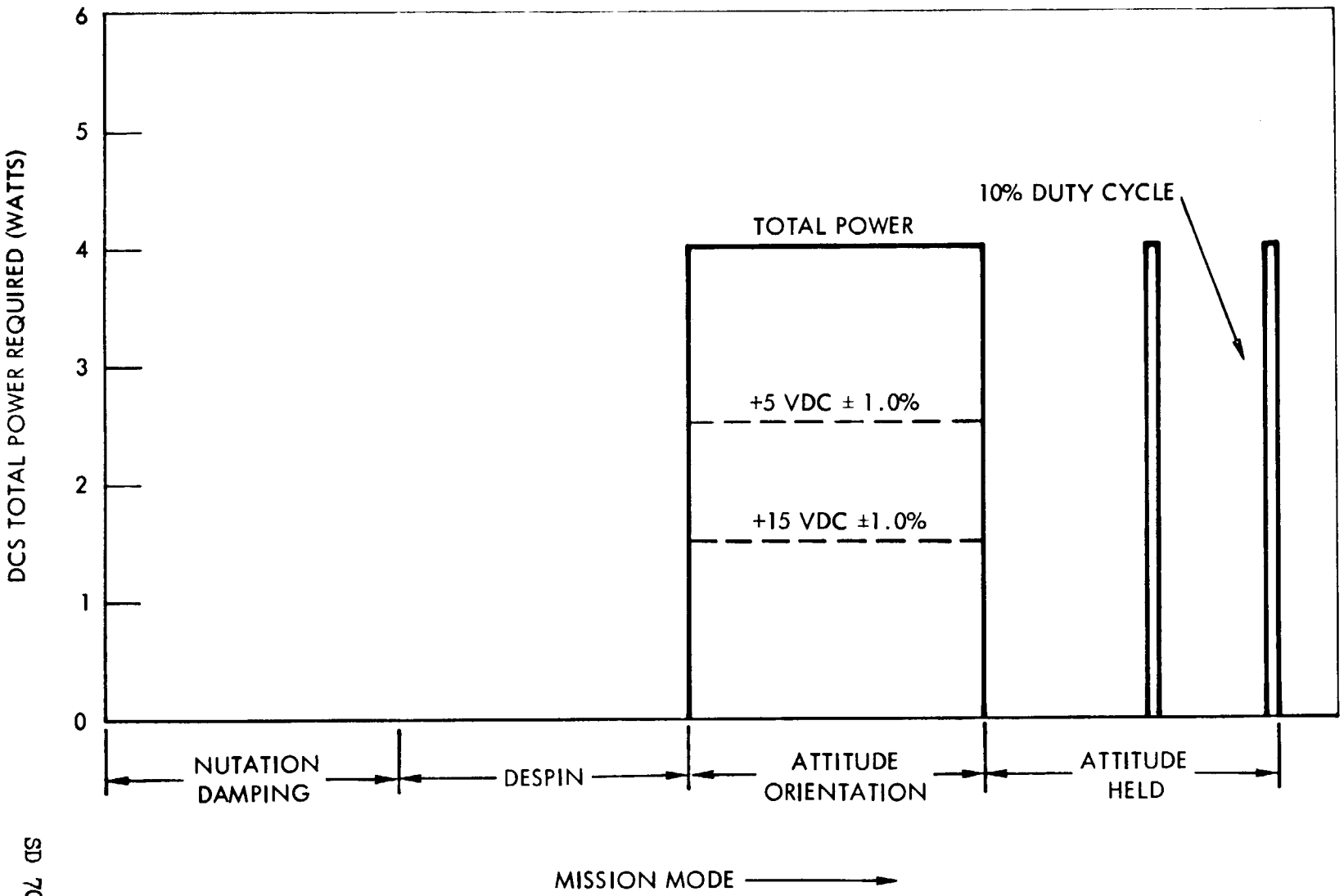

Figure 111. Mission Mode Power Profile for Dynamic Control System

Space Division
North American Rockwell

remain on continually until the desired orbital attitude orientation is achieved. At this point, power to the DCS is turned off until a spin rate or attitude correction is required, which is estimated to be a few times a week after the proper bias is selected for the MBC. A duty cycle of 10% is referred to in Figure 111 ; however, this is considered a conservative estimate if no unforeseen events occur during the mission.

Conclusion

The size, weight and power requirements of the proposed dynamic control subsystem to accommodate the UV and MW experimental satellite requirements is nominal even at peak demand. The low duty cycle of power demand for the system, over most of the mission, ensures minimal drain from the power system.

Operational Capability

Orbit Altitude Range

The system shall operate for any orbit in the altitude range of 400 to 800 nautical miles.

Orbit Inclination

The system shall operate within a range of orbital inclination from 80 to 102 degrees.

Nutation Damping

Orbit injection spin axis nutation shall be reduced to less than

0.5 degree half-cone angle within five minutes after separation from the boost vehicle and shall be maintained as such for the duration of the mission.

Spin Rate Attenuation

The orbit injection spin rate (which may be as high as 180 rpm) shall be reduced, within 1 second after command, to less than 7 rpm.

Spin Vector Maneuvering

The system shall be capable of orienting the spin-axis normal to the orbit plane, from its injection orientation (which may have the spin axis in the orbit plane) in 15 orbits or less. It shall be possible to reverse or repeat this process an unlimited number of times during the mission.

Spin Vector Pointing

The system shall control the spin-vector orientation normal to the orbit plane within ± 2 degrees half-cone angle for an indefinite period of time within the design lifetime of the satellite. This tolerance includes spin axis nutation and orbit regression as well as the effect of attitude disturbance torques.

Spin Vector Magnitude

It shall be possible to control the spin rate of the vehicle to within 0.5% of the selected 4 rpm nominal rate, which may vary between 1 and 7 rpm as selected.

Design Life

On-orbit design life of the system shall be one year.

Operational Requirements

Size

The total onboard control actuation system shall require less than 1000 in.^{3}.

Weight

The control actuation system shall weigh less than 15 pounds.

Maximum Power

The total peak power required at any time by the attitude control system shall be 5 watts or less.

Average Power

The average power consumption of control actuation system shall be 1.5 watts or less.

Standby Power

The control actuation system standby power shall not exceed 0.25 watt.

Conclusion

The operational capability and requirements specified will provide attitude control capability which is sufficiently accurate and has a long enough lifetime to perform the UV/MW experimental satellite mission at a low cost.

Operations Plan

The philosophy used to derive the Operations Plan for the Dynamic Control System (DCS) is based on the assumption that one master control station will provide all attitude error computation and generate all control commands to the satellite through the STADAN network. The ground tracking stations used would act as relay stations between the satellite and the master control station. The operations plan includes GSE, TT&C, Logistics, Data Reduction, and Data Analysis Requirements.

On-Orbit Ground Support Equipment Requirements

The ground effort required, during the on-orbit mission phase, to support the dynamic control system consists of:

(1) Attitude error computation and control command generation

(2) Spin rate error computation and control command generation

(3) Drift rate measurement and compensation

(4) DCS housekeeping status measurements

(5) Error computer self-test.

The primary data reduction mode will be automatic, with manual computation as a backup and/or checking mode. Dynamic control system status information will be provided, through the telemetry link, from the "V-head" attitude sensors, the Ultra Violet experimental sensor, and the Digital Solar Aspect Sensor (DSAS). The signals from the "V-head" attitude sensor and the UV sensor will be transmitted frequently so that sufficient monitoring of the dynamic control system can be modeled to determine long-term trends and observe short-term fluctuations.

The automatic data reduction hardware (GSE) will consist of a main frame computer with

(1) sufficient scratch pad memory to store past value data and interim computations as required to accommodate information contingencies and multi-cycle averaging, consistent with desired error confidence level 5,

(2) sufficient read-only memory to store all constants required for computation and all look-up tables,

(3) sufficient arithmetic and logical commands to reduce raw status data to error signals,

an input capability which

(4) provides for data handling of telemetry commands into storage for use by iterative dynamic control sub-routines in updating respective attitude and spin rate errors,

(5) has self-test override,

and an output capability which

(6) displays total attitude error (Γ) in degrees, continuously in digital format,

(7) displays spin rate error continuously (in rpm) in digital format,

(8) displays computed start angle (β) in seconds of time for current attitude error and spin rate,

(9) displays computed start time (in seconds) for spin correction based on current spin rate,

(10) displays "error too large",

(11) displays "correction in process",

(12) displays "number of cycles of correction",

(13) displays transmission parity "Go" and "No-Go",

(14) can have its automatic command mode overridden by a manual command mode,

(15) will drive an analog strip chart recorder for plotting spin rate vs. time,

(16) will drive an analog strip chart recorder for plotting attitude error vs. time,

(17) will drive an analog strip chart recorder for plotting orbital phasing parameter vs. time,

(18) will drive an X-Y plotter for recorder Γ vs. λ in degrees,

(19) displays self-test error,

(20) displays housekeeping error.

Figure 112 shows a preliminary conception of the DCS status and control panel.

TT&C Requirements

Communication Requirements

The Dynamic Control System (DCS) requires communication between the ground station and the satellite in both directions - up-link and down-link. The up-link data are command signals employed to activate the DCS for on-orbit correction or initial acquisition. The following

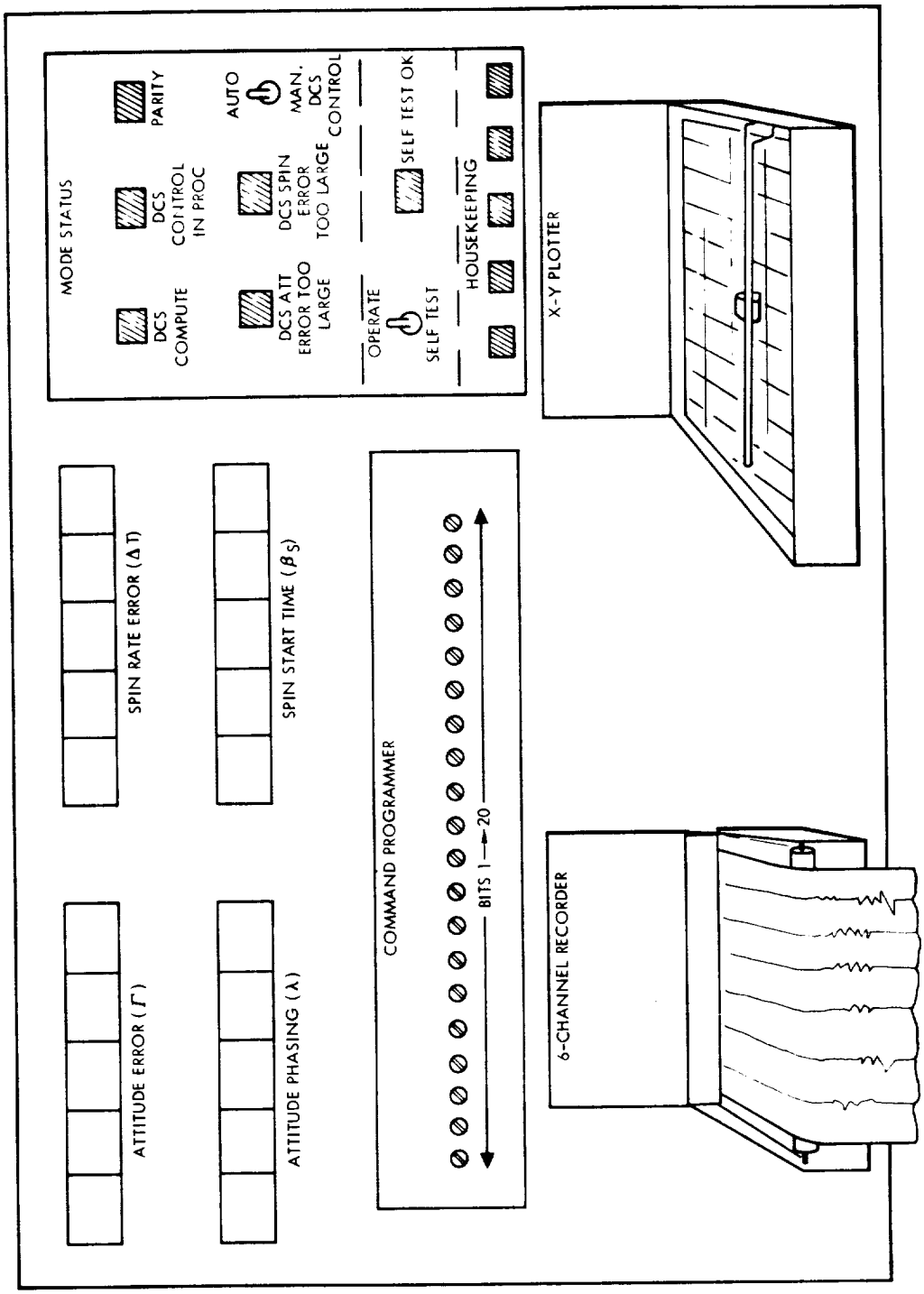

Figure 112 Dynamic Control System Status and Control Panel

is the command list for control of the DCS:

- Spin-up Command
- Spin-down Command
- Attitude Correction Command
- Attitude Bias Control Command

Down-link signals contain two types of information - the operational parameter signals, and test point signals. These signals form a complete set of down-link data required for effective DCS system status monitoring and are listed below:

- Channel 1 of "V-head" Attitude Sensor
- Channel 2 of "V-head" Attitude Sensor
- UV Horizon Scanner Output
- Digital Solar Aspect Sensor (DSAS) Output
- QOMAC Coil Current
- MASC Coil Current
- MBC Coil Current
- Test Points (housekeeping)

Word Format

The standard telemetry word available contains 20 bits of data information. Format of the required commands and down-link signals are tentative and are given in Tables 25 and 26 , respectively.

TABLE 25
UP-LINK SIGNAL FORMAT

Format / Command	Timing Bits	# Cycle	Address			
	20 ← 8	7 6 5	4	3	2	1
Attitude Correction	2's complement of to @ 0.4777 Hz	No. of cycle	X	0	1	1
Spin-up	"	No. of cycle	0	1	1	1
Spin-down	"	No. of cycle	1	1	1	1
Step MBC	X — X	X X X	X	1	0	1

TABLE 26
DOWN-LINK SIGNAL FORMAT

Format / Signal	Timing Bits				
	20 ← 5	4	3	2	1
V-Head Sens. Channel 1	Data	0	0	0	1
V-Head Sens. Channel 2	Data	0	0	1	1
UV Scanner	Data	0	1	0	1
DSAI	Data	0	1	1	1
QOMAC Coil Current	Data	1	0	0	1
MASC Coil Current	Data	1	0	1	1

Signal Conditioning

All the up-link commands are generated in digital format (as shown in Table 25) and are received and used in digital format, so that no signal conversion is required on up-link data.

Down-link data requirements are composed of three types of data:

(1) Serial digital data (horizon scanners)

(2) Parallel digital data (DSAI)

(3) Analog data (coil pick-offs)

This data must be accepted, converted and transmitted by the data system electronics on-board the satellite. The information must be converted into the twenty bit data word which is standard format for the transmitter/receiver and decoding electronics.

Logistics Support Requirements

The attitude and spin rate determination and control system will be automatic with a manual override. Assuming that there is at least one full-time man to monitor the flight status by computer display, the attitude and spin rate control system should require about 20 percent of his time. Periodically (once a week), the operator should perform a manual verification of the attitude and spin rate information being processed.

The attitude error and spin rate error are displayed by the computer, as well as the torquing start angle (β), in seconds of time from the ascending node to the correct start time for torquing at the present spin rate. In the manual override mode, these computations are still made and displayed; however, automatic corrective commands are inhibited. Additionally, a strip chart recorder (2-channel) records "V-head" horizon sensor data as long as the manual override exists. The precise error computation, by manual means, requires approximately one hour of the operator's time.

Transmission of attitude control commands will have parity verification which will be computed automatically and parity "GO" displayed. This will require continuous monitoring by the operator when data are being transmitted. Computer self-test will be conducted by the operator at periodic intervals.

Continuous graphs with the following information should be kept throughout the mission:

(1) Spin rate (in RPM) referenced to orbit number

(2) Maximum roll angle (Γ) referenced to orbit number

(3) Orbital phasing parameter (degrees) referenced to orbit number

(4) Polar plot of the maximum roll angle (Γ) in degrees against λ in degrees.

These plots may be either made by the computer or at least tabulated pointwise so that manual plotting is facilitated by the operator. If manual plotting is required, additional operator time is necessary.

Data Reduction Requirements

The data reduction will normally be done in the data reduction computer; however, provision for manual reduction as a checking technique should be available. The algorithms for data reduction are given here. Where nomographs and overlays are shown, they become table lookup functions or equation solutions in the automatic mode.

Manual Data Reduction

Marking of raw data. - The markup procedure which follows is to be applied to the recordings of both channels of attitude data prior to making attitude measurements. To mark the raw data, proceed as follows:

a. Mount the recording chart on the Gerber Scanner* and advance to the beginning of the chart.

b. Select the first clearly usable set of horizon-crossing pulses and draw in the slope and zero-reference lines (as shown in Figure 113). For the dual-channel case, a set of usable pulses consists of three consecutive, well-defined crossing pulses on each of both channels.

c. Identify the sky-earth crossing of the first set of horizon-crossing pulses as rotation No. 000.

d. Determine the real time of the first sky-earth-crossing pulse of rotation No. 000 of Channel No. 2 in GMT as follows:

   (1) Draw a line on the chart parallel to a chart gridline, through the point of intersection of the slope and zero-reference lines of the first sky-earth-crossing pulse and across the line of time marks.

   (2) Note the point of intersection of the line on the coded time scale. Convert the coded time value into GMT in accordance with the system described subsequently, and record this value of time on the Attitude Data Sheet.

e. Advance the chart, and add slope lines and zero-reference lines to the set of horizon-crossing pulses associated with rotation No. 005. If judgment indicates that this is not a usable set, advance or back up one or, if necessary, two sets of pulses to make a selection. Label the choice with its correct rotation number. If no usable set of pulses exists within two rotations of rotation No. 005, advance to rotation No. 010.

---

* A data reduction tool which is provided for manual evaluation.

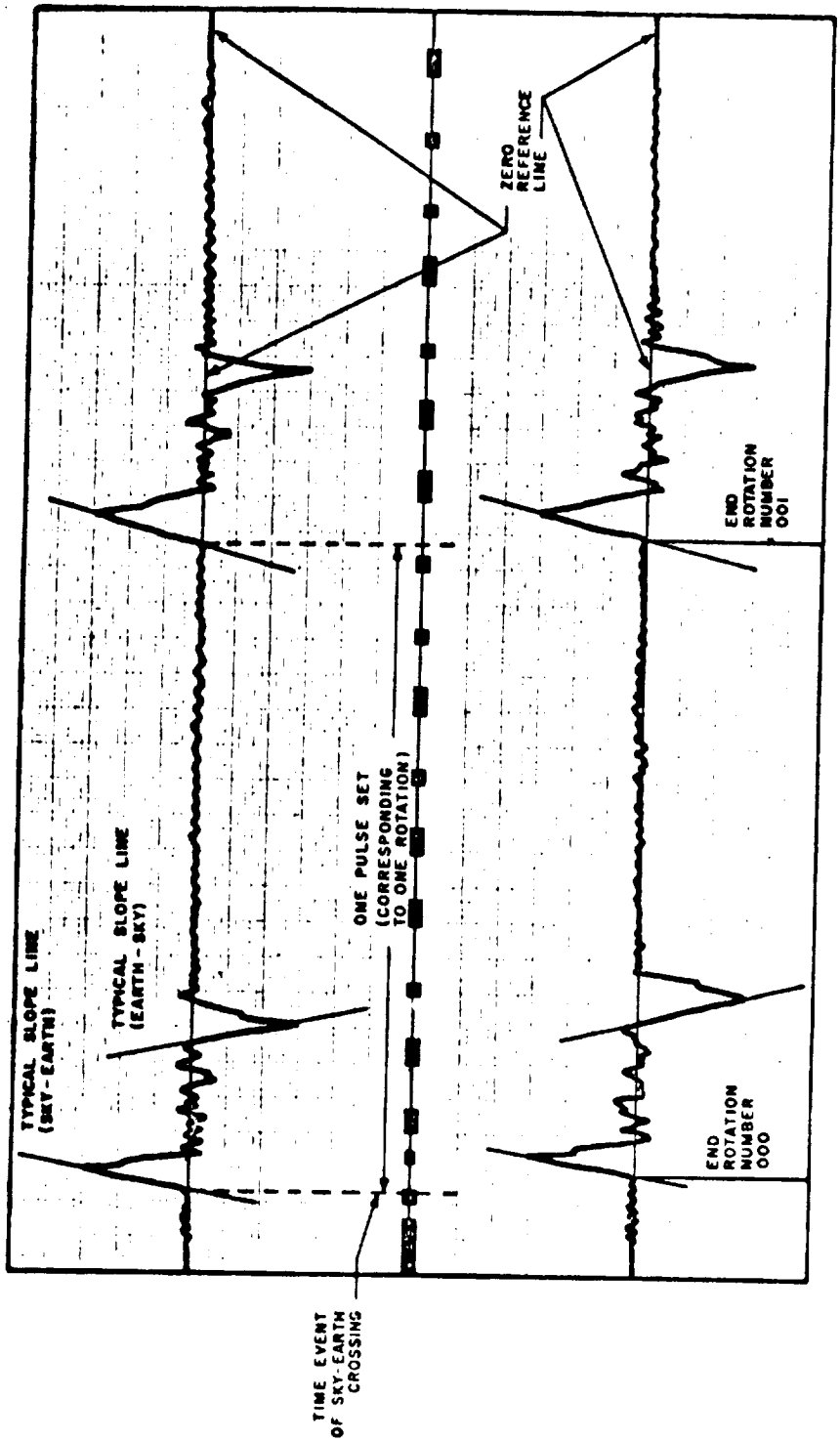

Figure 113. Marking of Raw Attitude-Sensor Data

f. Repeat the selection and marking process at every fifth set of horizon-crossing pulses (i.e., at rotation numbers 000, 005, 010, 015, etc.) until all the available sets are marked.

g. Using the procedure of Step d, determine the GMT of the last sky-earth-crossing pulse in the last set of pulses of Channel No. 2. Record this time value and the corresponding rotation number on the Attitude Data Sheet.

Determination of Earth-to-Spin Time (T_E/T_{SPIN}) Ratios. - Proceed as follows:

a. Adjust the Gerber Variable Scale so that the length represented by its scale reading of 0 to 10 is equal to the linear distance (L) between two consecutive sky-earth crossings.

b. Place the Gerber Variable Scale on the chart recording so that its left index is at the point of intersection of the slope line and zero-reference line for the sky-earth-crossing pulse of rotation number 000 on Channel No. 2. Align the edge of the Gerber Variable Scale with the zero-reference line, and read the T_E/T_{SPIN} ratio off the variable scale marker which is directly opposite the intersection of the slope line and zero-reference line of the earth-sky-crossing pulse. Record the measured value of T_E/T_{SPIN}, in three digits, in the appropriate place in the Attitude Data Sheet.

c. Select from the following list the digit whose corresponding description most nearly meets the description of the data used in the determination of the T_E/T_{SPIN} ratio of Step b. If the character of the data is such that a choice of more than one data description digit is possible, the one that should be chosen is the one which appears to be the most damaging to the accuracy of the measurement.

0 Clean

1 Noisy

2 Probable cloud interference at earth-sky transition

3 Probable sun interference at earth-sky transition

4 Probable cloud interference at sky-earth transition

5 Probable sun interference at sky-earth transition

6 Low amplitude signal

7 Jamming by another transmitter (crosstalk, beats, etc.)

Record on the Attitude Data Sheet the selected data description digit with the three-digit number representing the T_E/T_{SPIN} ratio of Step b. This digit should be placed in the position of a least significant digit (in the far right position).

d. Repeat the procedures of Steps b and c for each set of data for both channels of all marked orbit numbers. Record all the T_E/T_{SPIN} ratios and the corresponding data description digits in the Attitude Data Sheet.

Determination of Instantaneous Roll Angles. - The Master Control Station has the responsibility for the determination of instantaneous roll angles from the ratios reported on the attitude message. The instantaneous roll angle for each rotation number marked in the data span is determined through the use of the proper roll angle nomogram. Once the T_E/T_{SPIN} ratios have been determined, the nomogram illustrated in Figure 114 may be entered using these ratios to obtain instantaneous roll angles.

The procedure for using a roll angle nomogram is as follows:

a. Line up the values of the two entering parameters using a transparent straight edge (be careful to note the direction of scaling on the parameter axes of the nomogram).

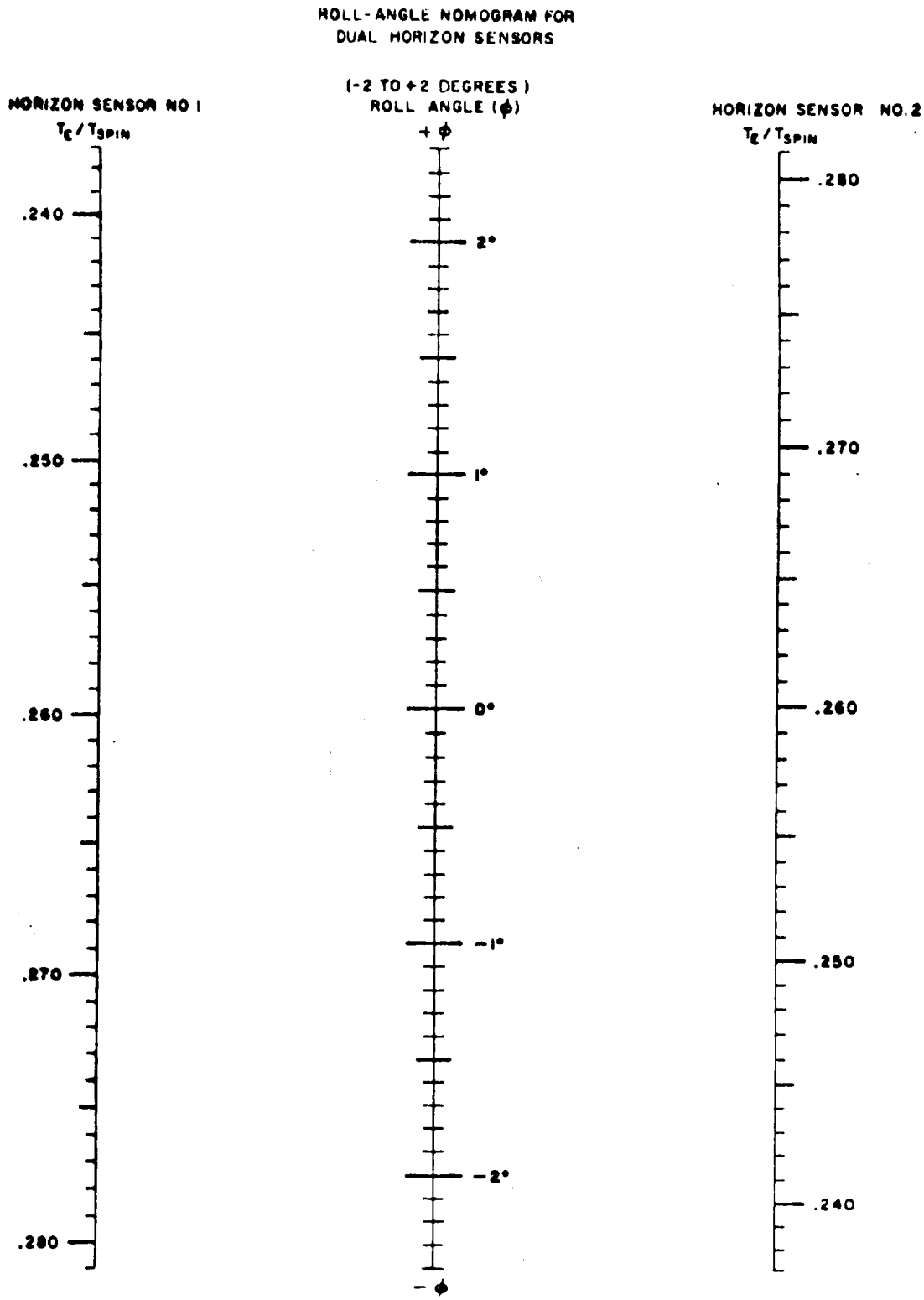

Notes:

1. T_E/T_{SPIN} is the ratio of earth time to spin time (duty cycle)
2. Sensor mounting angles are 30 and 130 degrees with respect to spin axis

Figure 114. Two-Degree Roll Angle Nomogram

b. Read the value of the instantaneous roll angle in degrees at the point where the transparent straight edge cross the roll angle axis. Record the value of instantaneous roll angle obtained on the Attitude Data Sheet (Be careful to indicate the polarity of the roll angle).

Normalization of Time - The time elapsed between the ascending node crossing and the moment of occurrence of each instantaneous roll angle must be divided by the orbital period, τ, in order to permit the use of a common overlay of roll curves in ascertaining the roll history. The quantities thus obtained are referred to as normalized time. The "zero" of normalized time will be taken as the time of the ascending node crossing. To calculate the value of normalized time associated with the moment of occurrence of the instantaneous roll angle of rotation number 000 at any of the CDA stations, use the relationship

$$(t_N)000 = \frac{GMT_{000} - GMT_{AN}}{\tau}$$

where:

GMT_{000} is the GMT of rotation number 000, and

GMT_{AN} is the GMT of the ascending node crossing.

To calculate the normalized time associated with succeeding rotation numbers, an incremental time value, Δt_N, is calculated which is added to the normalized time of rotation number 000. The incremental time (Δt_N) associated with rotation number n is given by

$$(t_N) = \frac{nP}{\tau}$$

where:

n is the rotation number,

P is the spacecraft spin period in minutes, and

τ is the anomalistic period in minutes.

Finally, to obtain the normalized time $(t_N)n$ associated with a particular rotation number, n, use the relationship

$$(t_N)n = (t_N)000 + (t_N)n$$

Plotting of Instantaneous Roll Angle against Normalized Time - For the character of the data and the accuracy of the results contemplated for the satellite, a sheet of 11- by 17-inch (or larger) graph paper with 10-by-10 grid lines to the 1/2-inch is required for plotting a single orbit, roll angle history, from the ascending node to the next ascending node.

The roll angle history is plotted as follows:

a. Set up a normalized-time scale on the abscissa so that the normalized time for one orbit is represented on a length of 10 inches.

b. Set up an instantaneous roll-angle scale on the ordinate to the same scale as the appropriate sine curve overlay used to aid in the curve-fitting procedure. Judgment and experience will dictate which sine curve is to be used.

c. Plot all data points listed on the Attitude Data Sheets associated with the STADAN stations that obtained data during the orbit under consideration.

d. Draw the locus using either of the following methods:

   (1) Sketch the curve of best fit, using personal judgment and experience as a guide, or

   (2) Use one of the three available sine curve overlays to obtain a curve which closely fits the data points, and trace in the curve (Figures 115, 116, 117 illustrate the three overlays available to cover maximum instantaneous roll angles of 2, 10 and 90 degrees, respectively).

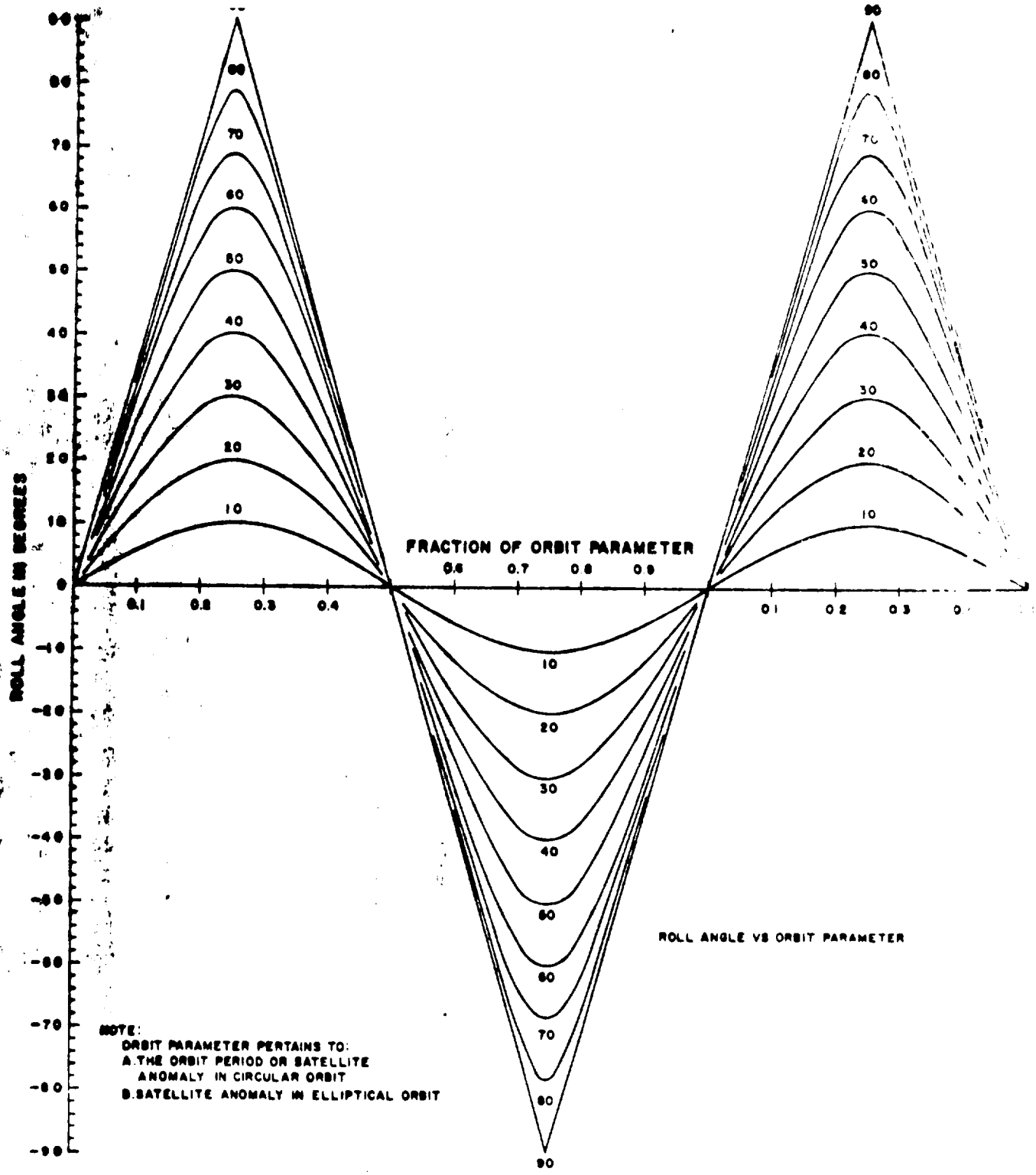

Figure 117. Example of 90-Degree Sine-Wave Template

ORIGINAL PAGE IS
OF POOR QUALITY

Determination of Maximum Roll Angle (Γ). - The maximum roll angle is the amplitude, in degrees, of the curve plotted in Step d-2. The amplitude is marked on the sine curve overlays used in construction of the data curve.

Determination of Orbital Phasing Parameter (λ). - To obtain the orbital phasing parameter (λ), in degrees, use the relationship

$$\lambda = 360\ (t_N)_\lambda$$

in which $(t_N)_\lambda$ is read from the plot of normalized roll angle history and is the normalized time from the ascending node to a zero value of roll angle at an upward crossing of the time axis (i.e., for the zero angle with a positive slope).

Automatic Mode

No continuous data is available to the computer from the two horizon scanner inputs. Data is only available during the data acquisition in addition to infrequent sampling during the mission. This data is used to compute all control system status (i.e., attitude, spin rate and drift).

The first computation is that of determining the T_{EARTH}/T_{SPIN} ratio. Data such as that shown in Figure 113 is received by the computer. The computer program will contain suitable slope detection logic to detect the horizon transitions with excellent resolution. It will also have the capability of determining whether or not a signal is clean enough to use for spin rate determination; how many cycles to average and, possibly, a stochastic filter for noise averaging. It should be able to determine sun interference, cloud interference, low amplitude signal conditions and a jamming (cross-talk) situation and reject the data as too inaccurate.

Once the credibility of the input data is established, a simple division is performed to compute T_E/T_S and, as many cycles as desired, averaged together to yield the appropriate confidence level.

Once T_E/T_S is known, roll angle error can be found by using a table lookup scheme (or can be computed) according to the nomograph shown in Figure 114.The points on the nomograph are coincident where they overlap.

Nominal and orbit correlated normalized time are computed by the simple algorithms given in the manual reduction section.

Maximum roll angle can be found by including the sinewave templates shown as table lookup numbers in the computer program.

The orbital phasing parameter is a simple computation as given previously.

From these calculations, the necessary plots can be generated by the computer on three strip recorders and an X-Y plotter for automatic continuous system status monitoring and flight history accumulation. These plots are delineated in the Data Analysis Requirements section.

Data Analysis Requirements

Actuation Command Analysis Procedure

The actuation command decisions are the same whether in the automatic mode or manual override. In one case, they are programmed as a subroutine in the data reduction computer and in the other, they are computed manually. Either way, the parametric relationships and actuation command decision criteria are the same.

The general method for arriving at each of the control decisions is as follows:

a. Compare the present condition of the satellite with the allowable error criteria.

b. Determine the amount of correction required to eliminate (or reduce) the error.

c. Determine, if applicable, the required time-of-application of the correcting control.

Four time histories should be maintained for evaluation of satellite spin rate and attitude. These are as follows:

(1) Spin rate (ordinate) in revolutions per minute referenced to orbit number.

(2) Maximum roll angle (ordinate) in degrees referenced to orbit number.

(3) Orbital phasing parameter (ordinate) in degrees referenced to orbit number.

(4) Polar plot of the maximum roll angle Γ (magnitude) in degrees against a λ' parameter (angle in degrees) as shown in Figure 118.

The data required is conveniently available from the following sources:

Spin rate is listed on the latest Telemetry Pass Summary

Maximum roll angle and orbital phasing parameter (λ) are obtained from the plot of the latest roll angle history, and

the λ' parameter in degrees is determined from the relationship

$$\lambda' = \lambda + 90°$$

Evaluation Criteria

QOMAC Decisions. - Whenever the maximum roll angle, Γ , of the satellite spin axis becomes equal to or greater than one degree, a QOMAC command should

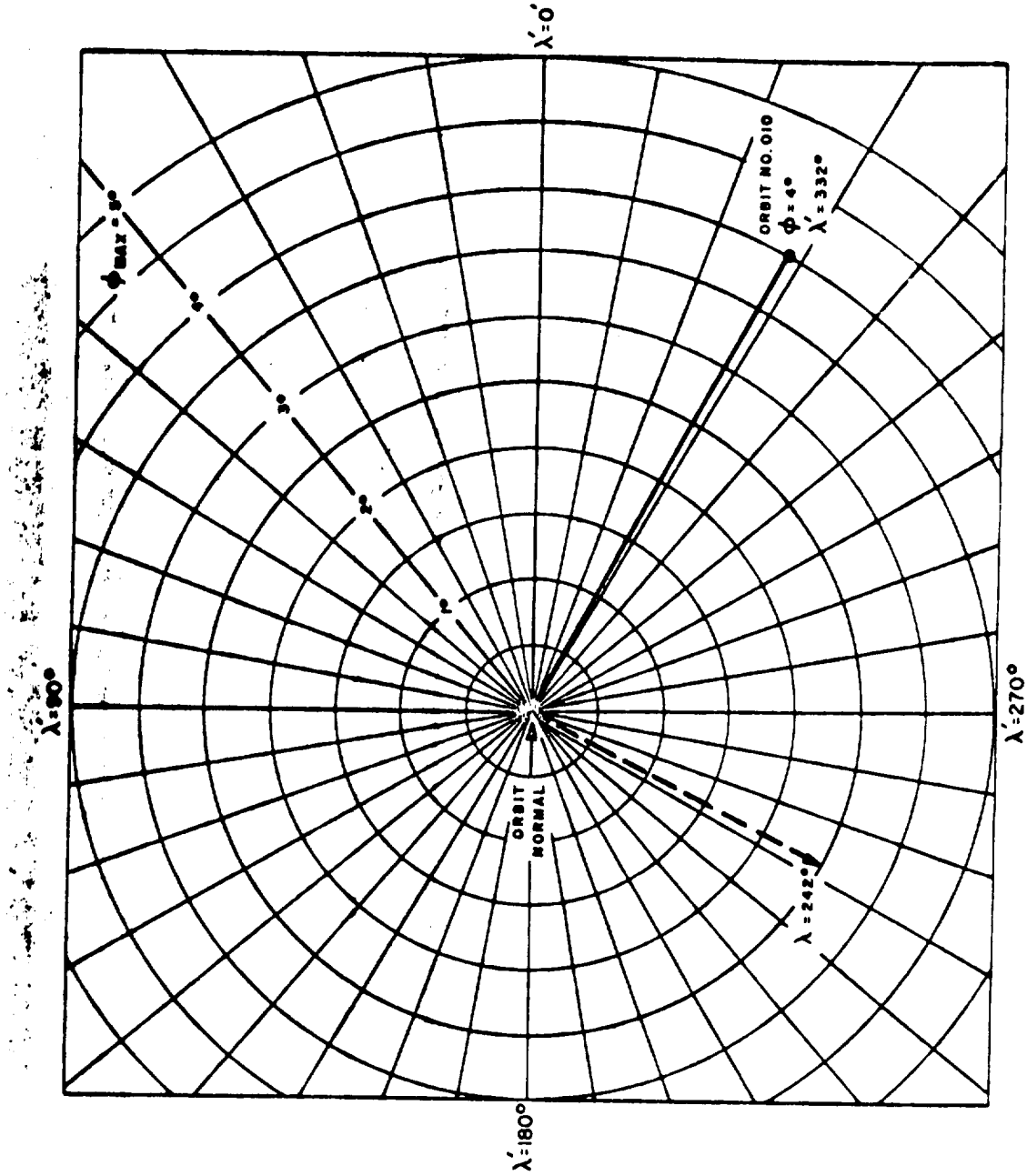

Figure 118. Sample Polar Graph of ϕ_{max} Versus λ'

ORIGINAL PAGE IS
OF POOR QUALITY

be prepared. The value of the existing maximum roll angle can be determined from the graph of maximum roll angle versus orbit number.

Operating Mode Selection .- Two modes of QOMAC operation are available*: high-torque (5 degrees per cycle) and low-torque (2 degrees per cycle). Select the mode of operation in accordance with the following criteria:

If the maximum roll angle is less than 15 degrees, select the low-torque mode of operation.

If the maximum roll angle is equal to or greater than 15 degrees, select the high-torque mode of operation.

Determination of Number of Correction Cycles Required .- If the low-torque mode of operation has been selected, use one of the two following alternative relationships to determine the required number of QOMAC cycles (N_Q).**

If the orbital phasing parameter (λ) is equal to or greater than 180 degrees (as determined from the graph of λ versus orbit number) use the relationship

$$N_Q = \frac{\Gamma}{2},$$

where Γ is the maximum roll angle (degrees).

If the orbital phasing parameter (λ) is less than 180 degrees, use the relationship

$$N_Q = \frac{\Gamma + 1}{2}$$

* The high-torque mode normally will be used only once during spacecraft life; the low torque mode should be used for routine torquing.

**A maximum of eight cycles can be programmed. Round-off the N_Q as computed above to the lower whole number.

If the high-torque mode of operation has been selected, use the following relationship to determine the required number of QOMAC cycles*:

$$N_Q = \frac{\Gamma}{5} ,$$

where Γ is the maximum roll angle (degrees).

Determination of the Required Alarm Time .- Calculate the time after ascending node T_{AAN} in minutes, for the start of a QOMAC sequence using the equation

$$T_{AAN} = \frac{\tau}{720} (\lambda - K) - (100 - \tau) \frac{N_Q}{4} ,$$

where

τ is the anomalistic period (minutes)

λ is the orbital phasing parameter (degrees), and

K is a correction angle (degrees) obtained from the graph of K versus the east longitude of the ascending node (E_{LAN}) on the west longitude of the ascending node** (W_{LAN}) (See Figure 119)

Calculate the GMT of the QOMAC alarm time using the equation

QOMAC alarm time*** = $GMT_{AN} + T_{ANN}$ = ___h ___M___s GMT,

where

GMT_{AN} is the time of the ascending node.

---

* When T_{ANN} as computed above is a negative number, add 50 minutes to the computed value to obtain the desired T_{AAN}.

** The longitude of the ascending node is obtained from ephemeral data.

*** If the QOMAC alarm time (in GMT) computed in paragraphs above occurs prior to the CDA station contact time, or so early in the contact period that sufficient time for QOMAC command transmission is not available, 50 minutes should be added to the computed QOMAC alarm time.

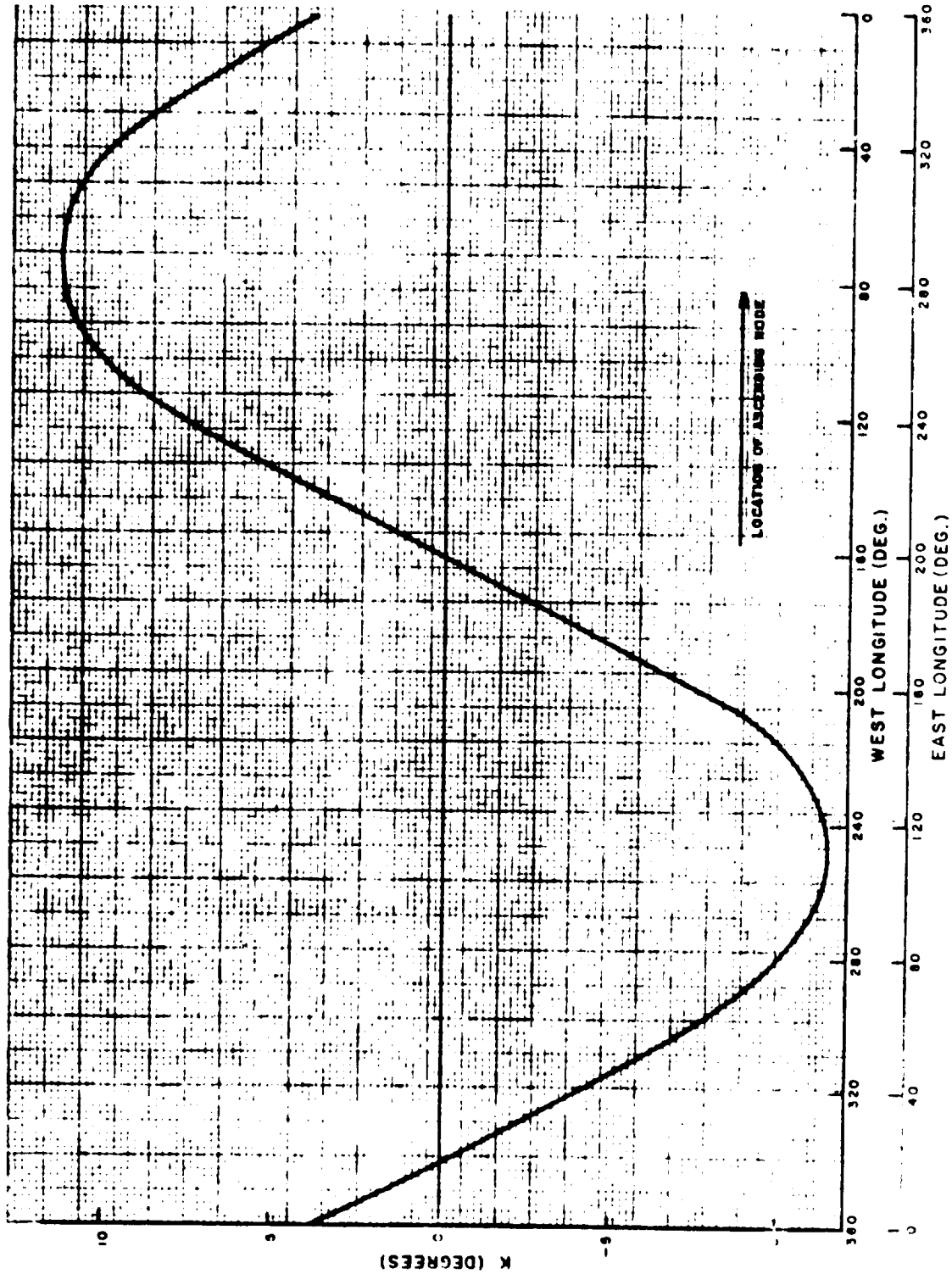

Figure 119. Correction Required to Compensate λ for Effect of Inclined Earth Dipole (K vs E_{LAN} and W_{LAN})

MBC Decisions. - Whenever the maximum roll angle of the satellite's spin axis is observed to increase at an average rate greater than 0.5 degree per day, a suitable MBC command must be derived.

Monitoring Spin-Axis Drift. - The rate of change of Γ is to be monitored through use of the polar graph of Γ versus λ'. To determine the rate an polarity of maximum roll angle drift, proceed as follows:

Store the Γ and λ' of the satellite at the beginning of the day.

Store the final Γ and λ' of the satellite at the end of the day.

Compute the distance between the initial and final maximum roll angles of the satellite spin axis. This is the absolute value (approximate) of the maximum roll angle drift per day, ω_D in degrees.

Determination of the Required Magnitude of Correction Moment. - Calculate the magnitude of magnetic moment (amp-turns-meters^2) which is to be programmed into the MBC coil of the satellite, using the relationship

$$M_{MB} = 0.344 - M_R$$

where

M_R is the approximate residual magnetic moment (ampere-turns-meters^2) of the satellite, M_R can be determined from the graph in Figure 120 which was plotted using the relationship

$$M_R \simeq 3.43 \times 10^{-2}\ \omega_S \left[1 + 1.01\ \omega_D\right]$$

where

ω_D is the maximum roll angle drift in degrees per day

and

ω_S is the present spin rate (revolutions-per-second) of the satellite.

MASC Decisions. - If desired, the MASC system can be used to control the spin rate within the limits of 1 to 7 RPM. The nominal spin rate for this mission is 4.0 RPM.

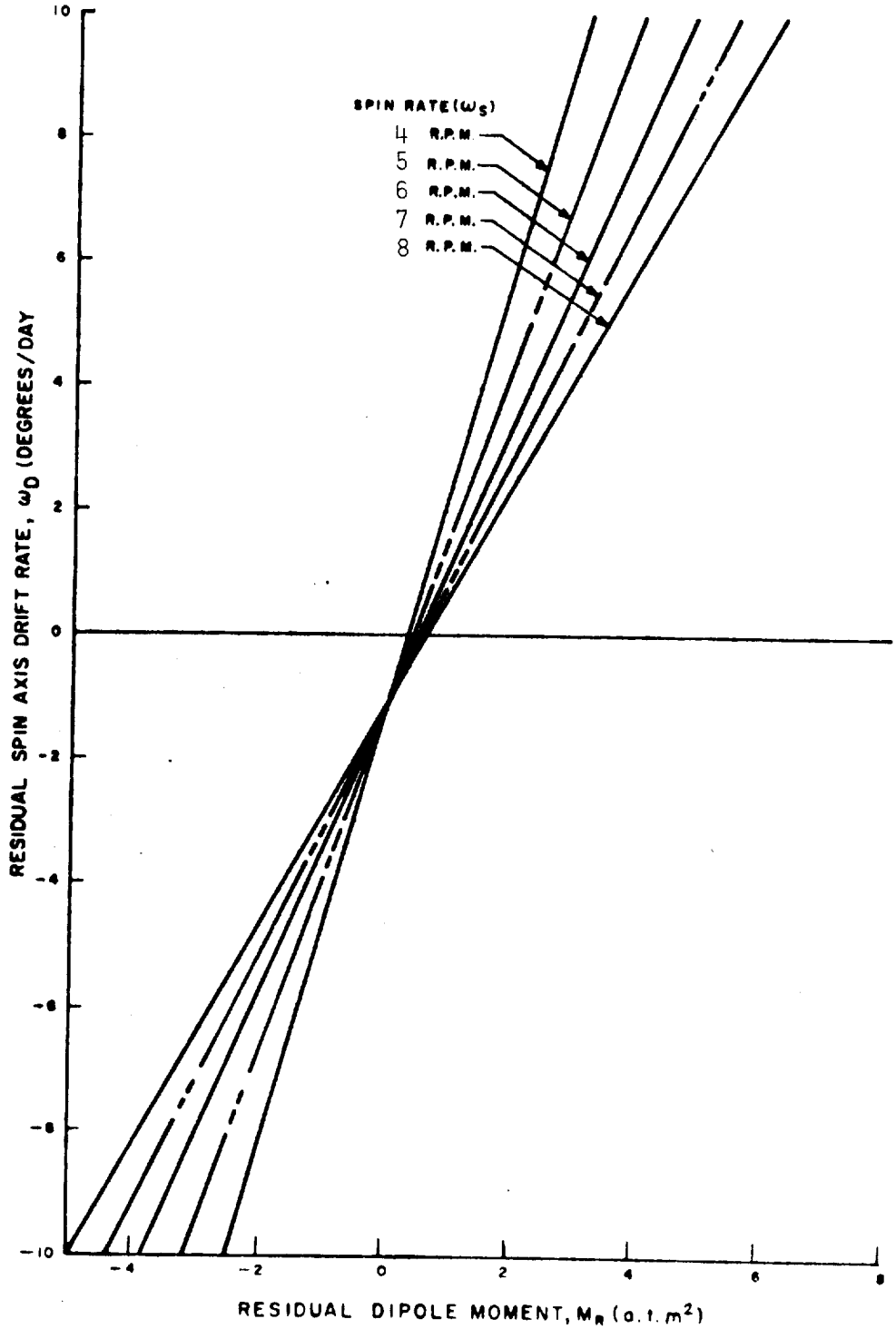

Figure 120. Residual Dipole Moment Versus Drift Rate

Determination of the Required Amount of Spin-Rate Correction. - If the satellite spin-rate is too slow, a spin-up command is formulated. If the satellite spin-rate is too fast, a spin-down command is formulated; however, spin-down commands are not normally required since the satellite spin-rate decays naturally.

Determine the desired spin rate increment (i.e., the difference between the desired spin-rate and the present spin rate).

Detailed Procedure. - For example, to demonstrate typical operation, assume only WALACO shall be used to command MASC sequences. Table 27 lists various spin rate increments which can be obtained for particular West Longitude of Ascending Node and the MASC Start Time after the Ascending Node (AAN).

TABLE 27

MASC PERFORMANCE (WALACO CONTACTS ONLY)

Start Time After Ascending Node, T_S	Spin Rate Increment (RPM) Versus Longitude of Ascending Node			
	10°W	40°W	70°W	100°W
8 min 20 sec	0.13	0.13	0.13	0.13
16 min 40 sec	0.12	0.12	0.12	0.12
25 min	0.09	0.08	0.07	0.07
33 min 20 sec	0.03	0.02	0.01	0.01

The procedure for formulation of a MASC command is as follows:

Determine the magnitude of the required change in spin-rate and whether a spin-up or spin-down is required.

Determine the longitude of the ascending node for the next orbit providing WALACO contact.

Choose a start time after ascending node, T_S, from table which most closely approximately spin-rate increment, or the closest value. If the desired spin-rate increment is greater than all values in the table, several cycles of the MASC sequence will be required. Select the number of cycles which will give the closest value to the desired spin rate increment; a maximum of eight cycles is available.

Determine the MASC alarm time, using the relationship

$$\text{MASC alarm time} = GMT_{AN} + T_S = ___h___m___s^{GMT}.$$

Actuation Command Format

Table 28 shows the word format for synthesizing control system commands. There are twenty usable bits for commanding the UV/MW experimental satellite from the ground control station. The first four and the mode address bits, which specify whether an attitude correction, spin-rate correction or bias correction is to be made. Bits 5-7 indicate how many correction cycles will be employed. The last 13 bits indicate the start time of the correction cycle in its orbit path with respect to the ascending node which is counted down. In the attitude control sequencer, from the time of the ascending node crossing the appropriate control coil is energized at the conclusion of the count.

TABLE 28

ATTITUDE CONTROL COMMAND WORD FORMAT

Bit No. / Control Mode	Cycle Start Time Data	No. of Cycle			Mode Address			
	20	8	7	6	5	4	3	2	1
Attitude Control	(2's complement of T_0 @ 0.4777 Hz)					X	0	1	1
Spin Control (Increase)	"					0	1	1	1
Spin Control (Decrease)	"					1	1	1	1
MBC Step						X	X	0	1

Conclusion

An automatic data reduction and analysis technique is highly desirable compared with a manual approach. Hours of hand plotting and computing will be saved, thereby significantly reducing the recurring cost of operating the satellite within its error limits, and accumulating a time history of its flight. Manual backup for the error computer is necessary in case of computer failure or for routine checking of accuracy. A software package is required to implement the automatic mode.

Example of the Determination of Γ & λ For TIROS IX

The attitude data given in the teletype messages of Figures 121-122 will be used for this example.

Three items of information not given in the teletype message are needed to carry out the determination. The first two, the GMT of the ascending node crossing and the satellite anomalistic period, are obtained from the Orbital Elements and Equator Crossings published by NASA. The third item of information, the satellite spin period, can be obtained either from the Telemetry Pass Summary Message or from the summary plot of Spin Period versus orbit number. For the example, the following values are assumed.

GMT_{AN} = 191903Z,

Orbital Period, τ, = 99.72 minutes, and

Satellite spin period, P, = 6.3158 seconds.

The data from WALACQ will be treated first since its real-time of occurrence is earlier than that from ALASKA. The procedure is as follows:

a. Determine the value of normalized time, $(t_N)_{000}$, associated with rotation number 000 at WALACO. To do this, use

$$(t_N)_{000} = \frac{(19h\ 24\ m\ 06s - 19h\ 19m\ 03s)}{99.72}$$

$$= \frac{5.05\ \text{min.}}{99.72\ \text{min.}}$$

WALACO, $(t_N)_{000} = 0.0506 \approx 0.051$

GHNJ01A
PP GOSI GULA GWEA GHNJ GOLA
DE GACQ 000A
28/0001Z

TIROS IX
ATTITUDE DATA SHEET
WALACQ ORBIT 0022 03 NOV 64

DATA SPAN: INITIAL ROTATION NO. 000 FINAL ROTATION NO. 105
TIME: 192406Z 193509Z

ROTATION NO.	T E/T SPIN CHAN 1	CHAN 2
000	2321	2801
005	2321	2781
010	2321	2801
015	2341	2781
020	2322	2761
025	2342	2741
030	2342	2721
035	2392	2711
040	2362	2731
045	2372	2721
050	2412	2701
055	2412	2681
060	2401	2670
068	2401	2670
070	2451	2670
076	2441	2640
080	2481	2630
090	2501	2650
094	2531	2640
100	2540	2610
105	2550	2600

28/0002Z NOV GACQ

Figure 121. Format of Teletype Message

GHN000A
PP GOSI GACQ GWEA GHNJ GOLA
DE GULA 000A
28/0000A

TIROS IX
ATTITUDE DATA SHEET
ULASKA ORBIT 0022 03 NOV 64

DATA SPAN: INITIAL ROTATION NO. 000 FINAL ROTATION NO. 040
TIME: 193706Z 194119Z

ROTATION NO.	T E/T SPIN CHAN 1	CHAN 2
000	2571	2561
005	2581	2541
010	2600	2531
015	2620	2491
020	2650	2470
025	2660	2500
031	2660	2480
035	2480	2460
040	2670	2450

28/0001Z NOV GULA

Figure 122. Format of Teletype Message

b. Determine the value of $P/_{\tau}$, associated with the determination of the normalized time increment Δt_N.

$$\frac{P}{\tau} = \frac{6.3158 \text{ sec.}}{(99.72 \text{ min.})\ 60 \text{ sec/min}} = 0.00106$$

c. Evaluate the normalized time increment $(\Delta t_N)_n$ for each rotation number for which time ratios, T_E/T_{SPIN}, have been measured. The Δt_n calculations for the sample data are shown in Table 29.

TABLE 29 SAMPLE CALCULATIONS OF NORMALIZED TIME INCREMENT

Rotation No.	$(\Delta t_N)_n = \frac{P}{\tau}(n)$
000	$(\Delta t_N)_{000} = 0.00106(0) = 0$
005	$(\Delta t_N)_{005} = 0.00106(5) = 0.0053 = 0.005$
010	$(\Delta t_N)_{010} = 0.00106(10) = 0.0106 = 0.011$
↓	↓
105	$(\Delta t_N)_{105} = 0.00106(105) = 0.1113 = 0.111$

d. Determine the normalized time of occurrence for each event of interest by adding its normalized time increment to the normalized time of rotation number 000. The t_n calculations for the sample data are shown in Table 30.

TABLE 30 SAMPLE CALCULATIONS OF NORMALIZED TIME

Rotation No.	$(\Delta t_N)_n + (t_N)_{000} = (t_N)_n$
000	$0 + 0.051 = 0.051$
005	$0.005 + 0.051 = 0.056$
010	$0.011 + 0.051 = 0.062$
↓	↓
105	$0.111 + 0.051 = 0.162$

e. Determine, by use of the appropriate nomogram, the instantaneous roll angles corresponding to the time ratios, T_E/T_{SPIN}. The instantaneous roll angles corresponding to several of the sample T_E/T_{SPIN} ratios are shown in Table 31.

TABLE 31 SAMPLE TABULATION OF INSTANTANEOUS ROLL ANGLE

Rotation No.	T_E/T_{SPIN}		Instantaneous Roll Angle
	Chan. 1	Chan. 2	
000	2321	2801	2.6
005	2321	2781	2.5
010	2321	2801	2.6
↓	↓	↓	↓
105	2550	2600	0.2

f. Record the reduced data in the format shown.

g. Repeat steps a through e using the data from the other STADAN stations for the pass under consideration.

h. The reduced attitude data, instantaneous roll angle and its associated normalized time, is then plotted. Normalized time is plotted as the abscicca to a scale of 0.1 unit of time to 1 inch of graph. The instantaneous roll angle is plotted as the ordinate. The ordinate scale is made to agree with that of the selected sine-curve overlay (i.e., the 2-degree, 10-degree, or 90-degree overlay). For the case at hand, the 10-degree overlay is used and 2 degrees of roll angle are taken equal to 1 inch. A completed data plot is shown in Figure 123.

TIROS IX ORBIT 0022 3 NOV. 1964 WALACO

Rotation No.	$(\Delta t_N)_n$	Normalized Time $\left[(t_N)_n = (t_N)_{000} + (\Delta t_N)_n\right]$	Instantaneous Roll Angle (Γ_1)
000	0	0.051	2.6
005	0.005	0.056	2.5
010	0.011	0.062	2.6
015	0.016	0.067	2.4
020	0.021	0.072	2.4
025	0.026	0.077	2.2
030	0.032	0.083	2.1
035	0.037	0.088	1.8
040	0.042	0.093	2.0
045	0.048	0.099	1.9
050	0.053	0.104	1.6
055	0.058	0.109	1.5
060	0.063	0.114	1.5
065	0.072	0.123	1.5
070	0.074	0.125	1.2
075	0.080	0.131	1.1
080	0.085	0.136	0.8
090	0.095	0.146	0.8
094	0.099	0.150	0.6
100	0.106	0.157	0.4
105	0.111	0.162	0.2

Figure 123. Example of Reduced Attitude Data Derived from WALACO Attitude Message

ORIGINAL PAGE IS
OF POOR QUALITY

i. Place the selected sine-wave overlay on the data plot and, by sliding the overlay to the left or right along the zero line, determine which sine-curve, either by a direct fit or by interpolation between the availabile sine-curves, most nearly fits the data points. Once this fit is achieved, Γ , is read directly from the graph. As shown in Figure 124, the Γ for the example is 4 degrees.

j. Obtain the orbit phasing parameter, λ , by multiplying the normalized time of the positive-going zero crossing of the roll angle by 360 degrees. For the case of the illustration this is:

$$\lambda = 3600\ (0.665) = 239.40 \text{ or } 239°$$

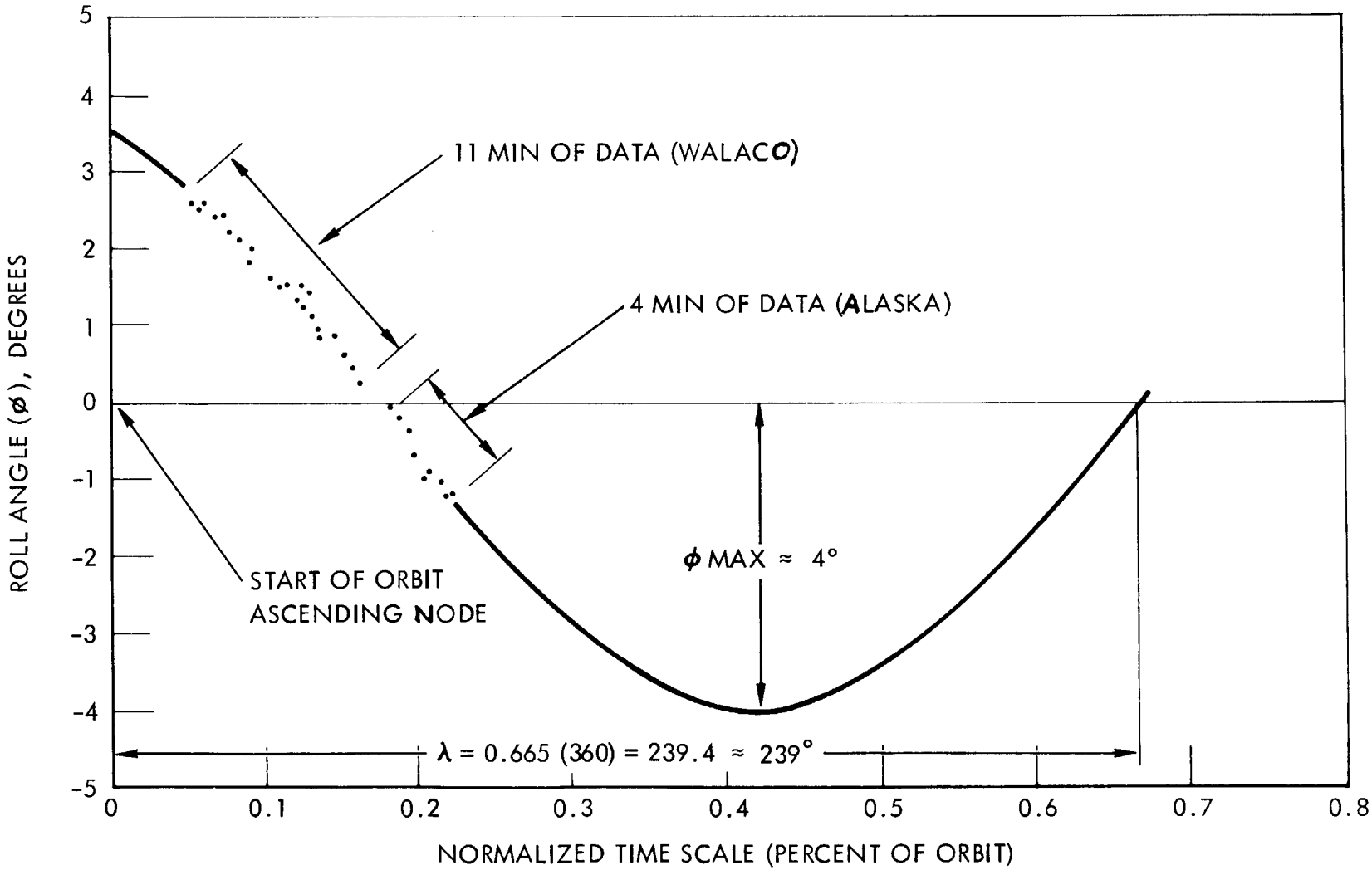

Figure 124. Example of Graphical Determination of Γ and λ

Other Aspects of Determining Γ and λ From Horizon Sensors

Use of Single Channel of Attitude Sensor

When both channels of the V-head attitude sensor are functioning correctly, the value for instantaneous roll angle for each set of data is determined using the nomograms contained in the main body of this report. In the event of interference or failure of one channel of the V-head sensor, additional procedures exist for determining the instantaneous roll angle, and therefore, Γ and λ.

If the attitude sensor is not operating properly, the following procedure may be followed.

> When one channel of the attitude sensor is inoperative, mark the data from the useful channel and determine the T_E/T_{SPIN} ratios as outlined in the main body of the report. Then, using these values along with the spacecraft altitude listed in the WMSAD for the corresponding measurement times, determine the corresponding values of instantaneous roll angle from the nomogram. Finally, plot these values of roll angle according to the procedures outlined in the main body of the report and determine Γ and λ.

Attitude Determination in the Presence of Nutation

A nutation, or wobbling motion, of the spin axis will introduce a modulation into successive readings of instantaneous roll angle. If this effect is permitted to remain uncompensated, it may lead to errors in attitude determination. Should the plot of instantaneous

roll angle versus normalized time exhibit a scatter in roll angle greater than ± 0.75 degree, indicating the possible presence of nutation, the following procedure may be used to compensate for the nutation scattering effect.

Whenever roll angle scatter is ± 0.75 degrees or greater, the procedure for determining instantaneous roll angle from the T_E/T_{SPIN} ratio described in the main body of the report (i.e., using every fifth satellite rotation, or Nos. 0, 5, 10....) should be augmented by the marking and measurement of two additional ratios for each original reading. These ratios should be measured from the rotation that is numbered two less than the originally selected rotation, and from the rotation numbered two greater than the originally selected rotation. For example, if the T_E/T_{SPIN} ratio from rotation No. 15 had originally been selected for use in attitude reduction, then the ratios from rotations 13 and 17 will also be included in the reduction treatment.

For each such group of three rotations (13, 15 and 17 shown in the example) the arithmetical average of the three T_E/T_{SPIN} ratios should be calculated. The resulting average is to be reported as the T_E/T_{SPIN} ratio associated with the original datum point (rotation 15 in the example given). The balance of the attitude-determination process is performed as described in the main body of this report.

TELEMETRY, TRACKING, COMMAND AND DATA HANDLING SYSTEM

The Telemetry, Tracking, Command, and Data Handling system study is presented in five separate sections.

- Data Handling System Analysis
- Telemetry, Tracking, and Command (TT&C) System Description
- Performance Specifications for TT&C System
- Communications Link Analysis
- Data Reduction Requirements

A brief summary is presented for each of these sections.

Data Handling System Analysis - The UV-MW satellite measurement system must acquire and format the performance data of the experiment sensors, attitude control and determination sensors, and the various on-board status sensors for subsequent transmission to the STADAN ground stations for analysis and corrective action. The UV sensor data, transmitted in real time, constrains the system bit rate while the fine sun sensor and IR horizon sensors constrain timing accuracy. The data handling techniques and accuracies required for the experiments and attitude determination devices necessitates digital data transmission. Systems implementation does not require spacecraft or ground station development or modification.

Telemetry, Tracking, and Command (TT&C) System Description - The TT&C system consists of a PCM transmission system, a command receiver-decoder unit and a timer. All hardware described is available as space-qualified

with little or no modification and the system is fully compatible with the selected STADAN stations. The timing unit provides accurate range time and events correlation, and the telemetry transmitter serves the dual purpose of tracking beacon and data transmission. Some unique features are incorporated in the design of attitude determination sensor signals to reduce sample rates while increasing timing precision.

Performance Specifications for TT&C System - Performance specifications are presented for the components of the TT&C subsyste. These consist of the sensor registers, timer, data conditioner, PCM encoder, pre-modulation filter, transmitter, diplexer, command receiver, and command decoder.

Communications Link Analysis - The communications link analysis was performed for the telemetry transmitter, tracking, and the command link. Adequate margins were obtained in all cases.

Data Reduction Requirements - Data reduction requirements are considered for the test and operational phases of the program. The telemetry signal content is described along with the planned method of data reduction and evaluation during the test phase. It is shown that the total data reduction task can be accomplished with existing equipment and software.

Data Handling System Analysis

The measurement system for the UV-MW satellite consists of the experiments, attitude determination and control, and status sensors; an analog to digital converter; multiplexers; signal conditioners; a formatter; timer; and registers.

This section delineates the design analysis and rationale employed to achieve a point design for the spacecraft TT&C data system. A tradeoff and method of obtaining sampled sensor data during horizon crossing versus zero crossing null only; an accuracy study of the on-board clock; sampling data rate analysis; and command and data requirements are featured.

Measurement Analysis

The UV-MW satellite measurement list is given in Table 32. This listing includes experiments, attitude determination and control, and housekeeping measurements. The experiments and attitude determination sensors are of prime importance and govern the design of the measurement system.

The ultraviolet and microwave sensors were described in detail with respect to functional and physical characteristics. The ensuing discussion is concerned only with conditioning and transmission of signals generated by these devices.

Ultraviolet Sensor Time Resolution Requirements

The primary purpose of the UV sensor is to provide data indicating the relative position of the UV horizon during any given revolution. These data can then be utilized along with tracking data (regarding satellite position) and attitude data (derived from IR sensors, Sun sensors, and Sun ephemeris) to determine the altitude of the UV horizon over specific points on the Earth's surface. Thus, the most significant datum that must be measured is the time at which the sensor scans through the UV horizon. The following discussion establishes the minimum allowable time uncertainty for measuring the horizon crossover time.

The stated objective is to locate the UV horizon to within ($\pm$) 1/2 kilometer. As shown in Figure 125 the slant range from the satellite to the horizon is approximately 2135 nmi., or 3960 km. The angle, θ, that subtends 1 km at the horizon is given by

TABLE 32

MEASUREMENT LIST

TITLE	QTY	RESPON	RANGE	SAMPLE RATE	REMARKS
MW Sensor Output	1	0.42 Sec	-5/+5 VDC	1/2 MS	None
UV Sensor Output	1	10 MS	-0.5/+1.0 VDC	1/MS	None
IR Sensors Temp. Meas.	2	DC	+40 to +140°C	1/320 MS	Temperature Bridge
Sun Sensor Output (DSAS)	1	±0.5 MS	7 Bit Binary	1/155 Sec	None
Sun Sensor Output (Fine)	2	±0.5 μS	29 Bit Binary	1/20μS	None
IR Sensor Output #1	1	± 0.5 μS	29 Bit Binary	1/20 μS	None
IR Sensor Output #2	1	±0.5 μS	29 Bit Binary	1/20 μS	None
Solar Array Temp	8	DC	-100 to +140 C	1/320 MS	Temperature Bridge
Structure Temp	10	DC	+40 to +140°C	1/320 MS	Temperature Bridge
Array Output Current	1	DC	0/1.0 Amp	1/320 MS	Operational Amplifier
Array Output Voltage	1	DC	0/24 VDC	1/320 MS	Voltage Divider
Battery Charge Status	1	DC	0/100%	1/320 MS	Voltage Divider
Battery Current	1	DC	0/10 Amp	1/320 MS	Operational Amplifier
Battery Temp	2	DC	40/120°F	1/320 MS	Temperature Bridge
Battery Voltage	1	DC	25/40 VDC	1/320 MS	Voltage Divider
Command Discretes	20	DC	0,2 VDC	1/320 MS	None
UV Sensor Temp	1	DC	+10 to +30°C	1/320 MS	Temperature Bridge
Bus Voltage (+5 Deg.)	1	DC	5 ±0.005 VDC	1/320 MS	DC-DC Conv.
Bus Voltage (+15 Deg.)	1	DC	15 ± .015 VDC	1/320 MS	DC-DC-Conv.
Bus Voltage (+24 Deg.)	1	DC	24 ± .024 VDC	1/320 MS	DC-DC Conv.
Bus Voltage (-15 Deg.)	1	DC	-15 ± .015 V	1/320 MS	DC-DC Conv.
Bus Voltage (+15)	1	DC	+15 ± .15 VDC	1/320 MS	DC-DC Conv.
Bus Voltage (+24)	1	DC	24 ±0.24 V	1/320 MS	DC-DC Conv.
QOMAC Coil Current	1	DC	0/100 MA	1/320 MS	Operational Amplifier
Spin Control Coil Current	1	DC	0/100 MA	1/210 MS	Operational Amplifier
Mag Bias Coil Current	1	DC	0/12 MA	1/320 MS	Operational Amplifier
Frame Sync	1	--	0/1.5 VDC	1/320 MS	None
Subframe Sync	1	--	0/1.5 VDC	1/10 MS	None
TOTAL	66				

Space Division
North American Rockwell

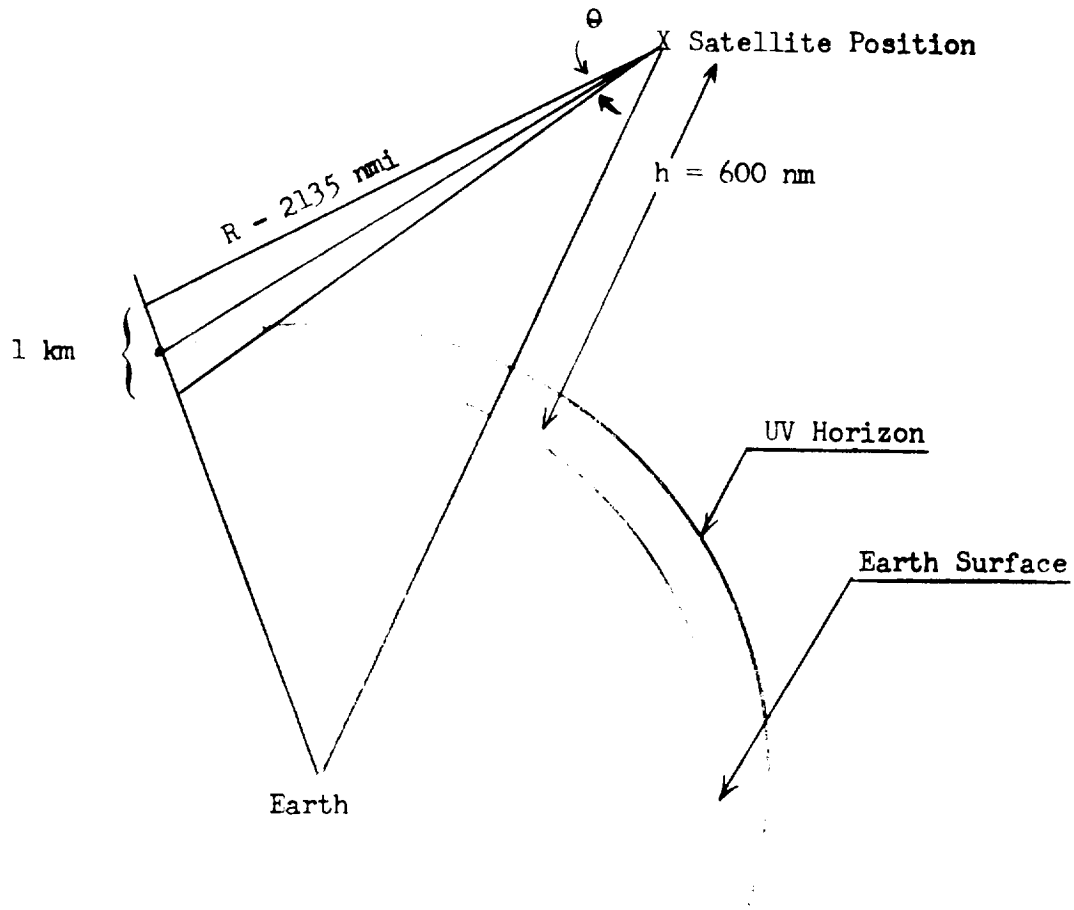

Figure 125. Satellite Geometry

$$\theta = \frac{1 \text{ km}}{R}$$

R = range in km

θ = angle in radians

$$\theta = \frac{1 \text{ km}}{3.96 \text{ km} \times 10^{3}} = 0.252 \times 10^{-3} \text{ radians}$$

(1.745×10^{-2} radians = 1 degree)

$$0 = \frac{0.252 \times 10^{-3}}{17.45 \times 10^{-3}} \text{ degrees} = 0.0145 \text{ degrees}$$

or, for an accuracy of ($\pm$) 1/2 km,

θ - 0.0073 degrees

The satellite rotation rate, ω, is nominally 4 rps or

$$\omega = 360°/15 \text{ sec} - 24°/\text{sec}$$

Thus, the minimum allowable time resolution, Δt, with respect to the required accuracy, is given by

$$\Delta t = \frac{0.0073}{24} = 0.00029 \text{ sec } (0.29 \text{ ms})$$

UV-MW Error Reduction Tradeoff Study

The above discussion delineates the maximum permissible time error to establish the locator height to within $\pm$ 0.5 km. The 0.29 ms value of Δt must be partitioned between all of the error contributing sources to achieve the desired precision. Typical error sources include mecahnical alignment, sensor noise, and transmission/data reduction systems errors. If these errors are partitioned equally between alignment-stability and noise transmission/reduction, the allowable time error for the latter is approximately 0.15 millisecond.

Recently acquired information indicates the signal slope for the UV sensor will be roughly 200 mv/sec, which will reduce the complexity of the data handling system. To analyze for the worst-case, the initial UV data is used in the following analysis.

Referring to Figure 126 it can be seen that the relationship of signal voltage to time results in a slope of $m = \frac{1.5\ V}{10\ ms}$ or 0.15 V/ms. Sensor noise of 60 millivolts peak-to-peak produces an equivalent full scale time error of $\frac{0.06}{0.15}$ ms or 0.4 ms, which exceeds the total allowable Δt of 0.29 ms. To reduce this error, statistical techniques are required. Statistical techniques require large sample sizes and either on-board processing or wide RF transmission bandwidths.

Figure 127 portrays the major candidate systems employing statistical analysis techniques for the UV and MW sensors. In Figure 127 a, the on-board processing candidate technique is shown, while Figure 127 b depicts a system which provides digital conversion and transmission in the spacecraft with ground station computation of the least squares curve fitting.

The on-board processing method permits data compression and results in low transmission data rates which, in turn, results in lower transmission power requirements and potentially lower primary power consumption. Large sample sizes commensurate with the "Law of Large Numbers" are possible, limited only by the calculation speed of the computer. The algorithm necessary to determine the best fitted line is relatively simple and can be achieved on a small machine (only addition is required).

The multiplexer, timer, and the analog-to-digital converter may be time-shared with the remainder of the PCM formatter to reduce equivalent complexity. The computation device is the only added part. The PCM transmitter input is a single data word which denotes the time of null crossing for each sensor. This data is required only once per revolution of the spacecraft for the MW experiment and twice per revolution for the UV experiment. Since only three data words per 15 seconds are required by the experiments and since the remainder of the data is low response status, the PCM bit rate is low enough to allow transmission of the RF bandwidth of 30 kHz.

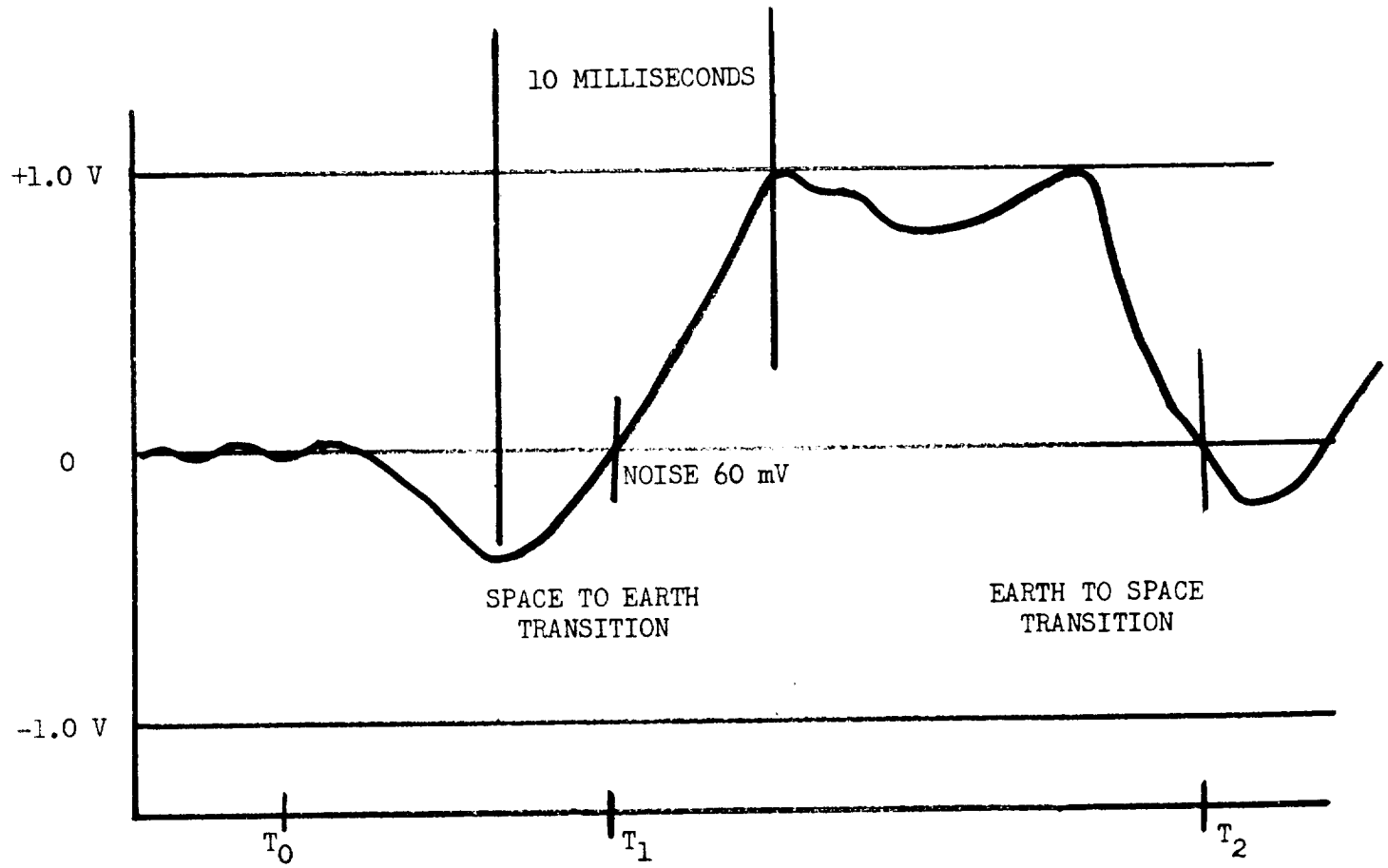

(Assuming 4 rpm Satellite Spin Rate)

Figure 126. UV Horizon Sensor Output Signal

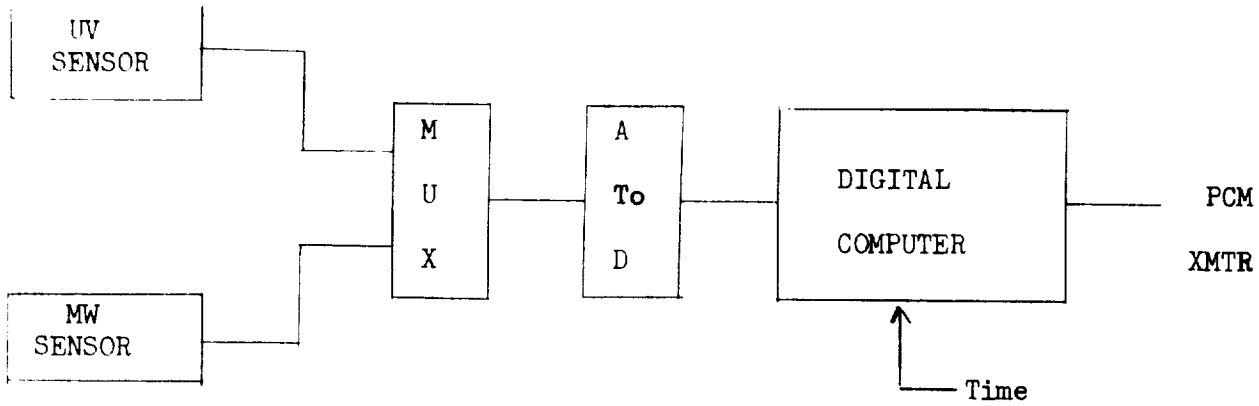

(a): On-Board Processor

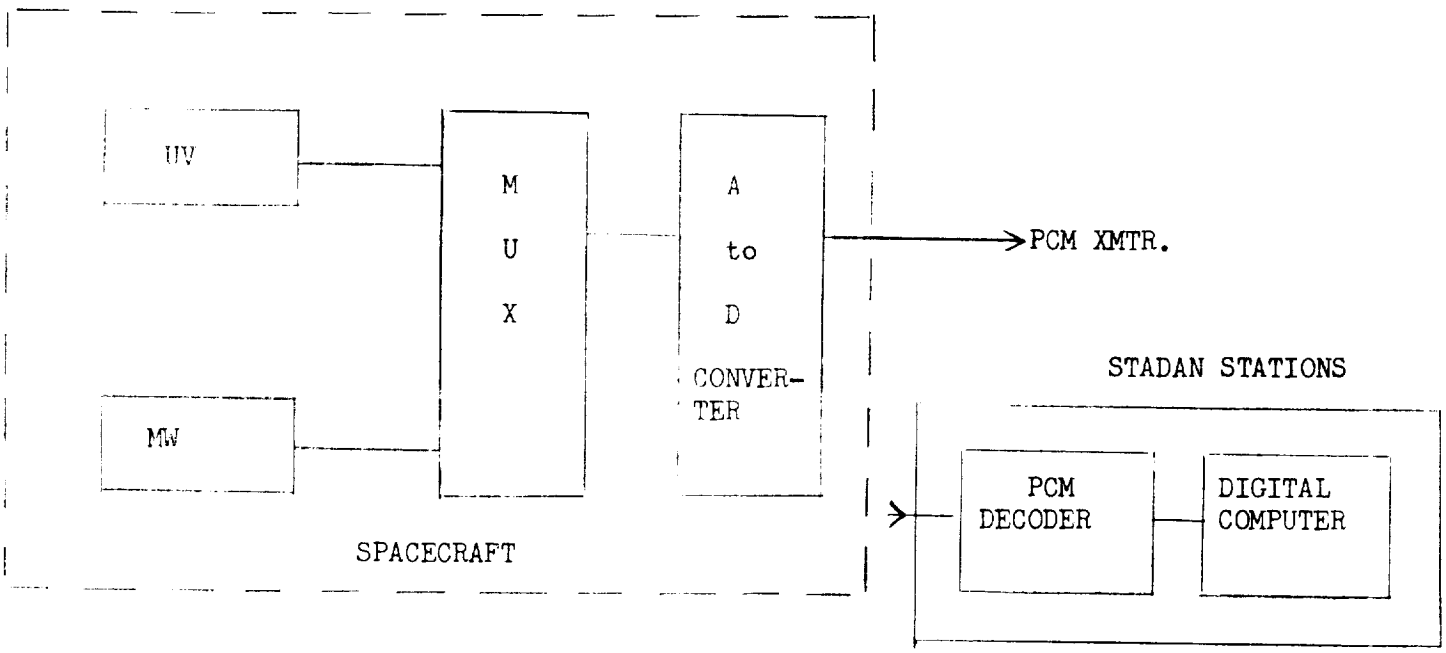

(b): STADAN Processor

Figure 127. Error Reduction Techniques

The ground station processing method does not require accurate timing or additional hardware. This system requires a high data sampling rate to provide an adequate sample size and elements of the sample set must be accurately transmitted. These constraints, imposed on the converter, translate into operation at increased speed and with increased quantization precision since the data must be emitted in "real time."

Fig. 126 shows the actual information period is of the order of 10 milliseconds. This is a very small time slice for either real time calculation or data transmission via PCM. The on-board processor can accept the data at some real time rate, store the time and data and perform the calculation over a more reasonable time span. This technique will simplify the on-board computer appreciably. This technique can be applied to ground processing as well if the buffer storage and control logic are added to the PCM system. This approach contains the features similar to operation with on-board computation and does not require additional analysis.

The real time data transmission technique cannot be analyzed without prior consideration of the sample size, sampling interval, and allowable timing quantization and transmission errors. These considerations for the UV-MW reference mission are given below.

Sample Size

The UV and MW sensors pace the data problem with respect to sampling rates and quantities. The UV sensor, in particular, requires a high data rate due to the extremely small time region of interest and the small permissible error which is further complicated by a rather large noise level.

The accuracy requirement dictates the use of curve fitting utilizing the least squares statistical techniques. To establish this curve to the desired precision, the sample size must be large enough to establish tolerable errors. Improvement in RMS error can be seen from the expression,

$$\bar{e}_{rms} = \frac{\sum \bar{R}\,(X_i)^2}{N+1}$$

where

$\bar{e}_{rms}$ measures the RMS deviation between the observed function and its calculated approximation over the N+1 points involved

N is the sample size

$R\,(X_i)^2$ is the i $\pm$h residual

The relative effect of sample size on the RMS deviation may be shown as:

N	$K_{\bar{e}\ rms}$
1	0.707
4	0.5
9	0.33
16	0.25
25	0.20
100	0.10
1000	0.03

A sample size of 1000 would require sampling at the rate of 1 sample per 10 microseconds. This requirement would tax most existing spacecraft equipment for on-board digitizing and storage is well beyond STADAN real time capabilities. Utilizing an 11 point sample, reduces the $K_{\bar{e}\ rms}$ by 71.2% of the full scale error, which results in a time error of,

(0.288) (0.4 millisecond) = 0.115 milliseconds

(Note: 0.4 milliseconds corresponds to the $\frac{0.06}{0.15}$ ms noise level given earlier.)

This error is satisfactory, provided all additional errors do not exceed 0.035 milliseconds (0.15 - 0.115 = 0.035).

Quantization

The 0.115 ms error is attributable to the sensor only. Additional errors arise in data transmission and reduction. To limit the magnitude of these errors, digital techniques (PCM) are required. The quantization error must be made small enough to be insignificant but the quantification should be commensurate with sample rate and bandwidth demands. Where the data has been quantized, the error can be considered fixed except for the bit error due to carrier-to-noise ratio (1 per 10^6 bits). This error is small and may be ignored. The rationale for quantization selection (8 bits) is derived from consideration of an error which corresponds to the least significant bit. The full scale percentage error as a function of the number of quantum levels was calculated and plotted in Figure 128.

The previously calculated slope indicates an equivalent time/voltage relationship of 1 ms/150 mv. The allowable error in time for the quantizer is approximately 0.035 milliseconds, which is the residue after consideration of the sample size. This time error is equivalent to a quantizing voltage error (X) of,

$$X = (.035 \text{ msec})\ (150 \text{ mv/msec}) = 5.3 \text{ mv}$$

It can be seen from the curve that the minimum number of bits required to provide this accuracy is 8 (0.0039 x 1.5 volts = 5.8 millivolts).

Real Time Requirements

The UV data sample period of 10 milliseconds necessitates high data rate to obtain sufficient data to establish the null at an Earth station after local statistical processing. One sample per millisecond produces approximately 11 data points over the locator sensing interval. Signals digitized at 8 bits per sample result in a data rate of 8 kilobits per second and require an RF bandwidth of approximately 16 kHz (using Carson's rule). This data rate increases the RF transmitter power requirements by about 3 db above the on-board technique.

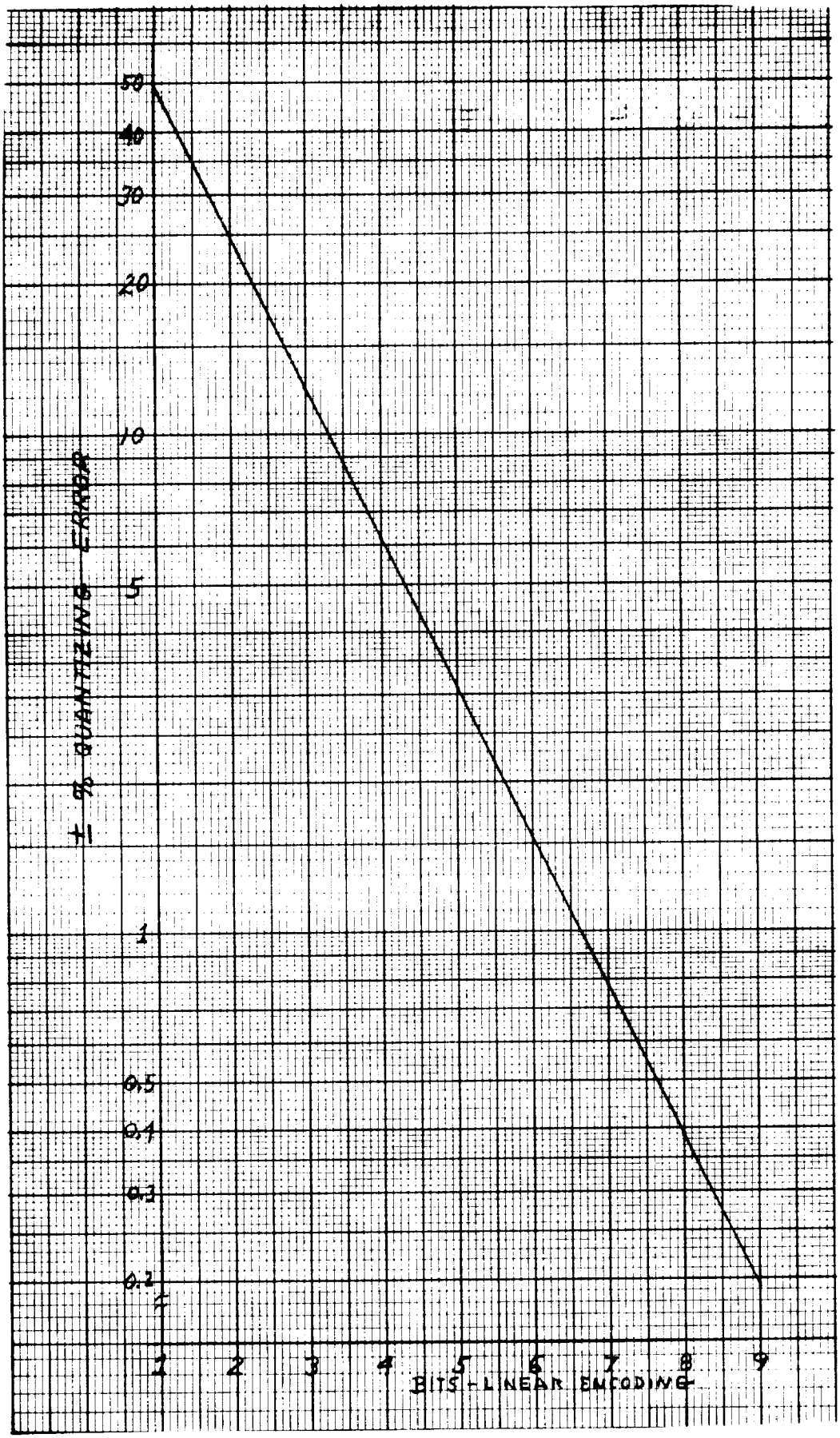

Figure 128. Error vs. Encoding Bits

However, the required power increase is less than 200 milliwatts of RF and about 400 milliwatts to the power source. This load penalty is considered small.

Tradeoff Matrix - The relative merits of each approach is summarized in Table 33.

TABLE 33

TRADEOFF SUMMARY

PARAMETER	ON-BOARD SYSTEM	GROUND SYSTEM
Performance	High	High
Weight	High	Low
Power	Low	Low
Flexibility	Low	High
Cost	High	None
Reliability	Low	High

Analysis of the table indicates that the on-board system out-performs the real time transmission system if it is sufficiently sophisticated. However, the real time system produces satisfactory results. In all other respects, the on-board system is inferior or only equal to the real time method. The real time system and the on-board unit utilize about the same amount of primary power; but the real time unit requires less hardware, does not depend upon additional equipment performance (timer and computer, saving cost of the items and their testing); it may be altered easily because all data is handled on the ground and algorithms are readily changed; weight is less; reliability is obviously greater. In addition, the raw data is recovered in this system and thus allows alternative methods of analysis of the data, if necessary.

Microwave Sensor

The output signal from the microwave sensor is given in Figure 129. Except for the longer transition times and larger excitation voltages and corresponding larger noise level, the microwave sensor output is similar to that of the UV sensor and the preceding analysis holds for it also. The MW experiment transitions

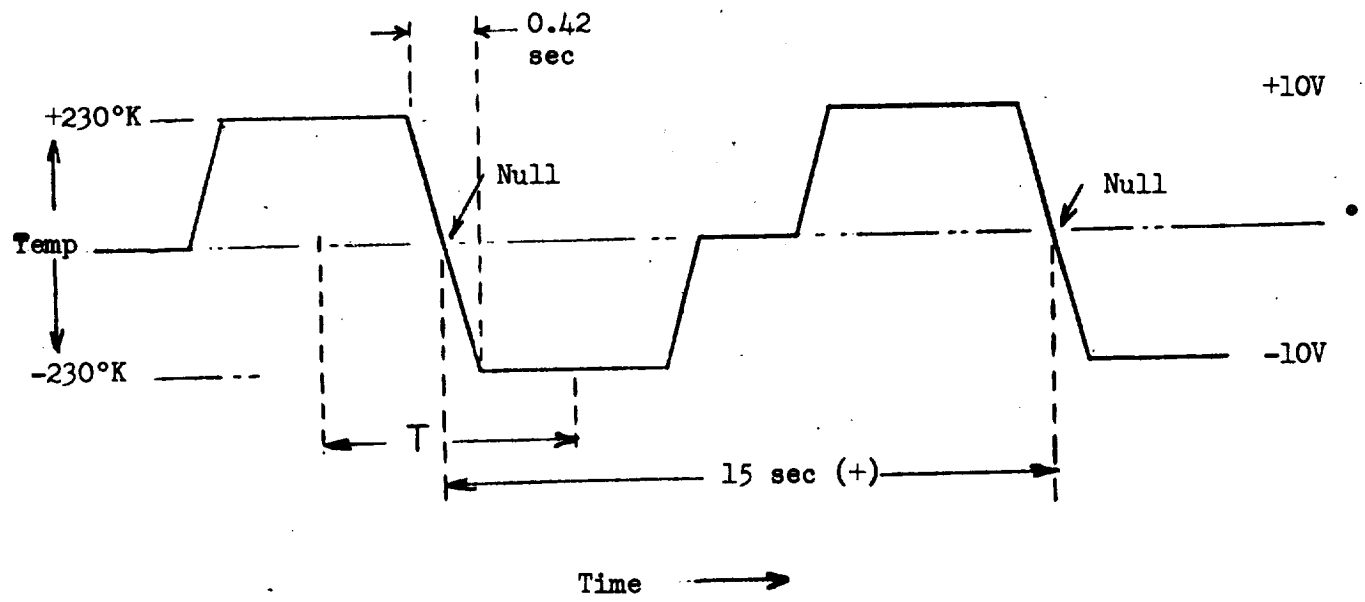

FIGURE 129. Microwave Sensor Output Signal

(4 rpm satellite spin rate)

will permit a much larger sample population (42 times larger) at the UV sampling rate so that the best fitting line derived by the least squares method is more accurately obtained.

Fine Sun Sensors and Horizon Sensors

The output signal from the sun sensors or horizon sensors is a rectangular pulse generated by a Schmitt trigger at the time of limb crossing. The pulse must be timed to within ± 2 microseconds to permit adequate time correlation between sensors to determine spacecraft attitude.

The timing system is described in a later section covering the required on-board clock accuracy. The system permits storage of a time value corresponding to the leading edge of the sensor pulse with a data update on each spacecraft revolution. Timing is extracted from the PCM clock and a series of bi-stable multivibrators arranged as an up-counter. The time stored in the up-counter registers is dumped into PCM parallel shift registers with the simultaneous appearance of a clock pulse and sensor signal. The leading edge and trailing edge pulse time for each sensor is stored separately; 8 data words are generated in this scanner (2 per sensor).

Housekeeping Data

Housekeeping data consists of status of the power busses, command functions, temperatures on the structures and the solar arrays, magnetic control coil signals for attitude control and bias, and coarse time.

Temperature measurement techniques include the use of thermistor sensors connected as a leg of a Wheatstone bridge which is in turn excited by a zener diode power supply. The output signal is amplified to provide a conditioned ± 1

vdc full-scale signal to the analog to digital converter. A potentiometer or selectable resistance sets the low temperature range for the measurement. A large number of temperature measurements are required early in the mission but are substantially reduced after the thermal control system has been evaluated under varying orbital conditions.

The bus voltages are combined for digitization by a voltage divider network with a bias voltage network to establish the necessary voltage range.

Current sensors consist of a small series resistor whose output is conditioned to the necessary levels by operational amplifiers.

The housekeeping data is derived from measurements whose outputs are relatively time invariant. While these functions are numerous they do not significantly affect the bit rate requirement for the PCM system. They may be sampled, in many cases, hourly or even daily if required. The sun and horizon sensors each provide two outputs per revolution. While these signals require extremely accurate time correlation, they do not require large sample sizes or high data rates.

Satellite Clock Accuracy

The sun sensor and horizon sensor require extremely fine timing accuracy to perform determination adequately. The sun sensor accuracy requirement is stated as ± 0.1 arc second. Considering the satellite rotation rate as 4 rpm, the ± 0.1 arc second error can be converted to a timing error by simple calculation considering

$$\frac{360°}{15 \text{ sec}} = \frac{(360)\ (60)\ (60)}{15} \frac{\text{arc sec}}{\text{sec}} = 0.1 \text{ arc sec} =$$

$$\frac{15 \text{ sec}}{(360)\ (60)\ (60)\ (10)} = 1.15 \text{ microseconds}$$

This timing accuracy is the most stringent requirement and consequently establishes the required clock accuracy. An additional consideration in the timing inaccuracy is introduced by the cross-track and altitude errors encountered in position determination utilizing Minitrack. This position uncertainty is of the order of ± 200 meters for each parameter. An uncertainty of 200 meters translates into a timing error of 0.66 microseconds, viz,

$$\frac{200}{C} = \frac{15 \text{ sec}}{300 \times 10^6 \text{ meters/sec}} = 0.66 \text{ msec}$$

Since the position time error is large, the clock error must be of the order of ± 0.5 usec (1.15 - 0.66 = 0.5 usec).

Small precision crystal oscillators are available that produce fundamental frequency outputs at 1 MHz with the following characteristics:

± 3 parts in 10^8 drift in 1-week period

± 2 parts in 10^6 per year

The PCM programmer clock can be designed to provide the pulse source of sufficient accuracy for the UV-MW satellite.

Command List

The required UV-MW spacecraft command functions are given in Table 34. These commands are largely concerned with power and attitude control. The attitude control functions consist of controlled currents whose magnitude and direction provide magnetic vectors which react with the magnetosphere to cause appropriate attitude correction, spin, and bias corrections.

The bus control functions permit power control over the experiment sensors, the attitude sensors, the timing system, and PCM devices. The PCM encoder is normally ON except in cases of power emergency. The sensors may be turned OFF during the battery charging cycles to reduce the load to a level to permit faster charging of the battery and may be dumped during even minor emergency, through ground control.

TABLE 34

COMMAND LIST

TITLE	SYSTEM	QTY	REMARKS
Battery Reconditioner	Power	2	On/Off
Cycled Loads Override	Power	2	On/Off
Fine Sun Sensor	Attitude Det	2	On/Off
IR #1 Horizon Sensor	Attitude Det/Control	2	On/Off
IR #2 Horizon Sensor	Attitude Det/Control	2	On/Off
Electronic Controller	Attitude Control	2	On/Off
Coarse Sun Sensor (DSAS)	Attitude Control	2	On/Off
Spin Rate MSC	Attitude Control	2	On/Off
QOMAC Coil	Attitude Control	2	On/Off
MBC Current Stepping Switch	Attitude Control	1	Step Pulse
UV Sensor	Exp /Att Control	2	On/Off
MW Sensor	Exp	2	On/Off
PCM Encoder	Commun	2	On/Off
Timer	Commun	2	On/Off
Timer Reset	Commun	1	Reset Pulse
Sensor Registers	Commun	2	On/Off
Data Conditioner	Commun	2	On/Off

Space Division
North American Rockwell

The timing unit is not required when the attitude sensors are not in use. Therefore, timing power may be removed when these sensors are OFF.

The UV and MW sensors cause the greatest power consumption and these sensors will be turned OFF when not in use to allow battery charing.

If data is required to be stored and transmitted at later orbital periods, the power control problem will become severe primarily due to the lack of global control and because more of the systems will be required within this mode of operation.

The remaining command is clock reset. This command resets the on-board clock and recycle time so that it may be correlated with time of day and other events at STADAN stations. The reset signal command may be given on each orbit or the clock will cycle through its two-hour count and reset automatically. The reset command can be read out in the coarse time signal to an accuracy of ± 0.1 millisecond.

Conclusion

The UV and MW locator height error of ± 0.5 km requires statistical computation of data. The sample sizes and allowable transmission error result in a sampling rate of 1 sample per millisecond and an 8-bit quantizer for the UV sensor with a sampling rate which can be 1 per 25 milliseconds at the 8-bit level for the MW device.

The fine sun sensors data must be transmitted with an accuracy equivalent to ± 0.1 part per second. This small error, coupled with tracking inaccuracy on the order of ± 200 meters, results in an on-board timer accuracy requirement of ± 0.5 microsecond. This is achieved by utilizing a precision 1 MHz PCM clock.

Approximately 42 analog measurements, 9 parallel digital words and approximately 19 discrete (ON-OFF) measurements are required.

Approximately 32 commands are required to provide power control during operations, particularly during battery charging; attitude and spin control; and to provide event markers to correlate range and spacecraft timing.

No significant development is required to implement the UV-MW measurement requirements. Modifications to existing STADAN facilities are not necessary.

Telemetry, Tracking, and Command System Description

The TT&C system consists of a PCM-PM telemetry system, an AM-AM command system, and a timing unit (see Figure 130).

The PCM-PM unit processes data generated by the experiments, attitude determination and various status sensors. This unit provides the format, digital conversion, synchronization, modulation, and other standard telemetry encoding and transmission functions. Approximately 42 analog, 9 digital-parallel and 20 bi-level measurements (Table 32) are telemetered by the system. The telemetry transmitter output is of the order of 0.6 watts with an RF bandwidth of approximately 100 kHz.

The AM-AM command system processes STADAN encoded functions to allow ground control over spacecraft spin rate, power control, attitude and time correlation (see Table 34). Command receiver sensitivity is of the order of 1.5 microvolts and is capable of processing 70 discrete command functions by decoding complex signal combinations of 7 audio tones. All outputs are momentary signals (24 volts dc @ 100 milliamperes for 50 milliseconds).

The timing unit provides fine and coarse time for range time and events correlation, for use in timing spacecraft events used in attitude determination, and for data processing of experiment information. Precise time is utilized by the fine sun sensors and the IR horizon sensors. The time counters may be cycled

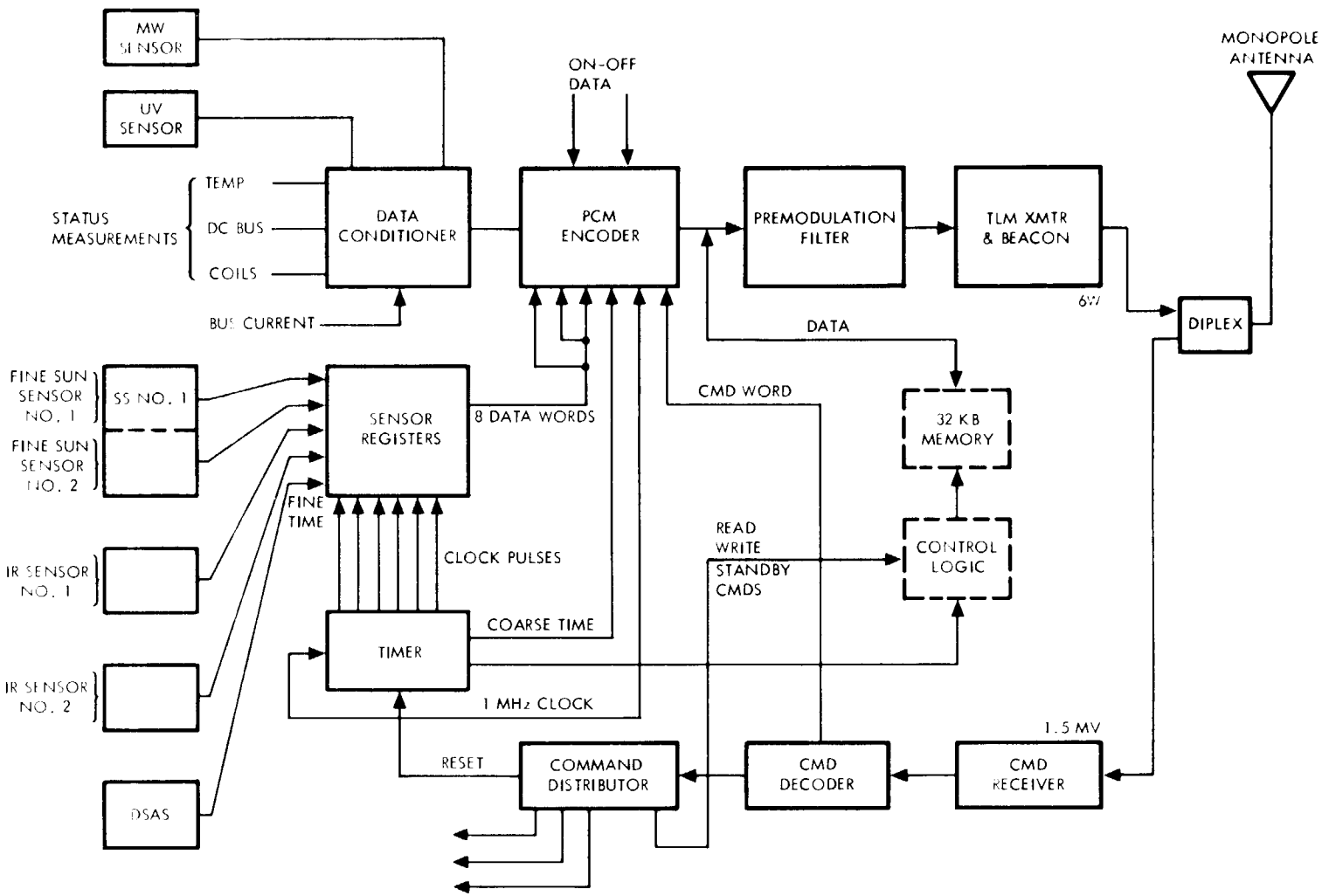

Figure 130. Avionics System Block Diagram

Space Division
North American Rockwell

under ground control to synchronize all data and significant events. Table 35 lists the general system characteristics.

Telemetry Subsystems

The telemetry system consists of the antenna, diplexer, transmitter, PCM formatter, data registers, and data conditioners. The antenna is a monopole (quarter-wave stub) which provides a pattern similar to that of a dipole. The diplexer is utilized to couple the antenna to both the telemetry transmitter and the command receiver, simultaneously, without internal interference.

The PCM formatter provides a serial NRZ mark data stream to the PM transmitter adding synchronization to the data stream together with the multiplexer-quantizer sampling and conversion process.

The data registers are utilized for the sensors. These data registers store sampled data which has been precisely timed and converted to corresponding sensor events for transmission at low bit rates. The data conditioners supply a standardized signal input voltage to the PCM quantizer. Data which has not been pre-converted to voltage by the sensors are conditioned to the acceptable signal by this unit (ex, temperature measurements converted to resistance by the transducer are converted to equivalent voltage by the data conditoner).

PCM Formatter

The PCM unit consists of an A to D converter (quantizer), multiplexer, sub-multiplexer, synch generator, clock, programmer, shift registers, and digital storage (see Figure 131).

PCM Format - The signal to the transmitter is formatted in NRZ-M with the output signal schedule shown in Figure 122 a,b. The multiplexer step is 3 samples per millisecond which permits cross-strapping of the channel inputs. The UV sensor

TABLE 35 T,T,&C SYSTEM CHARACTERISTICS

Antenna Type:	Monopole
Pattern:	Toroidal, 120° between half power points
Gain:	2.2 db at beam center
Characteristic Impedance:	50 ohms
Transmitter Frequency:	136.0 - 137.0 Megahertz
Power Output:	0.6 Watts
Modulation:	PCM-PM
Modulation Index:	1 Radian
Bandwidth:	100K Hz to allow for doppler and instability
Stability:	±.0037%
Command Receiver Type:	FM
Frequency:	148 Megahertz
Sensitivity:	1.5 Microvolts
Tone Modulation:	AM-AM, 7 tones
Command Outputs:	70 each On/Off, 200 ma @ 50 milliseconds
Telemetry Data Format:	NR Z-M at 24 Kilobits/second
Input Data:	42 analog 9 binary 20 discretes (multiplexed and sub-multiplexed)
Synchronization:	24 bit frame with supplementary sub-frame synch and identification
Word Length:	1 frame equal 32 sub-frames; 32 words/sub-frame
Timing:	Precision (±1 microsecond) Coarse (±10 milliseconds)
Volume:	250 cubic inches
Weight:	12 lbs
Power Dissipation:	6.4 Watts
Component Design:	Space qualified hardware pretested on NASA Programs

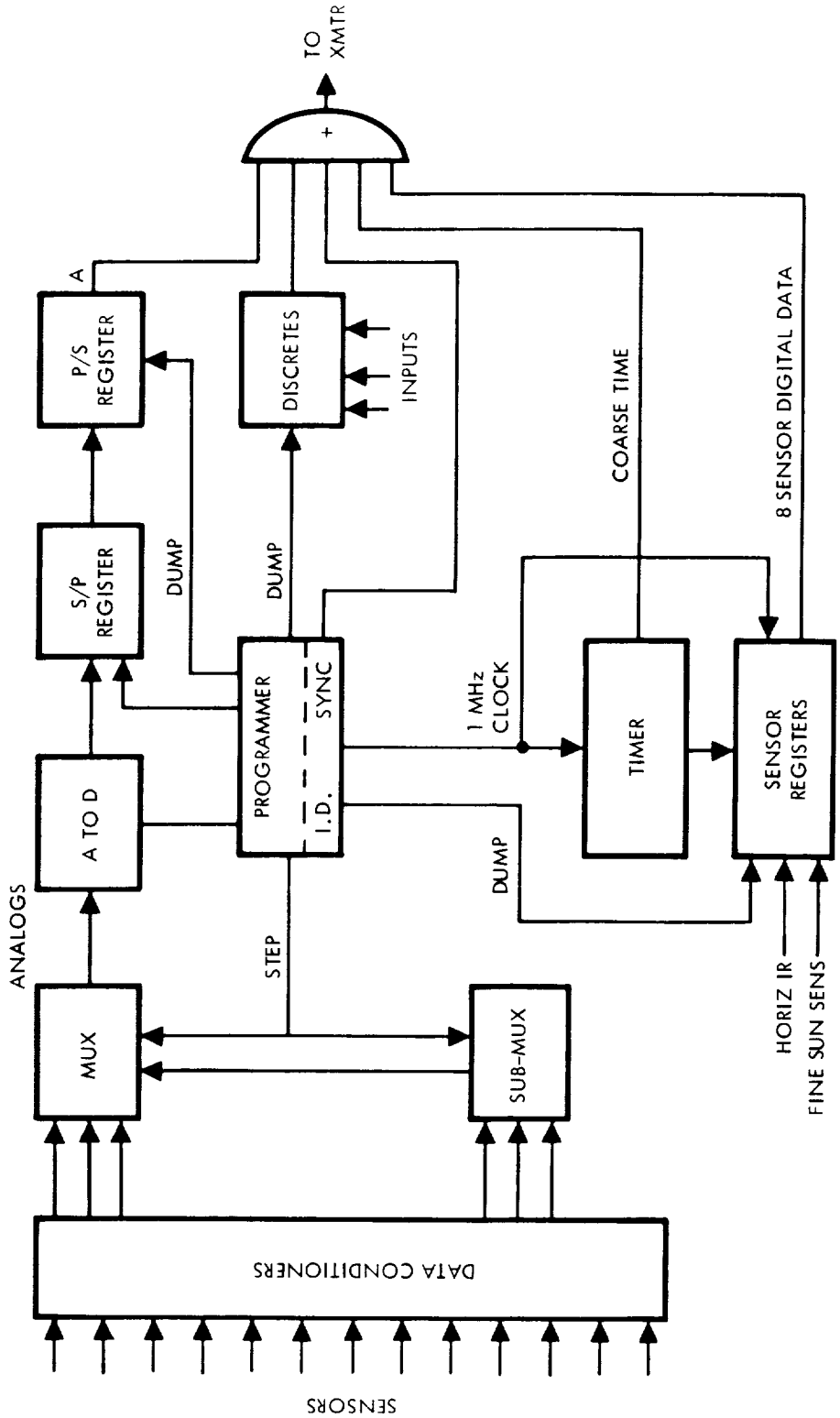

Figure 131. PCM Formatter

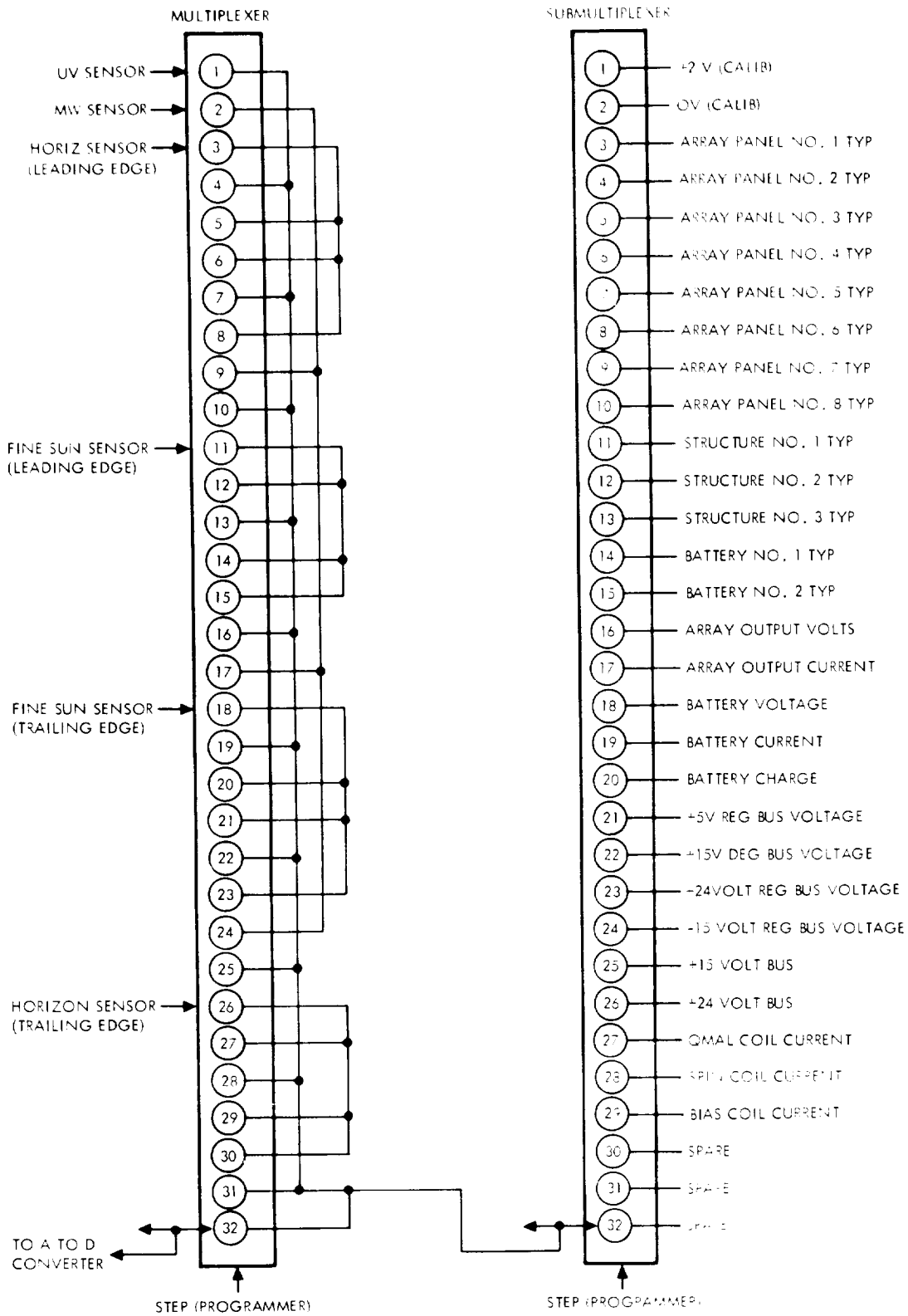

Figure 132 a. Analog Signal Format

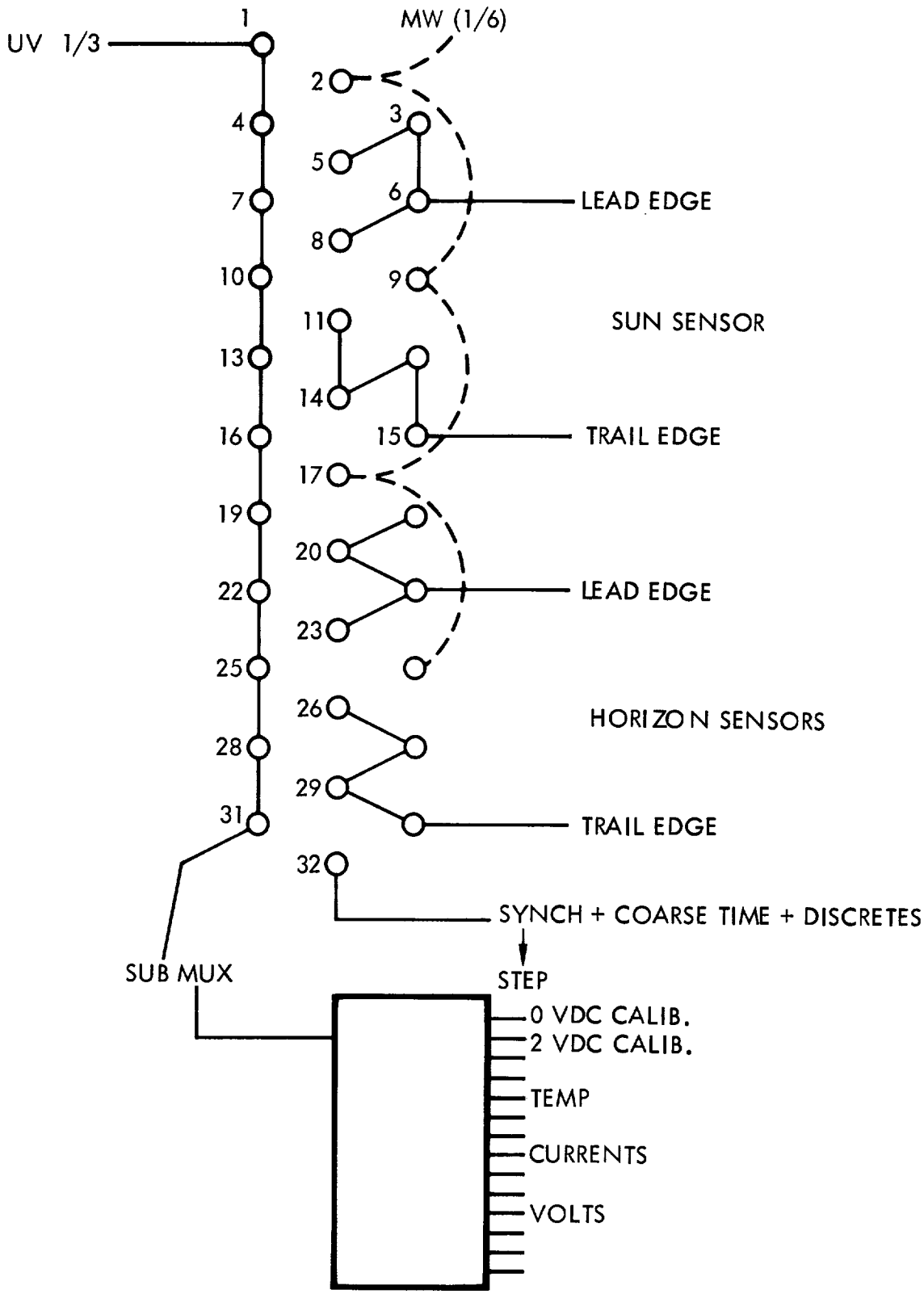

Figure 132 b. Signal Format

output is sampled every third step of the multiplexer while the MW sensor is sampled every 6th step of the multiplexer (1 sample per 2 milliseconds). On every other subframe, the leading and trailing edge times of an appropriate sun sensor/horizon sensor pair will be shifted out and coarse time emitted at the end of each subframe together with synchronization and subframe identification.

The sub-multiplexer advances one step for every 32 steps of the multiplexer. All data on these channels are housekeeping functions and do not require more frequent transmission. The sub-multiplexer completes a revolution in approximately 320 milliseconds. This rate provides a heavy load of undesirable data but since the ground station can analyze channels selectively, the load need not be greater than the demand.

The sub-multiplexer calibrate signals appear often enough to compensate the data for internal drift, if necessary.

This format consists of 32 subframes to a master frame with approximately 44 words per subframe. The word length is 8 bits and the bit rate, 24 kilobits/sec. Each subframe is identified with a 5-bit coded designation, and the subframe synch is the complement of frame synch.

Programmer - The PCM programmer generates most of the control functions for the PCM system. Step signals from the programmer timers advance the multiplexers and sub-multiplexers. In this manner, the programmer selectes the input signal to the 8-bit quantizer. The unit controls the signal injection into the data stream by asserting the unit from which an output is desired while inhibiting all others. All functions are precisely timed by the programmer to provide an orderly sequence of information requiring the least amount of synchronization. The programmer selectively introduces quantized data, digital data, discrete functions, coarse time, synchronization and identification data into the PM transmitter to form the ordered PCM data stream.

Quantizer - The analog to digital converter provides an 8-bit digital output signal corresponding to the amplitude of the input signal voltage. The device contains sample and hold provisions to enhance the quantization process and appropriate registers for serial digital data stream injection upon completion of digitization.

Multiplexer and Sub-Multiplexer - The multiplexer and sub-multiplexer are identical devices except for the step rate of advance. Each unit has the capacity for accepting 32 separate input signals; isolating the signals from each other; and sequentially presenting multiple input data to a single output. The selected channel dwell time exceeds the quantization period, but is synchronized with the data stream output rate.

Timer

The timer unit provides coarse and precise timing to synchronize spacecraft conditions and events with ground station operations. The timer is utilized specifically by the fine sun sensors and the IR horizon sensors to provide attitude reference information for experiments data analysis. The timer utilizes the PCM programmer clock to provide the necessarily stable timing source and is essentially a decimal up-counter (see Figure 133).

The 1 MHz input signal is divided down to provide a total count equivalent to a 2-hour period. The first seven scaling units are decade scalers (divided by 10) to provide outputs in microseconds, tens of microseconds, hundreds of milliseconds, tens of milliseconds, hundreds of milliseconds and seconds. These decades are followed by a scale of 6 divider which provides "tens of seconds." These dividers constitute the "precision time" section of the timer which is employed for use in sun and horizon sensor timing. The outputs from these scalers, true and complements, are cabled to the sensor registers for parallel shifting on demand (pulsed sensor events).

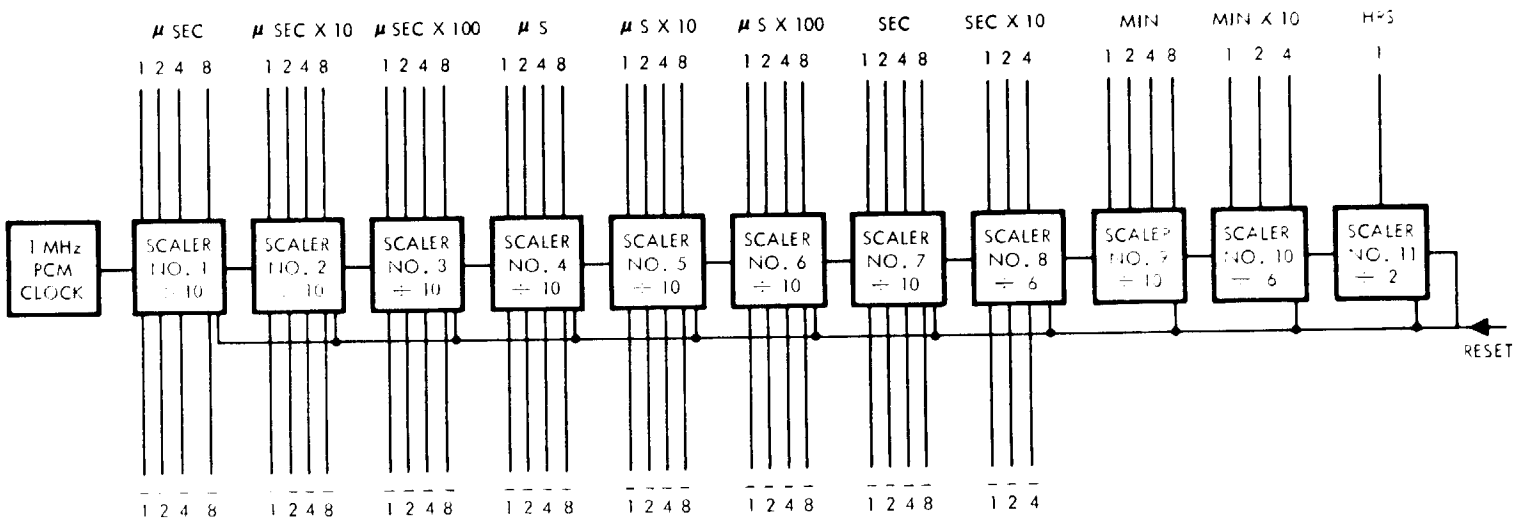

Figure 133. UV-MW Timer

Space Division
North American Rockwell

The tens of milliseconds, hundreds of milliseconds, seconds, and tens of seconds scalers are utilized for coarse time also, together with the minutes, tens of minutes, and hours dividers. The decimal scaling requires additional bi-stable multivibrators over a binary system and was selected because of the convenience of keeping time in seconds, hours, and minutes.

Only the time outputs from the dividers are delivered to the PCM data stream, since a serial data shift may be readily accomplished over these comparatively long time periods.

The timer is accurate to ± 0.5 microsecond while the source accuracy is the crystal short-term and aging error (1 part in 10^8 short term, 2 parts per million/year long-term error). The total clock countdown lasts two hours if a manual reset is not issued earlier by a STADAN control station. A STADAN command reset permits time correlation to desired events. The reset clears the count on all registers simultaneously.

Sensor Registers

The fine sun sensors and the horizon sensors require events timing which would result in enormous bandwidth if the data were processed in real time. To overcome the attendant spectral and power dissipation requirements necessary for broad bandwidth transmission, on-board buffering has been incorporated. The buffers consist of bi-stable multi-vibrators (RST flip-flops) constructed in integrated circuit form to conserve weight and power (see Figure 134). The buffer registers accept the true and complementary outputs from the precision time scalers of the timer. The contents of the time scalers are parallel shifted to the sensor storage registers when coincidence between a sensor pulse and a clock pulse occurs.

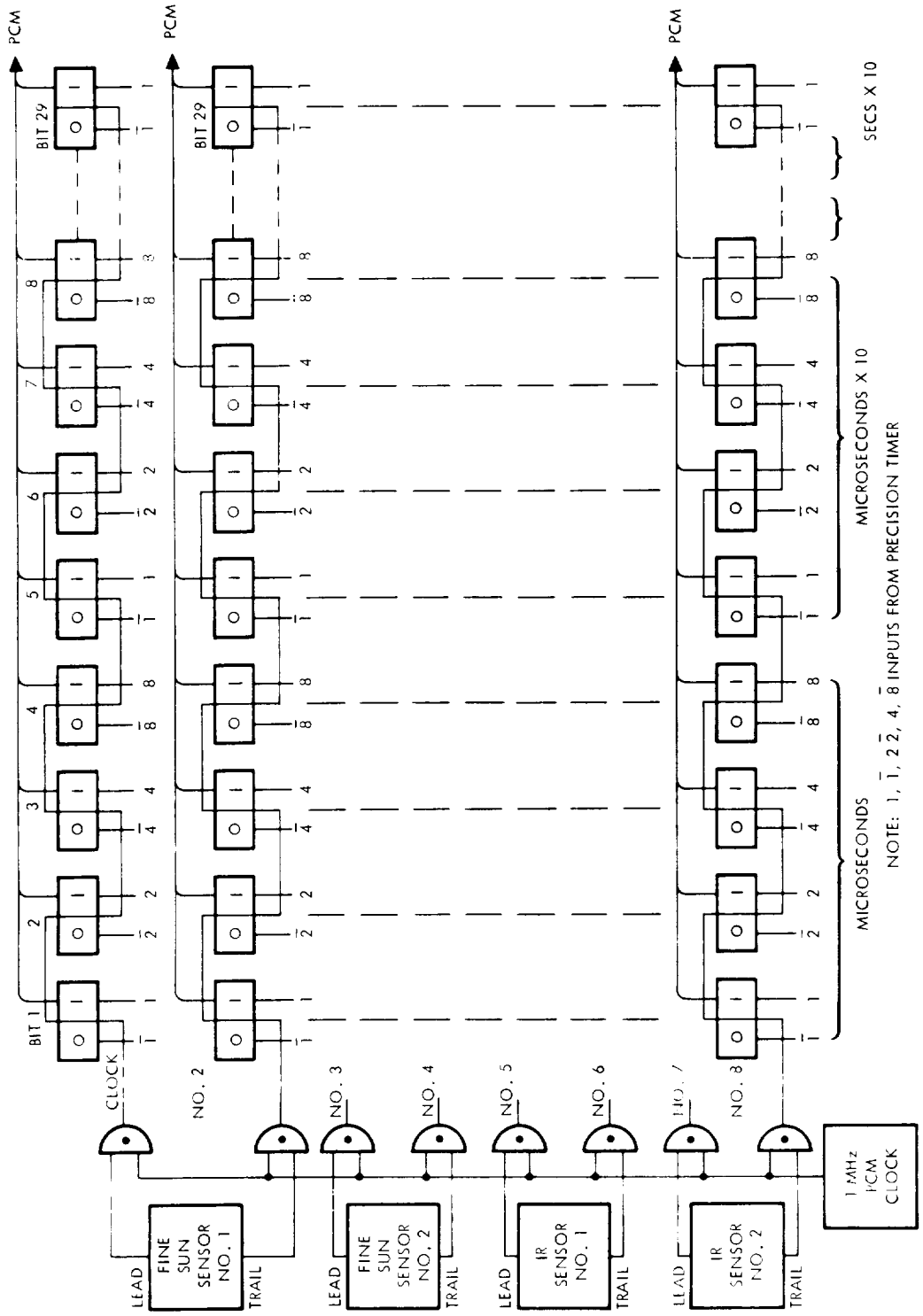

Figure 134. Sensor Registers

The clock frequency is 1 MHz and the gating speed is accomplished in tenths of nanoseconds to be consistent with the overall pulse timing error of ± 0.5 microsecond required by the sun sensors (± 0.1 arc second error). The true two-legged gate inputs assert all storage flip-flops concurrently. The sensor signal is a rectangular pulse generated by a Schmitt trigger when the sensor achieves the desired signal.

The registers store 29 bits of precise time information which is serially shifted out at the proper subframe time and rate by the PCM programmer. The programmer shifts the leading and trailing edge time information for a sun sensor/IR horizon sensor pair on alternate subframes (four registers are dumped per subframe).

RF Section

The TT&C RF section consists of the antenna, diplexer, PM transmitter and command receiver. The PM transmitter accepts the formatted PCM digital signal train and phase modulates a VHF carrier, which is impressed on the antenna by means of the diplexer. The diplexer efficiently couples both the command receiver and the transmitter to the monopole antenna and contains the necessary filters to isolate these units from each other. The command receiver is utilized to demodulate coded VHF signals to the baseband coded command signal.

Telemetry-Command Antenna

The telemetry-command antenna is required to provide omnidirectional coverage in an Earth plane normal to the orbit consistent with the ground station viewing angle and system RF power requirements. In addition to coverage, other considerations are weight, size, stowage, erection, solar cell shadowing, polarization, frequency and design compatible with the satellite geometry. Because of limited space, simplicity in design and stowage capability, linear antennas were considered.

Four basic and proven antennas were considered; a turnstile, dipole, sleeve, and a monopole. The antennas are illustrated in Figures 135 through 138. The sleeve, monopole and dipole antennas are mounted co-linear with the longitudinal axis of the satellite; i.e., the polarization vector is parallel to the satellite's longitudinal axis.

Except for the turnstile antenna, the pattern coverage provided is essentially the same. The best coverage is provided by the turnstile antenna, which provides near omnidirectional coverage. However, the dipole and turnstile antennas were eliminated because of the number of elements that must be stowed and the need for space-consuming balance-to-unbalance transformers (balans). In addition, a turnstile antenna would shadow the solar cells. The sleeve antenna was discarded because of stowage problems.

The antenna selected for the satellite was the monopole (Fig. 138). The monopole antenna provides approximately +2.2 db gain at broadside, and a pattern nearly like that of a halfwave dipole, which is consistent with the system requirements. The monopole can be readily stowed and impedance matching can be performed on the antenna base. To substantiate that the monopole antenna would satisfy system requirements, pattern measurements were performed on a full-scale cardboard model covered entirely with aluminum foil, and again with aluminum foil covering only the antenna mounting plane. Figures 139 & 140 demonstrate, in terms of relative db, the radiation pattern that can be anticipated. Figure 139 is a principal plane pattern where the antenna is in the plane. Figure 139 illustrates that the pattern will be a figure 8 revolved around the longitudinal axis of the vehicle. This is further demonstrated by Figure 140 which is a conical cut pattern, measured 45 degrees off the longitudinal axis of the satellite.

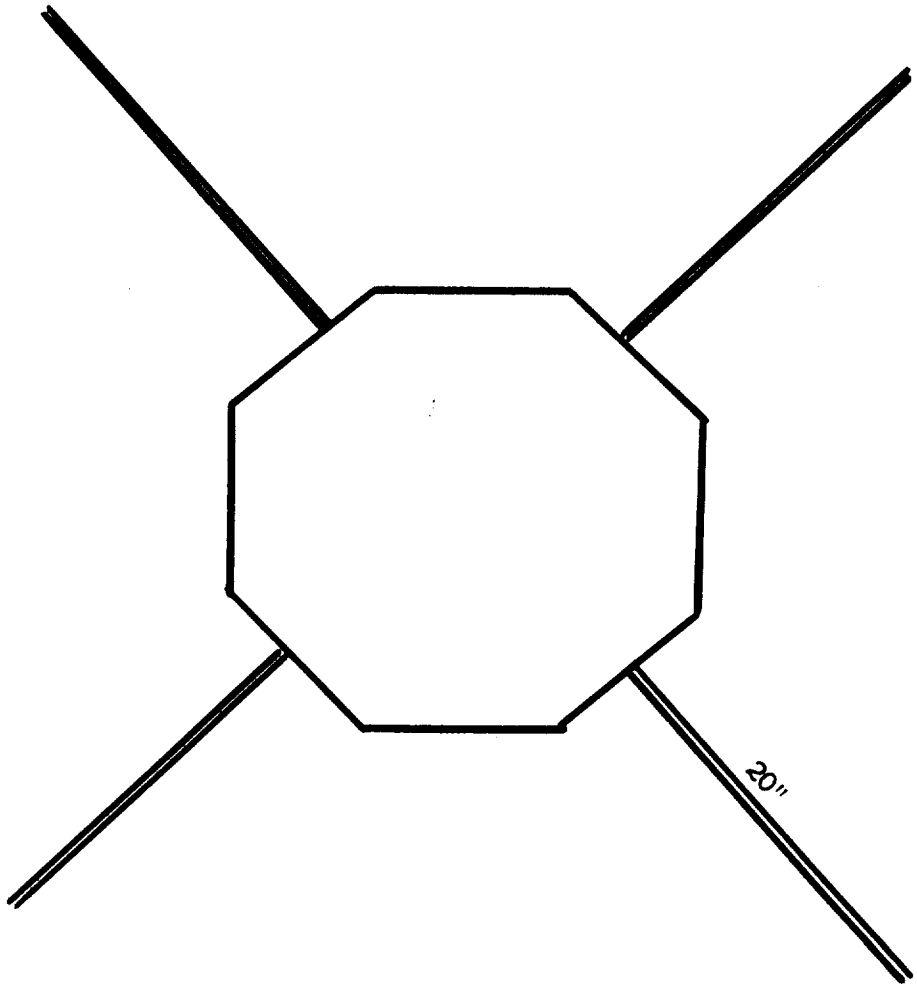

Figure 135. Turnstile Antenna

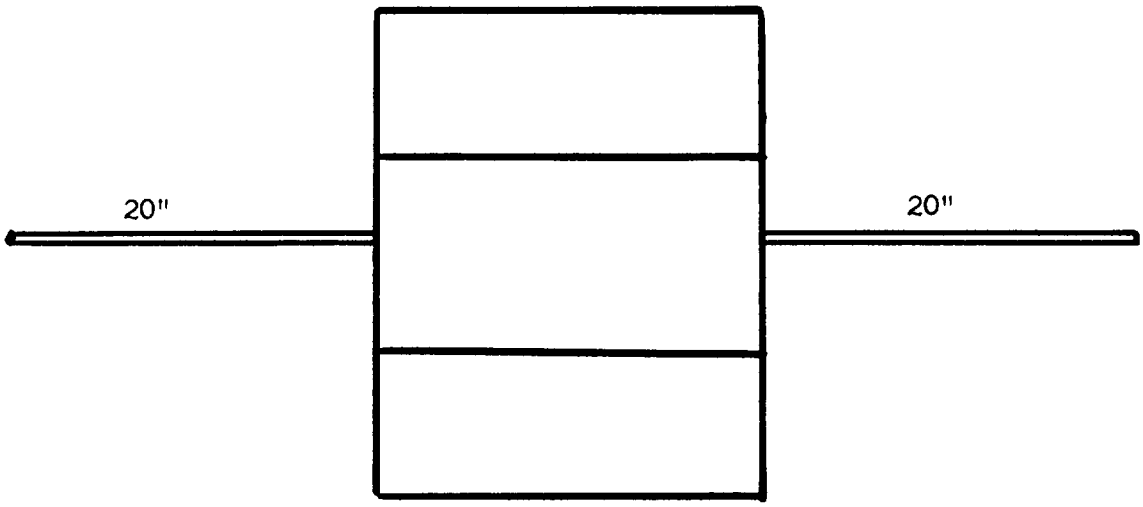

Figure 136. Dipole Antenna

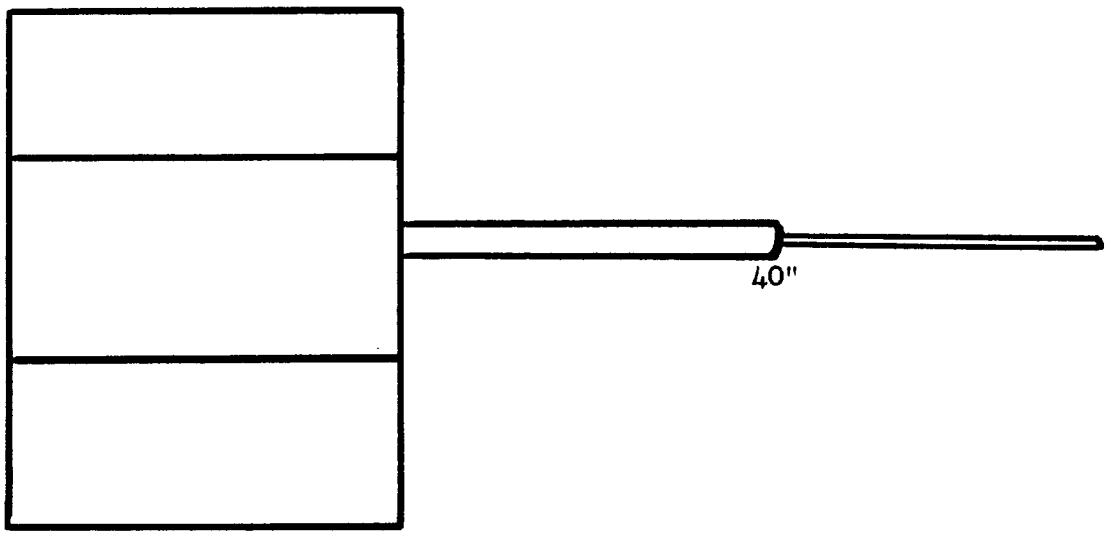

Figure 137. Sleeve Antenna

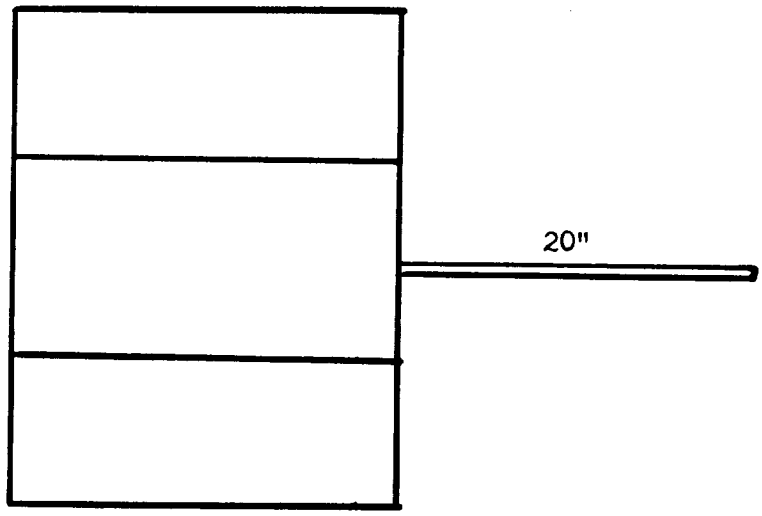

Figure 138. Monopole Antenna

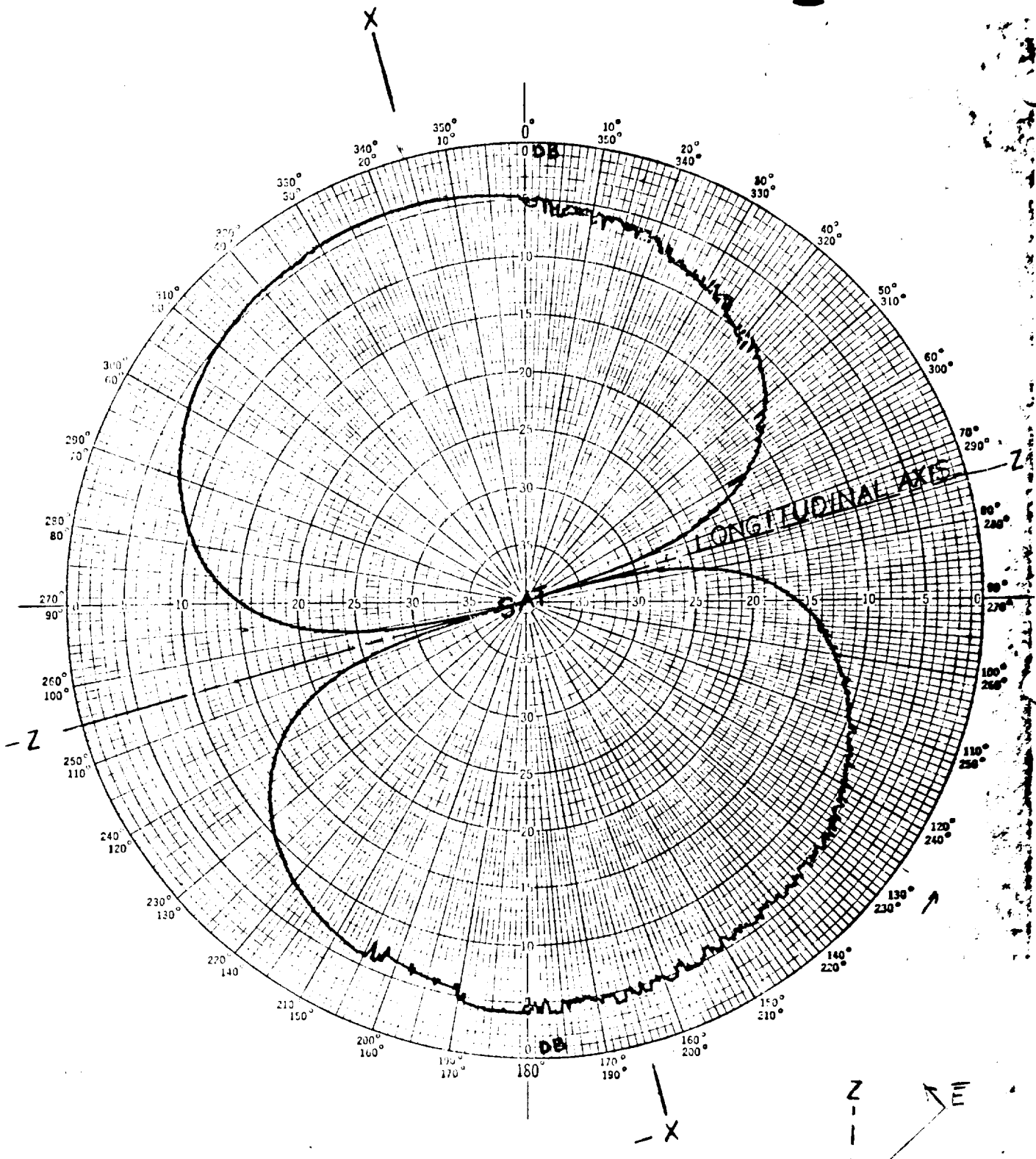

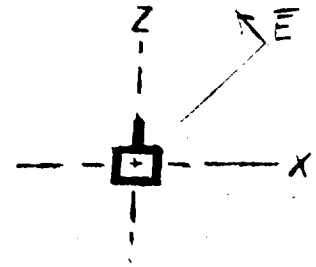

FIGURE 139. MONOPOLE ANTENNA RADIATION PATTERN
- PRINCIPAL PLANE

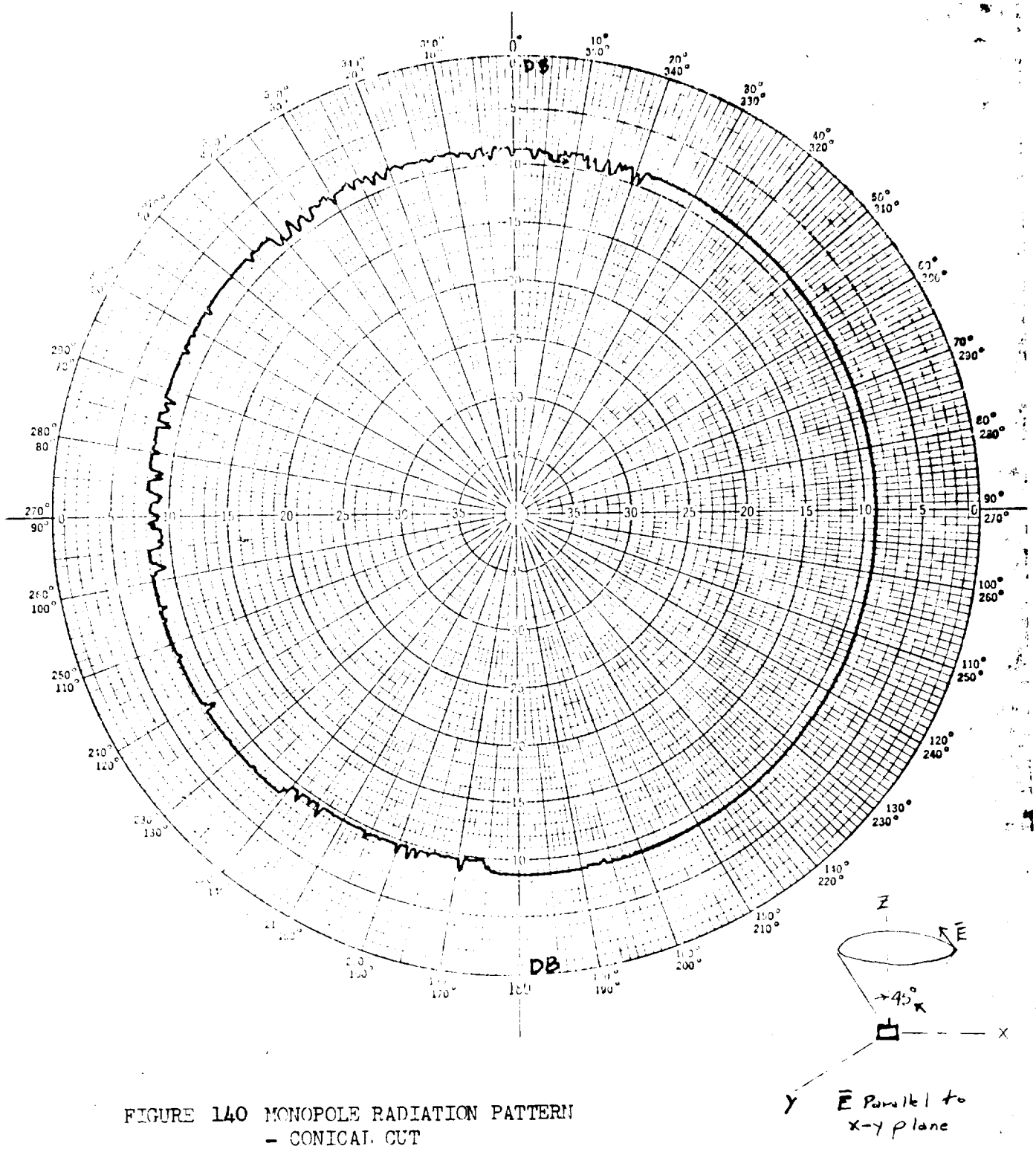

FIGURE 140 MONOPOLE RADIATION PATTERN
- CONICAL CUT

Diplexer

The Ball Brothers Research Corporation (BBRC) Orbiting Solar Observatory (OSO) diplexer is a passive unit designed to work with the specific transmitter and command receivers. It is small and light, and provides the required 50 ohm impedance to the RF units with over 70 db of isolation between the 136 MHz transmitter and the 148 MHz command receivers. The units required for the UV-MW satellite differ from the OSO units in that the required range of operating antenna VSWR will be relaxed. The OSO antenna is complex, and telemetry and command are required with the antenna in various stages of deployment. The resulting VSWR range is extreme. The UV-MW satellite antenna, a simple stub, will present a nominal 1.2:1 or better VSWR to the diplexer under all operational conditions.

Telemetry and Beacon Transmitter

A 136 MHz transmitter, qualified for satellite use with the STADAN ground system and meeting the UV-MW satellite requirements, is the OSO unit manufactured by BBRC. The OSO telemetry operates at 800 bits per second in a real time mode and at 14,400 bits per second in a playback mode. The PCM is Manchester-coded with a resulting premodulation filter cutoff frequency of 1.2 times the bit rate. The UV-MW subsystem will operate at 24,000 bits/sec only, and will use an NRZ format. The NRZ filtering is half the bit rate, so that optimum filtering will be 12 kHz. The resultant variation from the OSO requirements are minor, and the equipment could be operated with no changes. Sufficient changes in the data will occur at the 24,000 bits/sec rate to clear the spectrum around the carrier for tracking, without requiring a Manchester code.

The transmitter is stable to within $\pm 0.0037\%$ in the OSO environmental requirements, which are more than adequate for the UV-MW satellite. The phase modulator

RF characteristics of the transmitter are designed around the low modulation index required for use as a combination beacon and telemetry transmitter, and to maintain the spectrum within the 90 kHz range required to ensure reception in the STADAN 100 kHz receiver bandwidth. The transmitter provides a minimum of 600 milliwatts to a 50-ohm load under operational conditions, and requires only 1.1 watts of power at 19 vdc.

Pre-Modulation Filter

Although the pre-modulation filter is a separate physical unit, it is designed to match the OSO transmitter. The filtering characteristics meet the IRIG PCM standards. The filter is usable at the OSO cutoff frequency of 16 kHz; however, little difficulty is expected in tuning the filter to the more optimum 12 kHz cutoff for the UV-MW satellite. The filter is an active design to avoid weight and size. It requires 0.3 watt at 19 vdc.

Command Receiver

The command receiver used on the OSO is the AVCO AED-301A. This receiver is small, light, and requires only 190 milliwatts of standby dc power, increasing to 400 milliwatts during interrogation. It has a proven history of operation with the STADAN 148 MHz tone command systems. Also, compatibility with the telemetry transmitter and diplexer has been demonstrated. The input is 50 ohms and the sensitivity is 1.5 microvolts. The rated dynamic range is to 10,000 microvolts, and successful operation with the STADAN system well into saturation has been demonstrated. The basic design, a single conversion miniaturized unit tunable over a 100 to 150 MHz range, was developed under a NASA contract for use with STADAN; 50 milliwatts of audio are provided as well as an IF output.

Command Decoder

The AVCO AED-403A command decoder is designed to match the receiver. Operation has been proven with the STADAN time command system on a number of satellites. Compatibility with the RF components has been demonstrated with the OSO. The decoder accepts the STADAN digital time signals from the receiver, identifies the access code associated with that specific decoder, accepts the specific digital command, and provides up to 200 milliamps to the command output identified. Seventy command outputs are available. The unit requires only 4.8 milliwatts in standby, with momentary power up to 6.25 watts for the 30 to 35 milliseconds during strobe of the register while commands are being received. The UV-MW satellite command list is given in Table 34.

Conclusion

The TT&C system is compatible with existing STADAN facilities and provides a straightforward solution to UV-MW satellite needs. The system provides data only in "real time" and only when the satellite is within a station field of view.

Other approaches could provide on-board data reduction and a data store and forward technique which would enhance total mission performance somewhat. If data were required in increments of 5° longitude as well as 5° latitude, on-board storage would be required until a satellite data relay network is made available. While data relay satellite systems are under consideration, these systems are not expected to be available in the UV-MW program time frame.

Reporting to on-board data store and forward would severely tax satellite size and weight constraints. A memory system could be installed, however, Trade-off studies conducted at NR indicate that computer memory devices are preferable to tape recording and that a memory size equivalent to 32K bits would satisfy the 5° longitude-latitude criteria (with appreciable increase in cost).

Performance Specification

Sensor Registers

Input:	a. True and false precision timer outputs (logic levels 0, 2 vdc) b. 1 MHz clock pulses c. Rectangular pulses from various sensors: rise time 20 nanoseconds, pulse duration; 2 nanoseconds
Storage Control:	8 precision time registers (29 bits) Register Clocking: Coincidence between clock pulse and sensor pulse (leading edges)
Register Output:	True side of flip-flops level 0, 2 VDC
Storage Period:	Approximately 15 seconds
Power:	24 ± 2.4 vdc
Maximum Power Dissipation:	1.9 watts
Volume:	64 cubic inches, maximum (4" x 4" x 4")
Weight:	16 ounces, maximum
Components:	Space proven integrated circuits

Timer

Input: 1 MHz crystal oscillator

Output: Precision time:

a. True and false outputs from microsecond, tens of microseconds, milliseconds, tens of milliseconds, hundreds of milliseconds, seconds and tens of seconds scales

b. Scaler format: BCD

c. Output levels: 0, 2 vdc

Coarse time: True outputs only from tens of milliseconds, milliseconds, hundreds of milliseconds, seconds, tens of seconds, minutes, tens of minutes, hours

Maximum count time: 2 hours

Reset: External command or 2 hours, automatic

Power: 24 vdc $\pm$ 2.4 vdc

Power description: 0.6 watts, maximum

Size: 12 cubic inches, maximum

Weight: 16 ounces, maximum

Components: space proven integrated circuits

Data Conditioner

Temperature Bridges: $\approx$ 12 required

a. Sensor input: Low temperature equivalent resistance $\approx$1 KΩ

High temperature equivalent resistance $\approx$ 2 KΩ

b. Bridge output: 20 V at low temperature

+20V at high temperature

c. Linearity: ±1% of full scale resistance

d. Bridge adjust: Low temp or high temperature range outputs to within ±1%

Voltage dividers: 6 required

a. Input voltage: 0-24 vdc

b. Output voltage: 0-24 vdc

c. Accuracy (full scale): ±1%

Current Amplifier: 6 required

a. Input voltage: 0-10 millivolts or 0-100 millivolts

b. Input impedance: ≥0.5 meg ohms

c. Output voltage: 0-2.0 vdc

d. Accuracy: ±1%

e. Size: 0.5 x 4.0 x 4.0 inches, maximum

f. Weight: 8 ounces, maximum

g. Input voltage: 24 vdc ± .24 vdc

h. Power distribution: 100 milliwatts, maximum

PCM Encoder

Input Signal Range: 0 to 2 vdc

Input Analog Channels: 32 miltiplexed

32 sub-multiplexed

Channel Sampling Rate: .33 milliseconds/channel

Analog to Digital Conversion: 8 bits ± 1 bit accuracy

Synchronization: 24 bit barker, frame and subframe

Subframe Identification: 5 bits (part of synchronization)

Digital Inputs:	9 each 30 bit words (parallel)
Discretes:	20 bi-level signals (0, 2 vdc)
Bit Rate:	24 Kilobits/sec. maximum
Word Format:	Flexible, through channel hardwire interlacing
Word Length:	32 words equal 1 subframe
	32 subframes equal 1 frame
Volume:	33 cubic inches, maximum
Power:	24 ± 2.4 vdc
Power Dissipation:	1.7 watts, maximum
Weight:	24 ounces, maximum
Components:	Space proven hardware

Premodulation Filter, PCM Transmitter

This unit limits the bandwidth of the PCM input to the satellite transmitter in order to restrict the transmitted RF spectrum.

Input:	a. PCM wave train, IRIG standard
	b. Design goal: NRZ 24,000 bits/sec ($\approx$12 kHz)
	c. Maximum: Manchester, 14,400 bits/sec ($\approx$16 kHz)
Output:	a. IRIG premodulation filter characteristics
	b. Matched to the transmitter-beacon and telemetry
Power Requirements:	0.3 watts at +19 to + 24 vdc
Physical Configuration:	a. Size: $\leq$1" x 4-1/4" x 3-1/2" exclusive of connection; or equivalent volume
	b. Weight: $\leq$1/2 pound

Qualification Status: Basic design qualified and successfully flown on satellite operating with the NASA STADAN ground stations

The BBRC unit has successfully flown in OSO satellites and fully complies with all requirements of this specification.

Transmitter Beacon and Telemetry

This unit transmits an RF signal phase modulated by the satellite PCM wave train, serving as a telemetry link and as a tracking beacon. It shares the satellite antenna with the command receiver through a diplexer. The telemetry and tracking will be compatible with NASA STADAN.

Output:	a.	Power: 700m watts nominal; 600 mw min.
	b.	Impedance: The transmitter will perform operating into a 50 ohm load with a VSWR $\leq 1.3:1$
Frequency Stability:	a.	$\pm$ 0.0037% under all operating conditions
Modulation:	a.	Type: Phase; 0 to 1.5 radius min.
	b.	Response: 100 Hz to 15 kHz nominal
Operating Frequency:	a.	Fixed: factory tuned to any frequency which may be required from 136 to 137 MHz
RF Bandwidth:	a.	90 kHz min.
Power Requirements:	a.	≤ 1.1 watts at min. output; +19 to 24 vdc
Physical Configuration:	a.	Size: 3-1/4" x 3-1/4" x 1-3/4" exclusive of connectors; or equivalent volume
	b.	Weight: 1.1 pounds nominal
Qualification Status:	a.	Basic design qualified and flown in satellite operating with the NASA STADAN ground system

The BBRC transmitter has successfully flown on the OSO satellite and fully complies with all requirements of this specification.

Diplexer Telemetry and Command

This diplexer provides the isolation and impedance matching required to allow operation of the telemetry and beacon transmitter and the command receiver from the single satellite antenna. The device is passive with no DC power required.

Antenna Port:	Matches 50 ohm impedance antenna with VSWR ≤1.3:1 from 136 MHz to 149 MHz.
Transmitter Port:	50 ohm nominal impedance to transmitter operating on any frequency from 136 MHz to 137 MHz
Receiver Port:	50 ohm nominal impedance to receiver operating on any frequency from 146 MHz to 149 MHz
Isolation:	≥70 db from transmitter to receiver
Power Handling Capability:	≥1.0 watt RF from transmitters over all operating conditions
Loss:	Transmit: Nominal 0.5 db; 0.7 db max. Rescue: ≤ 1.5 db
Physical Configuration:	Size: ≤ 1 x 1-1/2" x 5" exclusive of connectors, or equivalent volume Weight: ≤ 1/3 pound
Qualification Status:	Basic design qualified and successfully flown on satellite operating with NASA STADAN ground stations

The BBRC diplexer has successfully flown on OSO satellites and meets or exceeds all requirements of this specification.

Command Receiver

This unit shows the satellite antenna with the telemetry and beacon transmitter through a diplexer. It receives VHF PCM time commands from the NASA STADAN and provides the tones or an audio input to the command decoder.

Frequency:	100 MHz to 150MHz - Factory tuned to specific frequency within this range.
Input Impedance:	50 ohms
6 db Bandwidth:	35 kHz min.
60 db Bandwidth:	110 kHz max.
Sensitivity:	1.5μ volts; 10 db S/N
Dynamic Range:	1.5μ volts to 10,000 μ volts
Overload:	100,000 μ volts
Image Rejection:	80 db
Spurious Response Rejection:	70 db
Local Oscillator Stability:	$\pm$4 kHz
Audio Response:	$\pm$2 db; 1.0 to 7 kHz
Output Signal:	50 MW nominal, 500 ohms
Power Required:	Standby: 0.180 watts + 19 to + 24 vdc Interrogation: 0.400 watts
Physical Characteristics:	Size: $\leq$ 3-1/2" x 5" x 1-1/8" exclusive of connectors, or equivalent volume Weight: $\leq$ 1-1/4 pounds
Qualification Status:	Qualified and successfully flown on satellite operating with the NASA STADAN command system

The AVCO AED-301A receiver has flown on the OSO and other satellites and meets all requirements of this specification.

Command Decoder

This unit receives the STADAN tm commands from the command receiver, recognizes the satellite access code and drives the command distributor with individual outputs corresponding to the command received.

Signal Input:	Audio output from UV-MW satellite command receiver
Format:	NASA STADAN PCM tone commands
Access Code:	Present by factory - To be assigned
Number of Commands:	> 70
Command Outputs:	200 m a nominal drive to command loads
Power Requirements:	Standby: $\leq$ 5.0 mW; + 19 to + 24 vdc
	Strobe: $\leq$ 6-1/4 W 40 m. sec max.
Physical Characteristics:	Size: 3.625" x 3.988" x 5" exclusive of connectors, or equivalent volume
	Weight: $\leq$ 3.3 pounds
Qualification Status:	Qualified and successfully flown on satellite operating with the NASA STADAN command system

The AVCO AEO 403-A decoder has flown on a number of satellites including the OSO, and fully meets all requirements of this specification.

Communications Link Analysis

Beacon and Telemetry Transmitter Output Power

The beacon and telemetry transmitter requirements are based on the STADAN equipment available at all stations intended for use with the satellite. Table 36, Link Margins - Calculated Minimum Requirements for Telemetry, shows the calculations made to establish a minimum telemetry transmitter power.

TABLE 36

LINK MARGINS - CALCULATED MINIMUM REQUIREMENTS FOR TELEMETRY

Transmitter Power		- 3.8 dbW (416 mW)
Feed Loss		- 0.5 db
S/C Antenna Gain		- 3.0 db
Path Loss		-147.3 db
Polarization Loss		- 3.0 db
Receiving System Loss (1600°K)		- 32.0 db
Ground Antenna Gain	+ 22.0 db	
Boltz. Const.	+228.6 dbW/°K-Hz	
	+250.6 db	-189.6 db
C/N_o = +61.0		
C/N_o = Required: 10^{-6} bit error rate E/N_o		11 db
	100 kHz noise	50 db
		61 db

MASK ANGLE deg	SAT. ALTITUDE nmi	MAX RANGE nmi	MARGIN @ 416 mW db
5°	800	2198.9	0
5°	600	1841.4	1.5
5°	400	1434.0	3.7
20°	800	1568.0	2.9
20°	600	1247.3	4.9
20°	400	896.6	7.8

The signal-to-noise power density required is based on a minimum signal-to-noise of 11 db in a 100 kHz bandwidth. For a PM system with a modulation index of 1, the 11 db is required for a bit error rate of 10^{-6}. The signal-to-noise power density is 11 db plus the 50 db above 1 Hz represented by 100 kHz, or 61 db. Link calculations are for a satellite at 800 miles altitude and a ground antenna elevation angle of 5°. Margins are included for satellite antenna gain and polarization loss of 3 db each. No other circuit margin for path anomalies such as scintillation and polar cap events are considered in this calculation. A required power of 416 milliwatts is indicated for the tabulated link. The table below the calculations indicates the additional circuit margin obtained at 600 and 500 nmi orbit ranges and at ranges for the three orbit altitudes considered at a 20° elevation angle.

A qualified transmitter, the BBRC OSO unit, delivers a minimum of 600 milliwatts. The link margins at this power for 5° and 20° elevation angles are shown in Table 37 , OSO Transmitter Link Margin - Telemetry. The transmitter should provide adequate margins for other than rare short-term scintillation fades and for polar cap event absorptions during solar flares, which may be as high as 8 db at low angles to the north of the Alaskan station. The telemetry loss due to these factors is expected to be rare in occurrence and limited to a small percentage of the time over a station in the worst case.

The beacon power is essentially determined by the modulation index of the PM transmitter. Table 38 , Tracking Margin, indicates the margin available for tracking with the SATAN systems operating with its 30 Hz loop, 300 kHz bandwidth, and 10 kHz sweep range. Power in the carrier is indicated for a case where the modulation index goes to 1.5, leaving only 26% of the power in the carrier. The margin above threshold at 2199 nmi is shown to be +23.6 db with the SATAN antenna,

TABLE 37

OSO TRANSMITTER LINK MARGIN - TELEMETRY

Transmitter Power, 600 mw	- 2.2 dbW
Feed Loss	- 0.5 db
S/C Antenna Gain	- 3.0 db
Polarization Loss	- 3.0 db
Path Loss (2199 nmi.)	-147.3 db
Receiving System T (1600°K Nominal)	- 32.0 db
	-188.0
Receiving Antenna Gain	+ 22.0 db
Boltz. Const.	+228.6 dbW/°K-Hz
C/N_o	62.6 db

For S/N = 11 db in 100 kHz Bandwidth

50 db + 11 db = 61 db

Margin: Max. Range; 1.6 db

MASK ANGLE deg	SAT. ALTITUDE nmi	MAX RANGE nmi	MARGIN db	MAX. DOPPLER Hz
5°	800	2198.9	1.6	2585
5°	600	1841.4	3.1	2860
5°	400	1434.0	5.3	3060
20°	800	1568.0	4.5	2380
20°	600	1247.3	6.5	2585
20°	400	896.6	9.4	2860

TABLE 38

TRACKING MARGIN (OSO TRANSMITTER)

Total Power Transmitted, P_t		600 mw
Mod Index, Max.		1.5 rad
Power in Carrier, Min. P_t, 26% P_t =		136 mw
SATAN System		
Threshold S/N in:	300 kHz Bandwidth 300 Hz Loop 10 kHz Sweep Range	
=	21.0 db	
300 mHz =	54.8 db	
C/N_o Threshold =	+33.8 db	
P_t	- 8.7 dbW	
Feed Loss	- 0.5 db	
S/C Antenna	- 3.0 db	
Polarization Loss	- 3.0 db	
Space Loss	-147.0 db	
System Receiving		
Temperature Nominal (1600°K)	- 32.0 db	
Boltz Constant		+228.6 dbW/°K-Hz
Antenna Gain		
SATAN, +22db		+ 22.0 db
C/N_o Required	- 33.8 db	
	-228.0 db	250.6 db
	250.6 -228.0	
SATAN Margin Above Threshold =	+ 22.6 db	
Margin with Minitrack Antenna 16 db Antenna	16.6 db	

or 16.6 db even with the 16 db Minitrack antenna. The tracking margins should be adequate for all conditions other than 40 to 50 db scintillation fades which may cause momentary loss on extremely rare occasions.

Command Link Margin

The command receiver is similar to that used by the OSO satellite. The receiver represents qualified and available hardware. Table 39, Command Link Margins, indicates the link margins using this receiver. The margin above noise is calculated assuming use of the SATAN 13 db antenna, maximum range of an 800 nmi altitude satellite, the 200 W command transmitter, and 6 db losses in the satellite antenna gain and polarization. This gives a margin of +14.3 db. Assuming a 400 nmi range, higher gain from the satellite antenna, and a 5000 watt command transmitter, the receiver will still be 27.4 db below saturation. This indicates that the link will be operational with the SATAN command equipment with no special considerations for the link margins.

Operating Frequencies of TT&C Subsystems

The conventional 136 MHz beacon and telemetry frequency and 148 MHz command frequency of the STADAN system were chosen from the standpoint that qualified equipment is available and compatibility with the ground network is assured. Alternate higher frequencies available would increase the complextiy of the satellite subsystems, with no observable increase in the subsystems performance.

Modulation and Coding

The modulation and coding is chosen to be compatible with the basic STADAN network. The command receiver and decoder will be essentially the same as the OSO equipment utilizing the STADAN tone command systems. The PCM will be standard IRIG with premodulation filtering at half the bit rate, again similar to the OSO equipment. The choice of PM for the telemetry simplifies the use of

TABLE 39

COMMAND LINK MARGINS

Nominal Frequency		149 MHz	
Modulation		PCM FM AM/AM	
Receiver Sens. (10 db S/N... > 10^{-6} bit error rate)		-133.5 db	
Receiver Saturation (76.5 db Dyn. Range)		- 57.0 db	
200W Trans. ERP (13 db Ant. Gain)	+36.5 db		
Path Loss, 2199 n.mi.			-147.7 db
S/C Ant. Gain			- 3.0 db
Polariz. Loss			- 3.0 db
Diplexer & Feed Loss			
	+36.5 db		-155.7 db
Power at Receiver		-119.2 db	
Receiver Sens.		-133.5 db	
•NOISE MARGIN		+ 14.3 db	

Max. Ant. Gain	= 2.0 db	+ 5 db
Polarization Loss	≈ 2.0 db	+ 1 db
Range; from 2199 to 400 n.mi.		+14.8 db
Trans. Pwr., from 200 to 5000 watts		+14 db
Signal at Receiver	-84.4 db	+34.8 db
Saturation	-57.0 db	
•SATURATION MARGIN	27.4 db	

equipment. The choice of PM for the telemetry simplifies the use of the transmitter for a tracking beacon, and is compatible with the STADAN ground systems.

Data Reduction Requirements

The spacecraft measurement and telemetry system will provide a composite PCM wavetrain that contains the following data: a sampled waveform of the experiment sensor outputs; discrete words indicative of Earth and Sun horizon crossover times for the IR and fine Sun sensors; discrete words regarding Sun angle from the coarse Sun sensor; and sampled outputs from voltage, current, and temperature transducers for systems evaluation.

Test Data

During the test phase, it will be necessary to process telemetry output data to evaluate systems performance. A simplified example of a functional test is outlined below.

Functional Test

1. Sequentially apply electrical loads; verify voltages, currents and applicable temperatures.
2. Exercise remaining commands; sequence attitude control and coil current values.
3. Verify internal alignment of FSS and IRS.
4. Initiate timer.
5. Pulse sensors with unclaibrated source; verify sensor outputs and appropriate timer values.
6. Sequentially remove loads.

During performance of this test, the telemetry signal will be decommutated and routed to an instrumentation rack. Individual measurements will be patched to strip charts where parameter values may be read in real time. If further

processing is felt to be necessary, the telemetry signal may be recorded on magnetic tape. The NR/Space Division facility is completely equipped to accommodate such a test.

Operational Data

Following launch and orbit injection, data must be reduced to accomplish attitude initialization, sensor evaluation, attitude determination, and periodic systems evaluation.

In the discussion regarding these requirements, the following assumptions have been made:

1. The spacecraft telemetry signal will be received at a given STADAN station and either relayed real-time to the Master Control Center (MCC) facility or recorded on magnetic tape and relayed at an appropriate later time. In either case, the spacecraft telemetry signal will be recorded on magnetic tape at the MCC facility for processing.
2. All operational data processing and subsequent analysis will be accomplished at the MCC Computer facility.

Operational data may be processed in real-time and presented in the same manner as that described for funtional test evaluation, i.e., simply decommutate the wavetrain, route the decommutated signal through D/A converters, and patch to individual, scaled strip charts. It should be noted that this scheme may be readily implemented at any STADAN facility.

As discussed in the Data Handling section, it will be necessary to apply the UV and MW data to a standard least squares fit program to achieve the required accuracy. However, if it is desired to process all data by computer

for subsequent data application to analysis programs, it will be necessary to generate a digital calibration tape. In addition, programs will be required to apply calibration to the raw data.

Calibrations will be established for voltage measurements prior to installation while current, temperature, and sensor calibrations will be accomplished at the supplier facility and delivered with each transducer. All calibration curves will be included in the qualification/acceptance test documentation.

Conclusions

The data processing task can be accomplished with existing equipment and software. If more elaborate evaluation schemes are desired, i.e., automated processing and evaluation, additional software (digital calibration tape, analysis programs and data reduction programs) will be required. However, since processing times and schedules are not critical, it is recommended that the manual evaluation scheme be used.

ELECTRICAL POWER GENERATION AND DISTRIBUTION SYSTEM (EPGDS)

The Electrical Power Generation and Distribution System is presented in four separate sections:

- System Analysis and Description
- Power Profile
- Performance Specifications
- Increased Power Trade-Off Analysis

A brief summary is presented for each of these sections:

System Analysis and Description - The recommended electrical power source for the orbiting earth satellite consists of eight solar panels with a two-piece secondary storage battery supplying the electrical power for the dark periods. A major feature of the recommended EPGDS is the use of a fully automatic adaptive power duty cycle that permits a highly flexible accommodating and efficient method for meeting the power requirements of the satellite. A low-voltage solar array with boost voltage regulation and peak power tracking provisions is utilized with a nickel-cadmium battery. The unique adaptive duty cycle relaxes the interfaces between solar arrays, battery, and the power conditioning equipment. Current limiters and microminiature latch relays are used for the control and protection of satellite loads. Satellite harness assembly features hard-wiring, wrapped kapton (H-film) nickel-clad copper wire and a wrapped, spot-tie configuration.

Power Profile - The baseline electrical load requirement for the orbiting earth satellite is shown. The baseline configuration is predicated on a sensor load of 8.5 watts. Maximum power demand (19.80 watts) occurs during day data acquisition with the required power being supplied by both the solar array and battery. Night data acquisition power (16.40 watts) is supplied entirely by the battery. Note that the system cannot charge the battery during data acquisition periods. Satellite standby loads average less than 7 watts and the power required for attitude control is around 16.70 watts. Maximum power requirements for initial orbit acquisition is about 15.85 watts. Power available for battery charging is approximately 11.5 watts.

Performance Specifications - Performance specifications were presented for the major components of the EPGDS. The components are the Solar Array, Peak Power Monitor, Boost Voltage Battery Charger, Nickel-Cadmium Battery, Battery Status and Charge Monitor, and the DC-DC Converters.

Increased Power Trade-Off Analysis - An analysis was performed using an experiment sensor system which required 30 watts of power while operating and a second system requiring 50 watts of power while operating. Using the mode of data acquisition proposed the proposed satellite and power system were adequate with no revision. In the case of the 50 watt sensor system the battery would be discharged to a maximum depth of 45%. It will be fully recharged in 17 orbits of approximately $1\frac{1}{4}$ days.

System Analysis and Description

The function of the electrical power generation and distribution subsystem (EPGDS) proposed for the UV-MW Horizon Sensor Orbital Experiment Satellite is to provide controlled conditioned electrical power to sensor payloads and other satellite subsystems for a minimum of a one-year period while in a 600 nautical mile circular sun-synchronous near-polar orbit. The EPGDS uses state-of-the-art previously qualified hardware materials and processes.

A solar cell/battery combination was selected for the EPGDS based on parametric studies that a photovoltaic (solar cell) power system yields the highest watts/pound capability for the required power range (less than 30 watts), its high state of current development, and the ready availability of components. In addition, the solar cell/battery combination is the least costly and most reliable power system.

The EPGDS block diagram is presented in Figure 141. The subsystem, using a combination nickel cadmium battery/silicon solar cell power source, provides DC power to all satellite loads. The combination of solar array shunting, peak power tracking, automatic battery monitor/charge control, power conditioning, and load protection and control network provides efficient use of the solar array output for (1) maintaining the satellite DC bus voltages at the required levels (+5 VDC, +15 VDC, +24 VDC and -15 VDC), (2) automatic battery recharge when not obtaining experiment data, and (3) the control, protection and distribution of the electrical power.

Design Parameters

In the choice of design parameters such as the solar array voltage, battery type, size and voltage, load bus voltages and regulation, duration of the duty cycle periods (data acquisition and battery charging times), battery depth of discharge (DOD), etc., a great deal of system flexibility and reliability has been obtained by the selection of an adaptive system that permits the maximum use of the available power from the solar array. The selected system automatically assures the maximum data acquisition and the minimum battery charging periods for any given operating constraints placed on the EPGDS. In addition, the recommended system permits, to a large degree, the separate optimization of the solar array and power conditioning equipment design.

Solar Array Voltage

Since the EPGDS uses a boost voltage battery charger, the principal voltage constraint on the solar array is that the value by less than the lowest battery charging voltage. No equipment harm results, however, if the solar array voltage is not lower.

The selected system configuration permits the battery charger to scavenge even small amounts of power and deliver it to the battery, and also allows a simple form of peak power tracking by which power from the array is converted into the maximum amount of battery charging current. This design deletes the requirement for a prescribed number of solar cells in a series string which may be difficult to obtain in small solar panels. It also provides each of the eight solar panels with its own individual boost charger. In

this case, it is not necessary that panel voltages or sizes be the same. The solar array voltage has been selected at 24 volts maximum. Lower voltages are also available from the solar array.

Battery Voltage

The battery voltage under full load will be nominally 24 volts, fluctuating a few volts as dark and light periods are encountered. On standby loads the battery voltage may rise to about 31 volts during the charge period, and may drop to around 26 volts during the discharge period. Thus, only fair regulation is provided for the cycled loads, and poor regulation for the standby loads requiring additional voltage regulation.

Battery voltage was selected to permit the use of a low-voltage solar array and reduce the required number of battery cells for increased reliability. The voltage was also selected to allow the possible use of series type non-dissipative regulated DC to DC converters for the satellite loads and for limiting the number of load buses. To minimize converter losses, two DC-DC converters are used, allowing the converter for the cycled loads to be cycled with the loads.

Battery Cycle Life and Selection

System design permits the battery to be automatically recharged whenever satellite loads do not require all of the available power from the solar array during the sun-lit portion of each orbit. Battery damage from excessive overcharging is unlikely because of the power limitations of the solar array, the limited power requirements of the loads, and the selection of a battery capable of

accepting continuously a given amount of battery overcharging current. Standby loads may be reduced during the life of the satellite, and data acquisition requirements could also be curtailed; therefore, it is probable that the battery could receive excessive overcharges. In this case, a provision for limiting battery overcharging is included. The maximum number of charge/discharge cycles expected in one year equals the number of orbits, or about 5,000. Figure 142 represents a load profile for a representative number of orbits which is described in another section of this report.

The battery is always discharged to some extent in every dark period, more so during the "data acquisition" than the "standby" phases. A typical discharge/charge cycle consists of a low depth of discharge (maximum DOD $< 7\%$ for a 6 A-H battery) followed by a low current ($\cong 0.5$ ampere) charge of approximately twice the duration of the discharge period. A silver cadmium battery could conceivably be used, but is considered marginal for this mission. Therefore, for reliability and from flight experience data, a nickel-cadmium battery is recommended. Battery rating (6 A-H) permits growth capability to the use of higher power sensors.

Average Power Output

Since the system is adaptive, all unused electrical energy generated by the solar panels during "standby" operations will go into recharging the battery. The mission requirements can be met by the solar array size selected for this application. Presently, for the loads shown, the battery will be fully recharged in four orbits following a data acquisition phase.

Distribution Bus Voltages and Regulation

An analysis of the loads and their requirements has developed into the following schedule of conditioned buses:

Standby DC-DC converter. - Input voltage (output of boost voltage battery charger, or, for dark periods, the battery voltage) to standby DC-DC converter is 25-31 VDC and the output voltages and maximum power requirements are shown below:

2.5 watts at +5 VDC ±1%

4.7 watts at +15 VDC ±1%

9.95 watts at +24 VDC ±1%

Of the total converter output (17.15 watts), the average load at any given time will not exceed 8 watts. For a regulator efficiency of 85% and allowing 4% line loss, the input power required would be about 9.8 watts.

Cycled DC-DC converter. - Input voltage to the cycled converter is also 25-31 volts and the output power requirements are shown below:

4.4 watts at +24 VDC ±0.1%

1.0 watts at +15 VDC ±0.1%

0.6 watts at -15 VDC ±0.1%

0.5 watts at +15 VDC ±1%

0.5 watts at -15 VDC ±1%

Assuming a cycled converter efficiency of 85% and 4% line loss, maximum input power required will be around 8.6 watts. Since about 6 of the 7 watts will require ±0.1% regulation a ±0.1% DC-DC converter will be used for these loads.

System Block Diagram and Description

A brief operational explanation of the EPGDS with expanded details of the principal components follows.

EPGDS Adaptive Mode of Operation

To illustrate the system's adaptive mode of operation, refer to the simplified block diagram shown below (Figure 143).

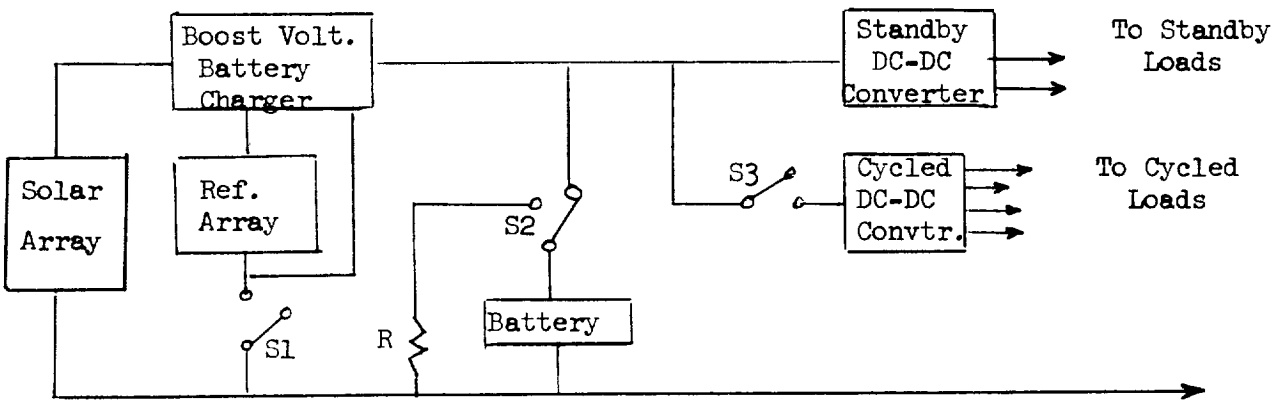

Figure 143. Simplified EPGDS Block Diagram

With S1 opened, the boost voltage battery charger is disabled and the solar array is connected (via a blocking diode in the boost voltage battery charger) to the battery by a contact of S2. This permits conventional battery float in the event of charger failure. S2 is the battery reconditioning switch used to restore the battery (by completely discharging it through resistor R and then fully recharging it) to its original capacity which may be required possibly several times a year. Switch S3 is controlled in three ways. On the assumption that the battery has been discharged to

the desired depth and S3 is in the open position, then data acquisition ceases and battery charging commences on the next light period of the orbit. When the battery reaches full charge (approximately four orbits later) as sensed by a battery status and charge monitor, the switch automatically closes to allow the data acquisition during which the battery discharges (both day and night). In the closed position, the battery supplies full power for the dark periods and part of the power during the light period to discharge the battery to a predetermined depth when the S3 automatically opens once again to repeat the duty cycle. Note that the closure of S3 is the only way of preventing battery overcharge unless resistor R is switched in by S2 by a ground command. Switch S3 can also be operated by an override command from the ground, thereby providing ground control of the data acquisition periods.

Solar Array

The detailed design of the solar array may be determined from parametric comparison of available panel areas and weights (including power conditioning). The solar array was simulated using a FORTRAN IV program similar to that cited in SD 68-760[1] for a representative orbit based upon preliminary data. The computer run provides the simulated response of output power and temperature as a function of orbit time. The computer program simulates the detailed performance of a photovoltaic solar array in a precise earth orbit. Relative

---

[1] NR Report SD 68-760, "Computer Simulation of a Photovoltaic Solar Array in Earth Orbit."

positions of the sun, the earth, and the satellite, as well as the satellite attitude, array temperature and available power, are continually calculated from a given set of input data.

Solar array design. - Eight solar array panels have a total area of about 6.5 square feet for mounting solar cells, or an average of 0.8 sq-ft of cells per panel. At 93 percent packing factor, this accommodates an average of up to 375 1x2 cm solar cells or 188 2x2 cm solar cells per panel. The maximum voltage of each solar cell degraded to 84.6 percent at the low temperature of -35°C is 0.536 volts. The boost charger must produce in excess of 25 volts while the battery is on float charge. This requires a solar array with no less than 47 solar cells in series or, allowing for a blocking diode and other losses, about 50 solar cells per series string. The number, fifty, does not divide evenly into either 188 or 375, which are average values; however, four panels have room for close to 400 1x2 cm cells (or 200 of 2x2 cm) and the others may have as few as 350. When a single boost regulator is used, four panels each have eight strings of 50 cells in series and the remaining four panels have three strings of 50 cells, for a total of up to 60 series strings in parallel. Should each panel be equipped with a boost regulator, the number of solar cells per series string is not critical and may be reduced on some panels; that is, eight series strings per panel and the number of cells per string may be the same for any one panel. In this latter configuration, four series strings per panel of 2x2 cm cells can also be utilized.

If the boost charger concept is not used, one may then either float the battery on the array or use bucking chargers. In that case, the minimum array voltage (at 31°C) must be 31 volts to charge the battery. This requires at least 68 solar cells per series string which reduces the total number of series strings to perhaps 40, or an average of five per panel. If a buck battery charger is used, the number of series strings that can be obtained is about the same, but now the possibility recurs of using peak power tracking either for the array or for each panel separately. Peak power tracking relaxes the problem of matching array voltage to the battery and, if it is done individually on each panel, the problem of matching panels to one another (in voltage) may be avoided. Each panel can then be packed as densely as possible with solar cells.

In addition to solar cells, each panel has a temperature sensor and, if peak power tracking is used, a peak power voltage sensor. The latter is a small array of miniature solar cells operating at the same temperature and illumination as the panel itself.

Boost Voltage Battery Charger

The boost-type battery charger is essentially a boost-type non-dissipative switching regulator as shown in the simplified schematic below (Figure 144).

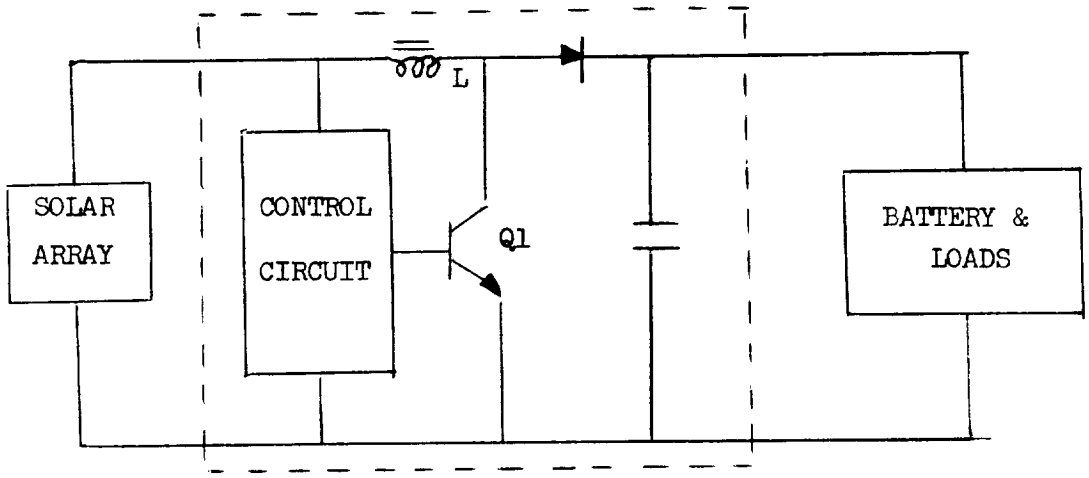

Figure 144. Simplified Boost Voltage Battery Charger Schematic

The purpose of this circuit is to obtain the maximum charging current for the battery from the solar array, whatever the voltage of the latter may be. This is the equivalent to operating at the peak power point of the array. Peak power point may be at an average voltage obtained by a fixed voltage reference device such as a zener diode or it could be the actual peak power voltage of the array as sensed by a peak power voltage sensor. In the latter case, it is possible to track the peak power voltage of the array as it changes with temperature and illumination. The peak power voltage sensor could be a small series string of solar cells, lightly loaded, installed in one or more of the solar panels.

There are three advantages of a boost over a buckling regulator: (1) current always flows through the array and no power is lost when the transistor switch is either "on" or "off"; (2) the flyback diode isolates the battery from the array during the dark periods (battery discharging); (3) should the switching transistor fail (open circuit - the usual failure mode), the array is still connected to the battery and satellite loads.

Peak Power Monitor

The peak power monitor is essentially a peak power tracking circuit consisting of a simple feedback method of switching the transistor to maintain the array voltage at optimum value. A simplified schematic of the circuit is shown below (Figure 145).

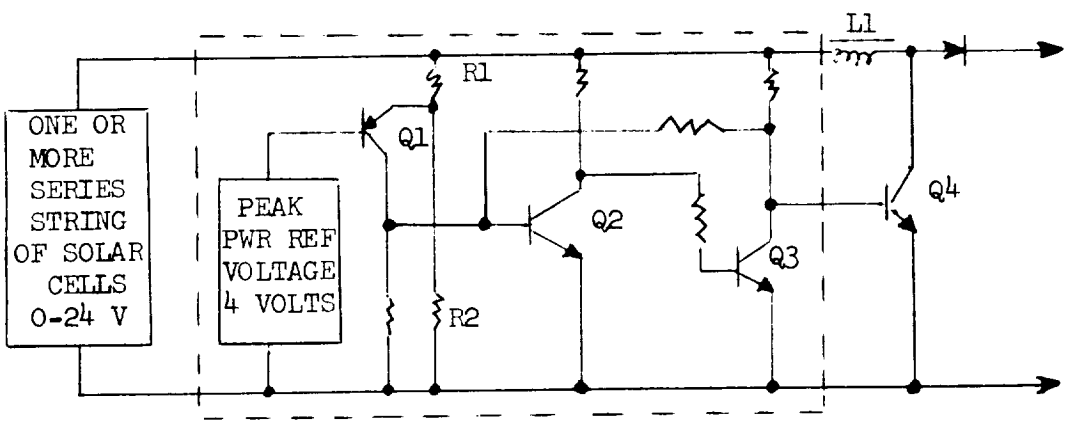

Figure 145. Peak Power Tracking Circuit

The same peak power reference voltage (generated as shown above) may be used for all the panels since this voltage is a function of temperature only and not illumination. Resistors R1 and R2 are a voltage divider to allow use of a lower and potentially more reliable reference voltage. Several reference arrays may be connected in parallel for greater reliability. Transistors Q2 and Q3 are a Schmitt trigger circuit, and Q4 is the power switching transistor. In operation, whenever the array voltage exceeds the peak power value, Q4 is switched ON and L1 (inductor) is connected across the array (or one panel of it, depending on the design). When the current in the inductor builds up to a point to drop the array voltage below the peak power value, Q4 is switched OFF. The current in L1 (and the array) is now forced to flow into the load. If the unregulated load bus voltage is high, the current decays rapidly, otherwise more slowly until the array voltage again exceeds the peak power value and the cycle is repeated. The circuit adapts both to array voltage changes due to temperature and to current changes due to illumination intensity variations, and essentially scavenges any power the solar array produces in excess of spacecraft demands.

Regulated DC-DC Converters

The candidate EPGDS produces unregulated and relatively wide-range voltage outputs from the power sources. The satellite loads require a variety of regulated voltages; therefore, line voltage regulated DC-DC converters are needed. The regulated function can best be met by a pulse modulated bucking type series regulator since the input voltage (25-31 VDC) is always higher than the output voltages (24 VDC

or less). Pulse modulation is preferred over the dissipative type of regulator whenever the ratio of input to output voltage is large. The basic block diagram for the bucking regulator is shown in Figure 146.

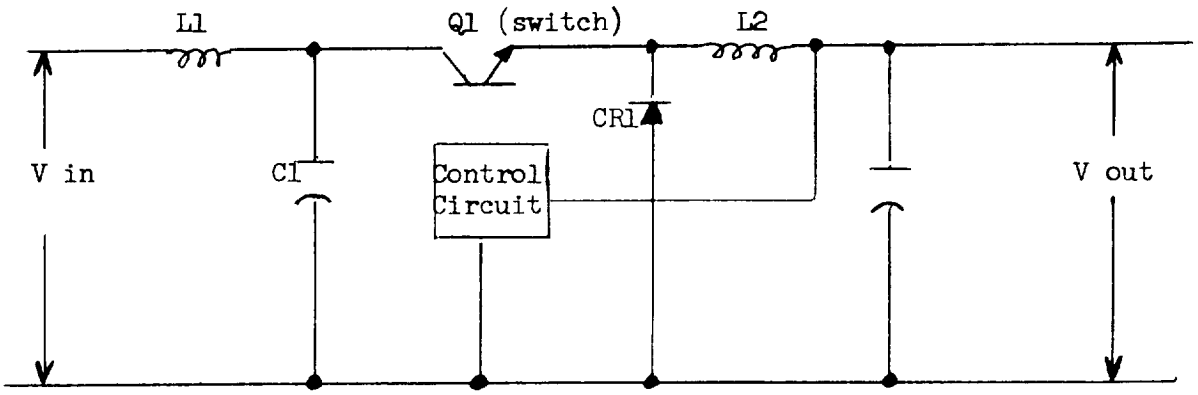

Figure 146. Pulsewidth Modulated (PWM) Bucking Regulator Block Diagram

The output voltage is related to the input voltage by the ratio of T_{ON}/T where T_{ON} is the "ON" time of the switch Q1 and T is the total drive period. Note that as the ratio of input to output voltage increases, the losses increase primarily as a result of greater switching losses. For maximum efficiency, the best switching frequency is in the range of 3 to 6 kHz.

For PWM series bucking line regulators, a voltage ratio V_{IN}/V_{OUT} of 2 is generally the accepted limits of operation. Beyond these limits, operating efficiencies tend to fall off very rapidly; therefore, for larger ratios, converters are used whenever the efficiency trade-off point is passed. A block diagram of a typical DC-DC converter is shown in Figure 147.

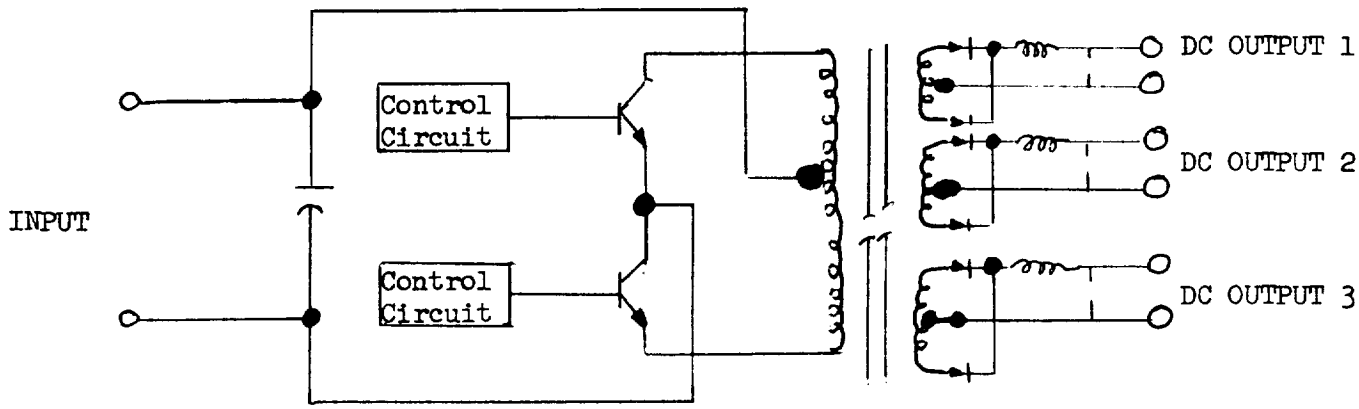

Figure 147 DC-DC Converter Block Diagram

Component Sizes and Weights

The following component dimensions and weights are tentative and subject to minor refinement as design requirements become firm.

Solar Array Panels

Eight rectangular panels will be employed to meet the satellite load requirements. Each rectangular panel is approximately 15.0 inches by 8.75 inches. The eight panels provide a maximum total usable area of approximately 6.5 square feet (only a portion of this area could be used at any one time) for supplying electrical power. Weight of the solar panels (including the peak power sensors) is estimated at eight pounds.

Battery

Battery selection is based on power and energy requirements, number of recharge cycles, depth of discharge, weight/volume comparisons, required battery life (reliability), and the degree of magnetic/nonmagnetic requirements. Figure 148 illustrates weight as a function of nominal energy capacities for the candidate batteries without consideration of operational requirements. Figure 149 compares the batteries on the basis of charging cycles versus depth of discharge and maximum available energy (lifetime configuration) versus discharge cycles. Figure 150 shows weight versus satellite loads power requirements, considering possible operational and mission constraints. Figures 151 and 152 compare candidate battery physical dimensions versus ratings. Trade-off parameters for the two battery finalists are summarized below.

Parameter	6 A-H Batt. DOD = 33-1/3%	
	Ni-Cad Batt.(20 Cells)	Sil-Cad Batt.(22 Cells)
Weight	14 pounds	10 pounds
Volume	136 in^3	120 in^3
Length	16.8 in	17.3 in
Width	2.1 in	2.1 in
Height	3.85 in	3.3 in
*Residual Magnetism	250-1500 gammas	10-23 gammas
Reliability	highest	fair
Technical Risk	low	medium

* One foot from center

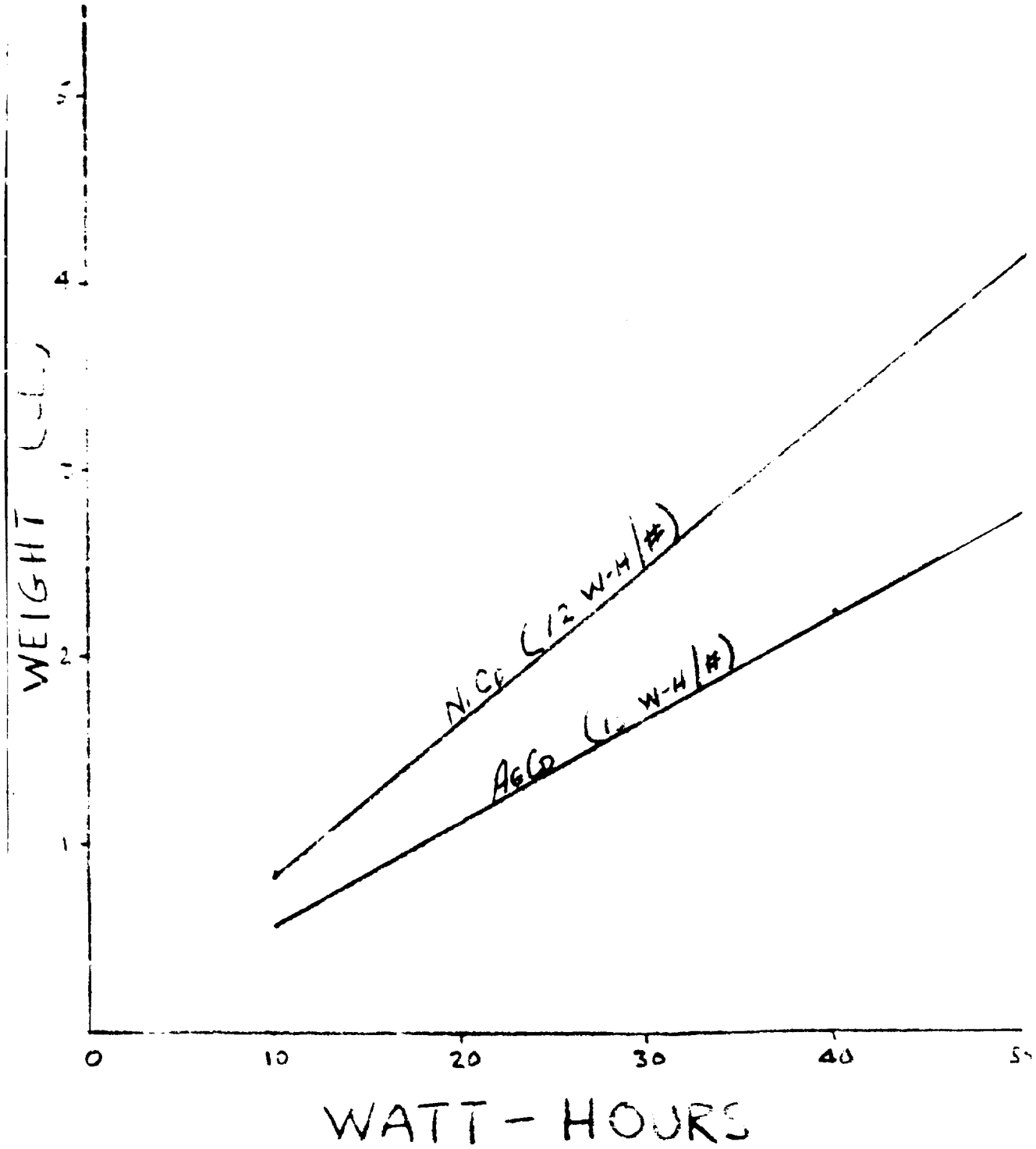

Figure 148 Comparison of Nickel-Cadmium and Silver-Cadmium Battery Weights

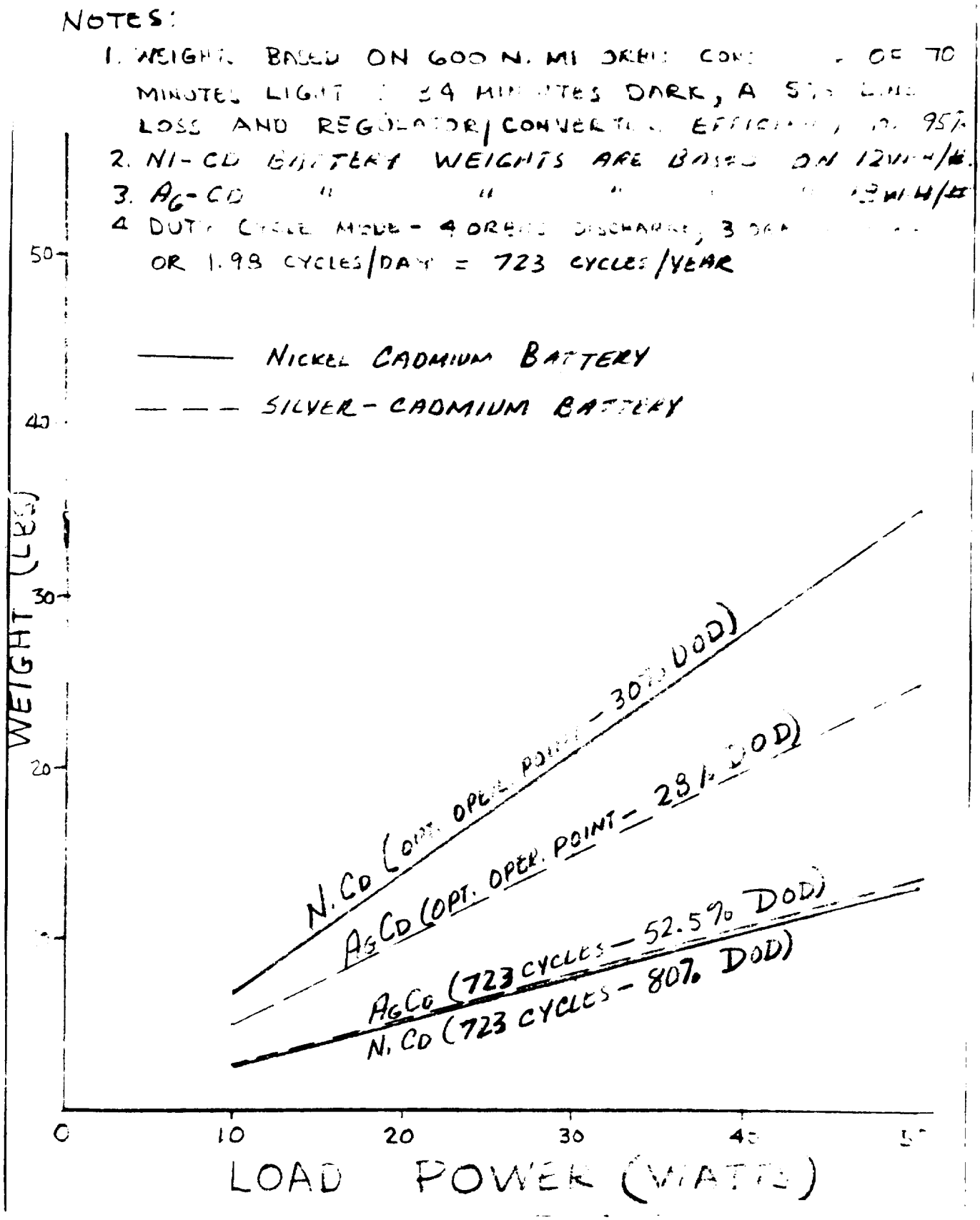

Figure 150 Battery Weights for Duty Cycle Mode

ORIGINAL PAGE IS
OF POOR QUALITY

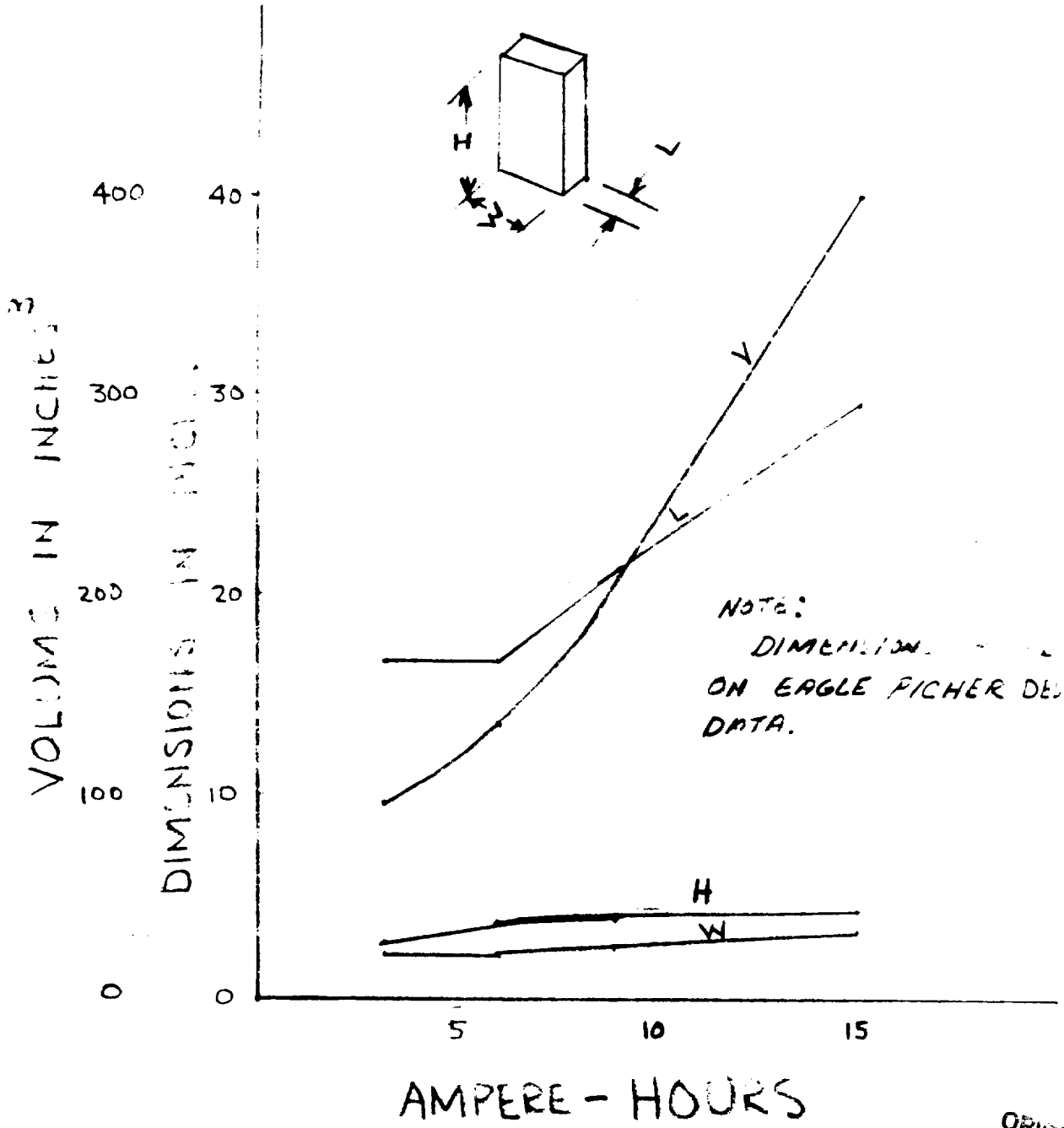

ORIGINAL PAGE IS
OF POOR QUALITY

Figure 151 Physical Dimensions for Nickel-Cadmium 20-Cell Hermetically Sealed Batteries

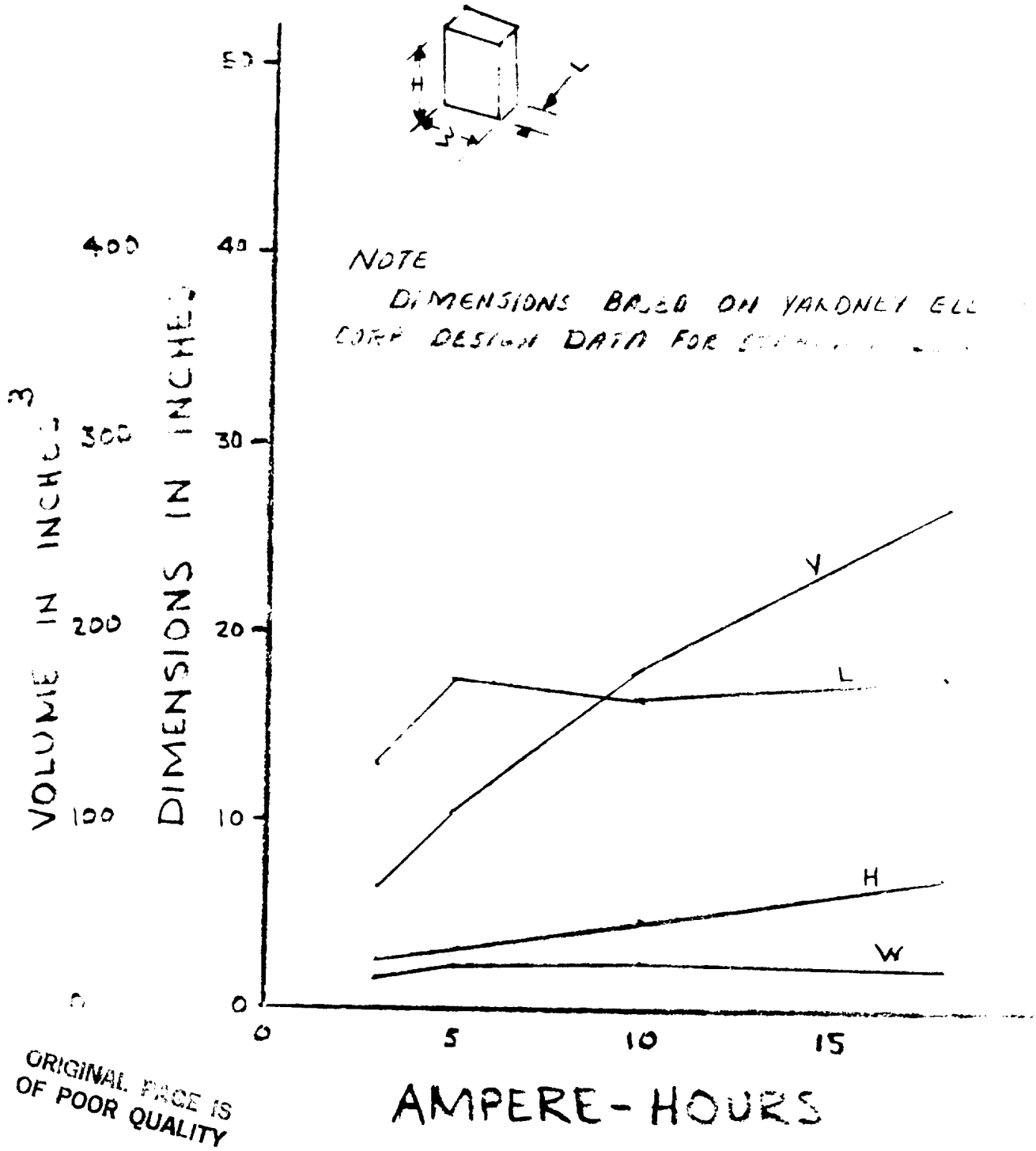

ORIGINAL PAGE IS
OF POOR QUALITY

Figure 152 Physical Dimensions for Silver-Cadmium 22-Cell Batteries

The parametric comparisons show that the use of silver-cadmium battery would provide the best advantage from a weight and volume standpoint. However, some (if not all) of the weight penalty in the use of nickel-cadmium battery can be recovered based on the capability of the battery to withstand greater depths of discharge as compared to silver-cadmium, although magnetic requirements could well decide the battery selection. A 6 A-H nickel-cadmium battery is recommended from a reliability standpoint and extensive flight data available for these batteries.

Battery Charger

The estimated dimensions and weight of the boost voltage battery charger are listed below:

Parameter	Value
Weight	1.0 pounds
Length	3.0 in
Width	2.0 in
Height	4.0 in
Volume	24 in^3

DC Converters

The EPGDS will employ two regulated DC-DC converters. The estimated dimensions and weight of each converter is shown below:

Parameter	Value
Weight	1.0 pounds
Length	3.0 in
Width	1.0 in
Height	4.0 in
Volume	12.0 in^3

Equipment Control and Protection

Two approaches, "on-the-shelf" versus "state-of-the-art", could be used in selecting hardware for equipment control and protection. Off-the-shelf hardware consists of current limiters and latching relays, whereas state-of-the-art employs solid-state switching devices. Dimensions and weights for the equipment control and protection are listed below:

Item	Weight (Oz.)	Volume (In^3)	Dimensions (In)		
			Length	Width	Height
Current Limiter	2.0	0.0625	1	0.25	0.25
Latching Relay	1.0	0.625	1	0.50	1.25
Solid-State SW Device	1.2	1.0	1	1.0	1

Since solid state switching devices will require costly test and development programs, off-the-shelf current limiters and latch relays are recommended.

Satellite Harness Assembly for EPGDS

Trade-Offs. - Fig. 153 illustrates in selection logic form the potential wire and hardness candidates evaluated for the satellite. The two wire-type finalists are extruded teflon (TFE) and wrapped kapton ("H"-film) nickel clad copper wire. The principle trade-offs are summarized below:

Parameter	Kapton	Teflon
Weight	6% lighter	6% heavier
Toughness	More rugged	Less rugged
Flammability	Self-propagating	Self-extinguishing

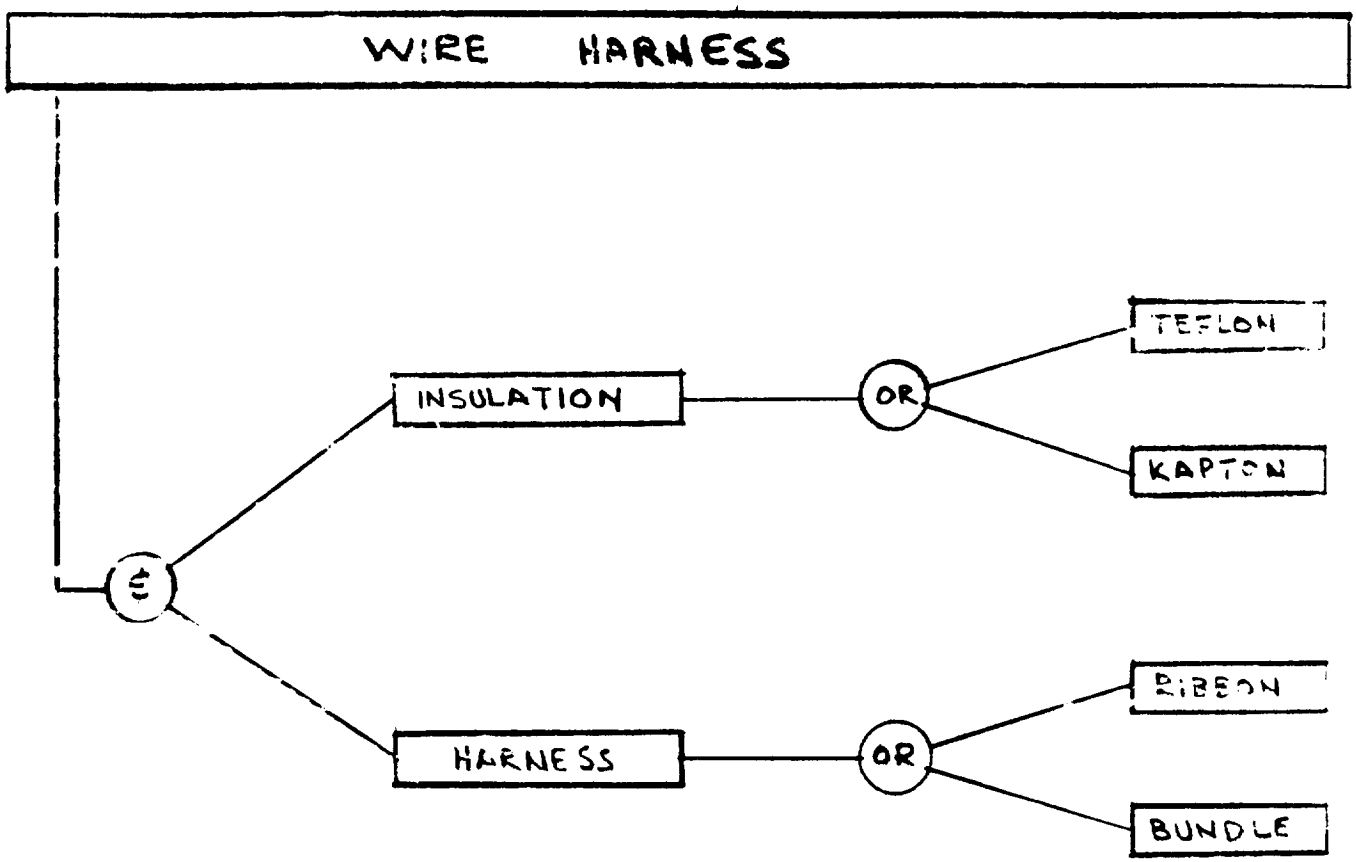

Figure 153 Wire and Harness Candidates for UV-MW Sensor Satellite

The wire harness can be fabricated and installed in many acceptable configurations. The two most attractive configurations are the wrapped, spot-tie bundle and the flat ribbon-type cable. The primary advantage of ribbon-type cable is the superior installation that is possible (cooler cable temperature). However, the cooler bundle temperature associated with flat cable is considerably reduced in high density areas, where several layers of ribbon must be stacked. The major disadvantage of the ribbon cable is in the terminations. However, the solutions to the anticipated difficulties are within the state-of-the-art and ribbon cables could be used advantageously where new equipment is being developed or repackaged.

The estimated weight for the satellite harness assembly is 3.5 pounds based on the assumption that hard-wiring will be used to the maximum extent possible.

Based upon weight and toughness considerations plus the fact that the satellite will operate in a non-oxygen atmosphere, kapton wire is recommended.

Since it is intended to maximize the use of existing equipment, spot-tied bundle construction is recommended for the satellite. This provides use of existing equipment designed to interface with circular bundle harnesses.

Power Profile

The baseline electrical load requirements for the orbiting earth satellite are shown in Table 40. The baseline configuration is predicated on a sensor load of 8.5 watts. Maximum power demand (19.80 watts) occurs during day data acquisition with the require power being supplied by both the solar array and battery. Night data acquisition power (16.40 watts) is supplied entirely by the battery. Note that the system cannot charge the battery during data acquisition periods. Satellite standby (continuous) loads average less than 7 watts and the power required for attitude control (changes) is around 16.70 watts. Maximum power requirements for initial orbit acquisition is about 15.85 watts. Power available for battery charging is approximately 11.5 watts.

A typical mission electrical load and battery charge profile is shown in Figure 142. Based on a 6 A-H battery, the maximum depth of discharge (DOD) is approximately 7%. Note that the number of charge/discharge cycles corresponds to the number of orbits or about 5,000 cycles per year. The large number of charge/discharge cycles supports the selection of a nickel-cadmium battery based on reliability factors.

Performance Specifications

Performance specifications are presented for the major subsystems of the EPGDS, the Solar Array, the Peak Power Monitor, the Boost Voltage Battery Charger, the Nickel-Cadmium Battery, the Battery Status and Charge Monitor, and the DC-DC Converters.

Solar Array

Number of Panels: 8

Solar Array Characteristics:

Average Power	-	19 watts
Rated Voltage	-	24.7 volts
Current (at rated voltage)	-	0.78 amps

Solar Cell Characteristics:

Type	-	N/P silicon, 12 mil, boron doped, solder dipped
Size	-	2 cm x 2 cm or 2 cm x 1 cm
Output Power	-	59.3 mw, average at 0.44 volts (for 2x2 cm cells)
Output Current	-	135 ma, average at 0.44 volts (for 2x2 cm cells)
Bulk Resistivity		10 ohm-cm nominal

Solar Cell Cover Slides:

Type	-	Fused silica, 6 mil
Adhesive	-	Dow Corning # XR6 3489

Radiation Protection

Outer Surface	-	Vacuum deposited magnesium fluoride anti-reflection coating to reduce energy reflection in the 0.4 to 1.2 micron wavelength region.
Inner Surface	-	Ultraviolet interference filter deposited to protect bonding adhesive from deterioration due to ultraviolet radiation.

Degradation and Manufacturer Allowances:

Series Resistance	- 3%
Standard Cell Errors	- 2%
Radiation Degradation	- 6% (maximum for 1 year)
Micrometeoroid Damage (contingency)	- 1.5%

Mechanical Characteristics:

Each panel includes series-parallel cell arrangements, blocking diodes, all cell interconnections, and provisions for hardpoint cabling connections from panel to a solar bus.

Temperature Sensor:

A thermistor or temperature sensitive resistor per panel.

Weight: < 8 pounds (8 panels)

Size: 15" x 8.75" (each panel)

Peak Power Monitor

Input Voltage: 0 to 24 VDC

Source Impedance: N/P silicon, 10 ohm/cm solar array

Power Consumption: 0.8 watt maximum

Output Characteristics:

Type	-	Continuous DC isolated analog signal
Range	-	0 (±0.5) VDC to 5 (±0.1) VDC
Linearity	-	±2% of maximum
Repeatability	-	+1% of full scale
Impedance	-	5 k-ohms maximum
Transient Response	-	Not responsive to input variations under 0.5 msec duration
Override Control	-	Inhibited in the presence of 5 VDC isolated event signal

Design: Shall be solid state, and use silicon semiconductors.

Weight: 1.0 pound (maximum)

Size: 2 x 4 x 3 inches (maximum)

Boost Voltage Battery Charger

Input:

Voltage	-	12-24 VDC
Power	-	25 watts maximum
Source Impedance	-	Supplied from silicon solar cell array/battery
Power Interruption	-	Transient output current to recover to and remain within ±10% of the steady state condition within 0.1 second following input power interruption.
Voltage	-	(Peak Power Monitor)

Output:

Current	-	0.8 amps maximum
Voltage	-	24 to 31 volts
Short Circuit	-	No damage when output short circuited for 1 hour with input of 24 VDC
Ripple Voltage	-	Not to exceed 0.8 volts peak-to-peak

Reflected Ripple:

Not to exceed 0.2 volt peak-to-peak for each watt of power rating.

Design:

Shall be solid-state and use silicon semiconductors.

Adjustments:

No external mechanical adjustment for currents or control (after final design levels are established).

Efficiency:

95% (minimum)

Weight:

1 pound maximum

Size:

4 x 3 x 2 inches

Battery

Type: Nickel-Cadmium, hermetically sealed, space qualified

Capacity: 6 ampere-hours

Voltages:

Open Circuit	- 28 volts @ 77°F (maximum)
Average delivering 1.2 amperes (full charge to 45% capacity remaining)	- 25 volts @ 77°F
Final voltage after discharging to 45% capacity remaining	- 24.2 volts @ 77°F (minimum)
Transients	- > 24.0 volts for 10 amperes 3-second load at up to 45% depth of discharge.

Operating Position and Gravity Conditions:

Rated operation in any position relative to an acceleration force/ field of up to 3G.

Sensors:

Temperature	- Thermistor or temperature sensitive resistor
Output Current	- Current sensing shunt (0-100 mv ±2% at 77°F corresponding to battery current of 0 to 10 amps)

Recharging:

Charge Rate	- < 0.5 ampere
Overcharge	- 0.5 ampere continuously without damage or degradation

Storage Life: Two years from date of manufacture

Intercell Connections:

Withstand a short circuit for minimum of 5 seconds and packaged to minimize the effect of residual and magnetic fields.

Weight: 14 pounds maximum (total - 2 units)

Size: 8.5 x 2 x 4 inches (each unit)

Battery Status and Charge Monitor

Input Power:

Source	-	Battery (operational) or battery charger (charging)
Voltage	-	24 to 28 volts (battery) and up to 31 volts (charger)
Power Consumption	-	0.8 watts maximum

Input Signals:

Battery Temperature	-	Thermistor or temperature sensitive resistor
Battery Current	-	0 to 100 mv (0 to 10 amperes battery current)

Output Signals:

Voltages	-	1) Zero (±0.05 v) to 5 volts (±0.1 v) isolated analog signal based on a zero to 6.0 ampere-hour integrated input. 2) A 5.0 volt (±0.1 v) DC isolated event signal at below TBD percent of the above analog signal. 3) A 5.0 volt (±0.1 v) DC isolated event signal at 100% of above analog signal. 4) A 5.0 volt (±0.1 v) DC isolated event signal corresponding to battery temperature of TBD °F.
Impedance	-	< 58 ohms
Linearity	-	< ±1.0%
Repeatability	-	±0.5% of full scale

Weight: < 8 ounces

Size: 2 x 2 x 1.5 inches

DC-DC Converters

Input Power:

Source	-	Battery or battery charger
Voltage	-	24 to 28 (battery) and up to 31 volts (charger)
Interruption	-	Shall recover within 50 microseconds after cessation of interruption and output voltages to be limited to 85% of their ratings during recovery over the entire input voltage range.

Output Power:

Unit #1	-	2.5 watts @ +5 VDC (±1% regulation) 4.7 watts @ +15 VDC (±1% regulation) 9.95 watts @ +24 VDC (±1% regulation)
Unit #2	-	1.5 watts @ +15 VDC (±0.1% regulation) 4.4 watts @ +24 VDC (±0.1% regulation) 1.1 watts @ -15 VDC (±0.1% regulation)

Normal Load Applications:

Unit #1	-	Continuous duty
Unit #2	-	68% operational and 32% inactive (continuous repetitive cycles)

Overload Capacity: 10% overload (output) for one hour

Short Circuit Capacity:

Sustain no damage after being subjected to a short circuit in the output for one hour with an input voltage of 31 VDC and an ambient temperature of plus 100°F.

Efficiency: > 85%

Design: Solid-state, using silicon semiconductors

Weight: 1.0 pound maximum (each)

Size: 4 x 3 x 1 inches (each)

Increased Power Trade-Off Analysis

An analysis was performed to determine the ability of the UV/MW Horizon Sensor Experiment Satellite to use sensors with a greater power requirement than the 8.5 watts used by the specified sensors. Sensor systems were assumed that might be typical of non solid state equipment and would use either 30 or 50 watts. A short 1.5 minute warmup period was assumed for these sensors.

The proposed mission has an operation profile with data acquisition occurring for approximately 55 minutes at night followed approximately 12 hours later by a day-light acquisition of 35 minutes. This cycle would be repeated every 7-9 days, or as desired. The orbits on which data was not acquired would be used to recharge the batteries. The power profile in this mode was described previously.

Using the same operating mode and the 30 and 50 watt sensors results in the power profile shown in Figure 154. The same solar cell area (6.5 ft^2) and battery (6 amp hour capacity) were considered as is in the proposed satellite.

Figure 154 shows that with the 30 watt sensor system, the maximum depth of discharge will be approximately 22% and the battery will be fully charged in 8 orbits. A 50 watt sensor system causes a maximum depth of discharge of approximately 45% and the battery will be fully charged in 17 orbits. The Ni-Cd battery can readily withstand the 50 discharges to this depth which will result if data is acquired every week.

INSTRUMENT ALIGNMENT ERROR ANALYSIS AND EFFECTS OF LAUNCH ON ALIGNMENT

It is very difficult to mount two or more optical devices on a spacecraft such as solar aspect sensors or space experiments which will maintain a relative boresight accuracy within 5-10 arc seconds after being subjected to the launch environment and the thermal stresses encountered during the mission. The optical components within the sensor or experiment must be located rigidly with respect to each other and must maintain a constant alignment to the experiment or sensor mounting surface. The sensor or experiment mounting surface must also maintain a constant alignment to the spacecraft mounting surface. Lastly, the spacecraft structure itself must not deflect between the locations of the sensors and/or experiments. Sensors having intrinsic accuracies in the 15 arc second range cannot be effectively utilized unless some means is established to either maintain all alignments in a rigid and constant manner over all environmental conditions or a technique is used to accurately measure the deflections caused by the launch and flight modes.

Alignment errors between sensors and within the individual optical subsystems may be divided into two categories, those induced by vibration and motion of mating surfaces and those caused by thermal changes and gradients. In order to ascertain the requirements for an in-flight alignment system, it will be useful to discuss the sources of alignment error in greater detail.

Mechanical considerations involve the physics of the interface between two objects which are fastened together mechanically (e.g., bolted structures). As the surfaces of two objects are forced against each other, contact is

initially made at the high points of surface irregularities. Since these areas are very small, high stress concentrations arise, and plastic yielding occurs until the contact areas are sufficiently large to support the applied load. If the objects are subsequently subjected to shock and vibration, local stress concentrations may cause further plastic yielding in particular areas, resulting in permanent alignment changes. Other phenomena such as creep and fatigue may contribute to the problem.

If the surfaces are of optical quality the surface irregularities will be so small that relatively large areas will be in contact. This would minimize the shock and vibration problems providing no distortions were introduced by the fasteners.

Fastening techniques incorporating removable components, e.g., bolts, introduce distortions adjacent to the fastener which largely offset the advantages of optical polishing.

These problems arise whenever two components are to be attached, such as in mirror or lens mounts, reticle mounts, or in mounting complete instruments to a base or each other.

The severity of the problem is illustrated by a few isolated tests which indicate that optical instruments designed for Aerobee rockets will typically undergo misalignments of 10 to 20 arc seconds after being subjected to the acceptance tests for sounding-rocket payloads.

Typically, some degree of burnishing is usually evident on mounting surfaces after subjecting the mounted article to shock and vibration tests. When it is realized that one arc-second alignment change represents only ten millionths of an inch change over a two-inch distance between mounting pads, and that visible burnishing may represent the removal of several tens

of microinches (one optical "fringe" is roughly 10 microinches), it is easy to visualize the reasons for the above test results and to see the difficulty in preventing alignment changes in demountable systems.

Angular misalignments can also be generated by thermal gradients. Consider a 24-inch aluminum base plate with sensors mounted on the rim. The misalignment due to thermal gradients will be:

$$\phi^{e} = \frac{12 \times 24 \times 10^{-6}}{10^{-5}} \times 1 \approx 28.7 \ \frac{\text{arc sec}}{°\text{C-inch}}$$

It is apparent from this result that while it may not be impossible to maintain the angular alignment of many elements in a sizable structure to within arc seconds it will be very difficult, requiring the use of materials such as quartz and invar which are undesirable from an economic, structural, or magnetic viewpoint. Very elaborate handling and assembly procedures must be invoked to ensure proper system performance. Furthermore, to detect and isolate a single unstable element in a complex system could be very time consuming and expensive.

One approach is to use simpler and more economical structures and mounting techniques which result in moderate alignment shifts through a space flight environment and to monitor these shifts using a small precise instrument of lower overall cost and complexity.

One possible approach with great flexibility utilizes a device developed by Exotech Inc. which consists of a pair of angular sensors fabricated within a monolithic quartz structure, or within several quartz blocks cemented together. Because of their small size and low coefficient of thermal expansion, mechanical and thermal problems are minimized; extensive tests and analysis show that the optical axes of the two sensors maintain their relative

alignment within a fraction of an arc second over a wide range of thermal and mechanical environments. These sensors may be solar sensors, autocollimators, collimated light sensors, or any combination of these with very stable axes relative to each other. Such devices could be employed in the following manner.

For this experiment, the sensor consists of a solar sensor with an integral electronic readout autocollimator in a monolithic quartz structure. Since the optical axes of the solar sensor and the autocollimator are rigidly maintained, the device can measure the angle between the solar vector and a reflective mounting surface on the UV-MW experiments to a precision independent of minor mounting errors and deflections induced by the launch environment. This concept was successfully implemented in a program for NASA Ames Research Center which is described in "A Precision Autocollimating Solar Sensor," AIAA Guidance Control and Flight Mechanics Conference, August 1969.

It is assumed that the reflective surface on the UV horizon sensor is rigidly attached to the UV and MW horizon sensors line-of-sight.

The monolithic quartz sun sensor-autocollimator will provide accurate aspect data despite alignment changes between the experiment and the solar sensor. This approach has the additional benefit of relaxing the mounting requirements of each device, and relaxing rigidity and stability of the spacecraft structure. Previous experience has indicated that the alignment error can be measured by this approach to an accuracy of 3 arc seconds.

SATELLITE STRUCTURES ANALYSIS

The satellite structures analysis is presented in four separate sections:

- Spacecraft Design
- Critical Interface Requirements between Reference Satellite and Launch Vehicle
- Mass Distribution Within The Satellite
- Balancing Requirements

A brief summary is presented for each of these sections:

Spacecraft Design - The spacecraft was configured to assure an economical and reliable satellite. The microwave and the ultraviolet horizon sensors, along with the fine sun sensor, the coarse sun sensor and the IR sensors are mounted to a common structural platform. This platform also supports the solar panels, the attitude control magnetic coils, the power packages and telemetry equipment.

Critical Interface Requirements between Reference Satellite and Launch Vehicle - This section of the study identifies the critical design interface requirements for the protective satellite canister and the launch vehicle. The canister provides for nitrogen purging of the satellite during the 30-day period of integration into the Delta second-stage engine (DSV 3L-4 T III C transtage) compartment prior to launch. Provision is made for connection of a battery charger and status monitor during this time period. Thermal and contamination protection for the satellite is also provided by the canister during second-stage motor firing. Launch loads are absorbed by the canister through the structural interface support frame of the

launch vehicle. Spacecraft separation occurs by releasing the stored energy in a spring and is commanded and monitored through the launch vehicle command and telemetry systems. The canister and hinged door covers remain with the launch vehicle after satellite ejection.

Mass Distribution Within The Satellite - A preliminary mass properties analysis was performed. The resultant spacecraft weighs 85 pounds, has a roll inertia of 1.28 slug-feet squared and roll and pitch inertias of 0.85 slug-feet squared. The center of gravity and principal axes inclinations are within differential equipment shifting and ballasting limits.

Balancing Requirements - A procedure of final spacecraft balancing has been established and is well within the capability of current analytical and mechanical equipment requirements.

Spacecraft Design

The satellite design involves the configuration, integration, and packaging alternatives to provide an assembly platform for equipment, sensors and spacecraft subsystems to meet the basic mission objectives. The design is simple and economical with maximum symmetry of structure for solar power and stabilization requirements. The spacecraft configuration chosen is an octagon with one rigid structural equipment shelf to accommodate the mounting of experiment packages and related systems.

Spacecraft Description

The spacecraft structure integrates and supports the two horizon experiments and the supporting subsystems. The structure includes the main center shelf support with the integrated tubular support which attaches to the booster, solar panel assemblies and required bracket and accessories to assemble the satellite.

The reference spacecraft structure is shown on (Fig. 155) Dwg 3026-A. It is an eight-sided cylinder with a rigid single central equipment shelf to which the UV and MW horizon sensors and all the spacecraft subsystems are attached. This mounting of all items on the single equipment shelf maximizes the moment of inertia ratio about the spin axis and insures a rigid structure to minimize vibration amplitude buildup.

The spacecraft structure has a single central octagonal equipment shelf supported at one edge by a tubular support. The solar panel structure assemblies are attached to this shelf by angles — and also by angles to each other.

The central tubular support in the lower half of the structure provides one-half the housing for the ejection spring and provides a guide for the spacecraft during ejection. The tubular support is bolted to the bottom edge of the equipment shelf and carries the primary structural loads from the equipment shelf to the booster attachment.

The structure shelf will be machined from a piece of stable, stress relieved, aluminum plate stock. The equipment shelf could also be machined from an aluminum or magnesium alloy billet to provide a rigid well dampened planar mounting surface for the sensors and subsystems. Integrally machined stiffening ribs provide minimum weight with high rigidity and mounting bosses are located for the sensor and subsystem attachment.

When assembled, the satellite consists of the central equipment shelf with eight solar panel assemblies mechanically fastened to each other as well as to the center shelf, providing a small, rigid structure to carry the loads into the booster attachment. The solar panels are required to carry only their own weight.

Each solar panel assembly consists of aluminum alloy angles to which and 0.40 thick aluminum substrate is attached. 2 x 2 CM. N/P silicon .012 thick solar cells with .012 quartz fused silicon cover glass are bonded to this surface.

Any solar panel can be readily removed from the central shelf to gain access to the internal components. This permits the central equipment shelf to be used as an assembly fixture for build-up and checkout of all equipment before assembling the solar panels around the equipment and closing it out.

Data gathering capabilities associated with the satellite configuration required that the microwave sensor and the ultra-violet horizon sensors be packaged on opposite sides of the structural plate, and to view the horizon at the same time. Since the MW sensor rotates through the horizon, it is mounted to the plate to give this mode of scanning. The UV sensor, being a line-of-sight type of optics, is mounted equal distance between the MW viewing optics on the null or vertical indication of the MW sensor.

The infrared sensors are mounted in a "vee" configuration, scanning the horizon at the same viewing direction as the UV sensor, and 90 degrees to the MW sensor scan path.

Both the fine and coarse sun sensors are mounted on the central structural plate, but with their viewing angles 180 degrees from the UV optics. Additional equipment required such as the batteries, controllers, decoders, and data conditioners were located on the support plate in the space available (as shown).

Attitude control is achieved by the utilization of the interaction of the Earth's magnetic field. To accomplish this, the satellite carries two coils, attached so the plane of the magnetic control coils (QOMAC & MBC)

PRECEDING PAGE BLANK NOT FILMED

are parallel to the spin axis. Conversely, to cause a change in direction of the spin vector, the magnetic spin coil (MASC) is mounted with its axis parallel to the moment vector.

Conclusions

The reference spacecraft structure is designed with conservative techniques to assure an economical reliable spacecraft system. The structure is rigid and designed to be lightweight, but utilizing proven state-of-the-art materials and conventional fabrication techniques. The equipment accessibility has been maximized by the approach of utilizing the equipment shelf as an assembly fixture and adding the outside structure after the equipment is installed.

Critical Interface Requirements between Reference Satellite and Launch Vehicle

The Thor/Delta second-stage engine (DSV 3L-4 T-III-C transtage) compartment shown in Figure 156 is considered, at this time, the best and most cost-effective approach to launch the UV-MW spin-stabilized satellite. The satellite is housed in a protective canister which is mounted in the engine compartment.

The canister provides the following functions:

1. Provides a container for the spacecraft during launch. The container is to consist of the canister and protective cover. The canister provides the interface with the launch vehicle. The size is compatible with spacecraft/launch vehicle interface.
2. Spacecraft and canister must be provided with venting to equalize pressure during launch.
3. Canister protective covers provide thermal protection from second-stage plume and engine compartment temperatures.

ORIGINAL PAGE
BLACK AND WHITE PHOTOGRAPH

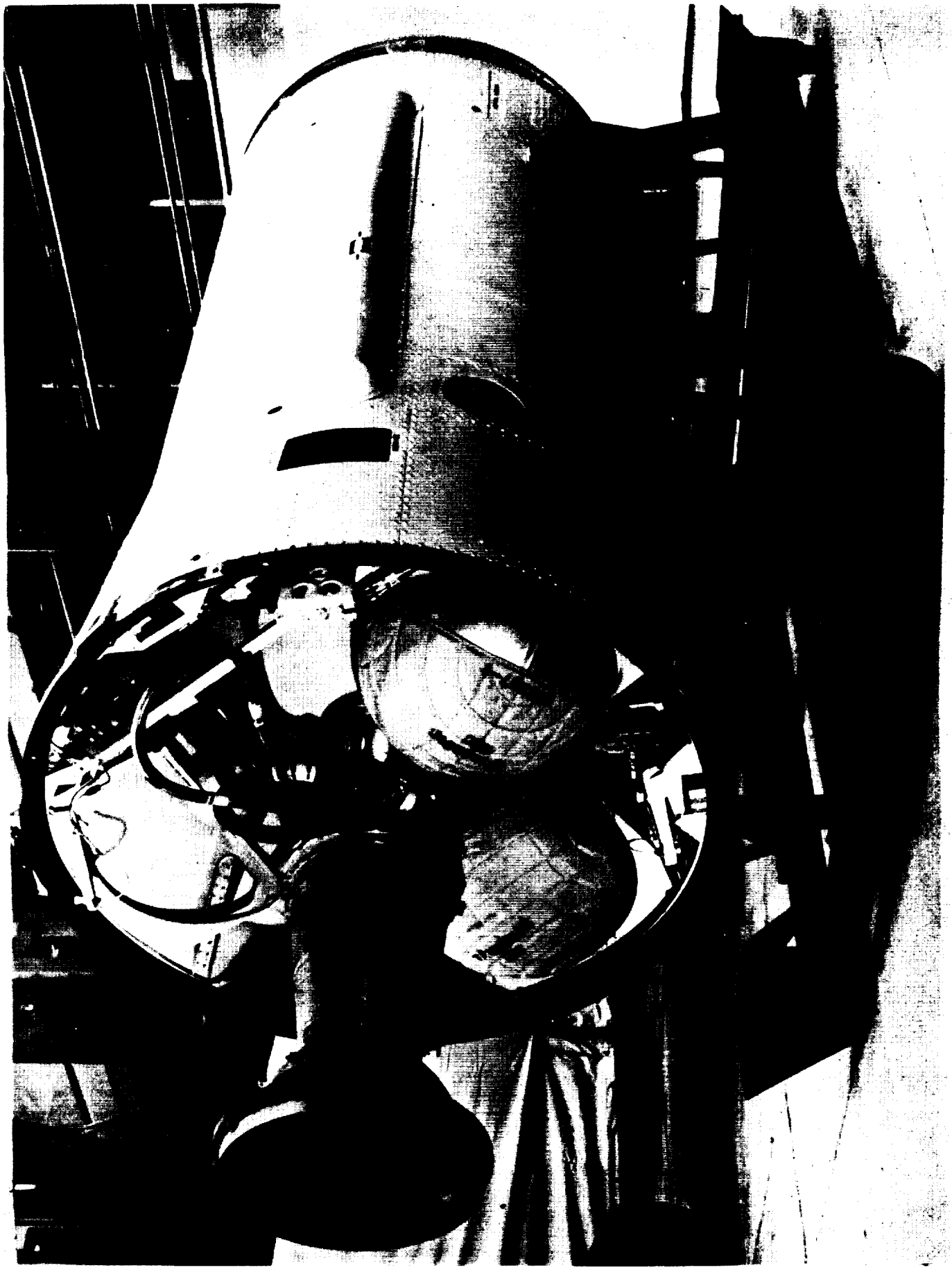

Figure 156 Thor/Delta Second-Stage Engine (DSV 3L-4
T-III-C Transtage) Compartment

4. Canister protects spacecraft from contamination of second-stage motor.
5. Canister remains with launch vehicle upon spacecraft separation.
6. Launch vehicle supplies separation signal.
7. Battery charging and monitoring through the canister.
8. Separation switch on canister - signal telemetered through launch vehicle telemetry system.
9. Redundant switches - remove spacecraft load from battery prior to launch and connect battery to spacecraft load upon ejection.
10. Dry nitrogen fitting on canister required.

Canister System

The spacecraft canister and protective covers are shown on Dwg. #3026-1(Fig. 157). The canister performs the mechanical interface with the parent launch vehicle as shown. It supports the spacecraft during launch and distributes the acceleration loads from the launch vehicle to the spacecraft. The protective cover protects the spacecraft from possible contamination from the candidate launch vehicle second-stage motor exhaust. It provides thermal protection to the spacecraft from the second-stage motor plume and engine compartment temperature.

The canister provides one-half the housing (the spacecraft control tube provides the other) for the ejection spring and supports the pin-puller separation mechanism. The canister and protective cover will remain with launch vehicle upon spacecraft separation.

The all aluminum alloy canister consists of a thin wall octagonal close-ended cylindrical compartment with ring frames and brackets carrying the loads

from the launch vehicle truss. The central tubular column provides the guide for the spacecraft for the first seven inches of travel as well as providing the housing for the ejection spring.

The protective cover consists of the flat door assemblies. The door sections are torsion spring loaded to the open position to provide clearance for the spacecraft during ejection. The doors are compression sealed at the edges when closed. Mechanical latching of the doors is accomplished by a center fitting assembly. A single pin-puller releases the spacecraft from the canister and the initial axial movement of the spacecraft during ejection releases the protective cover doors. The doors in the open position are shown in View B-B of Dwg. 3026-1.

Adjustable load take-out fittings are incorporated in the sides of the canister to preload the spacecraft along all three axes as installed within the canister, as shown in Detail C-C.

The canister is equipped with a fitting through which dry nitrogen is pumped for environmental protection during the 30-day period between satellite installation and launch.

Redundant switches are mounted on the canister to remove the spacecraft electrical load from the power sources while the spacecraft is mounted in the canister. Upon ejection of the spacecraft, closure of either switch permits the connection of the power source to this spacecraft load. After separation, or once the switches are closed, they are so mounted that they cannot be opened.

The canister design features a conventional approach to containment of the spacecraft. Only two doors are used for the protective cover and no

PRECEDING PAGE BLANK NOT FILMED

separate release and actuating mechanism are required. The initial axial movement of the spacecraft subsequent to actuation of the pin-puller unlatches the doors.

Upon receiving a command signal from the launch vehicle system, a squib is fired and the pin-puller releases the satellite from the canister. An off-the-shelf flight proven pin-puller is used.

Ejection of the spacecraft is accomplished by a single compression spring contained within the two-element telescoping tubular central column which provides primary structural support of the spacecraft to the launch canister. The spring exerts sufficient force to provide the required separation velocity. The length of the telescoping tubular members are greater in length than the extended spring to eliminate tip off of the spacecraft as it leaves the canister.

Imparting the desired rotational rate to the spacecraft is accomplished by canting the tubular central column so that when the stored energy of the compressed spring is released, the small moment imparted to the satellite will cause the initial rotation upon ejection from the canister of approximately 4 rpm. An alternate approach would be to use a rail system to guide the spacecraft out of the canister with canted fittings on the forward end of the guide rails which would rotate the spacecraft body as it clears the end of the rails.

Power is supplied by the launch vehicle through the microswitches which are either held open or closed as required by the booster telemetry system interface. The switches are wired through a connector mounted on the canister. Upon ejection of the satellite, the switches function to give a positive indication of separation from the boost vehicle at the proper time in the launch sequence.

The piggyback concept of packaging the horizon sensor equipment in the second stage engine compartment presents the possible problem areas as listed below:

1. The AGC part number 095832 (helium tank bracket) would have to be removed or modified approximately as shown

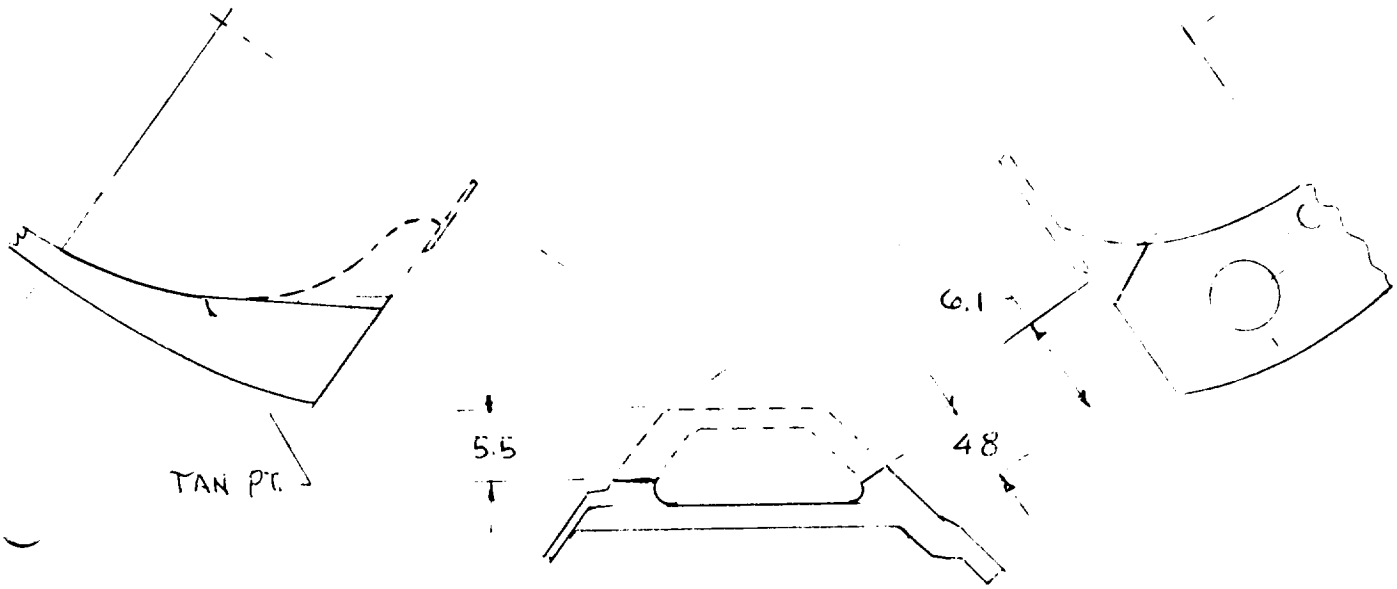

2. The truss support interfaced with the delta separation ring appears to present no restraints except for the attachment and location of the hardware in order to clear adjacent equipment.

3. Clearance problems may occur with existing plumbing lines in the engine compartment requiring rerouting to avoid interference.

4. Possible problems with attitude control jets may exist, but the canister/spacecraft installation (Dwg. No. 3026-1) appears to clear any jet plume impingement.

5. Installation of the supporting canister/satellite onto the support truss and the connection of lines, switches and connectors may present accessibility restraints.

6. Estimated weight of the support truss assembly is approximately 28 lbs., assuming thin wall steel tubing with attached brackets are used.

Conclusion

The canister configuration utilizes a simple approach to containment and release of the satellite. Upon actuation of the pin-puller, the spring in the ejection housing moves the spacecraft forward which, in turn, releases the spring-loaded protective doors of the canister allowing the spacecraft to be thrown clear of the canister and the launch vehicle.

The launch support truss, as pictured on Dwg. 3026-1, shows a configuration which attaches the canister/spacecraft assembly to the boost vehicle. The framework and its attach brackets were drawn as a support truss concept. The final configuration will have to be interfaced through appropriate NASA, Aerojet General, and the Douglas Aircraft Division offices, with the latter company supplying the actual design and modifications to the Delta transtage.

Mass Distribution Within The Satellite

An analysis of mass properties in the preliminary phase of a project is necessary to establish the feasibility of concept and illustrate the areas of the concept requiring additional analysis or definition.

This section of the report contains a summary of the results of a preliminary mass properties analysis.

Mass Properties

The mass properties analysis indicates that a satisfactory set of weight, CG, inertial data and angular axis inclinations have been found for the UV/MW satellite. The configuration is presented in Table 41. The satellite will weight about 85 pounds and have a roll inertia of about 1.3 slug-feet^2 and pitch and yaw inertias of about 0.85 slug-feet^2. The center of gravities and the two critical axes inclinations will be reduced to approximately zero by judicious ballasting.

TABLE 41

PRELIMINARY SATELLITE WEIGHT STATEMENT

SUBSYSTEM	Qty	Total Wt-Lb	Center of Gravity- Inches		
			X	Y	Z
UV Sensor	1	5.0	-1.8	-3.5	4.5
MW Sensor	1	7.5	-1.0	1.9	2.2
Diplexer	1	0.2	-0.9	3.7	2.0
Antenna	1	0.2	0	5.0	0
Nutation Dampers	2	1.2	±4.0	-1.3	±9.4
Pre-Mod. Filter	1	1.1	6.0	1.3	6.3
TLM Transmitter	1	1.3	8.5	2.6	1.8
Data Controller	1	0.5	8.2	1.5	0
Sensor Register	1	1.0	7.3	2.8	-4.1
PCM Encoder	1	1.5	4.6	2.3	-6.0
Timer	1	1.0	3.7	2.8	-7.9
CMD Receiver	1	1.3	-4.9	2.0	-7.2
CMD Distributer	1	0.5	-5.4	2.1	-6.2
CMD Decoder	1	3.3	-6.9	2.2	-4.1
IR Sensors	2	2.0	-8.0	±3.0	2.7
QOMAC/MB Coils	1	3.0	0	6.0	0

TABLE 41 CONT'D

Subsystem	Qty	Total Wt-Lb	Center of Gravity- Inches X	Y	Z
MASC Coil	1	1.5	-0.4	0	0.7
Batteries	2	14.0	±4.9	-1.8	±5.3
Latch & Limiter Assys	2	0.6	±2.2	-1.0	±3.3
DC Voltage Regulators	2	1.0	±4.6	-0.9	±1.4
Battery Charger	1	1.0	8.8	-1.5	0.7
Peak Power Monitor	1	1.0	8.2	-1.5	-2.3
Electronic Controller	1	3.8	4.1	-2.4	-3.3
Coarse Sun Sensor	1	0.5	9.7	-2.0	-4.7
CSS Electronic Register	1	2.5	6.5	-2.4	-6.4
Fine Sun Sensor	1	0.5	3.9	-2.4	-8.8
MBC Switch	1	1.0	-5.9	-2.4	4.5
Battery Status Monitor	1	1.0	0.2	-2.0	9.4
Wire Harness	1	3.5	0	0	0
Solar Panels	8	8.0	0	0	0
Ejection Socket	1	1.0	0	0	-8.2
Center Mounting Plate	1	10.0	0	0	0
Misc. Hardware	-	3.5	0	0	0
TOTALS		85.0	+0.29	-0.30	-0.43

From the available lists of equipments and spacecraft components supplied by the several disciplines and the configuration arrangement of the satellite (Drawing 3026-2), an analytical mass properties evaluation was performed. Table 41 presents a list of the spacecraft components and their location in the spacecraft. Table 42 presents a summary of the mass properties of the spacecraft and a diagram illustrating the axes nomenclature used in the analysis.

The computed center of gravity of the spacecraft is located about 0.6 inch from the geometric center in the +X, -Y, -Z sector. The moment of inertia in the spin axis is about 50 percent greater than that in the pitch or yaw planes. The principal axis inclinations parallel to the geometric roll axis are small, while the axis perpendicular is large. However, the inclination is not critical to spacecraft stability. This evaluation would indicate that a proper arrangement of components has been found and that final correction to zero out the CG's and angular inclinations can be performed with a small amount of rearrangement and ballasting. This indication is based on the assumption that the delivered components and installation estimates will not vary considerably from those of the analysis. Strict attention to component weight, CG and individual inertias and their effect on the gross spacecraft must be practiced in order to assure final spacecraft stability.

Balancing Requirements

One of the prime requirements in the concept of attitude determination for the satellite is the limitation of the spacecraft "wobble" due to mass unbalance and misalignment of the spacecraft principal axes of inertia with the geometric axes, to which the reference sensors are aligned. This section of the report will summarize the expected accuracy of alignment and the method of testing.

TABLE 42

PRELIMINARY SATELLITE MASS PROPERTIES

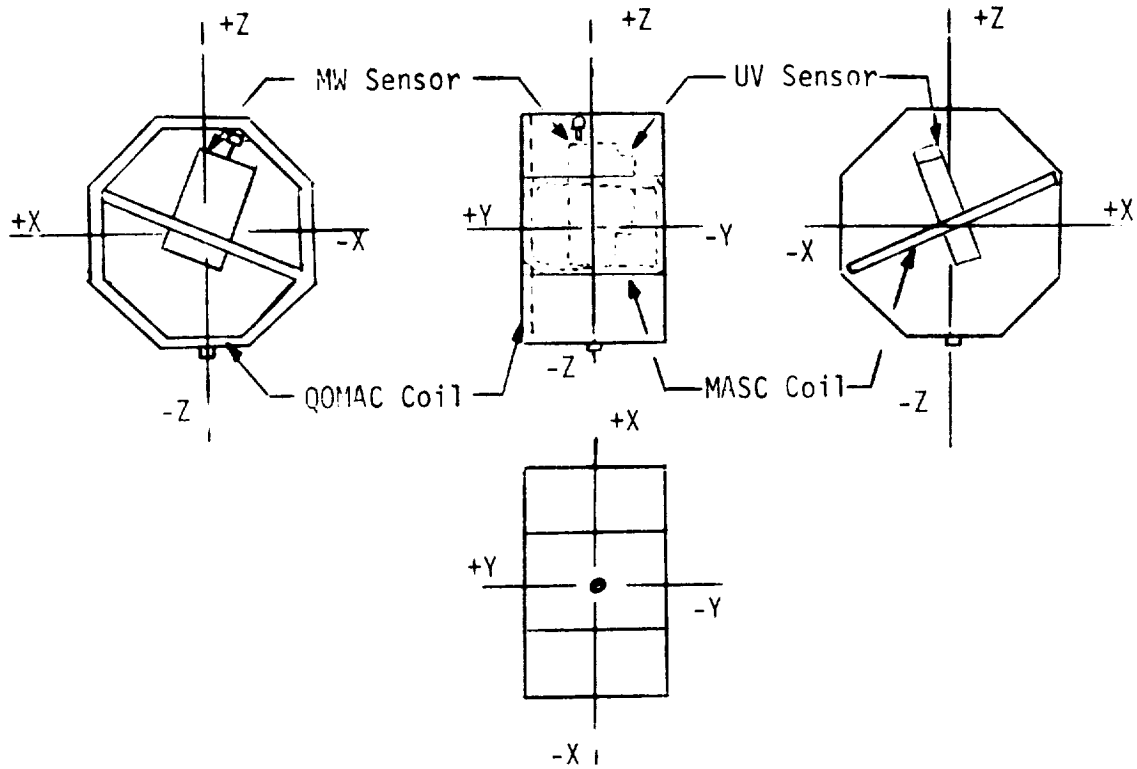

Total S/C Weight	- W	85.0 Pounds
Center of Gravity	- $\bar{X}$	+0.29 Inch
	$\bar{Y}$	-0.43 Inch
	$\bar{Z}$	-0.30 Inch
Moment of Inertia	- I_{xx}	0.870 Slug Ft^2
	I_{yy}	1.279 Slug Ft^2
	I_{zz}	0.819 Slug Ft^2
Product of Inertia	- I_{xz}	0.159 Slug Ft^2
	I_{xy}	-0.064 Slug Ft^2
	I_{yz}	-0.041 Slug Ft^2
Principal Axes	- xz	-36.3°
	xy	-4.5°
	yz	-2.5°

Analysis

Misalignment of the principal axis of inertia to the geometric axis (spin axis) results in a periodic wobble of any sensor line-of-sight (LOS). The relation between the mass unbalance leading to principal axis misalignment is described here.

Define the $\hat{Y}$-axis as the geometric spin axis. The $\hat{X}$ and $\hat{Z}$ axes are the transverse axes through the rotor center of mass (CM). These axes will be nominally equal and also define the $\hat{X}$ axis as the transverse axis in the plane of the mass unbalance. The $\hat{X}'$, $\hat{Y}'$, $\hat{Z}'$ axes are the principal axes of the rotor displaced from the $\hat{X}$, $\hat{Y}$, $\hat{Z}$ set by an angle ϵ about the $\hat{Z}$ axis. Since all cross products of inertia are zero in the primed set, the angle ϵ is constrained as

$$\tan 2\epsilon = \frac{2 I_{xy}}{I_x - I_y} \tag{1}$$

and for small ϵ

$$\epsilon = \frac{I_{xy}}{I_x - I_y} \tag{2}$$

where ϵ = the angular misalignment of the principal axis of inertia to its geometric axis, and I_{xy} = rotor cross product of inertia in the $\hat{X}$, $\hat{Y}$, $\hat{Z}$ set. Thus the angular misalignment of the rotor can be related to the inertia properties of the rotor. With I_x and I_y known, I_{xy} may be calculated based on the accuracy of the balance capability of the dynamic balance machine and expected mass shifts during boost.

Balancing Procedure

Without going into complete detail, several factors are critical in the spacecraft balancing procedure.

1. The alignment of the spacecraft geometric axis with respect to the balance machine axis is critical. Typically, optical collimation procedures are used and permit alignment to within 10 arc sec.
2. The second critical factor is the residual unbalance remaining after dynamic balancing. This unbalance is principally due to instrumentation noise. The resulting I_{xy} due to machine resolution limits is given by

$$I_{xy} = 2\ Td \qquad (3)$$

Where d = the distance between the plane of the spacecraft CM and the planes containing the balance masses, and T = residual unbalance of the machine.

The factor of 2 is a worst case assumption that the two plane unbalances are directly opposite.

Estimation of Misalignment

From the attitude determination error budget, it has been estimated that the maximum allowable misalignment (ϵ) is 0.5 degree. From Equations (2) and (3) then, we find

$$T = \pm \frac{\epsilon\ (I_x - I_y)}{2d} \qquad (4)$$

From the preliminary mass properties analysis of the UV/MW satellite, the expected values of I_x and I_y are 0.85 and 1.28 slug-feet^2, respectively.

Also $d \simeq 0.5$ feet

For $\epsilon \leq 0.5$ deg.

The maximum allowable mass unbalance, T, is

$$T = \pm \frac{0.5\ (0.85 - 12.8)}{(57.3)\ 2\ (0.5)} = 37.6 \times 10^{-3} \text{ slug ft}$$

or $T \simeq 27.5$ oz-in.

This indicates that the machine tolerance plus expected mass shifts must be less than 27.5 oz-in. Discussions with various balancing machine manufacturers and testing facilities indicate that if the spacecraft is balanced at 200 rpm, the machine tolerance can be held to less than 1.0 oz-in (Schenck Trebel Corp., Farmingdale, N.Y.). The spacecraft will be balanced before and after vibration and shock testing to maintain the mass unbalance to less that 25 oz-in.

Thermal Control Analysis and Design Requirements

The object of the thermal control design is to insure a long-life reliability of all components by maintaining their temperatures within specified limits.

The approach taken in the study was to demonstrate the feasibility of a thermal design which is to have the following characteristics:

(1) It is to be a passive system.

(2) It must employ state-of-the-art techniques having a long life with high reliability.

(3) It is to have a minimum impact on the other satellite subsystems.

Thermal Requirements

The thermal requirements of the satellite electronics and payload are given in Table 43.

TABLE 43

EQUIPMENT TEMPERATURE LIMITS

COMPONENT	TEMPERATURE LIMITS °F	
	Non-Operating (°F)	Operating (°F)
Satellite Electronics	40 to 120	40 to 120
Battery (Nickel-Cadmium)	30 to 120	40 to 120
UV Sensor	30 to 95	50 to 95
MW Sensor	32 to 120	32 to 120
IR Sensor	32 to 120	32 to 120
Coarse Sun Sensor	-60 to 160	-40 to 120
Fine Sun Sensor	-60 to 160	-40 to 120

In addition, thermal gradients must not result in misalignment of the experiments. These requirements are to be satisfied for the following flight conditions.

(1) The satellite is spin-stabilized and must operate in a near-polar sun synchronous orbit. The spin axis is maintained normal to the orbit plane with a nominal spin rate of 4 rpm. The nominal orbit is 600 n mi circular with an inclination of 100 degrees. The right ascension of the ascending node is equal to 220 degrees.

(2) The satellite initially can be oriented with the spin axis in the plane of the orbit. The most severe case for thermal control is when the spin axis is parallel to the sun vector. This orientation can exist for up to two hours. Within 14 orbits, the spacecraft will be positioned into its operating orientation.

Thermal Design and Performance

Thermal Design

The thermal control system was designed to provide a nearly isothermal satellite structure. This is necessary so that the wide fluctuations in skin (solar panel) temperature do not:

(1) Create expansion problems and thermal leakage paths from the structure.

(2) Set up fluctuating stresses which can lead to metal fatigue and thermal ratcheting.

(3) Cause misalignment of the experiments.

The essential feature of the design is the adoption of a completely passive system in which the internal heat dissipated by the equipment is transferred to the outer skins of the spacecraft (solar panels) by conduction through the aluminum mounting platform. The two ends of the satellite are thermally isolated from the equipment by thermal blankets.

All the systems equipment and the experiments are mounted on a thick aluminum platform which distributes the internal heat to non-operating or non-dissipating equipment and structures by conduction. Good thermal contact between the platform and equipment is provided by means (for example) of silicone rubber compound (RTV40 with 25% alumina). In addition, the internal radiation is maximized by painting the equipment, mounting platform and internal structure black. The equipment is arranged on the platform, as possible, to provide uniform heat dissipation. However, the present thermal design is capable of maintaining thermal gradients at an acceptable level without this provision.

The mounting platform is thermally isolated from the outer skins of the satellite by rigid gold-coated fiberglass mounts. The inner surface of these skins are polished to minimize thermal radiation between the skins (which fluctuate widely in temperature) and the equipment. Rigid thermal shields can be used to eliminate cold spots within the compartment if required. The requirements for these shields will be determined by detailed thermal analyses and testing.

The internal heat dissipated by the equipment is conducted through the platform to the skins where it is emitted to space. The mean temperature of the equipment is maintained at the desired level by designing the platform mounts to have the desired values of thermal conductance.

The temperature variations of the equipment caused by the fluctuations in solar flux absorbed by the skins will be small because of the relatively large thermal inertia of the equipment.

The two ends of the satellite are closed with thermal blankets which consist of layers of mylar coated on both sides with vacuum deposited

aluminum separated by nylon netting. The outer layers of the blankets are made of aluminized FEP teflon (one side only). The purpose of the teflon is twofold. First, it increases the heat capacity of the outer portion of the blanket, which may experience high temperatures during ascent as a result of the heat transfer from the booster. Second, the teflon has a low α/ϵ which is necessary because significant sunlight may impinge on the blanket during the first two orbits. The blanket effectiveness is not only reduced at high temperatures, but an aluminized surface exposed to direct sunlight will run hot and may damage the insulation. All edges of the blanket are bound with aluminized glass tape and a strip of velco is sewn to the perimeter to close the blanket. The blanket is attached to the satellite by metal strips which are attached to the blanket.

The antenna, which extends twenty inches outside the satellite, is thermally isolated from the equipment by fiberglass struts and by means of an optical reflector (polished surface).

The QOMAC and MBC coils are thermally decoupled from the temperature fluctuating skins in the same manner as the equipment mounting - by suitable mounts.

Thermal Performance

The performance of the thermal control design was determined for the following design conditions:

(1) The satellite is in a near-polar, sun synchronous orbit (reference orbit) with the spin axis normal to the orbit plane. The internal heat dissipation is 5 watts.

(2) The transient condition which exists with the satellite in the reference orbit, when the internal heat dissipation is

suddenly increased to its maximum value of 20 watts. This represents the hottest environment to be experienced by the equipment.

(3) The transient condition between launch and attitude acquisition of the spacecraft. It is assumed that immediately after launch, the spin axis is in the plane of the orbit with the spin axis pointing at the sun. The vehicle can remain in this attitude for one complete orbit. This is the coldest enviornment to be experienced by the equipment.

The thermal environment of the satellite while it is in an earth orbit consists of heat input from the external sources: direct solar heating, indirect solar heating (albedo) and infrared radiation emitted by the earth. The amount of this thermal energy incident on the solar panels for the reference orbit is given in Figure 158. A computer program[1] was used to obtain these values.

The temperatures of the equipment and the solar panels are given in Figure 159 for the reference orbit when the internal power is 5 watts. These results were calculated by a thermal analyzer computer program[2] for a 10-node system. Although the skin temperature fluctuates between -62 and 102°F, the equipment temperature remains stable between 70 and 90°F.

The temperature-time history of the equipment after the internal power has been increased to 20 watts is shown in Figure 160. After one orbit (the time during which the maximum electrical load is on), the average equipment temperature has increased to 95°F.

1. Space Vehicle Thermal Environment Program, SD 69-507, July 1969
2. General Thermal Analyzer Program, No. AF0014, SD 68-760, December, 1968

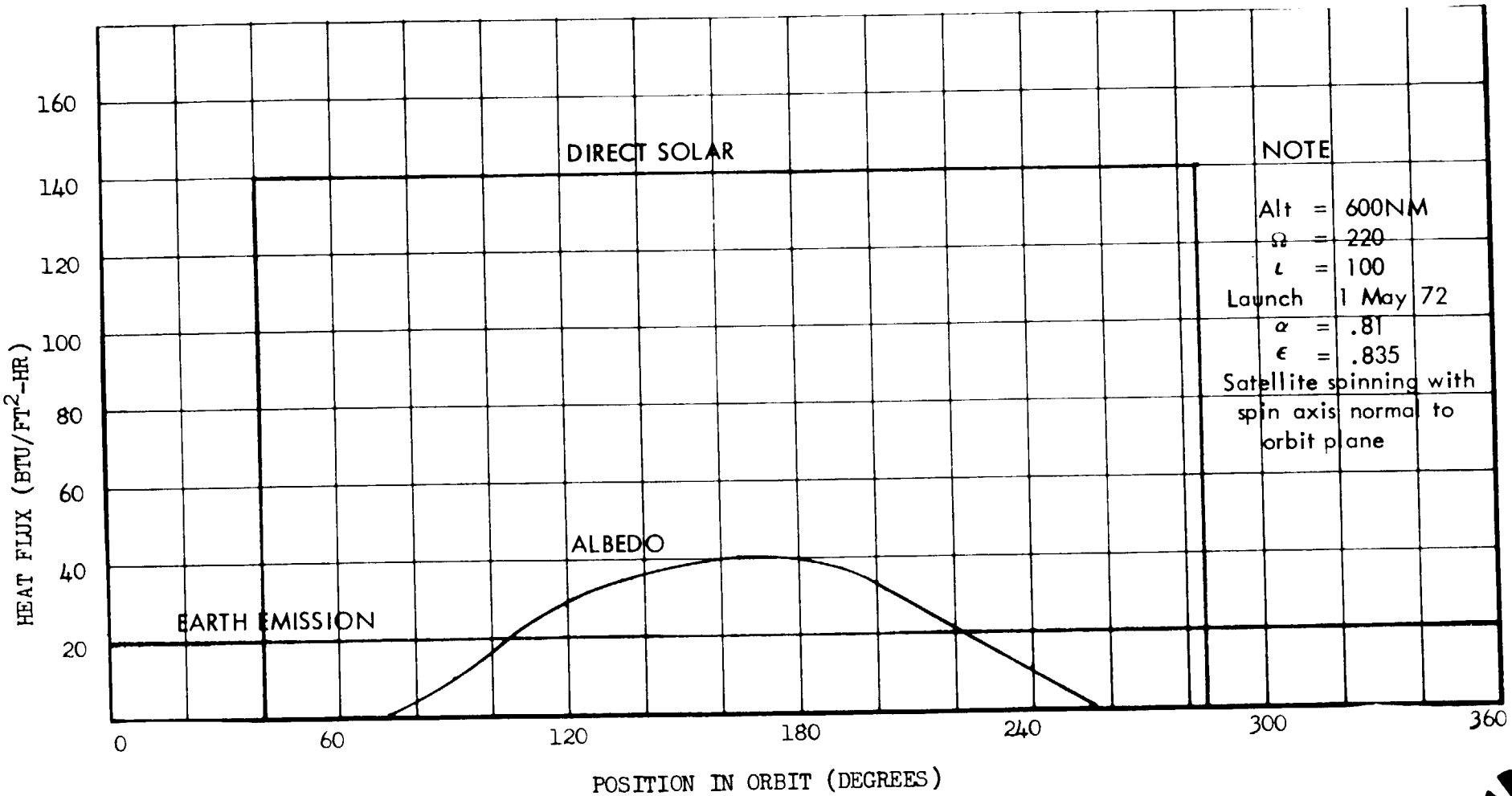

Figure 158. Incident Heat Flux on Solar Panels

Space Division
North American Rockwell

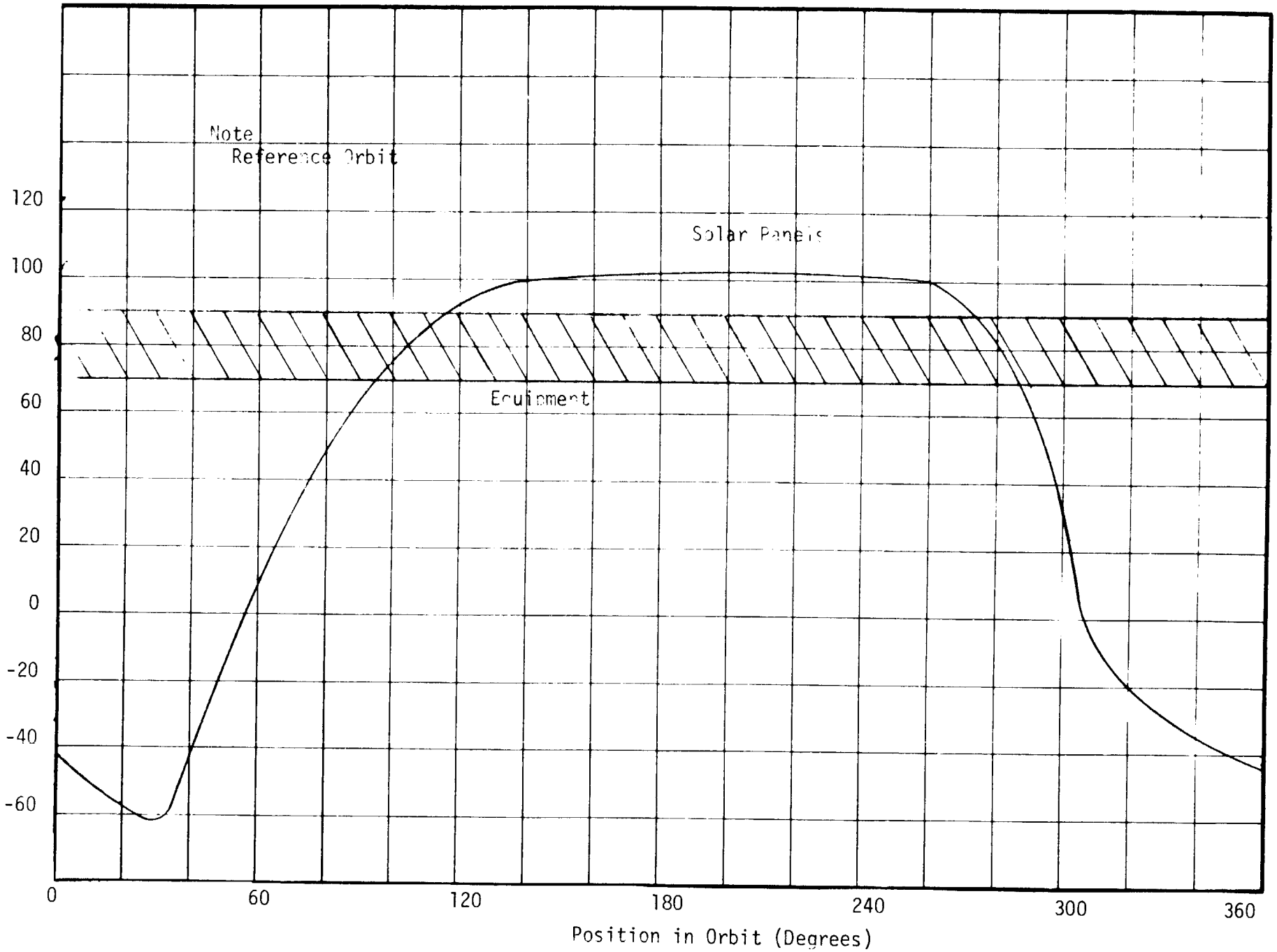

Figure 159 Solar Panel and Equipment Temperature

Space Division
North American Rockwell

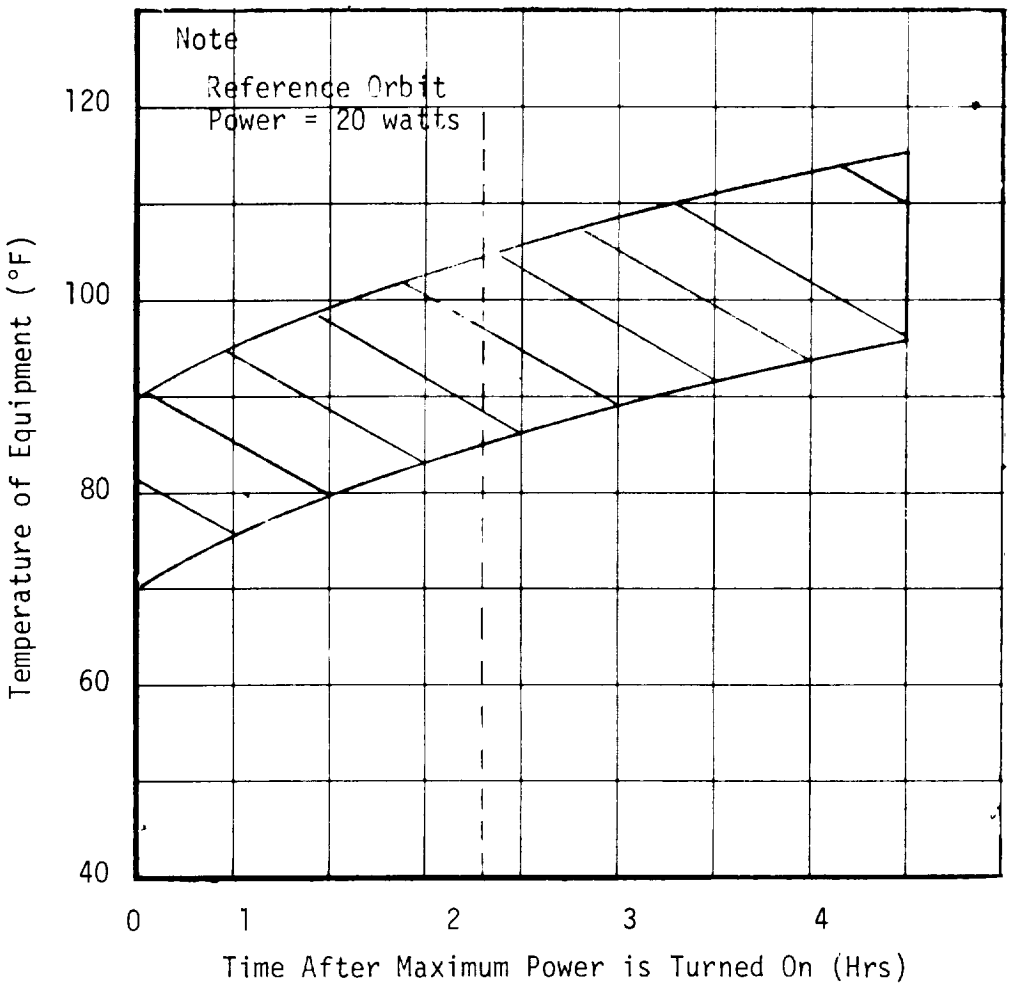

Figure 160 Temperature-Time History of Equipment After Maximum Power is Turned On

The analysis of the system during the period between launch and attitude acquisition is based on the following assumptions:

(1) During the first orbit, the spin axis is in the plane of the orbit and is pointing at the sun.

(2) During the second orbit, the spin axis begins rotating to its normal attitude - with the spin axis normal to the orbit plane.

The thermal control design is able to maintain a proper thermal environment for the satellite equipment during alternate orbits. The results of this analysis, presented in Table 44, show that the mean temperature of the equipment will change by no more than 20°F if the orbit is altered.

TABLE 44

MEAN TEMPERATURE EFFECTS OF CANDIDATE ORBITS

MISSION	ALTITUDE (N MI)	INCLINATION OF ORBIT (DEG)	RA OF ASCENDING NODE (DEG)	AVG TEMP OF EQUIP (°F)
Reference	600	100	220	80
Alternate	496	100	232.5	65
Alternate	790	102	107	60

Conclusion

The thermal environment of the temperature-sensitive equipment carried by the UV/MW satellite can readily be controlled passively, with little or no impact on the major subsystems of the satellite. Only state-of-the-art techniques are required to maintain the equipment between 30 and 95°F during flight in the reference orbit.

MISSION OPERATIONS PLAN

A mission operations plan containing the required tasks from the prelaunch phases through a portion of the orbital data-collecting period, sufficient to establish a repetitive cycle, was developed to establish the feasibility of the spacecraft concept and the procedures for its utilization. The operational phases are identified and described followed by a task/time sequence yielding an operational plan.

The plan is divided into the following phases:

- Prelaunch
- Launch
- Orbital
  - Attitude trim and magnetic moment compensation
  - Initial attitude determination
  - Data collection
  - Attitude and spin correction

PRELAUNCH

The prelaunch phase includes the operations required by the launch vehicle and the spacecraft following their delivery to the launch site (Western Test Range). The launch vehicle operations are the sequence of events established by the Delta booster into which the necessary spacecraft requirements must be mated. Spacecraft development and qualification proceeds in parallel with launch vehicle modification.

The spacecraft is delivered to the launch site in a flight-qualified status approximately 60 days prior to launch. All spacecraft systems are checked and functionally verified. The spacecraft is placed in a sealed,

transportable container provided with an inert, dry atmosphere for shipment. Spacecraft testing at the launch site is primarily at the system level to verify that the spacecraft is functioning properly prior to launch. The spacecraft test phases at the launch site are as follows:

1. Receive and inspect spacecraft (S/C) and subassemblies.
2. Check mechanical operation.
3. Check sensor alignment.
4. Conduct S/C electrical checkout.
5. Conduct S/C subsystem functional checkout.
6. Conduct S/C integrated systems test.
7. Weight S/C and conduct dynamic balance.
8. Install canister to second stage.
9. Install S/C into canister.
10. Conduct simulated countdown.
11. Conduct final countdown operations.

The launch vehicle is delivered to the launch site approximately 30 days prior to launch. The first and second-stage boosters are checked out individually, and the first-stage is erected on the launch pad. Prior to first- and second-stage mate, the spacecraft canister is installed on the second-stage and the spacecraft installed in the canister. The second-stage is mated to the first-stage. The canister installation is offset approximately 30 degrees (in azimuth) from the Delta aft skirt access hatch; thus it is not planned to access the spacecraft following first and second stage mating.

LAUNCH

The launch phase includes all the launch vehicle flight operations which are boost, injection, orientation and spin-up (See Table 45). The boost and injection are functions common to all launches, whereas the orientation and spin-up operations are peculiar to the spacecraft requirements. Orientation may require a yaw maneuver to position the spacecraft spin axis normal to the orbit plane. The spacecraft canister is opened and the spacecraft ejected with a spin rate of approximately 4 rpm. The course sun sensor is used to establish the spin vector after which the spacecraft is torqued into near-proper alignment. The course sun sensor is then switched OFF.

ORBITAL

Orbital operations begin with the attitude trim and magnetic moment compensation phase. This phase requires telemetry of attitude information, transmission to a computing facility, computation of a correction command, and implementation from the STADAN command station.

Following the initial torquing period, the spacecraft attitude is measured by using the IR horizon sensors and the fine sun sensor. These measurements are telemetered to STADAN stations with direct communication to Goddard to evaluate the spacecraft's actual magnetic moment. The pre-flight prediction accuracy of the spacecraft's magnetic moment is not considered to be sufficiently accurate for mission operation; however, commands to activate the magnetic compensation coil produce the required level of residual spacecraft torque.

TABLE 45

LAUNCH SEQUENCE - DELTA BOOSTER

TIME Sec	TIME :Hr :Min	EVENT	S/C FUNCTION	INITIATED BY	COMMENTS	
-T		Prelaunch turn-on	Telecon on Battery power on Status verified	Checkout equipment	Hardline connection to booster via umbilical	
T + 0	00:00	Vehicle liftoff Start Stage 1 programmer Uncage Stage 1 gyros	Monitoring status only	Liftoff switch	T + 0 First burn	T + 0 Solids burn
T + 2	00:00	Start roll program		Stage 1 programmer		
T + 13	00:00	End roll program				
T + 14	00:00	Start first pitch program				
T + 34	00:00	End first pitch program				
T + 35	00:00	Start second pitch program				
T + 64	00:01	End second pitch program				
T + 65	00:01	Start third pitch program				
T + 80	00:01	Solid motor separation command		Solid motor separation timer		
T + 115	00:02	End third pitch program				
T + 115	00:02	Start fourth pitch program				
T + 200	00:03	End fourth pitch program				
T + 220	00:03	Main engine cutoff (MECO)		Stage 1 programmer	MECO	
M + 0	00:03	Start Stage 2 programmer				
M + 4	00:04	Start Stage 2 engine Fire separation bolts Initiate VCS Channel 1		Stage 2 programmer	Second-Stage burn Velocity	cutoff system (backup)
M + 9	00:04	Start first pitch program				
M + 16	00:04	End first pitch program				
M + 17	00:04	Start second pitch program				
M + 21	00:04	Fairing separation				
M +		Acquire tracking ship				
M + 111	00:07	Lose sight of WTR				
M + 370	00:10	Second-stage engine cutoff End second pitch program End VCS Channel 1 Start coast phase			SECO 1 - Perigee of transfer orbi	

Space Division
North American Rockwell

TABLE 45 - LAUNCH SEQUENCE - DELTA BOOSTER (Continued)

TIME Sec	TIME : Hr :Min	EVENT	S/C FUNCTION	INITIATED BY	COMMENTS
M + 979	00:20	Start coast pitch program			
M +		Lose sight of tracking ship			
M + 2778	00:50	End coast pitch program	No ground stations		
M + 3320	00:59	Come in sight of Johannesburg	Status monitor		
M + 3407	01:00	Initiate ullage jets Initiate VCS Channel 2			
M + 3442	01:01	Restart Stage 2 engine			Circulation burn
M + 3455	01:01	Stage 2 engine cutoff End VCS Channel 2 Start coast phase			SECO 2- Altitude:600nm
M + 3467	01:01	Begin turn in yaw	Spin axis turned perpendicular to orbit plane		Location: In sight of Johannesburg station
M + 3460	01:04	Complete yaw turn and open canister			
M + 3687	01:05	Separate satellite and spin up to 4 rpm	Turn on S/C power	Stage 2 programmer	
		Begin spacecraft deployment activities			
M + 4107	01:12	Lose sight of Johannesburg			

Space Division
North American Rockwell

The initial attitude determination is expected to be completed during the first seven days of orbital operation. During this period, activities are directed primarily toward reduction and analysis of attitude data. Spacecraft data is collected from all STADAN stations with direct data communication capability with Goddard. This period is complete when the spacecraft attitude uncertainties are within the required limits.

The data collection period is the typical data-taking sequence with telemetry contact when over a tracking station. Spacecraft status data provides the information to predict the frequency of the attitude correction phase. The intervals between these corrections are estimated to be approximately five days. Telemetry contacts will be scheduled according to existing STADAN priorities; however, the seven available stations are expected to yield the necessary coverage flexibility to prevent losses of necessary telemetry data.

The data collection phases alternate with the attitude and spin correction phase. Attitude correction will be required at intervals of approximately five days or longer, while spin correction to maintain 4 rpm is expected to be at longer intervals. Each of these corrections is implemented by commanding the spacecraft when over a station. Although the periods of expected correction are not equal, spin correction will be phased with an attitude correction. The necessity to re-establish the spacecraft attitude following each correction, and the invalidating of sensor data during either of these magnetic torquing programs, identify the reasons for minimizing the total torquing intervals. One-half orbit is adequate to accomplish both corrections.

TASK/TIME SEQUENCE

A chronological task sequence of the previously identified phases will be discussed herein to establish the feasibility of the measurement program by demonstrating task compatibility.

Fig. 161 illustrates the prelaunch phase from spacecraft delivery to WTR through two days prior to launch. Fig. 162 details the 48-hour countdown terminating at lift-off. Figure 163, launch phase, establishes the timing interval of 12 minutes as the expected duration, during which time all booster functions will be accomplished through orientation, separation and spin-up of the spacecraft.

The third phase, attitude trim and magnetic moment compensation, is accomplished during the first day in orbit. The telemetry contacts for a typical day are shown in Figure 164. The stations at Rosman and Fairbanks can accomplish the entire program; however, due to possible conflicts and priority considerations, the other stations provide a complete range of STADAN alternatives. These will be of greater significance during the repetitive profile collection phases extending over the entire mission duration of one year.

The period required for the initial attitude determination is estimated to require approximately six days (seven days in orbit). The sequence is similar to the previous phase, in that direct communication with the mission control location is required for near realtime input of data from the attitude determination instruments to produce coverage to the solution as rapidly as possible; therefore, the telemetry contacts from Alaska and Rosman, possessing direct communication with Goddard, will be utilized. The other data contacts,

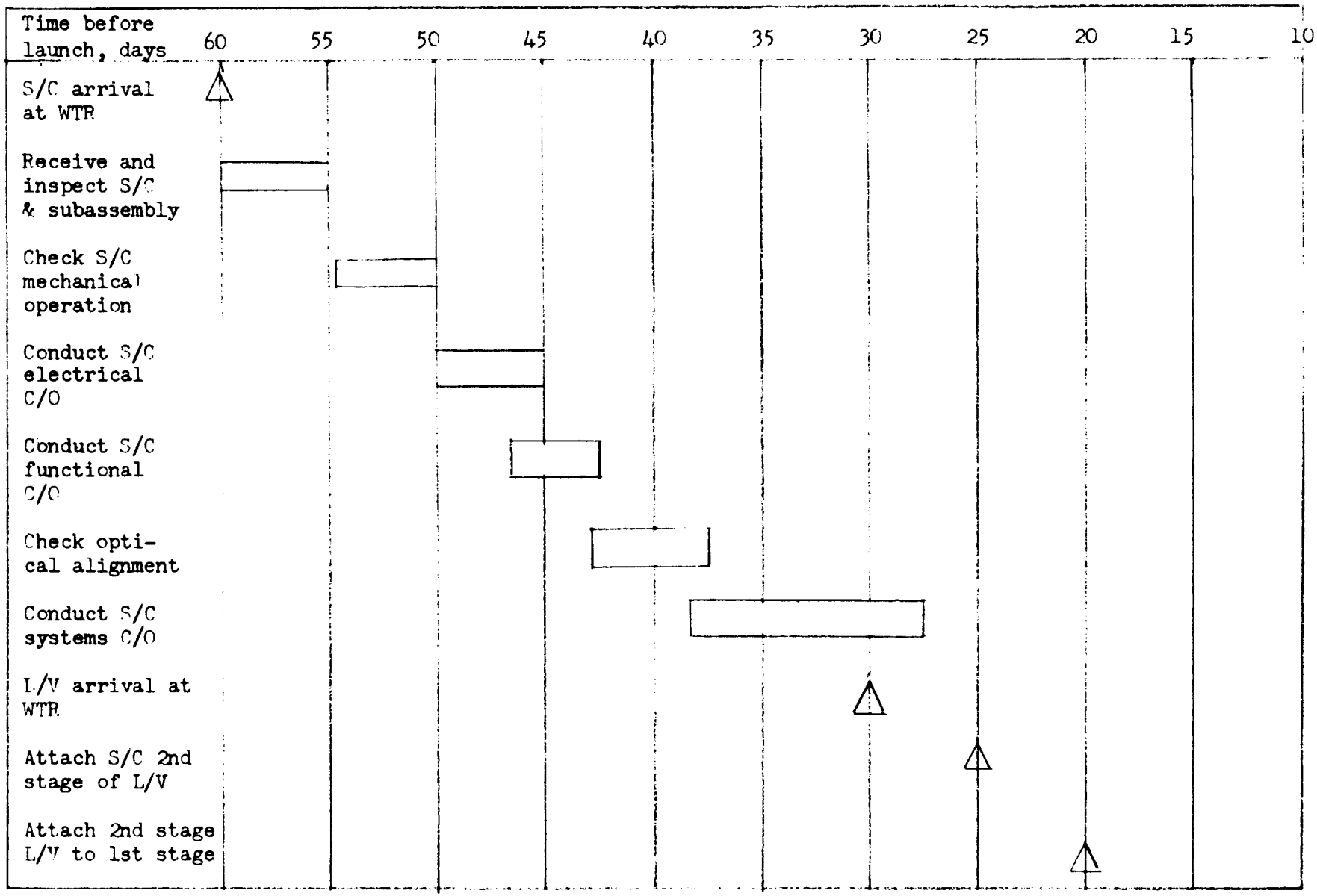

Figure 161 Operations Plan, Prelaunch Phase

Space Division
North American Rockwell

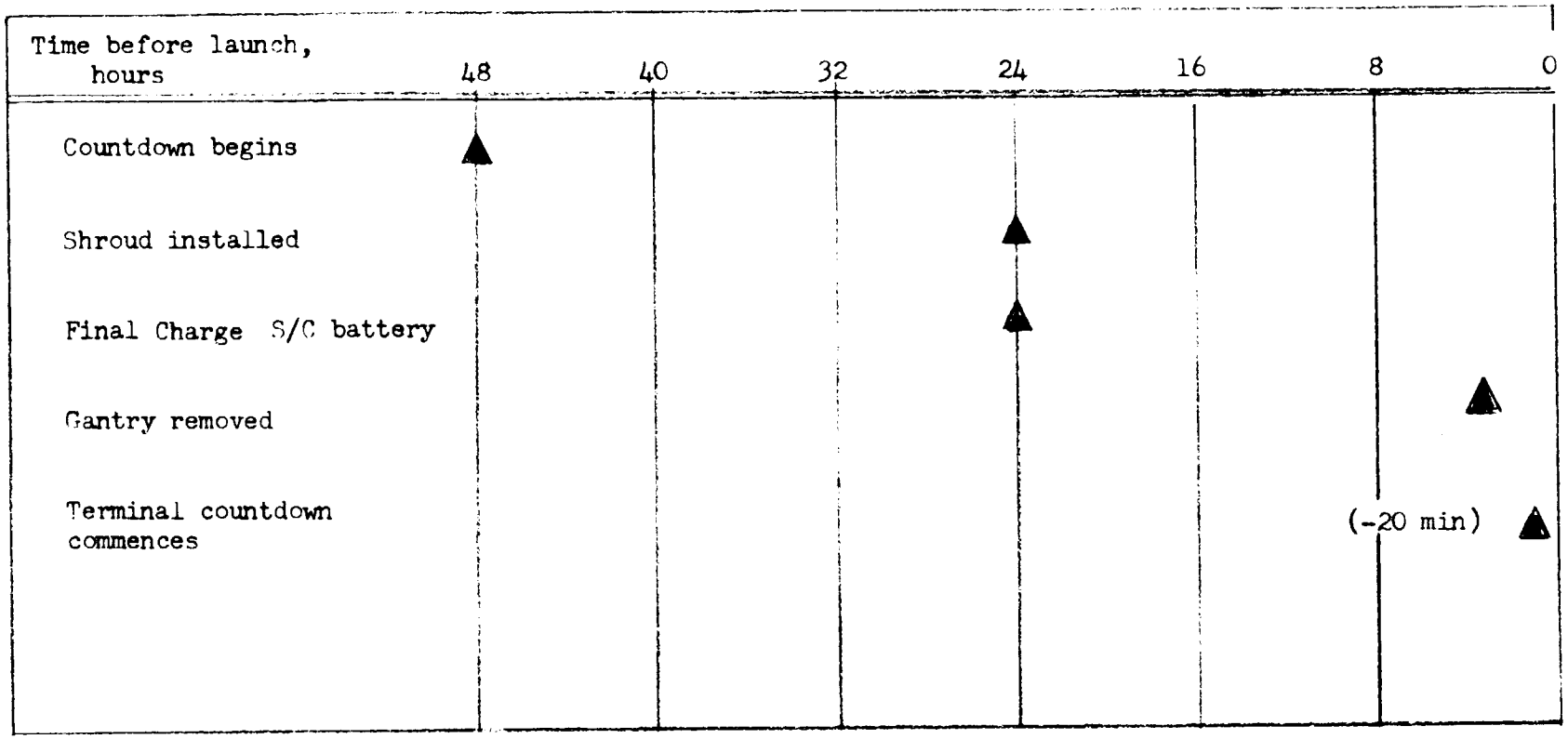

Figure 162 Operations Plan, Prelaunch Phase, Final 48 Hours

Space Division
North American Rockwell

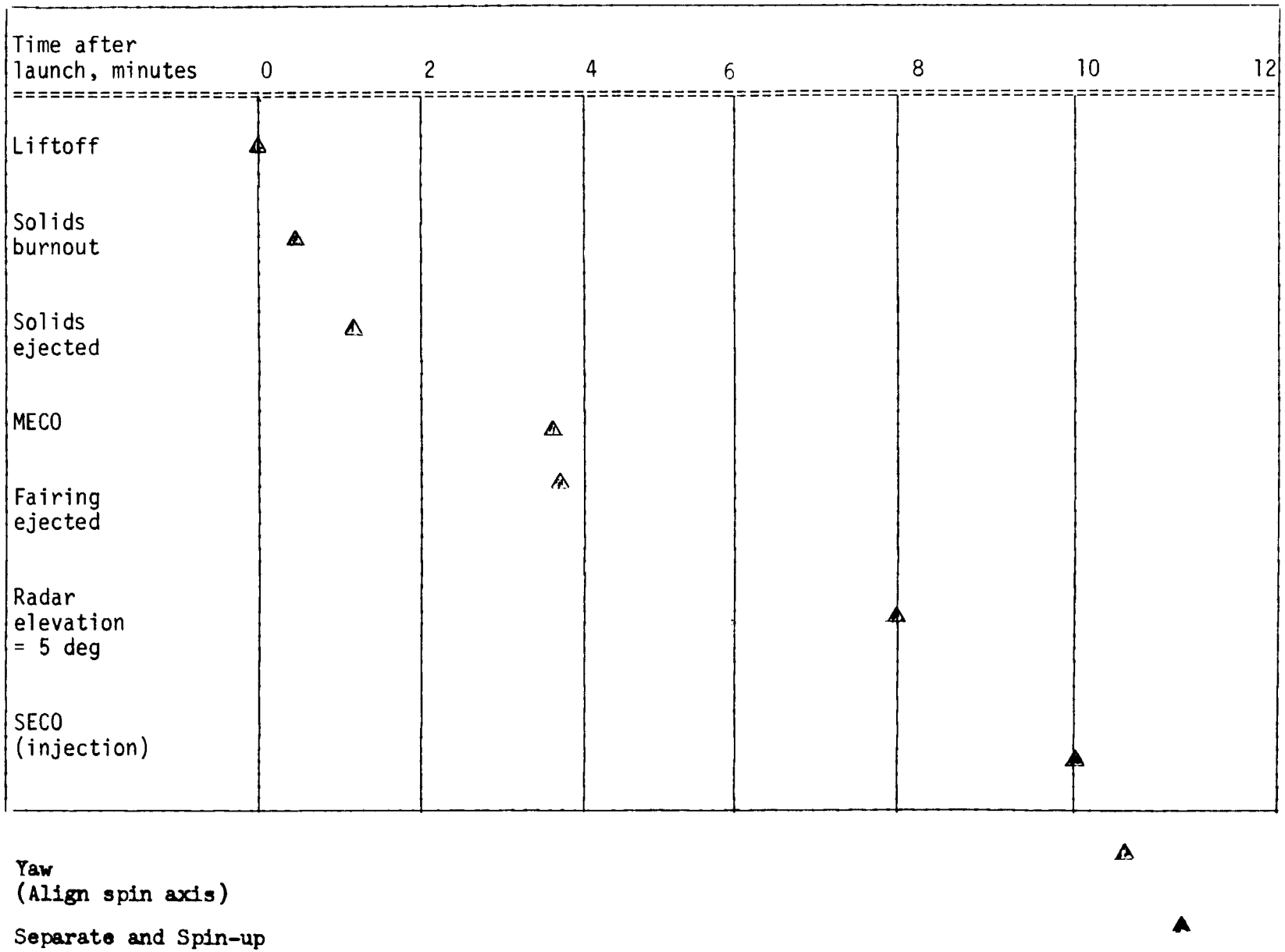

Figure 163 Operations Plan, Launch Phase

Space Division
North American Rockwell

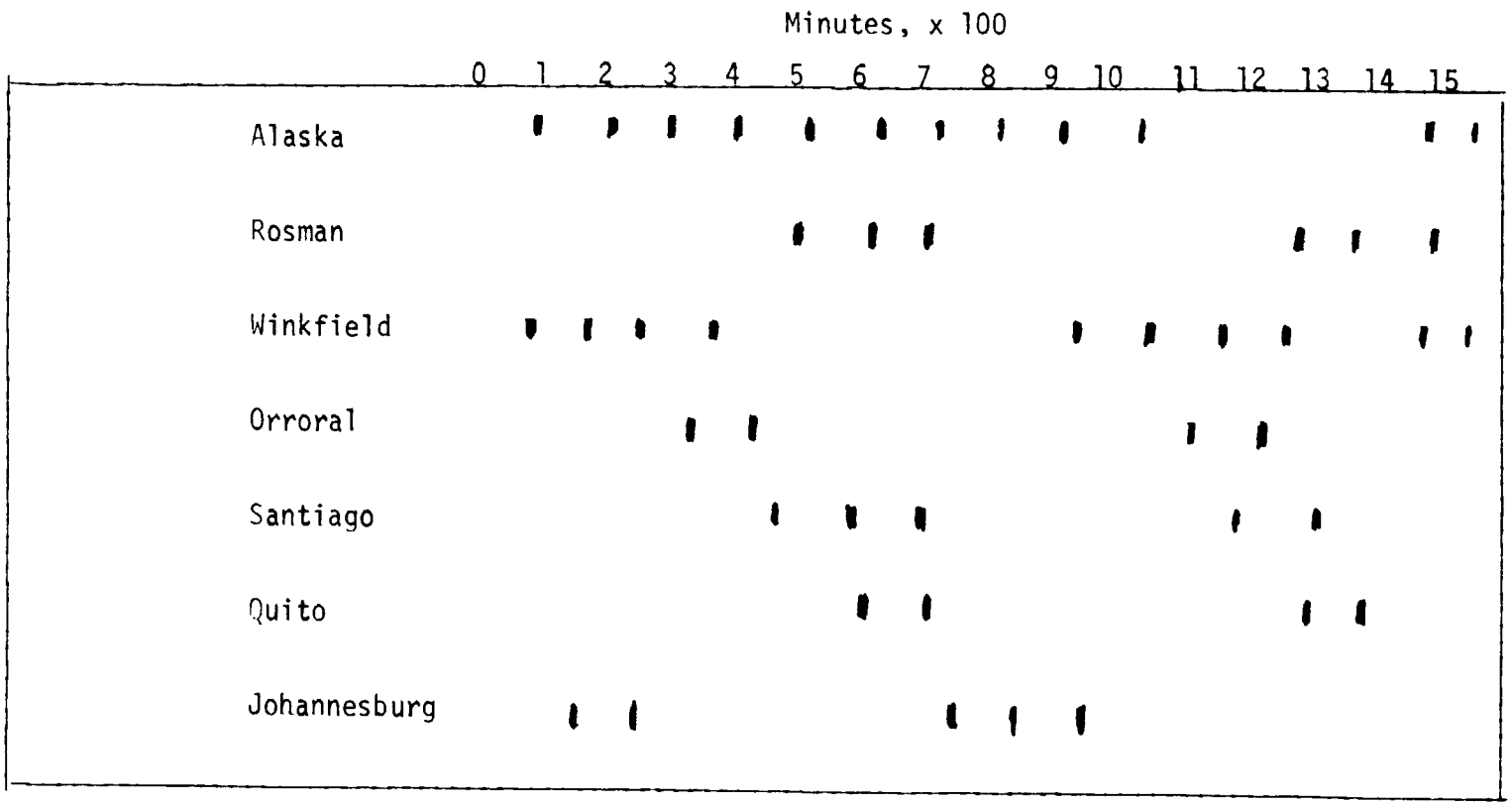

Figure 164. Telemetry Contacts for a Typical Day of Operation (Orbits 27 - 41)

Space Division
North American Rockwell

completing the record, are not required for the initial solution. The collection of this data provides for contingency analysis in the event of failure or anomalies.

Command requirements could be required during this phase in the event the spacecraft attitude exceeds the $\pm 2°$ limits.

The data collection phase will be repetitive at irregular intervals as desired.

The attitude and spin-correction phase has the following sequence:

1. Evaluation of status data from Alaska and Rosman stations and prediction of time to reach the attitude limit.
2. Selection of the appropriate command program for both attitude change and spin correction.
3. Determine Alaska contact immediately prior to predicted time to reach attitude limit.
4. Transmit command requirement to Alaska.
5. Transmit command to spacecraft.
6. Command implementation by spacecraft. One-half orbit required.
7. Resume normal operation (data collection).

The operational plan presented above provides for the elements of the measurement program to be completed within all program requirements. The actual plan for the one-year mission will evolve from spacecraft performance data. The actual STADAN coverage sequences can only be predicted for periods of several days in order to maintain adequate timing accuracies. A mission control function, therefore, is the determination at periodic intervals (approximately one week) of the coverage sequence and priorities.

Conclusion

The UV and MW Horizon Sensor Orbital Experiment mission functions can be conducted in a compatible, chronological manner as established by the existing operational plan.

The actual tracking telemetry and command functions will be established at approximately weekly intervals, according to the priorities in existence at the time.

PROGRAM IMPLEMENTATION PLAN

This section is furnished in response to task 2(d) of the contract for the UV/MW Horizon Sensor Satellite Phase B study. The purpose of the program development plan (PDP) is to describe a logical, integrated and orderly sequence of activities. The PDP includes schesules, cost estimates, and essential related information for a one flight spacecraft program. The PDP covers design, manufacture, test, ground support equipment, facilities, launch and flight operations support, and related activities for the spacecraft (i.e., NASA Phases C and D).

The PDP is an integrated document, consisting of seven principal elements:

- Program Management
- Work Breakdown Structure
- Program Development Schedule
- Subsidiary Program Plans
    - Engineering Development
    - Manufacturing
    - Program Test
    - Configuration Management
    - Quality Assurance
    - Facilities
- Ground Support Equipment Requirements
- Hardware Utilization List
- Program Cost Estimates

NR Space Division prepared the PDP using the approach shown in Figure 165. This approach is discussed in detail under the various sections of the PDP.

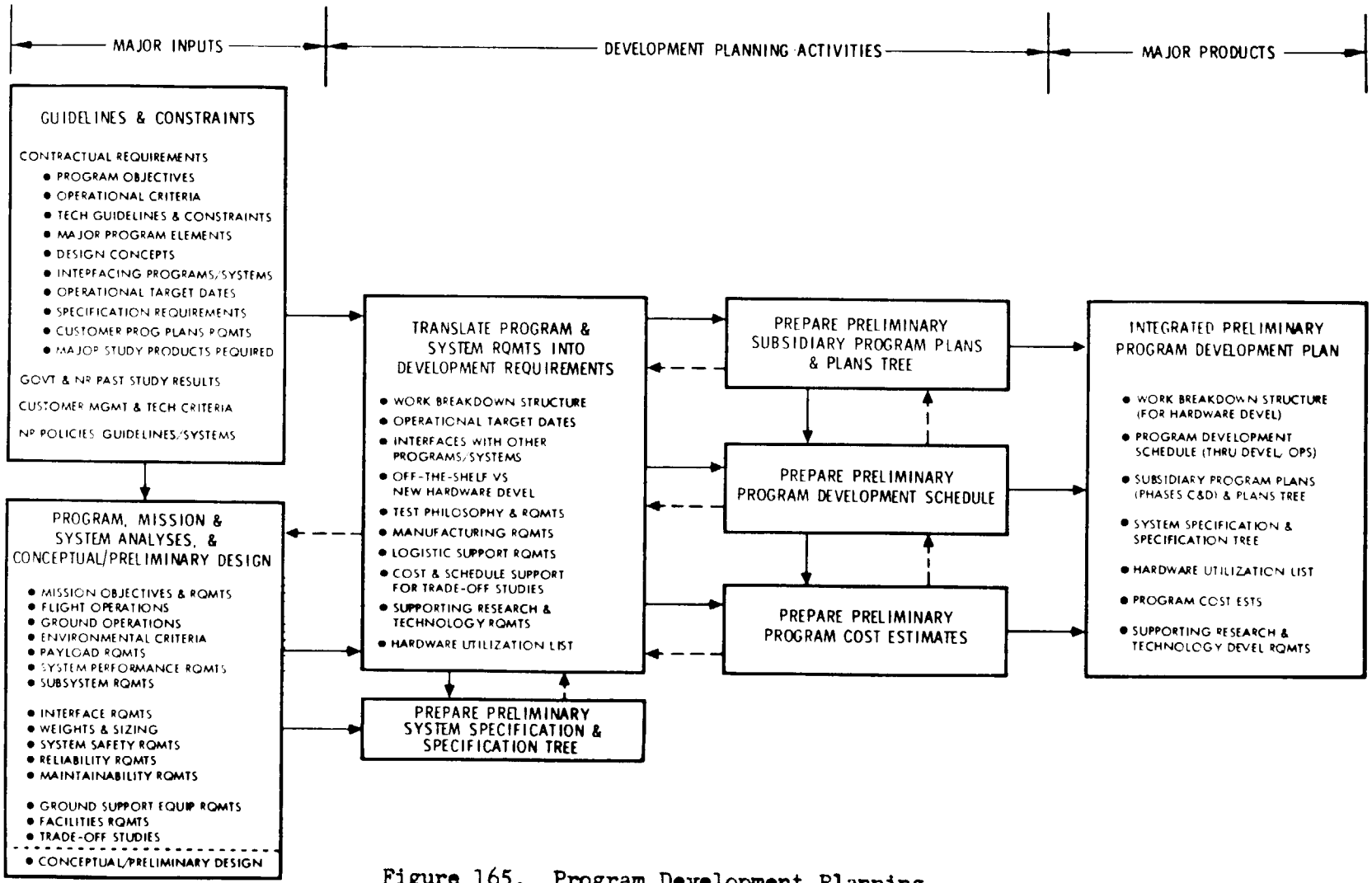

Figure 165. Program Development Planning

Space Division
North American Rockwell

PROJECT MANAGEMENT PLAN

The purpose of the Project Management Plan is to ensure economical and effective overall planning, organization, staffing, direction, and control of the spacecraft project activities of the UV/MW Horizon Sensor Satellite Program.

The Project Management Plan covers the Project Manager's responsibilities for project-wide cost and schedule control, configuration management, subcontract management, data management and make-or-buy determinations. This Plan is specifically applicable to Phases C (Design) and D (Development/Operations).

Management Approach

The size of this project must be kept in focus in planning, organizing, staffing, directing, and controlling the program. There will be a minimum number of management personnel. Staffing for control functions will be adequate but austere. Responsibility assignments for work effort will be on the basis of work packages derived from the Work Breakdown Structure. The services of qualified supportive personnel will be obtained from cognizant central functional organizations throughout the company--for specific tasks and for specific time periods. These personnel will be returned promptly to their central functional organizations when their assignment is completed.

The contractor shall be responsive to NASA management and technical criteria. Maximum use should be made of existing company management systems and procedures, tailored to this project, paperwork being kept to a minimum. There will be minimum requirements for new facilities and support equipment.

The Spacecraft Project Manager shall have complete authority and responsibility for all personnel working on the Project for the life of the Project. In the interests of efficiency, all personnel (other than off-site) working on the project shall be centralized in one location.

Task Summary

Spacecraft Project Manager. - The Spacecraft Project Manager will be directly accountable to Division executive management and carry the delegated authority of the President when directing project personnel in achieving project objectives. The Project Manager shall be specifically responsible for:

- Directing the UV/MW Satellite Program toward successful completion as dictated by the contract.
- Participating in contract negotiations.
- Establishing overall project performance baselines to meet contractual requirements on project cost, schedule, and technical performance.
- Approving all project plans, specifications, and schedules.
- Approving project implementing instructions and assuring that such instructions are within the guidelines of Division policy.
- Authorizing and controlling all project funds with sole accountability to Division executive management.
- Assessing actual performance against plans and providing remedial action when required.

- Acting as the prime customer interface for all matters that directly affect the project.
- Organizing the project for effective management.
- Selecting and approving management personnel assigned to the project.
- Approving the Project Master (Program Development) Plan and ensuring that revisions to it are properly authorized, issued, and implemented.
- Directing and approving the issuance of work authorizations to assigned work package managers.
- Maintaining constant awareness of overall project status and taking appropriate action on critical problems.
- Assuring that work package authorizations conform to project objectives.
- Assuring that the management system identifies problems and potential problems, and approving corrective action.
- Providing a forecast to the work package managers and central functional organizations regarding future project requirements for manpower, facilities, etc.
- Serving as Chairman of the Project Make-or-Buy Committee, and approving decisions made by the Committee.
- Defining the requirements for a project management system necessary to satisfy contractual obligations.

- Reviewing all aspects of the project with the Division executive management on a scheduled basis.
- Approving correspondence and other communications with the NASA.

Cost and Schedule Control

Total budgetary responsibility shall be assigned to the Project Manager. He shall direct the project effort by issuing work package authorizations to responsible work package managers or subcontractors. These work package authorizations shall identify specific effort, time-phased budgets including all direct costs, specific schedule activity, and required interfaces with other work package managers in accordance with the Work Breakdown Structure. After entering these cost and schedule baselines into the computer module, the cost data will be available for comparison with actual expenditures, and integration with schedule data from the automated schedule module. Project cost visibility can be obtained through variance analysis of budgeted costs for work scheduled against actual costs of work performed. Project summary and functional/product oriented reports shall be prepared and made available to the Project Manager, the work package managers and functional managers on both a weekly and monthly basis. These reports will provide the basis for management analyses of project cost status and accomplishment of cost objectives. The basic computer data will also provide a cost trade-off capability to assist in making cost effective decisions. Required cost status reports shall be submitted to the NASA (Financial Management 533 Series).

The Master Program Schedule shall be the baseline for the iterative process of developing and later monitoring detailed subordinate schedules for each work package. Detailed schedules shall also be developed and monitored for subcontract items. Schedule control shall also include: reviewing schedule status and program milestones, revising the Master Schedule, coordinating schedule data, updating schedule logic networks, performing schedule analysis, preparing biweekly computer inputs, providing work package schedule status/analysis biweekly to the Project Manager and work package managers, and preparing schedule status reports for submittal to the NASA.

Subcontract Management

The basic tool for control of subcontractor's effort shall be work package authorizations which require the subcontractors to prepare cost, schedule and performance reports. Each subcontractor work package shall identify time spans and release schedules, performance specifications, configuration management requirements, and specific reporting requirements. Reporting information shall be incorporated into the project integrated management system for planning and control visibility.

Configuration Management

The Configuration Management (CM) organization will be initiated and shall invoke CM on all functional organizations such as Engineering, Manufacturing, Test, Material, Quality and Reliability Assurance, Logistics, and the subcontractors.

Data Management

Data Management for this project shall consist of the planning, programming, organizing and implementing of a minimum data and documentation requirement throughout the contractual period. Data shall be submitted to the NASA in compliance with the Contract Data Requirements List and Data Requirements Descriptions.

Make-or-Buy Determinations

The prime contractor shall be responsible for integrating, assembling and checking out the spacecraft. As may be noted from an examination of the Hardware Utilization List, it is anticipated that the prime contractor would also manufacture the structural components; power distribution system; the mechanical devices; and some of the Ground Support Equipment.

It is anticipated that the payload and a few articles of Ground Support Equipment will be Government-Furnished.

WORK BREAKDOWN STRUCTURE

The Work Breakdown Structures (WBS - Figures 166 & 167) depict the principal categories of hardware, software, services and other work tasks that comprise the UV/MW Horizon Sensor Satellite Program for Phases C and D. The WBS is product-oriented, to the major component level. The WBS provides a frame of reference for the preparation of the Program Development Schedule, subsidiary program plans and program cost estimates and control.

The spacecraft hardware portion of the WBS is the reflection of a Hardware Tree derived from an analysis of the spacecraft design. To facilitate identification of development and production costs, the WBS contains separate breakdowns for design, and test hardware.

The WBS does not include the launch vehicle or STADAN operation. The WBS does, however, provide for their technical, management, and operational interfaces with the spacecraft under Test and Launch Operations and Support Services.

The other entries on the WBS (i.e., Program Management, System Engineering and Integration, Facilities, etc.) are based on NR Space Division past experience, tailored to this program.

PROGRAM DEVELOPMENT SCHEDULE

The preliminary Program Development Schedule (PDS) shown in Fig 168 demonstrates a total integrated set of activities and milestones for the design, development, fabrication, test and launch of the UV/MW Horizon Sensor Satellite. The schedule is predicated on the reference concept described in the R.F.P., the proposal (SD-69-524) and the technical sections of this report. It is predicated on the concept that all non-mission critical functions and requirements will be modified, relaxed or waived to allow the realization of an operational program within 18 months from contract go-ahead. For example, there is no structural model or development model spacecraft called out or proposed. It is felt that any required development testing can be done on the subsystem level and the spacecraft and systems qualified simultaneously with the engineering model and combined prototype/flight model.

The quality and reliability assurance and configuration management documentation aspects of the program assumes waivers from the standard NASA and NR requirements. No downgrading in work standards is implied; only that program costs can be substantially reduced by relaxation of certain subsidiary program software requirements.

Ground Rules and Assumptions

NR established specific ground rules and planning assumptions in order to maintain a program baseline and frame of reference in the preparation of the Program Development Schedule. The ground rules and assumptions are, as follows:

1. A single schedule is required covering a one (1) flight spacecraft program.
2. The current contract is Phase B (Definition).
3. A single contract will be awarded for both Phases C (Design) and D (Development/Operations) with no gap between these two phases.
4. Launch is assumed to take place from the Western Test Range.
5. The flight spacecraft will be ready at the launch range 30 days prior to launch.
6. Current North American Rockwell facilities (or equivalent) and nearby Government installations will be utilized; requirements for modified or additional facilities and related equipment will be kept to the minimum.
7. Some Government owned GSE and STE will be made available to the program.
8. Certain long lead time items (i.e. reference sensors) will be ordered during Phase C.
9. The Program Development Schedule defines an orderly, economical evolution of events leading to the realization of mission objectives with a highly quality operational system. The phasing of the program should not be considered as fixed.

10. The Program Development Schedule was prepared on the basis of close coordination with all functional activities. Action was taken to ensure that the Program Development Schedule and the schedules in the individual subsidiary program plans are consistent.

Task Summary

The preliminary program development schedule designates the desired delivery of test spacecraft and flight spacecraft, but does not portray precise Manufacturing, Test, and other functional milestones. Detailed schedules for each of the major functions are part of the subsidiary program plans.

The Program Development Schedule shows the proposed phasing of the principal development activities and milestones, the time scale being measured in calendar months.

The Program Development Schedule depicts the major milestones for each of the principal program functions during Phase D. Program Plans will be updated and implemented early after Phase C go-ahead. Program Management will implement the schedule, and cost and technical performance functions. Detail design effort will commence at the start of Phase D with the Critical Design Review (CDR) scheduled 8 weeks later. Eighty percent of the detail drawings are scheduled for release at this point in the program with the remaining twenty percent scheduled for release within the next two months to support Manufacturing scheduling requirements.

This Program Development Schedule is feasible. The time spans for each of the concurrent system development requirements are realistic. There is a minimum time

slack for unforeseeable program delays or test failures. Phasing for various activities and milestones is based on consultation with design engineers; with test operations, manufacturing and facilities engineers and schedules; and with other functional support personnel.

Major program pacing factors are: component procurement lead time, and precision sun sensor development.

SUBSIDIARY PROGRAM PLANS

The purpose of the subsidiary program plans for the program is to set a course of action for achieving mission objectives and to communicate that course, in order to accomplish the objectives: (1) at the lowest practical overall development and production costs; (2) on time with respect to a target launch date; and (3) in accordance with the NASA's quality standards. The plans also provide a basis for identification of deliverable products, and realistic program cost estimates and development schedules; and ensure functional integration of the various parts and activities of the program.

The scope of the planning activity required for this program encompasses all program technical and management functions. NR Space Division has selected a limited number of key functional areas for which preliminary plans are considered useful at this time and commensurate with the depth of this short study contract. These functional areas and corresponding plans consist of: Project Management, Engineering Development, Manufacturing, Program Test, Configuration Management, Quality Assurance and Facilities. During subsequent phases of this program these plans will be updated and expanded, and additional program plans if required will be prepared.

Engineering Development Plan

The Engineering Development Plan (EDP) summarizes the orderly progression of engineering activities required for conducting the UV/MW Satellite Program. The EDP also serves as the basis for engineering planning, organizing, staffing, directing, and controlling activities to achieve the objectives of the program in an efficient and effective manner.

The EDP spans the engineering activities of: (1) definition of system performance and configuration requirements, (2) preliminary design definition, and (3) design completion and verification. Continuous engineering planning and control is maintained through all phases.

Task Descriptions.- The Program Engineering Process (Fig 169) includes the technical functions required to fulfill the engineering commitments in the developed program. Activities have been organized into the basic modules; i.e., Requirements Definition, Planning and Control, Design and Integration, and Verification.

Requirements Definition.-

Analyze Program and System Functions.- Establish the approach and portray graphically and sequentially all detail functions for effective integration of engineering effort in developing, testing, supporting, and maintaining the system.

Analyze Program Requirements.- Establish the manner in which contractor resources and experience will be applied to satisfy the objectives and tasks in the statement of work.

Analyze Mission Operations Requirements.- Identify those operations requirements to be satisfied by a comgination of system elements; obtain parameters of design, design constraints, and system effectiveness factors; establish mission guidelines, operational constraints and reliability goals; prepare and review plans and procedures for horizon sensor data programming.

Develop Facilities and System Activation Requirements.- Identify facilities and activation requirements (including transportation, assembly, installation and check-out) to be satisfied by a combination of system elements.

Accomplish Preliminary Design.- Support the determination of an approach to system design; support establishment of the initial System Requirements Baseline.

Integrate System Requirements.- Select, and provide system end items equipment lists; identify and control interface requirements including launch vehicle-spacecraft, experiment-spacecraft subsystem, and spacecraft-support equipment, and establish compatibility between system plans.

Planning and Control.-

Plan Engineering Program.- Identify the tasks and align them to program milestones and production schedules, and provide inputs to the Program Management Networks.

Integrate Engineering Planning.- Establish and assess compatibility and consistency between schedules, budget breakdowns and work packages; provide an adequate and clearly defined interface with the Program Planning and Control function.

PRECEDING PAGE BLANK NOT FILMED

Design & Integration.-

Accomplish Detail Design. - Translate "design-to" requirements into "build-to" requirements; identify detailed constraints and additional design requirements applicable to production and maintenance effort; determine the design approach; and conduct synthesis of alternate approaches.

Establish Interface Control.- Assure physical, functional, and procedural compatibility between interfacing equipment/facilities; establish customer/contractor/subcontractor responsibilities for external interfaces; establish organizational responsibilities for internal interfaces.

Integrate Detail Design.- Assure compatibility between and within equipment end items including launch vehicle-spacecraft, experiment-spacecraft subsystem, and spacecraft-support equipment; identify additional feedback changes to system functions and design requirements; further refine interface definition; derive maximum benefits from development testing.

Verification.-

Conduct Engineering Breadboard and Mockup Operations.- For the purposes of (1) verification of design configurations, interface considerations, equipment installation locations, and clearances; (2) aiding in the manufacture of cable harnesses; and (3) supporting design reviews by customer personnel.

Support Development and System Test Program. - Verify the integrity of designs under static and dynamic conditions; assure qualification requirements are satisfied; assure achievement of reliability goals; determine suitability of design configurations physically, functionally, and procedurally; and verify selected materials and processes.

Conduct System and Product Performance Evaluation - Prepare tolerance model to allocate performance accuracies to system and subsystem elements. Evaluate variations between system and product performance requirements and actual performance measurements to determine potential impacts on system and product operations and capabilities.

Associated Activities.- The EDP, when fully expanded during Phase C, shall include coverage of the following and possibly additional, essential activities:

Reliability Program Plan.- The Reliability Program Plan will be the master planning and control document for the reliability program for development of spacecraft. It shall include a time-phased description of all tasks to be performed and the procedures for implementing, monitoring, and controlling these tasks. The document shall follow the outline and intent of NPC 250-1. The plan shall include the following significant tasks, as applicable:

(1) Reliability Program Management

(2) Reliability Analysis

(3) Specification Evaluation

(4) Test Planning

(5) Supplier Reliability Program Management

(6) Failure Analysis

(7) Reliability Program Reviews

System Safety Plan.- This plan will identify the tasks that will be performed throughout the program to assure the application of system safety principles.

Value Engineering.- Contractor-developed techniques and methods will be used to enhance design quality and cost effectiveness throughout all phases of the program.

Implementation and Management.-

Program Engineering Process.- In tailoring the PEP to the UV/MW Horizon Sensor Satellite program, a major consideration will be its cost-effective application. Therefore, a minimum of documentation will be adequate for clearly recording engineering decisions so that traceability of design solutions to basic requirements will be provided.

Manufacturing Plan

Purpose and Scope. - The Manufacturing Plan presents the initial manufacturing approach and summarizes the planned orderly progression of manufacturing activities for Phase C (Design) and D (Development/Operations). It has been tailored to meet the specific requirements of the Ultraviolet/Microwave Horizon Sensor Orbital Experiment Satellite (UV/MW Satellite).

The objective is to identify and define the manufacturing approach and functions for the fabrication, assembly, and installation of a combined structural/engineering model, and a combined prototype/flight spacecraft.

This plan will be expanded to levels of greater detail and finalized during Phase C.

Implementation and Management. - A Manufacturing/Facilities Manager will be appointed at the beginning of Phase C. He will direct all activities through a program-type organization. He will report to the NR/SD UV/MW Program Manager for program direction and to the Vice President of Manufacturing and Facilities for functional direction and support.

Fabrication, assembly, and installation effort will be accomplished in the Engineering Support Shop. This facility has the equipment, manufacturing specialists, and in-built flexibility required for programs such as the UV/MW Satellite.

Systems testing will be accomplished by Laboratories and Test Engineering utilizing existing test equipment.

Task Requirements. - The major items of hardware defined during Phase B consist of one structural/engineering UV/MW Satellite vehicle, one structural/engineering UV/MW Satellite cannister, one prototype/flight UV/MW Satellite spacecraft, and one prototype/flight UV/MW Satellite spacecraft cannister.

Task Descriptions.

Prototype/Flight Spacecraft Fabrication. - The satellite spacecraft structure is comprised of a machined or cast aluminum alloy mounting plate, solar cell array assemblies, ejection guide tube, and mounting clips. The subsystems, communications, data handling, electrical power, attitude control, etc. are attached to the mounting plate. Assembly of the structure and installation of the subsystems is by mechanical fasteners. A manufacturing breakdown is shown in Figure 170.

Detail fabrication will utilize existing equipment and manufacturing skills utilizing minimal tooling described elsewhere in this plan.

Assembly of the structural components will be accomplished using the tooling and shop aids described elsewhere in this plan.

The subsystems will be installed and wired as required on a progressive basis. Checkout by Manufacturing will be limited to the mechanical installation, and a continuity check on the wiring.

UV & MW SATELLITE

DRW-3026-Z (1-21-70)

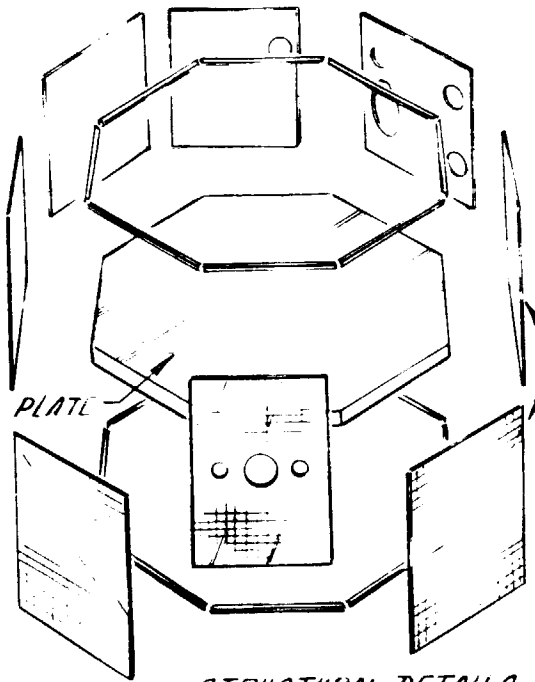

• STRUCTURAL DETAILS

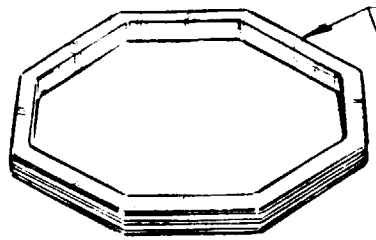

• QOMAC AND MBC COIL

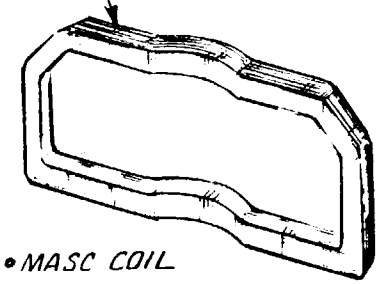

• MASC COIL

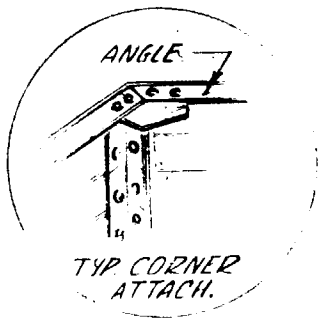

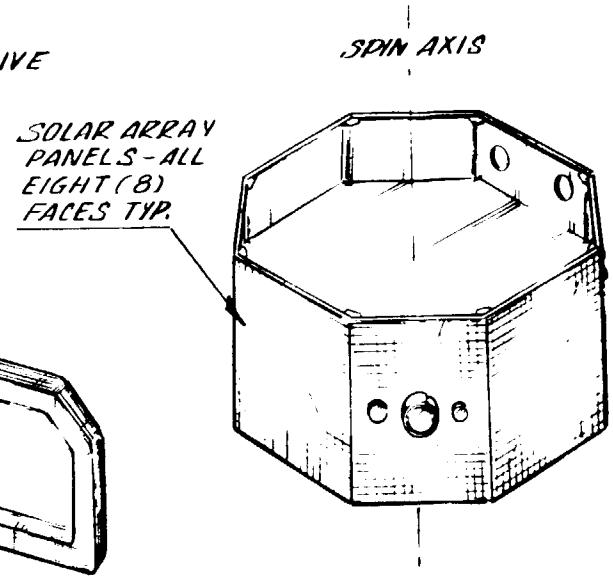

• STRUCTURAL ASSEMBLY

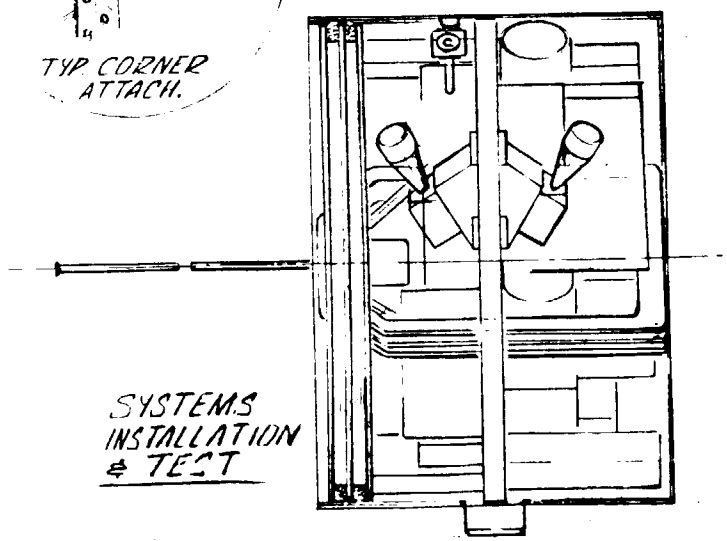

NR MAKE ITEMS - SUB-SYSTEMS

- SENSOR REGISTER ASSY.
- DATA CONDITIONER
- TIMER
- COMMAND DISTRIBUTOR
- NUTATION DAMPER
- DESPIN YO YO
- ELECTRONIC CONTROLLER

NOTES:

- MAJOR TESTING WILL BE PERFORMED BY ENGINEERING L & T.
- WIRE HARNESS TO BE INSTALLED INCREMENTALLY AS REQ'D.

FIGURE 170

MANUFACTURING BREAKDOWN

E.E.S.
JAN 22 '70
D-070

Weight and balance, thermal balance, electrical, mechanical, electromechanical, or other subsystems/systems checkout will be conducted by Laboratory and Test Engineering.

Prototype/Flight Cannister Fabrication. - The satellite cannister structure is comprised of aluminum alloy L-shaped extrusions, sheet metal panels, ejection spring housing assembly, support rods, and miscellaneous hardware consisting of door latches, and spring loaded hinges. Mechanical fasteners are used in assembly. Fig. 171 depicts the manufacturing breakdown.

Detail fabrication will utilize existing equipment and skills with tooling requirements kept to a minimum.

Assembly of the components will be accomplished using the tooling and shop aids described elsewhere in this plan. Functional operation of the clam shell doors will be verified by Manufacturing.

Test Article Fabrication. - Structural assemblies for the structural/engineering satellite vehicle, and the structural/engineering satellite cannister will be fabricated and assembled using flight spacecraft details and tooling. Subsystems/systems installations will be per Design Engineering requirements. Testing will be performed by Laboratory and Test Engineering.

Support Equipment Fabrication. - Minimum support equipment, such as Special Tooling and Shop Aids is required. These are listed and described in the Support Equipment section of this plan.

UV & MW SATELLITE CANNISTER

DRW. - -026-1 (1-15-70)

NOTE:
- ALL PARTS SHOWN ARE ALUM. MATERIAL.
- RIVET AND BOLT TO SUIT.

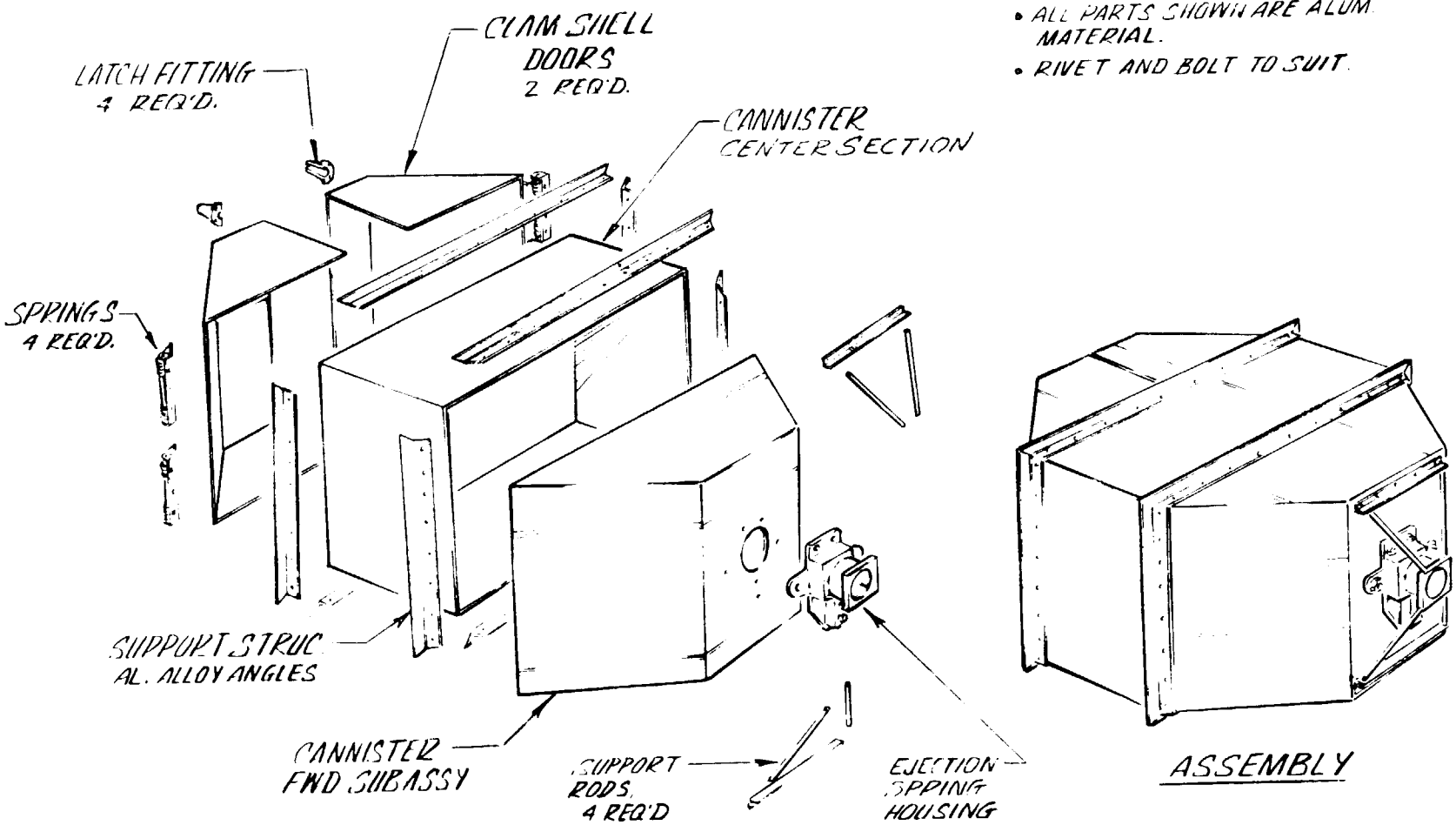

ASSEMBLY

MANUFACTURING BREAKDOWN

E.E.S.
JAN. 22 '70
D-070

FIGURE 171

Space Division
North American Rockwell

Manufacturing Engineering. - Manufacturing Engineers will serve as producibility consultants to Design Engineering during Phase C to provide analysis of designs from a fabrication and tooling feasibility viewpoint and also to recommend the optimum practical approach for facilitating machining, forming, processing, assembly, and installation operations.

Technical support will be provided to Manufacturing during fabrication, assembly, and installation.

Production Control. - Master programming/scheduling charts depicting long leadtime procurement requirements will be prepared during Phase C. Also during Phase C, a master composite schedule will be prepared to depict a coordinated plan for the fabrication of flight spacecraft and test articles. A preliminary schedule is shown in Figure 172.

UV/MW HORIZON SENSOR SATELLITE
PROPOSED MFG. COMPOSITE SCHEDULE

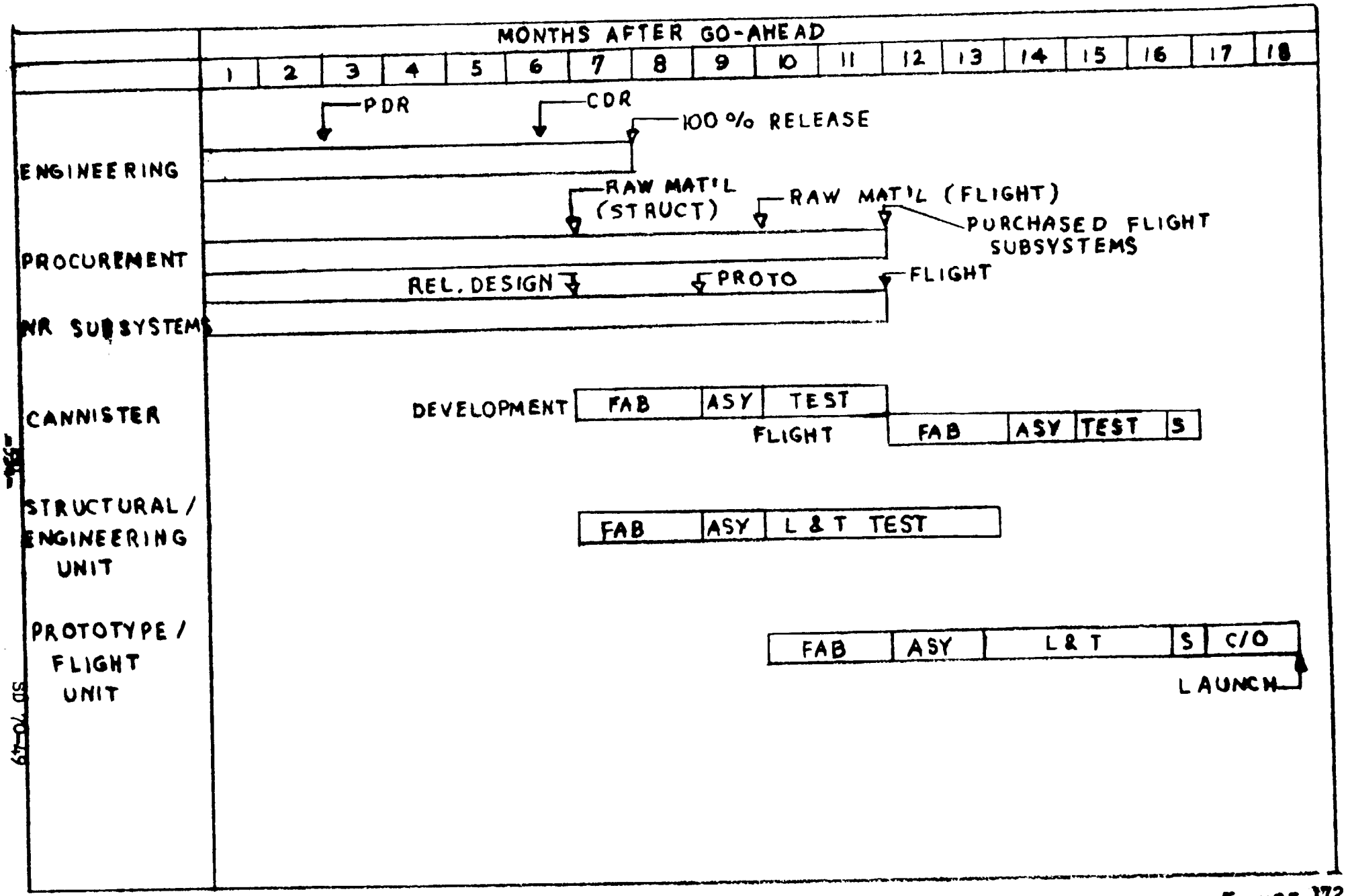

FIGURE 172

SD 70-49

Support Equipment.

Cannister Assembly (Drawing 3026-1).

Tooling/Shop Aids.

One (1) flat pattern template for LH/RH clam shell doors.

One (1) holding fixture (Non-design-type to be built by Model Shop) to position housing support rods (4) for welding.

Note: Miscellaneous shop aids will be fabricated as required to support the limited detail and subassembly operations.

Satellite Structural Assembly (Drawing 3026-2A).

Tooling.

One (1) template for center plate periphery.

One (1) drill template for plate, location of support brackets and subsystem components.

Two (2) form tools (non-design-type) for nonconductive housings for QOMAC/MBC and MASC coil assemblies.

One (1) (non-design-type) holding fixture to position solar array panels, ejection guide tube, and miscellaneous hardware to plate during the assembly operations.

Satellite Systems Fabrication (Drawing 3026-2).-

Tooling/Shop Aids.

Miscellaneous shop aids will be fabricated as required.

Special Test Equipment (STE).

None required. (Major testing will be performed by L&T Engineering.) Manufacturing will only perform continuity checks, utilizing standard equipment to suit requirements.

Test Plan

Purpose.- The test plan presents the basic test philosophy and test requirements, and outlines the activities and test sequences necessary to satisfy those requirements.

Scope.- Initial sections of the Test Plan describe the test approach, test requirements, and the necessary test articles. The final sections provide brief descriptions of the actual tests along with facility and test equipment requirements.

Test Approach.- The test plan is designed to achieve maximum confidence with minimum cost consistent with the available budget. Development costs are minimized by selection of fully developed, previously qualified components. In addition, no NR acceptance or qualification tests are planned at the flight qualified component level. Instead, qualification and acceptance testing will be accomplished simultaneously on the completed flight article. Thus, costs are diminished primarily by careful component selection and minimizing the number of test articles; however, significant savings are also realized by eliminating redundant environmental and functional tests.

Purchased parts will be subjected to a functional test at the supplier facility prior to shipment. Receiving/Inspection at NR/Space Division will consist of visual inspection for identification and obvious damage during transportation.

Components and subsystems manufactured by NR/Space Division will be functionally tested following fabrication.

It should be noted that the concept of combining qualification and acceptance testing has been implemented successfully on four previous satellite programs; thus, it is felt that this approach provides the highest degree of confidence for the allowable time and budget.

Test Categories. - The tests described in this plan are divided into three categories: development, qualification/acceptance, and pre-launch.

Development Tests.- Developmental tests are defined as those tests performed to informal procedures and intended to empirically optimize or verify the design. These tests provide an early indication of problem areas difficult or impossible to determine through analysis.

Qualification/Acceptance (Q/A) Tests.- Q/A tests will be conducted to satisfy two primary objectives: The first is to establish design capability to satisfy functional performance requirements over the complete range of anticipated environments. Actual test conditions will be slightly more stringent than predicted environments; however, this will provide assurance that there are no design weaknesses and that there is adequate performance margin to allow for manufacturing tolerances and predicted environment uncertainties.

The second objective is to disclose workmanship defects and manufacturing tolerance accumulation to unacceptable levels. Q/A tests will be performed at the top assembly level; i.e., on the complete spacecraft, thus ensuring a flight article capable of performing all mission requirements.

Pre-Launch Tests. - Pre-launch tests will be conducted following shipment to the launch site but prior to installation on the boost vehicle. The objective of these tests will be to ensure no degradation due to transportation and provide full verification of functional performance, including alignment and calibration.

Test Requirements.-

Development Tests.- As previously mentioned, fully developed, qualified hardware is utilized wherever practicable; however, in some cases "off-the-shelf" components are not available. The following paragraphs summarize the planned development tests for each system.

Communications and Data Handling.- The sensor register assembly, data conditioner, and timer are new designs, and while each will consist of qualified components, it is planned to breadboard each item, perform functional tests, and limited environmental tests such as vibration, temperature and thermal vacuum to provide early confirmation of the soundness of packaging and functional performance. Upon completion of development tests, these items will receive a functional test and visual inspection and be stored for subsequent spares support.

Electrical Power.- It is planned to assemble a complete electrical power system with simulated spacecraft loads, and perform functional tests to verify system response over the anticipated load profile. A DC power supply will be substituted for the solar array during these tests. It should be noted that with the exception of batteries, flight components will be utilized for electrical system development tests.

Structure.- Development test plans for the spacecraft structure entail dynamic testing only to identify potential harmful resonance characteristics. Confirmation of static load characteristics will be accomplished through a combination of analysis and over-design.

The dynamic test structure will consist of the primary structural components including bracketry, the center bulkhead and simulated solar array structure. Dummy masses will be substituted for significant components to provide a valid simulation of inertial characteristics, i.e: c.g., and moment of inertia.

Dynamic testing will be performed with the spacecraft installed in the development canister model.

Canister and Ejection.- The basic ejection system has been utilized successfully on previous programs. However, due to the criticality of this function to the overall mission, it is planned to conduct ejection tests during the development period. The structural development spacecraft will be installed in the canister and ejected under simulated operational conditions to confirm the fundamental design objectives of ejection and spin initiation.

Qualification/Acceptance Tests.- These tests will verify that the spacecraft will perform as an integrated system and will meet the functional performance requirements during or after exposure to environmental conditions as severe or more severe than any conditions expected during the mission life. Prior to exposure to the various environments, the spacecraft will receive a comprehensive functional performance test. This will establish the performance baseline. The functional test will be repeated during or after exposure to the various environments depending upon its status in the mission sequence. If a component fails during the series of qualification testing, it may be replaced by a spare which has undergone equivalent testing. The impact of any such component failure on the qualification of the spacecraft will be evaluated at the time of failure. Redesign and or retest requirements will have to take into consideration the nature of the failure, the test history of the part, and the criticality of the failure.

Qualification/Acceptance tests will be performed on the flight spacecraft consisting entirely of flight configured components. However, on completion of qualification/acceptance testing, the batteries will be removed, and replaced with new batteries at an appropriate time prior to spacecraft installation in the booster.

The planned qualification/acceptance tests are listed below:

(1) Functional Performance

(2) Vibration, Acoustic & Shock

(3) Temperature

(4) Thermal Balance & Thermal Vacuum

(5) Electromagnetic Interference

(6) Spin & Balance

(7) Weight, C/G, Moment of Inertia

(8) Magnetic Field Measurement

(9) Antenna Radiation Patterns

(10) TT&C Compatibility

The planned tests are consistent with the NASA General Environment Test Specification, S-320-G-1, with the following exceptions.

Humidity tests will not be performed. The spacecraft will be assembled in a controlled environment, and subsequent storage or shipment will be accomplished with the spacecraft installed in the pressurized canister. In addition, the lack of pyrogens eliminates pyrotechnic test requirements.

The majority of qualification/acceptance tests will be performed in the NR/SD, Downey environmental labs; however, it is planned to accomplish spin and balancing tests at an outside facility in the LosAngeles area. Antenna pattern tests will be performed on the NR/SD, El Toro antenna test range.

Functional Performance Tests.- Following each environmental check a functional test or portions thereof, will be performed to verify proper system operation. The spacecraft will be subjected to an operational sequence of ejection, antenna deployment, sequential application of electrical loads through the command system, and verification of systems operation through the telemetry link.

During functional tests, data readout and evaluation will be accomplished by coupling the telemetry signal into a receiver/decommutator, and routing the decommutated signals to D/A converters. The converter outputs will be patched to individual scaled strip charts to permit real time parameter readout.

System commands will be initiated from a test switch panel. Individual switch outputs will be routed to a tone encoder whose output is connected to a modulator/transmitter. The transmitter output will be coupled to the spacecraft antenna.

Solar cell panels will not be illuminated by a solar simulator during functional tests; consequently, the solar cell function will be provided by a DC power supply connected to the solar power bus.

Following ejection and antenna deployment, all functional parameters will be noted to be in the proper state; e.g., bus voltages, currents and switch status.

Telemetry system performance will then be verified by energizing appropriate power busses and measuring parameters such as carrier deviation, bit rate and synch words. Following severe environment tests, all functional checks will be preceded by VSWR tests on the RF system. On completion of telemetry verification, power will be applied to the attitude control components. The magnetic torque

control will be stepped through its full range control and coil currents will be monitored for proper values. Finally, all remaining loads will be applied and each sensor pulsed with an uncalibrated source to provide a gross indication of sensor operation. During full load conditions electrical power system checks will be completed by confirming bus voltage and current values, and regulation capability.

After completing all system checks, bus loads will be sequentially removed and the power system will be commanded to a charging mode to recharge the batteries.

On completion of systems tests sensor alignments will be checked. Alignment will be verified for each sensor with respect to the spacecraft axes. This test will be accomplished by the use of a theodolite, special targets on the sensors, and reference marks on the spacecraft. The final functional test will verify solar array integrity. This test will require determination of the approximate level of voltage and current generated when a known number of array cells are illuminated. This will be accomplished by mounting the spacecraft on a spin table and connecting a load to the solar power bus (the spacecraft load will be decoupled from the solar power bus) by the utilization of spin table slip rings. An uncalibrated illumination source, containing no ultraviolet radiation, will be impinged on a series parallel group of cells and the spacecraft will be rotated. Cell output voltage and current levels will be recorded on a continuous strip chart recorder. The resulting traces will consist of unidirectional pulses. An unvarying pulse amplitude for both cell parameters will verify functional performance of each series parallel cell group.

Vibration and Acoustic Dynamic Tests.- The objective of the vibration-acoustic tests is to verify that the spacecraft will not suffer detrimental effects during launch operations. A complete functional performance verification test will have been made on the spacecraft prior to initiation of vibration testing. The dynamic environment simulating transient vibration, engine ignition, and shutdown will consist of sinusoidal vibration in three axis and a vibro/acoustic test. During these tests, all cycled loads will be off, consistent with the spacecraft configuration during boost.

Test instrumentation will consist of accelerometers. Data will be recorded on magnetic tape and reduced to acceleration vs. frequency plots. Following vibration tests, the spacecraft will be subjected to acoustical noise simulating the launch environment.

During the acoustic test, instrumentation will consist of accelerometers, microphones, and strain gages. The sound pressure level spectrum will be controlled by microphones located in selected positions around the vehicle. Data will be recorded on magnetic tape and reduced to 1/3 octave data analyses plots.

A functional performance test and visual examination of the vehicle will be performed after exposure to the dynamic environment to verify that no degradation of the structure and systems has occurred.

Temperature.- A temperature test will be performed to ensure that the spacecraft can withstand the effects of base heating during second stage boost. The spacecraft will be installed in the canister and subjected to the maximum anticipated temperature environment for the entire boost interval. During this test, all cycled loads will be deenergized. Upon test completion a functional test will be performed to verify proper systems operation.

Thermal Vacuum Tests.- Thermal vacuum testing will be performed to verify systems performance in the operational environment and to prove the spacecraft thermal control design. During the simulated orbital thermal vacuum conditions, the spacecraft's systems will be operated to verify functional performance.

In considering the possible alternatives for producing the required simulated solar thermal environment, it was determined that a cost savings could be realized by maintaining the spacecraft stationary rather than spinning it during the thermal vacuum testing. This precludes the use of a collimated solar simulator. Infrared tubular quartz heating lamps provide the flexibility to apply simulated solar energy to the entire spacecraft body. The infrared lamp array will be divided into several zones of control to accurately produce the specified temperature distribution over the spacecraft body.

No thermal development test spacecraft vehicle is planned, since the costs for simulating the thermal characteristics of all of the spacecraft components becomes prohibitively high when weighed against the value and timeliness of the results. The baseline thermal analysis and the thermal control techniques which were used to develop this spacecraft design were based on previous experience and testing results.

The thermal vacuum qualification testing of the spacecraft will be performed in the SD 16' diameter by 18' "Belljar" vacuum chamber, which will be maintained at a pressure of 1×10^{-5} torr or less during all thermal balance testing. Thermal environment will be supplied by liquid nitrogen cold shrouds with attached

infrared heating lamps. The heating lamps are regulated from a system of ignitron power controllers which utilize automatic temperature control and will maintain a constant or programmed temperature profile on the test article. Automatic shut down occurs in the event that critical components reach their maximum allowable operating temperature. All spacecraft-to-support structure attachments as well as cable harnesses will be provided with thermostatically controlled heating and cooling systems to offset potential thermal unbalance.

Continuous monitoring of the vacuum chamber pressure is assured through the use of an automatic ranging vacuum gauging system. The test article will be instrumented with 30 gauge copper-constantan thermocouples at flight sensor locations and other critical points indicated by analysis and previous component and subsystem testing. Temperatures will be recorded by an automatic digital system which provides for rapid data reduction.

Electromagnetic Compatibility (EMC) Test.- The purpose of electromagnetic compatibility test is to determine whether the function of any spacecraft subsystem is disturbed by the operation of any other subsystem through the medium of electromagnetic coupling.

The spacecrcraft will be placed in the NR/SD, Downey facility screen room to demonstrate electromagnetic compatibility between all subsystems. The spacecraft will be in the in-flight configuration.

Radiated interference tests will be conducted by operating the spacecraft in the orbital mode of transmission while scanning the applicable frequency spectrum. Test data will include a plot of radiation level vs. frequency. Radiated susceptibility tests shall be performed by exposing the spacecraft to the orbital electromagnetic interference levels. Specific attention will be given to potential effects on the attitude control coils during this test.

Mass Properties Determination and Spin Balance Verification.- There are two major objectives to be achieved in this test. The first is to determine the actual mass properties of the satellite and compare them to the calculated mass properties. Mass properties that will be obtained are as follows:

(a) Weight

(b) Center of Gravity

(c) Moment of Inertia

(d) Products of Inertia

(e) Principle Axes

The second objective is to spin balance the vehicle to ensure that dynamic unbalance conditions are reduced to or are less than the specified maximum allowable values.

Static balance will be established initially along with weight and center of gravity. Next, the moment of inertia and products of inertia will be determined and finally, the spacecraft will be dynamically balanced.

Center of gravity location will be obtained with the mass properties table by measuring the unbalance moment in each plane or axis. Based upon these results, the center of gravity location will be calculated. A special fixture that will allow the assembled spacecraft to be oriented on its side as well as in the vertical position will be required for the various mass properties measurements. Adjustments of the spacecraft center of gravity will be accomplished as required to align the geometric center and the center of gravity. Moment of inertia measurements in three mutually perpendicular axes will be determined by utilizing the period of free swing associated with the torsional pendulum feature built into the mass properties table.

The complete spacecraft will then be subjected to a spin test. The spin rate will be incrementally increased to approximately 200 rpm. Geometric concentric measurements will be made of the spacecraft in its spin axis to verify that the value is within design requirements. Following spin and dynamic balance tests, a complete functional performance test will be performed on the spacecraft and the results compared to the baseline test.

Antenna Radiation Pattern Tests.- The purpose of antenna pattern tests is to verify antenna gain characteristics, and that the antenna mounting configuration provides adequate coverage for command reception and telemetry transmission. Two sets of radiation patterns will be measured, one set at the center frequency of the telemetry band, and one set at the center frequency of the command band. Each set will consist of 360° azimuth cuts measured about the spin axis at 10° intervals.

Following pattern measurements, antenna gain will be calculated. Pattern tests will be conducted on the NR/SD, El Toro antenna test range utilizing the flight antenna mounted on the dynamic test structure. Upon test completion, the antenna will be installed on the flight article.

Magnetic Field Measurements.- The spacecraft will be subjected to a magnetic field measurement to determine the permanent, induced, and stray magnetic moments of the spacecraft. This test will determine the moment orientation and magnitude (with respect to the local geomagnetic field) to allow prediction of the overall effect on spacecraft attitude caused by magnetic torque. The test will be performed by positioning the spacecraft in a non-magnetic fixture and making appropriate measurements with a magnetometer.

Following determination of the natural magnetic moment, it is planned to evaluate magnetic torque induced by the attitude control system. Magnitude and orientation of magnetic moment will be measured at each discrete level of the control system, and the resultant torque will be calculated. These tests will be performed at the NR/SD, Downey facility.

Telemetry, Tracking and Command Compatibility Test.- The final Q/A test to be performed will be the TT&C compatibility test between the spacecraft and the Space Tracking and Data Network (STADAN). It is planned to conduct compatibility tests in the STADAN test van, either in the Los Angeles area or after arrival at WTR. The objective of the compatibility test is to establish that the spacecraft can in fact achieve complete information exchanges with operational STADAN stations for telemetry, tracking, and command purposes. In addition, such a test

will provide advance magnetic tapes, strip charts, and other data suitable for verifying that the resulting STADAN outputs are compatible with NASA data-handling equipment.

Compatibility tests will be performed to the procedures outlined in the NASA-GSFC STADAN-Spacecraft Compatibility Test Procedures Document, X-531-69-27(A). A summary of significant tests is presented below.

Spacecraft transmission tests will be accomplished first where fundamental measurements of frequency, phase stability and power output are made. Next, the modulated signal will be tested for proper operation into the receiving phase-lock circuitry and discriminator. Thresholds (loss-of-lock points) will be determined for the spacecraft signal.

On completion of spacecraft transmission tests, commands will be initiated from the STADAN command equipment to verify proper spacecraft response to all commands. During this test the telemetry signal will be recorded for command system evaluation.

Pre-Launch Tests.- Pre-launch testing will consist primarily of functional performance tests at the system level, flight battery preparations, and battery charge and status monitoring following installation on the booster.

It is planned to transport the spacecraft and associated test equipment to WTR approximately 30 days prior to launch, (T-30 days) as shown in Figure 173. On arrival the cannister will be fit checked with the 2nd stage booster, and the spacecraft subjected to a comprehensive functional test similar to that described in the Q/A test section. The spacecraft must be installed in the 2nd stage booster at approximately T-21 days, therefore flight-batteries will be energized, subjected to load tests and installed in the spacecraft at T-22 days. Following battery installation the spacecraft

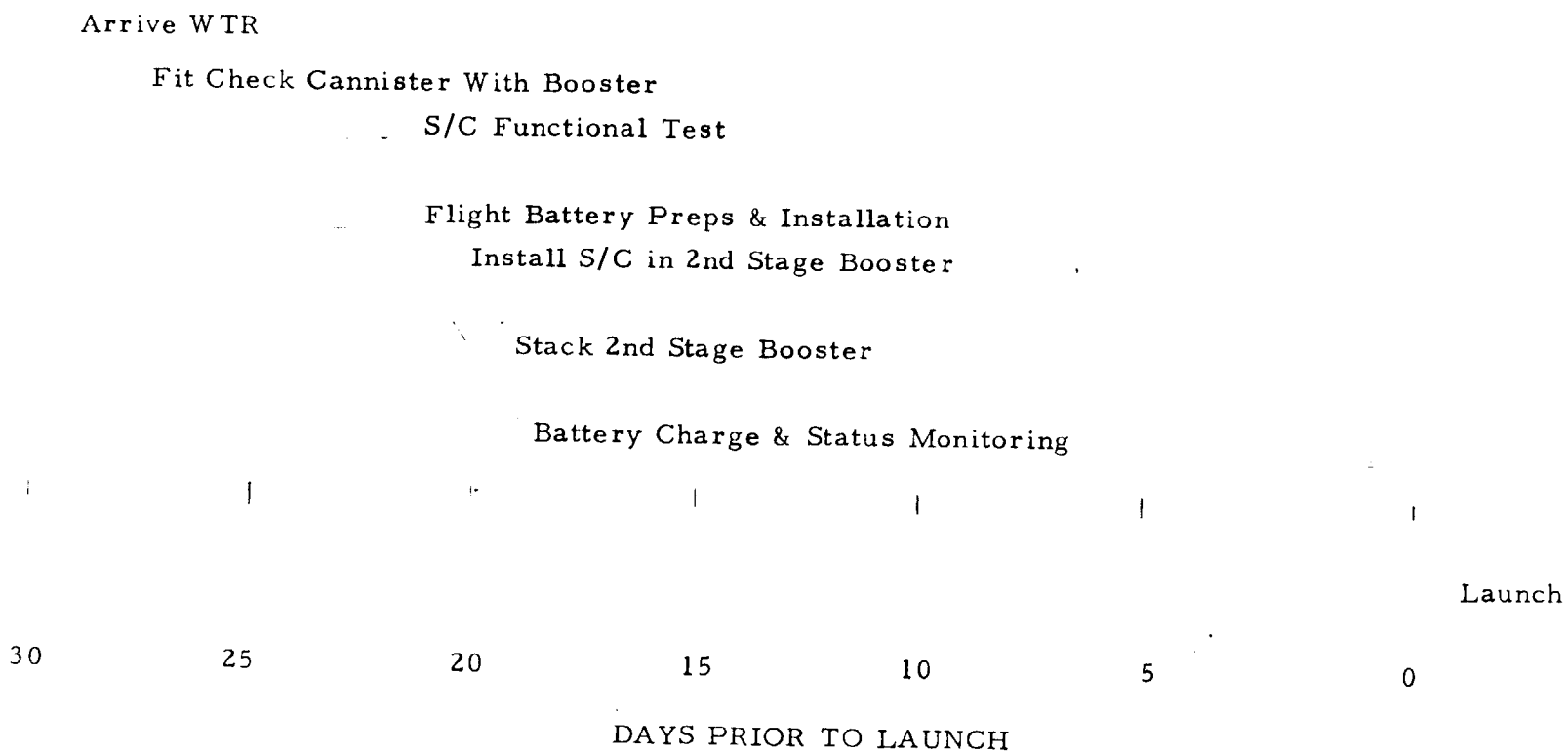

Figure 173 Pre Launch Test Operations Schedule

Space Division
North American Rockwell

will be closed out and installed in the cannister for subsequent installation on the booster. The spacecraft installation on the booster is located next to the thrust chamber, approximately 30° radially from the aft skirt access hatch. In reviewing the mounting configuration it was decided that no physical access to the spacecraft can be achieved after the booster is stacked. Therefore, it is planned to provide hardwire access from the spacecraft to the access door. This will consist of a cable attached to the cannister feed through connector to permit battery charge and charge status monitoring. Therefore, during final launch operations it will be necessary to provide a final charge and remove the cable prior to closing out the aft skirt hatch.

If such an operation cannot be accomplished, an electrical interface must be established between the spacecraft and the booster to permit battery charging and monitoring functions.

Configuration Management Plan

Organization.- The Configuration Management organization will report to the Program Manager but, in order to be cost effective, will be under the control of Division Configuration Management. Personnel responsible for Program Configuration Management will be permanently assigned but, in order to keep costs down, will not charge to the program on a full-time basis. However, support will be supplied as needed to fulfill the requirements of the program. All of the main elements of CM will be in effect, but requirements will be selected specifically to support the approach (philosophy) for a low-cost product. For simplicity and reduction in costs, a Configuration Management Requirements Plan, per se, will be non-existent. However, critical requirements will be identified in CMRP format as designated by the Space Division Configuration Management Manual. Requirements will be deleted, tailored, etc. to fit the philosophy of a low-cost approach for program management.

Identification. -

Specifications.- DCM proposes that only one CEI specification be prepared to control the program. This specification would be one part in nature and would specify the design and performance requirements as well as those testing parameters necessary to support the requirements. The concept to be utilized in the CEI will be basically derived from the contract statement of work and modified as necessary. Since basically all hardware or equipment to be utilized on the subject program is either of a qualified nature or off-the-shelf type equipment, specifications of a lower level may not be needed.

However, as of this date, some six items have been identified as new development-type equipment and will be controlled at a much lower spec level, with any critical components being controlled by a development-type specification for a prime item. Normal identification procedures will be used for each of the specifications pending their type and nature. By reducing the quantity of program specifications, maintenance will be reduced and cost savings will be realized.

Drawings.- The quantity of drawings to support this program are considered to be small (approximately 50) and their identification will be to current DRM and Engineering Operations Manual procedures and shall follow through a modified release cycle. DCM will control specification and drawing release with close coordination existing between Engineering and the DCM organization. This is in lieu of two organizations having overlapping responsibilities which would create additional costs to the program.

Control.- Control activity as normally known within NR/SD will be non-existent since there will be no formal CCB or change management system, as such. DCM proposes that once basic release has been made on specifications and drawings, that no additional engineering of a formal nature will be generated on these documents. Should any changes be necessary, they will be handled by redline changes to the individual drawing/specifications when approved by the Program Manager and Engineering. Furthermore, it will be necessary to maintain a master redlined copy of each specification and production drawing. All NR/SD-initiated changes will be considered in scope to the contract with no ECP activity being initiated except when customer-initiated requirements modify the basic contract. Should customer changes originate, they will be

handled via the normal ECP route with DCM providing all control and coordination with functional departments involved. The incorporation of all redline changes into a specification or drawing will not be accomplished unless so directed by customer. Should this condition occur, contract price will be subject to re-negotiation.

Accounting.- A simplified method of accounting will be utilized whereby a direct correlation between the as-built to the as-designed configuration will be verified. There will be no formal acceptance data package at time of customer acceptance. However, a complete set of drawings plus delta redline changes and specifications plus delta redline changes will be available along with an indentured parts list for presentation to the customer. Inspection buy-off will be made at the subassembly and assembly level, with inspection stamps of approval being placed on the master set of drawings and/or specifications, thus verifying the product configuration.

Assurance.- There will be no formal assurance conducted by Configuration Management during the life cycle of the proposed program.

Subcontractor Surveillance.- Subcontractor surveillance will be non-existent from the Configuration Management viewpoint and will be left entirely up to the Material, Quality and Engineering divisions to assure that each subcontracted part or assembly complies with the fabrication, inspection and test requirements necessary to support their next assembly. Where practical or possible, the subcontractor specifications will be utilized for final acceptance since no subcontractor PDR or CDR is expected.

Quality and Reliability Assurance Plan

The Space Division's Quality and Reliability Assurance organization maintains an effective and timely quality system, planned and developed in conjunction with all other functions (Fig. 174). This quality system will be tailored to meet the needs and requirements of the UV and MW Horizon Sensor Satellite experiment and for the successful accomplishment of the program objectives at a minimum cost.

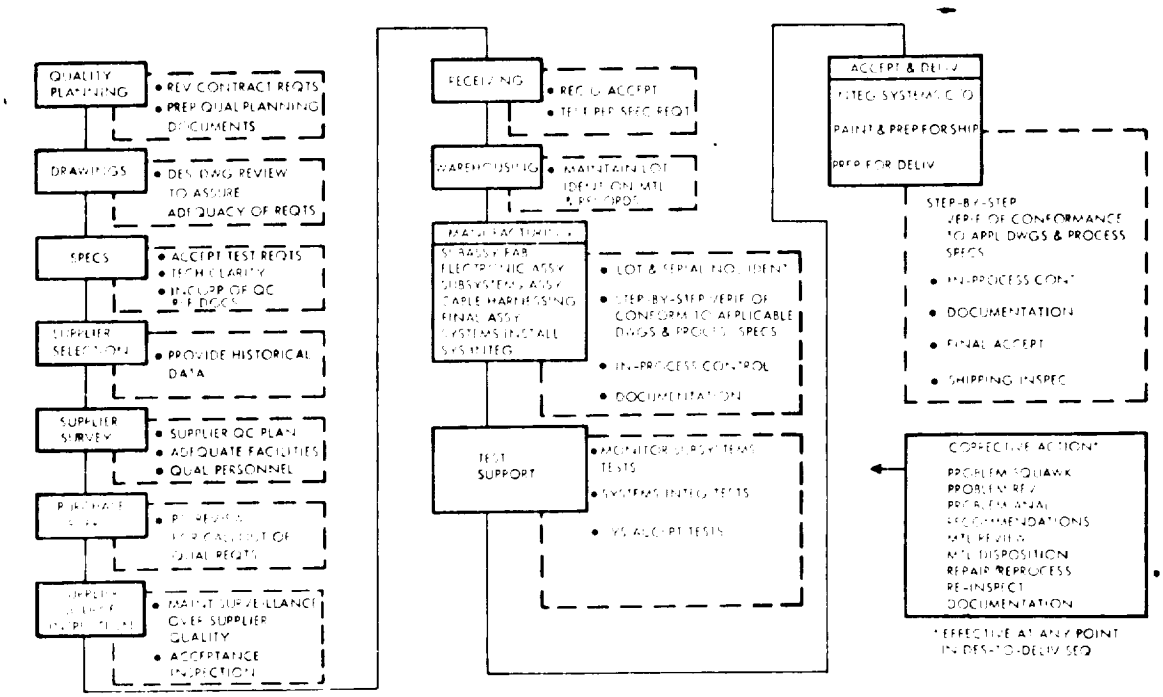

Figure 174 -Major Quality Assurance Functions

The Space Division is currently engaged in performance (50% complete) of an operation of similiar scope (Flying Lunar Excursion Experimental Plat-

form program for NASA/LRC), where new and flexible systems have been implemented towards achieving program contract and schedule requirements in an expeditious manner, while assuring that quality is maintained.

Considerable savings in both schedule and cost have been realized in the areas of (1) procurement planning (2) purchase order requirements (3) receiving inspection (4) drawing control, including drawing release and change control (5) test program documentation and (6) nonconforming material processing, including Material Review Board actions. These systems will be utilized for the UV/MW Sensor Satellite Program.

Phase C - Design.-

During this phase, over-all program review, design/specification review, procurement planning, and PDR participation will be performed by the assigned Quality Assurance Program Administrator in conformance with requirements of the program work breakdown structure, Phase C-Design. Functions of particular concern will be quality program management, system engineering and integration, and spacecraft design.

Phase D - Development/Operations.-

A quality assurance plan will be developed which will establish the specific responsibilities of Quality & Reliability Assurance for verifying that customer requirements have been satisfied and that deliverable materials are acceptable under the terms of the contract.

Requirements and Tasks.- The plan will include the following significant tasks:

1. Quality Management
2. Design and Development Control
3. Procurement Quality Control
4. Fabrication Quality Control
5. Nonconformance Control
6. Calibration and Standards
7. Acceptance and Delivery
8. Test Support
9. Documentation
10. Launch Support

Quality Management.- The Quality and Reliability Assurance organization maintains a system, which is planned and implemented in conjunction with other concerned functions, to assure quality requirements are determined and satisfied. Management of the UV/MW Horizon Sensor Satellite Program quality activities will be administrated through a program-type organization with the Program Quality Administrator reporting to the UV/MW Program Manager for program direction, but functionally responsible to the Quality & Reliability Assurance Manager.

Design & Development Control.- A system of controlled prints will be implemented to expedite program performance while maintaining drawing control. A complete set of released assembly drawings will be furnished

to the customer upon delivery of the satellite spacecraft.

Procurement Quality Control.- Quality level requirements for all incoming items will be assured by procurement document review. Identification and damage inspection will be imposed on all non-critical items. A requirement for supplier certification in accordance with procurement terms and conditions defined by Engineering will be imposed for all critical items. Items that require source inspection will be specified on the purchase order by the Quality Assurance Administrator. Vendors must certify compliance with the purchase order requirements. Received items will be stored in a controlled stockroom located in the manufacturing area.

Fabrication Quality Control.- Inspection will be made of all required tooling, detail parts, and assemblies for all hardware, including test operations, ensuring conformance to engineering drawings and applicable specifications.

Nonconformance Control.- Nonconforming items of minor nature which do not affect product function or structural integrity may be dispositioned for "use as is" by Program Engineering. The use of these items requires the signature approval of the Program Manager and the Program Quality Administrator. Copies of squawk sheets will be forwarded immediately to the appropriate NASA office for review and approval/disapproval action.

All significant items determined to be discrepant by the Program Manager or the Quality Administrator, and equipment failures or test failures will be documented and processed by the Quality Administrator for Material

Review Board Action.

Calibration and Standards.- Test specifications will be reviewed, and all test equipment calibration verified by inspection.

Acceptance and Delivery.- Each shipment shall include evidence that final acceptance was accomplished prior to shipment. This is to be documented on Government Form DD-250. Prior to shipment, each packing sheet DD-250, will be verified for contractual quality requirements by the Quality Administrator.

Test Support.- The program test plan will be reviewed by the Quality Administrator prior to implementation to verify the adequacy of test tolerances and quality criteria.

Inspection will verify that tests are conducted in accordance with established specifications and procedures during test performance and documented in the equipment logbooks.

Documentation.- Records will be maintained of in-process inspections, nonconformance controlled material/parts, failures, and their causes, and of all test activities. Data will be furnished to the customer at the time of delivery as negotiated for in the contract.

Launch Support.- Quality & Reliability Assurance support will be provided during pre-launch and launch operations for receiving inspection, check-out, and verification of configuration prior to vehicle launch.

Facilities Management Plan

The purpose of the Facilities Plan is to identify plant and related equipment requirements, and to describe the Facilities and Industrial Engineering support to the design, manufacture, and test of the UV/MW Horizon Sensor Experiment Satellite Program.

Scope. - The scope of activities will include the identification of facility requirements for design, manufacturing, testing, launch operation, ground operations, information management and support facilities. The plan will list the Government and Contractor dependent facilities required. Facility and equipment requirements established by Manufacturing and Test Operations will be analyzed to provide optimum results and maximum use of available facilities and equipment.

Approach. - The approach is to emphasize the application of facilities/industrial engineering techniques as an integral part of technical design, subsystem trade-off, and ground operations planning activities. Total resource requirements for subsequent phases of the program will be identified as early as is practical. Facilities-sensitive decisions will reflect the minimum new and/or modifications/augmentations necessary, as shown in Figure 175.

Task Summary. - The facility/industrial engineering analysis will provide data that will permit appraisal of program requirements, baseline documents, design, etc., as well as an evaluation of the man-machine facility interfaces with major program function and supporting contractors. Significant aspects of this evaluation include: producibility, work content, assembly complexity, handling, transportability, and safety.

F&IE PROPERTY MANAGEMENT SYSTEMS

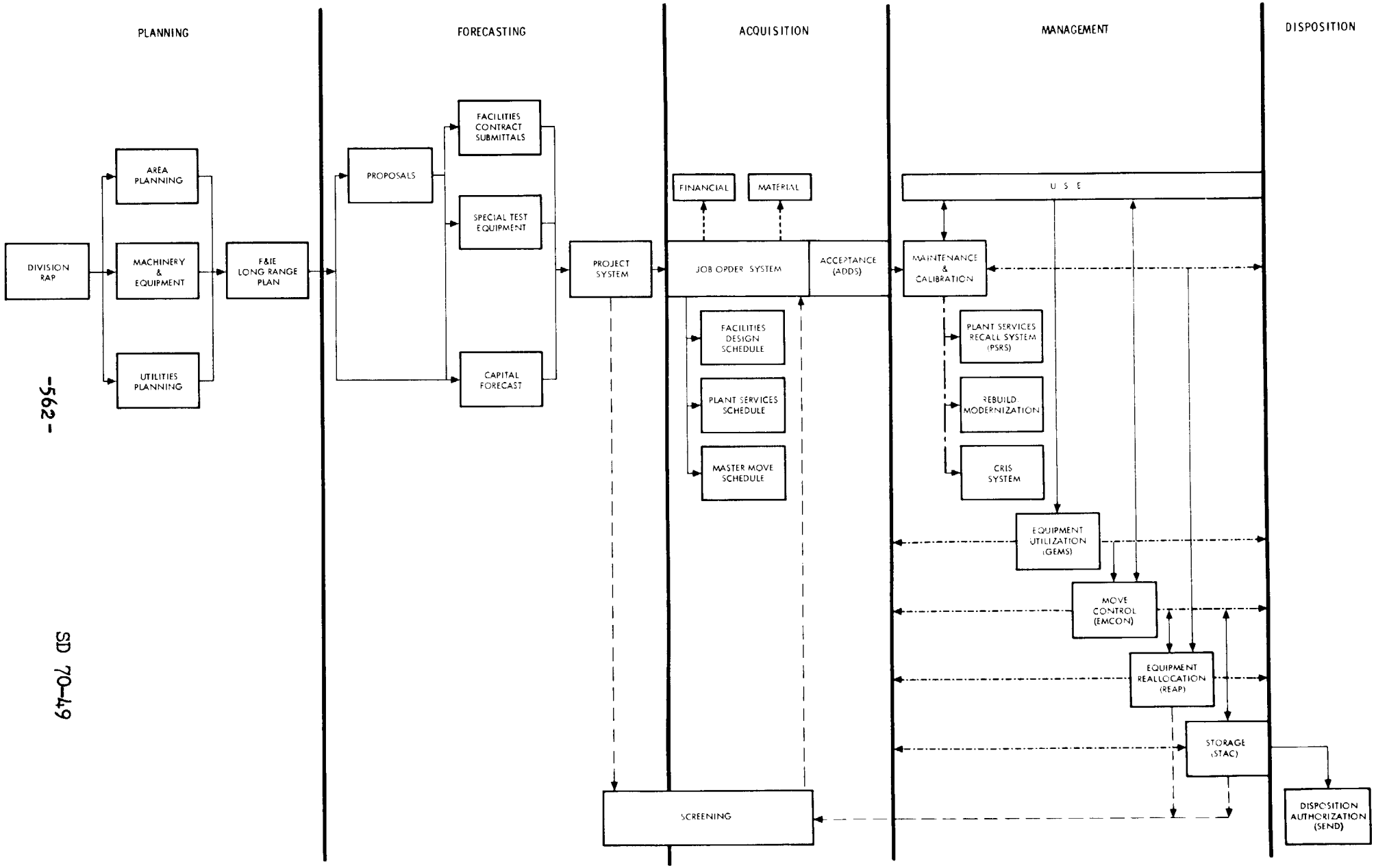

Figure 175

Ground Support Equipment (GSE) Requirements

GSE is defined as that equipment required to support functional performance tests during development, qualification/acceptance, and pre-launch testing. Environmental test equipment is not included.

A preliminary list of GSE is shown in Table 46. With the exception of handling fixtures, shipping containers and the command test panel, the required equipment is existing laboratory equipment in current NR/SD inventories. It is exptected that customer equipment inventories might also be utilized, if required.

Handling fixtures will be required to support magnetic moment measurements, spin-balance and vibration tests. In addition, a fixture will be utilized to support the spacecraft during functional tests. Where feasible, multipurpose fixtures will be utilized.

Shipping containers designed to commercial standards will be required to transport the spacecraft and its associated support equipment to WTR. A minimum of test equipment will be shipped (discussed in the Logistics requirements section). The WTR central equipment pool will be utilized to the greatest extent possible.

A command test panel will be required during performance functional tests. This panel will permit initiation of commands through the tone encoder. The test panel will consist of a single panel with ON/OFF toggle switches for each command. A wire harness will connect switch outputs to the appropriate terminals on the tone encoder. Power will be provided by a rack mounted supply.

Table 46 GSE Requirements List

	Model No. or Equiv.
1. Audio Oscillator	HP 200 CD
2. Pulse Generator	HP 222 A
3. VHF Signal Generator	HP 608 E/F
4. Dual-Trace Oscilloscope	132 A HP (Tektronics)
5. Electronic Counter	HP 5245
6. Frequency Converter	HP 5253 B
7. Receiver Nems Clarke (PM Rcvr)	
8. Receiver Plug IN (T/M Band 136-138 MHz)	
9. Spectrum Analyzer	
10. RF Power Meter	HP 432 A
11. Thermistor Mount	HP 478 A
12. Colorimetric Power Meter	HP 434 A
13. Directional Coupler	HP 774
14. Variable Coaxial Attenuator	HP 355 C/D
15. Diplexer	136/144
16. SWR Indicator	HP 415 E
17. Magnetic Moment Sensor	
18. Portable Recorder (3)	HP 7100 B
19. Magnetic Tape Recorder	Ampex FR 1400
20. Command Test Set (Tone Code)	
21. Command Test Switch Panel	NR Make Item
22. Power Supply (3)	HP 6433 B

23. Digital Voltmeter — HP 3430 A

24. VOM — Simpson

25. Battery Charger

26. Handling Fixtures

27. Shipping Containers

28. N_2 Purge Bottle & Cart

29. Autocollimator, Theodolite, Optical Flats

Logistics Requirements.-

Test operations for the UV/MW program necessitates logistics support in three areas: Documentation support, supply support (spares and usage materials), and transportation.

Documentation.-

Documentation support will entail the preparation and maintenance of an operations document which will include the installation drawings, schematics, and procedures necessary to process the spacecraft through the test phase.

Supply Support.-

Supply support will include that effort necessary to provide spares and usage materials as required for test operations. In an effort to provide adequate spares support and maintain minimum costs, the following spares criteria was established:

(a) All development test articles will be given a detailed visual inspection and functional test following development testing and stored for spares support.

(b) New designs with long procurement times will be spared.

(c) Proven designs of relatively high cost will not be spared; if such an item fails, it will be returned to the supplier for repair.

The planned spares list is shown in Table 47 along with the number of flight and development items. A complete usage materials list will be established following design completion, however it is planned to utilize excess material to existing NASA contracts wherever possible. In addition, a usage spares list will be submitted for review with respect to existing customer inventories.

Transportation.-

Following completion of tests at the NR/SD facility, the spacecraft and its support equipment will be packaged for shipment to the Western Test Range -- it is expected that shipment will be arranged through commercial transportation facilities. The feasibility of using Government Bill of Lading will be investigated by the NR/SD Transportation Department and coordinated with the appropriate customer representatives. It is planned to transport a minimum of laboratory-type equipment to WTR; arrangements will be made to access the WTR central equipment pool in every case possible. In addition, the WTR calibration facilities will be utilized to support test equipment requirements as well as flight transducer and sensors where applicable.

TABLE 47. UV-MW SENSOR EXPERIMENT SPARES LIST

NOMENCLATURE	QTY. REQUIRED		
	DEVEL.	FLIGHT ARTICLE	SPARE
Antenna	-0-	-1-	-1-
Diplexer	-0-	-1-	-0-
Pre-Modulation Filter	-0-	-1-	-1-
PCM Encoder	-0-	-1-	-0-
Transmitter	-0-	-1-	-0-
Sensor Register Assy.	-1-	-1-	-0-
Data Conditioner	-1-	-1-	-0-
Timer	-1-	-1-	-0-
Command Receiver	-0-	-1-	-0-
Command Decoder	-0-	-1-	-0-
Command Distributor	-1-	-1-	-0-
QOMAC & MBC Coil Assy.	-1-	-1-	-0-
MASC Coil	-1-	-1-	-0-
Nutation Damper	-1-	-1-	-0-
Despin Yo-Yo	-1-	-1-	-0-
MBC Switch	-1-	-1-	-0-
Electronic Controller	-1-	-1-	-0-
Fine Sun Sensor	-1-	-1-	-0-
IR Sensor	-0-	-2-	-1-
Coarse Sun Sensor	-0-	-1-	-0-
Coarse Sun Sensor Register	-0-	-1-	-0-

TABLE 47. UV-MW SENSOR EXPERIMENT SPARES LIST (cont'd)

NOMENCLATURE	QTY. REQUIRED		
	DEVEL.	FLIGHT ARTICLE	SPARE
Battery Halves	-2-	-2-	-1-
Battery Charger	-1-	-1-	-0-
Solar Cell Panel (8 panels/SC)	-1-	-8-	-0-
DC-DC Converter	-2-	-2-	-0-
Power Distribution Assy.	-1-	-1-	-0-
Harness Assy.	-1-	-1-	-0-
Battery Status Monitor	-1-	-1-	-0-
Canister Assy.	-1-	-1-	-0-
Structure Assy.	-1-	-1-	-0-
UV Sensor (GFE)	-0-	-1-	-0-
MW Sensor (GFE)	-0-	-1-	-0-

PROGRAM COST ESTIMATES

A budgetary and planning (B&P) cost estimate for the C&D phases of the UV/MW satellite program has been prepared based on the program management philosophy presented in this Program Development Plan. In order to be as accurate as possible within the short time span available, the NR method of "grass roots" estimating was used.

"Grass Roots" - Each estimating functional organization that would be involved in the subsequent phases of the program estimated their contribution to the program based on functional work package tasks defined under the Work Breakdown Structure. The detail estimates were prepared by first-line supervisory personnel, reviewed by successive levels of management, and ultimately reviewed and approved by the Spacecraft Project Manager.

Preliminary equipment specifications were prepared and furnished to the Purchasing Department who, in turn, obtained estimates for subcontract effort per specification requirements from prospective subcontractors and suppliers. The Hardware Utilization List defines the major components and required quantities.

Labor estimates are categorized by discipline, i.e., Engineering, Testing, Manufacturing, etc. Current 1970 dollar values were used.

Cost Estimating Ground Rules:

The cost estimate study covers a flight spacecraft program consisting of the following:

(1) One Flight Spacecraft (Delta Piggyback Launch)

(2) One Engineering Model

(3) Operational Software for Attitude Control Only

(4) GSE and STE as required

(5) Launch Support Services

(6) Facilities

Not included as part of the cost study are the following:

(1) Fee or Profit

(2) Flight Operations Support

(3) STADAN Support

(4) Attitude Determination Software

(5) Launch Vehicle Cost

(Launch vehicle contractor integration costs are estimated)

(6) GFE Experimental Sensors (UV and MW)

The program estimates given are separated into NASA phases C(Design) and D (Development).

The estimates were made based on the assumption that minimum program software support (Configuration Management, Quality Assurance, Data Management, etc.) will be required. Should waivers from the standard NASA requirements in these areas not be relaxed, a cost increment will be required. It is felt by NR that for a program of this type the plans outlined in this Program Development Plan are completely adequate to assure mission success without adding unnecessary costs.

Cost Estimate:

Results of the cost study using the above groundrules indicate a program cost as follows:

Phase C	$330,000
Phase D	$1,480,000
Total Spacecraft	$1,810,000
Launch Integration	$200,000 (Delta Contractor)
Spacecraft & Launch Integration	$2,010,000

NR has a high confidence in the Phase C estimates. The Phase D estimate, however, does include some non-firm vendor quotes.

The ordering of certain long lead time items (especially the fine sun sensor and the IR horizon sensors) early during Phase C is a requirements in order to meet the program schedule. Potential supplier sources have quoted delivery estimates of eight months for these items.

The launch integration cost of $200K was a verbal estimate by McDonnell-Douglas Corp. (Delta Contractor) personnel and cannot be considered firm.

Launch on a Scout or Thor/Burner II increases the launch costs to $1.4M. The cannister for the reference concept is not required, and therefore represents a spacecraft cost decrease of about $100,000.

Of the $1.81M spacecraft program cost approximately 30 percent is for material and spares and 44 percent is for engineering and development. The total management and management software costs have been held to less than 7 percent.

BIBLIOGRAPHY

- Tiros IX Final Engineering Report - Vol. I, dated August 31, 1965, Radio Corporation of America, AED-R-2568.
- TIROS IX Meteorological Satellite System Final Engineering Report, Radio Corp. of America, AED-R-2568, August 31, 1965.
- Attitude Handbook for the TIROS IX Meteorological Satellite System, Radio Corp. of America, AED-M-2036, October 7, 1964.
- Bandeen, W. and Manger, W. P., Angular Motions of the Spin Axis of the TIROS I Meteorological Satellite Due to Magnetic and Gravitational Torques, Journal of Geophysical Research, September 1960.
- Hecht, E. and Manger, W. P., Magnetic Attitude Control of the TIROS Satellites, Torques and Attitude Sensing, S. F. Singer, Editor, Academic Press, 1961.
- Wilson, R. H. Jr., Magnetic Damping of Satellite 1958 Beta 2, Journal of Science, Vol. 130, p. 791, 1959.
- Mobley, F. F., Attitude Control System for the Atmosphere Explorer-B Satellite, AIAA Paper No. 65-432, AIAA 2nd Annual Meeting, July 1965.
- Brown, R. D., A Magnetic-Inertial Attitude Control System, 12th Annual East Coast Conference on Aerospace and Navigational Electronics, IEEE, October 1965.
- Fischell, R. E., Spin Control for Earth Satellites, APL Technical Digest, Vol. 5, No. 1, September-October 1965.

- Tossman, B. E., Resonance Technique for Measurement of Satellite-Magnetic Dipole Moment, Proceedings of Magnetics Workshop, JPL Technical Memo. No. 33-216, p. 125, April 1965.
- Newkirk, H. L., Haseltine, R. R., and Pratt, A. V., Stability of Rotating Space Vehicles, Proceedings of the IRE, Vol. 48, p. 943, April 1960.
- Haseltine, W. R., Nutation Damping Rates for a Spinning Satellite, Aerospace Engineering, p. 10, March 1962.
- Schnapf, Abraham, The TIROS Global System, N. Y. Academy of Sciences, January 1965.
- Manger, Warren P., Attitude Control for the TIROS Weather Satellites, IFAC Symposium on Automatic Control in the Peaceful Uses of SPACE, June 1965.
- Schnapf, Abraham, The Performance of the TIROS IX Wheel Satellite, SVI International Astronautical Congress, Athens, Greece, September 1965.
- Hecht, E., and Manger, W. P., Magnetic Attitude Control of TIROS Satellites, American Astronautical Society, Paper No. 62-44, March 1962.
- Nidey, R. A., Gravitational Torque on a Satellite of Arbitrary Shape, ARS, February 1960.
- Rosner, Q. E., and Manger, W. P., Spin Axis Motion of TIROS I Meteorological Satellite Caused by Magnetic, Gravitational, and Eddy Current Torque, TIROS I Post-Launch Evaluation Report, July 1, 1961.

- Theory & Design Curves for a Yo-Yo Despin Mechanism for Satellites, NASA TN-D708, by J. V. Fedor.
- Performance of the Support Systems Aboard the DME-A Satellite, John Hopkins University Applied Physics Laboratory, TG-907, April 1967.
- Renard, Marc L., Attitude Perturbations and Magnetic Control of a Spin-Stabilized Satellite (Parts I & II), European Space Technology Center, January 1966.
- Spacecraft Magnetic Torques, NASA SP-8018, March 1969.
- UV-MW Horizon Sensor Orbital Experiment Phase B Study, Space Division, North American Rockwell, SD 69-524, Technical Proposal.
- Request for Proposal No. ERC/R&D TCG-0003 , NASA/ERC.
- A Proposal to Flight Test Ultraviolet and Microwave Components of Horizon Sensors for Navigation and Attitude Determination, NASA PM-61.

APPENDIX

A. LIST OF INTERIM REPORTS (TPRs) SUBMITTED TO ERC

Contract Task No.	Report Title	Author(s)
1	FLIGHT ALTERNATIVES	D. F. Adamski
2(a)	ORBIT ANALYSIS/HORIZON SENSOR SATELLITE - TDR 2(a)	T. Rudiger
2(b)	SCANNING MECHANISMS FOR EXPERIMENT INTEGRATION ON 3-AXIS STABILIZED VEHICLES - TDR 2(b)	A. R. Halbardier
2(c)	SYSTEM AND SUBSYSTEM DESCRIPTION AND PERFORMANCE SPECIFICATIONS - TDR 2(c)	M. Cantor
2(c)	PRELIMINARY SPACECRAFT SPECIFICATION	J. D. Ashley
2(c)	SPACECRAFT DESCRIPTION - TDR 2(c)	R. Thompson
2(c)	DESIGN ANALYSIS OF ELECTRICAL POWER GENERATION AND DISTRIBUTION SUBSYSTEM (EPGDS) PROPOSED FOR THE UV/MW HORIZON SENSOR ORBITAL SATELLITE - TDR 2(c)	L. Ule/J. Ambrose
2(c)	DESIGN ANALYSIS, MEASUREMENT SYSTEM - TDR 2(c)	D. S. Mercadante
2(c)	UV/MW TT&C SYSTEM DESCRIPTION-TDR 2(c)	D. S. Mercadante
2(c)	PERFORMANCE SPECIFICATIONS, ELECTRICAL POWER GENERATION & DISTRIBUTION SUBSYSTEM - TDR 2(c)	J. Ambrose
2(c)	PERFORMANCE SPECIFICATIONS, TT&C SYSTEM - TDR 2(c)	D. S. Mercadante
2(c-1)	DYNAMIC CONTROL SYSTEM DESCRIPTION - TDR 2(c-1)	W. Lanning
2(c-2)	DYNAMIC CONTROL SYSTEM SIZE, WEIGHT AND POWER REQUIREMENTS - TDR 2(c-2)	W. Lanning

Contract Task No.	Report Title	Author(s)
2(c-3)	PERFORMANCE SPECIFICATION FOR THE ATTITUDE CONTROL SYSTEM - TDR 2(c-3)	W. Lanning
2(d)	PROGRAM IMPLEMENTATION PLAN FOR UV/MW HORIZON SENSOR SATELLITE - TDR 2(d)	J. F. Farrell
2(e)	SUMMARY OF MASS DISTRIBUTION FOR THE SATELLITE AND BALANCING REQUIREMENTS - TDR 2(e)	F. G. Chapel
2(f)	POWER PROFILE - TDR 2(f)	J. Ambrose
2(g)	MISSION OPERATIONS PLAN - TDR 2(g)	M. A. Cantor
2(g)	OPERATIONS PLAN FOR DYNAMIC CONTROL SYSTEM - TDR 2(g)	W. Lanning
2(h) & 2(k)	INSTRUMENT ALIGNMENT ERROR ANALYSIS- TDR 2(h) ANALYSIS OF CRITICAL STRUCTURAL LOADS DURING BOOST AND THEIR EFFECT ON INSTRUMENT ALIGNMENT - TDR 2(k)	M. A. Cantor
2(i)	COMMUNICATIONS LINK ANALYSIS - TDR 2(i)	D. Mercadante
2(j)	THERMAL CONTROL ANALYSIS - TDR 2(j)	J. McClintic
2(l)	SYSTEM BLOOK DIAGRAM UV/MW REFERENCE SATELLITE CONCEPT - TDR 2(l)	A. R. Halbardier
2(m)	TELEMETRY, TRACKING AND COMMAND REQUIREMENTS, LOGISTICS REQUIREMENTS, AND GSE REQUIREMENTS - TDR 2(m)	J. Ashley
2(n)	UV/MW HORIZON SENSOR EXPERIMENT MISSION SUCCESS ANALYSIS - TDR 2(n)	N. Williams
2(o)	ATTITUDE CONTROL SYSTEM ANALYSIS - TDR 2(o)	W. Lanning
2(p)	DATA REDUCTION REQUIREMENTS - TDR 2(p)	J. Ashley
2(q)	ATTITUDE DETERMINATION AND EXPERIMENT POINTING SYSTEMS - TDR 2(q)	T. Rudiger, L.G. Larson/W.Dixon

Contract Task No.	Report Title	Author(s)
3(a)	EXPERIMENT POWER TRADEOFF - TDR 3(a)	M. Cantor J. Ambrose
3(b)	DATA HANDLING - DATA ACQUISITION AND TRANSMISSION OPPORTUNITIES - TDR 3(b)	M. Cantor
3(c)	TRADEOFF ANALYSIS OF AN ONBOARD VS. GROUND-CONTROLLED ERROR COMPUTER FOR MAGNETIC ATTITUDE CONTROL SYSTEM - TDR 3(c)	W. Lanning
3(d)	CRITICAL INTERFACE REQUIREMENTS BETWEEN REFERENCE SATELLITE AND LAUNCH VEHICLE - TDR 3(d)	R. Thompson